

Analogies Between Microplastics and Natural Particles for Inventory Mapping in Aquatic Sediments

Kumulative Dissertation
zur Erlangung des Akademischen Grades
Doctor rerum naturalium (Dr. rer. nat.)
der Mathematisch-Naturwissenschaftlichen Fakultät
der Universität Rostock

vorgelegt von Kristina Enders, geb. am 23. Juli 1988 in Karl-Marx-Stadt (Chemnitz)

2025-08-12

Note

A digital version of this thesis including supporting information is available in the accompanying repository which you can find at <https://doi.org/10.5281/zenodo.16790144>.



Table of contents

Summary	1
Zusammenfassung	3
List of publications	5
Articles in peer-reviewed scientific journals	5
Conference presentations	7
Synopsis	9
The short history of plastic (debris)	9
The generation of persistent polymeric particles	10
Physicochemical impacts of MP	12
Plastics share in crossing planetary boundaries	14
Tracing human impact in geological records	14
Sediments as passive MP samplers: an untapped potential for monitoring	15
MP particle transport dynamics	16
Surface water transport	16
Transport in suspension	16
Bed load transport	17
Post-depositional reworking	17
Aggregation	19
Biofouling	19
Challenges in quantifying and predicting MP transport	20
Proxy-based empirical predictive modelling	21
Characteristics of potential proxies	22
Proxy-normalisation	24
Prediction	26
Estuaries as model and indicator environments in the Baltic	27
Knowledge gaps and objectives	29
Focus 1: Tracing microplastics through sediment analogies	31
Focus 2: Machine-learning assisted mapping the microplastic legacy	33
Focus 3: Methodological advancements	35
MP extraction from matter-rich samples	35
Analytical accuracy validation and procedural reality check	37
Perspectives and closing remarks	39
References	41
Publications	61
Appendix	319
Abbreviations	319
Statement on the usage of language tools	320
Eigenständigkeitserklärung	321
Acknowledgement	322

Summary

The history of plastic is only about as long as a human life. Yet its intensive use has led to an omnipresence of small particle fragments - known as microplastics (MP) - worldwide. Their dispersal in the environment follows the natural laws of physics, as does natural particulate matter. This way, they have eventually entered the geological record of the Earth as a novel persistent anthropogenic entity. Sediments are considered an ultimate sink for MP in the aquatic environment. However, investigations of this matter- and particle-rich compartment are rare and it is currently impossible to reliably quantify MP inventories and draw MP distribution maps as the knowledge on transport behaviour is very limited.

This thesis takes the route of searching the parallels in the transport behaviour of MP and natural particulates. Hydrodynamic driving forces act on this pool of particles present in the aquatic environment and generate characteristic distribution patterns for different particle sizes, shapes and densities. Sediment grain size is a known indicator of the hydrodynamic conditions in aquatic sedimentary environments and has been applied in normalisation procedures for dissolved contaminants. Herein, it is investigated whether MP as a particulate pollutant spatially correlates with sediment properties and how such correlations could be applied to yield more accurate estimates of pollution levels when accounting for the hydrodynamic regime effect.

Geographically, the focus of the presented work is estuaries (or transitional systems in a broader context) of the Baltic Sea, with case studies in the Warnow and the Schlei. Estuaries are thereby highlighted as key indicator environments for monitoring trends in microplastic pollution. They constitute a bottleneck for plastic transport pathways. The high hydrodynamic diversity of estuaries provides a pronounced depositional behaviour in these systems. In both estuaries investigated, clear correlations between MP and sediment grain size, for example, expressed by the percentage of grains below 63 μm in size (i.e. the mud fraction) could be identified. Bed shear stress was the dominant force of particle sorting, explaining the observed shift in particle size between MP and sediment, as they have different typical material density ranges. By reviewing sampling designs and methods used in available studies, it could be shown that several factors can be detrimental to the identification and accuracy of MP sediment relationships. In particular, the spatio-temporal connectivity of the study area and sufficient sample size with representative coverage of the hydrodynamic conditions, e.g. proxied through grain size variability, are critical. MP concentrations that significantly deviate from the granulometric normalisation regression provide valuable information on the major MP sources in a system, which can then be further monitored and regulated. It is concluded that granulometric normalisation can correct for the hydrodynamic regime bias, allowing for a more reliable data interpretation of sinks and sources and for comparisons of MP levels within and across aquatic sedimentary systems.

In a second step, it was investigated whether granulometric proxies are sufficient predictors in empirical predictive modelling to spatially predict MP. Contrary to the former study on the Warnow, the Schlei, a more complex system, was selected where the spatio-temporal connectivity assumption was severely constrained. A large number of generated predictors (multiple natural particulate proxies, spatio-temporal discontinuity and geographic variables) and the different model classes (generalised linear models, linear and tree-based Extreme Gradient Boosting and Random Forest) were used in the development of a machine learning (ML) modelling pipeline. This endeavour was challenged by the small sample number ($n = 26$), which is much lower than in most ML applications but typical for MP surveys. The goal was to obtain reliable and rigorously validated predictions at locations where observed MP concentrations are not available. The presented pipeline accommodates this by adapting and combining nested cross-validation with adjustable stratification and ensembling for predictive stability. This concept is reflected in the acronym NIXVEGS (Nested Iterative stratified X-Validation-to-Ensemble-modelling through Grid Searches). Again, the percentage of mud was identified as one of the most suitable granulometric proxies, on par with a derived variable representing the first principal coordinate of the grain size distribution. However, the data reflect the recency of a significant localised MP input event and the higher geomorphological and hydrodynamic complexity, which necessitated the introduction of a predictor to account for the discontinuity in MP propagation. Based on a hydronumeric model, predictors

were generated of which one describing the mean traveling time of a passive tracer (i.e. a water molecule) provided the best fit in combination with the granulometric proxy. At more than 180 stations with available grain size data, NIXVEGS estimated that ~20 trillion MP particles (50 - 5000 μm) reside in the Schlei sediments, extending to a layer depth most relevant for the ‘plastic age’ (0 - 15 cm). Based on advancements in the analysis of all three dimensions of MP particles, a more reliably mass estimate of MP was provided, amounting to ~14.4 tonnes. These model estimates represent the highest resolution picture of an MP inventory for an entire geomorphological region to date. The generalisation score (on unseen data) reached a R^2 of 0.7 and proved robust in a sensitivity analysis. The entire data-analytical workflow follows FAIR principles (findability, accessibility, interoperability, reusability). The co-development of an MP database enabled structured data management across projects and allowed error-free querying of data by reproducible executable Jupyter notebooks and Python scripts that build the model environment. A web application is provided that allows readers to comprehensively explore the entire raw particle data in various visualisations.

While the theoretical and model-conceptual developments represent the main scientific contributions of this thesis, they would not have been possible without further methodological advances. This concerns the optimisation of purification techniques for solid-matter-rich samples, which were required to increase sample throughput. A modular protocol scheme was developed, adaptable to different sample matrix compositions. A conical spiral conveyor was invented that can assist gentle agitation of sediments in density separation. Several other publications on method and model development or evaluation are described as part of the foci in this thesis, i.e. on electrostatic MP separation, a novel immobilised laboratory ring-trial design, digestion method validations, error estimation of subsampling strategies, evaluation on environmental representativeness of MP exposure studies and an uncertainty analysis for hydronumeric MP models.

Zusammenfassung

Die Geschichte des Plastiks ist nur etwa so lang wie ein Menschenleben. Doch seine intensive Nutzung hat zu einer weltweiten Verbreitung von kleinen Partikelfragmenten - bekannt als Mikroplastik (MP) - geführt. Deren Ausbreitung in der Umwelt unterliegt denselben physikochemischen Prozessen wie natürliche Partikel. Auf diesem Weg gehen sie schließlich als neuartige persistente anthropogene Partikelklasse in die Bildung geologischer Schichten ein. Sedimente gelten als ultimative Senke für MP in der aquatischen Umwelt. Untersuchungen dieses Kompartiments sind jedoch selten, und es ist derzeit weitgehend unmöglich, MP-Bestände zuverlässig zu quantifizieren und MP-Verteilungskarten zu erstellen, auch da das Wissen über das Transportverhalten sehr begrenzt ist.

Diese Dissertation verfolgt den Ansatz, die Analogien im Transportverhalten von MP zu natürlichen Partikeln zu untersuchen. Hydrodynamische Kräfte wirken auf diese Partikelvorkommen in der aquatischen Umwelt und erzeugen charakteristische Verteilungsmuster für verschiedene Partikelgrößen, -formen und -dichten. Die Sedimentkörnung ist ein häufig verwendeter Indikator für die hydrodynamischen Bedingungen und wurde bereits für Normalisierungsverfahren von gelösten Schadstoffen angewendet. Mittels empirischer statistischer Verfahren wurde untersucht, ob MP als partikulärer Schadstoff räumlich mit bestimmten Sedimenteigenschaften korreliert und wie solche Korrelationen genutzt werden können, um unter Berücksichtigung der lokalen Auswirkungen des hydrodynamischen Regimes genauere Abschätzungen der Belastung des Systems zu gewinnen.

Geografisch liegt der Fokus der vorgestellten Arbeiten auf den Ästuaren (oder transitionalen Systemen im weiteren Sinne) der Ostsee mit Fallstudien in der Warnow und der Schlei. Die Rolle der Ästuarie als wichtige Indikatorgebiete für die Beurteilung der MP-Belastung und deren Entwicklung wird dabei hervorgehoben. Ästuarie stellen einen dynamischen Filter für den Transport von Partikeln auf dem Weg zum Meer dar. Die hohe hydrodynamische Vielfalt und biogeochemische Reaktivität in Ästuaren sorgt für ein ausgeprägtes Ablagerungsverhalten dieser Systeme. In beiden untersuchten Ästuaren konnten eindeutige Korrelationen zwischen MP und der Sedimentkorngröße, z. B. ausgedrückt durch den prozentualen Anteil an Feinsediment (Korngrößen $< 63 \mu\text{m}$), festgestellt werden. Die Bodenschubspannung war die dominierende Kraft der Partikelsortierung. Sie erklärt den beobachteten Größenunterschied zwischen MP und Sedimenten, da beide Partikeltypen unterschiedliche charakteristische Materialdichten aufweisen. In einer Metaanalyse von Beprobungs- und Analysemethoden früherer Studien konnte gezeigt werden, dass mehrere Faktoren die Identifizierung und Genauigkeit der MP-Sediment-Beziehung beeinträchtigen können. Entscheidend sind dabei insbesondere die räumliche und zeitliche hydrologische Konnektivität des Untersuchungsgebiets und eine ausreichende Stichprobengröße mit einer repräsentativen Abdeckung der hydrodynamischen Bedingungen, z. B. über die Variabilität der Korngröße. MP-Werte, die signifikant von der granulometrischen Normalisierungsregression abweichen, können wertvolle Informationen über die Hauptquellen von MP in einem System liefern, die dann weiter überwacht und reguliert werden können. Es wird gezeigt, dass eine granulometrische Normalisierung die durch das hydrodynamische Regime verursachten Verzerrungen in den MP-Konzentrationsdaten ausgleicht und so eine zuverlässigere Interpretation der Daten ermöglicht. Dies ermöglicht die Beurteilung von Senken und Quellen sowie einen Vergleich von MP-Belastungen innerhalb eines oder zwischen verschiedenen aquatischen Sedimentsystemen.

In einem zweiten Schritt wurde untersucht, ob granulometrische Proxys in empirischen Modellen ausreichen, um MP räumlich vorherzusagen. Im Gegensatz zur früheren Studie in der Warnow wurde ein komplexeres System, die Schlei, ausgewählt, in dem die Annahme einer hinreichenden räumlichen und zeitlichen Konnektivität stark eingeschränkt ist. Eine Vielzahl generierter Prädiktoren (mehrere natürliche Partikelproxys, räumliche und zeitliche Diskontinuitäts- sowie geografische Variablen) und verschiedene Modellklassen (generalisierte lineare Modelle, lineares und baumbasiertes Gradient Boosting und Random Forest) wurden in der Entwicklung einer auf maschinellem Lernen (ML) basierenden Modellierungspipeline verwendet. Dies wurde durch die geringe Probenanzahl (hier $n = 26$) erschwert, die zwar für MP-Studien typisch ist, jedoch weit unter anderen Anwendungsfällen von ML-Techniken liegt. Ziel war es, validierte Vorhersagen an Orten zu erhalten, an denen keine beobachteten MP-Konzentrationen verfügbar sind. Die vorgestellte Pipeline berücksichtigt dies durch die Anpassung und Kombination von algorithmischen

Komponenten wie “Nested Cross-Validation” mit regulierbarer Stratifikation und Ensemblebildung für bessere Modellstabilität. Dieses Konzept spiegelt sich im Akronym NIXVEGS (Nested Iterative stratified X-Validation-to-Ensemble-modelling through Grid Searches) wider. Wie bereits in der Warnow wurde auch hier der prozentuale Feinsediment-Anteil als einer der am besten geeigneten granulometrischen Proxys identifiziert, gleichauf mit einer abgeleiteten Variable, die die erste Hauptkoordinate der Korngrößenverteilung repräsentiert. Allerdings spiegelt sich in den Daten der Einfluss eines kürzlich erfolgten signifikanten lokalen MP-Eintragsereignisses wider. Zusammen mit der höheren geomorphologischen und hydrodynamischen Komplexität der Schlei erforderte dies die Einführung eines Prädiktors, der diese Diskontinuität der MP-Ausbreitung berücksichtigt. Auf Basis eines hydronumerischen Modells wurde eine Reihe potenzieller Prädiktoren generiert. Einer, welcher die mittlere Transportdauer eines passiven Tracers (d.h. Wassermolekül) beschreibt, wurde als am besten passend identifiziert, in Kombination mit dem granulometrischen Proxy. An über 180 Stationen mit verfügbaren Korngrößendaten schätzte NIXVEGS, dass sich ~20 Billionen MP-Partikel (50 - 5000 μm) in den Schlei-Sedimenten befinden, die sich bis zu einer Schichttiefe erstrecken, welche für das ‘Plastikzeitalter’ am relevantesten ist (0 - 15 cm). Basierend auf Fortschritten in der Analyse aller MP-Partikel aller drei Dimensionen konnte eine genauere Masseabschätzung von MP ermittelt werden, die etwa 14,4 Tonnen für das MP-Inventar der Schlei beträgt. Dieser Modellansatz ermöglicht ein hochaufgelöstes Bild eines MP-Bestands für eine gesamte geomorphologische Region. Die Generalisierungsgenauigkeit (d.h. die Vorhersagegenauigkeit auf ungesehenen Daten) wurde durch NIXVEGS auf einen R^2 von 0,7 geschätzt und erwies sich als robust in einer Sensitivitätsanalyse. Der gesamte datenanalytische Workflow folgt den FAIR-Prinzipien (findability, accessibility, interoperability, reusability). Diese Studie stützt sich dazu auf eine parallel entwickelte Datenbank für MP-Partikel, welche eine strukturierte Datenverwaltung über Projekte hinweg und eine fehlerfreie Abfrage der Daten durch reproduzierbar ausführbare Jupyter-Notebooks und Python-Skripte erlaubt. Darüber hinaus wird eine Webanwendung bereitgestellt, die es dem Nutzer ermöglicht, die gesamten Partikel-Rohdaten umfassend in verschiedenen Visualisierungen zu untersuchen.

Die theoretischen und modellkonzeptionellen Entwicklungen stellen die wesentlichen wissenschaftlichen Beiträge dieser Dissertation dar. Sie wären jedoch ohne weitere methodische Fortschritte nicht möglich gewesen. Dazu gehört die Optimierung von Aufreinigungsverfahren für partikelreiche Proben, um den Probendurchsatz zu erhöhen. Es wurde ein modulares Protokollschema entwickelt, das an verschiedene Probenmatrizen angepasst werden kann. Ein konischer Spiralförderer wurde entwickelt, der eine schonende Durchmischung von Sedimenten bei der Dichte-Trennung ermöglicht.

Mehrere andere Veröffentlichungen zur Methoden- und Modellentwicklung bzw. -evaluierung werden im Rahmen der Foki dieser Arbeit beschrieben. Dies umfasst unter anderem Untersuchungen zur elektrostatischen MP-Abscheidung, ein neuartiges Design für Labor-Ringversuche unter Nutzung immobilisierter Partikel, zwei Verfahren zur Validierung von Aufschlussmethoden, Fehlerbestimmungen von Probenteilungsstrategien, eine Evaluierung der Umweltrepräsentativität von MP-Expositionsstudien und eine Unsicherheitsanalyse anhand eines hydronumerischen MP-Transportmodells.

List of publications

Articles in peer-reviewed scientific journals

Publications are included in full length in the appendix of this thesis

- **Enders, K.**, Lenz, R., Fischer, F., Schwarzer, K., Seiß, G., Fischer, D., Labrenz, M.,
Mapping the plastic legacy: Machine-learning enabled microplastic inventory prediction in aquatic sedimentary systems (submitted)
Major contribution: Conceptualisation, method development, sedimentological and geo-chemical analysis, data curation, analysis and interpretation, manuscript writing
Minor contribution: NIXVEGS model development, visualisation, spectroscopic chemical MP analysis
The estimated combined contribution to the written manuscript was ~70%
- Lenz, R., **Enders, K.**, Vizsolyi, E.C., Schumacher, M., Lötsch, J., Löder, M.G.J., Eder, G., Voronko, Y., Andrade-Garda, J.M., Muniategui-Lorenzo, S., Laforsch, C., Fischer, D., Labrenz, M. (2024)
What goes around should not move around: immobilising microplastics as a new approach for analytical ring trials, Environmental Science and Technology, 58, 22224–22234 | doi:10.1021/acs.est.4c09427
Major contribution: Conceptualisation of filtration immobilisation approach, data curation
Minor contribution: interpretation and visualisation data, statistical approach and interpretation of quantitative data, spectroscopic chemical MP analysis, manuscript writing
The estimated combined contribution to the written manuscript was ~30%
- Čerkasova, N., **Enders, K.**, Lenz, R., Oberbeckmann, S., Brandt, J., Fischer, D., Fischer, F., Labrenz, M., Schernewski, G. (2023)
A Public Database for Microplastics in the Environment, Microplastics, 2, 132-146 | doi:10.3390/microplastics2010010
Minor contribution: database structure conceptualisation, support of database development, visualisations, editing, manuscript writing
The estimated combined contribution to the written manuscript was ~25%
- Lenz, R., **Enders, K.**, Fischer, F., Brandt, J., Fischer, D., Labrenz, M. (2021)
Measuring impacts of microplastic treatments via image recognition on immobilised particles below 100 µm, Microplastics and Nanoplastics, 1, 12 | doi:10.1186/s43591-021-00012-0
Major contribution: Interpretation and visualisation of qualitative data and respective manuscript section
Minor contribution: Conceptualisation, practical work, statistical approach and interpretation of quantitative data, manuscript writing

The estimated combined contribution to the written manuscript was ~30%

- Brandt, J., Fischer, F., Kanaki, E., **Enders, K.**, Labrenz, M., Fischer, D. (2021)
Assessment of subsampling strategies in microspectroscopy of environmental microplastic samples, *Frontiers in Environmental Sciences*, 8, 579676 | doi:10.3389/fenvs.2020.579676
Major contribution: Data interpretation and discussion of results
Minor contribution: Manuscript writing
The estimated combined contribution to the written manuscript was ~10%
- **Enders, K.**, Tagg, A.S., Labrenz, M. (2020)
Evaluation of Electrostatic Separation of Microplastics From Mineral-Rich Environmental Samples, *Frontiers in Environmental Science*, 8, 112 | doi:10.3389/fenvs.2020.00112
Major contribution: Conceptualisation, data acquisition, analysis and interpretation, method validation, visualisation, manuscript writing
The estimated combined contribution to the written manuscript was ~80%
- **Enders, K.**, Lenz, R., Ivar do Sul, J.A., Tagg, A.S., Labrenz, M. (2020)
When every particle matters: A QuEChERS approach to extract microplastics from environmental samples, *MethodsX*, 7, 100784 | doi:10.1016/j.mex.2020.100784
Major contribution: Protocol compilation and development, development of conical spiral conveyor and adaptation of associated laboratory equipment, method validation, manuscript writing
Minor contribution: Conceptualisation, visualisation
The estimated combined contribution to the written manuscript was ~65%
- Osinski, R.D., **Enders, K.**, Gräwe, U., Klingbeil, K., Radtke, H. (2020)
Model uncertainties of a storm and their influence on microplastics and sediment transport in the Baltic Sea, *Ocean Science*, 16, 1491-1507 | doi:10.5194/os-16-1491-2020
Major contribution: Integration and interpretation of sediment-MP proxy approach
Minor contribution: Manuscript writing
The estimated combined contribution to the written manuscript was ~15%
- **Enders, K.**, Käßler, A., Biniash, O., Feldens, P., Stollberg, N., Lange, X., Fischer, D., Eichhorn, K.-J., Pollehne, F., Oberbeckmann, S., Labrenz, M. (2019)
Tracing microplastics in aquatic environments based on sediment analogies, *Scientific Reports - Nature*, 9, 15207 | doi: 10.1038/s41598-019-50508-2
Major contribution: Conceptualisation, sedimentological analysis, data curation, analysis and interpretation, visualisation, manuscript writing
Minor contribution: Theoretical validation, Spectroscopic chemical MP analysis, geo-chemical analysis
The estimated combined contribution to the written manuscript was ~85%
- **Enders, K.**, Lenz, R., Beer, S., Stedmon, C.A., (2017)
Extraction of microplastic from biota: recommended acidic digestion destroys common plastic polymers, *ICES Journal of Marine Science*, 74, 326-331 | doi:10.1093/icesjms/fsw173
Major contribution: conceptualisation, data acquisition, data curation, visualisation,

manuscript writing

The estimated combined contribution to the written manuscript was ~60%

- Lenz, R., **Enders, K.**, Nielsen, T.G., (2016)

Microplastic exposure studies should be environmentally realistic, Proceedings of the National Academy of Science (PNAS), 113 | doi:10.1073/pnas.1606615113 (letter to the editor)

Major contribution: conceptualisation

Minor contribution: discussion, manuscript writing

The estimated combined contribution to the written manuscript was ~25%

The full publication record can be viewed on ORCID: <https://orcid.org/0000-0002-2710-7591>

Conference presentations

- **Enders, K.**, Mapping the Plastic Legacy: Geospatial Predictions of a Microplastic Inventory in a Complex Estuarine System Using Machine Learning, Poster | MICRO, Arrecife, 2024
- **Enders, K.**, From Sample to Insight – Streamlining the Microplastics Data Processing Pipeline, Presentation, Podium Discussion | Mini-Symposium: cornet project MICROPLEXFOOD, Vienna 2024
- **Enders, K.**, Round robin goes around - immobilizing microplastics as a new approach for analytical ring trials, Presentation | ESOPS, Berlin, 2024
- **Enders, K.**, Mapping the Plastic Legacy: Geospatial Predictions of a Microplastic Inventory in a Complex Estuarine System Using Machine Learning, Poster | NFDI for Earth, Dresden, 2024
- **Enders, K.**, Mapping the Plastic Legacy: Geospatial Predictions of a Microplastic Inventory in a Complex Estuarine System Using Machine Learning, Presentation | EGU General Assembly, Vienna, 2024
- **Enders, K.**, Granulometric Proxy-based Geo-spatial Prediction of Microplastic Inventories in Sediments, Presentation | SETAC, Dublin, 2023
- **Enders, K.**, Different software for different samples? Comparison of two automated approaches for the fast analysis of microplastics with Raman microspectroscopy, Poster | SETAC, Copenhagen, 2022
- **Enders, K.**, Tracing microplastics in aquatic environments based on sediment analogies, Presentation | Baltic Sea Science Congress, Stockholm, 2019
- **Enders, K.**, Tracing microplastics in aquatic environments based on sediment analogies, Presentation | MICRO, Arrecife, 2018
- **Enders, K.**, and Lenz, R., Plastik in der Umwelt - Aktuelle Forschung und Lösungsansätze, Presentation and Discussion | Hans-Böckler foundation, Greifswald, 2018

Co-authored conference contributions are not included in this list.

Synopsis

The short history of plastic (debris)

The first semi-synthetic plastics, Parkesine and celluloid, were invented in the 1860s and ought to replace constrained materials such as horn or ivory. The onset of plastics came with the promise to make manufacturing independent of limited natural resources. The first fully synthetic plastic (no natural molecules involved), Bakelite, was invented in 1907, at the start of the electrification period in Europe and Northern America, as a substitute for shellac for electrical insulators. This innovation stimulated synthetic polymer research, leading to the development of many new polymer types over the coming decades ([Freinkel, 2011](#)). Plastics represent a material group with seemingly unlimited transformability, which can be moulded into nearly anything and has virtually become accessible to everyone. During the 1950s, plastics began an exponential rise to become global mass products ([Geyer et al., 2017](#)). Human society benefits from the versatility, durability and relatively low cost of these materials ([Andrady & Neal, 2009](#)). Many technological innovations, human health and prosperity depend on and have been built with the help of synthetic polymers. It appears hard to imagine modern medicine and research, or packaging and electronic devices in our daily lives, without plastics. However, formerly positively connoted product properties - strong, lightweight and durable - turn into persistent and potentially hazardous complex debris when interacting with organisms in the environment ([Rochman et al., 2013a](#)).

Already shortly after the beginning rise of plastics, in the late 1960s, plastic debris was found in marine biota and first negative effects were associated, such as the reduction in digestive efficiency, meal size and body mass ([Kenyon & Kridler, 1969](#); [Harper & Fowler, 1987](#); [Ryan, 2015](#)). Certain species of marine mammals and sea birds were found to be especially prone, to be affected by floating plastic debris. For example, the entanglement in plastic debris has been identified as a driver for the decline of a local seal population ([Fowler, 1987](#)).

A decade later, small synthetic fibres, pellets and small fragments, nowadays termed ‘microplastics’ (MP), were reported in surface water samples from the North Sea and the North West Atlantic ([Buchanan, 1971](#); [Carpenter & Smith, 1972](#); [Colton et al., 1974](#)). Carpenter & Smith (1972) already highlighted the potential risk of intestinal blockage and transfer of plasticisers and persistent organic pollutants (e.g. polychlorinated biphenyls) to organisms. In response to the initial publications on marine plastic pollution, a multilateral treaty, MARPOL 73/78 ([IMO, 1988](#)) on the reduction of ship-generated litter, as well as industry initiatives on plastic pellets and recycling, were drawn up. While these measures had some effect, they were outweighed by the ongoing increase in plastic production and land-based waste generation volumes in the years to follow ([Ryan, 2015](#)).

In the 2000s, reports on large garbage patches in ocean surface water gyres (e.g. [Moore et al., 2001](#); [Law et al., 2010](#)) and the increasing accumulation of MP in coastal environments ([Thompson et al., 2004](#)), drew the attention of a broader scientific community and the public to these pervasive particulate pollutants ([Carpenter, 2022](#)). In retrospect, it is remarkable that what made people aware of the consequences of plastic handling and consuming practices was the discovery of these tiny remnants of modern life in assumingly pristine areas like places such as remote islands and the open marine environment far from human habitation ([Ivar Do Sul et al., 2009](#)), even though their intimate surroundings had long been affected by this pollution.

Over the next two decades, numerous research studies have identified MP in various environments, from ocean surface and sub-surface waters ([Law et al., 2010](#); [Enders et al., 2015](#)) and coastal areas ([Browne et al., 2011](#)) to the deep sea ([Van Cauwenberghe et al., 2013](#)), from marine environment to lakes ([Eriksen et al., 2013](#); [Imhof et al., 2013](#)), rivers ([Mani et al., 2015](#)), the atmosphere ([Dris et al., 2016](#)) and terrestrial soils ([Piehl et al., 2018](#)). Research began to focus on identifying sources to the aquatic system such as waste water treatment plants (WWTP) ([Murphy et al., 2016](#)) as well as direct human exposure pathways through food intake ([Rochman et al., 2015](#); [Yang et al., 2015](#); [Mason et al., 2018](#)) and inhalation via household dust ([Vianello et al., 2019](#)). More recently, human excrement ([Schwabl et al., 2019](#)), blood ([Leslie et al., 2022](#)) and various organs were analysed, although quantification in parts remain limited by methodological constraints (as

reviewed in [Roslan et al., 2024](#)). In essence, MP were found wherever researchers looked. Over the last decade, significant efforts have been made to identify ever smaller particles of plastic pollution, beyond what can be reliably identified visually ([Lenz et al., 2015](#); [Käppler et al., 2015](#); [Ivleva, 2021](#)). Simultaneously, purification and quality control techniques were developed and adapted to enable the chemical identification of MP in various sample types ([Hidalgo-Ruz et al., 2012](#); [Löder et al., 2017](#); [Enders et al., 2020b](#)).

Today, the global plastic production volume has reached 414 million tonnes ([PlasticsEurope, 2024](#)). Under current projections, approximately 1,100 million tonnes per year would be reached in 2050, amounting to 33.000 million tonnes of plastics produced in total ([Geyer, 2020](#)). While in the past only 10% were recycled, the significant share of plastic waste was discarded to landfills and open dumpsites (76%) including the losses to the environment, and a minor part was handled in incineration plants (14%) ([Geyer, 2020](#)). It is estimated that approximately 20 million tonnes of plastic enter aquatic ecosystems annually ([Borrelle et al., 2020](#)). However, these estimates do not include MP and remain generally difficult to validate. Although relative recycling and incineration rates are projected to increase ([Geyer, 2020](#)), the continued acceleration of plastic production and inadequate waste management, and the persistence and irreversible discharge of (micro)plastics to ecosystems prospect an exacerbation scenario. Under a business-as-usual trajectory, over 60 million tonnes of plastic could be discharged annually by 2050 ([Yan et al., 2024](#)), which represents a conservative estimate compared to other projections that reach two or three times higher numbers ([Lebreton & Andrady, 2019](#); [Lau et al., 2020](#); [OECD, 2022](#)). These projections greatly vary globally depending on economic and population growth ([OECD, 2022](#)). According to the environmental Kuznets Curve, there is an inverse U-shaped relationship between the deterioration of the environment and economic income per capita, based on global gross domestic product (GDP) ([Grossman & Krueger, 1991](#); [Shafik & Bandyopadhyay, 1992](#); [Barnes, 2019](#)). The model developed by Yan et al. ([2024](#)), incorporating changes in population demographics, economic activity, and technological advancements ([Dietz & Rosa, 1997](#)) into the Kuznets Curve, projects that plastic pollution will be significantly reduced in higher-income countries, whereas lower-income countries are likely to initially experience increased environmental inputs. However, even countries with more advanced waste management systems targeting macroplastics face the problem that MP is less easily mitigated ([Thompson et al., 2024](#)).

Along with this second wave of scientific and public awareness on marine plastic pollution, a new momentum started for finding global solutions to this global problem. In 2022, a resolution was adopted to establish an internationally legally binding instrument to address plastic pollution at all stages of the lifecycle; however, there is currently still no final agreement on concrete measures ([UNEP, 2022, 2025](#)). Developing appropriate monitoring procedures is essential for reliably quantifying (micro)plastic pollution levels and evaluating the effectiveness of measures at regional and cross-national levels, which have yet to be implemented.

The generation of persistent polymeric particles

Plastic debris has been defined as ‘objects consisting of synthetic or heavily modified natural polymers as an essential ingredient that, when present in natural environments without fulfilling an intended function, are solid and insoluble at 20 °C’ ([Hartmann et al., 2019](#)). Polymers are macromolecules, repetitively connected chains of subunits (monomers) in a process called polymerisation. Although polymers can contain substantial amounts of heteroatoms, carbon typically forms their backbone except for some cases such as silicone rubber. Chain length, arrangement and type of monomers determine their properties. Generally, polymers with higher molecular weights tend to be stronger and more durable ([Carraher Jr., 2017](#)).

Most natural polymers, such as deoxyribonucleic acid (DNA), cellulose and lignin, have functional groups that make them accessible to biodegradation ([Zhao et al., 2022](#)). Lignin is an example of a complex and variable natural polymer which evolved to fulfil structural functions in plants and to provide resistivity against microbial attack ([Hahn & Hennecke, 2023](#)). Over long time periods, complex ecosystems of fungal and microbial organisms have co-evolved that work in a sequential or complementary manner to effectively degrade it with the help of secondary metabolites and intracellular and extracellular enzymes ([Janusz et al., 2017](#)). The vast abundance of lignin in nature, coupled with its chemical structure and configuration consisting of multiple reactive functional groups, makes it accessible for enzymatic attack. Most synthetic polymers are chemically more uniform and lack such functional groups that act as chemical handles for enzymatic attack ([Hahn & Hennecke, 2023](#)). Often they are equipped with additives to increase resistance towards certain environmental conditions. On evolutionary time scales, they have only existed for a short period and for most plastic polymers natural degradation mechanisms have not evolved to be able to consume them at rates at which we release them into the environment.

Despite their better resistance towards biodegradation, as any matter, living or non-living, plastics undergo an inevitable deterioration process under environmental exposure. Photo-, oxidative and

mechanical forces (for certain polymers also hydrolysis) work in tandem to fragment the polymer backbone down to micro- and nanometre scales (Andrady, 2011). Polymer chemistry, morphology as well as environmental conditions fundamentally determine surface degradation rates. Chamas et al. (2020) exemplarily calculated fragmentation rates under different environmental settings: while for high-density polyethylene (HDPE) bottles an average material thickness reduction of 4.3 μm per year (ranging from 0 - 11 μm) was measured under marine conditions, low-density polyethylene (LDPE) plastic bags reached between 1.6 and 83 μm per year under photo-thermal composting conditions on land. Three-dimensional disintegration such as cracks were not considered by this study which would further increase surface area and degradation rates. Based on initial volumes and surface area, half-lives varied between months to thousands of years (Chamas et al., 2020). However, realistic lifetime estimates for MP do not exist due to the limitations in conducting long-term studies that adequately represent the high diversity of environmental pathways and actual exposure to degradative forces. Conditions span from relatively rapid mechanical break down and UV exposure on beaches to nearly complete conservation in deep sea environments characterised by limited light, low temperature and oxygen levels (Zalasiewicz et al., 2016). Replicating those in a test setting is difficult. The conservative conditions deep in the sea are illustrated by plastic pellets that were found unchanged, conserved for 29 years within a shipwreck in the Red Sea, Egypt. In contrast, companion pellets that had beached nearby showed various structural changes (Brümmer et al., 2022). Also in analogy to the natural polymer amber which can be preserved for millions of years on the sea bed, similarly long life spans for plastics under conserving conditions are reasonable (Chubarenko & Stepanova, 2017).

Thus, depending on the environmental conditions and chemical structure, most synthetic polymers can only be biodegraded once their molecular weight is small enough (Gewert et al., 2015). Microorganisms can remineralise polymers into inorganic substances (Guggenberger, 2005), foremost carbon dioxide, water and salts, although many natural polymers are also integrated into biomass or humic substances under aerobic conditions or methane under anaerobic conditions. Remineralisation represents the final stage in the degradation process, from which the remaining compounds are re-integrated into biogeochemical cycles (Hahn & Hennecke, 2023). Certainly, degradation mechanisms appear not to be able to cope with the current production pace, leading to a steady accumulation in the environment (Thompson et al., 2024).

In recent years more bacteria and fungal genera were identified that are capable of degrading various synthetic polymers (Ibrahim et al., 2024). Although the mechanisms involved are largely unknown (Hahn & Hennecke, 2023), given the various abilities and high adaptability of microorganisms to degrade other complex energy-rich organic structures, it seems reasonable that similar versatile and complex webs of degrading mechanisms evolve for plastic polymers (Andler et al., 2022). However, synthetic polymers are still a niche carbon source compared to other organic compounds, implying that evolutionary pressure for organisms to evolve suitable enzymatic attack mechanisms remain low outside of substantial pollution hotspots (Oberbeckmann & Labrenz, 2020). Yoshida et al. (2016) identified polyethylene terephthalate (PET)-degrading bacteria in the sediments near a PET bottle recycling facility in Japan. Microbial and enzymatic degradation are interesting for technical recycling applications due to enhanced, cleaner recyclates and improved sustainability (Akram et al., 2024). A first enzymatic bio-recycling plant in France has been installed (Tournier et al., 2020).

Studying these processes in the environment is difficult, also because many bacterial communities growing on polymers are not directly metabolising their constituents. While some might be important for involved processes e.g. by feeding on plastic degradation products, others just use the opportunity to colonise a floating surface as a hitchhiking vehicle through the ocean in order to consume water solutes and organic matter (Oberbeckmann et al., 2021). The complex and ever-changing interplay of physicochemical and biological degradation processes introduces considerable uncertainties in degradation rates (Gewert et al., 2015; Hahn & Hennecke, 2023). For instance, it has been noted that degradation efficiencies may be overestimated due to the relatively rapid initial breakdown of monomeric or oligomeric residues within the polymeric matrix (Klaeger et al., 2019). On the other hand, natural communities of degraders and their metabolic supporters may be more efficient than individual representatives extracted for study (Hahn & Hennecke, 2023). Yet, if and where environmental biodegradation of plastic polymers can contribute a quantitatively significant effect to its removal is unclear.

As a result of this continuous but foremost physicochemically driven fragmentation process, MP are being created as an intermediary size unit, often defined as being between 1 μm and 1 or 5 mm in their longest dimension. While the upper limit of 1 mm complies with the metric system (Hartmann et al., 2019), 5 mm is a more practical limit coined when scientists found plastic pieces in nature that escaped reliable identification and characterisation by the naked eye (Thompson et al., 2004). The effective lower size limit is mainly determined by the capabilities of the analytical detection limits. Although some analytical techniques can achieve sub-micron scale such as Raman spectroscopy (Gillibert et al., 2019), they are not yet widely applied, and practical limits arise concerning increasing self-contamination in the processing pipeline when working with particles in the sub 10 μm range under typical laboratory conditions (i.e. no certified cleanroom facilities). The

chemical analysis of MP is a large research field on its own with multiple analytical approaches that were customised to MP characterisation as summarised by several comprehensive reviews on the topic (Ivleva, 2021; Primpke et al., 2020). In the context of this thesis foremost Raman spectroscopy has been used. This technique coupled to microscopy and highly automated particle recognition routines is applied in state-of-the-art MP particle quantification methods, achieving particle detection limits in the lower micron size range, 1 μm theoretically, 4 μm practically (Brandt et al., 2020). The identification thereby is facilitated by collecting the spectral Raman scattering signal induced by an incident laser on a particle surface. The bands of varying intensity reveal the vibrational frequencies of excited Raman-active chemical groups and together form a chemical fingerprint of the material present at the measurement spot (Käppler et al., 2016). The high-throughput collection and evaluation of spectra on tens of thousands of particles per sample is the basis for the complete quantification and characterisation of the MP load in entire sample sets (Brandt et al., 2020). In contrast to mass-based methods such as pyrolysis-gas chromatography coupled mass-spectrometry, Raman and other vibrational spectroscopic methods such as Fourier transform infrared (FTIR) operate particle-based and provide information on particle characteristics such as size and shape, which are fundamental information regarding the study of particle transport processes.

In recent years, efforts were devoted to detect nanometer-sized plastic particles. The scales and occurrences of nanoplastics, however, have so far been explored primarily through theoretical models and under laboratory experiments, as isolating these particles from environmental matrices becomes increasingly challenging at smaller sizes (Koelmans et al., 2015; Mattsson et al., 2021). The existence of nanoplastics seems plausible, due to the continuous breakdown of matter, resulting in increasingly numerous and smaller particles which approach the smallest possible polymer and eventually oligomer units ranging in the lower nanometer scales (as a comparative example: the length of a CC-bond is 0.154 nm, a polyvinyl chloride (PVC) monomer unit measures 0.25 nm, Wunderlich, 2005). Under ultraviolet (UV) radiation in the laboratory, Pfohl et al. (2022) demonstrated that polymers continuously fragmented down to 10 nm suggesting that the formation of water-soluble organics and internalisation by microbes is possible. Yet, the stability of micro- and nanoplastics in the natural environment remains largely unknown. A certain size range could exist where they exhibit enhanced stability, being sufficiently small to avoid physical damage due to increased mobility, yet large enough to resist microbial degradation. Given the analytical challenges that already arise for small MP (e.g. single particle handling and characterisation), protocols adopted for MP appear mostly inapplicable for nanoplastics (Zhang et al., 2022; Azeem et al., 2023). The focus of this thesis lies within the MP size spectrum.

Physicochemical impacts of MP

Plastic production demands large quantities of chemicals. Additives are commonly applied to impart or enhance specific properties, e.g. plasticisers, flame retardants, surfactants, thermal and UV stabilisers, antioxidants, pigments, antistatics, nanoparticles or nanofibres, biocides, and fragrances. Residues of processing aids such as lubricants, solvents and catalysts facilitate plastic production or processing and can be retained in the plastic products. Unpolymerised monomers, breakdown and by-products of the reactions can remain in the polymers due to incomplete or impure production processes (Wiesinger et al., 2021). According to a review by Wagner et al. (2024), more than 16,000 different chemical substances are associated with the production and manufacturing of synthetic polymers. 15 chemical groups related to plastics are categorised as hazardous, e.g. phthalates, bisphenols, parabenes, aromatic amides, benzotriazoles. However, these numbers are incomplete due to the problem of missing characterisation, usage declaration and harmonisation of information and regulations (Wagner et al., 2024).

Under EU criteria, approximately a fourth of the plastic-associated chemicals are categorised as substances of potential concern due to their persistence, bioaccumulation and toxicity (Wiesinger et al., 2021). For over 10,000 plastic-associated compounds hazard information is missing. Half of those are assigned a high level of concern, due to high production volumes exceeding 1,000 tonnes annually (Wagner et al., 2024). The additive content in common technical polymers ranges between 0.05% - 70%. Many compounds are not covalently bound to the polymer matrix and leak throughout all stages of a (micro)plastic life cycle from production, transport, usage, potential recycling stages to the dump site, and as part of a chemical degradation process leading to ecosystem exposure. Continued fragmentation increases the exposure potential to a larger range of organisms due to increased mobility and the increase of particle numbers and exposure surface. Associated chemicals still entrapped in the polymer matrix experience a time-delayed release, also referred to as the ‘plastic toxicity debt’ (Rillig et al., 2021), as newly exposed larger relative polymer surface areas are created. Thus, ecosystem implications can be expected long-term and outlast the materials operating life.

The effects of the hazardous chemicals associated with plastics span from carcinogenicity, muta-

genicity, endocrine disruption, reproductive toxicity, developmental toxicity, ecotoxicity to aquatic organisms, nerve damage, metabolic effects, and biocidal effects (Groh et al., 2019). Chemical cocktail effects can occur from intendedly added substances during production as well as substances absorbed during their life cycle. The creation of new chemical additives and their potential chemical cocktail effects outpace the capacity in toxicological exposure risk assessments (Wiesinger et al., 2021; Wagner et al., 2024). Recent leachate toxicity tests that are capable of capturing the mixture effect of MP revealed that polycarbonate (PC), rubber, polyurethane (PU) and PVC induce highest toxicity, polypropylene (PP) and polyamide (PA) showed lowest toxicities across studies and organisms tested, as summarised by Wagner et al. (2024). These leachate tests also showed that preproduction pellets are less toxic than the final products, which were equipped with further additives.

Human exposure to plastic-related chemicals (additives, residual monomers, degradation products) is supposedly highest in situations involving direct contact, for instance, among workers in the plastic or recycling industry (Koch & Calafat, 2009; He et al., 2015). Elevated exposure is also linked to household products such as dust from carpets and other textiles (Soltani et al., 2021; Abb et al., 2009) and leachables from food-contact materials (Muncke et al., 2020; Hutter et al., 2016). A recent review classified the effects of MP on humans as suspected to be harmful for the reproductive, digestive, and respiratory system, however, the current body of evidence is rated low (Chartres et al., 2024).

There are documented physicochemical effects of plastics at all sizes on a broad range of biota. Among the most relevant are internal (intestinal blockage, injury) and external physical damage (entanglement, suffocation, mobility loss), accumulation and resulting reduction of food intake and oxidative stress (Koelmans et al., 2022a). Although there are more adverse effects described in the literature (e.g. inflammation, see also a comprehensive review by Koelmans et al. (2022a)) they currently suffer a low weight of evidence (de Ruijter et al., 2020). Overall the physical harm posed by MP is not fully explored. It is plausible that, analogous to asbestos fibres, combustion-derived particles and mineral dust, certain shapes and sizes of MP can inflict similarly severe adverse health outcomes (Wilber & Clarke, 2001; Newcombe & Macdonald, 1991; Bour et al., 2018; Rillig et al., 2019; Koelmans et al., 2022a; Wieland et al., 2022). Under most environmental conditions, however, MP are vastly outnumbered by other anthropogenic and natural particulates, and dose-effect studies typically test concentrations orders of magnitude above environmentally relevant levels (Lenz et al., 2016). Only few studies exist that included natural particles as references at similar concentrations in order to discriminate between the mechanical stress and the chemical exposure (Casado et al., 2013; Watts et al., 2016; Ogonowski et al., 2016; Straub et al., 2017; Scherer et al., 2020). In Scherer et al. (2020) and the critical review by Ogonowski et al. (2018) it was concluded that MP effects were largely indistinguishable from those of natural particles, pointing towards a primarily physical mechanism of action - a conclusion that is also supported by studies on the effects of suspended sediment (Wilber & Clarke, 2001; Newcombe & Macdonald, 1991). Furthermore, the lower effect levels observed for MP compared to minerals were explained by their longer relative suspension time in water. However, open questions remain, particularly concerning environmentally realistic MP morphology and ageing stages, chronic and population-level effects, and the use of standardised, realistic dose metrics (Ogonowski et al., 2018).

Physical particle properties are relevant for the damage they can cause on different organisms, requiring particle-based analysis to produce the data. In this context, Rillig et al. (2019) hypothesised that synthetic particles with shapes most dissimilar to natural particles at equivalent size scales pose the highest risk to organisms. However, this depends on the morphology of particles to which the organisms are adapted to handle. The multidimensionality of physical and chemical configurations of MP complicates a comprehensive risk assessment, yet the context of other environmental factors, such as the natural suspended particle load, should always be considered (Ogonowski et al., 2018; Kooi et al., 2021; Koelmans et al., 2022a). This includes the relatively recent exploration of presence and effects of MP in the human body, where the general particle effect has not yet been put in this context, aside from current methodological limitations of small sample volumes and insufficient blind control (Leslie et al., 2022; Noonan et al., 2023).

MP particles can act as carriers for environmental pollutants, particularly hydrophobic organic chemicals such as polycyclic aromatic hydrocarbons (PAH) and polychlorinated biphenyls (PCB), which has been documented by several studies analysing MP from marine environments (Teuten et al., 2009; Rochman et al., 2013b; Sørensen et al., 2020). Fragmented and aged plastics typically exhibit higher absorption capacities, owing to their larger relative surface-area-to-volume ratio of MP compared to larger plastic debris. The property of MP to attract and retain hydrophobic organic pollutants is even utilised in toxicological screenings to sample these chemicals and assess water pollution levels (Fries & Zarfl, 2012). Adsorption and desorption of chemicals is governed by equilibrium partition coefficients. Consequently, MP can have either a cleansing or contaminating effect. Koelmans et al. (2016) showed that the partitioning coefficients between organic pollutants and MP typically do not reach equilibrium in marine environments and that the total share of organic pollutants adsorbed to natural matter by far outweighs those adsorbed to MP, mainly

because MP are far less abundant. As a result, MP make only a minor contribution in transferring organic pollutants to organisms as the uptake of (contaminated) natural food is by far higher (Gouin et al., 2011; Koelmans et al., 2016, 2022b). Thus, while chemicals inherently associated with plastic production and MP composition pose relevant concerns when exposed to organisms as addressed above, MP represent only one of many particulate vectors that transport persistent organic pollutants (POP).

Knowledge on the extent, composition and distribution of MP is pivotal to determine exposure rates and perform meaningful risk assessments of this emerging contaminant that potentially jeopardises ecosystem integrity (Lenz et al., 2016; Koelmans et al., 2022a).

Plastics share in crossing planetary boundaries

MP are not an isolated environmental problem but deeply interconnected with several major contemporary threats to human and ecosystem well-being. Within the concept of planetary boundaries (Rockström et al., 2009) the relevance and problem areas of this globally emerging contaminant can be outlined (Steffen et al., 2015; Persson et al., 2022; Richardson et al., 2023). This framework defines measurable control parameters of several key processes to trace the scale of change in Earth system processes, aiming to keep them within ‘safe’ operating spaces, i.e. conditions similar to those of the Holocene epoch, to which the human and many other contemporary species are adapted. Abruptly crossing these safe planetary boundaries provokes persistent changes in the current state of natural systems, known as regime shifts, thereby jeopardising life as it exists today. These processes can lead to irreversible changes such as extinction, or can be long-lasting such as climate change and persistent contamination (Zalasiewicz et al., 2024). Within the concept, (micro)plastics are defined as novel entities, i.e. introduced substances which are not readily compatible with natural systems or whose abundance and cycling are substantially altered by anthropogenic activities (Steffen et al., 2015; Villarrubia-Gómez et al., 2024). The following key processes regarded by the planetary boundaries framework are particularly relevant in the context of plastic pollution (Carney Almroth et al., 2022; Schmidt et al., 2024; Villarrubia-Gómez et al., 2024):

- Chemical pollution: the uncontrolled release of chemical substances of known or unknown toxic effects associated to plastic manufacturing, recycling, usage and disposal is persistent in the environment and incompatible with natural systems
- Biodiversity loss: the ongoing loss of biodiversity is exacerbated by plastic pollution, for instance, when already endangered species ingest (micro)plastic debris or become entangled in it
- Climate change: the alteration of global climate patterns due to increased greenhouse gas emissions, which are linked to plastic production and waste management practices. Nearly all plastics (98 - 99%) today are produced from fossil-carbon resources, i.e. reactivated storage carbon (Walker & Fequet, 2023). Plastics are roughly 80% carbon by mass, underscoring their role in global carbon cycling in the context of climate change (Bazargan et al., 2013). By 2024, atmospheric carbon dioxide (CO₂) reached ~427 ppm (520 ppm, including CO₂ equivalents of other greenhouse gases) with mean surface temperatures 1.6°C above pre-industrial levels (Rohde, 2025). Plastics contribute about 7% of global greenhouse gas emissions, comparable to emissions from the cement industry (8%, Mishra et al. (2022)). Projections expect a 10 - 13% share by 2050 from plastic production and incineration alone (Shen et al., 2020). These estimates omit emissions from plastic degradation, secondary effects of fossil fuel extraction such as wood clearing or pipeline leakage, and biogeochemical feedback (e.g. impacts on the phytoplankton carbon pump), which remain to be quantified (Shen et al., 2020).

Hence, there is a clear incentive to investigate the effects of this novel entity. Understanding its distribution processes and abundance is an important prerequisite for generating the necessary motivation to respond when and where impacts of plastic pollution become attributable and evident.

Tracing human impact in geological records

On geological time scales, synthetic plastic has existed only for a very short moment in time. However, due to its persistence in environmental systems, it will remain evident in Earth’s historical geological records. Sediment cores taken around the world show a temporal MP distribution that resembles global plastic production trends, if undisturbed conditions are selected and minimum dating standards are applied (Brandon et al., 2019; Dong et al., 2020; Chen et al., 2022; Martin et al., 2022; Turner et al., 2019). Future archaeologists could take this material as one of the key signals of our times. MP have already been discussed as a supplementary marker under the Anthropocene concept, as their rise coincides with the increased acceleration of resource usage and cycling Zalasiewicz et al. (2016). The Anthropocene, coined by Crutzen (2002) in his publication ‘the geology of humankind’, is proposed as the point in time when human influence significantly

accelerated and became dominant over natural processes, as a clear deviation from stable Holocene conditions, that the current biosphere is adapted to. The close linkage to the planetary boundary concept is apparent (Zalasiewicz et al., 2024), and the search for geostratigraphic markers of the Anthropocene could be interpreted as its sedimentary manifestation.

MP are an interesting candidate in this context as they are an entirely novel anthropogenic material, also termed ‘technofossil’ (Chen et al., 2022), absent in geological records before production began. Besides, many other markers have been identified, for instance, black carbon from increased fossil fuel combustion, pesticides and plutonium from hydrogen-bomb tests in 1952, the latter of which has been found to be the most favourable primary marker (Waters et al., 2022). The formalisation of the Anthropocene as a geological epoch, aiming at defining a starting point for this proposed ‘stratigraphic unit’, has not been agreed upon. While there is clear evidence of the distinct anthropogenic changes and acceleration of resource usage which are preserved in sediments (Subramanian, 2019), the extent of these changes cannot currently be foreseen. Epochs are traditionally defined in retrospect, when their propagation and extent can be evaluated based on geological time scales. Currently existing strata of the proposed epoch are very young and represent only the potential lower boundary (Prillaman, 2023). Nevertheless, this demonstrates the ability of the sediment to archive and document human-induced change, reflected in the increasing trends of multiple constituents including particulates as MP. Even if plastic emission were to substantially decrease, the existing plastic legacy in land and water repositories would lead to further MP deposition on the sediment beds over centuries (Waters et al., 2022). A review paper by Chen et al. (2022) aligned specific strata with polymer types that were invented and subsequently introduced in the respective time period. Four layers were distinguishable: rayon (from 1910s), mixed polymer types (from 1930s), PP and polystyrene (PS) (from 1950s), and PET (from 1970s), despite the overall marked quantitative increase from the 1950s onwards. Together with the above mentioned studies, this shows clear evidence for chrono-stratigraphic preservation of MP in sediments. Yet, it has to be noted that potential vertical particle migration, dating uncertainties and contamination constitute reoccurring problems in these analyses (Barsanti et al., 2020; Dimante-Deimantovica et al., 2024). MP samples from sediment cores are especially prone to erroneous results, as sample volumes are typically too small to deliver statistically robust MP numbers. As new layers of sediment continue to accumulate over time, pressure increases, expels pore water and compacts the sediment (Parga Martínez et al., 2024). If the sediment is not disrupted by extreme storm events, bioturbation or anthropogenic influences, MP can be regarded as ultimately removed from active cycling in the ecosystem. This kind of long term storage or sequestration is considered the major sink mechanism and predominantly occurs in deep sea environments (Woodall et al., 2014; Einsele, 2000).

Sediments as passive MP samplers: an untapped potential for monitoring

Despite their relevance as the potentially largest MP reservoir, spanning more than 70% of Earth’s surface, sediments are greatly understudied and MP estimates are subject to major uncertainties, as reliable quantification and monitoring remain challenging (Alimi et al., 2018). In contrast to sediments, surface and intermediate waters have a highly dynamic nature which hampers reliable spatio-temporal comparisons of MP abundances and determination of MP inventories. This is reflected in the many publications finding contradicting or unexplained temporal or spatial trends (Tekman et al., 2022) and the search for the missing plastic fraction (van Sebille et al., 2020). Several multi-decade studies exist, for instance, surface water monitoring of the Western North Atlantic and the North Pacific subtropical gyre showed an increase in MP abundance (Goldstein et al., 2012; Wilcox et al., 2020), whereas beach litter surveys from the North Sea (Schulz et al., 2015), water and fish stomachs from the Baltic Sea (Beer et al., 2018) and waters within the North Atlantic subtropical gyres (Law et al., 2010, 2014) showed no clear temporal trends. Overall, water bodies represent intermediate ‘pass-through’ compartments with high spatio-temporal variability, and together with the high dilution factor, they appear disadvantageous for long-term monitoring particulates. When entering the aquatic environment, MP begin their journey to the sediments, governed by the physics of natural particle transport. This ‘top-down’ movement of MP is also supported by a modelling study that estimated a residence time for plastic at the ocean surface layer to lie just within a few years, with 99% of aquatic plastic debris expected to be found in the deep sea (Koelmans et al., 2017). This process can occur over shorter or longer time scales and may involve multiple intermediate reservoirs and cycles, such as interactions with biota, resuspension, re-attachment cycles of biofilms, as explained in more detail below (‘MP particle transport dynamics’). As the lower boundary of all aquatic environments, sediments are characterised by continuous particle deposition and accumulation (Dutkiewicz et al., 2015). This makes them a particularly suitable compartment for monitoring, as they act as passive particle samplers with a natural archiving function. With the ability to document the time-resolved emergence and vanishing of contaminants, sediments can offer valuable feedback on environmental management interventions.

Accordingly, they have been widely used to assess long-term trends of various pollutants, including organic contaminants, heavy metals and trace elements (Chiaia-Hernández et al., 2022). The characteristics and hence the distribution and deposition behaviour of macroplastic debris vary greatly, resulting in non-linear trends and localised occurrences in sediments (Canals et al., 2021). In contrast, MP are smaller, more abundant, more mobile, and share physical property ranges with naturally occurring particulates. As a result, their spatial distribution is broader and more finely resolved, enabling more representative and feasible monitoring. In the context of this thesis, estuarine sedimentary environments are identified as largely overlooked intermediate MP reservoirs that need to be approached by improvements in the quantification of MP in this complex particulate matrix.

MP particle transport dynamics

Reliably determining plastic inventories in the aquatic environment is difficult, not only because of the sheer scale. Plastic-particle distribution in water is highly dynamic in space and time - hydrodynamic. The multidimensionality of physical properties of plastic particles adds up to this (Kooi et al., 2021). Although atmospheric transport to the aquatic environment also plays a role, the focus here lies on hydrodynamic processes on a particle's path from the surface into and along the sediments. To better understand the distribution and sorting of MP in the aquatic environment, an overarching research question of this thesis is whether and how sediment qualities, grain size distributions in particular, reveal MP distribution patterns. In order to provide the necessary background, a brief overview of major particle transport mechanisms is provided here.

Surface water transport

Plastic distribution in surface waters is influenced by a multitude of physical processes: large-scale and sub-meso-scale open ocean processes (geostrophic flow, eddies), Stokes drift, internal tides, windage, Langmuir circulation or coastal currents and waves, ice formation processes, river plumes, coastal fronts and extreme events as well as biology; scaling with water depth and size of an aquatic region (van Sebille et al., 2020). It has been shown that the large-scale distribution of positively buoyant MP can be largely explained by the Ekman theory or geostrophic circulation, which is capable of describing the accumulation of macro to micro-scale plastic in the subtropical gyres, although many smaller scale processes are involved and influence their distribution (Kubota, 1994; Martinez et al., 2009; Onink et al., 2019). Yet, due to the strong sensitivity to particle density near that of water, reliable predictions, especially on smaller regional scales, remain difficult. Many of these physical processes were already intensively studied in other contexts such as plankton, ice, oil pollution and sediments distribution. As plastic is a unique anthropogenic tracer it aids to further understand physical processes, validate and improve ocean circulation models. A comprehensive review on these physical processes affecting (micro)plastic transport in surface waters is provided by van Sebille et al. (2020). While many aquatic MP sampling campaigns have focused on surface waters, considerably less data are available on their vertical distribution (Liu et al., 2020). Actual surface MP concentrations greatly depend on the turbulence level, primarily driven by wind forcing or geostrophic circulation. As a result, surface sampling is influenced not only by momentary horizontal variability but also prone to inconsistencies related to the vertical distribution of MP (Kukulka et al., 2012). Despite having higher densities than water, denser MP and other fine particulates are often found in surface waters, when sufficient diffusivity keeps them suspended (Enders et al., 2015). Under low-diffusivity conditions, a sea surface microlayer can establish concentrating particulate matter and biofilm aggregates through surface tension effects and air enclosure (Valero et al., 2022).

Transport in suspension

Suspended MP distribution patterns largely mirror prevailing oceanographic conditions (van Sebille et al., 2020). In the convergence zones of oceanic gyres, for instance, sub-surface waters exhibit a more pronounced separation of polymer type (i.e. high vs. low densities), in concentrations and size, reflecting the mixing processes, i.e. wind-driven Ekman transport and downwelling, at the surface ocean. A one-dimensional vertical diffusion-advection model can simulate the size dependence of low-density MP, supporting their vertical distribution in the sub-surface waters (Enders et al., 2015). Overall physical mechanisms that determine the vertical net transport of a particle - sinking or not sinking - are described by the downward gravitational forces and upward Stokes drag, predominantly governed by the densities of the particle and water, particle size and shape (Stokes, 1851). For larger particles in the micrometre range Stokes' law becomes inaccurate (e.g. for quartz > 100 μm) and semi-empirical equations more suitable, as inertial forces start to dominate over viscous forces, a transition from laminar towards turbulent flow as described by the Reynolds number (Ferguson & Church, 2004). For MP this transitional size would be larger, depending on the specific density. While striving towards neutral buoyancy through sinking or rising, the particle's motion can be

counteracted by turbulent mixing, a force that keeps particles in suspension. When the turbulence level falls below a particle's drag threshold, the particle settles onto the sediment bed (Khatmullina & Isachenko, 2017).

Terminal settling velocity has been an intensively studied parameter in sedimentology and hydrodynamics. More recently, studies determined settling and rising velocities for MP with a range of physical properties under laboratory conditions (e.g. Khatmullina & Isachenko, 2017; Kaiser et al., 2019; Waldschläger & Schüttrumpf, 2019). Although irregular particles tend to orient with their smallest cross-section to the flow to minimise resistance, this orientation can be regularly interrupted by a variety of secondary movements such as oscillation and rotation (Gram et al., 2016; Bagaev et al., 2017). It is thus argued that hydrodynamic drag models for MP need to incorporate shape descriptors (Waldschläger & Schüttrumpf, 2019; Chubarenko et al., 2024). Among the available descriptors, sphericity was found to be the most suitable due to its capability to also describe thin films (Van Melkebeke et al., 2020). The shape-dependent drag model of Dioguardi et al. (2018) suited best for a large variety of shapes of 140 MP tested by Van Melkebeke et al. (2020). The findings underscore the importance of a detailed shape determination in MP analysis, when aiming to describe the pathway of MP in water. Ideally the extent in three spatial dimensions needs to be known, yet particle height is not typically determined in MP studies. As part of this thesis height measurement methods were refined and validated (Enders et al., *subm.*).

Bed load transport

Once a particle is deposited on the sediment bed, it remains subject to near-bed turbulence induced by currents or wave action. This can lead to repeated re-initiation of motion. Such particle remobilisation is part of near-bottom, short-distance transport, known as bed load transport, which excerpts different modes of motion: rolling, saltation and sliding (Van Rijn, 1984). During extreme storm events or other periods of intense hydrodynamic forcing, particles may be resuspended to the water column, potentially enabling longer distance transport. The hydrodynamic force required to remobilise a specific particle is described by the critical bed shear stress. One of the most widely applied empirically derived equations to describe the onset of particle motion on the sediment bed is the modified Shields' diagram by Soulsby (Shields, 1936; Soulsby, 1997).

This function expresses that the critical bed shear stress mainly depends on grain size, where smaller grains are more likely to be transported than larger ones, however, finer sediment tends to compress i.e. consolidate over time which reduces the initiation of motion of single particles. Yet, it neglects further complexities associated with the sediment such as particle - particle interactions of different grain sizes, the variability of specific particle densities and shapes other than spherical, sorting, peak turbulence, interlocking, bed morphology, bed armouring or grain exposure (Yang et al., 2019).

First measurements of MP resuspension thresholds show a dependence on the same parameters as natural particles (Ballent et al., 2012; Waldschläger & Schüttrumpf, 2019). Waldschläger & Schüttrumpf (2019) derived critical bed shear stress values for four different shapes of virgin MP and varying sizes $> 500 \mu\text{m}$ and set up a customised formula. However, these equations cover only a limited range of MP characteristics and sediment grain sizes, with notable limitations for smaller MP.

Post-depositional reworking

Multiple processes can disturb sediments, leading to resorting of sediments that disrupt their chronological integrity and group formerly unrelated particles. These disturbances reduce stratigraphic resolution and vertically homogenise dating profiles, stratigraphic markers, as well as MP contents.

Hydrodynamic mixing

Wind, wave and current generate turbulent forces that lead to re-suspension of deposited sediment. In shallow estuaries, without tidal activity, waves and storms are the primary drivers (Green & Coco, 2014). Depending on the hydrodynamic force, short (bed load transport) or long term (suspended) transport of matter can be induced, as described above. In practice, it is not trivial to distinguish between suspended and bed load transport in the field as well as in the laboratory due to interference and overlaps in temporal and spatial scales (Ancy, 2020a).

Bioturbation and anthroturbation

Bioturbation refers to the mixing of particles within the sediment or their resuspension into the water column due to biological activity. Some organisms simply move through the sediments in search of food or shelter, while others ingest sediment and subsequently defecate it, thereby dislodging sediment volume (Meysman et al., 2006; Kristensen et al., 2012). Biogenic sediment

displacement and bubble formation have also been shown to promote granular size segregation (Srivastava et al., 2021; Savranskaia et al., 2022). Through these processes benthic organisms can facilitate both the burial as well as the remobilisation of archived MP, either directly via bioturbation or through ingestion and subsequent transfer to higher trophic levels (Sandgaard et al., 2023). Several laboratory and mesocosm studies have demonstrated that bioturbation also applies to MP (Näkki et al., 2017; Cozzoli et al., 2019; Pantó et al., 2024, 2025). While it may be regionally relevant in some natural environments, the larger scale extent and impact remains hard to predict (You et al., 2023). Although, there is a lack of studies comparing natural sediment grains to MP concerning burial depth and efficiency, there is no evidence suggesting that MP is disproportionately affected by bioturbation (Gebhardt & Forster, 2018).

Direct anthropogenic sediment disturbances originate from fishing activities such as bottom trawling, from hydraulic modifications such as dredging (extraction and redeposition of sediment) or construction of coastal or offshore infrastructure as well as from mining and drilling (Bruns et al., 2023; Chen et al., 2022; Bailey et al., 2024; Gazis et al., 2025; Jones et al., 2021). Such interventions not only actively displace sediments, but can also lead to long-term alterations in hydrodynamics, resulting in the reorganisation of sediment layers. Also indirect anthropogenically altered conditions can rework the sediments by reshaping benthic community extension and composition, with effects on local hydrodynamics, erosion and bioturbation intensity (Widdows & Brinsley, 2002). As for instance through nutrient-driven eutrophication which typically initially enhances productivity, over longer periods creates anoxic dead zones (Middelburg & Levin, 2009; Murray et al., 2019). Similarly, pollutants can influence the benthic community with a shift towards more tolerant or functional organisms. This has been observed in the vicinity of munition dump sites of the two world wars, where the bacteria community is significantly different to areas without pollution impact (Janßen et al., 2021). Yet the presence of physical structures typically leads to a local increase of biological activity and biodiversity (Vedenin et al., 2024).

Infiltration

The vertical transport of finer particles into existing pore spaces between coarser sediments has been demonstrated, both for MP (e.g. Waldschläger & Schüttrumpf, 2020; Mancini et al., 2023; Munz et al., 2024) and clastic sediments (see reviewed papers in Packman & MacKay, 2003; or Jaiswal et al., 2024), with the first systematic flume study performed by Einstein (1968). Infiltration can lead to temporary or long term retention of fine sediments and changes the sediment stratigraphy. Existing studies investigating the infiltration mechanism of MP, are in overall agreement with the former sedimentological observations concluding on particle size ratios, shape and infiltration depth profile (Waldschläger & Schüttrumpf, 2020). The median grain size ratio of the infiltrating fines to the coarser substrate, termed the infiltration size ratio depends on the hydrodynamic forcing on the sediment bed and the resulting hyporheic flow (Jaiswal et al., 2024). Stream beds can become clogged when interstitial pores are fill up, then inhibiting further infiltration and effectively clogging the sediment bed. Infiltration of fine sediments and MP has been described in laboratory studies to occur at infiltration size ratios between 0.32 and 0.11 (Schruff, 2018; Waldschläger & Schüttrumpf, 2020). Below 0.11, particles tended to percolate through. Generally, the infiltration potential and depth are higher for particles with higher sphericity, whereas density differences of the fine infiltrating particles appear not to be determining (Mancini et al., 2023). As density is a main difference between MP and clastic sediment grains, MP is unlikely to be more prone to infiltration.

Most studies describe the infiltration behaviour of fines in fluvial systems, typically dominated by coarse gravel, due to their relevance in stream bed management (Schruff, 2018). Their experimental designs typically use simulated stream beds in the form of open-circuit or recirculating flumes, with relatively large hydrodynamic forcing and non-representative model particles such as spherical-shaped glass spheres as sediment infiltrated by non-degraded MP (Boos et al., 2024). More realistic environmental particles with higher particle angularity and multimodal size distributions would reduce the likelihood of infiltration (Waldschläger & Schüttrumpf, 2020). Furthermore, organic matter presence and quickly established biofilms on particles exposed to the aquatic environment, makes them more prone to agglomerate to larger material composites, reduce single particle transport as well as pore spaces, and thus infiltration of particles in the lower micrometre scale (Boos et al., 2024). The relevance of this process in other environments besides coarse stream bed and energetic coastal swash zones, such as estuaries and marine waters with calmer hydrodynamic forcing on the sediment bed and smaller median grain sizes, infiltration is likely to play a minor role (Tian et al., 2023). This is supported by a median size comparison of MP and sediments of samples taken in the Schlei (Enders et al., *subm.*), where an effective infiltration ratio in coarser sediment regions was not reached. Overall, it often remains a challenge to distinguish between infiltration and hydrodynamic mixing in sedimentology, while bioturbation can leave traces of fossils, speckles and burrow structures or a speckled stratigraphy, infiltration is more difficult to identify.

Aggregation

Despite the large fraction of initially positively buoyant MP (PE and PP), many studies find equal shares of high and low-density polymers, reflecting the full range of produced polymers, in sediment samples (Enders et al., 2019; Klein et al., 2015). That is largely because, over time and with ongoing fragmentation a majority of MP are transported in aggregates such as other suspended fine particles. These aggregates or flocs can consist of a variety of inorganic (clay, silt) and organic dead (detritus, faeces, organic debris) and alive (microorganisms) particulate matter (Droppo, 2001; Papenmeier et al., 2014). Flocs occur in the water column as well as on the sediment bed surface (Droppo, 2001). Microflocs (referred to up to an upper size limit between 100 - 160 μm) are considered relatively dense and stable. They can aggregate to macroflocs which can reach sizes orders of magnitude larger than their constituent particles, yet are more porous and fragile. Organic-rich flocs can grow up to several millimetres, containing up to the order of one million of inorganic particles (Eisma, 1986; Papenmeier et al., 2014).

Floc properties can greatly deviate from those of the constituting particles and alter their net transport behaviour. Non-permeable flocs have a higher terminal velocity than its individual parts, but lower than an equally sized sediment particle of equivalent-volumetric diameter (Strom & Keyvani, 2011). Therefore floc formation constitutes a major contribution to a faster deposition of MP (Long et al., 2015; Thit et al., 2022). Floc composition and size is constantly changing, as a response to environmental conditions and available building components. Smaller particles sizes become more influenced by particle-particle interactions, due to their increased surface-area-to-volume ratio and usually longer time in suspension. The formation of flocs depends on the collision probability, which in turn depends on the hydrodynamic turbulence and concentrations of dissolved ions and other solutes, as well as particle abundance, coatings and electro-chemical forces between them (attraction by van der Waals, repulsion by electrical double layer forces) (Mhashhash et al., 2018; Papenmeier et al., 2014; Thit et al., 2022; Alimi et al., 2018). While a certain level of turbulence fosters flocculation as it increases collision probability, with stronger turbulences, however, disintegration becomes more likely (Eisma, 1986; Mhashhash et al., 2018). Estuaries are particularly effective flocculation and particle trapping zones. The large volumes of material transported through estuaries, combined with the mixing of freshwater and seawater, create sharp salinity gradients and ionic shifts that promote floc formation especially at the turbidity maximum (Burchard et al., 2018).

Experimental results demonstrate that high density polymers are integrated into aggregates with fine-grained sediment particles, leading to an increase in settling velocity compared to the individual PVC particles (Andersen et al., 2021). It has been shown that MP < 162 μm are predominantly transported within aggregates, independent of their density, even though floc sinking velocity may decrease due to the reduced net density. MP integration did not significantly influence overall floc size compared to flocs formed without MP (Leiser et al., 2021; Wu et al., 2024). Given the low relative number of MP compared to natural particles, their impact on the reduction or acceleration of organic matter and carbon sequestration appears relatively minor. A recent study determined that plastic-derived carbon accounted for between 0.3% to 3.8% of the total particulate organic carbon flux exported via the biological carbon pump in the North Atlantic Ocean (Galgani et al., 2022).

Biofouling

The formation of an eco-corona, layers of various biomolecules such as proteins, nucleic acids, surfactants and lipids on the surface of particles occurs rapidly in the aquatic environment (Galloway et al., 2017; Yang et al., 2025). This nutritional layer attracts bacteria attaching to these surfaces to take the advantage of increased nutrient availability compared to the surrounding water. The colonisation by microorganisms accompanied by the self-production of extracellular polymeric substances composed of polysaccharides, is referred to as biofilm formation (Thit et al., 2022). Studies have shown that within a few weeks of exposure, mature biofilms can develop on the MP surface in the aquatic environment (Kaiser et al., 2017). The presence of organic matter and microorganisms enhances particle stickiness and early biofouling (Eisma, 1986), accelerating aggregation, continued biofouling and ultimately promoting faster sinking. Biofilm formation has been shown to be one of the main drivers for vertical transport of intrinsically buoyant MP (Kaiser et al., 2017). However, this net increase in settling velocity, can also be temporarily reversed upon detachment, remineralisation or grazing by biota, leading to up- and downcycling in the water column (Kooi et al., 2017). Most plastic materials are characterised by hydrophobic surface properties. Yet, biofouling can change the polarity of MP towards hydrophilic behaviour, which has been experimentally determined by a significant reduction in wetting contact angle down to below 40° (Van Melkebeke et al., 2020). As a result, this increases the likelihood of aggregation and sinking.

Despite concerns that plastic could serve as a transport vector for pathogenic bacteria (Zettler et al., 2013), recent metagenomic studies, which used natural particles as reference material, showed

that the species were not plastic-specific but merely followed biogeographical and environmental vectors (e.g. nutrients, light, temperature, salinity) (Oberbeckmann et al., 2021). While specific surface properties play a role in the initial attachment of microorganisms, e.g. species capable of attaching on very smooth surfaces via polysaccharide holdfasts are reported as early colonisers on MP, the species composition and biofilm extent are in continuous change, depending on the respective environmental conditions and the evolution of competing as well as synergistic processes within these self-sustaining communities (Oberbeckmann & Labrenz, 2020). This indicates that MP in the aquatic environment act mainly as a surface for opportunistic colonists as it is also known for other particulates (Zobell, 1943; Oberbeckmann & Labrenz, 2020). The biofouled appearance mimics natural particles which leads to non-selective uptake by various biota, such as filter or deposit feeders. Depending on the intestinal system conditions (e.g. pH, enzymes, passage time) MP particles can deteriorate, leach chemicals or fragment and thereby further change their physical properties (Dawson et al., 2018). Egestion incorporates MP in faecal matter, usually facilitating particle sinking, and thereby affecting the place of deposition.

Challenges in quantifying and predicting MP transport

Experimentally gained knowledge at single particle level and derived transport functions can be applied in hydrodynamic numerical modelling (HNM) to describe the particles' pathway from sources to sinks and would constitute one approach to estimate inventories from limited data sets (Shiravani et al., 2023). However, these models are only as good as the data available for individual particles, particle interactions, hydrodynamic and environmental processes. Due to the scarcity of MP experimental data, modelling studies often use knowledge and functions gained from sediment transport (Osinski et al., 2020; Waldschläger et al., 2022). First experimental studies have determined parameters of sedimentary MP transport of selected MP particles as summarised above (e.g. Khatmullina & Isachenko, 2017; Ballent et al., 2012; Kaiser et al., 2019; Waldschläger & Schüttrumpf, 2019).

For a comprehensive parametrisation of HNM, able to couple MP transport over larger areas and across compartments, the available observed or experimental data are far from sufficient and thus requires far-reaching extrapolations and assumptions. In order to generate a detailed picture of realistic MP transport dynamics in sedimentary environments, necessary experiments would need to cover large parameter ranges. Process equations need to cover MP intrinsic properties like sizes, shapes, densities and chemical compositions, as well as surface charges and zeta potentials (Khatmullina & Chubarenko, 2019; Thit et al., 2022). However, these particle properties are subject to analytical uncertainties that increase as the analysed particle size ranges become smaller. For example, the size and shape measurement may be subject to larger relative errors when fitted particle outlines miss the correct particle boundaries due to a lack of optical features (Schnepf et al., 2023). The number and accuracy of acquired size dimensions and shape descriptors, either as categorical, numerical or continuous, strongly vary between studies (Kooi & Koelmans, 2019; Kooi et al., 2021; Waldschläger et al., 2022). They depend on analytical capabilities whose uncertainties propagate to prediction results. Density is usually inferred from the bulk density of the assigned polymer type, rather than being measured directly, as the latter would be too time-consuming and impractical for environmental MP samples (Stead et al., 2024).

Fragmentation, leaching, biofilm coatings, or hetero- and homoaggregation, inevitably alter and expand the already large diversity of intrinsic MP particle properties and states. Obviously, this constitutes an immense complexity that is difficult to cover through experimental measurement (Khatmullina & Chubarenko, 2019). *In situ*, natural particulates and MP form unstable particle aggregates, whose overall physical characteristics determine transport behaviour (Droppo, 2001; Wu et al., 2024). A few of these characteristics have been described in the literature (Thit et al., 2022). These include the effects of temperature and water viscosity on flocs, their sinking velocities and internal molecular reactivity and mobility. Several key processes, such as stability and degradation of aggregates and rates of leaching, however, remain largely unknown, as summarised and discussed in detail in a recent review (Thit et al., 2022). Along the pipeline of extraction (i.e. sampling and purification) and analysis, the natural state of aggregates is not conserved, as the aim of MP particle analysis is to obtain well-separated and purified single particles for material identification and property measurements (Droppo, 2001; Munz et al., 2024). In addition, the individual particles may undergo alterations due to laboratory processing (Lenz et al., 2021). Consequently, the properties of particles and the behaviour deduced from these properties do not accurately reflect the actual fate of the particles in nature.

Even if the intrinsic particle properties could be sufficiently determined, the presence and characteristics of the sediments such as grain size, stratification, inorganic and organic content influence how MP and other particulates can be effectively transported. Experimental estimation of mechanistic MP characteristics can cover only a tiny fraction of the existing diversity. Oftentimes studies employ generic particles, e.g. smooth spheres of pristine PS or glass beads as a substrate, to investigate

transport behaviour (Thit et al., 2022). In fact many sedimentological studies have used PS beads as tracer particles to study sediment transport behaviour (Bizmark et al., 2020). While such simplifications are inevitable to obtain experimental results under controlled settings, they limit the representativeness for the particles actually present in the environment (Thit et al., 2022). In consequence of the above limitations, models are often restricted to describing MP distribution only qualitatively (e.g. for localisation of deposition areas) or if concentration levels are reported, these are subject to high uncertainties (Schernewski et al., 2021; Sandgaard et al., 2023). Above all, hydrodynamic modelling does not spare taking sufficient environmental samples and high-quality *in situ* measurements, each as separate sets for calibration or validation purposes, respectively (Wright et al., 2017). HNM can make highly valuable contributions by forecasting potential contamination levels and future MP fluxes under various scenarios, only by adapting or updating relevant input parameters, however, current concerns regarding the parametrisation and validation of MP HNM need to be addressed (Wichmann et al., 2019). High-resolution coupled HNM is not widely available as they pose high developmental and computational costs, with only three-dimensional HNM being able to depict complex flow regimes with sufficient accuracy (Papanicolaou et al., 2008). A recent comprehensive review summarises the existing literature on models concerning MP transport (Waldschläger et al., 2022). The difficulty in achieving accurate model predictions arises from the fact that MP transport is characterised by non-linearity and feedback loops (Fersch et al., 2020). These are part of dynamic earth system processes, in which interactions across the different spheres are difficult to track. The hydrosphere, atmosphere, geosphere, and biosphere are intricately connected, each contributing to model uncertainty.

As an example of effects of processes in the **atmosphere**, Osinski et al. (2020) showed that uncertainties in weather inputs can substantially influence predictions on MP concentrations in Baltic Sea sediments.

Interactions within the **geosphere**, including mixing of sediment layers or beaching are usually not represented in HNM (She et al., 2023; Peleg et al., 2024). Factors such as sediment composition (grain size, stratification, inorganic and organic particulates) influence deposition and erosion behaviour of sediments, with lacking predictability in the transition from non-cohesive to cohesive sediments (Grabowski et al., 2011). The composition and hydrodynamic regime shape geomorphology by creating specific bedforms and sorting patterns or armouring (Ferdowsi et al., 2017). This demonstrates the interconnectivity of the geosphere and **hydrosphere**, where sedimentary structures are not only shaped by water movement but also feed back into it by modifying local flow conditions (Ancey, 2020b). In turn, these geomorphological features affect particle motion by shielding or exposing particles to flow direction. However, small geomorphological features such as certain bedforms or ripples remain unaccounted for in HNM, as their spatial extent is below typical model grid resolutions. While bedforms are a result of hydrodynamic processes, they in turn influence local threshold bed shear stress highlighting the inter-connectivity between the flow regime, geomorphology and individual particles (Ancey, 2020a).

Interactions with the **biosphere** may remain some of the greatest challenges for simulation: macrophytes, for example, modify local hydrodynamics by attenuating flow and stabilising sediments through root systems and canopy drag. This can reduce bed shear stress and promote fine sediment and MP deposition (Kerpen et al., 2024). Conversely, vegetation patches can also channel flow, increasing erosion in surrounding zones (Cozzoli et al., 2019; Le Hir et al., 2007). Similarly, biofilms can stabilise sediment beds while gas production by microorganisms or macrobenthic activity (bioturbation) can induce granular segregation, bed destabilisation, and even resuspension (Cozzoli et al., 2019; Van Melkebeke et al., 2020; Srivastava et al., 2021). These interactions are spatially variable on small scales, species-dependent, and subject to seasonal cycles, making them particularly difficult to generalise or incorporate into deterministic models (Le Hir et al., 2007).

Anthropogenic influences, i.e. effects of the **technosphere**, on the sediment bed stratigraphy can be equally multifaceted as bioturbation, which are yet hard to monitor or integrate into hydrodynamic models (Zalasiewicz et al., 2014; De Borger et al., 2021).

Earth scientists proclaim that the intensively studied field of sediment dynamics is still among the least understood within the discipline, which manifests in the mismatches between empirically and theoretically derived results (Zhang, 2014). This elucidates that we are yet far from reaching a deep understanding of MP transport dynamics. Empirical models, which are commonly applied in water research can here complement HNM especially for purposes of spatial prediction and inventory estimations (Martin et al., 1999; Moodley et al., 2024).

Proxy-based empirical predictive modelling

Reliable quantification and long-term monitoring of MP remain notoriously challenging. Sampling, purification and analysis of MP samples always involve the trade-off between time and cost on the one hand versus data quantity, accuracy and size range coverage on the other (Hidalgo-Ruz

et al., 2012). This results in a scarcity of MP data and makes it interesting to look for parallels between MP and the natural particles that surround them in order to establish potential proxies, i.e. quantities that are easier to obtain yet strongly predictive of MP abundance or other MP-related variables. Mineral grain-size distributions and organic-matter contents are controlled by the same hydrodynamic forces that sort MP. Because these parameters are routinely measured during standard sediment surveys, and can be obtained far more quickly and cheaply than MP, they are available at much higher spatial resolution than current MP data sets (Blott & Pye, 2001; Heiri et al., 2001). By building on these relationships, proxy-based empirical models allow to interpolate MP loads across entire aquatic systems like estuaries and coastal basins. By combining a dense grid of proxy measurements with only a modest number of direct MP determinations, high-resolution maps of MP inventories can be generated while analysing far fewer samples than direct measurement alone would demand for the same scale, resolution and accuracy.

The remainder of this chapter covers the qualities of potential proxies and how they can be used to normalise the variability in MP data introduced by the hydrodynamic regime. This enables to reveal actual MP sources and sinks and track spatial and temporal trends in sedimentary systems.

Characteristics of potential proxies

MP can be regarded as a unique contaminant class, namely due to its large variety of physical and chemical properties and the resulting complexity of transport behaviour and risk (Koelmans et al., 2022a). New chemical interactions and metabolites with unknown distribution, persistence and risks can occur in the environment with the introduction of these novel human-made materials. However, the physical properties of MP particles, which are relevant for their transport behaviour and distribution pattern, largely overlap with that of other natural particulates (Koelmans et al., 2022a), which suggests their usage in normalisation and proxy analysis as the conceptual basis of this thesis.

- **Density**

In the literature, clastic sediment density is often reported to average 2.65 g cm^{-3} . Due to its resistance to mechanical and chemical decomposition, quartz is the mineral with the highest overall prevalence in coastal and riverine aquatic sediments and therefore often used as a reference value. This simplification, however, neglects the large range of the various mineral and respective densities between $1.7 - 3.1 \text{ g cm}^{-3}$ (montmorillonite to apatite or the biogenic aragonite) (Harris, 2020).

Different density ranges are reported for organic matter, for instance, between $0.9 - 1.3 \text{ g cm}^{-3}$ (Harris, 2020). An exact determination can be challenging, due to the fragility and their permeability to the fluid medium of many organic components. Organics buried in sediments are referenced as $1 - 1.5 \text{ g cm}^{-3}$, therefore usually higher density separation thresholds of 1.6 or 1.8 g cm^{-3} are used for the fractionation between organics and minerals (Mayer et al., 2004; Kreyling et al., 2013; Wakeham & Canuel, 2016).

The density of MP is commonly found between $0.89 - 1.6 \text{ g cm}^{-3}$ (from PE to various paint resins, Enders et al. (2019)), although, there are exceptions, such as expanded PS with 0.05 g cm^{-3} or polytetrafluoroethylene (PTFE) with 2.3 g cm^{-3} (Chubarenko et al., 2016). The density range of organic matter largely overlaps with MP, while minerals show nearly no overlap. Therefore density separation is an important step in sample purification from sedimentary matrices (Enders et al., 2020b).

- **Shape**

Description of particle or grain shape is common in MP studies and sedimentology. Minerals, organic matter and MP all exhibit a wide range of shapes. For minerals these are determined by the crystal structure, which is a result of the chemical composition and the conditions under which the mineral formed (Aydinalp, 2012). Blott & Pye (2008) highlighted that form (in three dimensions), roundness (angularity), irregularity (deviations from regular shape) and sphericity (similarity to a sphere), together can describe all appearances of grains. Biogenic minerals express a large variety of bio-designed shapes and geometric features that fulfil specific ecological functions, such as providing structural support or protection (Hamm et al., 2003).

Particulate organic matter comes in various shapes. As it is produced by living organisms, its shapes are often more complex and diverse than those of clastic minerals, exhibiting shapes from ellipsoidal or spherical to filaments, plates and clusters of cells as well as various forms of appendages (Reynolds, 1984; Kruk et al., 2010). As organic matter degrades it re-agglomerates into porous flocs which are highly irregular and variable (Alldredge & Silver, 1988; Droppo, 2001).

MP shapes can be highly irregular, often showing cues from their original application even in the micrometre range. Many studies manage shape analysis through non-standardised categories (fibre, granule, bead, pellet, flake, film, etc.) which are of limited use for comparative analysis. Similar to mineral grains, MP shapes can be expressed through geometric descriptors, such as elongation, roundness and solidity (Schnepf et al., 2023). Alternatively, Kooi & Koelmans (2019) proposed the use of parameters of continuous probability density functions to represent MP shapes (and other properties), allowing for better mathematical comparability of particle properties across studies, albeit at the cost of intuitive interpretability of the discrete shape categories. For identification and quantification of MP, visual shape characteristics alone are in most cases not sufficiently distinct. While Ismayilova et al. (2021) were able to discriminate fresh industrial MP from soil particles with > 80% certainty, for environmentally fragmented MP such attempts are insufficient to characterise MP purely morphologically (Lenz et al., 2015). This indicates that MP shapes are no unique feature.

- **Size**

All non-living solid matter in the environment is subject to fragmentation processes that generate continuously smaller particles from larger, although at very different rates. They are countered by formation, aggregation and growth, i.e. processes that facilitate the regeneration of larger compounds. The size of particles is a key factor in determining their transport behaviour and distance, as it influences settling velocities, bed shear stress, and the likelihood of aggregation. In sedimentology, particle size is often classified into three main categories: sand (2000 - 63 μm), silt (< 63 - 4 μm), and clay (< 4 μm) (Wentworth, 1922). Various size parameters are typically determined, such as mean, mode, sorting, skewness, kurtosis, among various cumulative percentile values (Blott & Pye, 2001). Size fractions can be determined e.g. by sieving (Folk & Ward, 1957). However, continuous grain size distributions are now routinely determined using laser diffraction instruments, which provide a volumetric grain size distribution averaged over multiple scans (ISO, 2020). Depending on the method and instrument, significant deviations in the size measurements can occur (Flemming, 2007; Varga et al., 2019).

In biogeochemistry organic matter of sizes > 0.7 μm are classified particulate organic matter (POM), the fraction below is classified as dissolved organic matter (DOM). Organic matter size determination is challenged by sufficiently conserving size during sampling and analysis. Therefore, the organic fraction usually still contains a substantial fraction of minerals (Arnarson & Keil, 2007; Kreyling et al., 2013; Wakeham & Canuel, 2016). As organic matter sizes undergo continuous change due to microbial and fungal degradation as well as agglomeration and growth, the representativeness of this property may be limited.

For MP, depending on the analytical method, different size dimensions (typically only the longest) are determined (Schnepf et al., 2023). Sizes are typically reported in count histograms, however, oftentimes relatively low numbers constitute an accuracy limitation for this physical property determination (Wagner et al., 2022). Due to technical limitations often no more than two dimensions are measured, which hinders an accurate size and shape description as well as mass calculations. Particle characterisation in three spatial dimensions is necessary for more accurate estimates of volume and mass, which are important for transport predictions (Enders et al., *subm.*). A conversion to MP mass has often been demanded as it enables validation and integration in HNM as well as potential comparability to mass-based analytical methods (Koelmans et al., 2020). Overall, due to the different methods applied for these three sediment components, comparability between these different materials is subject to uncertainties.

As particle size decreases, transport in aquatic environments increasingly occurs in aggregates, thereby reducing the relative importance of individual particle properties.

- **Source**

The largest fraction are clastic sediments which are weathered rocks of various sources, such as solidified magma (igneous), lithified mineral or organic matter (sedimentary) and recrystallised minerals upon high pressure and heat (metamorphic) (Huggett, 2011). Most clastic sediment (85%) originates from land-based sources (terrigenous), which is comparable to known entry pathways and quantities for MP. Minerals of biological origin, bioclastic sediments, consist of leftovers from structure-building organisms (e.g. calcareous algae, corals) and are often composed of calcium carbonate CaCO_3 (Holden, 2017).

Particulate organic matter is derived from a variety of sources, including terrestrial plants, aquatic vegetation, animals and their faeces, and microbial biomass. Similar to MP, its composition is highly diverse, but due to its evolutionary long existence, pathways of microbial degradation and consumption of its stored carbon are well established for almost all types of organic matter, with few exceptions like biologically derived pyrogenic carbon (char coal,

Bowring et al., 2022) or sporopollenin (spore wall polymers, Wellman, 2004).

MP by definition have no natural sources, and are predominantly derived from land, with estimates suggesting that around 80% of MP originates from terrestrial environments (Andrady, 2011). This includes a wide range of materials, such as fragments and films from larger plastic items (secondary MP), fibres from textiles, shredded paint flakes from ships and other coated constructions and microbeads from personal care products or technical applications (primary MP). As silicones or heavily modified elastomers like tyre wear particles are often considered MP, there are basically no chemical constraints to what can be classified as MP other than containing > 1% of a synthetic polymer (European Parliament and of the Council, 2023).

- **Omnipresence**

Minerals and organic matter occur ubiquitously in all aquatic sedimentary environments. Their prevalence reflects repeated deposition - resuspension cycles, and their small sizes provide high mobility and long transport distances (Prothero et al., 2004).

MP are also found everywhere, while their numbers are still orders of magnitude lower than those of natural particles (Koelmans et al., 2016; Gorokhova et al., 2020). For instance, measurements of particulate organic carbon (POC) in water usually range between mg to g per kg sediment (Leipe et al., 2011), whereas MP typically ranges between ng to µg per kg dry weight of sediment (Fischer & Scholz-Böttcher, 2019; Bouzid et al., 2025).

- **Persistence**

The persistence of a material is defined by its resistance to degradation, which is determined by its chemical structure and the environmental conditions it is exposed to. Minerals fragment during transport as a result of collision and chemical dissolution, the latter of which varies greatly depending on the mineral type. For instance, a highly polymerised silicate like quartz dissolves at rates on the order of 10^{-16} mol cm⁻² s⁻¹, whereas carbonate minerals such as calcite dissolve with $\sim 10^{-10}$ mol cm⁻² s⁻¹, making quartz 100,000 times more persistent (White & Brantley, 1995; Morse & Arvidson, 2002). Especially in the sand size fraction, quartz appears as relatively stable, while with smaller sizes dissolution increases due to the larger surface-to-volume ratio (Boggs, 2006).

Organic matter, on the other hand, is generally more susceptible to microbial degradation, leading to a faster breakdown compared to MP and minerals, but is also regenerated at a faster rate. Degradation rates vary for different organic matter between $10^{1.2}$ - $10^{4.5}$ days as summarised by Koelmans et al. (2022a).

Similar to natural matter, the fragmentation of (micro)plastic is an ongoing process which highly depends on environmental conditions (see section ‘The generation of persistent polymeric particles’). As full mineralisation is to date only observed for very few synthetic polymers, MP are considered highly persistent. Although the atomic building blocks of MP greatly overlap with organic matter, their arrangement and invariability, provide MP with a stability ($\sim 10^5$ days, ranging from $10^{1.8}$ - $10^{7.2}$) that is closer to that of inorganic materials ($10^{6.3}$ days, ranging from $10^{4.3}$ - 10^9 , as summarised by Koelmans et al., 2022a), dominated by mechanical abrasion and chemical dissolution.

While there is a large variety of other particulates present in natural sediments, such as amber and black carbon as well as other anthropogenic pollutants that adsorb onto natural matter (e.g. Hg), they do not fulfil all proxy requirements. In some cases their overall presence in aquatic environments in sufficient quantities is not guaranteed, in others they are not routinely measured. Organic matter and clastic sediment grain size distribution are the most promising proxies for normalisation and prediction due to their omnipresence in all aquatic environments and overlapping physical property ranges. A good proxy is one that behaves conservatively with respect to the processes that govern MP distribution, i.e. it is not significantly impacted by other creation or removal processes over relevant time scales (Liss, 1976). In that regard, sediment grain size has an advantage for being a universal MP proxy compared to organic matter content.

Proxy-normalisation

Spatio-temporal analysis is fundamental for understanding transport and deposition processes of contaminants (Chiaia-Hernández et al., 2022). The application of normalisation procedures in pollution studies is a valuable tool to identify zones of higher or lower pollution. What the data is normalised for depends on the processes that govern the distribution of the pollutant other than the pollutant’s own introduction (Kersten & Smedes, 2002). In the context of pollution of aquatic habitats, this is mostly the hydrodynamic regime. Similar to studies concerning dissolved and sorptive pollutants, MP studies can benefit from a normalised view into MP concentration data. The study of the transport behaviour of the dissolved measurands may require multi-step

normalisation, e.g. accounting for the additive effects of preferred sorption to particles with a larger surface-area-to-volume ratio and hydrodynamic sorting (Kersten & Smedes, 2002). MP, being particulate pollutants, can be normalised with a suitable proxy of natural particles in order to identify pollution levels in relation to hydrodynamics. Sources and sinks can then be identified as deviations either below or above the normalisation line which can either be a regression or the connection between the end-members (i.e. minimum and maximum of the proxy) (Kersten & Smedes, 2002). As such, this concept is an adaptation of the conservative mixing theory applied to describe the source and sink characteristics in estuaries in regard to certain dissolved compounds where for instance salinity is often used as the property that behaves conservatively towards the estuarine mixing of fresh- and saltwater (Liss, 1976; Stedmon & Markager, 2003).

Viewing or comparing MP sediment data directly, i.e. without normalisation, may obfuscate actual patterns due to the inherent hydrodynamic regime bias (Enders et al., 2019). In consequence, one may observe large ranges of MP concentrations within and across studies (as can be seen in the review by Harris, 2020), with variance on small spatial scales potentially exceeding those of larger spatial scales (Barrett et al., 2020; Martin et al., 2017). This has implications for the interpretation of MP levels, for spatially as well as temporal comparisons and the determination of inventories of MP. Higher MP levels of a specific site are not necessarily an indication of high local MP input, a sink or a ‘hotspot’, but could exist due to the distribution dynamics if the present hydrodynamic conditions favour smaller, thus more abundant MP (i.e. align well along the normalisation line as shown in Figure 1).

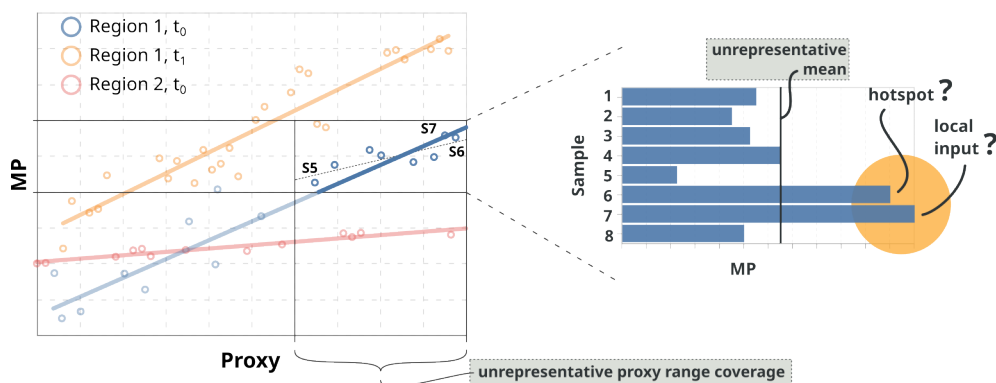


Figure 1: Proxy-normalised view on MP data can reveal actual areas of increased pollution inputs. Without proxy normalisation, interpretations with respect to spatial and temporal trends, sources and sinks or hotspots are likely to be inaccurate. Incomplete coverage of the present range of the proxy may lead to inrepresentative results and biased MP pollution level estimations

MP is omnipresent but patchy. As there is no ‘natural background MP’ the pristine baseline is zero MP. Whether high concentrations found at a certain location indicate an actual source or are the expected state formed by the hydrodynamic regime is not discernible from MP data itself. Proxy normalisation means viewing the MP distribution relative to that of one or several conservative properties, i.e. a quantity that ideally has no other influences than the effect it is used to normalise for (Liss, 1976). Applying this concept helps to avoid misinterpretations of MP dynamics like the identification of sink or source areas and ‘hotspots’ (Van Cauwenberghe et al., 2013; Hurley et al., 2018).

Under the proxy-normalisation framework, a **source** is an area whose MP storage is above its dynamic-equilibrium line (i.e. with significant excess MP relative to the normalisation line). This surplus remained as it has not been sufficiently mixed and sorted at the time of sampling due to insufficient mixing since introduction to the respective sedimentary system and hence with a tendency to cede the pollutant to connected regions Figure 2. It is crucial to note that the term ‘source’ is commonly used more broadly. Original input zones or entry points to the environment (e.g. an industrial site, WWTP, etc.), as well as processes or subsystems that facilitate net MP fluxes between environmental compartments are termed sources in the available MP literature (Woodward et al., 2021). Snow melt and flooding events are sources of MP to the river; the river is a source of MP to the sea (Hurley et al., 2018; Woodall et al., 2014).

A **sink** is an area with an unsaturated potential for MP uptake in the sense of the proxy-normalisation concept Figure 2. Equivalently to sources, the term sink can describe processes or subsystems. Biological processes such as biofouling that facilitate sinking of MP from the surface to the sea bed or the sediment bed that functions as a sink for matter residing in the water column (Kvale et al., 2020; Woodall et al., 2014). The term sink can refer to either intermediate or temporal sinks, or ultimate sinks, depending on the time horizon (Sandgaard et al., 2023).

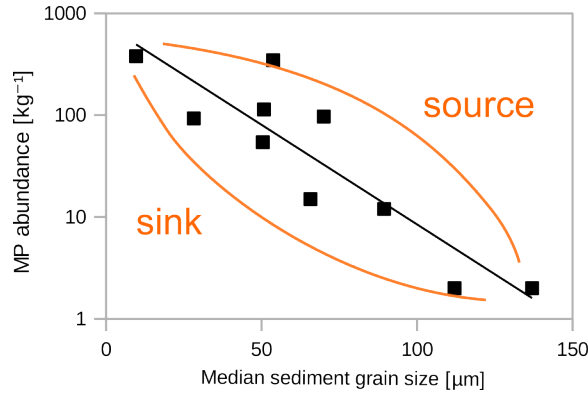


Figure 2: Regional sink source analysis applying the proxy normalisation concept

A cross-disciplinary definition is that a source or sink is a subsystem with a measurable net export or import of a target entity (Loreau et al., 2013). The analysis of sink-source dynamics is only meaningful when the temporal and spatial context is clearly defined. For instance, typical sinks in a narrower spatial context can also act as sources and vice versa: in case of resuspension events sub-regions of ocean sediments can act as a MP source to the water column and the organisms feeding there. Apart from some attempts using hydrodynamic models (e.g. Kvale et al., 2020), the terms sources and sinks remain descriptive and little quantified. The proposed proxy normalisation concept provides a more quantifiable method to define sink and source dynamics Figure 2.

Prediction

Commonly performed basic statistical analysis (mean, standard deviation, etc.) of non-normalised MP data may yield non-representative estimations of MP concentration. Comparing these estimates across different studies or areas (as e.g. in Harris, 2020) would imply a certain representativeness of values, which is however not guaranteed if the regional hydrodynamic ranges are not fully and equally covered. Also extrapolation from a non-representative data set includes potentially large error ranges. Yet, no systematic and comprehensive data interpretation scheme has evolved as a basis for a reliable MP level assessment that accounts for the hydrodynamic regime bias.

Applying normalisation to the data enables modelling MP distribution in a connected, albeit hydrodynamically heterogeneous system as one spatially well-resolved inventory, allowing one to depict the geographic legacy of the local MP pollution. Two studies in this thesis (described in detail in Focus 1 [page 31] and Focus 2 [page 33]), explore the modelling approach first for a simple well-connected system (Enders et al., 2019), and in extension for a geomorphologically and hydrodynamically more complex system containing discontinuities (Enders et al., *subm.*). In general, the application of the normalisation concept can show whether modelling with a natural particulate proxy alone is sufficient (i.e. in well-connected systems) or if there are discontinuities which necessitate the inclusion of further variables (more complex systems).

Once potential proxy variables are found, they can be used as predictor variables in an empirical modelling approach. As both, the choice of which variables to use as well as the model algorithm and its setup (e.g. model hyperparameters) are decision points with a potential impact on the model output, it is useful to avoid human bias by employing a data-driven approach (Cawley & Talbot, 2010). Here, certain practices from the field of machine learning (ML) models (e.g. nested cross-validation, stratification, ensembling) can be useful when adapted using meaningful settings for the sparse data scenarios typical for MP studies. Applying such practices allows for an efficient model selection as well as a rigorous validation and safeguards against the risk of overfitting (Varma & Simon, 2006).

ML has advanced rapidly within the Earth sciences (Bergen et al., 2019) and has likewise been employed across multiple facets of MP research from spectral noise reduction to polymer-type identification and image classification (Zhen et al., 2023; Brandt et al., 2021b; Ramanna et al., 2023). A recent study has demonstrated the development of a classifier for MP pollution levels on compiled data sets in surface seawater at global scale and used it for inference of predictor variable importance (Chen et al., 2023). In the context of the present work, empirical predictive modelling (EPM) based on ML principles are a key development that facilitates the identification of patterns in data that would otherwise be difficult to detect using classical statistical approaches. This includes testing and evaluating large combinatorial parameter spaces through the application of grid-search, as well as deducing the explanatory power of input variables, thereby increasing our understanding of the processes that drive MP distribution.

A predictive instance of such a proxy model (i.e. the model equation with fitted coefficients or weights) is not universal. The relationship between MP and natural particulates depends on the characteristics of the MP stock and the processes that dominate its distribution in the region being studied. For example, sorting may be dominated by sinking velocity, shear stress or the ratio of aggregates versus single particle sinking. If MP and sediment sorting is dominated by the sinking velocity (as they can be in calmer regions such as stagnant waters) the size offset between MP and sediment grains would be smaller compared to regions where sorting is predominantly driven by bed shear stress (Enders et al., 2019). Since particle abundance is related to particle size, these processes affect the relationships present in the respective model instances used to predict the spatial distribution of MP concentrations. The modelling pipeline used to train and validate the empirical model has the flexibility to adapt to different these regional particularities.

Estuaries as model and indicator environments in the Baltic

The study regions selected for this thesis are two Baltic Sea estuaries: the Schlei and the Warnow. Like most of the Baltic they are minimally influenced by tidal activity and water level changes occur primarily due to wind conditions (Medvedev et al., 2013). Yet they differ in their hydro-geomorphological character and anthropogenic pressures. Whereas the Warnow estuary (~10 km in length) is a partially mixed, hydro-geomorphologically simple estuary with a relatively continuous salinity gradient (Winkel, 2003), the Schlei (~42 km in length) features several narrowings and bays forming discontinuities in the hydrodynamic connectivity between inner and outer sub-systems. The freshwater input to the Warnow (527 million m³ annually) is about double that of the Schlei (250 million m³ annually), whereas the Warnow has relatively greater exchange with the Baltic Sea, for the Schlei it appears more restricted (Rönspieß et al., 2020; Schwarzer et al., 2019). The Warnow estuary at the city of Rostock is densely populated (~210,000), accommodates mass tourism, and is affected by urban, maritime and industrial pollution. In contrast, the Schlei is mostly surrounded by rural and provincial settlements (largest city Schleswig, population: ~24,000), and is affected by strong agricultural impacts. However, the Schlei has experienced a significant plastic pollution incident in recent history (NABU, 2018). There is little and mostly modelling-derived qualitative information in the relevant scientific literature on MP pollution in either estuary (Schernewski et al., 2021; Piehl et al., 2021; Siegel et al., 2021; Escobar-Sánchez et al., 2025), and no studies besides (Enders et al., 2019; Enders et al., *subm.*) have specifically addressed the sediment compartment or provided quantitative *in situ* data. To the knowledge of the author, this data gap applied equally to other Baltic Sea estuaries.

Estuaries, in a broader sense, are semi-enclosed coastal water bodies where freshwater from land mixes with saltwater from the open sea (Cameron & Pritchard, 1963; Fischer, 1976). They are sensitive environments with large natural fluctuations of physicochemical properties that challenge the natural adaptability of inhabiting organisms (Wolowicz et al., 2007). Many estuaries are already exposed to multiple stress factors (e.g. major shipping activities, coastal engineering, agricultural inlets) due to an intensive anthropogenic usage. An increasing majority of the human population (8.5 billion predicted for 2050) lives at and affects estuaries and other ocean-draining water systems (Bianchi, 2007). Here, MP constitutes a newly emerging pollutant, relevant from a socio-ecological perspective. These areas, where the river meets the sea, are also referred to as transitional waters as an overarching term (McLusky & Elliott, 2007). Although, due to the high variability in estuarine physiography, there is some ambiguity regarding a single definition, for instance, in cases where there is inconsistent freshwater inflow or periodic closures to the sea. Other classifications emphasise tidal range as a key feature (Potter et al., 2010).

The Baltic Sea itself is often considered one of the largest estuaries in the world. It is a semi-enclosed sea with a significant surplus of freshwater input, fostering estuarine circulation (Kullenberg & Jacobsen, 1981; Blenckner et al., 2021). With an area of 1.7 million km², the drainage basin of the Baltic Sea is over four times the size of the Baltic Sea itself, and is inhabited by around 85 million people from 14 countries (Sweitzer et al., 1996). Only rare inflow events from the North Sea through the Danish Straits deliver larger saltwater masses into the Baltic's deeper basins. Consequently, the Baltic Sea has a long water residence time of up to 30 years (Döös et al., 2004), making it susceptible to accumulation of pollutants of all kinds. Its isolated geography and significant human impact, such as chemical pollution and eutrophication caused by agricultural runoff and wastewater (Kanwischer et al., 2022; Murray et al., 2019), or chemical leaching from ammunition dump sites (Beldowski et al., 2016), together with an increased seawater temperature rise, have led to the Baltic Sea being described as a 'time machine' and a model environment for studying changes caused by human activity before they occur elsewhere (Reusch et al., 2018). At the same time, the region also benefits from decades of cross-national cooperation and management experience in addressing these environmental issues. Similar accumulation effects are expected for MP, however, little is known about MP retention and distribution of MP in the Baltic Sea and its estuaries (Schernewski et al., 2021). Sampling campaigns performed in the Baltic Sea found MP ranges between 0.07 to 3300 MP m⁻³ in water and 0 to 10179 MP kg⁻¹ dry weight in sediments (Enders et al., 2019; Esiukova

et al., 2020; Narloch et al., 2022). Yet, due to the described limitations in sample purification and analysis, sample number and coverage remain insufficient and it remains unrealistic to gain a comprehensive picture of the spatial distribution of MP in the Baltic Sea region. Grain size, even though it is one of the fundamental properties of sediment as it bears information on the respective hydrodynamic conditions, has rarely been explicitly analysed in sedimentary MP studies of the Baltic Sea and its estuaries. Tracking MP in larger sea environments such as the Baltic Sea is limited as many interacting processes and a greater temporal delay obscure the link between sources and depositions. With more than 105 major watersheds discharging into the Baltic Sea (Mörth et al., 2007) and delivering their MP loads into currents that disperse them across the sea, monitoring becomes difficult. In contrast, estuaries comprise a more confined area and their MP inventories reflect pollution levels closer to the terrestrial sources, offering clearer trends and better prospects for management interventions. Additionally, their strong gradients in biogeochemistry and hydrodynamic conditions render estuaries unique model environments (Bianchi, 2007) for investigating particulate MP proxies. Conclusively, comprehensive and reliable evaluation of MP levels of estuaries not only provides knowledge on the respective environment itself, but can be used as key indicator systems for changing MP level inputs to the marine environment.

Rivers and estuaries are recognised as major carriers of MP to the marine environment (Duis & Coors, 2016; Biltcliff-Ward et al., 2022). While MP abundances of sedimentary systems in the fluvial hinterlands spread over larger areas and have been shown to be highly fluctuating due to comparatively high sensitivities towards flooding events (Hurley et al., 2018), estuaries represent bottlenecks for MP sources deriving from land. Despite their prominent role in trapping particles and contaminants (Kennedy, 1984), they have not yet been a major focus in MP research and monitoring campaigns (Biltcliff-Ward et al., 2022). The trapping function of estuaries for suspended particulate matter, especially organic and fine-grained material, by flocculation and sedimentation is well-known (Wollast, 2003). On geological time scales estuaries are ephemeral: they evolve and continuously fill up with sediments, which might never reach the open sea. The trapping efficiency for natural particles, is known to depend, among other factors, on discharge volumes, residence times and tidal influence (Kennedy, 1984; Jay et al., 2007). Similarly, estuaries are thought to play a key functional role in controlling MP trapping mechanisms and release to the sea (López et al., 2021). In addition to the studies on MP and sediment floc formation discussed under ‘Aggregation’, another laboratory study demonstrated that MP sedimentation is generally enhanced in the presence of high loads of suspended matter (Möhlenkamp et al., 2018), a condition characteristic of estuaries. A recent model calculation of emission sources to the Baltic Sea found that most MP remained in the vicinity of river mouths and cities and recommended these regions for designing monitoring strategies (Schernewski et al., 2021). This indicates a strong need to develop suitable sampling and monitoring schemes including relevant proxies with a stronger focus on estuaries to receive a better picture of the evolution of this particulate pollutant.

MP has already been incorporated into several regulations aimed at protecting aquatic environments. In the European Union, the Marine Strategy Framework Directive (MSFD) (The European Parliament and of the Council, 2008) mandates member states to achieve ‘good environmental status’. In the MSFD, MP is integrated under Descriptor 10 aiming to ensure that: ‘properties and quantities of marine litter do not cause harm to the coastal and marine environment’. For the Baltic Sea region, this is integrated in the Helsinki Commission (HELCOM) Baltic Sea Action Plan on Marine Litter, which emphasises the need for the collection of baseline data on the extent and impacts of MP and systematic monitoring programmes in the Baltic Sea region (HELCOM, 2015). Worldwide, many regional action plans now address marine litter mitigation (Vince & Hardesty, 2018), including the previously mentioned resolution for a binding plastic treaty as a United Nations instrument (UNEP, 2022).

Knowledge gaps and objectives

As demonstrated in the background section, sediments can present a time-integrative archive of overall plastic pollution in aquatic ecosystems. However, knowledge of their actual MP loads is scarce and the data-analytical methods for understanding MP distribution processes, both towards and within the compartment remain underexplored. Especially, there is a lack of investigation into the relationship between MP and other natural particulates that may reveal a hydrodynamic regime bias in MP data. Determination of environmental plastic inventories and spatio-temporal monitoring strategies are needed in the light of recent policy advances. However, their implementation requires further theoretical advancements and technical developments. The former involves data-analytical procedures that address MP in relation to the transport of natural particulates, and provide modelling and mapping approaches. The latter concerns laboratory methodology, like techniques suitable for extraction of the smaller MP fractions from complex matrices, the abilities to estimate measurement-associated uncertainties, or improvements in applied routines of analytical chemistry that enhance quality and speed of the high-throughput data acquisition in MP particle characterisation.

The publications that form the canon of this thesis, aim to address these knowledge gaps by fulfilling the following objectives:

1. to develop a conceptual framework and data analytical procedure accounting for hydrodynamic variability in MP data via proxies of natural particulates ([Enders et al., 2019](#); [Enders et al., subm.](#); [Osinski et al., 2020](#))
2. to determine regional MP inventories via spatial prediction from proxy-calibrated small precursory MP data sets and predictive modelling following FAIR data principles ([Enders et al., subm.](#); [Čerkasova et al., 2023](#))
3. to adapt and evaluate purification protocols to extract small MP from particle-rich matrices and define best practises for the field ([Enders et al., 2020b, 2016](#); [Enders et al., 2020a](#); [Lenz et al., 2021](#))
4. to assess the quality and comparability of procedures applied in MP quantification or exposure studies ([Lenz et al., 2021, 2024, 2016](#); [Enders et al., 2020b](#); [Enders et al., 2020a](#))

Focus 1: Tracing microplastics through sediment analogies

This focus explores the scientific potential to establish environmental proxies for MP in sediments. Empirically found correlations between MP ($> 500 \mu\text{m}$) and grain size fractions are interpreted in the context of the theory of initiation of motion of sediments. The observation of grain size MP relationships are used to derive the methodological prerequisites which enable the deduction of MP distributions from sediment analogies for modelling purposes. Besides exploring the EPM potential, the application of HNM in the context of MP distribution is investigated with respect to its abilities for qualitative and quantitative predictive performance and uncertainty.

Enders et al. (2019): Tracing microplastics in aquatic environments based on sediment analogies

Previously published results were contradictory regarding the existence of an MP - sediment relationship (Vianello et al., 2013; Strand et al., 2013; Romeo et al., 2015; Ballent et al., 2016; Alomar et al., 2016; Fastelli et al., 2016; Blašković et al., 2017; Peng et al., 2017; Maes et al., 2018; Renzi et al., 2018) and the use of granulometric normalisers had not been systematically explored. In the Warnow estuary, we found that certain size-fractionated groups of MP ($> 500 \mu\text{m}$, density $> 1 \text{ g cm}^{-3}$) significantly correlated with sediment classes with a shift in size that could be explained by the density difference of the two particulate materials (see Fig. 4 A, B; Fig. 5 in Enders et al. (2019)). This empirically derived relationship was in general agreement with the theory of the onset of motion of sediments (threshold bed shear stress), which appeared to dominate the sorting mechanisms for MP and sediments. By using generalised linear models several predictors were tested, of which grain size, percent mud (i.e. the share of grains $< 63 \mu\text{m}$) in particular, was the most determining factor to explain MP distribution patterns. For most functional classes of MP such as paint flakes and ordinary polymers, the introduction of a source factor such as distance to marinas and the WWTP, respectively, further improved statistical power. This source factor represents the surplus MP fraction that remains unmixed and unsorted because post-depositional bed shear stresses have been too low.

Based on the data from this study and reviewing sample designs and methods employed in existing studies, we demonstrated that several factors can distort the identification and accuracy of the relationship between MP and sediment. Especially, the spatio-temporal connectivity of the study area and a sufficient sample size with a representative coverage of the hydrodynamic conditions, i.e. grain size variability, are critical for a proxy calibration of sufficient accuracy.

For the Warnow estuary we could show that at hydrodynamic equivalence MP abundances in this Baltic Sea estuary were higher by nearly two orders of magnitude compared to the two closest Baltic Sea basins. These results suggest that there is a high potential of estuarine sediments and other near-source depositional regions to function as potential long- or intermediate-term MP storage. Overall, this focus showed that MP level interpretation, e.g. source and sink determination or inter-region comparisons are only meaningful when the hydrodynamic regime is accounted for. Otherwise, MP variability may be falsely attributed to source load differences, MP-specific accumulation or erosion processes. It is concluded that granulometric normalisation can correct for the hydrodynamic regime bias, which allows a more reliable data interpretation and comparison within and across aquatic sedimentary systems. The measurement of granulometric proxies is recommended for future studies along with MP determination and used as a basis for sample selection as well as normalisation of MP levels.

Osinski et al. (2020): Model uncertainties of a storm and their influence on microplastics and sediment transport in the Baltic Sea

A numerical model of the Baltic Sea was developed to investigate how uncertainties in meteorological forcing fields, i.e. atmospheric conditions, propagate to affect erosional and depositional conditions for MP. The starting point of the model was a storm event, which was necessary to initiate sufficient

sediment transport. Throughout the four-step model cascade, the uncertainties originating from the atmospheric model propagated further to variability in storm tracks. This in turn influenced the direction of ocean waves and currents, ultimately impacting the bottom shear stress that initiates sediment and MP transport. As a result, significant quantitative variations in the transported MP loads among the ensemble members (i.e. multiple realisations predicting MP transport pathways) became visible. Uncertainty increased with decreasing MP sizes and densities. The authors concluded that, even if the deposition and resuspension behaviour of MP were fully understood (for simplification only spherical model MP were used), uncertainties relating to atmospheric conditions and their propagation through the ocean circulation model cascade would still impede a reliable quantitative MP estimation. Despite these limitations, the model could provide a valuable qualitative evaluation regarding potential depositional and erosional areas. This information can assist future monitoring studies, for instance, by optimising the location and coverage of sampling station across different hydrodynamic, depositional, and erosional conditions. Further research is needed to determine how sensitive the spatial distribution of erosional and depositional regions is under storm scenarios or multiple storm succession.

Focus 2: Machine-learning assisted mapping the microplastic legacy

The finding of correlations of MP to natural particulates motivated an investigation on proxy candidates for spatial prediction of MP distributions and the calculation of system-wide inventories. By integrating an environmental MP-targeted database, a reproducible model pipeline was developed, aided by procedures typically used in ML workflows. This enabled rigorous validation of the model performance in a combined nested cross-validation scheme that included, besides the actual model fit, the data-driven design decisions of the model selection (model types, hyperparameters and predictors chosen among multiple sediment constituents).

Enders et al. (subm.): Machine-learning enabled microplastic inventory prediction in aquatic sedimentary systems

Based on the findings of the study of the Warnow estuary (Enders et al., 2019), it was hypothesised that granulometric proxies are sufficient predictors of sedimentary MP spatial concentration distributions in EPM. As a case study region for developing such a modelling approach, the Schlei (Schleswig-Holstein, Germany), was selected. The Schlei recently made headlines due to a local plastic pollution incident (NABU, 2018). Being geomorphologically and hydrodynamically more complex than the previously studied Warnow estuary, it challenges the spatio-temporal connectivity assumption, yet offers the opportunity to develop a more universal model framework. Due to improvements in the preparation techniques of matter-rich samples (Enders et al., 2020b), a wider MP size spectrum and larger data set size could be included. The high number of generated predictors: multiple natural particulate proxies, spatio-temporal discontinuity and geographic variables; the tested model classes: generalised linear models (GLM), linear and tree-based Extreme Gradient Boosting (XGB linear, XGB tree) and Random Forest (RF); inspired the exploitation of modern ML concepts for the development of a model application. This endeavour was challenged by the yet relatively small sample size ($n = 26$), as it is typically the case for environmental MP data. Many ML algorithms operate best in the context of thousands of samples or more, which is not realistically achievable for environmental MP studies. Therefore, measures were implemented to adapt certain ML techniques specifically to small data set scenarios, such as nested cross-validation (NCV) with adjustable stratification, and ensembling for predictive stability. For referring to the resulting model selection, validation and prediction pipeline, the included components or concepts were used together to form the acronym NIXVEGS (Nested Iterative (stratified) X-Validation-to-Ensemble-modelling through Grid Searches). Correlations with several granulometric proxies (e.g. the first principal coordinate of grain size [PCo1] and the percentage of the mud fraction [perc_MUD] fitted best) could be confirmed for these smaller MP sizes. However, due to the hydrodynamic complexity of the studied system, including its geomorphological peculiarities, size, and recent localised heterogeneous MP inputs, it was found indispensable to have a predictor that accounted for discontinuities in MP propagation. Based on a hydronumeric model (provided by the Federal Waterways Engineering and Research Institute, BAW) predictors were generated, one of which (describing the mean travelling time of a passive tracer, i.e. a water molecule) was identified to be the best fitting in combination with the granulometric proxy for prediction of spatial MP distribution in the Schlei sediments, based on NIXVEGS' nested cross-validation. At over 180 stations with available grain size data (provided by the Christian-Albrechts-University of Kiel, CAU), NIXVEGS estimated that a total inventory of ~20 trillion MP particles (50 - 5000 μm) residing in the Schlei sediments, extending to a depth covering nearly the entire 'plastic age', as estimated from the sedimentation rates calculated by Schwarzer et al. (2019). Yet, due to a potential for deeper mixing activity in the Schlei sediments, MP extending beyond the 15 cm horizon cannot be excluded. It should be noted that the lower depth layers used in our model (samples extending down to a sediment depth of 15 cm) are subject to greater uncertainty as they are based on only four sampling stations. However, we observed that these deeper samples largely reflected the MP and sediment characteristics of their corresponding top-layer samples. This warranted merging them and estimating the total MP inventory of the Schlei sediments at a layer thickness of 15 cm.

As part of this study, advancements in the analysis of all three dimensions of MP particles (i.e. particle length, width and height) could be integrated in the employed micro-spectroscopic analysis software [GEPARD](#) ([Brandt et al., 2020](#)). Previous studies tried to estimate the third dimension from those available in 2-dimensional representations. In the data of this study (see exploratory data analysis web application) it can be seen that the first and second dimension do not carry sufficient information to predict the third dimension at satisfying accuracy. Thus, it can be concluded that measuring the third dimension is indispensable for a reliable estimate of volume and mass of MP. Based on the mass conversion, the MP inventory of the Schlei surface sediments was calculated to comprise ~14.4 tonnes. Overall, these estimates represent the highest resolution picture of an MP inventory for an entire geomorphological region to date. The generalisation score (i.e. the performance of the regression model on unseen data) reached R^2 of 0.7 based on NCV (i.e. including method selection decision into the validation) and proved robust in the sensitivity analysis (e.g. ranging from 0.63 to 0.72 under different perturbations input variations: +10%, $\pm 5\%$, max. value exclusion).

The entire data-analytical workflow follows FAIR principles (findability, accessibility, interoperability, reusability ([Wilkinson et al., 2016](#))). The data-analytical work for this study included the development of retrieval and processing tools for data stored in a dedicated MP database ([Čerkasova et al., 2023](#)). This enabled structured data management through a transparent, reproducible and validatable workflow of querying, managing and transforming data using Jupyter notebooks and Python scripts that build the model environment. An [exploratory data analysis web application](#) allows the readers of the study to comprehensively explore the entire MP and model data.

Following on from Focus 1, a comparison of grain size normalised data from the literature, confirmed that estuaries and fjords exhibit the highest accumulation of MP, as compared to beaches, rivers, lakes and the open sea. This establishes their pivotal role and key position in the context of monitoring.

Čerkasova et al. (2023): A public database for microplastics in the environment

The multitude of data and metadata recorded in one research project can be enormous and requires large efforts to prevent errors during all steps of data handling. These challenges inspired the development of a relational MP database to streamline data management and handling across data contributors, projects and institutions facilitating an efficient data transfer. The database schema ‘Marine Plastic Database’ (MPDB) is structured to be highly versatile for the kind of particle-based MP data. It ensures data integrity (invalid data is detected), consistency and security, and is referenced in the public-facing [meta-database](#) which makes the information findable for other public research data portals, aligning with FAIR principles. The MPDB allows to track the entire analytical history of a particle: from the particle properties (e.g. polymer type, size, shape) over preparational techniques (e.g. density separation, splitting, chemical treatment) back to sampling location and methods. This way all MP data can be related, stored, updated and queried for data-analytical and statistical applications. Additionally, a blind sample subtraction script has been developed in order to streamline and automate the procedure for self-contamination during sample preparation and analysis ([Enders et al., subm.](#); [Čerkasova et al., 2023](#)). It bases on matching phenotypes, i.e. particles with identical values in **sample**, **colour**, **shape**, and **polymer type**. Control for internal contamination is an integral part of MP studies, transparent and consistent procedures much-needed. To the knowledge of the authors, the MPDB is the first public MP database designed to preserve the entire analytical workflow, from spectra to harmonised particle metadata, so that the full data pipeline remains transparent, traceable and reusable. The data stored in the MPDB has been used by several studies (e.g. [Piehl et al., 2021](#); [Siegel et al., 2021](#); [Enders et al., subm.](#)) and reports ([Bertling et al., 2021](#)) and sparked interest in further developments of such databases in the scientific MP community ([Sherrod et al., 2024](#)).

Focus 3: Methodological advancements

The efficiency and reproducibility of extraction and analysis methods are a bottleneck to generate larger scale and reliable data sets ([Martin et al., 2022](#)). To realise the studies concerned with the proxy model methodological advancements were necessary. Focus 3 presents the outcome of method developments from sample processing to analytical measurement validation and data analytics. These advancements improved the extraction and characterisation of smaller MP from larger sample numbers with lower uncertainties from various matter-rich matrices.

MP extraction from matter-rich samples

Enders et al. (2020b): When every particle matters: A QuEChERS approach to extract microplastics from environmental samples

At the baseline stands the optimisation of purification techniques for matter-rich samples, like sediments, sludge, and soils, which was required to increase sample throughput, harmonise MP sample work up of diverse environmental matrices in a standard laboratory while ensuring sufficient analytical accuracy. Therefore, a universal framework of modular protocols was developed adaptable to various environmental sample compositions. It was designed to be used in a standard laboratory and meet predefined user requirements: Quick, Easy, Cheap, Effective, Rugged, Safe (QuEChERS). This modular extraction pipeline targets MP in a size spectrum between 10 μm and 5 mm. The reduction of non-MP matter is a crucial step for state-of-the-art particle-based analysis methods, such as Raman or FTIR spectroscopy. The analysis time is directly proportional to the number of particles, as every single one undergoes spectral evaluation.

A conical spiral conveyor was developed that assists gentle agitation of the sediment while being in the density separation medium, which enhances the recovery rates of MP from particle-rich matrices. This is advantageous compared to formerly applied techniques which used stirring blades or manual shaking which, however, bear the risk to disintegrate particles due to harsh grinding forces or are ineffective for larger sample volumes. Generally, only minor adaptations had to be made on standard laboratory equipment e.g. widening of separation funnel inlet and outlet for the conveyor to be applied and the sediment to pass. To adhere to QuEChERS targets, the need for specialised equipment was to be kept at a minimum, thereby lowering the barriers for other laboratories to adopt and implement these protocols. Recovery tests have been performed using differently sized fluorescent MP particles covering the entire treatment pipeline for a typical sub-aquatic sediment sample, which showed a size dependent recovery, i.e. lower recovery for smaller size classes of MP. Comprehensive quality assurance and control measures were defined and implemented, e.g. working in a laminar flow bench, micro-filtration of all solutions, implementation of a water-tap-filtration device, parallel blind sampling, MP-free laboratory utensils and room air filtering. An overall aim was to contribute towards a standardisation of MP purification techniques. With new protocols evolving, the modular structure provides the flexibility to be extended and can be used as a foundation to selectively extract MP from matrices beyond environmental samples. The development and implementation of this modular MP extraction pipeline was crucial for the systematic work up and analysis of MP samples for the development of a robust MP EPM in the Schlei described above, extending size and sample number ranges. Above that, the modular extraction approach has helped to realise multiple studies in IOW laboratories (e.g. [Brandt et al., 2020](#); [Enders et al., 2020a](#); [Siegel et al., 2021](#); [Piehl et al., 2021](#); [Tagg et al., 2022](#); [Kaiser et al., 2023](#)).

Lenz et al. (2021): Measuring impacts of microplastic treatments via image recognition on immobilised particles below 100 μm

It is an immanent goal in MP purification procedures to effectively reduce non-MP matter, while keeping MP unaltered and retained for analysis. The effectiveness of the matrix removal is evaluated

by measuring reductions in both sample volume and the number of non-MP particles during spectral analysis. However, each stage of sample processing carries inherent risks, MP loss, structural changes, aggregation or disintegration, which can falsify results. As particles below 100 μm easily cannot be handled individually, available evaluation study concepts rely on bulk analysis, where recovered particle numbers in relation to the count of originally spiked particles are evaluated, as for instance done in Enders et al. (2020b). However, these kind of tests come without the possibility to distinguish between chemical treatment loss (e.g. dissolution) and handling loss (e.g. sticking to glassware, filtration loss), which are less constant as they depended on the individual operator and handling variability. Additionally, the evaluation of losses and changes on the respective polymer types is challenging when target particle sizes are $< 100 \mu\text{m}$. If particles could, instead, be evaluated on an individual basis with respect to their alterations upon chemical treatment, higher detail and insight could be gained, e.g. on size dependent recoveries, or morphology and surface changes including spectroscopic effects. Having stationary particles with an attachment to a surface that can withstand the treatment steps would allow for such evaluations also for particles resembling environmental occurring MP instead of specifically labelled or spherical laboratory-grade fluorescent test beads of distinct properties in order to be found again. To address this, a novel approach was developed where MP particles between 10 and 70 μm were immobilised on a silicon substrate, which allowed pre-post evaluation of treatment methods on individual particles via image analysis. This included an evaluation of quantitative parameters such as particle loss, particle size and morphology. A qualitative complementary evaluation of spectral changes that compromise polymer recognition via spectroscopic analysis on bulk MP samples has also been performed.

These advancements in polymer resistivity testing specifically of small MP increased the reliability of the chemical treatment protocols as described for use on MP in this size range in the former publication by Enders et al. (2020b). Overall, polymer resistivity could be confirmed for most of the 19 different polymer types tested, with minor restrictions. Significant polymeric degradation has been observed for epoxy resins and PC under strong oxidative treatment (particle loss of 46% and 25%, respectively). Acrylonitrile-butadiene-styrene (ABS) particle loss of 30% was observed under density separation solution (sodium polytungstate, pH 3). Generally, Raman spectra of post-treatment measurements showed fewer recognition hindering artefacts like changes in band position and intensity than FTIR. Interestingly, for three of the five paint resins (PU-, Alkyd-, Rosin-based) no spectra of sufficient quality could be exploited prior to treatment by both applied analytical techniques, questioning their exhaustive quantification in environmental samples using current methods. This underpins existing analytical limitations: certain MP particles can be systematically underdetermined or lost due to size reduction between sampling and analysis, indicating that reported MP abundances are to be considered as conservative lower estimates, assuming sound analytical procedures and rigour were applied.

Enders et al. (2020a): Evaluation of electrostatic separation of microplastics from mineral-rich environmental samples

The application of a modular MP purification pipeline is efficient and targeted for matter-rich samples, yet, for certain sample types larger volumes need to be processed to yield sufficient statistical robustness. The MP abundances present in the sample determines the initial sample volume that would be necessary to enable a robust statistical analysis (Cowger et al., 2024). Extrapolation errors can be substantial when MP numbers are low, as investigated by Brandt et al. (2021a). Thus, for known low-MP regions higher sample volumes would be advantageous. Following the granulometric dependency of MP numbers in sediments, samples with coarser grain sizes and relatively low organic matter content are those with lower MP numbers.

A promising recently published MP separation method via electrostatic separation (Felsing et al., 2018) was evaluated for application of matter-rich samples. However, the formerly found MP recovery rates of nearly 100% across different MP sizes and mass reduction of 99% across various matter-rich matrices could not be reproduced. In finer grained sediments with high organic matter content such as the case for soils and many aquatic sediments, mass recovery rates greatly varied between 1% for soils, 17% for commercial calcite rich sand and 93% for beach sand. Especially the influence of fine organic matter and fine calcite particles may impede sufficient separation. Concerning MP recovery rates a strong size-dependency has been observed. In beach sands, 95% and 90% of MP particles of 2 mm and 0.45 mm are recovered, while for $\sim 125 \mu\text{m}$, $\sim 63 \mu\text{m}$, and $\sim 20 \mu\text{m}$ sized MP the recovery falls below 80%, 60%, and 50%, respectively. These deviations in results from the pioneering study were in overall agreement with another study, recognising their averagely higher recovery rates and mass reduction due to differences in sediment composition, larger MP and grain sizes, different polymer types and analytical overestimation (Kurzweg et al., 2022).

It is concluded that the application of electrostatic separation can be useful for coarse-grained samples of low organic matter content, which are also typically scarcer in small MP $< 100 \mu\text{m}$. As such beach monitoring could profit from the faster throughput of larger sample volumes. However, a subsequent density separation for the elimination of the remaining matter fraction is still required. More research would be needed to safely apply this method for larger application ranges, especially

with respect to matrix effects, polymer types and shapes, as well as other test parameters such as humidity. This study shows the importance of reproducibility in science in general.

Enders et al. (2016): Extraction of microplastic from biota: recommended acidic digestion destroys common plastic polymers

In the early 2010s, monitoring fish for (micro)plastics was integrated into the MSFD and OSPAR guidelines (Hanke et al., 2013). ICES issued a preliminary monitoring protocol for the digestion of organic matter for MP purification in 2015 (ICES, 2015), recommending the use of a 4:1 mixture of nitric and perchloric acid, as well as application at 80°C. However, during the Danish national monitoring campaign, the acidic mixture was found to have detrimental effects on multiple polymer types when this protocol was followed. Of the 21 polymer types tested, only six (PP, LDPE, HDPE, PTFE, one type of PVC and ethylene-vinyl acetate (EVA)) showed no changes. Others exhibited changes ranging from surface alterations to near-complete dissolution (e.g. PA, PU, ABS, three rubber elastomers and polymethylmethacrylate (PMMA)). A protocol involving a mixture of potassium hydroxide and sodium hypochlorite (1:1, 30%) was found to be an effective alternative MP-preserving digestion method, as validated via visual inspection and Raman spectroscopic measurements before and after treatment. The destructive effects observed in the digestion trials in this study were carried out using plastic items within the macroscopic size range. Even more severe effects are expected on a microscopic scale. Dedicated testing in this size range is therefore warranted, as for instance demonstrated by subsequent studies (Lenz et al., 2021). Consequently, this study is an early example of the importance of method validation in MP quantification.

Analytical accuracy validation and procedural reality check

Brandt et al. (2021a): Assessment of subsampling strategies in microspectroscopy of environmental microplastic samples

Particle-based spectroscopic methods such as Raman or FTIR have a high accuracy regarding the chemical classification of polymers. However, instrumental and software limitations can lead to measurement times on the order of hours to days per sample, hindering the analysis of large sample sets. In order to increase sample throughput, it is common practice to measure only a subset of the purified sample on a filter substrate, especially in case of particle-rich samples. However, usually less than 1% of the particles on the analytical substrate are identified as MP, which often means that absolute numbers of MP particles are so low that subsampling and subsequent extrapolation bear unacceptable errors. This is further aggravated when total MP results are segregated into sub-fractions by polymer, colour, shape or size category. The authors provide a quantitative analysis on the statistical robustness of commonly applied subsampling strategies during analysis. Based on the evaluation of 27 different environmental samples it was found that a minimum 50% of particles should be analysed, when accepting a subsampling error of no more than 20%. In scenarios with very low MP numbers or uneven distribution on the filter, statistical subsampling where every *n*th particle is measured proved most accurate. When statistical analysis on sub-fractions is targeted, the entire filter should be analysed to ensure sufficient statistical robustness.

Lenz et al. (2024): What goes around should not move around: immobilizing microplastics as a new approach for analytical ring trials

There are multiple methods available to analyse MP < 100 µm. Their comparability is one of the major challenges in the chemical analysis of MP. Several ring trials approach this issue by adapting procedures often used for benchmarking analytical proficiency for liquid or dissolved analytes. Typically, individual sample specimens are prepared by a host and sent to the trial participants. Hence all participants work in parallel, each measuring their own independent specimen. Adapting such a concept to MP in the lower micrometre ranges includes the problem that potential uncertainties on the contained MP numbers are hard to control completely and are indistinguishable from actual differences in the detection proficiency of a participant, i.e. the specific analytical uncertainty. This can lead to vastly deviating results among ring trial participants (Müller et al., 2020; Van Mourik et al., 2021; Belz et al., 2021; Ciornii et al., 2025). Herein, a novel ring trial design is being presented which is based on permanently immobilised MP on one sample which is then circulated among participants for sequential evaluation. This way production differences and pretreatment effects become obsolete and the specific analytical uncertainty can be identified. In the group of participants in a proof of concept application of the serial ring trial design, the relative standard deviation of 5% was ascertained. In comparison, the parallel design ring trial, including the potential additive errors described above, resulted in 23% relative standard deviation on average. A pre- and post-measurement by the ring trial host ensures a quality check that no significant particle loss occurred. The approach for creating the immobilised sample is based on filtration immobilisation using an inorganic binder, which leads to an optimal distribution of particles on the filter (avoiding particle conglomeration) and instant adherence of the particles on the filter substrate, with minimal remaining of the adhesive. In contrast to the previously used organic

binder ([Lenz et al., 2021](#)), potassium silicate does not interfere with spectral bands of polymers. The serial ring trial design directly helps to further improve MP analysis methods also at the lower end of the detection limits, as it enables analytical comparisons based on the same particle. It provides certainty on the comparability of analysis results of analytical consortia. The uncertainty coming from the purification and handling of the sample can now be separated from the purely analytical uncertainty. Besides their use in ring trials, the immobilisation-filtration technique can find further applications in correlative microscopy (as is currently tested for fluorescence microscopy and correlation of mass- and particle-based analysis techniques), sample archiving and the creation of analytical calibration samples for particulate analytes, potentially also beyond MP. It is currently filed for a patent.

Lenz et al. (2016): Microplastic exposure studies should be environmentally realistic

Besides accuracy and uncertainty of study results in MP experiments, another critical aspect is the environmental relevance. Multiple toxicological dose-response studies were performed during the last decades, in order to investigate the potential effect of MP on various organisms. In a response letter in PNAS to one of these studies ([Sussarellu et al., 2016](#)), Lenz et al. (2016) shared the observation that when reviewing the concentrations used by toxicological studies with environmentally identified levels, large differences became apparent. Experimental concentrations were, on average, two to seven orders of magnitude higher than those identified in environmental surveys. Clearly, working with respective environmental concentrations would in many setups be hindered by practical limitations. For instance, the highest concentrations reported in an Atlantic surface water survey with a lower mesh size of 10 μm were at the order of one MP particle per 2 L of water ([Enders et al., 2015](#)). Depending on the experimental setup (exposed species, toxicological endpoint, exposure time), this could easily lead to situations where it becomes challenging or impossible to draw statistically significant conclusions, be it due to limited encounter rates or too weak effects. However, that does not mean that effects established at higher concentrations are not relevant, but it is important to keep in mind that current environmental MP concentrations are often lower than those where measurable acute toxicological effects are observed. Notably, chronic or additive effects of so-called ‘chemical cocktails’ are difficult to address in these studies and are important issues to be addressed in future research.

Perspectives and closing remarks

The publications presented in this thesis contribute new insights and methodological advances for the quantification of MP pollution in sediments. The concept of grain size normalisation is introduced in the context of MP abundance assessment, which allows for comparative pollution level assessments in sediments. With it, a robust and adaptable model framework is developed which is applied to regional distribution analysis and inventory determination and can be a valuable toolkit in MP monitoring studies.

Granulometric proxy-based modelling is based on the assumption that the processes that drive particle transport are the same for MP as for sediments. This means that any MP-specific process would disrupt the relationship, appearing as smaller-scale deviations that increase model uncertainty if they occur in a non-continuous manner or cannot be represented by additional variables. Larger-scale MP attenuation effects, such as those observed due to the geomorphological obstacles in the Schlei, were accounted for by introducing a spatio-temporal discontinuity variable.

Several limitations and challenges could occur when applying the model to other environments where the primary hydrodynamics are occasionally interrupted. For instance, continental slopes and sub-marine canyons repeatedly experience turbidity currents that deliver high loads of MP to the deeper sediments (Kane et al., 2020). In theory, they represent a pronounced spatial and temporal discontinuity; therefore, an attempt should be made to demarcate the spatially and temporally connected sub-area. However, this may be difficult, as the sorting processes within turbidity currents are rather chaotic (Symons et al., 2017). They overlap with ocean-current-driven bed load transport processes and are difficult to model (Salles et al., 2008). It is up to future research to determine whether the presented modelling pipeline is applicable in such hydrodynamically highly variable environments, where several major sorting mechanisms overlap. Similarly, singular or local events, whether of natural (e.g. local flora or fauna) or anthropogenic origin (e.g. dredging) are difficult to incorporate in prediction models. A comprehensive analysis of local processes and exploratory data analysis based on a granulometric normalisation plot is necessary prior to modelling in order to identify and potentially exclude technically justified outliers for a better model robustness regarding the entire region studied.

As any model can only be as good as the data that are provided, a reliable MP extraction and analysis pipeline is essential. Several methodological improvements have been made as part of this thesis to increase sample throughput and method validity, ultimately fostering data comparability. However, there is still room for further improvements in purification techniques as typically far less than 1% of the analysed particles in a purified sample are confirmed MP. At the same time, analytical methods should be further automated in order to accelerate sample throughput. Measurement and spectral assessment are still very time-consuming tasks, which include manual work by experts. It must be acknowledged that MP < 5 μm (including nanoplastics) must be handled in a certified clean room facility in order to effectively prevent contamination of overall particle numbers in these size ranges. Although high-throughput analysis as it is known from grain size or organic matter analysis seems currently unrealistic for MP, an increase in sample numbers and measurement accuracy would directly improve model accuracy.

Dedicated campaigns for spatio-temporal monitoring of sedimentary MP would require sampling more recent layers for higher temporal resolution and keeping layer depth constant with respect to sedimentation rates. Therefore box corers are preferable, as they better preserve sediment layers and sample a larger surface area compared to grab samplers. Although the entire range of grain size variability should be covered, finer cohesive sediment regions are especially valuable with respect to temporal comparability as they are less prone to vertical movement and disturbance during sampling.

Empirically found correlations between MP (> 500 μm) and grain size fractions are interpreted in the context of the theory of initiation of motion of sediments. In Schlei sediments an extended and more precise size correlation was possible as exact particle sizes were retrieved in three dimensions. Here, finer sediments (< 63 μm) showed a shift relative to MP sizes, similar to what was found

in the Warnow sediments. However, in coarser sediments the size relationship changed and grain sizes were larger relative to MP. This could indicate that larger MP particles are not available in the Schlei at sufficient concentrations while under increased hydrodynamic forcing smaller sized particles get trapped between pore spaces (beginning infiltration). Kane et al. (2020) observed that MP did not deposit above a certain threshold bed shear stress. However, this observation was not made in Warnow sediments where only MP > 500 µm were explored and correlated well with bed load particle transport behaviour.

Only a few particles ($n < 10$) in the size range of those that dominated the shorelines of the Schlei after the pollution event (NABU, 2018), were present in the analysed sediment samples. One reason for this observation could be that our sampling design, using a grab sampler covering only 0.04 cm², may have missed these larger and consequently less abundant size fractions. On the other hand, especially larger low-density sheets (typical shape of food-packaging derived plastic debris) were more likely to stay at the surface for a reasonable time to leave the Schlei towards the Baltic Sea. Intercepted by coastal vegetation and beaching, plenty of these larger snippets were visible around the coastal zone where multiple clean-up events predominantly targeted this fraction, potentially removing them before they would end up in larger amounts on the sediment bed.

Literature data reviewed here (see Fig. 4 Enders et al., *subm.*) indicate that the granulometric normalisation approach is applicable to other sedimentary environments, such as lakes and rivers. Also for Baltic Sea beaches it can be hypothesised that the hydrodynamic effect dominates the MP distribution in contrast to degrading macroplastics or direct local pollution at these sites. This means that degraded macroplastics probably take an indirect route through the sea or air before coming to rest on the beach again, where they are then sorted by means of hydro- and aerodynamics. Such a hypothesis would be supported by recent modelling studies which describe mechanisms of repeated beaching (e.g. Schernewski et al., 2021). The model concept developed for the Schlei can be adapted to other systems, as long as sufficient grain size data are obtainable and the spatio-temporal connectivity assumption holds or can be adequately represented through available variables. It can be used to predict MP abundances in sediments based on grain size distributions, which can be derived from standard sedimentological surveys. This allows for a more efficient and cost-effective monitoring of MP in sediments, as it reduces the need for extensive sampling and analysis of MP particles.

The concept as presented in Enders et al. (2019) has been picked up in a relevant review paper (Harris, 2020) and other MP sediment studies confirming the MP-sediment relationship and recommending further use of such normalisation procedures (e.g. Vermeiren et al., 2021; Croiset et al., 2024; Van Daele et al., 2024), demonstrating that now more studies acknowledge the importance of grain size normalisation and test it for further sedimentary settings. As rivers are often characterised by high topographic variability and large water-level fluctuations (Rolf et al., 2022), the identification of a normalisation line can be challenging. Even at small spatial scales, temporal changes can be substantial, for instance, when floodplains are included in a streambed data set, which are not constantly submerged and therefore not continuously connected to the river flow (Croiset et al., 2024). Assessing spatio-temporal connectivity, even at small spatial scales, is essential for meaningful normalisation. Van Daele et al. (2024) applied granulometric proxy normalisation in a river bed, and successfully distinguished between depositional and erosional areas. The authors proposed that a constant normalisation factor could exist based on the similar factor found between the two studies. However, currently available data are not sufficient to support this. The two studies used different preparation methods and different lower MP size limits which significantly affect the composition of the MP pool, and influence the statistical relationship between the two constituents. This problem had already been addressed in Enders et al. (2019) as well as in (Enders et al., *subm.*) where the authors compared data from available studies, showing largely variable normalisation factors. Although there is an indication from the data in Enders et al. (2019) that MP represent a size scale where polymer-type distribution broadly mirror the global plastic production shares thus representing the universal stock of plastic polymers. Yet, site-specific differences in particle shape, polymer type, and size distribution are inevitable.

The application of the developed concepts in monitoring and environmental management can contribute to the containment of the plastic pollution problem by providing a more accurate assessments and information needed for targeted mitigation measures. However, as long as the current linear economic model of plastic mass production and consumption remains in place, the problem of plastic pollution will persist. With preventive measures in place and better recycling practices, a certain plateau of MP discharge to the environment will not be exceeded due to non-avoidable wear of plastic materials in use. A transition to safe-by-design applications and increasing circular economies that close material cycles are necessary to reduce the overall plastic pollution burden in the environment (UNEP, 2023; Brander et al., 2024).

References

- Abb, M., Heinrich, T., Sorkau, E., & Lorenz, W. (2009). Phthalates in house dust. *Environment International*, 35(6), 965–970. <https://doi.org/10.1016/j.envint.2009.04.007>
- Akram, M. A., Savitha, R., Kinsella, G. K., Nolan, K., Ryan, B. J., & Henehan, G. T. (2024). Microbial and enzymatic biodegradation of plastic waste for a circular economy. *Applied Sciences*, 14(24), 11942. <https://doi.org/10.3390/app142411942>
- Alimi, O. S., Farner Budarz, J., Hernandez, L. M., & Tufenkji, N. (2018). Microplastics and nanoplastics in aquatic environments: Aggregation, deposition, and enhanced contaminant transport. *Environmental Science & Technology*, 52(4), 1704–1724. <https://doi.org/10.1021/acs.est.7b05559>
- Allredge, A. L., & Silver, M. W. (1988). Characteristics, dynamics and significance of marine snow. *Progress in Oceanography*, 20(1), 41–82. [https://doi.org/10.1016/0079-6611\(88\)90053-5](https://doi.org/10.1016/0079-6611(88)90053-5)
- Alomar, C., Estarellas, F., & Deudero, S. (2016). Microplastics in the mediterranean sea: Deposition in coastal shallow sediments, spatial variation and preferential grain size. *Marine Environmental Research*, 115, 1–10. <https://doi.org/10.1016/j.marenvres.2016.01.005>
- Ancey, C. (2020a). Bedload transport: A walk between randomness and determinism. Part 1. The state of the art. *Journal of Hydraulic Research*, 58(1), 1–17. <https://doi.org/10.1080/00221686.2019.1702594>
- Ancey, C. (2020b). Bedload transport: A walk between randomness and determinism. Part 2. Challenges and prospects. *Journal of Hydraulic Research*, 58(1), 18–33. <https://doi.org/10.1080/00221686.2019.1702595>
- Andersen, T. J., Rominikan, S., Olsen, I. S., Skinnebach, K. H., & Fruergaard, M. (2021). Flocculation of PVC microplastic and fine-grained cohesive sediment at environmentally realistic concentrations. *The Biological Bulletin*, 240(1), 42–51. <https://doi.org/10.1086/712929>
- Andler, R., Tiso, T., Blank, L., Andreeßen, C., Zampolli, J., D’Afonseca, V., et al. (2022). Current progress on the biodegradation of synthetic plastics: From fundamentals to biotechnological applications. *Reviews in Environmental Science and Bio/Technology*, 21(4), 829–850. <https://doi.org/10.1007/s11157-022-09631-2>
- Andrady, A. L. (2011). Microplastics in the marine environment. *Marine Pollution Bulletin*, 62(8), 1596–1605. <https://doi.org/10.1016/j.marpolbul.2011.05.030>
- Andrady, A. L., & Neal, M. A. (2009). Applications and societal benefits of plastics. *Philosophical Transactions of the Royal Society B: Biological Sciences*, 364(1526), 1977–1984. <https://doi.org/10.1098/rstb.2008.0304>
- Arnarson, T. S., & Keil, R. G. (2007). Changes in organic matter–mineral interactions for marine sediments with varying oxygen exposure times. *Geochimica Et Cosmochimica Acta*, 71(14), 3545–3556. <https://doi.org/10.1016/j.gca.2007.04.027>
- Aydinalp, C. (Ed.). (2012). *An introduction to the study of mineralogy*. IntechOpen.
- Azeem, I., Shakoor, N., Chaudhary, S., Adeel, M., Zain, M., Ahmad, M. A., et al. (2023). Analytical challenges in detecting microplastics and nanoplastics in soil-plant systems. *Plant Physiology and Biochemistry*, 204, 108132. <https://doi.org/10.1016/j.plaphy.2023.108132>
- Bagaev, A., Mizyuk, A., Khatmullina, L., Isachenko, I., & Chubarenko, I. (2017). Anthropogenic fibres in the baltic sea water column: Field data, laboratory and numerical testing of their motion. *Science of The Total Environment*, 599–600, 560–571. <https://doi.org/10.1016/j.scitotenv.2017.04.185>
- Bailey, L. P., Dorrell, R. M., Kostakis, I., McKee, D., Parsons, D., Rees, J., et al. (2024). Monopile-induced turbulence and sediment redistribution form visible wakes in offshore wind farms. *Frontiers in Earth Science*, 12, 1383726. <https://doi.org/10.3389/feart.2024.1383726>
- Ballent, A., Purser, A., de Jesus Mendes, P., Pando, S., & Thomsen, L. (2012). *Physical transport*

- properties of marine microplastic pollution* (Preprint). Biodiversity and Ecosystem Function: Marine. <https://doi.org/10.5194/bgd-9-18755-2012>
- Ballent, A., Corcoran, P. L., Madden, O., Helm, P. A., & Longstaffe, F. J. (2016). Sources and sinks of microplastics in canadian lake ontario nearshore, tributary and beach sediments. *Marine Pollution Bulletin*, 110(1), 383–395. <https://doi.org/10.1016/j.marpolbul.2016.06.037>
- Barnes, S. J. (2019). Understanding plastics pollution: The role of economic development and technological research. *Environmental Pollution*, 249, 812–821. <https://doi.org/10.1016/j.envpol.2019.03.108>
- Barrett, J., Chase, Z., Zhang, J., Holl, M. M. B., Willis, K., Williams, A., et al. (2020). Microplastic pollution in deep-sea sediments from the great australian bight. *Frontiers in Marine Science*, 7. <https://doi.org/10.3389/fmars.2020.576170>
- Barsanti, M., Garcia-Tenorio, R., Schirone, A., Rozmaric, M., Ruiz-Fernández, A. C., Sanchez-Cabeza, J. A., et al. (2020). Challenges and limitations of the ²¹⁰Pb sediment dating method: Results from an IAEA modelling interlaboratory comparison exercise. *Quaternary Geochronology*, 59, 101093. <https://doi.org/10.1016/j.quageo.2020.101093>
- Bazargan, A., Hui, D., McKay, G., Bazargan, A., Hui, C., & McKay, G. (2013). Porous carbons from plastic waste. In *Advances in polymer science* (Vol. 266, pp. 1–26). Springer. https://doi.org/10.1007/12_2013_253
- Beer, S., Garm, A., Huwer, B., Dierking, J., & Nielsen, T. G. (2018). No increase in marine microplastic concentration over the last three decades – a case study from the baltic sea. *Science of The Total Environment*, 621, 1272–1279. <https://doi.org/10.1016/j.scitotenv.2017.10.101>
- Bełdowski, J., Klusek, Z., Szubska, M., Turja, R., Bulczak, A. I., Rak, D., et al. (2016). Chemical munitions search & assessment—an evaluation of the dumped munitions problem in the baltic sea. *Deep Sea Research Part II: Topical Studies in Oceanography*, 128, 85–95. <https://doi.org/10.1016/j.dsr2.2015.01.017>
- Belz, S., Bianchi, I., Cella, C., Emteborg, H., Fumagalli, F. S., Geiss, O., et al. (2021). *Current status of the quantification of microplastics in water: Results of a JRC/BAM interlaboratory comparison study on PET in water*. LU: Publications Office. Retrieved from <https://data.europa.eu/doi/10.2760/27641>
- Bergen, K. J., Johnson, P. A., De Hoop, M. V., & Beroza, G. C. (2019). Machine learning for data-driven discovery in solid earth geoscience. *Science*, 363(6433), eaau0323. <https://doi.org/10.1126/science.aau0323>
- Bertling, J., Dau, K., Selig, U., & Werner, S. (2021). *Release of microplastics in the marine environment – state of knowledge and options for action*. Fraunhofer-Gesellschaft. <https://doi.org/10.24406/UMSICHT-N-648144>
- Bianchi, T. S. (2007). *Biochemistry of estuaries*. Oxford University Press.
- Biltcliff-Ward, A., Stead, J. L., & Hudson, M. D. (2022). The estuarine plastics budget: A conceptual model and meta-analysis of microplastic abundance in estuarine systems. *Estuarine, Coastal and Shelf Science*, 275, 107963. <https://doi.org/10.1016/j.ecss.2022.107963>
- Bizmark, N., Schneider, J., Priestley, R. D., & Datta, S. S. (2020). Multiscale dynamics of colloidal deposition and erosion in porous media. *Science Advances*, 6(46), eabc2530. <https://doi.org/10.1126/sciadv.abc2530>
- Blašković, A., Fastelli, P., Čizmek, H., Guerranti, C., & Renzi, M. (2017). Plastic litter in sediments from the croatian marine protected area of the natural park of telaščica bay (adriatic sea). *Marine Pollution Bulletin*, 114(1), 583–586. <https://doi.org/10.1016/j.marpolbul.2016.09.018>
- Blenckner, T., Ammar, Y., Müller-Karulis, B., Niiranen, S., Arneborg, L., & Li, Q. (2021). The risk for novel and disappearing environmental conditions in the baltic sea. *Frontiers in Marine Science*, 8, 745722. <https://doi.org/10.3389/fmars.2021.745722>
- Blott, S. J., & Pye, K. (2001). GRADISTAT: A grain size distribution and statistics package for the analysis of unconsolidated sediments. *Earth Surface Processes and Landforms*, 26(11), 1237–1248. <https://doi.org/10.1002/esp.261>
- Blott, S. J., & Pye, K. (2008). Particle shape: A review and new methods of characterization and classification. *Sedimentology*, 55(1), 31–63. <https://doi.org/10.1111/j.1365-3091.2007.00892.x>
- Boggs, S. (2006). *Principles of sedimentology and stratigraphy* (4th ed). Upper Saddle River (N.J.): Pearson prentice hall.
- Boos, J.-P., Dichgans, F., Fleckenstein, J. H., Gilfedder, B. S., & Frei, S. (2024). Assessing the behavior of

- microplastics in fluvial systems: Infiltration and retention dynamics in streambed sediments. *Water Resources Research*, 60(2), e2023WR035532. <https://doi.org/10.1029/2023WR035532>
- Borrelle, S. B., Ringma, J., Law, K. L., Monnahan, C. C., Lebreton, L., McGivern, A., et al. (2020). Predicted growth in plastic waste exceeds efforts to mitigate plastic pollution. *Science*, 369(6510), 1515–1518. <https://doi.org/10.1126/science.aba3656>
- Bour, A., Haarr, A., Keiter, S., & Hylland, K. (2018). Environmentally relevant microplastic exposure affects sediment-dwelling bivalves. *Environmental Pollution*, 236, 652–660. <https://doi.org/10.1016/j.envpol.2018.02.006>
- Bouzid, N., Tassin, B., Gasperi, J., & Dris, R. (2025). Sequential combination of micro-FTIR imaging spectroscopy and pyrolysis-GC/MS for microplastic quantification. Application to river sediments. *Analytical Methods*, 17(18), 3781–3792. <https://doi.org/10.1039/D5AY00237K>
- Bowring, S. P. K., Jones, M. W., Ciais, P., Guenet, B., & Abiven, S. (2022). Pyrogenic carbon decomposition critical to resolving fire's role in the earth system. *Nature Geoscience*, 15(2), 135–142. <https://doi.org/10.1038/s41561-021-00892-0>
- Brander, S. M., Senathirajah, K., Fernandez, M. O., Weis, J. S., Kumar, E., Jahnke, A., et al. (2024). The time for ambitious action is now: Science-based recommendations for plastic chemicals to inform an effective global plastic treaty. *Science of The Total Environment*, 949, 174881. <https://doi.org/10.1016/j.scitotenv.2024.174881>
- Brandon, J. A., Jones, W., & Ohman, M. D. (2019). Multidecadal increase in plastic particles in coastal ocean sediments. *Science Advances*, 5(9), eaax0587. <https://doi.org/10.1126/sciadv.aax0587>
- Brandt, J., Bittrich, L., Fischer, F., Kanaki, E., Tagg, A., Lenz, R., et al. (2020). High-throughput analyses of microplastic samples using fourier transform infrared and raman spectrometry. *Applied Spectroscopy*, 74(9), 1185–1197. <https://doi.org/10.1177/0003702820932926>
- Brandt, J., Fischer, F., Kanaki, E., Enders, K., Labrenz, M., & Fischer, D. (2021a). Assessment of subsampling strategies in microspectroscopy of environmental microplastic samples. *Frontiers in Environmental Science*, 8, 579676. <https://doi.org/10.3389/fenvs.2020.579676>
- Brandt, J., Mattsson, K., & Hassellöv, M. (2021b). Deep learning for reconstructing low-quality FTIR and raman spectra—a case study in microplastic analyses. *Analytical Chemistry*, 93(49), 16360–16368. <https://doi.org/10.1021/acs.analchem.1c02618>
- Browne, M. A., Crump, P., Niven, S. J., Teuten, E., Tonkin, A., Galloway, T., & Thompson, R. (2011). Accumulation of microplastic on shorelines worldwide: Sources and sinks. *Environmental Science & Technology*, 45(21), 9175–9179. <https://doi.org/10.1021/es201811s>
- Brümmer, F., Schnepf, U., Resch, J., Jemmali, R., Abdi, R., Kamel, H. M., et al. (2022). In situ laboratory for plastic degradation in the red sea. *Scientific Reports*, 12(1), 11956. <https://doi.org/10.1038/s41598-022-15310-7>
- Bruns, I., Bartholomä, A., Menjua, F., & Kopf, A. (2023). Physical impact of bottom trawling on seafloor sediments in the german north sea. *Frontiers in Earth Science*, 11, 1233163. <https://doi.org/10.3389/feart.2023.1233163>
- Buchanan, J. B. (1971). Pollution by synthetic fibres. *Marine Pollution Bulletin*, 2(2), 23. [https://doi.org/10.1016/0025-326X\(71\)90136-6](https://doi.org/10.1016/0025-326X(71)90136-6)
- Burchard, H., Schuttelaars, H. M., & Ralston, D. K. (2018). Sediment trapping in estuaries. *Annual Review of Marine Science*, 10(1), 371–395. <https://doi.org/10.1146/annurev-marine-010816-060535>
- Cameron, W. M., & Pritchard, D. (1963). Estuaries. In M. N. Hill (Ed.), *The sea* (pp. 306–324). New York: John Wiley and Sons.
- Canals, M., Pham, C. K., Bergmann, M., Gutow, L., Hanke, G., van Sebille, E., et al. (2021). The quest for seafloor macrolitter: A critical review of background knowledge, current methods and future prospects. *Environmental Research Letters*. <https://doi.org/10.1088/1748-9326/abc6d4>
- Carney Almroth, B., Cornell, S. E., Diamond, M. L., De Wit, C. A., Fantke, P., & Wang, Z. (2022). Understanding and addressing the planetary crisis of chemicals and plastics. *One Earth*, 5(10), 1070–1074. <https://doi.org/10.1016/j.oneear.2022.09.012>
- Carpenter, E. J. (2022). A very short informal history of marine plastic pollution. *Limnology and Oceanography Bulletin*, 31(4), 107–109. <https://doi.org/10.1002/lob.10518>
- Carpenter, E. J., & Smith, K. L. (1972). Plastics on the sargasso sea surface. *Science*, 175(4027), 1240–1241. <https://doi.org/10.1126/science.175.4027.1240>

- Carraher Jr., C. E. (2017). *Introduction to polymer chemistry* (4th ed.). CRC Press. <https://doi.org/10.1201/9781315369488>
- Casado, M. P., Macken, A., & Byrne, H. J. (2013). Ecotoxicological assessment of silica and polystyrene nanoparticles assessed by a multitrophic test battery. *Environment International*, 51, 97–105. <https://doi.org/10.1016/j.envint.2012.11.001>
- Cawley, G. C., & Talbot, N. L. C. (2010). On over-fitting in model selection and subsequent selection bias in performance evaluation. *Journal of Machine Learning Research*, 11(70), 2079–2107. <https://doi.org/10.5555/1756006.1859921>
- Čerkasova, N., Enders, K., Lenz, R., Oberbeckmann, S., Brandt, J., Fischer, D., et al. (2023). A public database for microplastics in the environment. *Microplastics*, 2(1), 132–146. <https://doi.org/10.3390/microplastics2010010>
- Chamas, A., Moon, H., Zheng, J., Qiu, Y., Tabassum, T., Jang, J. H., et al. (2020). Degradation rates of plastics in the environment. *ACS Sustainable Chemistry & Engineering*, 8(9), 3494–3511. <https://doi.org/10.1021/acssuschemeng.9b06635>
- Chartres, N., Cooper, C. B., Bland, G., Pelch, K. E., Gandhi, S. A., BakenRa, A., & Woodruff, T. J. (2024). Effects of microplastic exposure on human digestive, reproductive, and respiratory health: A rapid systematic review. *Environmental Science & Technology*, acs.est.3c09524. <https://doi.org/10.1021/acs.est.3c09524>
- Chen, B., Zhang, Z., Wang, T., Hu, H., Qin, G., Lu, T., et al. (2023). Global distribution of marine microplastics and potential for biodegradation. *Journal of Hazardous Materials*, 451, 131198. <https://doi.org/10.1016/j.jhazmat.2023.131198>
- Chen, H., Zou, X., Ding, Y., Wang, Y., Fu, G., & Yuan, F. (2022). Are microplastics the “technofossils” of the anthropocene? *Anthropocene Coasts*, 5(1), 8. <https://doi.org/10.1007/s44218-022-00007-1>
- Chiaia-Hernández, A. C., Casado-Martinez, C., Lara-Martin, P., & Bucheli, T. D. (2022). Sediments: Sink, archive, and source of contaminants. *Environmental Science and Pollution Research*, 29(57), 85761–85765. <https://doi.org/10.1007/s11356-022-24041-1>
- Chubarenko, I., & Stepanova, N. (2017). Microplastics in sea coastal zone: Lessons learned from the baltic amber. *Environmental Pollution*, 224, 243–254. <https://doi.org/10.1016/j.envpol.2017.01.085>
- Chubarenko, I., Bagaev, A., Zobkov, M., & Esiukova, E. (2016). On some physical and dynamical properties of microplastic particles in marine environment. *Marine Pollution Bulletin*, 108(1–2), 105–112. <https://doi.org/10.1016/j.marpolbul.2016.04.048>
- Chubarenko, I., Esiukova, E., Bagaev, A., Isachenko, I., Zobkov, M., Bagaeva, M., et al. (2024). Microplastics particles in coastal zone: Approach of physical oceanography. In *Microplastic contamination in aquatic environments* (pp. 249–310). Elsevier. <https://doi.org/10.1016/B978-0-443-15332-7.00005-3>
- Ciornii, D., Hodoroba, V.-D., Benismail, N., Maltseva, A., Ferrer, J. F., Wang, J., et al. (2025). Interlaboratory comparison reveals state of the art in microplastic detection and quantification methods. *Analytical Chemistry*, 97(16), 8719–8728. <https://doi.org/10.1021/acs.analchem.4c05403>
- Colton, J. B., Burns, B. R., & Knapp, F. D. (1974). Plastic particles in surface waters of the northwestern atlantic: The abundance, distribution, source, and significance of various types of plastics are discussed. *Science*, 185(4150), 491–497. <https://doi.org/10.1126/science.185.4150.491>
- Cowger, W., Markley, L. A. T., Moore, S., Gray, A. B., Upadhyay, K., & Koelmans, A. A. (2024). How many microplastics do you need to (sub)sample? *Ecotoxicology and Environmental Safety*, 275, 116243. <https://doi.org/10.1016/j.ecoenv.2024.116243>
- Cozzoli, F., Gjoni, V., Del Pasqua, M., Hu, Z., Ysebaert, T., Herman, P. M. J., & Bouma, T. J. (2019). A process based model of cohesive sediment resuspension under bioturbators’ influence. *Science of The Total Environment*, 670, 18–30. <https://doi.org/10.1016/j.scitotenv.2019.03.085>
- Croiset, C., Dhivert, E., Phuong, N.-N., Grosbois, C., Zalouk-Vergnoux, A., Baltzer, A., & Gasperi, J. (2024). Exploring possible controlling factors of spatial distribution of microplastics in sediments of a river segment (loire river, france). *Science of The Total Environment*, 956, 177328. <https://doi.org/10.1016/j.scitotenv.2024.177328>
- Crutzen, P. J. (2002). Geology of mankind. *Nature*, (415), 23. <https://doi.org/10.1038/415023a>
- Dawson, A. L., Kawaguchi, S., King, C. K., Townsend, K. A., King, R., Huston, W. M., & Bengtson Nash, S. M. (2018). Turning microplastics into nanoplastics through digestive fragmentation by antarctic krill. *Nature Communications*, 9(1), 1001. <https://doi.org/10.1038/s41467-018-03465-9>

- De Borger, E., Tiano, J., Braeckman, U., Rijnsdorp, A. D., & Soetaert, K. (2021). Impact of bottom trawling on sediment biogeochemistry: A modelling approach. *Biogeosciences*, 18(8), 2539–2557. <https://doi.org/10.5194/bg-18-2539-2021>
- Dietz, T., & Rosa, E. A. (1997). Effects of population and affluence on CO₂ emissions. *Proceedings of the National Academy of Sciences*, 94(1), 175–179. <https://doi.org/10.1073/pnas.94.1.175>
- Dimante-Deimantovica, I., Saarni, S., Barone, M., Buhhalko, N., Stivrins, N., Suhareva, N., et al. (2024). Downward migrating microplastics in lake sediments are a tricky indicator for the onset of the anthropocene. *Science Advances*, 10(8), eadi8136. <https://doi.org/10.1126/sciadv.adi8136>
- Dioguardi, F., Mele, D., & Dellino, P. (2018). A new one-equation model of fluid drag for irregularly shaped particles valid over a wide range of reynolds number. *Journal of Geophysical Research: Solid Earth*, 123(1), 144–156. <https://doi.org/10.1002/2017JB014926>
- Dong, M., Luo, Z., Jiang, Q., Xing, X., Zhang, Q., & Sun, Y. (2020). The rapid increases in microplastics in urban lake sediments. *Scientific Reports*, 10(1), 848. <https://doi.org/10.1038/s41598-020-57933-8>
- Döös, K., Meier, H. E. M., & Döscher, R. (2004). The baltic haline conveyor belt or the overturning circulation and mixing in the baltic. *AMBIO: A Journal of the Human Environment*, 33(4), 261–266. <https://doi.org/10.1579/0044-7447-33.4.261>
- Dris, R., Gasperi, J., Saad, M., Mirande, C., & Tassin, B. (2016). Synthetic fibers in atmospheric fallout: A source of microplastics in the environment? *Marine Pollution Bulletin*, 104(1–2), 290–293. <https://doi.org/10.1016/j.marpolbul.2016.01.006>
- Droppo, I. G. (2001). Rethinking what constitutes suspended sediment. *Hydrological Processes*, 15(9), 1551–1564. <https://doi.org/10.1002/hyp.228>
- Duis, K., & Coors, A. (2016). Microplastics in the aquatic and terrestrial environment: Sources (with a specific focus on personal care products), fate and effects. *Environmental Sciences Europe*, 28(1), 2. <https://doi.org/10.1186/s12302-015-0069-y>
- Dutkiewicz, A., Müller, R. D., O’Callaghan, S., & Jónasson, H. (2015). Census of seafloor sediments in the world’s ocean. *Geology*, 43(9), 795–798. <https://doi.org/10.1130/G36883.1>
- Einsele, G. (Ed.). (2000). Oceanic sediments. In *Sedimentary basins*. Berlin, Heidelberg: Springer Berlin Heidelberg. https://doi.org/10.1007/978-3-662-04029-4_5
- Einstein, H. A. (1968). Deposition of suspended particles in a gravel bed. *Journal of the Hydraulics Division*, 94(5), 1197–1206. <https://doi.org/10.1061/JYCEAJ.0001868>
- Eisma, D. (1986). Flocculation and de-flocculation of suspended matter in estuaries. *Netherlands Journal of Sea Research*, 20(2–3), 183–199. [https://doi.org/10.1016/0077-7579\(86\)90041-4](https://doi.org/10.1016/0077-7579(86)90041-4)
- Enders, K. (2025). *Analogies between microplastics and natural particles for inventory mapping in aquatic sediments* (PhD thesis). Universität Rostock. Retrieved from <https://doi.org/10.5281/zenodo.16790144>
- Enders, K., Lenz, R., Stedmon, C. A., & Nielsen, T. G. (2015). Abundance, size and polymer composition of marine microplastics > 10 µm in the atlantic ocean and their modelled vertical distribution. *Marine Pollution Bulletin*, 100(1), 70–81. <https://doi.org/10.1016/j.marpolbul.2015.09.027>
- Enders, K., Lenz, R., Beer, S., & Stedmon, C. A. (2016). Extraction of microplastic from biota: Recommended acidic digestion destroys common plastic polymers. *ICES Journal of Marine Science*, 74(1), 326–331. <https://doi.org/10.1093/icesjms/fsw173>
- Enders, K., K  ppler, A., Bini  sch, O., Feldens, P., Stollberg, N., Lange, X., et al. (2019). Tracing microplastics in aquatic environments based on sediment analogies. *Scientific Reports*, 9(1), 15207. <https://doi.org/10.1038/s41598-019-50508-2>
- Enders, K., Tagg, A. S., & Labrenz, M. (2020a). Evaluation of electrostatic separation of microplastics from mineral-rich environmental samples. *Frontiers in Environmental Science*, 8, 112. <https://doi.org/10.3389/fenvs.2020.00112>
- Enders, K., Lenz, R., Ivar do Sul, J. A., Tagg, A. S., & Labrenz, M. (2020b). When every particle matters: A QuEChERS approach to extract microplastics from environmental samples. *MethodsX*, 7, 100784. <https://doi.org/10.1016/j.mex.2020.100784>
- Enders, K., Lenz, R., Fischer, F., Schwarzer, K., Se   , G., Fischer, D., & Labrenz, M. (subm.subm.). *Mapping the plastic legacy with NIXVEGS: Machine-learning enabled microplastics prediction in sediments*.
- Eriksen, M., Mason, S., Wilson, S., Box, C., Zellers, A., Edwards, W., et al. (2013). Microplastic pollution

- in the surface waters of the laurentian great lakes. *Marine Pollution Bulletin*, 77(1–2), 177–182. <https://doi.org/10.1016/j.marpolbul.2013.10.007>
- Escobar-Sánchez, G., De Ramos, B., Lange, X., Piehl, S., Haseler, M., & Schernewski, G. (2025, March 15). Plastics in estuaries: Estimating an emission budget, transport and fate of plastics through high resolution model simulations. <https://doi.org/10.5194/egusphere-egu25-18892>
- Esiukova, E., Zobkov, M., & Chubarenko, I. (2020). Data on microplastic contamination of the baltic sea bottom sediment samples in 2015–2016. *Data in Brief*, 28, 104887. <https://doi.org/10.1016/j.dib.2019.104887>
- European Parliament and of the Council. Commission regulation (EU) 2023/2055 of 25 september 2023 amending annex XVII to regulation (EC) no 1907/2006 of the european parliament and of the council concerning the registration, evaluation, authorisation and restriction of chemicals (REACH) as regards synthetic polymer microparticles (2023). Retrieved from <https://eur-lex.europa.eu/eli/reg/2023/2055/oj>
- Fastelli, P., Blašković, A., Bernardi, G., Romeo, T., Čížmek, H., Andaloro, F., et al. (2016). Plastic litter in sediments from a marine area likely to become protected (aeolian archipelago's islands, tyrrhenian sea). *Marine Pollution Bulletin*, 113(1–2), 526–529. <https://doi.org/10.1016/j.marpolbul.2016.08.054>
- Felsing, S., Kochleus, C., Buchinger, S., Brennholt, N., Stock, F., & Reifferscheid, G. (2018). A new approach in separating microplastics from environmental samples based on their electrostatic behavior. *Environmental Pollution*, 234, 20–28. <https://doi.org/10.1016/j.envpol.2017.11.013>
- Ferdowski, B., Ortiz, C. P., Houssais, M., & Jerolmack, D. J. (2017). River-bed armouring as a granular segregation phenomenon. *Nature Communications*, 8(1), 1363. <https://doi.org/10.1038/s41467-017-01681-3>
- Ferguson, R. I., & Church, M. (2004). A simple universal equation for grain settling velocity. *Journal of Sedimentary Research*, 74(6), 933–937. <https://doi.org/10.1306/051204740933>
- Fersch, B., Senatore, A., Adler, B., Arnault, J., Mauder, M., Schneider, K., et al. (2020). High-resolution fully coupled atmospheric–hydrological modeling: A cross-compartment regional water and energy cycle evaluation. *Hydrology and Earth System Sciences*, 24(5), 2457–2481. <https://doi.org/10.5194/hess-24-2457-2020>
- Fischer, H. B. (1976). Mixing and dispersion in estuaries. *Annual Review of Fluid Mechanics*, 8(1), 107–133. <https://doi.org/10.1146/annurev.fl.08.010176.000543>
- Fischer, M., & Scholz-Böttcher, B. M. (2019). Microplastics analysis in environmental samples – recent pyrolysis-gas chromatography-mass spectrometry method improvements to increase the reliability of mass-related data. *Analytical Methods*, 11(18), 2489–2497. <https://doi.org/10.1039/C9AY00600A>
- Flemming, B. W. (2007). The influence of grain-size analysis methods and sediment mixing on curve shapes and textural parameters: Implications for sediment trend analysis. *Sedimentary Geology*, 202(3), 425–435. <https://doi.org/10.1016/j.sedgeo.2007.03.018>
- Folk, R. L., & Ward, W. C. (1957). Brazos river bar [texas]; a study in the significance of grain size parameters. *Journal of Sedimentary Research*, 27(1), 3–26. <https://doi.org/10.1306/74D70646-2B21-11D7-8648000102C1865D>
- Fowler, C. W. (1987). Marine debris and northern fur seals: A case study. *Marine Pollution Bulletin*, 18(6), 326–335. [https://doi.org/10.1016/S0025-326X\(87\)80020-6](https://doi.org/10.1016/S0025-326X(87)80020-6)
- Freinkel, S. (2011). *Plastic: A toxic love story*. Boston: Houghton Mifflin Harcourt.
- Fries, E., & Zarfl, C. (2012). Sorption of polycyclic aromatic hydrocarbons (PAHs) to low and high density polyethylene (PE). *Environmental Science and Pollution Research*, 19(4), 1296–1304. <https://doi.org/10.1007/s11356-011-0655-5>
- Galgani, L., Goßmann, I., Scholz-Böttcher, B., Jiang, X., Liu, Z., Scheidemann, L., et al. (2022). Hitchhiking into the deep: How microplastic particles are exported through the biological carbon pump in the north atlantic ocean. *Environmental Science & Technology*, 56(22), 15638–15649. <https://doi.org/10.1021/acs.est.2c04712>
- Galloway, T. S., Cole, M., & Lewis, C. (2017). Interactions of microplastic debris throughout the marine ecosystem. *Nature Ecology & Evolution*, 1(5), 0116. <https://doi.org/10.1038/s41559-017-0116>
- Gazis, I.-Z., De Stigter, H., Mohrmann, J., Heger, K., Diaz, M., Gillard, B., et al. (2025). Monitoring benthic plumes, sediment redeposition and seafloor imprints caused by deep-sea polymetallic nodule mining. *Nature Communications*, 16(1), 1229. <https://doi.org/10.1038/s41467-025-56311-0>
- Gebhardt, C., & Forster, S. (2018). Size-selective feeding of arenicola marina promotes long-term burial

- of microplastic particles in marine sediments. *Environmental Pollution*, 242, 1777–1786. <https://doi.org/10.1016/j.envpol.2018.07.090>
- Gewert, B., Plassmann, M. M., & MacLeod, M. (2015). Pathways for degradation of plastic polymers floating in the marine environment. *Environmental Science: Processes & Impacts*, 17(9), 1513–1521. <https://doi.org/10.1039/C5EM00207A>
- Geyer, R. (2020). Production, use, and fate of synthetic polymers. In *Plastic waste and recycling* (pp. 13–32). Elsevier. <https://doi.org/10.1016/B978-0-12-817880-5.00002-5>
- Geyer, R., Jambeck, J. R., & Law, K. L. (2017). Production, use, and fate of all plastics ever made. *Science Advances*, 3(7), e1700782. <https://doi.org/10.1126/sciadv.1700782>
- Gillibert, R., Balakrishnan, G., Deshoules, Q., Tardivel, M., Magazzù, A., Donato, M. G., et al. (2019). Raman tweezers for small microplastics and nanoplastics identification in seawater. *Environmental Science & Technology*, 53(15), 9003–9013. <https://doi.org/10.1021/acs.est.9b03105>
- Goldstein, M. C., Rosenberg, M., & Cheng, L. (2012). Increased oceanic microplastic debris enhances oviposition in an endemic pelagic insect. *Biology Letters*, 8(5), 817–820. <https://doi.org/10.1098/rsbl.2012.0298>
- Gorokhova, E., Ek, K., & Reichelt, S. (2020). Algal growth at environmentally relevant concentrations of suspended solids: Implications for microplastic hazard assessment. *Frontiers in Environmental Science*, 8, 551075. <https://doi.org/10.3389/fenvs.2020.551075>
- Gouin, T., Roche, N., Lohmann, R., & Hodges, G. (2011). A thermodynamic approach for assessing the environmental exposure of chemicals absorbed to microplastic. *Environmental Science & Technology*, 45(4), 1466–1472. <https://doi.org/10.1021/es1032025>
- Grabowski, R. C., Droppo, I. G., & Wharton, G. (2011). Erodibility of cohesive sediment: The importance of sediment properties. *Earth-Science Reviews*, 105(3–4), 101–120. <https://doi.org/10.1016/j.earscirev.2011.01.008>
- Gram, A., Silfwerbrand, J., & Lagerblad, B. (2016). Particle motion in fluid - analytical and numerical study. *Applied Rheology*. <https://doi.org/10.3933/APPLRHEOL-26-23326>
- Green, M. O., & Coco, G. (2014). Review of wave-driven sediment resuspension and transport in estuaries: WAVE-DRIVEN SEDIMENT TRANSPORT. *Reviews of Geophysics*, 52(1), 77–117. <https://doi.org/10.1002/2013RG000437>
- Groh, K. J., Backhaus, T., Carney-Almroth, B., Geueke, B., Inostroza, P. A., Lennquist, A., et al. (2019). Overview of known plastic packaging-associated chemicals and their hazards. *Science of The Total Environment*, 651, 3253–3268. <https://doi.org/10.1016/j.scitotenv.2018.10.015>
- Grossman, G., & Krueger, A. (1991). *Environmental impacts of a north american free trade agreement* (No. w3914). Cambridge, MA: National Bureau of Economic Research. <https://doi.org/10.3386/w3914>
- Guggenberger, G. (2005). Humification and mineralization in soils. In A. Varma & F. Buscot (Eds.), *Microorganisms in soils: Roles in genesis and functions* (Vol. 3, pp. 85–106). Berlin/Heidelberg: Springer-Verlag. https://doi.org/10.1007/3-540-26609-7_4
- Hahn, S., & Hennecke, D. (2023). What can we learn from biodegradation of natural polymers for regulation? *Environmental Sciences Europe*, 35(1), 50. <https://doi.org/10.1186/s12302-023-00755-y>
- Hamm, C. E., Merkel, R., Springer, O., Jurkojc, P., Maier, C., Prechtel, K., & Smetacek, V. (2003). Architecture and material properties of diatom shells provide effective mechanical protection. *Nature*, 421(6925), 841–843. <https://doi.org/10.1038/nature01416>
- Hanke, G., Galgani, F., Werner, S., Oosterbaan, L., Nilsson, P., Fleet, D., et al. (2013). *Guidance on monitoring of marine litter in european seas* (No. EUR 26113) (pp. 1–6). Luxembourg: Publications Office of the European Union. <https://doi.org/10.2788/99475>
- Harper, P. C., & Fowler, J. A. (1987). PLASTIC PELLETS IN NEW ZEALAND STORM-KILLED PRIONS (pachyptila spp.) 1958-1977. *NOTORNIS*, (34), 65–70.
- Harris, P. T. (2020). The fate of microplastic in marine sedimentary environments: A review and synthesis. *Marine Pollution Bulletin*, 158, 111398. <https://doi.org/10.1016/j.marpolbul.2020.111398>
- Hartmann, N. B., Hüffer, T., Thompson, R. C., Hassellöv, M., Verschoor, A., Dagaard, A. E., et al. (2019). Are we speaking the same language? Recommendations for a definition and categorization framework for plastic debris. *Environmental Science & Technology*, 53(3), 1039–1047. <https://doi.org/10.1021/acs.est.8b05297>

- He, Z., Li, G., Chen, J., Huang, Y., An, T., & Zhang, C. (2015). Pollution characteristics and health risk assessment of volatile organic compounds emitted from different plastic solid waste recycling workshops. *Environment International*, 77, 85–94. <https://doi.org/10.1016/j.envint.2015.01.004>
- Heiri, O., Lotter, A. F., & Lemcke, G. (2001). Loss on ignition as a method for estimating organic and carbonate content in sediments: Reproducibility and comparability of results. *Journal of Paleolimnology*, 25(1), 101–110. <https://doi.org/10.1023/a:1008119611481>
- HELCOM. (2015). *Regional action plan for marine litter in the baltic sea*. (p. 22). Helsinki Commission, Baltic Marine Environment Protection Commission. Retrieved from <https://www.helcom.fi/wp-content/uploads/2019/08/Regional-Action-Plan-for-Marine-Litter.pdf>
- Hidalgo-Ruz, V., Gutow, L., Thompson, R. C., & Thiel, M. (2012). Microplastics in the marine environment: A review of the methods used for identification and quantification. *Environmental Science & Technology*, 46(6), 3060–3075. <https://doi.org/10.1021/es2031505>
- Holden, J. (2017). *An introduction to physical geography and the environment*. Harlow: Pearson Education.
- Huggett, R. J. (2011). *Fundamentals of geomorphology* (3. ed). London: Routledge.
- Hurley, R., Woodward, J., & Rothwell, J. J. (2018). Microplastic contamination of river beds significantly reduced by catchment-wide flooding. *Nature Geoscience*, 11(4), 251–257. <https://doi.org/10.1038/s41561-018-0080-1>
- Hutter, H.-P., Kundi, M., Hohenblum, P., Scharf, S., Shelton, J. F., Piegler, K., & Wallner, P. (2016). Life without plastic: A family experiment and biomonitoring study. *Environmental Research*, 150, 639–644. <https://doi.org/10.1016/j.envres.2016.05.028>
- Ibrahim, S. S., Ionescu, D., & Grossart, H.-P. (2024). Tapping into fungal potential: Biodegradation of plastic and rubber by potent fungi. *Science of The Total Environment*, 934, 173188. <https://doi.org/10.1016/j.scitotenv.2024.173188>
- ICES. (2015). *ICES special request advice northeast atlantic and arctic ocean. OSPAR request on development of a common monitoring protocol for plastic particles in fish stomachs and selected shellfish on the basis of existing fish disease surveys* (pp. 1–6). LU: Publications Office. Retrieved from <https://data.europa.eu/doi/10.2788/99475>
- Imhof, H. K., Ivleva, N. P., Schmid, J., Niessner, R., & Laforsch, C. (2013). Contamination of beach sediments of a subalpine lake with microplastic particles. *Current Biology*, 23(19), R867–R868. <https://doi.org/10.1016/j.cub.2013.09.001>
- IMO. (1988). Protocol of 1978 relating to the international convention for the prevention of pollution from ships, 1973 with annex v prevention of pollution by garbage from ships. International Maritime Organization (IMO).
- Ismayilova, I., Zeyer, T., & Timpf, S. (2021). Identification of microplastics in soils using 2D geometric shape descriptors. *AGILE: GIScience Series*, 2, 1–6. <https://doi.org/10.5194/agile-giss-2-32-2021>
- ISO. Particle size analysis — laser diffraction methods (Version 2), Pub. L. No. ISO 13320:2020 (2020). Geneva: ISO.
- Ivar Do Sul, J. A., Spengler, Â., & Costa, M. F. (2009). Here, there and everywhere. Small plastic fragments and pellets on beaches of fernando de noronha (equatorial western atlantic). *Marine Pollution Bulletin*, 58(8), 1236–1238. <https://doi.org/10.1016/j.marpolbul.2009.05.004>
- Ivleva, N. P. (2021). Chemical analysis of microplastics and nanoplastics: Challenges, advanced methods, and perspectives. *Chemical Reviews*, 121(19), 11886–11936. <https://doi.org/10.1021/acs.chemrev.1c00178>
- Jaiswal, A., Bui, M. D., & Rutschmann, P. (2024). On the process of fine sediment infiltration into static gravel bed: A CFD–DEM modelling perspective. *River Research and Applications*, 40(1), 29–48. <https://doi.org/10.1002/rra.4215>
- Janßen, R., Beck, A. J., Werner, J., Dellwig, O., Alneberg, J., Kreikemeyer, B., et al. (2021). Machine learning predicts the presence of 2,4,6-trinitrotoluene in sediments of a baltic sea munitions dumpsite using microbial community compositions. *Frontiers in Microbiology*, 12, 626048. <https://doi.org/10.3389/fmicb.2021.626048>
- Janusz, G., Pawlik, A., Sulej, J., Świdarska-Burek, U., Jarosz-Wilkolazka, A., & Paszczyński, A. (2017). Lignin degradation: Microorganisms, enzymes involved, genomes analysis and evolution. *FEMS Microbiology Reviews*, 41(6), 941–962. <https://doi.org/10.1093/femsre/fux049>
- Jay, D. A., Orton, P. M., Chisholm, T., Wilson, D. J., & Fain, A. M. V. (2007). Particle trapping in stratified estuaries: Application to observations. *Estuaries and Coasts*, 30(6), 1106–1125. <https://doi.org/10.1007/s12237-007-9048-1>

- Jones, R., Wakeford, M., Currey-Randall, L., Miller, K., & Tonin, H. (2021). Drill cuttings and drilling fluids (muds) transport, fate and effects near a coral reef mesophotic zone. *Marine Pollution Bulletin*, 172, 112717. <https://doi.org/10.1016/j.marpolbul.2021.112717>
- Kaiser, D., Kowalski, N., & Waniek, J. J. (2017). Effects of biofouling on the sinking behavior of microplastics. *Environmental Research Letters*, 12(12), 124003. <https://doi.org/10.1088/1748-9326/aa8e8b>
- Kaiser, D., Estelmann, A., Kowalski, N., Glockzin, M., & Waniek, J. J. (2019). Sinking velocity of sub-millimeter microplastic. *Marine Pollution Bulletin*, 139, 214–220. <https://doi.org/10.1016/j.marpolbul.2018.12.035>
- Kaiser, J., Abel, S., Arz, H. W., Cundy, A. B., Dellwig, O., Gaca, P., et al. (2023). The east gotland basin (baltic sea) as a candidate global boundary stratotype section and point for the anthropocene series. *The Anthropocene Review*, 10(1), 25–48. <https://doi.org/10.1177/20530196221132709>
- Kane, I. A., Clare, M. A., Miramontes, E., Wogelius, R., Rothwell, J. J., Garreau, P., & Pohl, F. (2020). Seafloor microplastic hotspots controlled by deep-sea circulation. *Science*, 368(6495), 1140–1145. <https://doi.org/10.1126/science.aba5899>
- Kanwischer, M., Asker, N., Wernersson, A.-S., Wirth, M. A., Fisch, K., Dahlgren, E., et al. (2022). Substances of emerging concern in baltic sea water: Review on methodological advances for the environmental assessment and proposal for future monitoring. *Ambio*, 51(6), 1588–1608. <https://doi.org/10.1007/s13280-021-01627-6>
- Käppler, A., Windrich, F., Löder, M. G. J., Malanin, M., Fischer, D., Labrenz, M., et al. (2015). Identification of microplastics by FTIR and raman microscopy: A novel silicon filter substrate opens the important spectral range below 1300 cm⁻¹ for FTIR transmission measurements. *Analytical and Bioanalytical Chemistry*, 407(22), 6791–6801. <https://doi.org/10.1007/s00216-015-8850-8>
- Käppler, A., Fischer, D., Oberbeckmann, S., Schernewski, G., Labrenz, M., Eichhorn, K.-J., & Voit, B. (2016). Analysis of environmental microplastics by vibrational microspectroscopy: FTIR, raman or both? *Analytical and Bioanalytical Chemistry*, 408(29), 8377–8391. <https://doi.org/10.1007/s00216-016-9956-3>
- Kennedy, V. S. (1984). *The estuary as a filter*. Orlando: Academic Press.
- Kenyon, K. W., & Kridler, E. (1969). Laysan albatrosses swallow indigestible matter. *The Auk*, 86(2), 339–343. <https://doi.org/10.2307/4083505>
- Kerpen, N. B., Larsen, B. E., Schlurmann, T., Paul, M., Guler, H. G., Goral, K. D., et al. (2024). Microplastic retention in marine vegetation canopies under breaking irregular waves. *Science of The Total Environment*, 912, 169280. <https://doi.org/10.1016/j.scitotenv.2023.169280>
- Kersten, M., & Smedes, F. (2002). Normalization procedures for sediment contaminants in spatial and temporal trend monitoring. *Journal of Environmental Monitoring*, 4(1), 109–115. <https://doi.org/10.1039/b108102k>
- Khatmullina, L., & Chubarenko, I. (2019). Transport of marine microplastic particles: Why is it so difficult to predict? *Anthropocene Coasts*, 2(1), 293–305. <https://doi.org/10.1139/anc-2018-0024>
- Khatmullina, L., & Isachenko, I. (2017). Settling velocity of microplastic particles of regular shapes. *Marine Pollution Bulletin*, 114(2), 871–880. <https://doi.org/10.1016/j.marpolbul.2016.11.024>
- Klaeager, F., Tagg, A. S., Otto, S., Bienmüller, M., Sartorius, I., & Labrenz, M. (2019). Residual monomer content affects the interpretation of plastic degradation. *Scientific Reports*, 9(1), 2120. <https://doi.org/10.1038/s41598-019-38685-6>
- Klein, S., Worch, E., & Knepper, T. P. (2015). Occurrence and spatial distribution of microplastics in river shore sediments of the rhine-main area in germany. *Environmental Science & Technology*, 49(10), 6070–6076. <https://doi.org/10.1021/acs.est.5b00492>
- Koch, H. M., & Calafat, A. M. (2009). Human body burdens of chemicals used in plastic manufacture. *Philosophical Transactions of the Royal Society B: Biological Sciences*, 364(1526), 2063–2078. <https://doi.org/10.1098/rstb.2008.0208>
- Koelmans, A. A., Besseling, E., & Shim, W. J. (2015). Nanoplastics in the aquatic environment. Critical review. In M. Bergmann, L. Gutow, & M. Klages (Eds.), *Marine anthropogenic litter* (pp. 325–340). Cham: Springer International Publishing. https://doi.org/10.1007/978-3-319-16510-3_12
- Koelmans, A. A., Bakir, A., Burton, G. A., & Janssen, C. R. (2016). Microplastic as a vector for chemicals in the aquatic environment: Critical review and model-supported reinterpretation of empirical studies. *Environmental Science & Technology*, 50(7), 3315–3326. <https://doi.org/10.1021/acs.est.5b06069>

- Koelmans, A. A., Kooi, M., Law, K. L., & van Sebille, E. (2017). All is not lost: Deriving a top-down mass budget of plastic at sea. *Environmental Research Letters*, 12(11), 114028. <https://doi.org/10.1088/1748-9326/aa9500>
- Koelmans, A. A., Redondo-Hasselerharm, P. E., Mohamed Nor, N. H., & Kooi, M. (2020). Solving the nonalignment of methods and approaches used in microplastic research to consistently characterize risk. *Environmental Science & Technology*, 54(19), 12307–12315. <https://doi.org/10.1021/acs.est.0c02982>
- Koelmans, A. A., Redondo-Hasselerharm, P. E., Nor, N. H. M., de Ruijter, V. N., Mintenig, S. M., & Kooi, M. (2022a). Risk assessment of microplastic particles. *Nature Reviews Materials*, 7(2), 138–152. <https://doi.org/10.1038/s41578-021-00411-y>
- Koelmans, A. A., Diepens, N. J., & Mohamed Nor, N. H. (2022b). Weight of evidence for the microplastic vector effect in the context of chemical risk assessment. In M. S. Bank (Ed.), *Microplastic in the environment: Pattern and process* (pp. 155–197). Cham: Springer International Publishing. https://doi.org/10.1007/978-3-030-78627-4_6
- Kooi, M., & Koelmans, A. A. (2019). Simplifying microplastic via continuous probability distributions for size, shape, and density. *Environmental Science & Technology Letters*, 6(9), 551–557. <https://doi.org/10.1021/acs.estlett.9b00379>
- Kooi, M., Nes, E. H. V., Scheffer, M., & Koelmans, A. A. (2017). Ups and downs in the ocean: Effects of biofouling on vertical transport of microplastics. *Environmental Science & Technology*, 51(14), 7963–7971. <https://doi.org/10.1021/acs.est.6b04702>
- Kooi, M., Primpke, S., Mintenig, S. M., Lorenz, C., Gerdt, G., & Koelmans, A. A. (2021). Characterizing the multidimensionality of microplastics across environmental compartments. *Water Research*, 202, 117429. <https://doi.org/10.1016/j.watres.2021.117429>
- Kreyling, O., Kölbl, A., Spielvogel, S., Rennert, T., Kaiser, K., & Kögel-Knabner, I. (2013). Density fractionation of organic matter in dolomite-derived soils. *Journal of Plant Nutrition and Soil Science*, 176(4), 509–519. <https://doi.org/10.1002/jpln.201200276>
- Kristensen, E., Penha-Lopes, G., Delefosse, M., Valdemarsen, T., Quintana, C., & Banta, G. (2012). What is bioturbation? The need for a precise definition for fauna in aquatic sciences. *Marine Ecology Progress Series*, 446, 285–302. <https://doi.org/10.3354/meps09506>
- Kruk, C., Huszar, V. L. M., Peeters, E. T. H. M., Bonilla, S., Costa, L., Lüring, M., et al. (2010). A morphological classification capturing functional variation in phytoplankton. *Freshwater Biology*, 55(3), 614–627. <https://doi.org/10.1111/j.1365-2427.2009.02298.x>
- Kubota, M. (1994). A mechanism for the accumulation of floating marine debris north of hawaii. *Journal of Physical Oceanography*, 24(5), 1059–1064. [https://doi.org/10.1175/1520-0485\(1994\)024%3C1059:AMFTAO%3E2.0.CO;2](https://doi.org/10.1175/1520-0485(1994)024%3C1059:AMFTAO%3E2.0.CO;2)
- Kukulka, T., Proskurowski, G., Morét-Ferguson, S., Meyer, D. W., & Law, K. L. (2012). The effect of wind mixing on the vertical distribution of buoyant plastic debris. *Geophysical Research Letters*, 39(7), 2012GL051116. <https://doi.org/10.1029/2012GL051116>
- Kullenberg, G., & Jacobsen, T. S. (1981). The baltic sea: An outline of its physical oceanography. *Marine Pollution Bulletin*, 12(6), 183–186. [https://doi.org/10.1016/0025-326X\(81\)90168-5](https://doi.org/10.1016/0025-326X(81)90168-5)
- Kurzweg, L., Schirrmeister, S., Hauße, M., Adomat, Y., Socher, M., & Harre, K. (2022). Application of electrostatic separation and differential scanning calorimetry for microplastic analysis in river sediments. *Frontiers in Environmental Science*, 10. <https://doi.org/10.3389/fenvs.2022.1032005>
- Kvale, K., Prowe, A. E. F., Chien, C.-T., Landolfi, A., & Oschlies, A. (2020). The global biological microplastic particle sink. *Scientific Reports*, 10(1). <https://doi.org/10.1038/s41598-020-72898-4>
- Lau, W. W. Y., Shiran, Y., Bailey, R. M., Cook, E., Stuchtey, M. R., Koskella, J., et al. (2020). Evaluating scenarios toward zero plastic pollution. *Science*, 369(6510), 1455–1461. <https://doi.org/10.1126/science.aba9475>
- Law, K. L., Morét-Ferguson, S., Maximenko, N. A., Proskurowski, G., Peacock, E. E., Hafner, J., & Reddy, C. M. (2010). Plastic accumulation in the north atlantic subtropical gyre. *Science*, 329(5996), 1185–1188. <https://doi.org/10.1126/science.1192321>
- Law, K. L., Morét-Ferguson, S. E., Goodwin, D. S., Zettler, E. R., DeForce, E., Kukulka, T., & Proskurowski, G. (2014). Distribution of surface plastic debris in the eastern pacific ocean from an 11-year data set. *Environmental Science & Technology*, 48(9), 4732–4738. <https://doi.org/10.1021/es4053076>
- Le Hir, P., Monbet, Y., & Orvain, F. (2007). Sediment erodability in sediment transport modelling: Can we account for biota effects? *Continental Shelf Research*, 27(8), 1116–1142. <https://doi.org/10.1016/j.csr.2007.05.001>

- Lebreton, L., & Andrady, A. (2019). Future scenarios of global plastic waste generation and disposal. *Palgrave Communications*, 5(1), 6. <https://doi.org/10.1057/s41599-018-0212-7>
- Leipe, T., Tauber, F., Vallius, H., Virtasalo, J., Uscinowicz, S., Kowalski, N., et al. (2011). Particulate organic carbon (POC) in surface sediments of the baltic sea. *Geo-Marine Letters*, 31(3), 175–188. <https://doi.org/10.1007/s00367-010-0223-x>
- Leiser, R., Schumann, M., Dadi, T., & Wendt-Potthoff, K. (2021). OPEN burial of microplastics. *Scientific Reports*. <https://doi.org/10.1038/s41598-021-02748-4>
- Lenz, R., Enders, K., Stedmon, C. A., Mackenzie, D. M. A., & Nielsen, T. G. (2015). A critical assessment of visual identification of marine microplastic using raman spectroscopy for analysis improvement. *Marine Pollution Bulletin*, 100(1), 82–91. <https://doi.org/10.1016/j.marpolbul.2015.09.026>
- Lenz, R., Enders, K., & Nielsen, T. G. (2016). Microplastic exposure studies should be environmentally realistic. *Proceedings of the National Academy of Sciences*, 113(29). <https://doi.org/10.1073/pnas.1606615113>
- Lenz, R., Enders, K., Fischer, F., Brandt, J., Fischer, D., & Labrenz, M. (2021). Measuring impacts of microplastic treatments via image recognition on immobilised particles below 100 μm . *Microplastics and Nanoplastics*, 1(1), 12. <https://doi.org/10.1186/s43591-021-00012-0>
- Lenz, R., Enders, K., Vizsolyi, E. C., Schumacher, M., Lötsch, J., Löder, M. G. J., et al. (2024). What goes around should not move around: Immobilizing microplastics as a new approach for analytical ring trials. *Environmental Science & Technology*, 58(50), 22224–22234. <https://doi.org/10.1021/acs.est.4c09427>
- Leslie, H. A., Van Velzen, M. J. M., Brandsma, S. H., Vethaak, A. D., Garcia-Vallejo, J. J., & Lamoree, M. H. (2022). Discovery and quantification of plastic particle pollution in human blood. *Environment International*, 163, 107199. <https://doi.org/10.1016/j.envint.2022.107199>
- Liss, P. S. (1976). Conservative and non-conservative behaviour of dissolved constituents during estuarine mixing. In J. D. Burton & P. S. Liss (Eds.), *Estuarine chemistry* (pp. 93–130). London: Academic Press.
- Liu, K., Courteney-Jones, W., Wang, X., Song, Z., Wei, N., & Li, D. (2020). Elucidating the vertical transport of microplastics in the water column: A review of sampling methodologies and distributions. *Water Research*, 186, 116403. <https://doi.org/10.1016/j.watres.2020.116403>
- Löder, M. G. J., Imhof, H. K., Ladehoff, M., Löschel, L. A., Lorenz, C., Mintenig, S., et al. (2017). Enzymatic purification of microplastics in environmental samples. *Environmental Science & Technology*, 51(24), 14283–14292. <https://doi.org/10.1021/acs.est.7b03055>
- Long, M., Moriceau, B., Gallinari, M., Lambert, C., Huvet, A., Raffray, J., & Soudant, P. (2015). Interactions between microplastics and phytoplankton aggregates: Impact on their respective fates. *Marine Chemistry*, 175, 39–46. <https://doi.org/10.1016/j.marchem.2015.04.003>
- López, A. G., Najjar, R. G., Friedrichs, M. A. M., Hickner, M. A., & Wardrop, D. H. (2021). Estuaries as filters for riverine microplastics: Simulations in a large, coastal-plain estuary. *Frontiers in Marine Science*, 8, 715924. <https://doi.org/10.3389/fmars.2021.715924>
- Loreau, M., Daufresne, T., Gonzalez, A., Gravel, D., Guichard, F., Leroux, S. J., et al. (2013). Unifying sources and sinks in ecology and Earth sciences. *Biological Reviews*, 88(2), 365–379. <https://doi.org/10.1111/brv.12003>
- Maes, T., Barry, J., Leslie, H. A., Vethaak, A. D., Nicolaus, E. E. M., Law, R. J., et al. (2018). Below the surface: Twenty-five years of seafloor litter monitoring in coastal seas of north west europe (1992–2017). *Science of The Total Environment*, 630, 790–798. <https://doi.org/10.1016/j.scitotenv.2018.02.245>
- Mancini, M., Francalanci, S., Innocenti, L., & Solari, L. (2023). Investigations on microplastic infiltration within natural riverbed sediments. *Science of The Total Environment*, 904, 167256. <https://doi.org/10.1016/j.scitotenv.2023.167256>
- Mani, T., Hauk, A., Walter, U., & Burkhardt-Holm, P. (2015). Microplastics profile along the rhine river. *Scientific Reports*, 5(1), 17988. <https://doi.org/10.1038/srep17988>
- Martin, J., Lusher, A., Thompson, R. C., & Morley, A. (2017). The deposition and accumulation of microplastics in marine sediments and bottom water from the irish continental shelf. *Scientific Reports*, 7(1). <https://doi.org/10.1038/s41598-017-11079-2>
- Martin, J., Lusher, A. L., & Nixon, F. C. (2022). A review of the use of microplastics in reconstructing dated sedimentary archives. *Science of The Total Environment*, 806, 150818. <https://doi.org/10.1016/j.scitotenv.2022.150818>

- Martin, J. L., McCutcheon, S. C., & Schottman, R. W. (1999). *Hydrodynamics and transport for water quality modeling*. Boca Raton: Lewis Publishers.
- Martinez, E., Maamaatuaiahutapu, K., & Taillandier, V. (2009). Floating marine debris surface drift: Convergence and accumulation toward the south pacific subtropical gyre. *Marine Pollution Bulletin*, 58(9), 1347–1355. <https://doi.org/10.1016/j.marpolbul.2009.04.022>
- Mason, S. A., Welch, V. G., & Neratko, J. (2018). Synthetic polymer contamination in bottled water. *Frontiers in Chemistry*, 6, 407. <https://doi.org/10.3389/fchem.2018.00407>
- Mattsson, K., Björkroth, F., Karlsson, T., & Hassellöv, M. (2021). Nanofragmentation of expanded polystyrene under simulated environmental weathering (thermooxidative degradation and hydrodynamic turbulence). *Frontiers in Marine Science*, 7, 578178. <https://doi.org/10.3389/fmars.2020.578178>
- Mayer, L. M., Schick, L. L., Hardy, K. R., Wagai, R., & McCarthy, J. (2004). Organic matter in small mesopores in sediments and soils. *Geochimica Et Cosmochimica Acta*, 68(19), 3863–3872. <https://doi.org/10.1016/j.gca.2004.03.019>
- McLusky, D. S., & Elliott, M. (2007). Transitional waters: A new approach, semantics or just muddying the waters? *Estuarine, Coastal and Shelf Science*, 71(3–4), 359–363. <https://doi.org/10.1016/j.ecss.2006.08.025>
- Medvedev, I. P., Rabinovich, A. B., & Kulikov, E. A. (2013). Tidal oscillations in the baltic sea. *Oceanology*, 53(5), 526–538. <https://doi.org/10.1134/S0001437013050123>
- Meysman, F., Middelburg, J., & Heip, C. (2006). Bioturbation: A fresh look at darwin's last idea. *Trends in Ecology & Evolution*, 21(12), 688–695. <https://doi.org/10.1016/j.tree.2006.08.002>
- Mhashhash, A., Bockelmann-Evans, B., & Pan, S. (2018). Effect of hydrodynamics factors on sediment flocculation processes in estuaries. *Journal of Soils and Sediments*, 18(10), 3094–3103. <https://doi.org/10.1007/s11368-017-1837-7>
- Middelburg, J. J., & Levin, L. A. (2009). Coastal hypoxia and sediment biogeochemistry. *Biogeosciences*, 6(7), 1273–1293. <https://doi.org/10.5194/bg-6-1273-2009>
- Mishra, U. C., Sarsaiya, S., & Gupta, A. (2022). A systematic review on the impact of cement industries on the natural environment. *Environmental Science and Pollution Research*, 29(13), 18440–18451. <https://doi.org/10.1007/s11356-022-18672-7>
- Möhlenkamp, P., Purser, A., & Thomsen, L. (2018). Plastic microbeads from cosmetic products: An experimental study of their hydrodynamic behaviour, vertical transport and resuspension in phytoplankton and sediment aggregates. *Elementa: Science of the Anthropocene*, 6, 61. <https://doi.org/10.1525/elementa.317>
- Moodley, T., Abunama, T., Kumari, S., Amoah, D., & Seyam, M. (2024). Applications of mathematical modelling for assessing microplastic transport and fate in water environments: A comparative review. *Environmental Monitoring and Assessment*, 196(7), 667. <https://doi.org/10.1007/s10661-024-12731-x>
- Moore, C. J., Moore, S. L., Leecaster, M. K., & Weisberg, S. B. (2001). A comparison of plastic and plankton in the north pacific central gyre. *Marine Pollution Bulletin*, 42(12), 1297–1300. [https://doi.org/10.1016/S0025-326X\(01\)00114-X](https://doi.org/10.1016/S0025-326X(01)00114-X)
- Morse, J. W., & Arvidson, R. S. (2002). The dissolution kinetics of major sedimentary carbonate minerals. *Earth-Science Reviews*, 58(1–2), 51–84. [https://doi.org/10.1016/s0012-8252\(01\)00083-6](https://doi.org/10.1016/s0012-8252(01)00083-6)
- Mörth, C.-M., Humborg, C., Eriksson, H., Danielsson, Å., Rodriguez Medina, M., Löfgren, S., et al. (2007). Modeling riverine nutrient transport to the baltic sea: A large-scale approach. *AMBIO: A Journal of the Human Environment*, 36(2), 124–133. [https://doi.org/10.1579/0044-7447\(2007\)36%5B124:MRNTTT%5D2.0.CO;2](https://doi.org/10.1579/0044-7447(2007)36%5B124:MRNTTT%5D2.0.CO;2)
- Müller, Y. K., Wernicke, T., Pittroff, M., Witzig, C. S., Storck, F. R., Klinger, J., & Zumbülte, N. (2020). Microplastic analysis—are we measuring the same? Results on the first global comparative study for microplastic analysis in a water sample. *Analytical and Bioanalytical Chemistry*, 412(3), 555–560. <https://doi.org/10.1007/s00216-019-02311-1>
- Muncke, J., Andersson, A.-M., Backhaus, T., Boucher, J. M., Carney Almroth, B., Castillo Castillo, A., et al. (2020). Impacts of food contact chemicals on human health: A consensus statement. *Environmental Health*, 19(1). <https://doi.org/10.1186/s12940-020-0572-5>
- Munz, M., Loui, C., Postler, D., Pittroff, M., & Oswald, S. E. (2024). Transport and retention of micro-polystyrene in coarse riverbed sediments: Effects of flow velocity, particle and sediment sizes.

- Murphy, F., Ewins, C., Carbonnier, F., & Quinn, B. (2016). Wastewater treatment works (WwTW) as a source of microplastics in the aquatic environment. *Environmental Science & Technology*, 50(11), 5800–5808. <https://doi.org/10.1021/acs.est.5b05416>
- Murray, C. J., Müller-Karulis, B., Carstensen, J., Conley, D. J., Gustafsson, B. G., & Andersen, J. H. (2019). Past, present and future eutrophication status of the baltic sea. *Frontiers in Marine Science*, 6, 2. <https://doi.org/10.3389/fmars.2019.00002>
- NABU. (2018). *Plastic in the schlei - wastewater treatment plant releases 5 tonnes to the environment (original: Plastik in der schlei - klärwerk entlässt fünf tonnen müll in die umwelt)*. Retrieved from <https://schleswig-holstein.nabu.de/news/2018/24614.html>
- Näkki, P., Setälä, O., & Lehtiniemi, M. (2017). Bioturbation transports secondary microplastics to deeper layers in soft marine sediments of the northern baltic sea. *Marine Pollution Bulletin*, 119(1), 255–261. <https://doi.org/10.1016/j.marpolbul.2017.03.065>
- Narloch, I., Gackowska, A., & Wejnerowska, G. (2022). Microplastic in the baltic sea: A review of distribution processes, sources, analysis methods and regulatory policies. *Environmental Pollution*, 315, 120453. <https://doi.org/10.1016/j.envpol.2022.120453>
- Newcombe, C. P., & Macdonald, D. D. (1991). Effects of suspended sediments on aquatic ecosystems. *North American Journal of Fisheries Management*, 11(1), 72–82. [https://doi.org/10.1577/1548-8675\(1991\)011%3C0072:eossoa%3E2.3.co;2](https://doi.org/10.1577/1548-8675(1991)011%3C0072:eossoa%3E2.3.co;2)
- Noonan, M. J., Grechi, N., Mills, C. L., & De A. M. M. Ferraz, M. (2023). Microplastics analytics: Why we should not underestimate the importance of blank controls. *Microplastics and Nanoplastics*, 3(1). <https://doi.org/10.1186/s43591-023-00065-3>
- Oberbeckmann, S., & Labrenz, M. (2020). Marine microbial assemblages on microplastics: Diversity, adaptation, and role in degradation. *Annual Review of Marine Science*, 12(1), 209–232. <https://doi.org/10.1146/annurev-marine-010419-010633>
- Oberbeckmann, S., Bartosik, D., Huang, S., Werner, J., Hirschfeld, C., Wibberg, D., et al. (2021). Genomic and proteomic profiles of biofilms on microplastics are decoupled from artificial surface properties. *Environmental Microbiology*, 23(6), 3099–3115. <https://doi.org/10.1111/1462-2920.15531>
- OECD. (2022). *Global plastics outlook: Policy scenarios to 2060*. OECD. <https://doi.org/10.1787/aa1edf33-en>
- Ogonowski, M., Schür, C., Jarsén, Å., & Gorokhova, E. (2016). The effects of natural and anthropogenic microparticles on individual fitness in daphnia magna. *PLOS ONE*, 11(5), e0155063. <https://doi.org/10.1371/journal.pone.0155063>
- Ogonowski, M., Gerdes, Z., & Gorokhova, E. (2018). What we know and what we think we know about microplastic effects – a critical perspective. *Current Opinion in Environmental Science & Health*, 1, 41–46. <https://doi.org/10.1016/j.coesh.2017.09.001>
- Onink, V., Wichmann, D., Delandmeter, P., & Van Sebille, E. (2019). The role of ekman currents, geostrophy, and stokes drift in the accumulation of floating microplastic. *Journal of Geophysical Research: Oceans*, 124(3), 1474–1490. <https://doi.org/10.1029/2018JC014547>
- Osinski, R. D., Enders, K., Gräwe, U., Klingbeil, K., & Radtke, H. (2020). Model uncertainties of a storm and their influence on microplastics and sediment transport in the baltic sea. *Ocean Science*, 16(6), 1491–1507. <https://doi.org/10.5194/os-16-1491-2020>
- Packman, A. I., & MacKay, J. S. (2003). Interplay of stream-subsurface exchange, clay particle deposition, and streambed evolution. *Water Resources Research*, 39(4), 2002WR001432. <https://doi.org/10.1029/2002WR001432>
- Pantó, G., Aguilera Dal Grande, P., Vanreusel, A., & Van Colen, C. (2024). Fauna – microplastics interactions: Empirical insights from benthos community exposure to marine plastic waste. *Marine Environmental Research*, 200, 106664. <https://doi.org/10.1016/j.marenvres.2024.106664>
- Pantó, G., Vanreusel, A., Vercauteren, M., Asselman, J., & Van Colen, C. (2025). Seabed microplastics in the european continental shelf: Unravelling physical and biological transport pathways and reciprocal fauna–polymer relationships. *Environmental Pollution*, 365, 125392. <https://doi.org/10.1016/j.envpol.2024.125392>
- Papanicolaou, A. (Thanos). N., Elhakeem, M., Krallis, G., Prakash, S., & Edinger, J. (2008). Sediment transport modeling review—current and future developments. *Journal of Hydraulic Engineering*, 134(1), 1–14. [https://doi.org/10.1061/\(ASCE\)0733-9429\(2008\)134:1\(1\)](https://doi.org/10.1061/(ASCE)0733-9429(2008)134:1(1))

- Papenmeier, S., Schrottke, K., & Bartholomä, A. (2014). Over time and space changing characteristics of estuarine suspended particles in the german weser and elbe estuaries. *Journal of Sea Research*, 85, 104–115. <https://doi.org/10.1016/j.seares.2013.03.010>
- Parga Martínez, K., Andersen, T. J., Da Silva, V., Strand, J., & Posth, N. R. (2024). Microplastics deposition in arctic sediments of greenland increases significantly after 1950. *Communications Earth & Environment*, 5(1), 584. <https://doi.org/10.1038/s43247-024-01768-y>
- Peleg, E., Teitelbaum, Y., & Arnon, S. (2024). Exploring the influence of sediment motion on microplastic deposition in streambeds. *Water Research*, 249, 120952. <https://doi.org/10.1016/j.watres.2023.120952>
- Peng, G., Zhu, B., Yang, D., Su, L., Shi, H., & Li, D. (2017). Microplastics in sediments of the changjiang estuary, china. *Environmental Pollution*, 225, 283–290. <https://doi.org/10.1016/j.envpol.2016.12.064>
- Persson, L., Carney Almroth, B. M., Collins, C. D., Cornell, S., de Wit, C. A., Diamond, M. L., et al. (2022). Outside the safe operating space of the planetary boundary for novel entities. *Environmental Science & Technology*, 56(3), 1510–1521. <https://doi.org/10.1021/acs.est.1c04158>
- Pfohl, P., Wagner, M., Meyer, L., Domercq, P., Praetorius, A., Hüffer, T., et al. (2022). Environmental degradation of microplastics: How to measure fragmentation rates to secondary micro- and nanoplastic fragments and dissociation into dissolved organics. *Environmental Science & Technology*, 56(16), 11323–11334. <https://doi.org/10.1021/acs.est.2c01228>
- Piehl, S., Leibner, A., Löder, M. G. J., Dris, R., Bogner, C., & Laforsch, C. (2018). Identification and quantification of macro- and microplastics on an agricultural farmland. *Scientific Reports*, 8(1), 17950. <https://doi.org/10.1038/s41598-018-36172-y>
- Piehl, S., Hauk, R., Robbe, E., Richter, B., Kachholz, F., Schilling, J., et al. (2021). Combined approaches to predict microplastic emissions within an urbanized estuary (warnow, southwestern baltic sea). *Frontiers in Environmental Science*, 9, 616765. <https://doi.org/10.3389/fenvs.2021.616765>
- PlasticsEurope. (2024). *Plastics – the fastFacts 2024*. Retrieved from <https://plasticseurope.org>
- Potter, I. C., Chuwen, B. M., Hoeksema, S. D., & Elliott, M. (2010). The concept of an estuary: A definition that incorporates systems which can become closed to the ocean and hypersaline. *Estuarine, Coastal and Shelf Science*, 87(3), 497–500. <https://doi.org/10.1016/j.ecss.2010.01.021>
- Prillaman, M. (2023). Are we in the anthropocene? Geologists could define new epoch for earth. *Nature*, 613(7942), 14–15. <https://doi.org/10.1038/d41586-022-04428-3>
- Primpke, S., Christiansen, S. H., Cowger, W., De Frond, H., Deshpande, A., Fischer, M., et al. (2020). Critical assessment of analytical methods for the harmonized and cost-efficient analysis of microplastics. *Applied Spectroscopy*, 74(9), 1012–1047. <https://doi.org/10.1177/0003702820921465>
- Prothero, D. R., Schwab, F. L., & Schwab, F. L. (2004). *Sedimentary geology: An introduction to sedimentary rocks and stratigraphy* (2. ed). New York: Freeman.
- Ramanna, S., Morozovskii, D., Swanson, S., & Bruneau, J. (2023). Machine learning of polymer types from the spectral signature of raman spectroscopy microplastics data. *Advances in Artificial Intelligence and Machine Learning*, 03(01), 647–668. <https://doi.org/10.54364/AAIML.2023.1144>
- Renzi, M., Blašković, A., Fastelli, P., Marcelli, M., Guerranti, C., Cannas, S., et al. (2018). Is the microplastic selective according to the habitat? Records in amphioxus sands, märl bed habitats and cymodocea nodosa habitats. *Marine Pollution Bulletin*, 130, 179–183. <https://doi.org/10.1016/j.marpolbul.2018.03.019>
- Reusch, T. B. H., Dierking, J., Andersson, H. C., Bonsdorff, E., Carstensen, J., Casini, M., et al. (2018). The baltic sea as a time machine for the future coastal ocean. *Science Advances*, 4(5), eaar8195. <https://doi.org/10.1126/sciadv.aar8195>
- Reynolds, C. S. (1984). Phytoplankton periodicity: The interactions of form, function and environmental variability. *Freshwater Biology*, 14(2), 111–142. <https://doi.org/10.1111/j.1365-2427.1984.tb00027.x>
- Richardson, K., Steffen, W., Lucht, W., Bendtsen, J., Cornell, S. E., Donges, J. F., et al. (2023). Earth beyond six of nine planetary boundaries. *Science Advances*, 9(37), eadh2458. <https://doi.org/10.1126/sciadv.adh2458>
- Rillig, M. C., Lehmann, A., Ryo, M., & Bergmann, J. (2019). Shaping up: Toward considering the shape and form of pollutants. *Environmental Science & Technology*, 53(14), 7925–7926. <https://doi.org/10.1021/acs.est.9b03520>
- Rillig, M. C., Kim, S. W., Kim, T.-Y., & Waldman, W. R. (2021). The global plastic toxicity debt. *Environmental Science & Technology*, 55(5), 2717–2719. <https://doi.org/10.1021/acs.est.0c07781>

- Rochman, C. M., Browne, M. A., Halpern, B. S., Hentschel, B. T., Hoh, E., Karapanagioti, H. K., et al. (2013a). Classify plastic waste as hazardous. *Nature*, 494(7436), 169–171. <https://doi.org/10.1038/494169a>
- Rochman, C. M., Hoh, E., Kurobe, T., & Teh, S. J. (2013b). Ingested plastic transfers hazardous chemicals to fish and induces hepatic stress. *Scientific Reports*, 3(1). <https://doi.org/10.1038/srep03263>
- Rochman, C. M., Tahir, A., Williams, S. L., Baxa, D. V., Lam, R., Miller, J. T., et al. (2015). Anthropogenic debris in seafood: Plastic debris and fibers from textiles in fish and bivalves sold for human consumption. *Scientific Reports*, 5(1), 14340. <https://doi.org/10.1038/srep14340>
- Rockström, J., Steffen, W., Noone, K., Persson, Å., Chapin, F. S., Lambin, E. F., et al. (2009). A safe operating space for humanity. *Nature*, 461(7263), 472–475. <https://doi.org/10.1038/461472a>
- Rohde, R. (2025). *Berkeley earth: Global temperature report for 2024*. Retrieved from <https://berkeleyearth.org/global-temperature-report-for-2024/>
- Rolf, M., Laermanns, H., Kienzler, L., Pohl, C., Möller, J. N., Laforsch, C., et al. (2022). Flooding frequency and floodplain topography determine abundance of microplastics in an alluvial rhine soil. *Science of The Total Environment*, 836, 155141. <https://doi.org/10.1016/j.scitotenv.2022.155141>
- Romeo, T., D'Alessandro, M., Esposito, V., Scotti, G., Berto, D., Formalewicz, M., et al. (2015). Environmental quality assessment of grand harbour (valletta, maltese islands): A case study of a busy harbour in the central mediterranean sea. *Environmental Monitoring and Assessment*, 187(12), 747. <https://doi.org/10.1007/s10661-015-4950-3>
- Rönspeiß, L., Dellwig, O., Lange, X., Nausch, G., & Schulz-Bull, D. (2020). Spatial and seasonal phosphorus dynamics in a eutrophic estuary of the southern baltic sea. *Estuarine, Coastal and Shelf Science*, 233, 106532. <https://doi.org/10.1016/j.ecss.2019.106532>
- Roslan, N. S., Lee, Y. Y., Ibrahim, Y. S., Tuan Anuar, S., Yusof, K. M. K. K., Lai, L. A., & Brentnall, T. (2024). Detection of microplastics in human tissues and organs: A scoping review. *Journal of Global Health*, 14, 04179. <https://doi.org/10.7189/jogh.14.04179>
- de Ruijter, V. N., Redondo-Hasselerharm, P. E., Gouin, T., & Koelmans, A. A. (2020). Quality criteria for microplastic effect studies in the context of risk assessment: A critical review. *Environmental Science & Technology*, 54(19), 11692–11705. <https://doi.org/10.1021/acs.est.0c03057>
- Ryan, P. G. (Ed.). (2015). A brief history of marine litter research. In *Marine anthropogenic litter* (Melanie Bergmann, Lars Gutow, Michael Klages). Bremerhaven, Fiskebäckskil: Springer.
- Salles, T., Lopez, S., Eschard, R., Lerat, O., Mulder, T., & Cacas, M. C. (2008). Turbidity current modelling on geological time scales. *Marine Geology*, 248(3–4), 127–150. <https://doi.org/10.1016/j.margeo.2007.10.004>
- Sandgaard, M. H., Palmqvist, A., Bour, A., Grønlund, S. N., Hooge, A., Selck, H., et al. (2023). Sediment matters as a route of microplastic exposure: A call for more research on the benthic compartment. *Frontiers in Marine Science*, 9, 1100567. <https://doi.org/10.3389/fmars.2022.1100567>
- Savranskaia, T., Egli, R., & Valet, J.-P. (2022). Multiscale brazil nut effects in bioturbated sediment. *Scientific Reports*, 12(1), 11450. <https://doi.org/10.1038/s41598-022-14276-w>
- Scherer, C., Wolf, R., Völker, J., Stock, F., Brennhold, N., Reifferscheid, G., & Wagner, M. (2020). Toxicity of microplastics and natural particles in the freshwater dipteran chironomus riparius: Same same but different? *Science of The Total Environment*, 711, 134604. <https://doi.org/10.1016/j.scitotenv.2019.134604>
- Schernewski, G., Radtke, H., Robbe, E., Haseler, M., Hauk, R., Meyer, L., et al. (2021). Emission, transport, and deposition of visible plastics in an estuary and the baltic sea—a monitoring and modeling approach. *Environmental Management*, 68(6), 860–881. <https://doi.org/10.1007/s00267-021-01534-2>
- Schmidt, C., Kühnel, D., Materić, D., Stubenrauch, J., Schubert, K., Luo, A., et al. (2024). A multi-disciplinary perspective on the role of plastic pollution in the triple planetary crisis. *Environment International*, 193, 109059. <https://doi.org/10.1016/j.envint.2024.109059>
- Schnepf, U., Von Moers-Meßmer, M. A. L., & Brümmer, F. (2023). A practical primer for image-based particle measurements in microplastic research. *Microplastics and Nanoplastics*, 3(1), 16. <https://doi.org/10.1186/s43591-023-00064-4>
- Schruff, T. (2018). *Taking a closer look at the causes and impacts of fine sediment infiltration into gravel beds : Development and application of an extended theory of fine sediment infiltration based on grain scale numerical simulations* (PhD thesis). Dissertation. RWTH Aachen University. <https://doi.org/10.18154/RWTH-2018-227229>

- Schulz, M., Clemens, T., Förster, H., Harder, T., Fleet, D., Gaus, S., et al. (2015). Statistical analyses of the results of 25 years of beach litter surveys on the south-eastern north sea coast. *Marine Environmental Research*, 109, 21–27. <https://doi.org/10.1016/j.marenvres.2015.04.007>
- Schwabl, P., Köppel, S., Königshofer, P., Bucsecs, T., Trauner, M., Reiberger, T., & Liebmann, B. (2019). Detection of various microplastics in human stool: A prospective case series. *Annals of Internal Medicine*, 171(7), 453–457. <https://doi.org/10.7326/M19-0618>
- Schwarzer, K., Ricklefs, K., & Höft, D. (2019). *Sediment inventory and hydromorphology of the schlei, (original: Sedimentinventar und hydromorphologie der schlei)* (p. 114). Institute of Geosciences, Kiel University. Retrieved from https://www.schleswig-holstein.de/DE/fachinhalte/M/meeresschutz/Downloads/Bericht_SedimentinventarHydromorphologieSchlei.pdf
- van Sebille, E., Aliani, S., Law, K. L., Maximenko, N., Alsina, J. M., Bagaev, A., et al. (2020). The physical oceanography of the transport of floating marine debris. *Environmental Research Letters*, 15(2), 023003. <https://doi.org/10.1088/1748-9326/ab6d7d>
- Shafik, N., & Bandyopadhyay, S. (1992). *Economic growth and environmental quality: Time series and cross-country evidence*. Background Paper for the World Development Report, WPS 904.
- She, J., Christensen, A., Garaventa, F., Lips, U., Murawski, J., Ntoumas, M., & Tsiaras, K. (2023). Developing realistic models for assessing marine plastic pollution in semi-enclosed seas. *Frontiers in Ocean Observing: Emerging Technologies for Understanding and Managing a Changing Ocean*. <https://doi.org/10.5670/oceanog.2023.s1.17>
- Shen, M., Huang, W., Chen, M., Song, B., Zeng, G., & Zhang, Y. (2020). (Micro)plastic crisis: Un-ignorable contribution to global greenhouse gas emissions and climate change. *Journal of Cleaner Production*, 254, 120138. <https://doi.org/10.1016/j.jclepro.2020.120138>
- Sherrod, H., Leong, N., Hapich, H., Gomez, F., Moore, S., Maurer, B., et al. (2024). One4All: An open source portal to validate and ShareMicroplastics data and beyond. *Journal of Open Source Software*, 9(99), 6715. <https://doi.org/10.21105/joss.06715>
- Shields, A. (1936). *Anwendung der aehnlichkeitsmechanik und der turbulenzforschung auf die geschiebebewegung*. Technische Hochschule Berlin, Berlin.
- Shiravani, G., Oberrecht, D., Roscher, L., Kernchen, S., Halbach, M., Gerriets, M., et al. (2023). Numerical modeling of microplastic interaction with fine sediment under estuarine conditions. *Water Research*, 231, 119564. <https://doi.org/10.1016/j.watres.2022.119564>
- Siegel, H., Fischer, F., Lenz, R., Fischer, D., Jekel, M., & Labrenz, M. (2021). Identification and quantification of microplastic particles in drinking water treatment sludge as an integrative approach to determine microplastic abundance in a freshwater river. *Environmental Pollution*, 286, 117524. <https://doi.org/10.1016/j.envpol.2021.117524>
- Soltani, N. S., Taylor, M. P., & Wilson, S. P. (2021). Quantification and exposure assessment of microplastics in australian indoor house dust. *Environmental Pollution*, 283, 117064. <https://doi.org/10.1016/j.envpol.2021.117064>
- Sørensen, L., Rogers, E., Altin, D., Salaberria, I., & Booth, A. M. (2020). Sorption of PAHs to microplastic and their bioavailability and toxicity to marine copepods under co-exposure conditions. *Environmental Pollution*, 258, 113844. <https://doi.org/10.1016/j.envpol.2019.113844>
- Soulsby, R. (1997). *Dynamics of marine sands : A manual for practical applications* (Vols. 1–1). London: Telford.
- Srivastava, A., Kikuchi, K., & Ishikawa, T. (2021). Microbial brazil nut effect. *Soft Matter*, 17(46), 10428–10436. <https://doi.org/10.1039/D1SM01327K>
- Stead, J. L., De Souza Leite, L., & Bond, T. (2024). Gradient columns to measure the density of microplastics. *Science of The Total Environment*, 953, 176176. <https://doi.org/10.1016/j.scitotenv.2024.176176>
- Stedmon, C. A., & Markager, S. (2003). Behaviour of the optical properties of coloured dissolved organic matter under conservative mixing. *Estuarine, Coastal and Shelf Science*, 57(5–6), 973–979. [https://doi.org/10.1016/S0272-7714\(03\)00003-9](https://doi.org/10.1016/S0272-7714(03)00003-9)
- Steffen, W., Richardson, K., Rockström, J., Cornell, S. E., Fetzer, I., Bennett, E. M., et al. (2015). Planetary boundaries: Guiding human development on a changing planet. *Science*, 347(6223), 1259855. <https://doi.org/10.1126/science.1259855>
- Stokes, G. G. (1851). On the effect of the internal friction of fluids on the motion of pendulums. In *Mathematical and physical papers* (1st ed., pp. 8–106). Cambridge University Press. <https://doi.org/10.1017/CBO9780511702266>

- Strand, J., Lassen, P., Shashoua, Y., & Andersen, J. H. (2013, September). *Microplastic particles in sediments from danish waters*. Poster presented at the ICES annual science conference, Reykjavík, Iceland. Retrieved from https://pure.au.dk/ws/portalfiles/portal/56618475/JAK_Microplastic_poster_20sep13jak_3a.pdf
- Straub, S., Hirsch, P. E., & Burkhardt-Holm, P. (2017). Biodegradable and petroleum-based microplastics do not differ in their ingestion and excretion but in their biological effects in a freshwater invertebrate *gammarus fossarum*. *International Journal of Environmental Research and Public Health*, 14(7), 774. <https://doi.org/10.3390/ijerph14070774>
- Strom, K., & Keyvani, A. (2011). An explicit full-range settling velocity equation for mud flocs. *Journal of Sedimentary Research*, 81(12), 921–934. <https://doi.org/10.2110/jsr.2011.62>
- Subramanian, M. (2019). Humans versus earth. *Nature*, 572, 168–170.
- Sussarellu, R., Suquet, M., Thomas, Y., Lambert, C., Fabioux, C., Pernet, M. E. J., et al. (2016). Oyster reproduction is affected by exposure to polystyrene microplastics. *Proceedings of the National Academy of Sciences*, 113(9), 2430–2435. <https://doi.org/10.1073/pnas.1519019113>
- Switzer, J., Langaas, S., & Folke, C. (1996). LAND USE AND POPULATION DENSITY IN THE BALTIC SEA DRAINAGE BASIN: A GIS DATABASE. *AMBIO*, (25), 191–198.
- Symons, W. O., Sumner, E. J., Paull, C. K., Cartigny, M. J. B., Xu, J. P., Maier, K. L., et al. (2017). A new model for turbidity current behavior based on integration of flow monitoring and precision coring in a submarine canyon. *Geology*, 45(4), 367–370. <https://doi.org/10.1130/g38764.1>
- Tagg, A. S., Brandes, E., Fischer, F., Fischer, D., Brandt, J., & Labrenz, M. (2022). Agricultural application of microplastic-rich sewage sludge leads to further uncontrolled contamination. *Science of The Total Environment*, 806, 150611. <https://doi.org/10.1016/j.scitotenv.2021.150611>
- Tekman, M. B., Walther, B. A., Peter, C., Gutow, L., & Bergmann, M. (2022). *Impacts of plastic pollution in the ocean on marine species, biodiversity and ecosystems: study*. Berlin: WWF Germany. <https://doi.org/10.5281/zenodo.5898684>
- Teuten, E. L., Saquing, J. M., Knappe, D. R. U., Barlaz, M. A., Jonsson, S., Björn, A., et al. (2009). Transport and release of chemicals from plastics to the environment and to wildlife. *Philosophical Transactions of the Royal Society B: Biological Sciences*, 364(1526), 2027–2045. <https://doi.org/10.1098/rstb.2008.0284>
- The European Parliament and of the Council. Directive 2008/56/EC, Official Journal of the European Union § (2008). Retrieved from <http://data.europa.eu/eli/dir/2008/56/oj>
- Thit, A., Grønlund, S. N., Trudsø, L. L., Hansen, B. W., Herzog, S. D., Nielsen, S. L., et al. (2022). Particles as carriers of matter in the aquatic environment: Challenges and ways ahead for transdisciplinary research. *Science of The Total Environment*, 838, 155831. <https://doi.org/10.1016/j.scitotenv.2022.155831>
- Thompson, R. C., Olsen, Y., Mitchell, R. P., Davis, A., Rowland, S. J., John, A. W. G., et al. (2004). Lost at sea: Where is all the plastic? *Science*, 304(5672), 838–838. <https://doi.org/10.1126/science.1094559>
- Thompson, R. C., Courtene-Jones, W., Boucher, J., Pahl, S., Raubenheimer, K., & Koelmans, A. A. (2024). Twenty years of microplastic pollution research—what have we learned? *Science*, 386(6720), ead12746. <https://doi.org/10.1126/science.adl2746>
- Tian, Z., Liu, C., Ren, Z., Guo, X., Zhang, M., Wang, X., et al. (2023). Impact of seepage flow on sediment resuspension by internal solitary waves: Parameterization and mechanism. *Journal of Oceanology and Limnology*, 41(2), 444–457. <https://doi.org/10.1007/s00343-022-2001-9>
- Tournier, V., Topham, C. M., Gilles, A., David, B., Folgoas, C., Moya-Leclair, E., et al. (2020). An engineered PET depolymerase to break down and recycle plastic bottles. *Nature*, 580(7802), 216–219. <https://doi.org/10.1038/s41586-020-2149-4>
- Turner, S., Horton, A. A., Rose, N. L., & Hall, C. (2019). A temporal sediment record of microplastics in an urban lake, London, UK. *Journal of Paleolimnology*, 61(4), 449–462. <https://doi.org/10.1007/s10933-019-00071-7>
- UNEP. (2022). *END PLASTIC POLLUTION - TOWARDS AN INTERNATIONAL LEGALLY BINDING INSTRUMENT*, united nations environment assembly of the united nations environment programme (Resolution No. UNEP/EA.5/Res.14) (p. 4). Nairobi: United Nations. Retrieved from <https://www.unep.org/inc-plastic-pollution>
- UNEP. (2023). *Turning off the tap: How the world can end plastic pollution and create a circular economy*. United Nations Environment Programme. Retrieved from <https://www.unep.org/resources/turning-off-tap-end-plastic-pollution-create-circular-economy>

- UNEP. (2025). *Draft report of the intergovernmental negotiating committee to develop an international legally binding instrument on plastic pollution, including in the marine environment, on the work of the first part of its fifth session* (Meeting Report No. UNEP/PP/INC.5/8) (pp. 1–33). Busan, Republic of Korea: United Nations Environment Programme. Retrieved from https://wedocs.unep.org/bitstream/handle/20.500.11822/47162/INC_5_1_Report.pdf
- Valero, D., Belay, B. S., Moreno-Rodenas, A., Kramer, M., & Franca, M. J. (2022). The key role of surface tension in the transport and quantification of plastic pollution in rivers. *Water Research*, 226, 119078. <https://doi.org/10.1016/j.watres.2022.119078>
- Van Cauwenberghe, L., Vanreusel, A., Mees, J., & Janssen, C. R. (2013). Microplastic pollution in deep-sea sediments. *Environmental Pollution*, 182, 495–499. <https://doi.org/10.1016/j.envpol.2013.08.013>
- Van Daele, M., Van Bastelaere, B., De Clercq, J., Meyer, I., Vercauteren, M., & Asselman, J. (2024). Mud and organic content are strongly correlated with microplastic contamination in a meandering riverbed. *Communications Earth & Environment*, 5(1). <https://doi.org/10.1038/s43247-024-01613-2>
- Van Melkebeke, M., Janssen, C., & De Meester, S. (2020). Characteristics and sinking behavior of typical microplastics including the potential effect of biofouling: Implications for remediation. *Environmental Science & Technology*, 54(14), 8668–8680. <https://doi.org/10.1021/acs.est.9b07378>
- Van Mourik, L. M., Crum, S., Martinez-Frances, E., Van Bavel, B., Leslie, H. A., De Boer, J., & Cofino, W. P. (2021). Results of WEPAL-QUASIMEME/NORMANs first global interlaboratory study on microplastics reveal urgent need for harmonization. *Science of The Total Environment*, 772, 145071. <https://doi.org/10.1016/j.scitotenv.2021.145071>
- Van Rijn, L. C. (1984). Sediment transport, part i: Bed load transport. *Journal of Hydraulic Engineering*, 110(10), 1431–1456. [https://doi.org/10.1061/\(ASCE\)0733-9429\(1984\)110:10\(1431\)](https://doi.org/10.1061/(ASCE)0733-9429(1984)110:10(1431))
- Varga, G., Gresina, F., Újvári, G., Kovács, J., & Szalai, Z. (2019). On the reliability and comparability of laser diffraction grain size measurements of paleosols in loess records. *Sedimentary Geology*, 389, 42–53. <https://doi.org/10.1016/j.sedgeo.2019.05.011>
- Varma, S., & Simon, R. (2006). Bias in error estimation when using cross-validation for model selection. *BMC Bioinformatics*, 7(1), 91. <https://doi.org/10.1186/1471-2105-7-91>
- Vedenin, A. A., Kröncke, I., Beck, A. J., Bodenbinder, A., Chrysagi, E., Gräwe, U., et al. (2024). Spatial structure and biodiversity of macrofauna around marine munition dumpsites – a case study from the baltic sea. *Marine Pollution Bulletin*, 198, 115865. <https://doi.org/10.1016/j.marpolbul.2023.115865>
- Vermeiren, P., Lercari, D., Muñoz, C. C., Ikejima, K., Celentano, E., Jorge-Romero, G., & Defeo, O. (2021). Sediment grain size determines microplastic exposure landscapes for sandy beach macroinfauna. *Environmental Pollution*, 286, 117308. <https://doi.org/10.1016/j.envpol.2021.117308>
- Vianello, A., Boldrin, A., Guerriero, P., Moschino, V., Rella, R., Sturaro, A., & Da Ros, L. (2013). Microplastic particles in sediments of lagoon of venice, italy: First observations on occurrence, spatial patterns and identification. *Estuarine, Coastal and Shelf Science*, 130, 54–61. <https://doi.org/10.1016/j.ecss.2013.03.022>
- Vianello, A., Jensen, R. L., Liu, L., & Vollertsen, J. (2019). Simulating human exposure to indoor airborne microplastics using a breathing thermal manikin. *Scientific Reports*, 9(1), 8670. <https://doi.org/10.1038/s41598-019-45054-w>
- Villarrubia-Gómez, P., Carney Almroth, B., Eriksen, M., Ryberg, M., & Cornell, S. E. (2024). Plastics pollution exacerbates the impacts of all planetary boundaries. *One Earth*, S2590332224005414. <https://doi.org/10.1016/j.oneear.2024.10.017>
- Vince, J., & Hardesty, B. D. (2018). Governance solutions to the tragedy of the commons that marine plastics have become. *Frontiers in Marine Science*, 5, 214. <https://doi.org/10.3389/fmars.2018.00214>
- Wagner, J., Robberson, W., & Allen, H. (2022). Analytical precision assessment for microplastic analyses. *Chemosphere*, 304, 135295. <https://doi.org/10.1016/j.chemosphere.2022.135295>
- Wagner, M., Monclús, L., Arp, H. P. H., Groh, K. J., Løseth, M. E., Muncke, J., et al. (2024). *State of the science on plastic chemicals - identifying and addressing chemicals and polymers of concern*. <https://doi.org/10.5281/ZENODO.10701706>
- Wakeham, S. G., & Canuel, E. A. (2016). The nature of organic carbon in density-fractionated sediments in the sacramento-san joaquin river delta (california). *Biogeosciences*, 13(2), 567–582. <https://doi.org/10.5194/bg-13-567-2016>
- Waldschläger, K., & Schüttrumpf, H. (2019). Effects of particle properties on the settling and rise velocities of microplastics in freshwater under laboratory conditions. *Environmental Science & Technology*, 53(4),

- 1958–1966. <https://doi.org/10.1021/acs.est.8b06794>
- Waldschläger, K., & Schüttrumpf, H. (2020). Infiltration behavior of microplastic particles with different densities, sizes, and shapes—from glass spheres to natural sediments. *Environmental Science & Technology*, 54(15), 9366–9373. <https://doi.org/10.1021/acs.est.0c01722>
- Waldschläger, K., Brückner, M. Z. M., Carney Almroth, B., Hackney, C. R., Adyel, T. M., Alimi, O. S., et al. (2022). Learning from natural sediments to tackle microplastics challenges: A multidisciplinary perspective. *Earth-Science Reviews*, 228, 104021. <https://doi.org/10.1016/j.earscirev.2022.104021>
- Walker, T. R., & Fequet, L. (2023). Current trends of unsustainable plastic production and micro(nano)plastic pollution. *TrAC Trends in Analytical Chemistry*, 160, 116984. <https://doi.org/10.1016/j.trac.2023.116984>
- Waters, C. N., Williams, M., Zalasiewicz, J., Turner, S. D., Barnosky, A. D., Head, M. J., et al. (2022). Epochs, events and episodes: Marking the geological impact of humans. *Earth-Science Reviews*, 234, 104171. <https://doi.org/10.1016/j.earscirev.2022.104171>
- Watts, A. J. R., Urbina, M. A., Goodhead, R., Moger, J., Lewis, C., & Galloway, T. S. (2016). Effect of microplastic on the gills of the shore crab *carcinus maenas*. *Environmental Science & Technology*, 50(10), 5364–5369. <https://doi.org/10.1021/acs.est.6b01187>
- Wellman, C. H. (2004). Origin, function and development of the spore wall in early land plants. In *The evolution of plant physiology* (pp. 43–63). Elsevier. <https://doi.org/10.1016/B978-012339552-8/50004-4>
- Wentworth, C. K. (1922). A scale of grade and class terms for clastic sediments. *The Journal of Geology*, 30(5), 377–392. <https://doi.org/10.1086/622910>
- White, A. F., & Brantley, S. L. (Eds.). (1995). *Chemical weathering rates of silicate minerals*. Washington, D.C: Mineralogical Society of America.
- Wichmann, D., Delandmeter, P., Dijkstra, H. A., & Van Sebille, E. (2019). Mixing of passive tracers at the ocean surface and its implications for plastic transport modelling. *Environmental Research Communications*, 1(11), 115001. <https://doi.org/10.1088/2515-7620/ab4e77>
- Widdows, J., & Brinsley, M. (2002). Impact of biotic and abiotic processes on sediment dynamics and the consequences to the structure and functioning of the intertidal zone. *Journal of Sea Research*, 48(2), 143–156. [https://doi.org/10.1016/S1385-1101\(02\)00148-X](https://doi.org/10.1016/S1385-1101(02)00148-X)
- Wieland, S., Balmes, A., Bender, J., Kitzinger, J., Meyer, F., Ramsperger, A. F., et al. (2022). From properties to toxicity: Comparing microplastics to other airborne microparticles. *Journal of Hazardous Materials*, 428, 128151. <https://doi.org/10.1016/j.jhazmat.2021.128151>
- Wiesinger, H., Wang, Z., & Hellweg, S. (2021). Deep dive into plastic monomers, additives, and processing aids. *Environmental Science & Technology*, 55(13), 9339–9351. <https://doi.org/10.1021/acs.est.1c00976>
- Wilber, D. H., & Clarke, D. G. (2001). Biological effects of suspended sediments: A review of suspended sediment impacts on fish and shellfish with relation to dredging activities in estuaries. *North American Journal of Fisheries Management*, 21(4), 855–875. [https://doi.org/10.1577/1548-8675\(2001\)021%3C0855:beossa%3E2.0.co;2](https://doi.org/10.1577/1548-8675(2001)021%3C0855:beossa%3E2.0.co;2)
- Wilcox, C., Hardesty, B. D., & Law, K. L. (2020). Abundance of floating plastic particles is increasing in the western north atlantic ocean. *Environmental Science & Technology*, 54(2), 790–796. <https://doi.org/10.1021/acs.est.9b04812>
- Wilkinson, M. D., Dumontier, M., Aalbersberg, Ij. J., Appleton, G., Axton, M., Baak, A., et al. (2016). The FAIR guiding principles for scientific data management and stewardship. *Scientific Data*, 3(1), 160018. <https://doi.org/10.1038/sdata.2016.18>
- Winkel, N. (2003). *Das morphologische system des warnow-ästuars* (Mitteilungsblatt No. 86) (pp. 65–67). Karlsruhe: Bundesanstalt für Wasserbau. Retrieved from <https://hdl.handle.net/20.500.11970/102634>
- Wollast, R. (2003). Biogeochemical processes in estuaries. In G. Wefer, F. Lamy, & F. Mantoura (Eds.), *Marine science frontiers for europe* (pp. 61–77). Berlin, Heidelberg: Springer Berlin Heidelberg. https://doi.org/10.1007/978-3-642-55862-7_5
- Wolowicz, M., Sokolowski, A., & Lasota, R. (2007). Estuaries — a biological point of view. *Oceanological and Hydrobiological Studies*, 36(3), 113–130. <https://doi.org/10.2478/v10009-007-0025-2>
- Woodall, L. C., Sanchez-Vidal, A., Canals, M., Paterson, G. L. J., Coppock, R., Sleight, V., et al. (2014). The deep sea is a major sink for microplastic debris. *Royal Society Open Science*, 1(4), 140317. <https://doi.org/10.1098/rsos.140317>

- Woodward, J., Li, J., Rothwell, J., & Hurley, R. (2021). Acute riverine microplastic contamination due to avoidable releases of untreated wastewater. *Nature Sustainability*, 4(9), 793–802. <https://doi.org/10.1038/s41893-021-00718-2>
- Wright, K. A., Goodman, D. H., Som, N. A., Alvarez, J., Martin, A., & Hardy, T. B. (2017). Improving hydrodynamic modelling: An analytical framework for assessment of two-dimensional hydrodynamic models. *River Research and Applications*, 33(1), 170–181. <https://doi.org/10.1002/rra.3067>
- Wu, N., Grieve, S. W. D., Manning, A. J., & Spencer, K. L. (2024). Flocs as vectors for microplastics in the aquatic environment. *Nature Water*, 2(11), 1082–1090. <https://doi.org/10.1038/s44221-024-00332-4>
- Wunderlich, B. (Ed.). (2005). *Thermal analysis of polymeric materials*. Berlin, Heidelberg: Springer Berlin Heidelberg. <https://doi.org/10.1007/b137476>
- Yan, H., Cordier, M., & Uehara, T. (2024). Future projections of global plastic pollution: Scenario analyses and policy implications. *Sustainability*, 16(2), 643. <https://doi.org/10.3390/su16020643>
- Yang, D., Shi, H., Li, L., Li, J., Jabeen, K., & Kolandhasamy, P. (2015). Microplastic pollution in table salts from china. *Environmental Science & Technology*, 49(22), 13622–13627. <https://doi.org/10.1021/acs.est.5b03163>
- Yang, H., Chen, Z., Kong, L., Xing, H., Yang, Q., & Wu, J. (2025). A review of eco-corona formation on micro/nanoplastics and its effects on stability, bioavailability, and toxicity. *Water*, 17(8), 1124. <https://doi.org/10.3390/w17081124>
- Yang, Y., Gao, S., Wang, Y. P., Jia, J., Xiong, J., & Zhou, L. (2019). Revisiting the problem of sediment motion threshold. *Continental Shelf Research*, 187, 103960. <https://doi.org/10.1016/j.csr.2019.103960>
- Yoshida, S., Hiraga, K., Takehana, T., Taniguchi, I., Yamaji, H., Maeda, Y., et al. (2016). A bacterium that degrades and assimilates poly(ethylene terephthalate). *Science*, 351(6278), 1196–1199. <https://doi.org/10.1126/science.aad6359>
- You, Y., Della Penna, A., & Thrush, S. F. (2023). Modelled broad-scale shifts on seafloor ecosystem functioning due to microplastic impacts on bioturbation. *Scientific Reports*, 13(1), 17121. <https://doi.org/10.1038/s41598-023-44425-8>
- Zalasiewicz, J., Waters, C. N., & Williams, M. (2014). Human bioturbation, and the subterranean landscape of the anthropocene. *Anthropocene*, 6, 3–9. <https://doi.org/10.1016/j.ancene.2014.07.002>
- Zalasiewicz, J., Waters, C. N., Ivar Do Sul, J. A., Corcoran, P. L., Barnosky, A. D., Cearreta, A., et al. (2016). The geological cycle of plastics and their use as a stratigraphic indicator of the anthropocene. *Anthropocene*, 13, 4–17. <https://doi.org/10.1016/j.ancene.2016.01.002>
- Zalasiewicz, J., Thomas, J. A., Waters, C. N., Turner, S., & Head, M. J. (2024). What should the anthropocene mean? *Nature*, 632, 980–984.
- Zettler, E. R., Mincer, T. J., & Amaral-Zettler, L. A. (2013). Life in the “plastisphere”: Microbial communities on plastic marine debris. *Environmental Science & Technology*, 47(13), 7137–7146. <https://doi.org/10.1021/es401288x>
- Zhang, W. (2014). Sediment dynamics. In J. Harff, M. Meschede, S. Petersen, & J. Thiede (Eds.), *Encyclopedia of marine geosciences* (pp. 1–6). Dordrecht: Springer Netherlands. https://doi.org/10.1007/978-94-007-6644-0_175-1
- Zhang, W., Wang, Q., & Chen, H. (2022). Challenges in characterization of nanoplastics in the environment. *Frontiers of Environmental Science & Engineering*, 16(1), 11. <https://doi.org/10.1007/s11783-021-1445-z>
- Zhao, L., Zhang, J., Zhao, D., Jia, L., Qin, B., Cao, X., et al. (2022). Biological degradation of lignin: A critical review on progress and perspectives. *Industrial Crops and Products*, 188, 115715. <https://doi.org/10.1016/j.indcrop.2022.115715>
- Zhen, Y., Wang, L., Sun, H., & Liu, C. (2023). Prediction of microplastic abundance in surface water of the ocean and influencing factors based on ensemble learning. *Environmental Pollution*, 331, 121834. <https://doi.org/10.1016/j.envpol.2023.121834>
- Zobell, C. E. (1943). The effect of solid surfaces upon bacterial activity. *Journal of Bacteriology*, 46(1), 39–56. <https://doi.org/10.1128/jb.46.1.39-56.1943>

Publications

A digital version of this doctoral thesis, including all supplementary information of the included publications omitted from the printed version due to formatting restrictions, is available under Enders ([2025](#)).

Mapping the plastic legacy with NIXVEGS: Machine-learning enabled microplastics prediction in sediments

Kristina Enders^{1,2*}, Robin Lenz^{1,2}, Franziska Fischer², Klaus Schwarzer³, Guntram Seiß⁴, Dieter Fischer², Matthias Labrenz^{1*}

¹ Leibniz Institute for Baltic Sea Research Warnemünde (IOW), 18119 Rostock, Germany

² Leibniz Institute for Polymer Research (IPF), 01069 Dresden, Germany

³ Christian-Albrechts-University of Kiel (CAU), 24118 Kiel, Germany

⁴ The Federal Waterways Engineering and Research Institute (BAW), 22559 Hamburg, Germany

*Corresponding authors. Emails: enders-kristina@ipfdd.de, matthias.labrenz@io-warnemuende.de

Abstract: Aquatic sediments act as major sinks for microplastic (MP) pollution, yet accurately quantifying their MP distributions and inventories on a regional scale remains challenging, especially in hydrodynamically complex estuarine environments. Existing distribution models focus on ocean basins or simple hydrodynamic systems but lack sufficient adaptability to the spatial heterogeneity typical of estuaries. To address this limitation, we developed NIXVEGS, an open-source empirical spatial prediction pipeline adapting machine learning components like nested cross-validation and ensemble modeling specifically for the sparse data characteristic of environmental MP studies. It integrates granulometric proxies and spatio-temporal connectivity to predict MP distributions and provides data-driven decisions in model selection combined with performance validation on unseen data under the best possible utilization of the available observations. The model predictions increased spatial data coverage 7.6-fold from an original set of 26 analyzed MP sediment concentration in the Schlei estuary (Baltic Sea coast, Northern Germany). We demonstrate the application of NIXVEGS and use its predictions to estimate the region's sedimentary MP inventory at ~20 trillion particles (50-5000 μm) or ~14.3 tons. Estuarine sediments are key environments for monitoring MP pollution evolution, where NIXVEGS can assist regional plastic management and contribute to the understanding of a global MP budget.

Keywords: Grain size, Proxy, Geological analysis, Spectroscopy, FAIR data, Cross-validation, Predictive modeling, Environmental monitoring

Synopsis: We developed NIXVEGS, a predictive modeling tool leveraging readily obtainable sediment proxies, to significantly enhance the spatial coverage of microplastic concentrations from limited direct measurements.

Introduction

Sediments as the largest passive MP samplers

Global plastic cycling is influenced by a multitude of physical processes ¹. Similar to natural debris, the majority of the global plastic legacy ends up in sediments – places of continuous particle deposition ^{2,3}. Even initially buoyant MP are found to deposit in sediments as a result of particle agglomeration, biofouling and degradation ⁴, which manifests in their frequent presence in sedimentary environments ^{5,6}. The distribution dynamics of MP, like other suspended solids, are governed by the physics of particle motion. The hydrodynamic regime determines the sediment grain size distribution: while finer sediment particles dominate low-energy environments, coarser ones prevail in high-energy regimes due to their higher threshold for initiating motion ^{5,7,8}. The same principles apply to the transport of MP, as evident from observed correlations in MP concentrations and sediment grain size ^{5,9–11}, yet, with an observable size shift due to the lower densities of plastics compared to natural sediment ⁵. Unlike surface or intermediate water compartments, where MP levels fluctuate spatially and temporally, making unambiguous trend analyses difficult, sediments provide a more stable and integrated record of the temporal evolution and spatial extent of plastic pollution ^{12–16}.

In systems of uninterrupted hydrodynamic connectivity and sufficient steady state with respect to distribution and sorting processes, granulometric normalization is an effective tool for studying sedimentary MP pollution levels ⁵. It helps in evaluating the influence of the hydrodynamic regime or in performing source and sink analyses. If the hydrodynamic connectivity can be assumed to be sufficient, the MP distribution could readily be predicted based on a granulometric proxy ⁵. However, for many environmental settings, this connectivity assumption does not hold. The local interplay between MP inputs, hydrodynamic forcing, geomorphological peculiarities, and spatial extent of the studied system may reveal spatio-temporal discontinuities in the granulometric normalized MP concentrations.

Reliably quantifying MP is crucial for assessing risk and changes in biogeochemical cycles ^{17–19}. While worldwide geological records show MP increasing in sediments since the 1950s ^{20–22}, we still lack fundamental understanding of the mechanisms driving their distribution ^{23,24}, and reliable quantification of MP inventories remains elusive. Indeed, sediments are among the least studied compartments for MP pollution ^{25,26} since quantifying this heterogeneous synthetic, polymeric material group ²⁷ embedded within diverse sediment matrices is highly demanding. Despite MP-analytical methods improving in efficiency, their laborious nature restricts exhaustive measurement campaigns resulting in overall small datasets, especially if the full spectrum of MP sizes, shapes and polymers is covered ⁵. Data scarcity spawns an incentive for MP distribution modeling, but it is challenged by the large material diversity and a lack of data analytical standards.

Given these challenges, hydrodynamic numerical models (HNMs) offer a promising approach to predicting sedimentary MP distributions and inventories by simulating particle transport dynamics directly. However, the accuracy of HNMs relies heavily on precise parameterization

of numerous complex processes, many of which remain incompletely understood ^{23,28,29}. Variables such as MP particle properties (e.g., shape, density, biofouling, degradation state) and environmental factors (such as sediment composition and biotic activity), require empirical data specific to MP for accurate representation. Additionally, directly transferring knowledge from sediment transport models to MP dynamics has notable limitations ^{23,24}. Sediment dynamics, despite extensively researched, continues to be acknowledged one of the least understood areas within Earth science ³⁰, which pertains all the more to models where MP is added to the equation. Consequently, while HNMs exhibit strong theoretical foundations, their ability to reliably simulate MP distributions is often constrained by necessary assumptions and simplifications. Furthermore, model generalizability remains limited, as parameterizations and process equations usually cannot be directly applied from one environmental setting to another without significant adjustments ²⁸.

For specific cases, state-of-the-art HNMs have helped to gain valuable first principle estimates of plastic pollution at ocean basin or global scales ^{18,31–33}. Others have provided detailed local insights based on hydro-numeric simulations of select key systems ^{34,35}. However, there is a lack of models for predicting MP distribution at regional scales, especially for systems of high geomorphological and hydrodynamic heterogeneity such as estuarine sediments. These ecosystems at the fluvial-marine interface, which typically represent bottlenecks for MP of terrestrial origin, and which are often affected by high anthropogenic activity, are ideal monitoring sites to study the evolution of (micro)plastic pollution. Hence, there is a clear need to model the regional-scale distribution pattern of MP and determine their inventories in these key indicator ecosystems. Empirical predictive modeling (EPM), relying on multivariate regression, can be harnessed in combination with selected techniques from modern machine learning (ML) methodology to provide a data-driven model and validation framework that can be applied to a wide range of systems. EPM facilitates a description of variable relations despite limited knowledge of the many underlying subprocesses involved by leveraging several easier-to-obtain covariates as predictors. EPM is often employed in water quality assessments ²⁸.

Here we report the development of NIXVEGS (Nested Iterative (stratified) X-Validation-to-Ensemble-modeling through Grid Search): an open-source empirical spatial prediction tool using ML techniques to determine MP abundances in complex sedimentary ecosystems. NIXVEGS encompasses the complete ML pipeline for model selection, evaluation and prediction (SI, Fig. S4). The model founds on the hydrodynamic equivalence principle between MP and sediment grains. It is an integral part of a data analysis workflow starting with data preparation (querying MP data from the database MPDB ³⁶, blind corrections and augmentation from external data sources) and concluding with geospatial interpolations and inventory estimation, all implemented as reproducibly executable Jupyter notebooks (see overview Fig. 1).

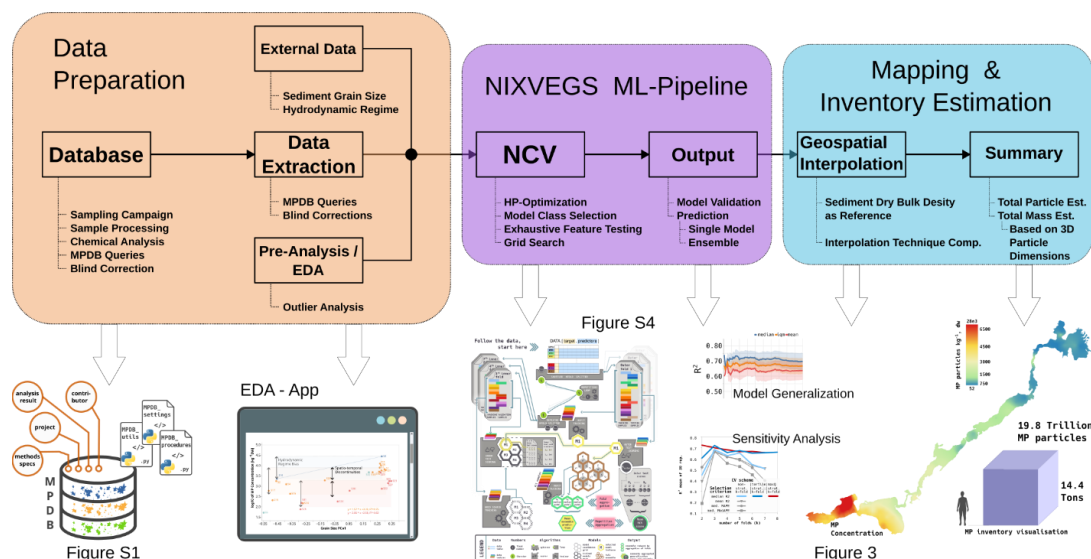


Figure 1. Overview of data analysis pipeline for prediction of the MP legacy in sedimentary systems. Insight into all underlying MP and sediment data is provided in the accompanying web application for exploratory data analysis ([EDA app](#)).

The model was established and validated on a MP dataset of 26 sediment samples in a field measurement campaign in spring 2018, taken along the 42 km long Schlei, and investigated using spectroscopic, geological and geo-chemical analyses (Fig. 2 A). The Schlei is influenced by the annual discharge of about 250 million m³ of freshwater from several tributaries and by wind-driven inflow of brackish water through its open connection to the non-tidal Baltic Sea, resulting in a slight estuarine circulation. The Schlei combines several aspects of a complex geomorphological and hydrodynamic setup, and has a high societal and ecosystemic value. It has moreover been impacted by a major source of MP pollution, with meso- and microplastic snippets, leftovers from shredded, packaged food used in the biogas plant in the city of Schleswig, which entered the Schlei waterbody via the local waste water treatment plant (WWTP). Local newspapers published estimates of several tons supposedly being released over the course of 2-3 years³⁷. A reliable model of MP pollution distribution could have supported knowledge-based decisions and effective regulatory interventions, but was lacking at the time of discovery of the pollution event.

NIXVEGS – a ML tool chain for empirical MP modeling

ML is now rapidly developing in the field of earth science³⁸ and has also been adopted in several areas of MP research, such as pollution level classification, spectral noise reduction, or polymer type and image classification^{39–42}. Regarding MP concentration regression, however, there is no protocol available to yield local predictions or geospatial interpolations thereof⁴³.

NIXVEGS addresses this gap and accounts for the typical properties and requirements of regional MP prediction. Most ML use cases involve datasets with several orders more

observations than the typically small MP environmental datasets, making it challenging for ML to achieve high predictive power while performing stably under rigorous testing. NIXVEGS encompasses several key elements including model configuration grid search, nested cross-validation (NCV) with adjustable stratification, and ensembling for predictive stability. While each of these methods have individually been described previously, NIXVEGS combines and balances these elements in a novel manner to compensate difficulties arising from modeling with small datasets. With NCV being at the core of NIXVEGS, it safeguards against overfitting not only in the actual model training, but also in selection of predictor variables, model algorithms, and hyperparameters. For NIXVEGS' other core components (i.e., grid search, stratified k-fold cross-validation [CV], regression algorithms, predictions) we rely on functionalities implemented in the widely recognized ML libraries *sci-kit-learn* and *xgboost* ^{44,45}. How these components are linked together is described in the supplementary information (SI, Fig. S4).

NIXVEGS uses sediment grain size proxy variables as predictors describing the similarities in the hydrodynamic deposition behavior between MP and natural particles. Where areas are hydrodynamically well-connected, correlations of MP abundance with certain sediment grain size fractions are clearly evident ⁵. However, if present, spatio-temporal discontinuities need to be accounted for by the EPM to effectively model the system's MP distribution, which is addressed by NIXVEGS. With this model framework we aim to provide the tools needed to generate realistic MP distribution maps, allowing us to estimate a sedimentary MP inventory for an entire geomorphological region.

Methods

We summarized the methodological steps crucial for the core of our analysis and model approach. Further details and reasoning for certain methodological choices are provided in a more comprehensive version of the methods section in the SI.

Sample collection

Sediment was collected at a total of 32 stations from May 14 – 16, 2018, using a Van Veen grab from aboard a ship (Klaashahn, IOW) in a transect from the Inner Schlei to the Baltic Sea opening ⁴⁶. The deliberate choice of the sampling locations aimed to balance grain size coverage (by consulting grain size maps of the Schlei ⁴⁶), spatial coverage (covering the entire extent and depths) and usage coverage (i.e., regions of more pristine and more anthropogenic character). After carefully opening the grab, the top 5 cm of sediment were transferred into a MP-free cleaned glass jars (one per sampling location and additionally also one sample of the 10-15 cm layer at S1, S2, S4, S10) and stored dark at 4°C. Of the 32 stations, 28 samples were later analyzed for MP, two only for sediment properties, and two were lost.

We used data on sediment properties from a second sample set, collected at 183 stations by an earlier sediment survey on courtesy of Kiel University. Information on sampling and analysis of this subset of data can be found in ⁴⁶. Principal procedural steps were comparable between the two studies. A van Veen grab was used to obtain 161 samples, whereas the 22

samples were taken using a gravity corer. For each core sample, sediment grain size measurements from the upper 5 cm were averaged for comparability to the grab samples.

MP sample preparation

The detailed MP extraction protocols, method validation and contamination prevention measures are documented in a separate method article ⁴⁷. We here report the essential procedural steps and refer to respective protocol modules (m1 – m6) as part of the modular decision tree (see Fig. 2 in ⁴⁷) as they are identical as described in these published protocols. Samples were freeze dried (m1), homogenized (m2) and defined dry masses (160 g on average) transferred into a density separation using sodium polytungstate (1.8 g cm^{-3} , m5). The application of the conical spiral conveyor (see Fig. 3 in ⁴⁷) in a customized glass separation funnel under addition of a few droplets of hydrogen peroxide allowed a gentle release and separation of lighter particles. Density and pH (3 – 3.4) were checked regularly and readjusted if necessary. Remaining organic constituents in the filtered supernatant were reduced by applying 30% hydrogen peroxide (m4.1). Samples were then filtered in the analytical laboratory (IPF Dresden) onto silicon filters with $\sim 50 \text{ }\mu\text{m}$ pore size using a custom-built glass filtration device ⁴⁸ under a laminar flow cabinet (Telstar Aeolus V3) ⁴⁹.

Larger MP suspects ($> 1 \text{ mm}$) were individually picked and rinsed. In cases of particle overloading, stacked sieve filtration was applied (m6). Blanks covering the entire MP extraction (using an MP free sediment matrix, $n = 8$) and spectroscopic analysis pipeline (one per sample) were prepared to account for own MP contamination.

Spectroscopic analysis

MP particles on the Si-filters were identified and quantified via particle analysis combined with Raman μ -spectroscopy using the GEPARD software ^{48,50}. On a WITec alpha 300R microscope (Oxford Instruments Group), using a 20x objective with a 532 nm excitation, Raman spectra were acquired as 5 accumulated scans of 5 mW and 0.5 s integration. Larger particles were individually measured with Raman spectroscopy (WITec alpha 300R, Renishaw inVia Qontor) or ATR-FTIR spectroscopy (Bruker ATR microscope Hyperion 2000, coupled to a FTIR spectrometer Vertex 70) ⁵¹.

Geological and geochemical analysis

On homogenized and freeze-dried subsamples, deprived of organic matter by 30% H_2O_2 , grain size distribution was analyzed in two replicates per sample using a Mastersizer 3000 (Malvern Panalytical) in wet dispersion mode with 10 s initial ultrasonication. Five consecutive measurements were performed and averaged for statistical analysis. Grain size data were exported in log scale in 116 histogram intervals.

TOC was calculated as averages of duplicates by subtraction of the total inorganic carbon (TIC) from the total carbon (TC). TIC and TC (TN, TS) determination was conducted on lyophilized, homogenized and ground sample material using the elemental analyzers multi-EA 4000 (Analytik Jena) and Euro-Vector EA (Hekatech).

The size distribution of organic matter was determined based on homogenized subsamples (5 – 40 g dry weight [dw]). The centrifuged supernatant of a density separation (sodium

polytungstate 1.8 g cm^{-3})⁵² was pipetted to a beaker. This process was repeated up to 10 times to ensure complete separation of the light fraction. Samples were filtered onto a $0.4 \mu\text{m}$ filter using MilliQ water⁵³, rinsed off and size analyzed using the laser-sizer Mastersizer 3000 in wet dispersion.

Data analysis and modeling summary

Reproducibly executable jupyter notebooks and python scripts (overview Fig. S1) were used to develop empirical and geospatial models and are available at <https://github.com/robna/MPSchleiSediments> under GNUv3 open-source license. This also includes a web app for exploratory data analysis ([EDA app](#)). More details and rationales on the development of the modeling pipeline are provided in the SI.

Response variable

We used the total particle- and mass-based MP abundances per kg sediment dw (*Concentration* (Fig. S2), *MassConcentration*, see [EDA app](#): sample domain data) as response variables for predictive modeling and spatial interpolation.

Database

MPDB, a MP-specific database³⁶ for FAIR-data compliant⁵⁴, particle-based analysis workflows (findable via the [IOW-META database](#)), was used to store MP related particle-, spectroscopic- and metadata (Fig. S1). The [MPDB notebook](#) contains the necessary functions to query the relevant entries from the MPDB. This includes the procedures of aggregating the particle-based raw data into sample-based data, according to the principles described in³⁶. All relevant information that was extracted from the MPDB for the model development can also be seen in the [EDA app](#).

Blank correction was done by matching MP phenotypes between environmental and blank samples (see also SI and³⁶ under 3.4. Data sanitation - Phenotyping and Blank Subtraction). In short, MP particle phenotypes were characterized by having the same sample, polymer type, shape and color properties.

Particle size, volume and mass and approximation

We advanced and validated (based on > 100 manual particle height measurements) the particle height determination algorithm in GEPARD to enable an accurate determination of all three spatial dimensions needed for more accurate conversion to volume, hence, mass-based data. The relevant changes can be comprehended in the [GEPARD repository](#).

Volumes of irregular shaped particles V_{irr} were calculated as ellipsoids based on particle length l , width w and height h , according to [Eq. 1](#). Fibers were approximated as cylindrical volumes V_{fib} ([Eq. 2](#)).

$$V_{irr} = \frac{\pi l w h}{6} \quad (1)$$

$$V_{fib} = \frac{\pi l w^2}{4} \quad (2)$$

7

Particle volumes were then multiplied by the density of the identified polymer type to yield particle masses (see “densities” in [settings.py](#) for used values).

Predictor variables

Predictors in the context of this study are vectors of non-MP related properties with values for each station (see SI for further details on their composition).

Geographic features

Depth, the water depth in meters at measured a sample’s location. In lack of measured depths in the prediction dataset, depth values were sampled from a bathymetry map (digital elevation model [DEM], 5 m grid, provided on courtesy of the BAW, based on comprehensive bathymetric echosounder and multibeam echosounder measurements, for details on validation see SI, Fig. S3). *Dist_Land* is measured as the shortest distance in meters between a sample’s location and the shoreline.

Sediment grain size properties

Grain size variables were generated using GRADISTAT⁵⁵ on the log-scaled binned volume-based grain size distributions. Median grain size in μm (*SED_D50*) and the percentage below $63 \mu\text{m}$ (*perc_MUD*) was used. In addition, a 2D representation of grain size was calculated and used as predictor variables (*PCo1*, *PCo2*). They were created from a principal coordinate analysis (*PCoA*) using Bray-Curtis dissimilarity⁵⁶ as a distance measure.

Samples with missing data in either in *TOC* ($n = 26$) or the grain size variables *SED_D50*, *perc_MUD*, *PCo1* and *PCo2* ($n = 11$) were imputed by regressions as described in the SI (also including explanations for the choice of specific granulometric proxies).

Spatio-temporal discontinuity

A numeric model⁵⁷, based on the unstructured finite volume code UnTRIM (Unstructured Tidal Residual Mudflat model⁵⁸), was used to simulate the hydrodynamic behavior of the Schlei. Simulated spherical drifters (300, 100, 50, 18 and $0 \mu\text{m}$ radius, 1.113 kg/m^3) were released for three different periods (2017-06-01 to 2017-08-01, 2017-10-15 to 2017-12-15, 2018-04-01 to 2018-06-01). They were traced forward⁵⁹ originating from $54^\circ 31' 31.499''\text{N}$, $9^\circ 36' 11.582''\text{E}$, a point at shore near the location of the highest granulometric normalized MP particle concentrations at S8 and S10 (see also [Fig. 3 D](#)). The resulting tracer paths were used to infer knowledge about how the tracers had moved through the system in respect to the sampling locations in four different implementations (see Table S1). Six variables (*Disco1* to *Disco6*) were generated using varying settings of these implementations (see Table S2). Tracks of location, depth and time step of each tracer are provided in the [data sources](#).

ML pipeline

Through NIXVEGS (implemented in a [jupyter notebook](#), [Fig. 1](#), [Fig. S4](#)) we create a model which has predictive capabilities for estimating the response variable *Concentration* for samples in the prediction set. Theoretically it is founded on the principles of cross-validation (CV)⁶⁰, or, more specifically, nested-cross-validation (NCV)⁶¹, and grid-search (GS), i.e., the

exhaustive model optimization on a given parameter space. NIXVEGS is structurally similar to the NCV proposed by ⁶², but extends the concept by adaptations specifically addressing the problems and needs arising under small dataset conditions.

NIXVEGS' adjustable components are:

1. CV scheme:
 - number of *repetitions* for the outer and inner loop
 - number of *folds* for the outer and inner CV
2. scoring scheme:
 - *selection scorer*: evaluation metric used to select a “best” model in the grid-search procedure, see Table S3
 - *inner fold aggregator* of the selection scorer: median, interquartile mean (iqm), or mean
 - *generalization scorer*: evaluation metric used as the final generalization score, see Table S3
 - *outer fold aggregator*: median, iqm, or mean
 - *repetitions aggregator*: median, iqm, or mean
3. model candidate configurations:
 - *predictor variable sets*: selection from allowed variable combinations
 - *model class*: generalized linear models (GLM), gradient boosting for linear regressors (XGBlinear), gradient boosting for tree regressors (XGBtree), random forests (RF)
 - *model hyperparameter values*: depending on model class

Model algorithms

The tested model algorithms included two from the linear family. A GLM has previously been used to model MP concentrations, based on granulometric proxies ⁵. In the present study the *GLM* was implemented for a gamma distribution with a log link using the TweedieRegressor class of the [scikit-learn library](#) with power=2 and a L2 regularization parameter alpha=0. A linear gradient boosting model, here referred to as *XGBlinear*, was implemented using the XGBRegressor class from the [xgboost library](#) ⁴⁵. It was set up with hyperparameters to resemble the settings of the GLM model, however, allowing ensembles of up to 300 base estimators with the fixed hyperparameter set: booster=gblinear, objective=reg:gamma, n_estimators=300, reg_alpha=0, reg_lambda=0. Two model classes of tree-based estimators were included for comparison to the linear models. *XGBtree* was also implemented from the XGBRegressor class of the [xgboost library](#), sharing the same hyperparameters as *XGBlinear*, but using booster=gbtrees. Additional decision-tree-related hyperparameters were varied and optimized within NIXVEGS based on the following allowed values: tree_method=exact, learning_rate=[0.1, 0.25], max_depth=[2, 3], min_child_weight=[5, 7]. A *RF* model ⁶³, implemented using the RandomForestRegressor class of the [scikit-learn library](#), was allowed to vary in the following hyperparameters: n_estimators=[10, 100, 300], max_depth=[None, 2, 4], max_features=[None, 1/3]. All non-mentioned hyperparameters were left at their default values.

Model composition

After consolidation of the sample set, 26 samples were found usable for the modeling dataset, 187 for the prediction dataset.

A set of 12 predictor variables was available for the automated feature selection inside NIXVEGS:

- **granulometric proxies:** *in situ* measured *SED_D50*, *perc_MUD* and the computed variable *PCo1* as descriptors of the sediment grain size, and hence, the hydrodynamic regime. *PCo2* was included for representing other, more oblique sediment characteristics.
- **discontinuity variables:** *Disco1* to *Disco6* generated from hydrodynamic tracer simulations (see SI). Parameter variations concerning passive or advective transport, seasonal coverage of the simulation time, sedimentation behavior and influence radius are described in SI
- **geographic properties:** water *Depth* and *Dist_Land* (distance to closest point at shore) were accepted as relevant geographical descriptors.

The choice of which combinations of predictor variables become part of the predictive model is left to the exhaustive feature selection of the CV optimization within NIXVEGS. Limitations on allowed predictor combinations (e.g., [mutually exclusive features](#) and [model class dependent restrictions](#), see also SI) were applied to avoid collinearities and unnecessary expense of computation. This resulted in 130 and 18 distinct predictor variable sets for linear and tree-based model candidates, respectively.

Model validation

The CV and scoring schemes were chosen under consideration of the small dataset size and modeling goal. We used 100 and 10 randomized repeats, each with $k = 3$ folds splitting for the outer and inner CV loop, respectively. We used the coefficient of determination (R^2) as scorer for both, the selection and generalization scoring scheme. When the GS had trained and selected the best models, their outer test set scores were calculated and aggregated first across folds within repetitions (*outer fold aggregator*) as median, then across repetitions (*repetitions aggregator*) as mean, to obtain the final NCV generalization score.

While R^2 is the main scorer used here in model selection and to assess overall model performance, we also evaluated other statistical metrics including the Mean Squared Error (MSE), Mean Absolute Error (MAE), and Mean Absolute Percentage Error (MAPE) and, for the latter two also their median-version (MedAE and MedAPE). These metrics provide complementary perspectives on the uncertainties associated with the model predictions: R^2 normalizes the explained variance relative to the total variance, MSE, MAE and MedAE quantify the absolute deviations between observed and predicted values, whereas MAPE and MedAPE express these errors in relative terms. Table S3 details mathematical definitions and range meanings of these metrics.

Adaptation for small datasets

For validation of our model results, NIXVEGS provides the CV scores. A range of CV-related settings i.e., the number of folds k , the type of scorer and the use of a stratification scheme, were evaluated (Fig. 3 F). We tested different stratification schemes (i.e., tertile and $\frac{n}{k}$ quantile) to evaluate performance estimation more independent of the described sensitivities towards k arising from small datasets. Based on this sensitivity analysis, we use a repeated stratified k -fold CV scheme, with $k = n_{folds} = [3,3]$ drawn from $s = n_{strata} = [3,3]$, repeated $r = n_{repetitions} = [100...500,10]$ times and scored using $scorer = [R^2, R^2]$, for the outer and inner CV of NIXVEGS, respectively (Fig. 3 F). This setup results in 300 to 1500 unique aggregable splits which is approximately on par with what a leave-two- or leave-three-out scheme would achieve (325 and 2600, respectively), but with the advantage that it allows for a more balanced response variable distribution. More details of the sensitivity analysis and reasoning for the chosen CV schemes are provided in the SI.

Prediction

EPM_{ensemble}

The ensemble of models is composed of $N_{outer\ repetitions} = 100$ members. Before predicting, every ensemble member was refit on the entire set of samples. Their individual predictions were then aggregated according to the *repetitions aggregator*, for each sample.

EPM_{single}

A single-model EPM was instantiated running a non-nested grid search CV with the same CV scheme and grid previously used in the inner NCV loop, selecting a ‘best candidate’ configuration. This configuration was then fitted to all data available before prediction.

MP mass calculations

The calculation of MP mass concentration was based on the summed observed MP particle masses per sample.

MassConcentration at the prediction stations was then approximated from the predicted numeric *Concentration* via an empirical regression ($R^2 = 0.910$, Eq. 3, Fig. S5)

$$MassConcentration = 0.1451 \cdot Concentration^{1.1894} \quad (3)$$

Geospatial interpolation and inventory estimation

The predicted and observed values (together $n = 213$), were used to interpolate the response variables on a regular 10 m grid over the entire Schlei area. Three grids were independently interpolated: *Concentration*, *MassConcentration* and *SedDBD*, i.e., sediment dry bulk density. For the final numeric- and mass inventory estimation, we used the interpolation method OK (Table S4), as it resulted in the lowest leave-one-out cross-validation (LOOCV) error in a comparison of several interpolation methods ($R^2 = 0.41$, for details see SI, Table S4). Sediment dry bulk density *SedDBD* was interpolated likewise. The total MP inventory estimates $E_{inventory}$ were then calculated according to Eq. 4,

$$E_{\text{inventory}}(\text{MP}|\text{Schlei}) = \sum_{x,y} d^2 \cdot l \cdot \text{SedDBD}_{xy} \cdot \text{MPconc}_{xy} \quad (4)$$

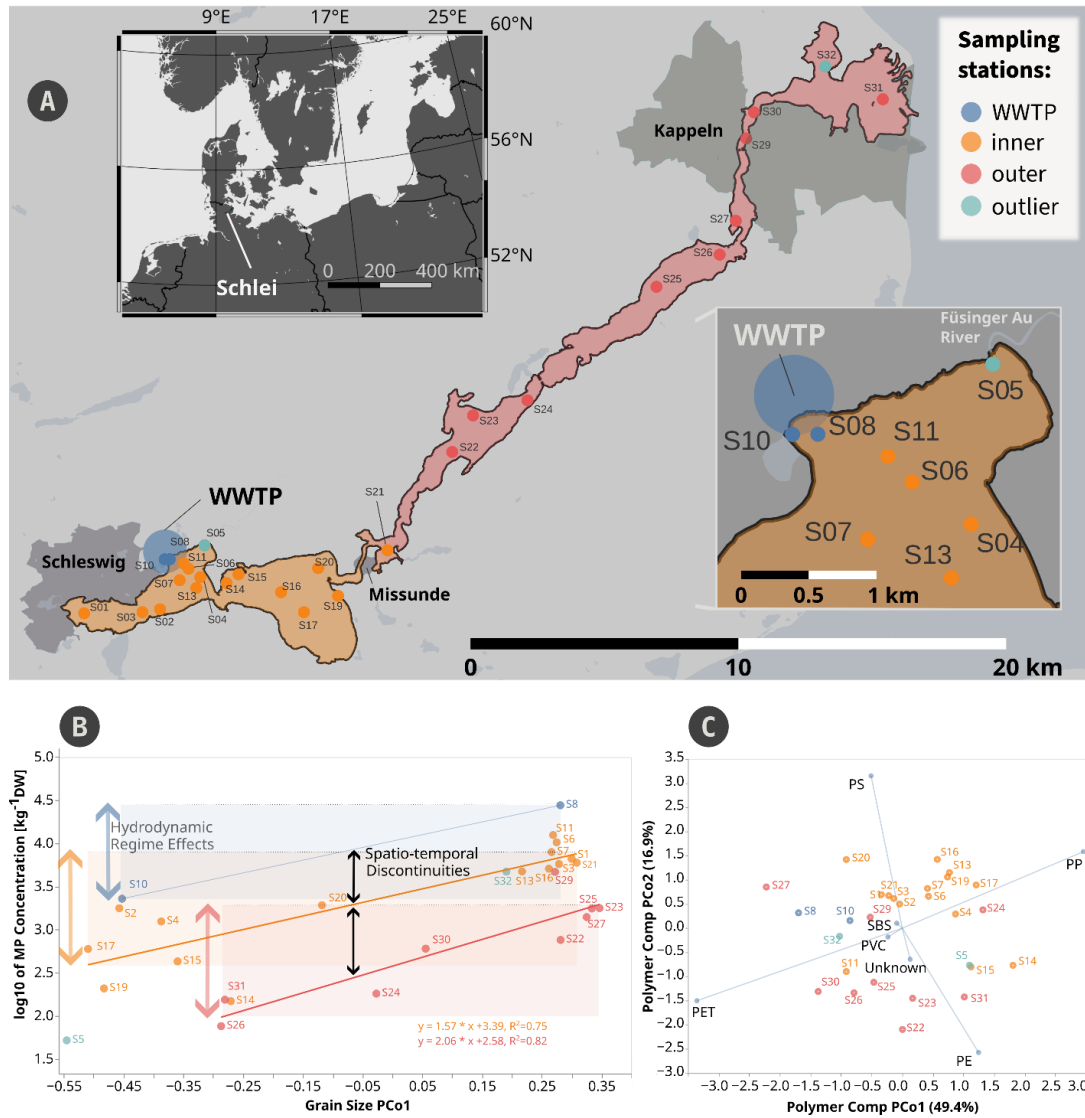
with (x, y) being the coordinate points of the MP concentration grid *MPconc* and *SedDBD*, d the grid point distance and l the relevant sediment layer thickness.

Results

MP concentrations quantified in 28 Schlei surface sediment samples in sizes 50–5000 μm range from 52 to 27610 MP kg^{-1} dw, with a mean and median at 3967 and 1771, respectively. All MP data on sample and particle level can be viewed in the accompanying [EDA app](#). Via NIXVEGS we achieve a 7.6-fold availability increase of MP data points in the Schlei ($n = 213$) and provide results of our model validation. Finally, we estimate MP concentrations on regular 10 m grid in the entire Schlei by geospatial interpolation and use the gridded data to obtain an approximate MP inventory within a sediment layer depth of 0–15 cm, relevant for the local time horizon of the plastic age.

Granulometric pre-analysis - proxy normalization reveals major discontinuities

Looking only within continuous subregions (e.g., Inner Schlei / Outer Schlei, [Fig. 2 A](#)), we see in the granulometric proxy-normalization of the MP concentrations that a significant fraction of the small-scale MP variability is explained by differences in hydrodynamic conditions ([Fig. 2 B](#)). This underscores the importance of taking local grain size distributions into consideration for planning MP sampling campaigns. If we sample only within a narrow part of the available grain size spectrum, we may inherit a substantial bias regarding the MP concentrations. This is referred to as the hydrodynamic regime bias. The following granulometric proxies, with their respective R^2 (average of Inner- and Outer Schlei) were found to be viable predictor candidates for an EPM: *PCo1*: 0.78 > *perc_MUD*: 0.76 > *SED_D50*: 0.63 > *TOC*: 0.61. This observation is in line with former study results of the well-connected Warnow estuary⁵, where comparable R^2 were found (*perc_MUD*: 0.73, *SED_D50*: 0.8). Note that reported R^2 values refer to linear correlations between \log_{10} of numeric MP concentration and the respective proxy. Discontinuities, however, result in an apparent segregation into different MP concentration levels ([Fig. 2 B](#)), that cannot be explained by the hydrodynamic regime effect. A comparison at hydrodynamic equivalence in fine-grained sediments, for instance, shows that stations S08, S03 and S22 span over two orders of magnitude.



When the MP dataset of the entire system is normalized with respect to the local hydrodynamic sorting conditions, spatio-temporal discontinuities become visible as deviations of the MP distribution pattern from the gradient of the granulometric proxy, demonstrated in [Fig. 2 B](#). While spatial and temporal discontinuities are intimately linked, for comprehensibility we consider them separately below. The Schlei sediments provide favorable conditions to study these effects as both, spatial and temporal continuity as an assumption for granulometric proxy prediction is challenged by the geomorphological and hydrodynamic complexity of this system. Spatio-temporal discontinuities are herein defined as the deviation from the ideal state of a continuous hydrodynamic connectivity of all parts of the system.

Spatial discontinuity: A major discontinuity can be observed by the segregation of proxy-normalized samples into different MP pollution levels in inner and outer Schlei samples ([Fig. 2 B](#)). A narrowing, at the village of Missunde, constitutes a major geomorphological barrier, which represents an obstacle for MP to distribute beyond at equal rate.

Temporal discontinuity: The observable singling out of station S08 and S10 as the stations of the highest grain size normalized MP concentrations ([Fig. 2 B](#)), indicated the proximity of a significant MP point source with an input rate above the system's distribution efficiency. Indeed, the point source (WWTP) of the reported pollution incident is located there at the inner Schlei basin ([Fig. 2 A](#)). Other stations close by (S11, S06 and S07, zoomed-in inset [Fig. 2 B](#)) follow this trend. MP concentrations decreasing with distance from this region of highest MP contamination, despite the absence of geomorphological barriers, point towards a temporal discontinuity.

The findings from the granulometric and discontinuity analyses are twofold. Firstly, granulometric properties reveal information on the hydrodynamic influence that also drives parts of the MP distribution processes. Hence, they are important predictive variables for our proxy-based EPM. Secondly, to adequately represent MP concentrations and reach sufficient explanatory power, the proxy-based EPM must be extended by another key class of predictor variables describing locally present spatio-temporal discontinuities in the hydrodynamic distribution efficiency.

The variability in polymer composition also reflects this spatio-temporal segregation ([Fig. 2 C](#)). The faster sinking denser polymer types as PET, PS, or PVC are proportionally more abundant near the high MP concentration areas, supporting the identification of the major source region. Less dense polymers as PP or PE can propagate further outwards, where they are more abundantly found. Interestingly, S27, a station nearby a smaller WWTP, is most like the polymer composition found at the major source region, indicating a general WWTP polymer type fingerprint.

NIXVEGS results

The path of integrating granulometric, geographic and hydrodynamic spatio-temporal discontinuity predictors to produce an interpolated MP concentration prediction of the Schlei sediments is schematically shown in [Fig. 3 A](#).

Model validation

The score of an NCV includes the evaluation of the selection process of model configurations, and is therefore an estimate of the performance (on unseen data) of the entire modeling pipeline. NCV ensures the evaluation is done on data that were not used during model training, providing a more realistic estimate of general performance. By contrast, with non-nested CV, there is no independent evaluation of the model selection, which entails the possibility of overfitting the model selection to the available data ⁶⁴. NIXVEGS achieved a generalization score of $R^2 = 0.70$ ($\sigma = 0.11$), aggregated as mean of 100 repetitions with 3 folds, aggregated as median (see Fig 3 B). Aggregating up to 500 repetitions showed no significant difference in performance. Other metrics show the model's overall error in absolute terms (~ 1000 and ~ 1700 MP particles kg^{-1} dw for MedAE and MAE, respectively) or as relative numbers ($\sim 54\%$, $\sim 110\%$). In NIXVEGS' [jupyter notebook](#), an interactive version of Fig. 3 E allows exploring the local error on a per sample basis, while an additional histogram unravels the votes cast by members of the $\text{EPM}_{\text{ensemble}}$ in relation to the original observed MP concentration for a selected station.

Model selection

NIXVEGS generates a predictive model instance by performing a non-nested grid search CV with the same CV scheme previously used in the inner NCV loop. The resulting best-performing model configuration (here: GLM of family gamma with log link and the predictor set *perc_MUD*, *Disco1*, *Depth*) is then fitted to all available data before making predictions. We refer to this as the single empirical predictive model ($\text{EPM}_{\text{single}}$), which aligns with recommendations from the NCV methodology literature for deriving a predictive model instance after obtaining a robust NCV performance estimate.

However, through NIXVEGS we also obtain an empirical predictive model ensemble ($\text{EPM}_{\text{ensemble}}$) composed of the “best candidate” configurations, refitted to all data, of the various folds and repetitions. Its aggregation resembles the procedure previously used to aggregate the generalization score. There are justifications for each type of predictive models, $\text{EPM}_{\text{single}}$ and $\text{EPM}_{\text{ensemble}}$ (details of justifications are provided in the SI). Notably, the $\text{EPM}_{\text{single}}$ predictor set coincides with the most abundantly selected predictors in the $\text{EPM}_{\text{ensemble}}$ (Fig. 3 C), indicating a good model stability with respect to the predictor selection process. The predictor variables *perc_MUD* and *PCo1* (being similar to each other, $R^2_{\text{PCo1}, \text{perc_MUD}} = 0.98$) were the most abundantly selected granulometric predictors in the different ensemble members, however, never together in a single member due to the restrictions on mutually exclusive predictors (see SI).

There was a clear preference for discontinuity predictor variables computed from the mean time that tracers travelled until their first appearance in a station's vicinity. The predominant selection of *Disco1* shows a preference for the longer time period 'allseasons'. A longer period is less sensitive to seasonal variations. The simulated drifter *Disco1* indicates that a passive tracer (i.e., no advection) is a genuine measure of the distribution efficiency through the system. This is plausible because the depositional component is already covered in the model in form of the granulometric proxy. The importance of the proxy and discontinuity predictors can also be seen when the geographic variables are excluded (NIXVEGS generalization $R^2 = 0.66$, $\sigma = 0.12$).

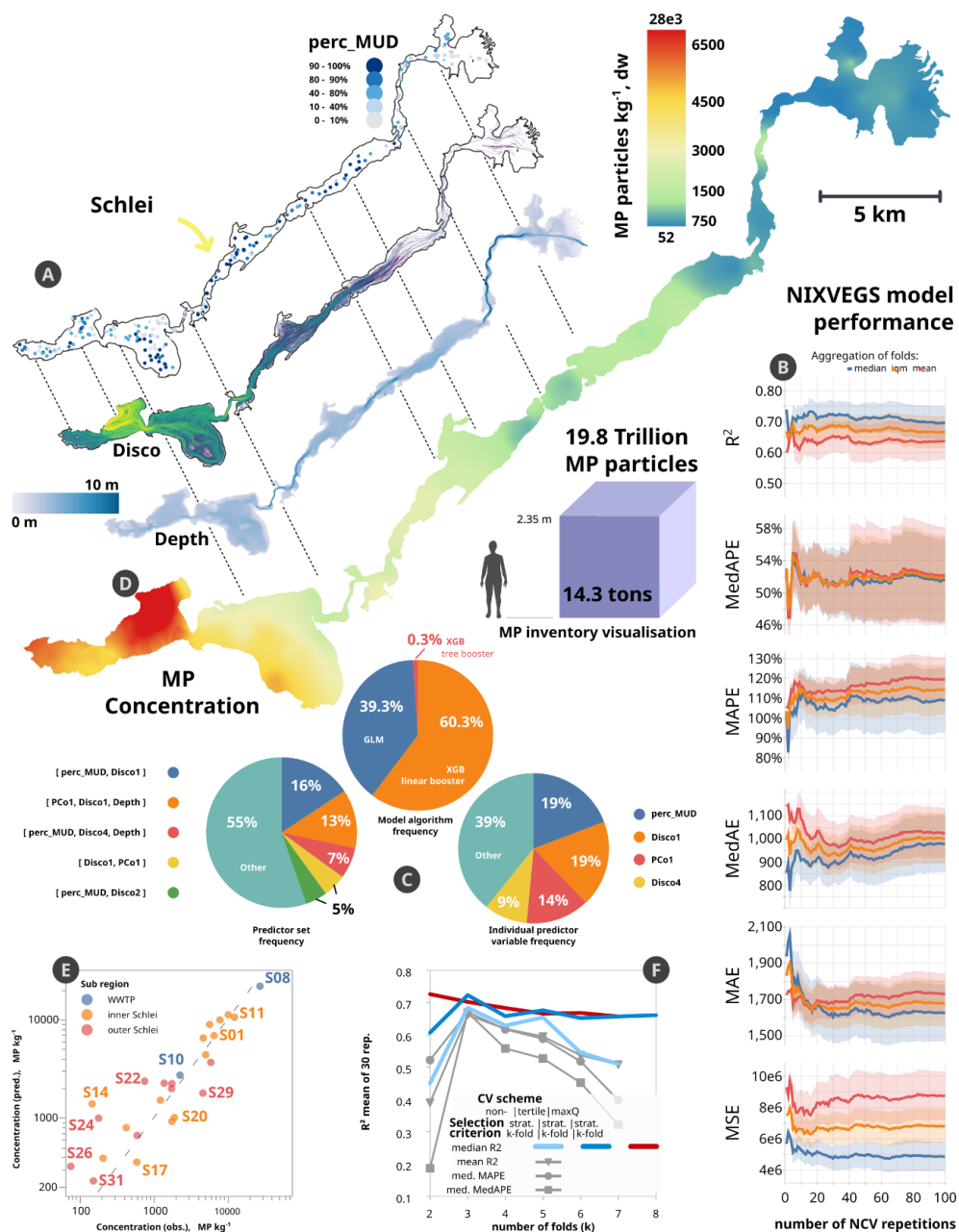


Figure 3. MP inventory estimation of the Schlei surface sediments (0-15cm). (A) The map was created based on an empirical predictive model ensemble. A NCV modeling pipeline (NIXVEGS) performed model selection including predictor choice from a range of sedimentological, hydrodynamic, and geographical variables. (B) Metrics of model performance: evolution of means of accumulating randomized repeats of the NCV showed

that a generalization performance of 0.70 (R^2 , median of folds) can be expected for unseen data. Other metrics show the error evolution in the unit of the response variable (MAE, MedAE), its square (MSE) or as relative deviation (MAPE, MedAPE). (C) The composition of the ensemble revealed that primarily model classes based on linear regressors were selected in combination with the predictors *perc_MUD* (sediment fraction < 63 μm) and *Disco1*, a tracer simulation derived variable accounting for spatio-temporal discontinuities present in the system (C). (D) Geospatial interpolation of the predicted and observed MP concentrations (213 stations) on a 10 m grid by Ordinary Kriging. Highest concentrations can be found in the inner Schlei in the vicinity of a WWTP (at the location of the letter “D”). (E) shows the prediction residuals as deviation from the identity line (dashed). (F) shows the sensitivity analysis as mean of $N_{\text{outer repetitions}} = 30$ using different cross-validation schemes: 2 to 8 folds combined with strong stratification (maxQ: quantile stratification with $\frac{n}{k}$ quantiles), medium stratification (tertile) and no stratification (the latter also in different variations of the model selection criterion: median R^2 , mean R^2 , median MAPE and median MedAPE).

In a more streamlined and less complex waterway structure, with a major water input and output, discontinuity could be simplified by determination of the shortest distance through water from the main source. However, for our dataset, replacing predictors related to spatio-temporal discontinuities (*Disco1* – 6) with a simple direct distance through water from the point of the trace release to each station, would result in a substantially lower R^2 score of 0.44. Indeed, for systems with a more complex hydrodynamic flow field such as the Schlei, major discontinuities occur that are better represented by the water’s mean traveling time. The importance of the spatio-temporal discontinuity variables corroborates the conclusions of an earlier study reviewing the relevant literature in search for a MP-sediment relationship⁵.

The two linear model algorithms (GLM, XGBlinear) vastly outperformed the tree models (XGBtree, RF) on the present regression problem (Fig. 3 C). In contrast to linear models, models using decision trees as base learners cannot predict outside the range of the response variable seen during training. The likelihood of the response extrema being excluded from the values seen during training of a particular split gets higher with decreasing size of the dataset. Tree-based models are especially strong in approximating highly-non-linear relationships and handling large predictor sets^{63,65}, neither of which apply here.

Model predictions

Given the size of the investigation area (51.2 km^2), with 213 predicted and observed stations, we reach a high-resolution picture of the inventory of ~ 4 MP stations per km^2 . Interpolated on a regular 10 m grid, MP concentrations indicate accumulations mainly in the vicinity of city of Schleswig, the WWTP, as well as the southern part of the Inner Schlei’s larger basin (“Große Breite”). The middle and outer stretches of the Schlei show 2 to 10-fold lower concentrations (Fig. 3 D).

Sensitivity analysis

The choice of the CV parameters, i.e., number of folds k , stratification scheme and model selection criterion, were based on theoretical considerations with respect to the small dataset size (see SI), aided by a sensitivity analysis of NIXVEGS' aggregated performance score towards changes in these CV parameters (Fig. 3 F). Both of the stratified schemes show a higher stability of the score for varying values of k , as compared to the non-stratified CV, signaling that a stratification is preferable to counteract the increased likelihood of drawing highly unrepresentative splits in small datasets. As the performance in stratified CV stays relatively stable for $k \geq 3$, the threefold tertile stratified CV emerges as a preferential choice allowing for robust performance evaluation while keeping computational demands low.

As the uncertainty associated with the model input is unknown (e.g., sampling, purification or measurement method uncertainties), we conducted sensitivity analyses, where we perturbed the target variable by adding 10% on all samples, or changing them $\pm 5\%$ (randomly repeated 5 times), or by excluding the most extreme value. The generalization score exhibited negligible changes, $R^2 = 0.7, 0.63 - 0.7$ and 0.72 , respectively. The inventory estimate varied only around $\pm 1.5\%$ (EPM_{ensemble}) when introducing the random variance, showing the robustness of the model.

Estimated Schlei MP inventories

Based on the upper 15 cm sediment layer, the total inventory of the Schlei is thus estimated at 19.8 trillion MP particles, equating to approximately 14.3 tons of MP. These numbers are based on the combined observed and predicted MP concentrations using the EPM_{ensemble} model. For EPM_{single} , the numbers are at 18.8 trillion MP particles and 14.3 tons, respectively. For reference and transparency, if we limit the inventory calculations strictly to the uppermost sediment layer (0–5 cm, from where most of our measured MP samples were taken), estimated MP numbers would be 6.6 and 6.3 trillion particles (~ 4.8 tons) for EPM_{ensemble} and EPM_{single} , respectively. As we argue in the discussion, however, the 15 cm layer provides a more realistic inventory approximation of the accumulated MP legacy.

To put this unimaginable number of MP into perspective, all MP in the Schlei sediments tightly compressed would form a cube with a side length of 2.35 m (Fig. 3 D). When visualized as easily graspable everyday (macro)plastic objects, it would approximate 1 thin plastic knot bag (typically used for fruits, 9 μm thick, see details in SI) per interpolation cell (10 x 10 m), roughly 5 million bags in total.

Discussion

Evidence-based decision-making in environmental management relies on sufficiently spatially resolved data⁶⁶. We demonstrate that robust EPMs of sedimentary MP distribution can be established using natural particulate and hydrodynamic proxies combined with rigorous validation techniques. Yet, a universal pre-trained model applicable to all sedimentary environments and MP compositions is neither realistic nor necessarily

desirable. Instead, EPMs offer the flexibility to adapt to regional MP levels, compositions, and the complex interactions of external factors (i.e., hydrodynamic forces, agglomeration, and biofouling) making them well-suited for targeted plastic management strategies. The developed modeling pipeline can be fed new data of other sedimentary systems, improving plastic monitoring and management in more regions at a significantly lower analytical expenditure. When planning sampling locations for modeling-ready datasets, it is important to consider both coverage of grain size variability and spatial extent. As a practical consideration, locations for labor-intensive MP-measured stations should prioritize granulometric diversity to improve normalization accuracy. Sediment-only stations, which are used as prediction points and from which more can be analyzed, should prioritize spatial coverage of the system and potential subsystems.

Mitigating systemic misestimations

Comparisons of MP pollution from several regions, as for example extensive meta-analyses⁶⁷, are often left with only average MP concentration values to establish pollution levels or inventories. In this study, sampling locations were deliberately chosen to broadly cover the available grain size spectrum. Yet, we see that simply projecting out the mean of our observed MP concentrations to estimate the system's MP inventory may yield results far from what we obtained through NIXVEGS. The average concentration of the 26 samples used to train the model lies at $3967 \text{ kg}^{-1} \text{ dw}$, approximating an inventory of 31.4 trillion MP particles, which would be an > 50% overestimation compared to NIXVEGS' mean concentration of 2499 kg^{-1} or 19.8 trillion MP. Although the means in the above comparison vary considerably, they could have been very close by chance. However, without the model we would still only have knowledge of the local MP concentration at the few observed stations, whereas with NIXVEGS we could use the available sediment data to infer the spatial distribution of MP concentrations at 213 sites in total. Until MP analyses with significantly higher sample numbers are feasible, proxy models that account for the hydrodynamic regime allow efficient MP inventory estimation and detailed pollution mapping.

Controlling validation overoptimism

Under the acronym NIXVEGS we presented a model selection and validation pipeline whose outputs are twofold: an estimate of model performance on unseen data (generalization score) and a predictive model instance. If the same model selection would be conducted inside a non-nested (i.e., ordinary) CV - be it LOOCV or another scheme - the obtained score is expected to be higher, but includes the risk of the model selection criterion to be overfitted to the available data⁶⁴. As such, NIXVEGS' nested CV score should be regarded as a conservative estimate on how good a model can be built to approximate the response variable, given a set of possible model configurations and the available data.

A non-nested CV is also run as part of NIXVEGS after the NCV score has been determined, but for a different purpose. Its score (being with $R^2 = 0.88$, as expected, higher than the NCV score) is neglected, knowing about its included bias. The resulting "best candidate" model configuration, however, is what gets utilized as the "EPM_{single}" predictive model instance.

The accompanying [EDA app](#) provides the possibility to approximate any of the available variables by a freely configurable GLM. The app's preset at loading shows the same model configuration found as NIXVEGS' "EPM_{single}". The LOOCV of this model can be seen further

down in the [EDA app](#) with an R^2 of 0.91, however, underlying the same caveat that such a score is less reliable due to the included bias.

Estuaries are key indicator environments

In a meta-analysis of various studies, we present a cross sedimentary compartment comparison normalized for the hydrodynamic regime which allows a reliable site-representative comparison of MP pollution levels ([Fig. 4](#)). We see that NIXVEGS' first principles of using granulometric proxies for spatial MP prediction may also find application in many other sedimentary environments. Yet, spatio-temporal discontinuities and multiple interfering major source inputs may be more difficult to track in the open sea, while beaches are additionally directly influenced by aerodynamic sorting processes and direct littering. Transitional systems⁶⁸ such as estuaries and fjords as well as riverine systems store some of the highest numeric MP concentrations, are closer to sources and may show changes faster in contrast to the open marine environment. While freshwater systems can reach exceptionally high pollution levels, it has been shown that they can be substantially diminished after flooding events^{26,69}, passing the MP load on to transitional systems that are usually more confined. This bottleneck effect positions estuaries as key indicator ecosystems for monitoring MP pollution, emphasizing the need for tools such as NIXVEGS to determine the MP inventory.

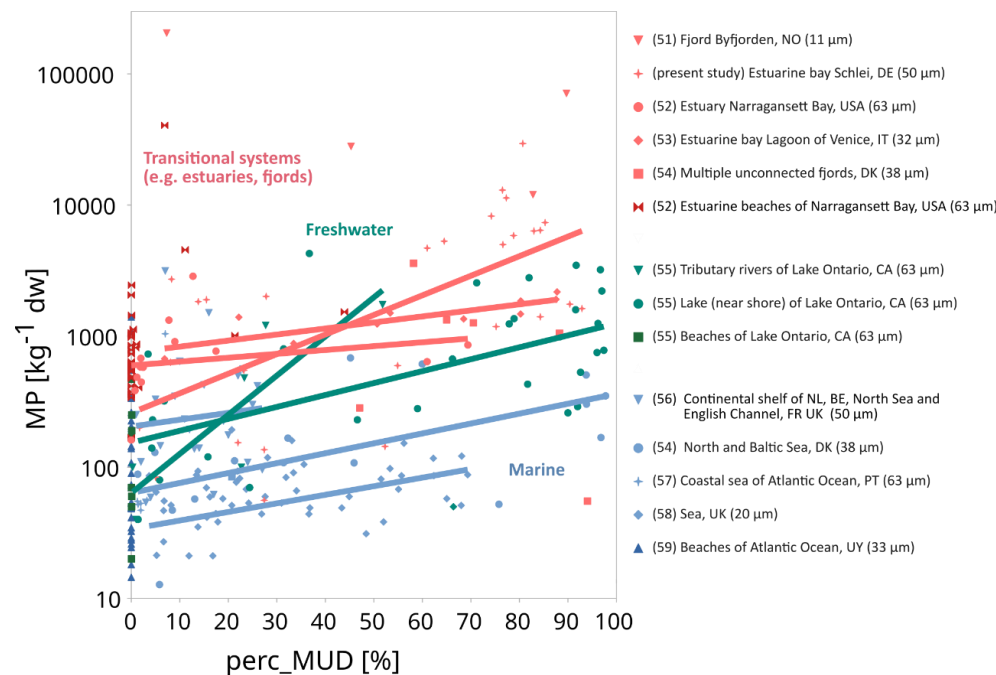


Figure 4. Meta-analysis of granulometric normalized MP concentrations of various representations of worldwide aquatic sediments^{9–11,70–75}. Transitional systems at the fluvial-marine interface (red), freshwater (rivers, lakes, and their beaches, green) and marine systems (open and coastal seas and their beaches, blue) are compared. Beaches of the

individual compartments are shown in opaque color. To allow comparability only studies with a lower size limit of $MP \leq 63 \mu m$ which reported grain size as perc_MUD (most common proxy for grain size) were included in the analysis. For studies with less than 5 stations per connected compartment or negligible variation in perc_MUD no regression line is displayed.

Limitations and uncertainties in inventory estimation and sediment layer depth

As NIXVEGS is an empirical predictive- and not a process-driven model, it estimates the state of an unknown variable based on the available input without a time component. It may be continuously re-run with new input (e.g., when a repeated monitoring campaign would provide new data) obtaining time series of MP distributions, however, it will by itself not allow a projection of the response variable's evolution into the future.

The choice of sediment depth horizon significantly influences MP inventory estimates. Here, we opted to calculate the inventory to a depth of 15 cm, based on sedimentation and granulometric data. The onset of widespread global plastic production around 1950 coincides with observations of increasing MP deposits in the sedimentary record ²⁰. Known sedimentation rates in the Schlei (2.2 mm a⁻¹, increasing up to 4.2 mm a⁻¹ pre-1980 ⁴⁶) suggest that this period corresponds roughly to the lower boundary of 10–20 cm.

To evaluate this assumption practically, we collected additional sediment samples from deeper layers (10-15 cm) at selected locations. Interestingly, MP concentrations and sediment grain sizes at these depths closely resembled those from the surface layer (0-5 cm) in sample S02 and S04, indicating vertical sediment mixing. Such mixing in the Schlei sediments foremost results from wind-driven hydrodynamic reworking and anthropogenic disturbances, both of which obscure distinct sedimentary chronologies. The intensity and depth of mixing may vary significantly throughout different locations of the Schlei. Station S10, located near the WWTP outlet showed inverse MP concentrations of 1200 and 11267 MP kg⁻¹ dw for the 0-5 cm and 10-15 cm layers, respectively.

An analysis of particle sizes (MP, organic matter, and sediment grains) demonstrated distinct patterns related to sediment type. In fine sediments, MP particle sizes were typically about one order of magnitude larger than the median sediment grain size, aligning with previous findings ⁵ as we elaborate in the SI (including Fig. S6). However, coarser sediments exhibit similar sizes of MPs and sediment grains, supporting observations of significant vertical mixing processes which trap MP intergranular. Infiltration, however, appears not to play a relevant role (for details see SI, Fig. S6). This granulometric complexity highlights the inherent difficulties in precisely defining an optimal sediment depth for MP inventory assessments.

Thus, while selecting 15 cm as a sedimentary depth horizon provides a pragmatic estimate of the MP legacy in the Schlei, we acknowledge inherent limitations. On the one hand, the limited number of deeper samples (10-15 cm) introduces uncertainties about sediment mixing intensity across the entire Schlei estuary. On the other hand, due to strong local differences in mixing, MP inventories could extend even deeper, implying that our reported

MP inventories may represent conservative estimates. Therefore, the presented inventory estimate based on a 0-15 cm sediment layer constitutes a workable approximation, balancing practical feasibility, empirical evidence, and historical context. Future studies focusing explicitly on deeper sediment sampling and higher vertically resolved profile analyses would help refine sedimentary MP inventories and provide stronger constraints on the vertical distribution of MPs.

Conclusion

Limited data availability remains a key challenge in accurately quantifying sedimentary MP. By using sediment properties as proxy variables, the predictive modeling approach presented here significantly improves the spatial data coverage of MP concentration estimates without requiring extensive direct MP analyses. For future studies, sampling strategies that combine a few MP-measured sites strategically chosen to represent local sedimentological diversity with numerous sediment-only samples targeted to maximize spatial coverage, can significantly reduce systemic uncertainties and enable the quantification of regional MP inventories. This combined methodological approach, presented as a fully open-source pipeline NIXVEGS, facilitates robust MP assessments, supports targeted management strategies, ultimately advancing our understanding of the role sedimentary environments play in the global MP budget.

Acknowledgments

We are grateful to the IOW workshop team for the operation of boat Klaashahn and technical customizations in the laboratory, municipal and port authorities for facilitation of the sampling campaign, Karl Walther (schleiinfozentrum.de) for local Schlei expertise, Svenja Papenmeier, Mischa Schönke, Peter Feldens and Helge Arz for access and knowledge exchange on grain size analysis, Thomas Leipe and Ines Scherff for assistance with Hg, TIC and CSN analysis, Julian Decker and Linnea Dawo for lab assistance, Franziska Klaeger for project coordination, Julia Lötsch, Anne Rödiger and Melinda Arnold for Raman analysis, Elisavet Kanaki, Robert Ohnmacht and Josef Brandt for assistance on the improvements of the GEPARD code, Christiane Hassenrück and Theodor Sperlea for helpful ML knowledge exchange and Sonja Oberbeckmann for project management.

Funding: M.L. and D.F. were supported by the German BMBF research program “Plastics in the environment”: MicroCatch_Balt “Investigation of Sinks and Sources of Microplastics from a Typical Catchment Area to the Open Baltic Sea”, grant number 03F0788A. D.F. and M.L. were supported by the EU-BONUS Programme “Blue Baltic”: MICROPOLL “Multilevel assessment of microplastics and associated pollutants in the Baltic Sea”, grant number 03F0775A

Author contributions: Conceptualization: K.E., R.L., M.L. - Funding: D.F., M.L. - Method development: K.E., R.L. - Data acquisition and analysis: K.E., R.L., F.F., K.S. - Interpretation and modeling (NIXVEGS): R.L., K.E. - Modeling (PARTRACE, UnTRIM): G.S. - Writing: All authors contributed to writing the manuscript.

Competing interests: The authors declare no competing interests.

Data and materials availability:

Supplementary Information file

EDA app (<https://robna.github.io/MPSchleiSediments>)

Code repository (<https://github.com/robna/MPSchleiSediments/>)

References

- (1) van Sebille, E.; Aliani, S.; Law, K. L.; Maximenko, N.; Alsina, J. M.; Bagaev, A.; Bergmann, M.; Chapron, B.; Chubarenko, I.; C  zar, A.; Delandmeter, P.; Egger, M.; Fox-Kemper, B.; Garaba, S. P.; Goddijn-Murphy, L.; Hardesty, B. D.; Hoffman, M. J.; Isobe, A.; Jongedijk, C. E.; Kaandorp, M. L. A.; Khatmullina, L.; Koelmans, A. A.; Kukulka, T.; Laufk  tter, C.; Lebreton, L.; Lobelle, D.; Maes, C.; Martinez-Vicente, V.; Morales Maqueda, M. A.; Poulain-Zarcos, M.; Rodr  guez, E.; Ryan, P. G.; Shanks, A. L.; Shim, W. J.; Suaria, G.; Thiel, M.; van den Bremer, T. S.; Wichmann, D. The Physical Oceanography of the Transport of Floating Marine Debris. *Environmental Research Letters* **2020**, *15* (2), 023003. <https://doi.org/10.1088/1748-9326/ab6d7d>.
- (2) Bagaev, A.; Mizyuk, A.; Khatmullina, L.; Isachenko, I.; Chubarenko, I. Anthropogenic Fibres in the Baltic Sea Water Column: Field Data, Laboratory and Numerical Testing of Their Motion. *Science of The Total Environment* **2017**, *599–600*, 560–571. <https://doi.org/10.1016/j.scitotenv.2017.04.185>.
- (3) Canals, M.; Pham, C. K.; Bergmann, M.; Gutow, L.; Hanke, G.; van Sebille, E.; Angiolillo, M.; Buhl-Mortensen, L.; Cau, A.; Ioakeimidis, C.; Kammann, U.; Lundsten, L.; Papatheodorou, G.; Purser, A.; Sanchez-Vidal, A.; Schulz, M.; Vinci, M.; Chiba, S.; Galgani, F.; Langenk  mper, D.; M  ller, T.; Nattkemper, T. W.; Ruiz, M.; Suikkanen, S.; Woodall, L.; Fakiris, E.; Molina Jack, M. E.; Giorgetti, A. The Quest for Seafloor Macrolitter: A Critical Review of Background Knowledge, Current Methods and Future Prospects. *Environmental Research Letters* **2021**. <https://doi.org/10.1088/1748-9326/abc6d4>.
- (4) Koelmans, A. A.; Kooi, M.; Law, K. L.; van Sebille, E. All Is Not Lost: Deriving a Top-down Mass Budget of Plastic at Sea. *Environmental Research Letters* **2017**, *12* (11), 114028. <https://doi.org/10.1088/1748-9326/aa9500>.
- (5) Enders, K.; K  ppler, A.; Bini  sch, O.; Feldens, P.; Stollberg, N.; Lange, X.; Fischer, D.; Eichhorn, K.-J.; Pollehne, F.; Oberbeckmann, S.; Labrenz, M. Tracing Microplastics in Aquatic Environments Based on Sediment Analogies. *Scientific Reports* **2019**, *9* (1), 15207. <https://doi.org/10.1038/s41598-019-50508-2>.
- (6) Klein, S.; Worch, E.; Knepper, T. P. Occurrence and Spatial Distribution of Microplastics in River Shore Sediments of the Rhine-Main Area in Germany. *Environmental Science & Technology* **2015**, *49* (10), 6070–6076. <https://doi.org/10.1021/acs.est.5b00492>.
- (7) Kersten, M.; Smedes, F. Normalization Procedures for Sediment Contaminants in Spatial and Temporal Trend Monitoring. *Journal of Environmental Monitoring* **2002**, *4* (1), 109–115. <https://doi.org/10.1039/b108102k>.
- (8) Soulsby, R. *Dynamics of Marine Sands: A Manual for Practical Applications*; Telford: London, 1997.
- (9) Strand, J.; Lassen, P.; Shashoua, Y.; Andersen, J. H. Microplastic Particles in Sediments from Danish Waters.
- (10) Vianello, A.; Boldrin, A.; Guerriero, P.; Moschino, V.; Rella, R.; Sturaro, A.; Da Ros, L. Microplastic Particles in Sediments of Lagoon of Venice, Italy: First Observations on

- Occurrence, Spatial Patterns and Identification. *Estuarine, Coastal and Shelf Science* **2013**, *130*, 54–61. <https://doi.org/10.1016/j.ecss.2013.03.022>.
- (11) Ballent, A.; Corcoran, P. L.; Madden, O.; Helm, P. A.; Longstaffe, F. J. Sources and Sinks of Microplastics in Canadian Lake Ontario Nearshore, Tributary and Beach Sediments. *Marine Pollution Bulletin* **2016**, *110* (1), 383–395. <https://doi.org/10.1016/j.marpolbul.2016.06.037>.
 - (12) Thompson, R. C.; Olsen, Y.; Mitchell, R. P.; Davis, A.; Rowland, S. J.; John, A. W. G.; McGonigle, D.; Russell, A. E. Lost at Sea: Where Is All the Plastic? *Science* **2004**, *304* (5672), 838–838. <https://doi.org/10.1126/science.1094559>.
 - (13) Eriksen, M.; Cowger, W.; Erdle, L. M.; Coffin, S.; Villarrubia-Gómez, P.; Moore, C. J.; Carpenter, E. J.; Day, R. H.; Thiel, M.; Wilcox, C. A Growing Plastic Smog, Now Estimated to Be over 170 Trillion Plastic Particles Afloat in the World's Oceans—Urgent Solutions Required. *PLOS ONE* **2023**, *18* (3), e0281596. <https://doi.org/10.1371/journal.pone.0281596>.
 - (14) Law, K. L.; Morét-Ferguson, S.; Maximenko, N. A.; Proskurowski, G.; Peacock, E. E.; Hafner, J.; Reddy, C. M. Plastic Accumulation in the North Atlantic Subtropical Gyre. *Science* **2010**, *329* (5996), 1185–1188. <https://doi.org/10.1126/science.1192321>.
 - (15) Beer, S.; Garm, A.; Huwer, B.; Dierking, J.; Nielsen, T. G. No Increase in Marine Microplastic Concentration over the Last Three Decades – A Case Study from the Baltic Sea. *Science of The Total Environment* **2018**, *621*, 1272–1279. <https://doi.org/10.1016/j.scitotenv.2017.10.101>.
 - (16) Galgani, F.; Brien, A. S.; Weis, J.; Ioakeimidis, C.; Schuyler, Q.; Makarenko, I.; Griffiths, H.; Bondareff, J.; Vethaak, D.; Deidun, A.; Sobral, P.; Topouzelis, K.; Vlahos, P.; Lana, F.; Hasselov, M.; Gerigny, O.; Arsonina, B.; Ambulkar, A.; Azzaro, M.; Bebianno, M. J. Are Litter, Plastic and Microplastic Quantities Increasing in the Ocean? *Microplastics and Nanoplastics* **2021**, *1* (1), 2. <https://doi.org/10.1186/s43591-020-00002-8>.
 - (17) Stubbins, A.; Law, K. L.; Muñoz, S. E.; Bianchi, T. S.; Zhu, L. Plastics in the Earth System. *Science* **2021**, *373* (6550), 51–55. <https://doi.org/10.1126/science.abb0354>.
 - (18) Lebreton, L. C. M.; Van Der Zwet, J.; Damsteeg, J.-W.; Slat, B.; Andrady, A.; Reisser, J. River Plastic Emissions to the World's Oceans. *Nat Commun* **2017**, *8* (1), 15611. <https://doi.org/10.1038/ncomms15611>.
 - (19) Koelmans, A. A.; Redondo-Hasselerharm, P. E.; Nor, N. H. M.; de Ruijter, V. N.; Mintenig, S. M.; Kooi, M. Risk Assessment of Microplastic Particles. *Nature Reviews Materials* **2022**, *7* (2), 138–152. <https://doi.org/10.1038/s41578-021-00411-y>.
 - (20) Brandon, J. A.; Jones, W.; Ohman, M. D. Multidecadal Increase in Plastic Particles in Coastal Ocean Sediments. *Science Advances* **2019**, *5* (9), eaax0587. <https://doi.org/10.1126/sciadv.aax0587>.
 - (21) Dong, M.; Luo, Z.; Jiang, Q.; Xing, X.; Zhang, Q.; Sun, Y. The Rapid Increases in Microplastics in Urban Lake Sediments. *Scientific Reports* **2020**, *10* (1), 848. <https://doi.org/10.1038/s41598-020-57933-8>.
 - (22) Turner, S.; Horton, A. A.; Rose, N. L.; Hall, C. A Temporal Sediment Record of Microplastics in an Urban Lake, London, UK. *Journal of Paleolimnology* **2019**, *61* (4), 449–462. <https://doi.org/10.1007/s10933-019-00071-7>.
 - (23) Khatmullina, L.; Chubarenko, I. Transport of Marine Microplastic Particles: Why Is It so Difficult to Predict? *Anthropocene Coasts* **2019**, *2* (1), 293–305. <https://doi.org/10.1139/anc-2018-0024>.

- (24) Waldschläger, K.; Brückner, M. Z. M.; Carney Almroth, B.; Hackney, C. R.; Adyel, T. M.; Alimi, O. S.; Belontz, S. L.; Cowger, W.; Doyle, D.; Gray, A.; Kane, I.; Kooi, M.; Kramer, M.; Lechthaler, S.; Michie, L.; Nordam, T.; Pohl, F.; Russell, C.; Thit, A.; Umar, W.; Valero, D.; Varrani, A.; Warriar, A. K.; Woodall, L. C.; Wu, N. Learning from Natural Sediments to Tackle Microplastics Challenges: A Multidisciplinary Perspective. *Earth-Science Reviews* **2022**, *228*, 104021. <https://doi.org/10.1016/j.earscirev.2022.104021>.
- (25) Alimi, O. S.; Farner Budarz, J.; Hernandez, L. M.; Tufenkji, N. Microplastics and Nanoplastics in Aquatic Environments: Aggregation, Deposition, and Enhanced Contaminant Transport. *Environmental Science & Technology* **2018**, *52* (4), 1704–1724. <https://doi.org/10.1021/acs.est.7b05559>.
- (26) Hurley, R.; Woodward, J.; Rothwell, J. J. Microplastic Contamination of River Beds Significantly Reduced by Catchment-Wide Flooding. *Nature Geoscience* **2018**, *11* (4), 251–257. <https://doi.org/10.1038/s41561-018-0080-1>.
- (27) Kooi, M.; Primpke, S.; Mintenig, S. M.; Lorenz, C.; Gerdts, G.; Koelmans, A. A. Characterizing the Multidimensionality of Microplastics across Environmental Compartments. *Water Research* **2021**, *202*, 117429. <https://doi.org/10.1016/j.watres.2021.117429>.
- (28) Martin, J. L.; McCutcheon, S. C.; Schottman, R. W. *Hydrodynamics and Transport for Water Quality Modeling*; Lewis Publishers: Boca Raton, 1999.
- (29) Besseling, E.; Quik, J. T. K.; Sun, M.; Koelmans, A. A. Fate of Nano- and Microplastic in Freshwater Systems: A Modeling Study. *Environmental Pollution* **2017**, *220*, 540–548. <https://doi.org/10.1016/j.envpol.2016.10.001>.
- (30) Zhang, W. Sediment Dynamics. In *Encyclopedia of Marine Geosciences*; Harff, J., Meschede, M., Petersen, S., Thiede, J., Eds.; Springer Netherlands: Dordrecht, 2014; pp 1–6. https://doi.org/10.1007/978-94-007-6644-0_175-1.
- (31) Jambeck, J. R.; Geyer, R.; Wilcox, C.; Siegler, T. R.; Perryman, M.; Andrady, A.; Narayan, R.; Law, K. L. Plastic Waste Inputs from Land into the Ocean. *Science* **2015**, *347* (6223), 768–771. <https://doi.org/10.1126/science.1260352>.
- (32) Mai, L.; Sun, X.-F.; Xia, L.-L.; Bao, L.-J.; Liu, L.-Y.; Zeng, E. Y. Global Riverine Plastic Outflows. *Environ. Sci. Technol.* **2020**, *54* (16), 10049–10056. <https://doi.org/10.1021/acs.est.0c02273>.
- (33) Stokal, M.; Vriend, P.; Bak, M. P.; Kroeze, C.; Van Wijnen, J.; Van Emmerik, T. River Export of Macro- and Microplastics to Seas by Sources Worldwide. *Nature Communications* **2023**, *14* (1), 4842. <https://doi.org/10.1038/s41467-023-40501-9>.
- (34) Shiravani, G.; Oberrecht, D.; Roscher, L.; Kernchen, S.; Halbach, M.; Gerriets, M.; Scholz-Böttcher, B. M.; Gerdts, G.; Badewien, T. H.; Wurpts, A. Numerical Modeling of Microplastic Interaction with Fine Sediment under Estuarine Conditions. *Water Research* **2023**, *231*, 119564. <https://doi.org/10.1016/j.watres.2022.119564>.
- (35) Osinski, R. D.; Enders, K.; Gräwe, U.; Klingbeil, K.; Radtke, H. Model Uncertainties of a Storm and Their Influence on Microplastics and Sediment Transport in the Baltic Sea. *Ocean Science* **2020**, *16* (6), 1491–1507. <https://doi.org/10.5194/os-16-1491-2020>.
- (36) Čerkasova, N.; Enders, K.; Lenz, R.; Oberbeckmann, S.; Brandt, J.; Fischer, D.; Fischer, F.; Labrenz, M.; Schernewski, G. A Public Database for Microplastics in the Environment.
- (37) NABU Schleswig-Holstein. *Plastic in the Schlei - Wastewater Treatment Plant Releases 5 Tonnes to the Environment (Original: Plastik in Der Schlei - Klärwerk Entlässt Fünf Tonnen*

- Müll in Die Umwelt); 2018. <https://schleswig-holstein.nabu.de/news/2018/24614.html>.
- (38) Bergen, K. J.; Johnson, P. A.; De Hoop, M. V.; Beroza, G. C. Machine Learning for Data-Driven Discovery in Solid Earth Geoscience. *Science* **2019**, 363 (6433), eaau0323. <https://doi.org/10.1126/science.aau0323>.
 - (39) Zhen, Y.; Wang, L.; Sun, H.; Liu, C. Prediction of Microplastic Abundance in Surface Water of the Ocean and Influencing Factors Based on Ensemble Learning. *Environmental Pollution* **2023**, 331, 121834. <https://doi.org/10.1016/j.envpol.2023.121834>.
 - (40) Brandt, J.; Mattsson, K.; Hassellöv, M. Deep Learning for Reconstructing Low-Quality FTIR and Raman Spectra-A Case Study in Microplastic Analyses. *Analytical Chemistry* **2021**, 93 (49), 16360–16368. <https://doi.org/10.1021/acs.analchem.1c02618>.
 - (41) Ramanna, S.; Morozovskii, D.; Swanson, S.; Bruneau, J. Machine Learning of Polymer Types from the Spectral Signature of Raman Spectroscopy Microplastics Data. *Advances in Artificial Intelligence and Machine Learning* **2023**, 03 (01), 647–668. <https://doi.org/10.54364/AAIML.2023.1144>.
 - (42) Phan, S.; Torrejon, D.; Furseth, J.; Mee, E.; Luscombe, C. Exploiting Weak Supervision to Facilitate Segmentation, Classification, and Analysis of Microplastics (<100 Mm) Using Raman Microspectroscopy Images. *Science of The Total Environment* **2023**, 886, 163786. <https://doi.org/10.1016/j.scitotenv.2023.163786>.
 - (43) Hu, B.; Dai, Y.; Zhou, H.; Sun, Y.; Yu, H.; Dai, Y.; Wang, M.; Ergu, D.; Zhou, P. Using Artificial Intelligence to Rapidly Identify Microplastics Pollution and Predict Microplastics Environmental Behaviors. *Journal of Hazardous Materials* **2024**, 474, 134865. <https://doi.org/10.1016/j.jhazmat.2024.134865>.
 - (44) Pedregosa, F.; Varoquaux, G.; Gramfort, A.; Michel, V.; Thirion, B.; Grisel, O.; Blondel, M.; Prettenhofer, P.; Weiss, R.; Dubourg, V.; Vanderplas, J.; Passos, A.; Cournapeau, D. Scikit-Learn: Machine Learning in Python. *MACHINE LEARNING IN PYTHON*.
 - (45) Chen, T.; Guestrin, C. XGBoost: A Scalable Tree Boosting System. In *Proceedings of the 22nd ACM SIGKDD International Conference on Knowledge Discovery and Data Mining*; ACM: San Francisco California USA, 2016; pp 785–794. <https://doi.org/10.1145/2939672.2939785>.
 - (46) Schwarzer, K.; Ricklefs, K.; Höft, D. *Sediment Inventory and Hydromorphology of the Schlei, (Original: Sedimentinventar Und Hydromorphologie Der Schlei)*; Institute of Geosciences, Kiel University, 2019; p 114. https://www.schleswig-holstein.de/DE/fachinhalte/M/meeresschutz/Downloads/Bericht_SedimentinventarHydromorphologieSchlei.pdf.
 - (47) Enders, K.; Lenz, R.; Ivar do Sul, J. A.; Tagg, A. S.; Labrenz, M. When Every Particle Matters: A QuEChERS Approach to Extract Microplastics from Environmental Samples. *MethodsX* **2020**, 7, 100784. <https://doi.org/10.1016/j.mex.2020.100784>.
 - (48) Brandt, J.; Bittrich, L.; Fischer, F.; Kanaki, E.; Tagg, A.; Lenz, R.; Labrenz, M.; Brandes, E.; Fischer, D.; Eichhorn, K.-J. High-Throughput Analyses of Microplastic Samples Using Fourier Transform Infrared and Raman Spectrometry. *Applied Spectroscopy* **2020**, 74 (9), 1185–1197. <https://doi.org/10.1177/0003702820932926>.
 - (49) Käßler, A.; Windrich, F.; Löder, M. G. J.; Malanin, M.; Fischer, D.; Labrenz, M.; Eichhorn, K.-J.; Voit, B. Identification of Microplastics by FTIR and Raman Microscopy: A Novel Silicon Filter Substrate Opens the Important Spectral Range below 1300 Cm⁻¹ for FTIR

- Transmission Measurements. *Analytical and Bioanalytical Chemistry* **2015**, 407 (22), 6791–6801. <https://doi.org/10.1007/s00216-015-8850-8>.
- (50) Bittrich, L.; Brandt, J. GEPARD - Gepard-Enabled PARticle Detection for Raman Microscopes. <https://gitlab.ipfdd.de/gepard/gepard>.
- (51) K  ppler, A.; Fischer, D.; Oberbeckmann, S.; Schernewski, G.; Labrenz, M.; Eichhorn, K.-J.; Voit, B. Analysis of Environmental Microplastics by Vibrational Microspectroscopy: FTIR, Raman or Both? *Analytical and Bioanalytical Chemistry* **2016**, 408 (29), 8377–8391. <https://doi.org/10.1007/s00216-016-9956-3>.
- (52) Kreyling, O.; K  lbl, A.; Spielvogel, S.; Rennert, T.; Kaiser, K.; K  gel-Knabner, I. Density Fractionation of Organic Matter in Dolomite-Derived Soils. *Journal of Plant Nutrition and Soil Science* **2013**, 176 (4), 509–519. <https://doi.org/10.1002/jpln.201200276>.
- (53) Wakeham, S. G.; Canuel, E. A. The Nature of Organic Carbon in Density-Fractionated Sediments in the Sacramento-San Joaquin River Delta (California). *Biogeosciences* **2016**, 13 (2), 567–582. <https://doi.org/10.5194/bg-13-567-2016>.
- (54) Wilkinson, M. D.; Dumontier, M.; Aalbersberg, Ij. J.; Appleton, G.; Axton, M.; Baak, A.; Blomberg, N.; Boiten, J.-W.; Da Silva Santos, L. B.; Bourne, P. E.; Bouwman, J.; Brookes, A. J.; Clark, T.; Crosas, M.; Dillo, I.; Dumon, O.; Edmunds, S.; Evelo, C. T.; Finkers, R.; Gonzalez-Beltran, A.; Gray, A. J. G.; Groth, P.; Goble, C.; Grethe, J. S.; Heringa, J.; 'T Hoen, P. A. C.; Hooft, R.; Kuhn, T.; Kok, R.; Kok, J.; Lusher, S. J.; Martone, M. E.; Mons, A.; Packer, A. L.; Persson, B.; Rocca-Serra, P.; Roos, M.; Van Schaik, R.; Sansone, S.-A.; Schultes, E.; Sengstag, T.; Slater, T.; Strawn, G.; Swertz, M. A.; Thompson, M.; Van Der Lei, J.; Van Mulligen, E.; Velterop, J.; Waagmeester, A.; Wittenburg, P.; Wolstencroft, K.; Zhao, J.; Mons, B. The FAIR Guiding Principles for Scientific Data Management and Stewardship. *Sci Data* **2016**, 3 (1), 160018. <https://doi.org/10.1038/sdata.2016.18>.
- (55) Blott, S. J.; Pye, K. GRADISTAT: A Grain Size Distribution and Statistics Package for the Analysis of Unconsolidated Sediments. *Earth Surface Processes and Landforms* **2001**, 26 (11), 1237–1248. <https://doi.org/10.1002/esp.261>.
- (56) Bray, J. R.; Curtis, J. T. An Ordination of the Upland Forest Communities of Southern Wisconsin. *Ecological Monographs* **1957**, 27 (4), 325–349. <https://doi.org/10.2307/1942268>.
- (57) Se  , G. Hydrodynamic Numerical Models Suitable for Application to the German Fairways and Ports at the Baltic Sea Coast. **2014**.
- (58) BAWiki. Mathematical Model UNTRIM.
- (59) BAWiki. PARTRACE.DAT.
- (60) Stone, M. Cross-Validatory Choice and Assessment of Statistical Predictions. *Journal of the Royal Statistical Society: Series B (Methodological)* **1974**, 36 (2), 111–133. <https://doi.org/10.1111/j.2517-6161.1974.tb00994.x>.
- (61) Varma, S.; Simon, R. Bias in Error Estimation When Using Cross-Validation for Model Selection. *BMC Bioinformatics* **2006**, 7 (1), 91. <https://doi.org/10.1186/1471-2105-7-91>.
- (62) Krstajic, D.; Buturovic, L. J.; Leahy, D. E.; Thomas, S. Cross-Validation Pitfalls When Selecting and Assessing Regression and Classification Models. *Journal of Cheminformatics* **2014**, 6 (1), 10. <https://doi.org/10.1186/1758-2946-6-10>.
- (63) Breiman, L. Random Forests. *Machine Learning* **2001**, 45 (1), 5–32. <https://doi.org/10.1023/A:1010933404324>.

- (64) Cawley, G. C.; Talbot, N. L. C. On Over-Fitting in Model Selection and Subsequent Selection Bias in Performance Evaluation. *Journal of Machine Learning Research* **2010**, *11* (70), 2079–2107. <https://doi.org/10.5555/1756006.1859921>.
- (65) Sperlea, T.; Kreuder, N.; Beisser, D.; Hattab, G.; Boenigk, J.; Heider, D. Quantification of the Covariation of Lake Microbiomes and Environmental Variables Using a Machine Learning-Based Framework. *Molecular Ecology* **2021**, *30* (9), 2131–2144. <https://doi.org/10.1111/mec.15872>.
- (66) Li, J. Predicting the Spatial Distribution of Seabed Gravel Content Using Random Forest, Spatial Interpolation Methods and Their Hybrid Methods. In *Piantadosi, J., Anderssen, R.S. and Boland J. (Eds) MODSIM2013, 20th International Congress on Modelling and Simulation*; Modelling and Simulation Society of Australia and New Zealand, 2013. <https://doi.org/10.36334/modsim.2013.A9.li>.
- (67) Harris, P. T. The Fate of Microplastic in Marine Sedimentary Environments: A Review and Synthesis. *Marine Pollution Bulletin* **2020**, *158*, 111398. <https://doi.org/10.1016/j.marpolbul.2020.111398>.
- (68) McLusky, D. S.; Elliott, M. Transitional Waters: A New Approach, Semantics or Just Muddying the Waters? *Estuarine, Coastal and Shelf Science* **2007**, *71* (3–4), 359–363. <https://doi.org/10.1016/j.ecss.2006.08.025>.
- (69) Woodward, J.; Li, J.; Rothwell, J.; Hurley, R. Acute Riverine Microplastic Contamination Due to Avoidable Releases of Untreated Wastewater. *Nature Sustainability* **2021**, *4* (9), 793–802. <https://doi.org/10.1038/s41893-021-00718-2>.
- (70) Haave, M.; Lorenz, C.; Primpke, S.; Gerdt, G. Different Stories Told by Small and Large Microplastics in Sediment - First Report of Microplastic Concentrations in an Urban Recipient in Norway. *Marine Pollution Bulletin* **2019**, *141*, 501–513. <https://doi.org/10.1016/j.marpolbul.2019.02.015>.
- (71) Fulfer, V. M.; Walsh, J. P. Extensive Estuarine Sedimentary Storage of Plastics from City to Sea: Narragansett Bay, Rhode Island, USA. *Sci Rep* **2023**, *13* (1), 10195. <https://doi.org/10.1038/s41598-023-36228-8>.
- (72) Maes, T.; Van Der Meulen, M. D.; Devriese, L. I.; Leslie, H. A.; Huvet, A.; Frère, L.; Robbens, J.; Vethaak, A. D. Microplastics Baseline Surveys at the Water Surface and in Sediments of the North-East Atlantic. *Frontiers in Marine Science* **2017**, *4*, 135. <https://doi.org/10.3389/fmars.2017.00135>.
- (73) Rodrigues, D.; Antunes, J.; Pais, J.; Pequeno, J.; Caetano, P. S.; Rocha, F.; Sobral, P.; Costa, M. H. Distribution Patterns of Microplastics in Subtidal Sediments from the Sado River Estuary and the Arrábida Marine Park, Portugal. *Front. Environ. Sci.* **2022**, *10*, 998513. <https://doi.org/10.3389/fenvs.2022.998513>.
- (74) Bakir, A.; Doran, D.; Silburn, B.; Russell, J.; Archer-Rand, S.; Barry, J.; Maes, T.; Limpenny, C.; Mason, C.; Barber, J.; Nicolaus, E. E. M. A Spatial and Temporal Assessment of Microplastics in Seafloor Sediments: A Case Study for the UK. *Front. Mar. Sci.* **2023**, *9*, 1093815. <https://doi.org/10.3389/fmars.2022.1093815>.
- (75) Vermeiren, P.; Lercari, D.; Muñoz, C. C.; Ikejima, K.; Celentano, E.; Jorge-Romero, G.; Defeo, O. Sediment Grain Size Determines Microplastic Exposure Landscapes for Sandy Beach Macroinfauna. *Environmental Pollution* **2021**, *286*, 117308. <https://doi.org/10.1016/j.envpol.2021.117308>.

Mapping the plastic legacy with NIXVEGS: Machine-learning enabled microplastics prediction in sediments

Kristina Enders^{1,2*}, Robin Lenz^{1,2}, Franziska Fischer², Klaus Schwarzer³, Guntram Seiß⁴, Dieter Fischer², Matthias Labrenz^{1*}

¹ Leibniz Institute for Baltic Sea Research Warnemünde (IOW), 18119 Rostock, Germany

² Leibniz Institute for Polymer Research (IPF), 01069 Dresden, Germany

³ Christian-Albrechts-University of Kiel (CAU), 24118 Kiel, Germany

⁴ The Federal Waterways Engineering and Research Institute (BAW), 22559 Hamburg, Germany

*Corresponding authors. Emails: enders-kristina@ipfdd.de, matthias.labrenz@io-warnemuende.de

Supplementary Information

Material and Methods

MP Sample collection

Sediment was collected at a total of 32 stations from May 14 – 16, 2018, using a Van Veen grab from aboard a ship (Klaashahn, IOW) in a transect from the Inner Schlei to the Baltic Sea opening ¹. The deliberate choice of the sampling locations aimed to balance grain size coverage (by consulting grain size maps of the Schlei ¹), spatial coverage (covering the entire extent and depths) and usage coverage (i.e. regions of more pristine and more anthropogenic character). After carefully opening the grab, the top 5 cm of sediment were transferred into a MP-free cleaned glass jars (one per sampling location and additionally also one sample of the 10-15 cm layer at S1, S2, S4, S10) and stored dark at 4°C. Of the 32 stations, 28 samples were later analyzed for MP, two only for sediment properties, and two were lost.

We used data on sediment properties from a second sample set, collected at 183 stations by an earlier sediment survey on courtesy of Kiel University. Information on sampling and analysis of this sub-dataset can be found in ¹. Principal procedural steps were comparable between the two studies. A van Veen grab was used to obtain 161 samples, whereas the 22 samples were taken using a gravity corer. For each core sample, sediment grain size measurements from the upper 5 cm were averaged for comparability to the grab samples.

Sample preparation

The detailed MP extraction protocols, documentation of the technical equipment, method validation and general contamination prevention measures are documented in the respective method article ². We here report the essential procedural steps and refer to respective protocol modules (m1 – m6) as part of the modular decision tree (see Fig. 2 in ²) as they are identical as described in these published protocols. Samples were freeze dried (m1), homogenized (m2) and defined dry masses (160 g on average) transferred into a density separation using sodium

S1

polytungstate (1.8 g cm^{-3} , m5). The application of the conical spiral conveyor (see Fig. 3 in ²) in a customized glass separation funnel under addition of a few droplets of hydrogen peroxide allowed a gentle release and separation of lighter particles. Density and pH (3 – 3.4) were checked regularly and readjusted if necessary. Remaining organic constituents in the filtered supernatant were then reduced by applying 30% hydrogen peroxide (m4.1). Samples were then filtered in the analytical laboratory (IPF Dresden) onto silicon filters with $\sim 50 \text{ }\mu\text{m}$ pore size using a custom-built glass filtration device ³ under a laminar flow cabinet (Telstar Aeolus V3) ⁴. In cases where samples contained too many particles and that would exceed the usage of more than 10 filters, samples were split using a glass sample splitter built at IPF which allows homogeneous subsampling of the poured to remaining fraction of averagely $52 \text{ to } 48 \pm 11\%$ SD (SI, ⁵). Liquid sample splitters are commonly used in plankton research and were already applied in previous MP studies ⁶. For most samples, $\geq 50\%$ or 100% were analyzed, which is favorable to reach a reasonable statistical robustness on MP numbers ⁷.

Larger MP suspects ($> 1 \text{ mm}$) were picked and rinsed individually or in case of particle overloading a stacked sieve filtration was applied (m6) as otherwise μ -spectroscopic analysis would be impaired. These individually picked particles were then transferred between glass slides for single particle analysis.

Blanks covering the entire MP extraction (using an MP free sediment matrix, $n = 8$) and spectroscopic analysis pipeline (one blank per sample) were prepared in an identical manner to account for MP contamination in the laboratories.

Spectroscopic analysis

Smaller MP particles applied to the Si-filters were identified and quantified via particle analysis combined with Raman μ -spectroscopy using the semi-automated software GEPARD developed at the IPF Dresden (for more details see ^{3,8}). The software recognizes particles on a substrate, captures particle properties such as size dimensions, shapes and color, among others and induces a spectroscopic measurement at every particle center coordinate. As a standard for Raman spectroscopic measurements, a WITec alpha 300R Raman microscope (Oxford Instruments Group) with a 20x objective and a 532 nm excitation laser at 5 mW, 0.5 s integration time and 5 scans were used. Using Raman μ -spectroscopy not only polymers but also pigments can be identified. In some cases the Raman scatter is more sensitive to the pigment than its polymeric binder and masks the polymer type signals ⁹. A shortlist of identified pigments was selected (i.e., PO7, PO13, PO34, PY185, PR214, PR254, PG7) which are majorly used in relation with synthetic polymers and classified as ‘unknown’ polymers (0.4% of all MP). Conservative criteria were applied for this selection process and most identified pigments were not counted (see ‘polyDropList’ in *MPDB_settings.py*). Larger particles were individually measured with Raman spectroscopy or ATR-FTIR spectroscopy ¹⁰. Raman measurements were performed either with the WITec alpha 300R Raman microscope (20x objective, 532 nm excitation laser at 5 mW, 0.5 s integration time, 10 to 100 scans) or with the Renishaw inVia Qontor Raman microscope (10x, 20x or 50x objective, 532 nm excitation laser at 0.1- 15 mW, 0.5-10 s integration time, 20 or 50 scans). ATR-FTIR measurements were performed using a Bruker ATR microscope Hyperion 2000 (20x ATR objective), coupled to a FTIR spectrometer Vertex 70 (100 scans, 4 cm^{-1} spectral resolution). Raman and FTIR spectra were identified using spectral reference databases. For Raman spectra, the WITec software TrueMatch and in-house curated databases for common polymers, pigments and dyes as well as selected inorganic and organic materials typical of environmental samples were used. For the FTIR spectra, the database search was performed using the Bruker OPUS software and the Hummel Polymer spectra library as well as in-house FTIR spectral libraries.

Geological and geochemical analysis

Based on homogenized and freeze-dried subsamples, grain size distribution was analyzed in two sample replicates with the laser-sizer Mastersizer 3000 (Malvern Panalytical) in wet dispersion mode. Priorly, organic matter was removed using 30% H₂O₂ as the physical and chemical instability of this fraction and conglomeration affect measurement accuracy and deviating physical properties hinder the consistency of the sediment fraction. During measurements 10s ultrasound was applied ensuring disintegration of particle conglomerates. Five consecutive measurements were performed and averaged for further statistical analysis. All grain size data were exported in log scale (0.0419 - 2096.5 µm) in 116 histogram intervals.

Total organic carbon (TOC) was calculated by subtraction of the total inorganic carbon (TIC) from the total carbon (TC). TIC and TC (TN, TS) determination was conducted on lyophilized, homogenized and ground sample material using the elemental analyzers multi-EA 4000 (Analytik Jena) and Euro-Vector EA (Hekatech). Averages were calculated from analytical duplicates.

The size distribution of organic matter was determined based on homogenized subsamples (5 – 40 g dw). Samples were transferred to centrifuge bottles filled with 1.8 g cm⁻³ sodium polytungstate which was priorly microfiltrated at 0.4 µm¹¹. Bottles were gently shaken on a shaker table for 30 min to ensure complete wetting of the material. Thereafter samples were centrifuged at 2500g rcf for 20 minutes. The supernatant was then pipetted to a beaker. Centrifugation and pipetting were repeated until no further light fraction could be separated (up to 10 repetitions). Samples were then filtered onto a 0.4 µm filter using MilliQ water¹². Sample material remaining on the filter was then rinsed off and size analyzed using the laser-sizer Mastersizer 3000 (Malvern Panalytical) in wet dispersion.

Hg analysis was performed using the direct mercury analyzer DMA-80 (MLS GmbH Milestone Lab).

Data analysis

This section details the data analytical procedures that were applied in the generation of estimates on the MP inventory of the Schlei sediments. The entire data analytical workflow of this study is available as [open source code](#). Reproducibly executable jupyter notebooks and python scripts were used to develop statistical and geospatial models and are available, including documentation of individual functions, at <https://github.com/robna/MPSchleiSediments>. The infographic (Fig. S1) provides an overview of how the code is structured.

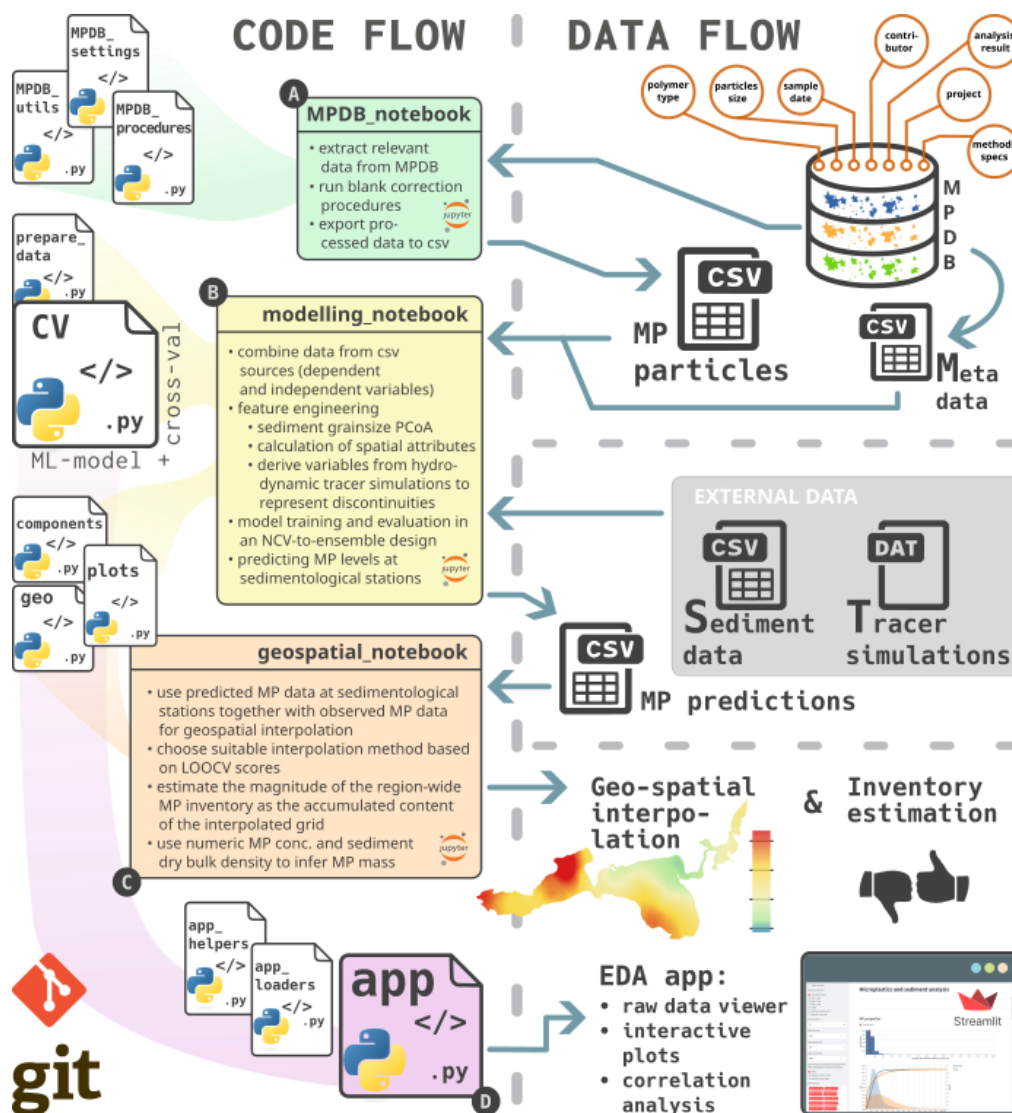


Figure S1: Overview of the analysis- (left panel) and data (right panel) flow. Raw data on MP samples and particles are stored in a public MP database (MPDB, ¹³). Data analysis was conducted in a collection of jupyter notebooks (A, B, C). For better readability of the notebooks, specific functions, integrating the MP- with sediment-, hydrodynamic tracer simulation- and geo data, were outsourced into python scripts. The functions in the scripts are then called from the notebooks. **A)** the *MPDB_notebook* queries MP particle data from the MPDB. Processing to account for potential contamination identified in blank controls happens here too. The extracted dataset is passed on as a csv file. **B)** the *modelling_notebook* ingests the data provided from **A** and establishes a machine learning model selection-validation-prediction pipeline and provides predictions of MP at sedimentological stations, as well as a detailed analysis of the model's validity. **C)** the *geospatial_notebook* uses the predictions from **B** and interpolates it to grid data covering the entire Schlei area. The summarized interpolated MP amounts give an estimation of the total MP inventory. **D)** an interactive exploratory data analysis webapp (EDA app) provides detailed insights into the dataset.

Model conception

The general modeling steps can be summarized as follows:

1. **Dataset assembly:** data management, preparation and feature engineering for response and predictor variable generation

2. **Model selection:** A nested cross-validation (NCV) and hyperparameter optimization approach was used to explore a finite grid of empirical models for their suitability to explain the dependence of response variables (numeric and gravimetric MP abundances) on predictor variables (geographic, spatio-temporal discontinuity and sediment properties).
3. **Evaluation and prediction:** A derived model ensemble from step 2 was used for prediction of the respective response variable at 187 sites where the same predictor variables were available from a prior sediment survey ¹.
4. **Geospatial interpolation:** The predicted response variables were used to estimate the MP load of the entire studied system using geospatial interpolation.

Dataset assembly

Two subsets of sample data, sharing the same structure, were assembled from the pool of available data sources. The *model set* contained all samples with complete response and predictor variables, suitable for model training. The *prediction set* consisted of samples with only complete predictor information.

Response variable generation

Any MP-related datum, aggregated at sample level from the obtained MP particle data, may be considered a potential response (commonly also referred to as dependent variable or target variable). We used the total particle- and mass-based MP abundances per kg sediment dw (*Concentration* (Fig. S2), *MassConcentration*, see [EDA app](#): sample domain data) as response variables for predictive modeling and spatial interpolation.

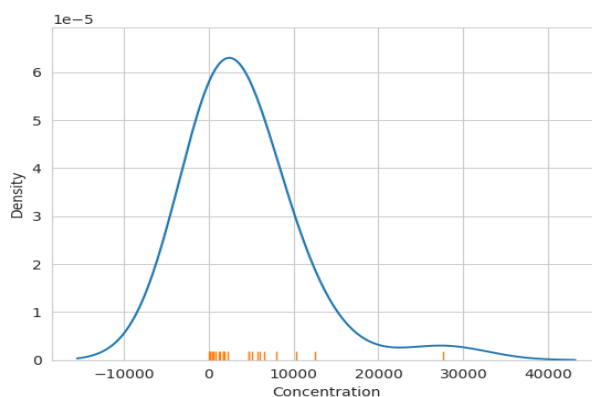


Figure S2: Kernel density estimation of the right-skewed response variable MP Concentration

Database

The recently published MPDB, a MP-specific database ¹³, was used to store and access MP related particle-, spectroscopic- and metadata (Fig. S1). This warrants data integrity, consistency and effective data management from the single MP particle (e.g., polymer type, size) to sample level (e.g., methods specifics, sampling dates and coordinates). The MPDB was developed for particle-based MP analysis workflows following the FAIR principles and is findable by international databases via the [IOW-META database](#) (for more details see ¹³). All relevant information that was extracted from the MPDB for the model development can also be seen in the [EDA app](#).

The [MPDB notebook](#) contains the necessary functions to query the relevant entries from the MPDB. This includes the procedures of aggregating the particle-based raw data into sample-based data, according to the principles described in ¹³. During this process, samples which were only analyzed in part, i.e., which had been sub-sampled before spectroscopic measurement, were extrapolated by replicating the respective entries on the particle level. The exact steps of this process can be inferred from the respective [function 'particle_amplification'](#).

Blank correction was done by matching MP phenotypes between environmental and blank samples (see also ¹³ under 3.4. Data sanitation - Phenotyping and Blank Subtraction). In short, MP particle phenotypes were characterized by having the same sample, polymer type, shape and color properties. Particle size was used as a continuous selection criterion, to facilitate matches on individual particle level, i.e., smallest absolute difference in 2D geometric mean, between blank- and sample particles of the same phenotype, implied a match.

Two types of blanks were used: analysis blanks (one per environmental sample) and process blanks (n = 8). For the latter, synthesized average blank samples were created for the blank subtraction process on each environmental sample. For details of the implementation of this concept the reader is referred to code and documentation in the [notebook](#) and [function script](#). In total, 12225 MP particles were found in the samples of which 237 particles were removed by the blank correction process.

Particle size, volume and mass and approximation

MP particle sizes were acquired by the open-source software GEPARD particle detection software ³. We advanced and validated (based on > 100 manual particle height measurements) the particle height determination algorithm in GEPARD to enable an accurate determination of all three spatial dimensions needed for more accurate conversion to volume hence mass based data. The relevant changes can be comprehended in the [GEPARD repository](#).

Particle heights up to 20 µm, however, could not be reliably determined in this manner, due to vertical resolution limitations of the microscopic measurements. For these particles a [function "height_vol_dens_mass"](#) was implemented, which estimates the height by re-sampling from a distribution generated from [50 manually measured particle heights in this size range](#). For the individually measured larger MP, size dimensions were retrieved by the respective microscope software, a Zeiss microscope (Axio Imager Z2, Carl Zeiss Microscopy GmbH) or using a ruler in case of long fibers.

Particle volumes were calculated from particle size measurements in three dimensions. Volumes of irregular shaped particles V_{irr} were calculated as ellipsoids based on particle length l , width w and height h , according to [Eq. 1](#). Fibers were approximated as cylindrical volumes V_{fib} ([Eq. 2](#)).

$$V_{irr} = \frac{\pi l w h}{6} \quad (1)$$

$$V_{fib} = \frac{\pi l w^2}{4} \quad (2)$$

Particle volumes were then multiplied by the density of the identified polymer type to yield particle masses (see ["densities" in settings.py](#) for used values). For data exploratory purposes, other MP size parameters (median, mode, mean, etc.) were calculated from the volume and number-based particle distributions and are available for investigations in the provided [EDA app](#).

Data preparation

Before modeling the MP response variables, we consolidated the available sample set based on theoretical considerations. This resulted in exclusion of samples S05 and S30 from the dataset used for model building, as they were considered environmental outliers. In both cases, spatio-temporal discontinuities could explain these deviations, however, at a much more localized scale, i.e., without effecting stations close by. Station S05 is situated in the fluvially coined outflow region from the tributary “Füsinger Au”, leading to a local spot of lower MP concentrations, visible as negative deviation from Inner Schlei proxy-normalization curve (see Fig 2 B). This indicates that the riverine MP load is much lower compared to the Inner Schlei levels, leading to local dilution effects. In contrast, station S32 deviates positively from the outer Schlei proxy-normalization curve. Situated in a lagoon-like embayment “Wormshöfter Noor”, S32 is having limited exchange with the main part of the Schlei, but likely receives increased MP input from local sources (harbor, shipyard). Instead, these outlier stations were used in the prediction set, along with all other samples with no available MP data.

In sampling locations for which a sample of the deeper sediment layer (10 - 15 cm) existed aside the 0 - 5 cm sample, data of the two samples were vertically merged i.e., combined into single samples per station. The combination was done by:

1. merging MP particle related data
2. summing analyzed sample mass
3. taking the mean of sediment data.

Predictor variable generation

Predictors in the context of this study are vectors of all non-MP-related properties with values for each station. This includes variables from three categories: *geographic features*, *sediment properties* and variables describing the *spatio-temporal discontinuity* of the studied system.

During model training, the predictors are composed in a “feature matrix” individually for each model configuration candidate in the grid search. For every candidate the predictor variables (columns) selected by the exhaustive feature selection algorithm contain the values for the 26 training samples (rows). Similarly, a “feature matrix” is created for the prediction step, however, containing the predictor variable values for the 187 sediment-only station (i.e. where no MP content was analyzed).

Geographic features

The selected geographic features were:

- *Dist_Land*, measured as the shortest distance in meters between a sample’s location and the shoreline
- *Depth*, the water depth in meters at a sample’s location. For the prediction dataset, the values were sampled from a bathymetry map (digital elevation model (DEM), 5 m grid, provided on courtesy of Federal Waterways Engineering and Research Institute [BAW]). The DEM is based on comprehensive bathymetric measurements using echosounder and multibeam echosounder surveys conducted over two decades by German waterways institutions (Federal Maritime and Hydrographic Agency [BSH], Federal Waterway and Shipping Administration [WSV]). Line soundings conducted

by the BSH are data from a single transducer along the ship's route. The resolution along the route is < 1 m, the resolution for several parallel voyages is usually between 20 and 50 m. The fairways are surveyed by the WSV using multibeam sounding or a multiple transducer system (beams with several independent transducers), which generally achieves a resolution of < 1 m both along and across the route. A real resolution of 5 m can be assumed within the fairway, as each grid point was served at least once by one of the newer multibeam soundings, while outside the fairway a real data density of about 20 m of the primary data points can be assumed. As the gradients outside the fairway are predominantly flat, the linearly interpolated DEM can be considered being sufficiently representative of the bathymetry. The horizontal position is determined by differential GPS, i.e. GPS with additional correction by a land-based reference station.

To control for the validity of the DEM derived depth values we show them sampled at the locations of our MP stations against the *in-situ* measured depth values available there (Fig. S3). Both types are in good agreement ($R^2 = 0.81$, linear regression) with only one deviating value (S29) being about 4 m deeper in the DEM depth. Without S29, the other stations are approximated by a linear regression of $R^2 = 0.97$.

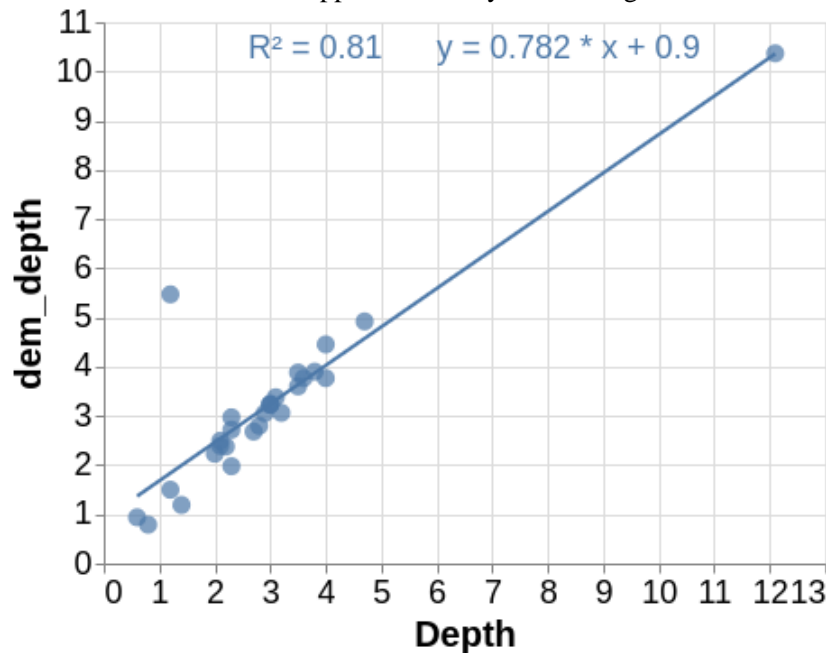


Figure S3: Control of validity of DEM sampled depth values. X-axis shows depths in meters manually measured at the MP stations, y-axis shows depths sampled from the DEM at the same coordinates.

Sediment grain size properties

From the vast possibilities of potential granulometric proxies, we chose sediment characteristics based on three key considerations:

1. Empirical evidence: Prior studies have consistently demonstrated a strong correlation between microplastic concentrations and sediment grain size, as well as related particulate properties, because both microplastics and sediment particles respond to similar hydrodynamic forces.

2. Practical availability: These parameters are routinely measured in sediment surveys, making them readily available and far less labor-intensive to obtain than direct microplastic measurements. This ease of acquisition is essential when scaling up to regional inventories.
3. Methodological rigor: We began with a broad list of candidate predictors and then curated a shortlist based on their availability across all sampling stations and their potential relevance.

Grain size variables were generated using GRADISTAT¹⁴ on the log-scaled binned volume-based grain size distributions as obtained by the laser sizer. Of the large number of calculated distribution moments of GRADISTAT, only median grain size in μm *SED_D50* and the share below $63 \mu\text{m}$ in percent *perc_MUD* was used. In addition, using a multidimensional scaling technique on the raw grain size data of 116 size bins, a 2D representation of grain size was calculated and used as predictor variables (*PCo1*, *PCo2*). They were created from a principal coordinate analysis (*PCoA*) using Bray-Curtis dissimilarity¹⁵ as a distance measure, to map the compositional, zero-inflated grain size data to the two-dimensional space which retains the largest share of dissimilarity between samples (here 77.3% and 12.1% for *PCo1* and *PCo2*, respectively). By definition the two are uncorrelated to each other.

PCo1 is highly correlated to variables like *perc_MUD* or *SED_D50*, i.e. some of the most common sediment properties descriptors used in sedimentological studies, which aligns with similar observations in the literature^{16,17}. We tested if *PCo2* correlated with more of the various sediment variables obtained through GRADISTAT (such as kurtosis, skewedness, sorting, etc.), but no strong correlations were observed. As *PCo2* had 12.1% explanatory value in the *PCo*-Analysis, we still included it as potential predictor to see its potential explanatory influence on the MP model. However, in only 4% of the ensemble members it was among the used predictor variables, as selected through the exhaustive feature selection of NIXVEGS (Nested Iterative (stratified) X-Validation-to-Ensemble-modeling through Grid Search).

Some of the 183 samples from the sediment-only survey used as prediction stations had missing values either in *TOC* ($n = 26$) or the grain size variables *SED_D50*, *perc_MUD*, *PCo1* and *PCo2* ($n = 11$). They were imputed by regressions from those variables available (Eq. 3 - Eq. 7).

$$\text{TOC} = 0.477 e^{0.039 \text{perc_MUD}} \quad R^2 = 0.77 \quad (3)$$

$$\text{SED_D50} = -99.342 \ln(\text{TOC}) + 235.451 \quad R^2 = 0.75 \quad (4)$$

$$\text{perc_MUD} = 27.147 \ln(\text{TOC}) + 22.62 \quad R^2 = 0.83 \quad (5)$$

$$\text{PCo1} = -0.274 \ln(\text{TOC}) + 0.337 \quad R^2 = 0.82 \quad (6)$$

$$\text{PCo2} = -0.01 \text{TOC} + 0.051 \quad R^2 = 0.05 \quad (7)$$

As can be seen in Eq. 3 - Eq. 7, most of the missing variables could be regressed from strong correlations to one of the available granulometric variables used in the model. No such correlation was found for *PCo2* (Eq. 7). With a R^2 close to zero, the imputed values were practically equivalent to a mean imputation of all available *PCo2* values.

Spatio-temporal discontinuity

To enable MP predictions via natural particulates proxies despite spatio-temporal discontinuities, it was necessary to introduce another class of predictor variables. A numeric

model¹⁸ was used to simulate the hydrodynamic behavior of the Schlei. It was set to a point at shore near the location of the highest granulometric normalized MP particle concentrations (S8 and S10). The so-identified simulation release point, in fact, coincided with the approximate point of discharge of the WWTP facility which has been found to emit unusually high amounts of meso- and microplastics. With the postprocessing method PARTRACE spherical drifters were released at location (latitude=54°31'31.499"N, longitude=9°36'11.582"E, Fig. 2 A and Fig. 3 D) into the hydrodynamic field and then traced forward. The transport behavior of the particles depends on the turbulence-advection regime and their own sinking rates (determined by their density and size). The hydrodynamic model covers the Schlei from Schleimünde to Schleswig and is based on the unstructured finite volume code UnTRIM (Unstructured Tidal Residual Mudflat model¹⁹). The horizontal resolution of the mesh is adapted to the bathymetry and the vertical resolution varies between 0.5 m and 1 m.

The particle tracing software PARTRACE was developed by BAW²⁰. The aim of this method is to trace idealized particles with defined sinking velocity. The particles are driven by the vertically averaged flow field of the Schlei hydrodynamic model. An idealized correction for the vertical structure of the flow (logarithmic profile) is assumed. The vertical movement of the particles is driven by vertical turbulence and sinking velocity, which depends on the density and size of the particles.

The hydrodynamic simulation period was 2017-05-01 to 2018-07-01. Particle tracing was simulated for three different periods: 2017-06-01 to 2017-08-01, 2017-10-15 to 2017-12-15 and 2018-04-01 to 2018-06-01. These three seasons were selected to assess the influence of wind- and wave-induced turbulence on MP redistribution and determine which period would be most determining for the model. The stormiest season ('autumn') preceding sampling was expected to have the strongest influence, while the most recent period ('spring') could also be a key determinant. In contrast, 'summer' represented the calmest conditions with minimal water turbulence and was included as a reference contrasting the two others.

Five different particle types were released with a density of 1.113 kg m⁻³ and different radii (300 µm, 100 µm, 50 µm, 18 µm) and passive tracer (no advection, i.e. equivalent to radius of 0 µm). The chosen density was derived from the mean density of all polymer particles identified in this study.

The resulting tracer paths were used to infer knowledge about how the tracers had moved through the system in respect to the sampling locations in four different implementations (see Table S1). Six variables (*Disco1* to *Disco6*) were generated using varying settings of these implementations (see Table S2). Tracks of location, depth and time step of each tracer are provided in the [data sources](#). Each of them was varied according to the following settings: simulated particle size and season, influence radius and sedimentation behavior.

Table S1: Discontinuity predictor variables derived from tracer simulations. Four main variable types were created, each with various alterations of simulation parameters. The function "[get_wwtp_influence](#)" is used for the calculations.

	Type	Description	Range / Unit	Meaning	Varied Parameters
Distance	tracer_mean_dist	mean straight-line distance of all drifters at all time steps to each sampling station	10 ^{2.8} – 10 ^{4.5} m	low values indicate high connectivity / low discontinuity	<ul style="list-style-type: none"> sedimentation [True, False] <ul style="list-style-type: none"> True: arrest drifters at location for all following time steps when valid sedimentation was observed

Buffer aggregates	endpoints_mean_dist	mean straight-line distance of drifter locations at last time step to each sampling station	$10^{2.8} - 10^{4.5}$ m	low values indicate high connectivity / low discontinuity	<ul style="list-style-type: none"> False: use tracks as simulated (never arrest drifters at sediment contact)
	cummulated_residence	summed occurrences of presence of all drifters at all time steps inside station buffer zones	$0 - 10^{5.9}$ observations	high values indicate high connectivity / low discontinuity	<ul style="list-style-type: none"> drifter sizes [0, 18, 50, 100, 300, all sizes] <ul style="list-style-type: none"> only include drifter simulations of the selected drifter particle size in μm volume-based ESD season [spring, summer, autumn, all seasons] <ul style="list-style-type: none"> only include drifter simulations from the selected season
	mean_time_travelled	mean of time steps of all drifters at first entrance to station buffer zones	$10^{0.7} - 10^{2.7}$ timesteps [3 h]	low values indicate high connectivity / low discontinuity	<ul style="list-style-type: none"> buffer radius [222, 444] <ul style="list-style-type: none"> radius in meters around each station used as an event horizon only for buffer aggregating variable types specific to sampling site density

Table S2: Discontinuity predictor variables with varied parameters in tracer simulations. See Table S1 for more information.

Variable	Type	Sedimentation	Drifter size	Season	Buffer radius
<i>Disco1</i>	mean_time_travelled	False	0 μm	allseasons	222
<i>Disco2</i>	mean_time_travelled	False	18 μm	allseasons	222
<i>Disco3</i>	mean_time_travelled	True	18 μm	autumn	222
<i>Disco4</i>	mean_time_travelled	True	18 μm	allseasons	444
<i>Disco5</i>	cummulated_residence	False	0 μm	allseasons	222
<i>Disco6</i>	cummulated_residence	False	18 μm	autumn	222

Model selection and evaluation

Through NIXVEGS (implemented in a [jupyter notebook](#), Fig. 1, Fig. S4) we create a model which has) predictive capabilities for estimating the response variable *Concentration* for samples in the prediction set. Theoretically it is founded on the principles of cross-validation (CV) ²¹, or NCV ²² more specifically, and grid-search (GS), i.e. the exhaustive optimization of a given parameter space with respect to a given performance metric. NIXVEGS is structurally similar to the NCV proposed by ²³, but extends the concept by creating a predictive ensemble in parallel to the generalization performance measure, and by adaptations specifically addressing the problems and needs arising under small dataset conditions.

The NIXVEGS modeling pipeline was implemented in a [jupyter notebook](#) with the goal to design a model selection, evaluation and prediction protocol, suitable for small datasets (i.e. $n_{\text{samples}} \sim 30$, an $n_{\text{predictors}}$ in the same order of magnitude), which is typical for MP field data.

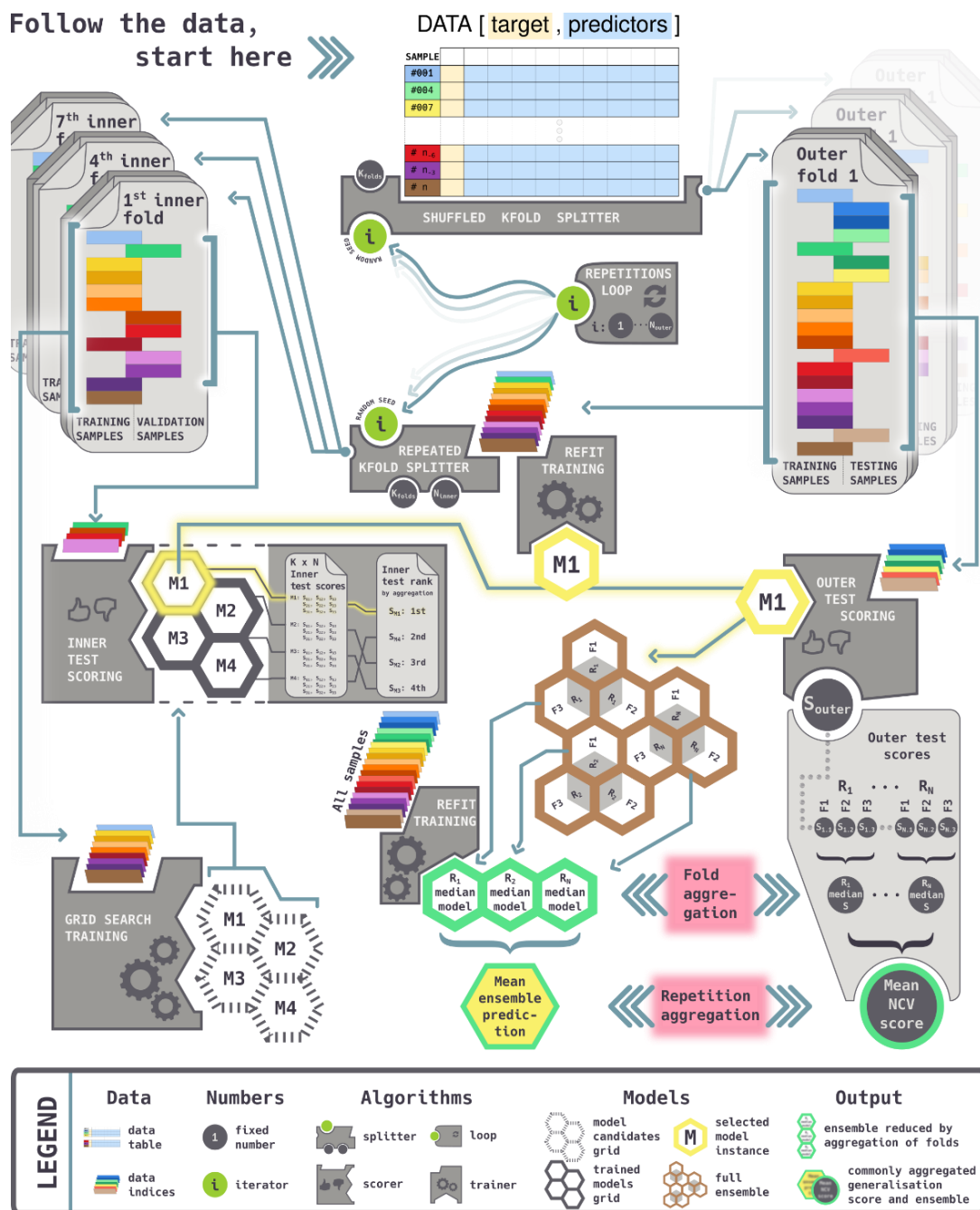


Figure S4: NIXVEGS model components and workflow: NIXVEGS performs selections of predictor variables, suitable model classes and hyperparameter settings synchronously with model training and validation. The final generalization score (“Mean NCV score”) indicates how the pipeline would perform on unseen data. The same logic of how the score (S) is aggregated is then used to construct an ensemble from individual trained model instances (M), which had been selected as the best performing ones, based on their respective inner test scores. For clarity, the infographic represents a simplified procedure of just three repetitions (R) and three folds (F), for the inner and outer cross-validations, respectively.

NIXVEGS' adjustable components are:

1. CV scheme:
 - number of *repetitions* for the outer and inner loop
 - number of *folds* for the outer and inner CV
2. scoring scheme:
 - *selection scorer*: evaluation metric used to select a “best” model in the grid-search procedure, see Table S3
 - *inner fold aggregator* of the selection scorer: median, interquartile mean (iqm), or mean
 - *generalization scorer*: evaluation metric used as the final generalization score, see Table S3
 - *outer fold aggregator*: median, iqm, or mean
 - *repetitions aggregator*: median, iqm, or mean
3. model candidate configurations:
 - *predictor variable sets*: feature selection from allowed variable combinations
 - *model class*: generalized linear models (*GLM*), gradient boosting for linear regressors (*XGBlinear*), gradient boosting for tree regressors (*XGBtree*), random forests (*RF*)
 - *model hyperparameter values*: depending on model class

The tested model algorithms included two from the linear ones. A GLM has previously been used to model MP concentrations, based on granulometric proxies²⁴. In the present study the *GLM* was implemented for a gamma distribution with a log link using the *TweedieRegressor* class of the [scikit-learn library](#) with *power=2* and a L2 regularization parameter *alpha=0*. A linear gradient boosting model, here referred to as *XGBlinear*, was implemented using the *XGBRegressor* class from the [xgboost library](#). It was set up with hyperparameters to resemble the settings of the GLM model, however, allowing ensembles of up to 300 base estimators with the fixed hyperparameter set: *booster=gblinear*, *objective=reg:gamma*, *n_estimators=300*, *reg_alpha=0*, *reg_lambda=0*. The hyperparameters for the two linear models were held fixed as they were chosen on theoretical considerations of the modelled response variable and based on residual analysis using our [EDA app](#). This could also further reduce computational time. Only predictor variable composition was varied. Two model classes of tree-based estimators were included for comparison to the linear models. *XGBtree* was also implemented from the *XGBRegressor* class of the [xgboost library](#), sharing the same hyperparameters as *XGBlinear*, but using *booster=gmtree*. Additional decision-tree-related hyperparameters were varied and optimized in NIXVEGS based on the following allowed values: *tree_method=exact*, *learning_rate=[0.1, 0.25]*, *max_depth=[2, 3]*, *min_child_weight=[5, 7]*. A *RF* model, implemented using the *RandomForestRegressor* class of the [scikit-learn library](#), was allowed to vary in the following hyperparameters: *n_estimators=[10, 100, 300]*, *max_depth=[None, 2, 4]*, *max_features=[None, 1/3]*. The hyperparameter range was narrowed based on sample and predictor size as well as their selection frequency. For the specific roles of the hyperparameters, we refer to the respective library documentation. All non-mentioned hyperparameters were left at their default values.

In order to identify viable predictors, while also keeping computational cost for model training within practical limits, the [EDA app](#) was used for screening the large number of possible discontinuity and granulometric proxy variables. Six discontinuity variables were selected which demonstrated sufficient spatio-temporal separation of the identified sub-regions (compare Fig. 2). For geographic and sediment variables, an initially high number of

candidates was reduced to four granulometric proxies (*SED_D50*, *perc_MUD*, *PCo1* and *PCo2*) and two geospatial properties (*Dist_Land*, *Depth*) by excluding those being infrequently selected by NIXVEGS' feature selection or being not available at the majority of stations (incl. the sediment-only prediction stations). In result, a set of 12 predictor variables was available for the automated feature selection inside NIXVEGS. For model parsimony and avoidance of potential collinearities, only one predictor for each per class (granulometric proxies and discontinuity variables) was allowed per model candidate. As an exception, *PCo2* was allowed in combination with any other granulometric proxy as it is, by definition, uncorrelated to the first principal coordinate of grain sizes *PCo1*. NIXVEGS' feature selection algorithm was to exhaustively test all possible combinations of two or three predictor variables for linear-based models. For tree-based models all possible sets of five predictors were tested, to allow more flexibility in feature variability for tree-building. For elaboration on the role of manual pre-selections in the context of information leakage see the following section.

The CV and scoring schemes were chosen manually under consideration of the small dataset size and modeling goal. We used 100 and 10 randomized repeats, each with $k = 3$ folds splitting for the outer and inner CV loop, respectively. Generally, a higher number of splits, such as $k = 10$, may be preferred for performance evaluations²⁵, but owing to the small dataset size this would lead to very low numbers of samples in the test sets. This would lead to scores that reflect more the favorable or unfavorable composition of the test set, rather than the model's ability to predict unseen data correctly. We used the coefficient of determination (R^2 , Eq. 8) as scorer for both, the selection and generalization scoring scheme. It can be regarded as a variant of the mean squared error (MSE), normalized by the sample variance. Thus, models minimizing a sum-of-squares loss, will be rewarded a better score. In particular, we argue that, because R^2 accounts for the sample variance, its use as evaluation metric in small dataset scenarios is preferable to using MSE, as it facilitates comparability of scores produced by test sets of possibly significantly different sample variance. The aggregation of the inner and outer folds' test scores was implemented as median. Using the median, instead of the (more commonly used) mean for the aggregation of folds, was chosen deliberately to adapt to the small sample number. Situations with such limited data resources will likely lead to few train/test-set combinations yielding egregiously bad test scores. These will affect a mean-aggregated score over proportionately, as the upper end of the score's scale is bound to 1.0, meaning perfect prediction, while the lower end is open towards negative infinity. Median (and also iqm) aggregation is more robust in such situations. Despite the use of median R^2 as the main scoring scheme, we report the evolution of scores (and their standard deviations) over the increasing number of NIXVEGS' outer repetitions for all aggregations of multiple scorers listed in Table S3.

Table S3: Regression metrics used in model evaluation, with y as observed values of targeted response variable and \hat{y} being its prediction, n as the number of samples and ϵ being an arbitrarily small positive number to avoid division by zero.

Metric	Definition	Range and meaning
Coefficient of determination	$R^2(y, \hat{y}) = 1 - \frac{\sum_{i=1}^n (y_i - \hat{y}_i)^2}{\sum_{i=1}^n (y_i - \bar{y})^2} \quad (8)$	$R^2 = 1$ (perfect prediction) $1 > R^2 > 0$ (imperfect prediction)
	with $\bar{y} = \frac{1}{n} \sum_{i=1}^n y_i \quad (9)$	$R^2 = 0$ (pred. == obs. mean) $0 > R^2 > -\infty$ (worse than mean)

Metric	Definition	Range and meaning
Mean absolute percentage error	$\text{MAPE}(y, \hat{y}) = \frac{1}{n} \sum_{i=1}^n \frac{ y_i - \hat{y}_i }{\max(\epsilon, y_i)} \quad (10)$	MAPE = 0 (perfect prediction) $0 < \text{MAPE} < \infty$ (increasingly imperfect) in percent of the response variable unit
Median absolute percentage error	$\text{MedAPE}(y, \hat{y}) = \text{median} \left(\frac{ y_1 - \hat{y}_1 }{\max(\epsilon, y_1)}, \dots, \frac{ y_n - \hat{y}_n }{\max(\epsilon, y_n)} \right) \quad (11)$	MedAPE = 0 (perfect prediction) $0 < \text{MedAPE} < \infty$ (increasingly imperfect) in percent of the response variable unit
Mean absolute error	$\text{MAE}(y, \hat{y}) = \frac{1}{n} \sum_{i=1}^n y_i - \hat{y}_i \quad (12)$	MAE = 0 (perfect prediction) $0 < \text{MAE} < \infty$ (increasingly imperfect) in response variable unit
Median absolute error	$\text{MedAE}(y, \hat{y}) = \text{median}(y_1 - \hat{y}_1 , \dots, y_n - \hat{y}_n) \quad (13)$	MedAE = 0 (perfect prediction) $0 < \text{MedAE} < \infty$ (increasingly imperfect) in response variable unit
Mean squared error	$\text{MSE}(y, \hat{y}) = \frac{1}{n} \sum_{i=1}^n (y_i - \hat{y}_i)^2 \quad (14)$	MSE = 0 (perfect prediction) $0 < \text{MSE} < \infty$ (increasingly imperfect) in response variable unit squared

When the GS had trained and selected the best models, their outer test set scores were calculated and aggregated first across folds within repetitions (*outer fold aggregator*), then across repetitions (*repetitions aggregator*), to obtain the final NCV generalization score. Afterwards, the model instances were not discarded, but used to recruit members for an ensemble, following the same logic as for the previous score aggregation. This process can be understood graphically in Fig. S4. In effect, this procedure integrates the steps of selecting between different model classes, with the optimization of their respective hyperparameters and the choice of the most suitable predictor variables set (i.e. feature selection).

Rational for the chosen model design

In contrast to classical hypotheses-driven statistical modeling, there are few prerequisites to a dataset when applying data-driven machine learning techniques, but a strong emphasis on posterior performance evaluation under avoidance of information leakage. This concept of information leakage refers to the notion, that for building a machine learning pipeline, any decision that has influence on the resulting model output becomes part of the model itself. This includes the parameters used to set up the model algorithm before fitting (often called hyperparameters), the way to choose which predictor variables are used (feature selection), or even the choice of the model algorithm itself.

In effect, all of the before listed aspects become essentially hyperparameters of the modeling pipeline. The combinations that can be created thereof, form a grid of possible model configurations in which the optimum shall be searched for. Any decision for or against a certain configuration, when taken under consideration of the entire available data, is potentially biased towards the statistical peculiarities of the dataset²⁶. In other words, when

all available information has leaked into the decision-making process, none is available to independently evaluate the decision.

It is important to note that the concept of avoiding information leakage has practical limitations. The grid of possible configurations is theoretically infinite. Some of the parameters to be chosen are real numbers and can thus be chosen arbitrarily dense or wide. On the other hand, the choice of which components (i.e., model algorithm classes or derived predictor variables) should or should not be variably tried out by the grid search is already a decision. Thus, when the pipeline is set up, a manual pre-restriction of the variable components is inevitable. This would also be the case if other methods, such as randomized search or Bayesian methods, were chosen instead of an exhaustive grid search CV.

CV provides an efficient way for either model evaluation, or to decide on a certain model configuration. When it is nested, it provides both under the best possible utilization of a confined dataset. It has been demonstrated that NCV, using k-fold splitting, can offer an almost unbiased estimate of the true generalization performance²². The cross-validated scheme itself also comes with a range of setup parameters, that need to be chosen depending on the dataset and type of problem, as there is no general optimal setting²³. These include the number of folds to split, how samples can be selected for a particular fold (e.g., using stratification), and how often to repeat the whole procedure in independent randomized trials that can be aggregated to reduce the evaluation variance.

In practice, the decision on which aspects of the modeling pipeline are allowed to adapt to the available data is likely based on knowledge about the problem to be modelled and its data structure, as well as relevant domain knowledge. This does not need to invalidate the estimated generalization performance. In fact, it has been shown on a range of modeling problems from real-life datasets, that many model decisions taken under consideration of all available data in a non-nested CV had negligible effects on the biasedness of the estimated generalization performance as compared to the computationally more expensive NCV²⁷. Nevertheless, the importance of NCV is elevated specifically with decreasing dataset size and increasing model flexibility²⁶ and is therefore seen as an indispensable component of NIXVEGS.

Sensitivity analysis and adaptations for small datasets

For validation of our model results, NIXVEGS provides the CV scores. Various CV settings were evaluated, including the number of folds k , the type of scorer and the use of a stratification scheme (Fig. 3 F).

For large ML-datasets, often higher values of k in k-fold CV are generally preferred as they reduce bias in performance estimation and provide a reliable CV score^{25,28}. However, when datasets are small (as in our case $n_{\text{samples}}=26$) and are skewed, stochastic instability in drawing of the sets can become a problem. With higher k , test sets become smaller and may not represent the observed data distribution, leading to erratic CV scores. Conversely, with lower k , the informational content of the training sets diminishes, making it less likely that the correct response distribution is learned during training. This can be observed in our data testing different values of k : the score is highly variable over different values of k (Fig. 3 F, non-stratified). We tested different stratification schemes (i.e., tertile and $\frac{n}{k}$ -quantile) to evaluate performance estimation more independent of the described sensitivities towards k arising from small datasets. At $k=3$ there was highest agreement between the different cases tested in the sensitivity analysis. When using stratification, however, only minor score deviations are observed for lower or higher k as compared to unstratified k-fold. Strict

stratification schemes, i.e., higher number of quantile strata, imply a higher confidence in the representativeness of distribution in the available data. With the small dataset at hand, it seemed more balanced to implement a weaker tertile stratification (Fig. 3 F). Based on this sensitivity analysis, we use a repeated stratified k-fold CV scheme, with $k = n_{folds} = [3,3]$ drawn from $s = n_{strata} = [3,3]$, repeated $r = n_{repetitions} = [100 \dots 500, 10]$ times and scored using $scorer = [R^2, R^2]$, for the outer and inner CV of NIXVEGS, respectively (Fig. 3 F). This setup results in 300 to 1500 unique aggregable splits which is approximately on par with what a leave-two- or leave-three-out scheme would achieve (325 and 2600, respectively), but with the advantage that it allows for a more balanced response variable distribution.

Prediction

EPM_{ensemble}

The ensemble of models, generated as described above, is composed of $N_{\text{outer repetitions}} = 100$ members. Before predicting, every ensemble member was refit on the entire model set of samples. The prediction was then carried out by each member individually using the prediction set of samples. The individual predictions were then aggregated according to the *repetitions aggregator*, for each sample. Since the entire ensemble was re-trained on the complete dataset, members that completely overlapped in their chosen predictor variables set, model class and corresponding hyperparameters were consequently identical models. The aggregated ensemble prediction, thus can be regarded as the weighted arithmetic mean of all unique model configurations, where the frequency of occurrence of a configuration in the ensemble constitutes its weighting factor. We use this logic also to infer the relative importance of partial configuration aspects in the ensemble, i.e., the model class (Fig. S4).

EPM_{single}

To obtain a predictive model instance, a non-nested grid search CV with the same CV scheme previously used in the inner NCV loop, is applied to the same grid of configurations, selecting a ‘best candidate’ configuration. This configuration is then fitted to all available data before prediction. We refer to this model as single empirical predictive model (EPM_{single}). It may seem counterintuitive, at first glance, that the EPM_{single}, as a model realized from one point on the configuration grid, shall be adequate to make predictions when its generalization performance has been calculated as an aggregate of model performances from potentially very different configurations. This becomes ever more salient the larger and the more diverse the configuration grid is (e.g., as in the present case with $n_{configs} = 728$, allowing for different algorithm classes, their respective hyperparameters and predictor sets to be selected). In comparison, the EPM_{ensemble}, which consists of models with the exact configurations that took part in the score construction, and whose predictions are aggregated in the same way as the score itself, may give the impression of being more directly related to the reported generalization performance, and thus more fit for prediction. It is, however, the EPM_{single} that is derived purely from first principals, i.e. the idea that model selection is an integral part of the model fitting procedure²⁶. This implies, that for making predictions the procedure should adapt to the full data available, just as during performance evaluation it had to adapt to each reduced set of training data. This logic would hold even if the very configuration found for the EPM_{single} was not present among those selected in the evaluation.

The reasons for creating the EPM_{ensemble} are therefore different and can be summarized as follows:

- the members of the ensemble have been selected as the optimal adaptations of the modeling procedure to various facets of the data available
- the aggregation of their predictions gives a weighted sum, where configurations that fitted more facets get a larger say
- it has been demonstrated that model ensembling can reduce instability, especially when datasets are small ²⁹
- in effect, ensembling takes into account the limited confidence one can have that the response variable distribution of a small dataset is representative of the unknown true distribution.

MP mass concentration prediction

The calculation of MP mass concentration was based on the summed observed MP particle masses per sample. See also the section on size, volume and mass approximation for the determination of all three spatial dimensions needed for the conversion to volume hence mass based data.

MassConcentration at the prediction stations was then approximated from the predicted numeric *Concentration* via an empirical regression established from the model set samples ($R^2 = 0.910$, Eq. 15, $R^2 = 0.89$ in LOOCV, Eq. 3).

$$\text{MassConcentration} = 0.1451 \cdot \text{Concentration}^{1.1894} \quad (15)$$

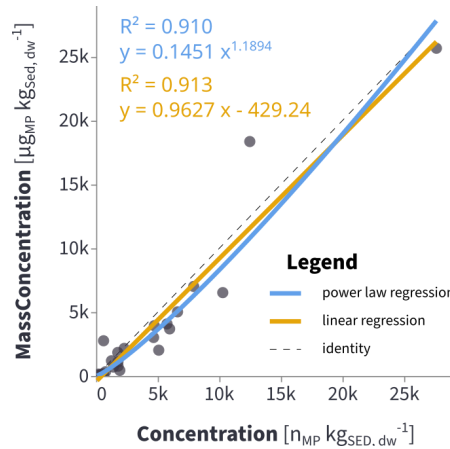


Figure S5: MP *MassConcentration* estimated through regression from numeric *Concentration*. The power law regression (blue) was used for estimation of MP *MassConcentration* at the predicted stations.

It should be noted, that this power law regression is very similar to a linear regression (which achieved a marginally higher R^2 of 0.913). The theoretical consideration for this choice is that samples with high numeric *Concentration* are more likely to include very rare, very large MP, which disproportionately increase *MassConcentration*. It also has the practical implication, that, in contrast to the linear equation, it avoids calculating negative values for *MassConcentration* in cases of very low numeric *Concentration*.

Both regressions are close to identity of the concentrations of MP number and MP mass in μg , indicating that the mass of an average MP particle in this study is on the order of 1 μg .

An attempt to use the NIXVEGS modeling pipeline to directly predict MP *MassConcentration* did not indicate that a generalization performance on unseen data would be able to get better than guessing the mean of the response ($R^2 = 0.01$ as median of three folds after 100 mean aggregated repetitions). This is surprising given that *MassConcentration* is highly correlated to MP numeric *Concentration* ($r = 0.95$, $p \leq 0.01$, Fig. S5). We attribute this observation to the sporadic occurrence of very large MP particles. They easily dominate the MP volume and thus the mass of their sample. This introduces an additional variance for *MassConcentration*, that cannot be explained sufficiently by the predictive resources with the sample number being on the verge of meaningful exploitability.

Number- and mass-based MP values are complementary reporting units, usually originating from different analytical approaches, such as particle analytical techniques (e.g., Raman or FTIR microscopy) on the one hand, and mass spectroscopic techniques (e.g., pyrolysis GC/MS) on the other hand. When a reliable conversion is possible between the two, reporting of both quantities can avoid misinterpretations. For instance, mass-based MP inventory estimations are more intuitively interpreted in the context of the extent of the studied system, its inputs or affected population. Number-based MP concentration are important for ecotoxicological risk assessments or particle distribution dynamics.

Geospatial interpolation and inventory estimation

The predicted and observed values were used together ($n = 213$ samples) to interpolate the response variables on a regular 10 m grid over the entire Schlei area. Three grids were independently interpolated: *Concentration* and *MassConcentration* as main response variable of interest and *SedDBD* (sediment dry bulk density), which was used to infer the total estimated MP numbers and masses from the concentrations. As *SedDBD* had not been measured on the samples, it was necessary to calculate it apriori. Two empirical equations, available in the literature (Eq. 18, Eq. 19^{30,31}), were suitable for *SedDBD* approximation. These studies were also conducted in sediments of coastal waterways (lagoon, tidal channel, laboratory), covering comparable percentages of mud i.e., hydrodynamic ranges. The former used percent organic matter (*perc_OM*) and percent silt (*perc_SILT*, i.e., the fraction between 4 and 63 μm grain size), obtained according to Eq. 16 and Eq. 17. *SedDBD* was then calculated at the sample locations as the mean output of both equations from the literature (Eq. 20).

$$\text{perc_OM} = \text{TOC} \cdot 2.22 \quad (16)$$

$$\text{perc_SILT} = \text{perc_MUD} - \text{perc_CLAY} \quad (17)$$

$$\begin{aligned} & \text{SedDBD}_{\text{vanRijn et al}} \\ &= \left(1 - \frac{\text{perc_OM}}{100}\right) \\ & \cdot \left(400 \cdot \frac{\text{perc_CLAY}}{100} + 800 \cdot \frac{\text{perc_SILT}}{100} + 1600 \cdot \frac{\text{perc_SAND}}{100}\right) \end{aligned} \quad (18)$$

$$\text{SedDBD}_{\text{Jia et al}} = -8.86 \cdot \text{perc_MUD} + 1518.91 \quad (19)$$

$$\text{SedDBD} = \frac{\text{SedDBD}_{\text{vanRijn et al}} + \text{SedDBD}_{\text{Jia et al}}}{2} \quad (20)$$

The interpolation procedure was implemented in a [jupyter notebook](#) and its associated script files. Several interpolation algorithms were tested and compared using a leave-one-out cross-validation (LOOCV) with *Concentration* as target. Every of the 213 points, where either observed or predicted MP values were available, was withheld in turns, while the grid was interpolated on the remaining data points. The resulting grid was then sampled at the coordinates of the held-out point. The sampled values were used to calculate error metrics against the original values (Table S4). For the final numeric- and mass inventory estimation, we used the *OK* interpolation.

Table S4: Interpolation algorithms.

	Description	Implementation	Settings	Ref
<i>NN</i>	Nearest Neighbor interpolation. Every grid point is assigned the value of the closest sample point. Akin to assigning the target values to subareas generated by Voronoi tessellation.	interpol.py, function "scipy_griddata" using scipy library	<i>method="nearest"</i>	32
<i>IDW</i>	Inverse Distance Weighted interpolation. With the Euclidean distance $d_{i,j}$ between the sample and grid coordinates i and j , respectively, weights were determined as $w = \frac{1}{d^p}$ (with p as the weighting power) and multiplied with the sample values to obtain the weighted mean at each grid point.	interpol.py, function "numpy_simple_idw"	<i>power=1.0</i>	—
<i>OK</i>	Ordinary Kriging. The empirical variogram was used to fit a theoretical variogram for the interpolation.	interpol.py, function "skgstat_ordkrig" using SciKit-GStat	<i>n_lags: 10, maxlag: 7000, model: "spherical", min_points: 20, max_points: 30, mode: "exact", normalize: False, use_nugget: True</i>	33

The total MP inventory estimates $E_{\text{inventory}}$ were then calculated according to [Eq. 21](#),

$$E_{\text{inventory}}(\text{MP}|\text{Schlei}) = \sum_{x,y} d^2 \cdot l \cdot \text{SedDBD}_{xy} \cdot \text{MPconc}_{xy} \quad (21)$$

with (x, y) being the coordinate points of the MP concentration grid *MPconc* and *SedDBD*, d the grid point distance and l the relevant sediment layer thickness.

Vertical MP mixing

Comparing the volumetric median size of MP and sediments allows an evaluation with respect to vertical mixing and infiltration processes (Fig. S6 A). A segregation of the data is observed, with fine sediments featuring relatively larger median MP sizes (see also sample-aggregated cumulative size distributions in Fig. S6 C) and coarse sediments with relatively smaller median MP sizes (with ample-aggregated cumulative size distributions in Fig. S6 B). It is described that infiltration increasingly occurs when the ratio between the size medians of coexisting finer and coarser fractions is 0.32 or less^{34,35}. Although Schlei samples almost approach this infiltration size ratio (Fig. S6 A, dashed infiltration line) with increasingly coarser sediment grain sizes, it does not fall below.

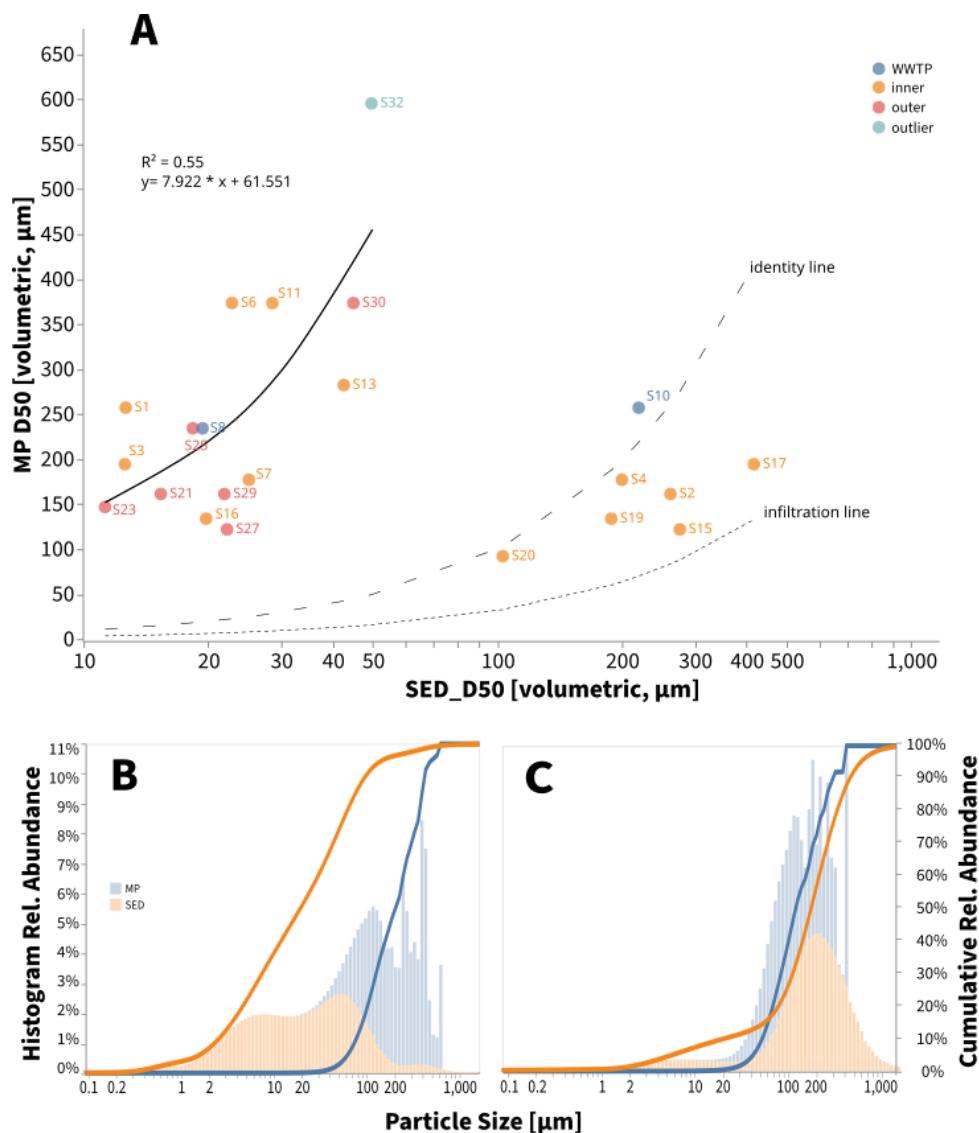


Figure S6: MP median versus sediment grain size median. For better projection of the fine sediment fraction the X-axis is shown in log-scale. Note that only samples with MP numbers > 50 are shown. (B, C) MP and sediment grain size histograms and cumulative relative abundance within fine and coarse sediments, showing interchanged size ratios, containing relatively larger and smaller MP, respectively.

The presence of additional factors in MP from environmental samples such as angularity of particles and multimodal size distributions further counteract infiltration³⁴. Thus, infiltration of MP in the studied size range appears not to be a dominating process in Schlei sediments. Equal MP levels found in greater depth are likely caused by hydrodynamic and anthropogenic sediment mixing as well as bioturbation.

Radiocarbon dating at four stations show varying degrees of mixing activities vertical across stratigraphic layers within fine sediment regions¹. Wide extents of the Schlei surface sediments are composed of a thick sapropel layer, characterized by organic-rich, fine and unconsolidated sediments. The shallow waters of the Schlei (average depth 2.5 - 3 m), foster wind-driven wave-induced sediment mixing. In fine sediments median MP sizes positively correlate with median sediment grain sizes ($R^2 = 0.55$ in linear regression) and are roughly 10

times larger. This size difference (Fig. S6) is consistent with the finding that MP distribution on the sediment bed is mainly driven by bedload transport as opposed to direct deposition ²⁴. At a given bed shear stress, relatively larger MP sizes can be mobilized compared to quartz grains due to the lower relative densities of polymers. The above considerations support the assumption that within wide parts of the Schlei, MP are subjected to sediment mixing processes which allows an extension of the MP projection to a depth of 15 cm (Fig. 3 D).

References

- (1) Schwarzer, K.; Ricklefs, K.; Höft, D. *Sediment Inventory and Hydromorphology of the Schlei, (Original: Sedimentinventar Und Hydromorphologie Der Schlei)*; Institute of Geosciences, Kiel University, 2019; p 114. https://www.schleswig-holstein.de/DE/fachinhalte/M/meeresschutz/Downloads/Bericht_SedimentinventarHydromorphologieSchlei.pdf.
- (2) Enders, K.; Lenz, R.; Ivar do Sul, J. A.; Tagg, A. S.; Labrenz, M. When Every Particle Matters: A QuEChERS Approach to Extract Microplastics from Environmental Samples. *MethodsX* **2020**, 7, 100784. <https://doi.org/10.1016/j.mex.2020.100784>.
- (3) Brandt, J.; Bittrich, L.; Fischer, F.; Kanaki, E.; Tagg, A.; Lenz, R.; Labrenz, M.; Brandes, E.; Fischer, D.; Eichhorn, K.-J. High-Throughput Analyses of Microplastic Samples Using Fourier Transform Infrared and Raman Spectrometry. *Applied Spectroscopy* **2020**, 74 (9), 1185–1197. <https://doi.org/10.1177/0003702820932926>.
- (4) Käppler, A.; Windrich, F.; Löder, M. G. J.; Malanin, M.; Fischer, D.; Labrenz, M.; Eichhorn, K.-J.; Voit, B. Identification of Microplastics by FTIR and Raman Microscopy: A Novel Silicon Filter Substrate Opens the Important Spectral Range below 1300 Cm⁻¹ for FTIR Transmission Measurements. *Analytical and Bioanalytical Chemistry* **2015**, 407 (22), 6791–6801. <https://doi.org/10.1007/s00216-015-8850-8>.
- (5) Tagg, A. S.; Brandes, E.; Fischer, F.; Fischer, D.; Brandt, J.; Labrenz, M. Agricultural Application of Microplastic-Rich Sewage Sludge Leads to Further Uncontrolled Contamination. *Science of The Total Environment* **2022**, 806, 150611. <https://doi.org/10.1016/j.scitotenv.2021.150611>.
- (6) Enders, K.; Lenz, R. How to Find the Small Plastic in the Big Sea, The Identification and Characterisation of Microplastic Larger 10 Micrometer from the Atlantic Ocean. **2014**, 98.
- (7) Brandt, J.; Fischer, F.; Kanaki, E.; Enders, K.; Labrenz, M.; Fischer, D. Assessment of Subsampling Strategies in Microspectroscopy of Environmental Microplastic Samples. *Frontiers in Environmental Science* **2021**, 8, 579676. <https://doi.org/10.3389/fenvs.2020.579676>.
- (8) Bittrich, L.; Brandt, J. GEPARD - Gepard-Enabled PARTicle Detection for Raman Microscopes. <https://gitlab.ipfdd.de/gepard/gepard>.
- (9) Lenz, R.; Enders, K.; Stedmon, C. A.; Mackenzie, D. M. A.; Nielsen, T. G. A Critical Assessment of Visual Identification of Marine Microplastic Using Raman Spectroscopy for Analysis Improvement. *Marine Pollution Bulletin* **2015**, 100 (1), 82–91. <https://doi.org/10.1016/j.marpolbul.2015.09.026>.
- (10) Käppler, A.; Fischer, D.; Oberbeckmann, S.; Schernewski, G.; Labrenz, M.; Eichhorn, K.-J.; Voit, B. Analysis of Environmental Microplastics by Vibrational Microspectroscopy: FTIR, Raman or Both? *Analytical and Bioanalytical Chemistry* **2016**, 408 (29), 8377–8391. <https://doi.org/10.1007/s00216-016-9956-3>.
- (11) Kreyling, O.; Kölbl, A.; Spielvogel, S.; Rennert, T.; Kaiser, K.; Kögel-Knabner, I. Density Fractionation of Organic Matter in Dolomite-Derived Soils. *Journal of Plant Nutrition and Soil Science* **2013**, 176 (4), 509–519. <https://doi.org/10.1002/jpln.201200276>.
- (12) Wakeham, S. G.; Canuel, E. A. The Nature of Organic Carbon in Density-Fractionated Sediments in the Sacramento-San Joaquin River Delta (California). *Biogeosciences* **2016**, 13 (2), 567–582. <https://doi.org/10.5194/bg-13-567-2016>.

- (13) Čerkasova, N.; Enders, K.; Lenz, R.; Oberbeckmann, S.; Brandt, J.; Fischer, D.; Fischer, F.; Labrenz, M.; Schernewski, G. A Public Database for Microplastics in the Environment.
- (14) Blott, S. J.; Pye, K. GRADISTAT: A Grain Size Distribution and Statistics Package for the Analysis of Unconsolidated Sediments. *Earth Surface Processes and Landforms* **2001**, *26* (11), 1237–1248. <https://doi.org/10.1002/esp.261>.
- (15) Bray, J. R.; Curtis, J. T. An Ordination of the Upland Forest Communities of Southern Wisconsin. *Ecological Monographs* **1957**, *27* (4), 325–349. <https://doi.org/10.2307/1942268>.
- (16) Su, Q.; Yu, H.; Xu, X.; Chen, B.; Yang, L.; Fu, T.; Liu, W.; Chen, G. Using Principal Component Analysis (PCA) Combined with Multivariate Change-Point Analysis to Identify Brine Layers Based on the Geochemistry of the Core Sediment. *Water* **2023**, *15* (10), 1926. <https://doi.org/10.3390/w15101926>.
- (17) Duquesne, A.; Carozza, J.-M. Improving Grain Size Analysis to Characterize Sedimentary Processes in a Low-Energy River: A Case Study of the Charente River (Southwest France). *Applied Sciences* **2023**, *13* (14), 8061. <https://doi.org/10.3390/app13148061>.
- (18) Seiß, G. Hydrodynamic Numerical Models Suitable for Application to the German Fairways and Ports at the Baltic Sea Coast. **2014**.
- (19) BAWiki. Mathematical Model UNTRIM.
- (20) BAWiki. PARTRACE.DAT.
- (21) Stone, M. Cross-Validatory Choice and Assessment of Statistical Predictions. *Journal of the Royal Statistical Society: Series B (Methodological)* **1974**, *36* (2), 111–133. <https://doi.org/10.1111/j.2517-6161.1974.tb00994.x>.
- (22) Varma, S.; Simon, R. Bias in Error Estimation When Using Cross-Validation for Model Selection. *BMC Bioinformatics* **2006**, *7* (1), 91. <https://doi.org/10.1186/1471-2105-7-91>.
- (23) Krstajic, D.; Buturovic, L. J.; Leahy, D. E.; Thomas, S. Cross-Validation Pitfalls When Selecting and Assessing Regression and Classification Models. *Journal of Cheminformatics* **2014**, *6* (1), 10. <https://doi.org/10.1186/1758-2946-6-10>.
- (24) Enders, K.; Käppler, A.; Biniash, O.; Feldens, P.; Stollberg, N.; Lange, X.; Fischer, D.; Eichhorn, K.-J.; Pollehne, F.; Oberbeckmann, S.; Labrenz, M. Tracing Microplastics in Aquatic Environments Based on Sediment Analogies. *Scientific Reports* **2019**, *9* (1), 15207. <https://doi.org/10.1038/s41598-019-50508-2>.
- (25) Yates, L. A.; Aandahl, Z.; Richards, S. A.; Brook, B. W. Cross Validation for Model Selection: A Review with Examples from Ecology. *Ecological Monographs* **2023**. <https://doi.org/10.1002/ecm.1557>.
- (26) Cawley, G. C.; Talbot, N. L. C. On Over-Fitting in Model Selection and Subsequent Selection Bias in Performance Evaluation. *Journal of Machine Learning Research* **2010**, *11* (70), 2079–2107. <https://doi.org/10.5555/1756006.1859921>.
- (27) Wainer, J.; Cawley, G. Nested Cross-Validation When Selecting Classifiers Is Overzealous for Most Practical Applications. *Expert Systems with Applications* **2021**, *182*, 115222. <https://doi.org/10.1016/j.eswa.2021.115222>.
- (28) Arlot, S.; Celisse, A. A Survey of Cross-Validation Procedures for Model Selection. *Statist. Surv.* **2010**, *4* (none). <https://doi.org/10.1214/09-SS054>.
- (29) Dietterich, T. G. Ensemble Methods in Machine Learning. In *Multiple Classifier Systems*; Goos, G., Hartmanis, J., Van Leeuwen, J., Eds.; Springer Berlin Heidelberg: Berlin, Heidelberg, 2000; Vol. 1857, pp 1–15. https://doi.org/10.1007/3-540-45014-9_1.
- (30) Van Rijn, L. C.; Barth, R. Settling and Consolidation of Soft Mud–Sand Layers. *Journal of Waterway, Port, Coastal, and Ocean Engineering* **2019**, *145* (1), 04018028. [https://doi.org/10.1061/\(ASCE\)WW.1943-5460.0000483](https://doi.org/10.1061/(ASCE)WW.1943-5460.0000483).
- (31) Jia, J.-J.; Gao, S.; Xue, Y.-C. Sediment Dynamic Processes of the Yuehu Inlet System, Shandong Peninsula, China. *Estuarine, Coastal and Shelf Science* **2003**, *57* (5–6), 783–801. [https://doi.org/10.1016/S0272-7714\(02\)00406-7](https://doi.org/10.1016/S0272-7714(02)00406-7).
- (32) Virtanen, P.; Gommers, R.; Oliphant, T. E.; Haberland, M.; Reddy, T.; Cournapeau, D.; Burovski, E.; Peterson, P.; Weckesser, W.; Bright, J.; van der Walt, S. J.; Brett, M.; Wilson, J.; Millman, K. J.; Mayorov, N.; Nelson, A. R. J.; Jones, E.; Kern, R.; Larson, E.; Carey, C. J.; Polat, İ.; Feng, Y.; Moore, E. W.; VanderPlas, J.; Laxalde, D.; Perktold, J.; Cimrman, R.; Henriksen, I.; Quintero, E. A.; Harris, C. R.; Archibald, A. M.; Ribeiro, A. H.; Pedregosa, F.;

- van Mulbregt, P.; SciPy 1.0 Contributors; Vijaykumar, A.; Bardelli, A. P.; Rothberg, A.; Hilboll, A.; Kloeckner, A.; Scopatz, A.; Lee, A.; Rokem, A.; Woods, C. N.; Fulton, C.; Masson, C.; Häggström, C.; Fitzgerald, C.; Nicholson, D. A.; Hagen, D. R.; Pasechnik, D. V.; Olivetti, E.; Martin, E.; Wieser, E.; Silva, F.; Lenders, F.; Wilhelm, F.; Young, G.; Price, G. A.; Ingold, G.-L.; Allen, G. E.; Lee, G. R.; Audren, H.; Probst, I.; Dietrich, J. P.; Silterra, J.; Webber, J. T.; Slavič, J.; Nothman, J.; Buchner, J.; Kulick, J.; Schönberger, J. L.; de Miranda Cardoso, J. V.; Reimer, J.; Harrington, J.; Rodríguez, J. L. C.; Nunez-Iglesias, J.; Kuczynski, J.; Tritz, K.; Thoma, M.; Newville, M.; Kümmerer, M.; Bolingbroke, M.; Tartre, M.; Pak, M.; Smith, N. J.; Nowaczyk, N.; Shebanov, N.; Pavlyk, O.; Brodtkorb, P. A.; Lee, P.; McGibbon, R. T.; Feldbauer, R.; Lewis, S.; Tygier, S.; Sievert, S.; Vigna, S.; Peterson, S.; More, S.; Pudlik, T.; Oshima, T.; Pingel, T. J.; Robitaille, T. P.; Spura, T.; Jones, T. R.; Cera, T.; Leslie, T.; Zito, T.; Krauss, T.; Upadhyay, U.; Halchenko, Y. O.; Vázquez-Baeza, Y. SciPy 1.0: Fundamental Algorithms for Scientific Computing in Python. *Nat Methods* **2020**, *17* (3), 261–272. <https://doi.org/10.1038/s41592-019-0686-2>.
- (33) Mälicke, M. SciKit-GStat 1.0: A SciPy-Flavored Geostatistical Variogram Estimation Toolbox Written in Python. *Geosci. Model Dev.* **2022**, *15* (6), 2505–2532. <https://doi.org/10.5194/gmd-15-2505-2022>.
- (34) Waldschläger, K.; Schüttrumpf, H. Infiltration Behavior of Microplastic Particles with Different Densities, Sizes, and Shapes—From Glass Spheres to Natural Sediments. *Environmental Science & Technology* **2020**, *54* (15), 9366–9373. <https://doi.org/10.1021/acs.est.0c01722>.
- (35) Schruoff, T. Taking a Closer Look at the Causes and Impacts of Fine Sediment Infiltration into Gravel Beds : Development and Application of an Extended Theory of Fine Sediment Infiltration Based on Grain Scale Numerical Simulations. PhD Thesis, RWTH Aachen University, 2018, Vol. RWTH Aachen University. <https://doi.org/10.18154/RWTH-2018-227229>.

What Goes Around Should Not Move Around: Immobilizing Microplastics as a New Approach for Analytical Ring Trials

Robin Lenz,* Kristina Enders, Eva Cseperke Vizsolyi, Mareike Schumacher, Julia Lötsch, Martin G. J. Löder, Gabriele Eder, Yuliya Voronko, José Manuel Andrade-Garda, Soledad Muniategui-Lorenzo, Christian Laforsch, Dieter Fischer,* and Matthias Labrenz*



Cite This: *Environ. Sci. Technol.* 2024, 58, 22224–22234



Read Online

ACCESS |

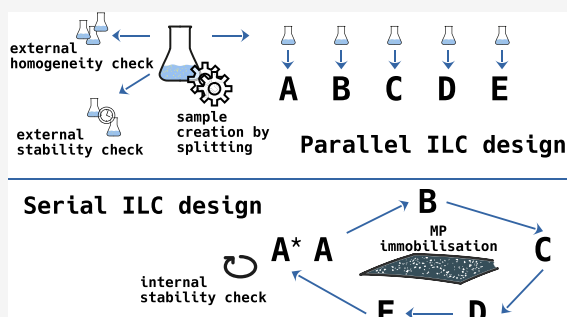
Metrics & More

Article Recommendations

Supporting Information

ABSTRACT: Microplastics have gained importance as pervasive environmental particulate pollutants. Their analysis demands precise quantification methods, with interlaboratory comparisons (ILCs) being crucial for performance assessment. Typically, ILCs follow a parallel design: participants each analyze their own sample specimen, often with significant variability due to challenges in producing identical subsamples of the particulate analyte, inseparably masking the relevant uncertainty sources the ILC intends to measure. We provide a filtration-immobilization approach for particles $\leq 100 \mu\text{m}$, creating permanently immobilized microplastics samples. This enables serial ILC designs where participants sequentially measure the same sample. Demonstrating the concept using 5 polymers immobilized on $10 \mu\text{m}$ pore-sized silicon filters, we expose the specific measurement uncertainty being 77% lower than the total combined uncertainty observed in a parallel ILC (relative standard deviations: 5 and 23%, respectively). Particle immobilization opens further applications in sample archiving and creation of durable reference samples also for other fields of particulate matter research beyond microplastics.

KEYWORDS: spectroscopy, microscopy, particles, colloid, proficiency, validation, round robin, fixation



INTRODUCTION

The contamination of the environment with microplastics (MPs), i.e., synthetic polymer particles commonly accepted to be between 1 and $1000 \mu\text{m}$,¹ has created a need for reliable data on the characteristics and quantities of MPs. This has led to a wide variety of methodological developments. The resulting significant differences in resolution and quality of analyses are impeding the comparability of data between studies^{2–4} and more comprehensive environmental risk assessments.⁵

To solve this issue, interlaboratory comparisons (ILCs) play a crucial role in evaluating the reliability and accuracy of methods for the characterization and quantification of MP particles in various samples,⁶ including environmental, food, and tissue matrices. Several ILC studies aimed at MP-analytical proficiency can be found in the recent literature^{6–14} using different sample types such as environmental matrices spiked with specific MP types,¹³ artificial samples such as suspensions,¹² or MP particles in solid media like tablets or ice cubes.^{6,11} These studies typically follow a parallel design, where each participant receives and analyzes their own sample specimen, assuming equality in MP numbers and composition. This design, based on reporting guidelines like DIN 38402-45:2014-06, as cited by ref 12, ISO 13528,¹⁵ or the IUPAC

technical report,¹⁶ resembles established procedures for soluble analytes, where homogeneity issues are less of a concern and accurate reference measurements are available. As particulate pollutants, MPs pose significant challenges to this equality assumption, especially for particle sizes in the lower micrometer range where individual handling of particles is impractical.¹⁷

The need for comparable and reliable MP quantification led to innovations in creating homogeneous sample specimens for ILCs and reference materials,^{11,18–20} as well as assessment and correction methods^{8,21} and reporting guidelines.^{22,23} Their perpetual integration in new ILCs can improve precision and reduce the uncertainty of the true MP content, gradually making the determination of analytical proficiency more reliable. However, the fundamental problem remains: parallel ILC designs capture compounded effects caused by a range of

Received: September 5, 2024

Revised: October 25, 2024

Accepted: October 25, 2024

Published: December 3, 2024



ACS Publications

© 2024 The Authors. Published by
American Chemical Society

22224

<https://doi.org/10.1021/acs.est.4c09427>
Environ. Sci. Technol. 2024, 58, 22224–22234

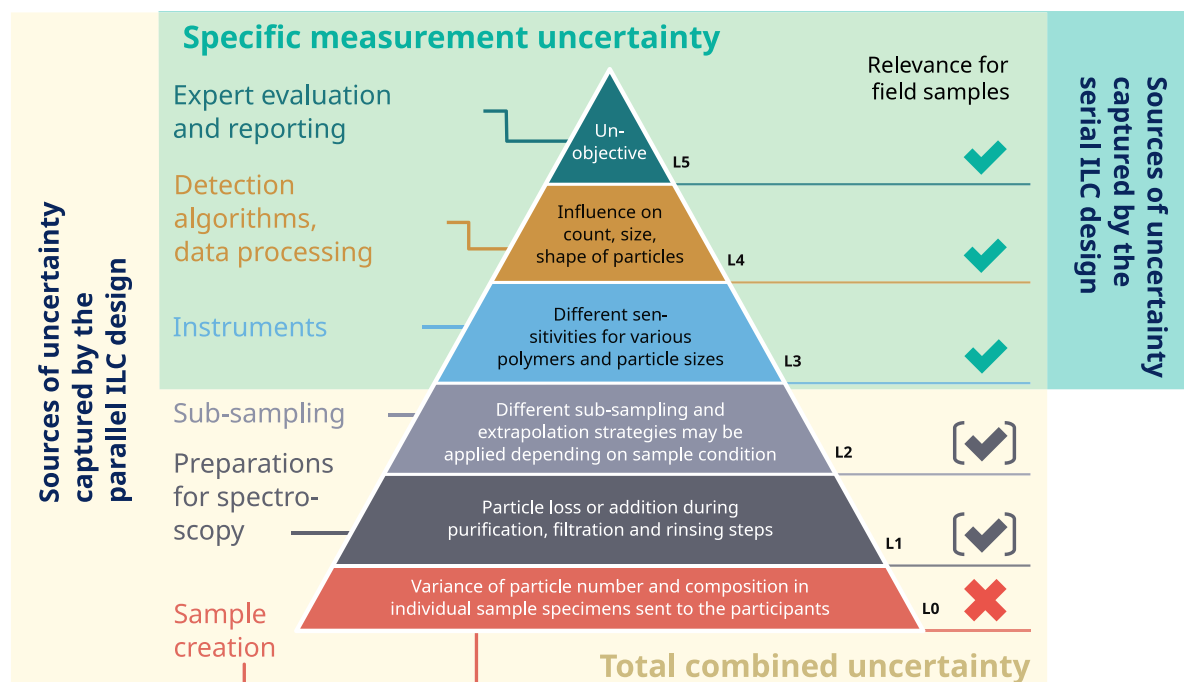


Figure 1. Uncertainties propagating through the pipeline of MP quantification. Colored areas enclose the shares captured by parallel (beige) and serial (mint) ILC design concepts. The relevance of the uncertainty contributors with regard to field samples is shown to the right of the pyramid. It is highlighted that uncertainties arising from the way in which the parallel ILC sample is produced (L0) are irrelevant to real samples and should therefore preferably be excluded by an ILC design. Other uncertainty sources (L1 and L2) can be relevant, but because they depend on the sample conditions, they should be addressed separately from an ILC estimating the specific measurement uncertainty.

uncertainty sources whose contributions cannot be further decomposed (Figure 1). At this point, it is important to emphasize the principles of metrology, such as uncertainty propagation according to the “Guide to the expression of uncertainty in measurement” (GUM)²⁴ by the Joint Committee for Guides in Metrology (JCGM) whose terminology we apply here to the field of MP analysis.

All steps from planning the sampling to evaluating and reporting the final data contribute to the combined uncertainty in the MP-analytical chain. Therefore, any uncertainties intrinsic to the production of the parallel sample specimens, e.g., from splitting or weighing, are included at the base of the final result (Figure 1). Here, we use the term “specific measurement uncertainty” to describe the combined uncertainty associated with the chemical measurement acquisitions (e.g., microspectroscopy), data evaluation, manual result control, and reporting (Figure 1, L3–L5). In parallel ILCs, the specific measurement uncertainty is inseparable from uncertainty contributions of production and distribution of sample specimens (Figure 1, L0), sample treatments like purification and measurement preparations (Figure 1, L1), and subsampling (Figure 1, L2). The first is specific to the ILC design itself and, as such, not informative about a participant’s proficiency to quantify MP field samples (compare Figure 1, “Relevance for field samples”). The latter two are of potential relevance when considering field samples but may vary depending on the pretreatment requirements of the matrix such as sediments, biota, or food samples. They should, therefore, be addressed by separate QA/QC measures²⁵ or a posteriori data alignments.⁵

Currently there is no approach available to investigate the specific measurement uncertainty in ILCs to build the basis for a subsequent evaluation of the total combined uncertainty of the whole sample preparation and analysis process. To address this gap, we adapt the concept of MP particle immobilizations, first described for experiments in the $\leq 100 \mu\text{m}$ size fraction,^{17,26} to the requirements of ILCs using an inorganic adhesive. For two common spectroscopic substrate types, porous Si wafers and alumina membranes, we describe an immobilization-by-filtration approach, leading to a permanent fixation of particles on the surface of the carrier. It can be measured sequentially by all ILC participants, with each laboratory measuring the same filter and passing it onto the next participant in the ILC consortium. This methodological paradigm shift renders the ILC literally a “ring trial”, or “round-robin test” as it is also often called, relating to its historic meaning of an institution of coordinated collective activity.^{27,28} We refer to this concept as the serial design to distinguish it from the parallel ILC design. It eliminates the unwanted uncertainty sources introduced by the repetitive sample specimen creation in the parallel design approach. Therefore, the observed variance of the results represents a more accurate magnitude of the specific measurement uncertainty.

METHODS

We conducted a comparison between a parallel design ILC where participants received independent sample specimens of samples P1–P3 and serial ILCs where participants received the same specimens of three different sample types subsequently: S1–S3 (Table 1).

Table 1. Sample Names and Their Poolings (Pool) that Were Prepared for the Parallel and Serial ILC Designs Are Listed with Their Key Specifications

Pool	Sample names	Design concepts		Immobilisation	Target area determined by	Substrate for transport	Particles
		parallel	serial				
P	P1	✓		n/a		aqueous suspension, 0.005% surfactant (TritonX)	cryo-milled fragments of
	P2	✓					
	P3	✓					
S2	S1		✓	potassium silicate solution 10%	coordinate definition	Si filter 10 µm	LDPE, PA12, PET, PP, PS retained in dry-sieving between 71 µm and 10 µm analytical stainless steel sieves
	S2.1		✓		laser engraving area A1 area A2 area A3 area A4	Si filter 1 µm	
	S2.2		✓				
	S2.3		✓				
	S2.4		✓				
S3	S3.1		✓		colour marking	alumina filter 0.2 µm (Anodisc)	
	S3.2		✓				

To encourage broader adoption, we emphasize that the proposed serial ILCs using immobilized particle samples can be conducted using standard laboratory equipment. Any special or custom-made devices, although detailed here for possible replication, can be replaced by commercially available alternatives without compromising the immobilization's success.

Sample Preparation. Sample preparation steps were conducted in specialized MP-analytical laboratories under laminar flow benches. As an exception, steps involving handling of dry MP powders such as grinding, mixing, or adding powders to suspension media were conducted outside the laminar flow bench to avoid workplace contamination. White cotton lab coats were used during all procedures.

We obtained the MP particles by sieving five previously cryo-milled (Cryomill, Retsch, Germany) environmentally relevant polymers. The resulting particle shapes were irregular (see also Figure S15.2). Fibers were not included in this study. We used low-density polyethylene (LDPE), polyamide 12 (PA12), polyethylene terephthalate (PET), polypropylene (PP), and polystyrene (PS). The raw materials and grinding and sieving procedures were identical as reported by a previous study.¹⁷

The creation of the aqueous suspension samples P1–P3 and the adhesive particle suspension for the immobilized samples S1 and S2 is described in full detail in S11. In the samples of the serial ILC design (S1–S3), the homogeneity of particle distribution on the filters was not assumed or required, as all participants measured the same defined area of each sample. The selected measurement areas were chosen based on their representativeness of the overall particle immobilization.

Immobilization on Si Wafers. Porous silicon wafers were inserted in the precleaned filtration apparatus,²⁹ connected to an adjustable vacuum pump (SC920, KNF Neuberger). The device contained red PTFE discs for sealing. For sample S1, a silicon wafer was used (11 mm length and width and 250 μm thickness) with conical pores (15/8 μm terminal diameters and 55 μm interpore distance) supplied by Fraunhofer Institute for Reliability and Microintegration, Moritzburg,

Germany; for more details, see ref 30. We refer to it as a nominal 10 μm filter.

For S2, we used a nominal 1 μm pore size filter (Si wafer: 10 mm length and width, 200 μm thickness, cylindrical 1 μm pore diameter, 1.5 μm interpore distance, from SmartMembranes GmbH, Halle, Germany).

The prepared potassium silicate adhesive particle suspension (S11) was placed on top of a high-frequency excentric shaker for homogenization, while volumes were being extracted for filtration using 1 mL Pasteur glass pipettes. We applied 2 and 6 mL for S1 and S2, respectively, where particle coverage was found to be suitable on visual inspection. Filtration was conducted at approximately 100 mbar. After curing in a vacuum drying oven (40 °C, 100 mbar, 12 h), filters were flushed with running MP-free water and compressed air to remove any loose particles. This rinsing process was repeated three times. Dark field microscopic images were acquired after each iteration to evaluate the removal of loose material. It was considered complete as no substantial further changes in the particle amounts could be manually observed between the images taken after the second and third rinse.

Immobilization on Alumina Filters. The dry powder mixture of MP particles was suspended in MP-free water and filtered onto an Al_2O_3 membrane (Anodisc, Whatman, polypropylene outer ring support, 45 μm height, 25 mm diameter, 60 μm membrane thickness, 0.2 μm pore size). The filter was then placed inside a glass Petri dish on top of a droplet of the potassium silicate adhesion medium (S11), which was allowed to soak through the filter material by capillary rising, wetting the particles from below. Two filters of this type were created and measured, S3.1 and S3.2, with different amounts of MP particles.

Target Area Definition. Measuring the entire filter area was not a viable approach for several participants in terms of measurement time and amount of data produced. Instead, rectangular areas of approximately 2 by 2 mm were defined for measurement by each participant. Three approaches to marking the specific target areas were investigated, coordinate definition, laser engraving, and color markings, for samples S1–S3, respectively (see also Table 1 and Figure 2 as well as details and dimensions provided in S12).

Serial ILC Round Trip. The filters were sent to the participants in custom-made filter holders (Figure S13) by standard mail. In the case of Si filter samples (S1 and S2), participants were advised to rinse the sample with MP-free water and dry it with compressed air prior to measurement to avoid contamination. For the Al_2O_3 membrane sample S3, this was not possible due to the fragile nature of the substrate. Al_2O_3 membranes provide a less smooth and less even surface than the samples prepared on Si filters. Hence, participants were advised to use adhesive tape on the outer ring support to improve surface flatness during measurement. Participants measured the samples using the method of their choice before repackaging them and sending them onto the next participant. Finally, the samples were received and remeasured by the host participant to assess potential particle losses from the repetitive handling and transport.

Sample Analysis. The samples from the parallel and serial ILCs were analyzed individually by each participant with no further requirements other than using their laboratory's state-of-the-art MP analysis techniques and parameters like they would use to analyze field samples. A total of eight participants were involved in the measurements; however, due to the

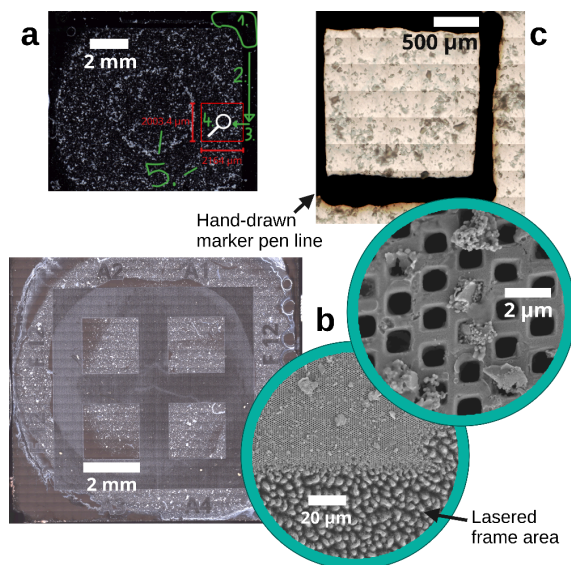


Figure 2. Approaches to defining the measurement area. (a) Dark field image of sample S1 with visual guidelines (green) provided to the participants for manual targeting. (b) Laser-engraved frame and resulting target areas A1–A4 of sample S2 shown as a dark field overview with insets showing SEM images of the area boundaries and the square 1 μm pores. (c) Bright field overview of the Al_2O_3 membrane sample S3 with the target area defined by a black marker.

developmental character of this study, not every participant measured every sample and the order of participants varied between samples. Table 2 details the chosen techniques and key parameters of the participants, as well as the samples they measured. A participant in the context of this study is a unique constellation of an institute, an analyst, a measurement instrument, and an analysis software. Participants A–D and G were located all at the same institute and differed only in the technical and analytical choices as described in Table 2.

Common Area Correction. The target area definition of samples S1 and S3 (compare Figure 2a and Figure 2c) resulted in slightly different areas measured by each participant. This was partly due to different rotation angles of the sample on the

instrument stages, different image acquisition modes of the instruments, and/or manual inaccuracies. To evaluate results from the same area only, the largest common area was defined by superimposing the obtained particle distribution images in the GNU image manipulation software (<https://gimp.org>). All images were manually registered to a common coordinate system. A rectangle contained within each image was then defined graphically as the common measurement area. Particles completely outside this common area were counted for each image and polymer type, and their numbers were subsequently subtracted from the original particle counts reported by each participant. The definition of the target area by laser engraving for sample S2 made such a correction unnecessary. The areas were sharply defined and macroscopically visible. As particles in the interstices were burnt off by the laser, a simple measurement of a slightly larger area gave the same particle numbers as measuring an area to its exact extent.

Statistical Analysis. Results were reported by participants as numbers of particles per polymer type, size range, and sample. Total MPs (TMPs) were calculated as the sum of particles of the five added polymers. We use the terms P, S2, and S3 to refer to mean aggregated results from samples P1–P3, S2.1–S2.4, and S3.1–S3.2, respectively. For results derived from Raman spectroscopy, only size classes $\geq 10 \mu\text{m}$ were considered to increase comparability to FTIR results, which were left untruncated.

In the absence of an unbiased reference value for the MP particle numbers in the samples, we used the arithmetic mean and standard deviation between participants as measures of centrality and agreement. To evaluate the deviation of the i^{th} participant's result (P_i) obtained for a sample from the overall mean of the results reported by all participants for that sample, we calculated a “relative deviation from the mean” (RMD, eq 1) where \bar{P} denotes the overall sample mean.

$$\text{RMD} = \left(\frac{P_i}{\bar{P}} - 1 \right) \cdot 100\% \quad (1)$$

Using the relative standard deviation among participants (RSD, eq 2), we compare the dispersion of reported results between the different ILC design concepts.

Table 2. ILC Participants with Spectroscopic Techniques and Measured Samples

	technique	instrument	measurement parameters	software	analyzed samples
participant A	Raman microscopy	WITec alpha300R	20 \times objective, 532 nm, 10 mW, 10 \times 0.5 s acquisitions	Gepard ³¹	all
B				Witec ParticleScout + Gepard ³¹	S1, S2, S3
C				Gepard ³¹ + ML-prototype Raman ^a	S1
D	micro-FTIR imaging	PerkinElmer Spotlight400	transmission, IR range of 4000–650, 8 cm^{-1} resolution, 4 scans/pixel (6.25 μm)	ML-prototype FTIR ^a	all
E					
F		Bruker Lumos II	transmission, IR range of 3600–1250, 8 cm^{-1} resolution, 2 scans/pixel (5.7 μm)	Bruker Opus v7.5 + BayreuthMicroplasticsFinder ³²	P1, P2, P3, S2, S3
G	Raman microscopy	Renishaw inVia Qontor	20 \times objective, 633 nm, 50% power, 7 \times 0.5 s acquisitions	Gepard ³¹	S1, S2, S3
H	LDIR imaging	Agilent 8700LDIR	quantum-cascade laser IR source, IR range of 1800–975, 8 cm^{-1} resolution, 1 scan/particle	Agilent Clarity software v1.5	S2

^aMachine learning-based prototypes for MP quantification developed by Purency GmbH, Vienna, Austria.

$$\text{RSD} = \frac{\sqrt{\frac{\sum_{i=1}^n (P_i - \bar{P})^2}{n}}}{\bar{P}} \cdot 100\% \quad (2)$$

Due to the low number of participants using Raman ($N \leq 4$) and FTIR ($N \leq 3$) spectroscopy, mean differences between these groups were evaluated by one-sided, nonpaired, exact permutation tests³³ and accepted as statistically significant for $p \leq 0.05$, i.e., the proportion where the mean of values assigned to the lower group was greater than the mean of values assigned to the higher group in not more than 5% of all possible permutations.

Results were regarded as statistical outliers where experimental values were more than 1.5 times the interquartile range below the first or above the third quartile of all participants. They were excluded where technically justified, i.e., where a limited compatibility between the properties of a certain ILC sample and the applied measurement technique was identified.

The stability of a sample was evaluated by comparing the TMP measurements, conducted by the same participant, at the beginning x_{pre} and at the end x_{post} of the serial ILC. We used a stability criterion c (eq 4) in adaptation from ISO 13528.¹⁵ Here, we used the ratio between the “two-sided” relative pre/postdeviation Δ_{rel} (eq 3) and the RSD among the participants as a stability criterion, accounting for the fact that samples with multiple measurement areas may not have comparable absolute MP particle numbers. “Two-sided” here indicates that we take the double of the difference from the mean as the expected deviation range would be centered around the mean going into positive and negative directions.

$$\Delta_{\text{rel}} = \frac{2 \cdot |\bar{x}_{\text{pre,post}} - x_{\text{pre}}|}{\bar{x}_{\text{pre,post}}}, \text{ with } \bar{x}_{\text{pre,post}} = \frac{x_{\text{pre}} + x_{\text{post}}}{2} \quad (3)$$

$$c = \frac{\Delta_{\text{rel}}}{\text{RSD}} \quad (4)$$

Acceptable stability was expected when $c \leq 0.3$. When the calculated stability was only marginally above this threshold, c had to be corrected to include the measurement uncertainty (u) according to eq 6 as recommended for testing against the same threshold.¹⁵ We determined u as the average relative distance of r replicate postmeasurements from their mean (eq 5).

$$u = \frac{\sum_{i=1}^r |\bar{x}_{\text{post}} - x_{\text{post},i}|}{r \cdot \bar{x}_{\text{post}}}, \text{ with } \bar{x}_{\text{post}} = \frac{\sum_{i=1}^r x_{\text{post},i}}{r} \quad (5)$$

$$c = \frac{\Delta_{\text{rel}}}{\text{RSD} + 2\sqrt{u^2 \cdot \Delta_{\text{rel}}}} \quad (6)$$

A spreadsheet file that was used for the calculations and figure generations and a Jupyter notebook containing the calculations of the permutation tests are provided in the data deposit.³⁴

RESULTS AND DISCUSSION

We report on a novel immobilization technique for MPs and its application in serial ILCs compared to parallel ILCs. As absolute numbers of particles varied significantly between samples, we show the numbers of MP particles reported by the participants here relative to their mean (Figure 3), but raw

count data are presented as bar charts in the Supporting Information (Figure SI4.1).

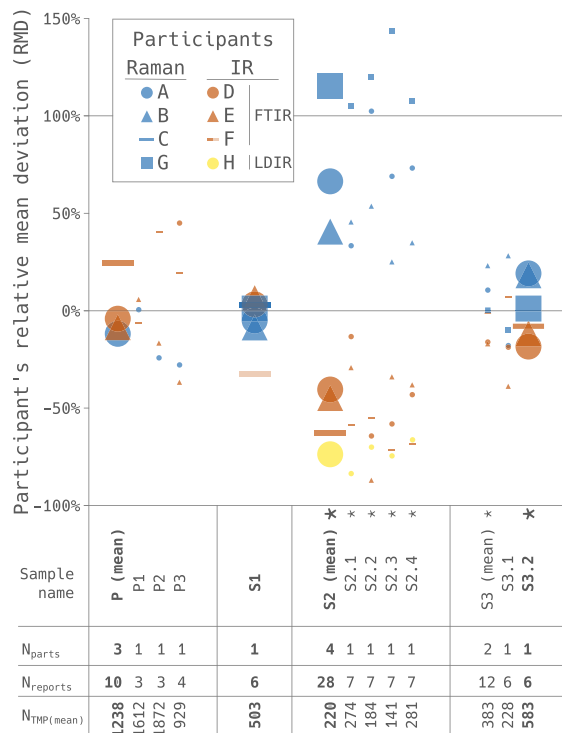


Figure 3. Particle numbers shown as percentage deviation from the participant mean per sample (RMD). Large symbols show the most important results per sample type. These are the pooled results for P and S2 where multiple sample parts were available and the single sample results S1 and S3.2. Sample S3.1 needed to be excluded for lack of stability. Small symbols indicate the RMDs for the constituting sample parts. Asterisks indicate significant differences between the subgroups' mean RMDs (Raman vs IR, see also Table 2 for references of the techniques used by each participant). Participant F's result for sample S1 was excluded as a statistically and technically justified outlier, and it is shown here semitransparently for reference only (not included in the mean calculation). Key data of the samples are provided below the horizontal axis. Sample name: terminology used according to Table 1 (P: samples used in parallel ILCs; S: samples used in serial ILCs). N_{parts} : number of parts that were pooled under this sample name. N_{reports} : number of reports returned by participants (for brevity showing the sum of reports in multipart samples). N_{TMP} : reported particle numbers of TMP as mean over participants (polymer and participant-specific results are provided in the data deposit³⁴). Absolute particle numbers are shown in Figure SI4.1.

The serial ILC design, by isolating the specific measurement uncertainty, significantly reduces observed variation among participants compared to the parallel ILC, with a 77% lower RSD in the small-scale ILC comparison we conducted here (Figure 4).

Isolation of the Specific Measurement Uncertainty by MP Immobilization. The parallel ILCs resulted in an RSD of 23% as derived from the mean of the three suspended samples, following Table 1 (pooled as sample P in Figure 4). The RSD spreads from 5% (P1) to 34% (P3) and is shown as whiskers in Figure 4. The high RSD, along with the absence of a consistent

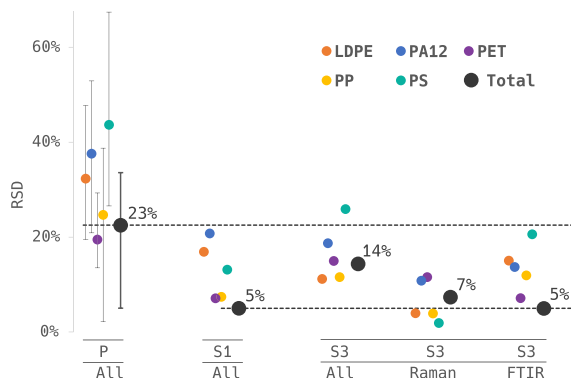


Figure 4. RSD among participants for the different ILC samples. Dashed lines indicate the RSD levels of TMP in the serial ILC of S1, which was 77% lower than in the parallel ILC design (results of samples P1, P2, and P3 were pooled as “P”). Whiskers show the extents to the minimum and maximum of the unpooled RSD values. RSD values of S2 can be seen in an extended version in the Supporting Information (Figure SI4.2). P, parallel samples; S, serial samples.

pattern among participants over the three samples (see Figure 4, P1–P3, for details), suggests that uncertainty sources like sample production, transport, and preparation for spectroscopy (see L0–L2 in Figure 1) may have contributed an important share of the overall variation of the results. Hence, the magnitude of the specific measurement uncertainty (L3–L5, Figure 1) cannot be estimated. The serial ILCs, with particles immobilized on the measurement substrates, exclude production- and preparation-derived uncertainties by design, as every participant measures the same sample. Thus, the specific measurement uncertainty can be investigated independently.

The S1 series on the 10 μm Si filter substrate resulted in an RSD of 5% (with participants A–E and G, Figure 4), giving an indication of the specific measurement uncertainty within the ILC consortium. It is observed that, generally, individual polymers have a larger RSD than TMP. The TMP individual values reported by the participants vary with RMDs between -9 and $+6\%$ around their mean (Figure 3). There was no significant difference between the RMD means of the ad hoc Raman and Fourier transform infrared (FTIR) subgroups for S1.

To test whether the serial ILC concept can be extended to other applications, a smaller pore size Si filter (S2) and aluminum oxide as another common filter substrate (S3) were explored in further ILCs. While the FTIR participants reported largely consistent results for the Al_2O_3 -based sample S3, participant F reported difficulties in obtaining a reliable measurement result for the Si sample S1. Their analysis technique is based on a machine-learning polymer recognition model trained on Al_2O_3 substrates, which can be expected to have limited compatibility with the Si substrate. This underlines the importance of taking filter substrate preferences into account when designing an ILC. The use of different filter substrates can help to make an equitable assessment.

The overall RSD of S3 is 14% with regard to all participants (A, B, and D–G). However, when separated by the spectroscopic technique, the RSD is comparable to what has been described for S1: 7 and 5% for Raman and FTIR spectroscopy, respectively (Figure 4). Raman-based measure-

ments of S3 have, on average, a significantly higher RMD of 25 percentage points (%pt) difference, significant at $p \leq 0.05$ (Figure 3) compared to FTIR-based techniques. The other filter S3.2 is excluded from analysis as a substantial particle loss of 21% has been recorded between pre- and postmeasurements of the host participant, indicating that the immobilization was not sufficient (see also Figure 6 and Stability of Filtration-Immobilization).

For the 1 μm Si filter (S2), an even stronger segregation can be observed with respect to the spectroscopic technique. On average, Raman participants are $>120\%$ pt higher in terms of RMD compared to FTIR and LDIR. Accordingly, the RSD is substantially higher: 71% for TMP and up to 91% for the individual polymers, exceeding the RSD of the parallel ILC. In order not to distort the scale of Figure 4, S2 was omitted there. An extended version including S2 is presented in the Supporting Information (Figure SI4.2). We assume that a reason for the observed systematically lower TMP estimates of the FTIR and LDIR participants for the 1 μm filter S2, and, although weaker, for the Al_2O_3 filters S3 (see also Figure SI4.1), is likely an excess of potassium silicate adhesive, which remains in the smaller pores due to capillary forces and thus adversely affects the FTIR signal intensity. Further, the properties of Si wafer filters like material thickness and pore diameter, pattern, and distance could cause interferences in the IR wavelengths.³⁰ In combination with the potassium silicate adhesive, this may have reduced polymer recognition for IR-based techniques. This was indeed the case when considering the LDIR transmittance measurements as the spectra of many particles appeared “blurred” or distorted due to the partial coverage by the adhesive. In transmittance, the IR light interacts twice with the surface of the particles plus with the reflecting substrate.

Radar charts in Figure 5 show the RMDs of the participants for the five polymer types. The closer the lines are to the most intense color region (RMD $\pm 10\%$), the higher the consensus within the consortium. The host or initial participant is located at the top of the polygon, and the other participants follow clockwise in the order the samples were sent around. The trials

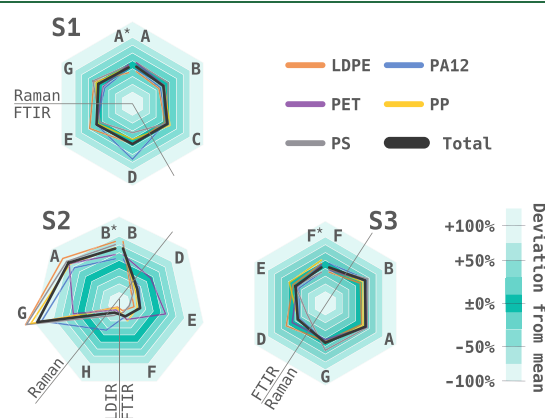


Figure 5. Reported results of the three serial ILC trials with samples S1–S3 as percentage deviation from the overall participant mean. Entries marked by asterisks indicate the post-transport control measurement of each ILC sample and do not constitute an own participant. Hairlines delineate the ad hoc subgroups of Raman, FTIR, and LDIR measurements.

finish with remeasurement by the host (marked with an asterisk in Figure 5) to determine the immobilization stability. The remeasurement results were not included in the mean for the RMD calculations.

S1 showed high consensus among the participants (Figure 5). Overall, we conclude that the use of the 10 μm Si filter, in contrast to 1 μm pore-sized filter S2, allowed better comparability between Raman and FTIR results. We attribute this observation to the resulting size range of particles (excluding the sub-10 μm fraction), which is better suited to the typical limits for FTIR, and to a lower capillary retention of the potassium silicate adhesive in the larger pores of S1.

As to the polymer type, the largest singular positive deviation from the overall participants mean in S1 occurs for the polyamide PA12, which has been identified as a software-caused false-positive problem by participant D. The machine learning-based analysis was sensitive to even weak presence of bands in the natural amide region, leading to pixels being erroneously classified as polyamide. This illustrates that the isolation of the specific measurement uncertainty achieved herein enables certain analysis pipelines to be debugged.

Neither parallel nor serial ILC designs can determine the absolute truth of the particle number present. This is clearly so when particle sizes get close to the instrumental detection limits, as it was the case here, at least for FTIR and LDIR at around 10 μm . Nevertheless, when only larger sizes are considered, agreement might be possible and very relevant. At least for the immobilized design, a theoretically viable—but very time-consuming—way to obtain an accepted true reference value would be an analysis with individual optical microscopy and manual spectroscopic assessment of all immobilized particles in a target area of a sample. However, even then, it would be difficult to achieve absolute certainty about the number of MP particles present. In borderline cases, it may be impossible even for human assessors to make a final decision about the extent of a single particle, because MPs do not always exhibit unequivocally visually separable particle boundaries.

The serial ILC performed here serves as a demonstrative proof of concept for the idea of using immobilized samples in serial ILCs. We recommend for benchmarking or standardizing ILCs, prepared in this manner, to use replicated samples as well as repetitions of the pre- and postmeasurements ($n \geq 3$). They serve as a control of successful immobilization and allow to estimate the intra-analytical measurement uncertainty. Furthermore, the number of participants was low and the apparent particle numbers varied between the different ILC types (see also the table within Figure 3). Presenting more equal particle numbers to a larger group of participants will lead to increased stability of the uncertainty estimations that can be attributed to the applied analysis techniques.

Stability of Filtration-Immobilization. The development of the immobilization method in the present study was adapted from a previous approach where spin-coating was used to distribute an adhesive on a carrier.¹⁷ The change to the filtration-immobilization principle proved advantageous as the amount of residual adhesive on the substrate surface is substantially reduced. We provide insights of spectroscopic effects of the remaining adhesive in S15.

In the serial ILC concept, the host participant repeats their measurements after the ring trial completion to ascertain whether particle loss occurred (Figure 6). Negligible differ-

ences indicate the adequate stability and permanence of the immobilization.

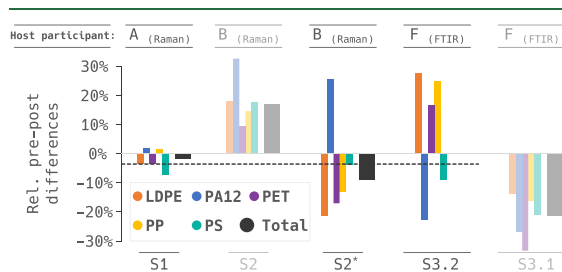


Figure 6. Relative differences of particle numbers per polymer identified by the host participant before and after the serial ILC. S2* was calculated only on the particle fraction $\geq 20 \mu\text{m}$ due to the reasons explained in the main text. The dashed line indicates the change in particle counts as the average “pre/postdifferences” of those samples with acceptable sample stability, i.e., only opaquely plotted bars. Note that the value for total MPs was very low in S3.2 (bar not visible).

Participant B, who made the pre/postcomparison of sample S2 using Raman spectroscopy, received a software upgrade from the manufacturer between the two measurements that improved the instrument’s ability to detect smallest particles. The stability of the immobilization was therefore only evaluated on the $\geq 20 \mu\text{m}$ particle fraction of the pre- and postmeasurements. The comparison including particles between 10 and 20 μm is presented for reference (Figure 6) and shows a spurious increase in the abundance of particles in the postmeasurement.

In adaptation of the ISO 13528¹⁵ stability criteria c (eqs 4 and 6) to the serial ILC, we observe that samples S1, S2, and S3.2 qualify for being included in the ILC results. Their relative pre/postdifferences are within the threshold for acceptable stability of $c \leq 30\%$, namely, at 25, 14, and 1% of the interparticipant RSDs, respectively. For sample S1, this result was obtained using eq 6 with an expected measurement uncertainty of 0.056 and would have been 32% when using eq 4.

In addition to actual changes in particle numbers due to sample transport, deviations between pre/postmeasurements are also influenced by the expected—and here unknown—intra-analytical variance of the host participants. However, the overall low pre/postdifference (Figure 6; dashed line: -4% on average of the samples accepted according to the “criterion c ”) implies that only relatively small intra-analytical variances are to be expected here.

There was an apparent difference of immobilization stability between the two Al_2O_3 filters (S3.1 and S3.2). In contrast to the Si filters, a rinsing procedure to remove insufficiently immobilized particles after curing was not applied due to the fragility of the material. Future studies aiming for immobilized samples on alumina membranes should explore other solutions for removing loose particles.

Pre/postdifferences in the individual polymer types appear to largely cancel out each other in TMP, which is especially obvious for samples S2 and S3.2. This indicates a differential polymer type misclassification problem, not only between participants (Figure 4) but also intra-analytically. This reveals an interesting research question on whether there is in general

a significantly lower uncertainty on TMP counts than on quantifications of individual polymers.

Perspective of Environmental Particle Evaluation.

Below, we summarize the lessons learned from the interlaboratory trials presented here and give recommendations to encourage much needed further methodological advancement in this area. The approach we present here is targeting the size range of about 10–100 μm . It would likely be suitable for MPs up to about 500 μm , but the effectiveness of the filtration immobilization is yet to be evaluated in this size range. As such, we only cover a part of the environmentally relevant MPs. For larger sizes, simpler methods like obtaining a true reference value by manual counting become viable and are therefore likely to be preferred.

With sample S1, we found a 10 μm filter well suited for comparative measurements with Raman, FTIR, and LDIR spectroscopy, while the 1 μm filter S2 posed several obstacles to FTIR and LDIR detection. This includes a higher presence of particles in size ranges where physical limitations restrict successful detection by these techniques. In Raman spectroscopy, potassium silicate shows distinct bands at 545 and 1029 cm^{-1} (Figure S1S.1), but they did not interfere with the polymer classification, primarily because Raman spectroscopy is acting on the up-facing surfaces of the particles, where little or no excess adhesive is expected. For FTIR and LDIR spectroscopy measured in transmission and transreflectance modes, respectively, any adhesive between the particles and the filter surface or inside the filter pores will interact with the IR light. However, this will not result in conjugate spectra (i.e., polymer spectra clearly superimposed inorganic bands of the adhesive) because the FTIR measurements for polymer identification were made against a background of potassium silicate on the filter material. Instead, the IR adsorption of the silica compounds manifests itself as increased noise because it limits the IR energy that can reach the detector. Regarding the concentration of potassium silicate, we chose the lowest tested concentration as the best option. It seems reasonable thinking that further dilutions may be a promising endeavor to decrease potential impacts to certain techniques.

Many analytical protocols employ subsampling measurement approaches due to instrumental or computational limitations or to reduce measurement time. This entails extensive extrapolation of the actual measurement result to the whole sample, contributing to the uncertainty propagation. In fact, subsampling approaches (see also Figure 1) have been demonstrated to cause substantial errors in the determination of the total particle numbers.²⁵ A major advantage of the immobilized serial ILC design is that such a subsampling error is eliminated by the precise definition of a commonly measured area. Here, the laser engraving technique developed for Si filter S2 proved to be highly useful in that it expedites and unifies measurements and result evaluations. Due to the particles being removed from the interstice, minor unavoidable differences in the size and positioning of the measurement areas will not significantly affect the results when all participants select areas slightly larger than the visible target areas.

For a permanently immobilized serial ILC sample, we consider three properties to be most desirable:

- The substrate and immobilization achieve sufficient stability, i.e., they withstand the repetitive handling, transportation, and measurement.

- Its physical properties do not interfere with or discriminate against certain measurement techniques, e.g., sufficient IR transparency is warranted.
- The sample allows for some form of return to original state, e.g., by rinsing off any adherent contaminating particles prior to each participant's measurement.

Compared to the creation of numerous sample specimens for parallel ILCs, the immobilized approach requires less strict contamination control during production. Contamination during sample generation is excluded by design as everything that gets immobilized becomes part of the sample. It is still advisable to prepare samples under reasonable analytical laboratory conditions to avoid unintentionally introduced particles, producing spurious results.

Outlook and Future Perspectives. The immobilized filters in our serial ILC were prepared at small research laboratory scale. While offering significant advantages over traditional parallel designs, they are not intended as a permanent solution. They serve as an intermediate step in establishing robust analytical protocols and identifying sources of measurement uncertainty. However, the concept should be taken up for the development and supply of certified reference materials (CRMs) that can be routinely used for method validation and quality control in laboratories worldwide. CRMs, produced and certified by accredited organizations such as the European Joint Research Centre (JRC), the German Federal Institute for Materials Research and Testing (BAM), the National Metrology Institute of Japan (NMIJ), the International Atomic Energy Agency (IAEA), or the United States National Institute of Standards and Technology (NIST), provide a standardized and traceable means of validating analytical methods and ensuring interlaboratory comparability. For MPs, however, the provision of CRMs presents unique challenges due to the particulate nature of the analyte. Collaboration between research institutions, regulatory bodies, and accredited reference material producers is essential to overcome these challenges and establish commercially available immobilized and suspended CRMs for MP analysis.

With immobilized MP CRMs available, automated reproducible measurements may be set up with minimal manual involvement. These procedures can run routinely on a periodic schedule or after any changes in measurement protocols, equipment, or personnel. Over time, the results can become highly valuable for the laboratory to monitor the relative analytical proficiency and spot any arising problems in MP detection.

Further questions should be addressed to establish a broader applicability of the immobilized samples. For instance, knowledge on immobilization stability of larger MP sizes (e.g., 100–1000 μm), fibers or natural particulates, may allow for an application also to field samples. This can reduce particle loss or disarrangement in the transition from sample preparation to spectroscopic measurement. Additionally, it may be used to build up persistent sample archives for repeatable measuring. At the current stage, however, we do not recommend the immobilization technique for quantitative sample preservation. We included here steps of sample flushing to remove incompletely immobilized particles, which would obviously not be an option in field samples intended for MP quantification. Provided that the objective is to conduct an ILC or similar experiment—where the total number of MPs present

in the sample prior to immobilization is not of interest—we may reasonably assume that the technique would work just as effectively if MPs from the environment were used instead of the milled and sieved pristine particles employed in this study.

Our results suggest that other research on particulate pollutants beyond like fly ashes, cement dust, soot, or spores can benefit from adapting the immobilization technique to yield reproducibly measurable samples. In particular, further developments targeting immobilization of atmospheric particulate matter samples will help in comparability studies of microspectroscopic and mass spectroscopic analyses^{35,36} (see also S16). Likewise, other multianalysis studies, such as correlative microscopy or spectroscopy, could benefit from enhanced precision and accuracy when working with particle immobilizations.

■ ASSOCIATED CONTENT

Data Availability Statement

Data of measured MP particles per sample and participant with statistical analysis and raw version of the figures created thereof are provided as a Microsoft Office Excel spreadsheet in the data and code deposit³⁴ at [10.5281/zenodo.10791088](https://doi.org/10.5281/zenodo.10791088).

■ Supporting Information

The Supporting Information is available free of charge at <https://pubs.acs.org/doi/10.1021/acs.est.4c09427>.

Material and methodological details, additional microspectroscopic and spectroscopic information, and an extended version of Figure 4 (PDF)

■ AUTHOR INFORMATION

Corresponding Authors

Robin Lenz — Leibniz Institute of Polymer Research Dresden, Dresden 01069, Germany; Leibniz Institute for Baltic Sea Research Warnemünde, Rostock 18119, Germany; orcid.org/0000-0003-4156-7380; Email: robin.lenz@ipfdd.de

Dieter Fischer — Leibniz Institute of Polymer Research Dresden, Dresden 01069, Germany; Email: fisch@ipfdd.de

Matthias Labrenz — Leibniz Institute for Baltic Sea Research Warnemünde, Rostock 18119, Germany; orcid.org/0000-0003-3452-8631; Email: matthias.labrenz@io-warnemuende.de

Authors

Kristina Enders — Leibniz Institute of Polymer Research Dresden, Dresden 01069, Germany; Leibniz Institute for Baltic Sea Research Warnemünde, Rostock 18119, Germany

Eva Cseperke Vizsolyi — University of Bayreuth, Bayreuth 95440, Germany

Mareike Schumacher — Leibniz Institute of Polymer Research Dresden, Dresden 01069, Germany

Julia Lötsch — Leibniz Institute of Polymer Research Dresden, Dresden 01069, Germany

Martin G. J. Löder — University of Bayreuth, Bayreuth 95440, Germany; orcid.org/0000-0001-9056-8254

Gabriele Eder — Österreichisches Forschungsinstitut für Chemie und Technik, Wien 1030, Austria

Yuliya Voronko — Österreichisches Forschungsinstitut für Chemie und Technik, Wien 1030, Austria

José Manuel Andrade-Garda — University of A Coruña, A Coruña 15071, Spain

Soledad Muniategui-Lorenzo — University of A Coruña, A Coruña 15071, Spain

Christian Laforsch — University of Bayreuth, Bayreuth 95440, Germany

Complete contact information is available at: <https://pubs.acs.org/10.1021/acs.est.4c09427>

Author Contributions

R.L. and K.E. invented the serial ILC concept and the silicon-based particle immobilizations, contributed to Raman and FTIR measurements, analyzed the data, and drafted the manuscript. E.C.V. and M. Löder contributed to FTIR measurements, created the samples for the parallel ILC, and developed the alumina-based particle immobilizations. M.S. and J.L. contributed to Raman measurements. G.E. and Y.V. contributed to FTIR measurements. J.M.A.G. and S.M.L. contributed to LDIR measurements. D.F. and M. Labrenz supervised the work. All authors reviewed the manuscript draft.

Funding

Financial support was received from the following: the CORNET project microplastics@food funded by the German Federal Ministry of Economic Affairs and Climate Action, IGF project no. 298 EBG; the JPI OCEANS project microplastiX funded by the German Federal Ministry of Education and Research under grant number 03F0852A, the Spanish Agencia Española de Investigación (grant PCI2020-112145, MCIN/AEI/10.13039/501100011033, and EU “Next Generation EU/PRTR”), and Galician Government (Xunta de Galicia, “Consolidación e Estructuración de Unidades de Investigación Competitivas”, ED431C 2021/56); the Deutsche Forschungsgemeinschaft (DFG, German Research Foundation), project number 391977956, SFB 1357; the German BMBF research program “Plastics in the environment”: MicroCatch_Balt “Investigation of Sinks and Sources of Microplastics from a Typical Catchment Area to the Open Baltic Sea”, grant number 03F0788A; the EU-BONUS Programme “Blue Baltic”: MICROPOLL “Multilevel assessment of microplastics and associated pollutants in the Baltic Sea”, grant number 03F0775A.

Notes

The authors declare no competing financial interest.

■ ACKNOWLEDGMENTS

We thank the following for their help: Melinda Arnold and Mikhail Malanin (IPF Dresden) for FTIR measurements; Christian Norkus (Werkstatt TU Dresden) for assistance with the laser engraving of the Si filters; Maria auf der Landwehr (IPF Dresden) for providing SEM images; Benedikt Hufnagl (Hufnagl Chemometrics GmbH) for providing access to ML-prototype Raman and FTIR spectroscopy; Elisavet Kanaki and Robert Ohmacht for continuous improvement of the Gepard measurement software; Alexander Tagg for helpful comments on the manuscript draft.

■ REFERENCES

- (1) ISO/TR 21960. *Plastics—Environmental Aspects—State of Knowledge and Methodologies*, 2020.
- (2) Hidalgo-Ruz, V.; Gutow, L.; Thompson, R. C.; Thiel, M. Microplastics in the Marine Environment: A Review of the Methods Used for Identification and Quantification. *Environ. Sci. Technol.* **2012**, *46* (6), 3060–3075.
- (3) Löder, M. G. J.; Gerds, G. Methodology Used for the Detection and Identification of Microplastics—A Critical Appraisal. In *Marine*

Anthropogenic Litter; Bergmann, M.; Gutow, L.; Klages, M., Eds.; Springer International Publishing: Cham, 2015; pp 201–227.

(4) Hermesen, E.; Mintenig, S. M.; Besseling, E.; Koelmans, A. A. Quality Criteria for the Analysis of Microplastic in Biota Samples: A Critical Review. *Environ. Sci. Technol.* **2018**, *52* (18), 10230–10240.

(5) Koelmans, A. A.; Redondo-Hasselerharm, P. E.; Mohamed Nor, N. H.; Kooi, M. Solving the Nonalignment of Methods and Approaches Used in Microplastic Research to Consistently Characterize Risk. *Environ. Sci. Technol.* **2020**, *54* (19), 12307–12315.

(6) van Mourik, L. M.; Crum, S. J. H.; Martinez-Frances, E.; Bavel, B. van; Leslie, A. A.; de Boer, J.; Cofino, W. P. Results of WEPAL-QUASIMEME/NORMANS First Global Interlaboratory Study on Microplastics Reveal Urgent Need for Harmonization. *Sci. Total Environ.* **2021**, *772*, No. 145071.

(7) Thornton Hampton, L. M.; De Frond, H.; Gesulga, K.; Kotar, S.; Lao, W.; Matuch, C.; Weisberg, S. B.; Wong, C. S.; Brander, S.; Christensen, S.; Cook, C. R.; Du, F.; Ghosal, S.; Gray, A. B.; Hankett, J.; Helm, P. A.; Ho, K. T.; Kefela, T.; Lattin, G.; Lusher, A.; Mai, L.; McNeish, R. E.; Mina, O.; Minor, E. C.; Primpke, S.; Rickabaugh, K.; Renick, V. C.; Singh, S.; Van Bavel, B.; Vollnhals, F.; Rochman, C. M. The Influence of Complex Matrices on Method Performance in Extracting and Monitoring for Microplastics. *Chemosphere* **2023**, *334*, No. 138875.

(8) Wagner, J.; Robberson, W.; Allen, H. Analytical Precision Assessment for Microplastic Analyses. *Chemosphere* **2022**, *304*, 135295–135295.

(9) Langknecht, T.; Lao, W.; Wong, C. S.; Kotar, S.; El Khatib, D.; Robinson, S.; Burgess, R. M.; Ho, K. T. Comparison of Two Procedures for Microplastics Analysis in Sediments Based on an Interlaboratory Exercise. *Chemosphere* **2023**, No. 137479.

(10) de Frond, H.; Hampton, L. T.; Kotar, S.; Gesulga, K.; Matuch, C.; Lao, W.; Weisberg, S. B.; Wong, C. S.; Rochman, C. M. Monitoring Microplastics in Drinking Water: An Interlaboratory Study to Inform Effective Methods for Quantifying and Characterizing Microplastics. *Chemosphere* **2022**, *298*, No. 134282.

(11) Deuke, A.-K.; Fischer, E. *Microplastics on the Rocks: Adaption of a Method for the Preparation and Storage of Reference Material*; Zenodo, 2022.

(12) Müller, Y. K.; Wernicke, T.; Pittroff, M.; Witzig, C. S.; Storck, F. R.; Klinger, J.; Zumbülte, N. Microplastic Analysis-Are We Measuring the Same? Results on the First Global Comparative Study for Microplastic Analysis in a Water Sample. *Anal. Bioanal. Chem.* **2020**, *412* (3), 555–560.

(13) Becker, R.; Altmann, K.; Sommerfeld, T.; Braun, U. Quantification of Microplastics in a Freshwater Suspended Organic Matter Using Different Thermoanalytical Methods – Outcome of an Interlaboratory Comparison. *J. Anal. Appl. Pyrolysis* **2020**, *148*, No. 104829.

(14) Isobe, A.; Buenaventura, N.; Chastain, S.; Chavanich, S.; Cózar, A.; DeLorenzo, M. E.; Hagmann, P.; Hinata, H.; Kozlovskii, N.; Lusher, A.; Martí, E.; Michida, Y.; Mu, J.; Ohno, M.; Potter, G.; Ross, P. S.; Sagawa, N.; Shim, W. J.; Song, Y. K.; Takada, H.; Tokai, T.; Torii, T.; Uchida, K.; Vassilenko, K.; Viyakarn, V.; Zhang, W. An Interlaboratory Comparison Exercise for the Determination of Microplastics in Standard Sample Bottles. *Mar. Pollut. Bull.* **2019**, *146*, 831–837.

(15) ISO 13528. *Statistical Methods for Use in Proficiency Testing by Interlaboratory Comparisons*, 2022.

(16) Thompson, M.; Ellison, S. L. R.; Wood, R. The International Harmonized Protocol for the Proficiency Testing of Analytical Chemistry Laboratories (IUPAC Technical Report). *Pure Appl. Chem.* **2006**, *78* (1), 145–196.

(17) Lenz, R.; Enders, K.; Fischer, F.; Brandt, J.; Fischer, D.; Labrenz, M. Measuring Impacts of Microplastic Treatments via Image Recognition on Immobilised Particles below 100 Mm. *Microplastics Nanoplastics* **2021**, *1* (1), 12.

(18) Seghers, J.; Stefaniak, E. A.; La Spina, R.; Cella, C.; Mehn, D.; Gilliland, D.; Held, A.; Jacobsson, U.; Emteborg, H. Preparation of a

Reference Material for Microplastics in Water—Evaluation of Homogeneity. *Anal. Bioanal. Chem.* **2022**, *414* (1), 385–397.

(19) Martínez-Francés, E.; Marie-Louise, T. M.; Craig, M.; Johansen, J. E.; Nizzetto, L.; Hurley, R.; Buenaventura, N.; Van Bavel, B. *Production of Microplastic Reference Materials*; Zenodo, 2022.

(20) Dehaut, A.; Himber, C.; Colin, M.; Duflos, G. Think Positive: Proposal of a Simple Method to Create Reference Materials in the Frame of Microplastics Research. *MethodsX* **2023**, *10*, No. 102030.

(21) Dawson, A. L.; Santana, M. F. M.; Nelis, J. L. D.; Motti, C. A. Taking Control of Microplastics Data: A Comparison of Control and Blank Data Correction Methods. *J. Hazard. Mater.* **2023**, *443*, No. 130218.

(22) Brander, S. M.; Renick, V. C.; Foley, M. M.; Steele, C.; Woo, M.; Lusher, A.; Carr, S.; Helm, P. A.; Box, C.; Cherniak, S. L. C.; Andrews, R. C.; Rochman, C. M. Sampling and Quality Assurance and Quality Control: A Guide for Scientists Investigating the Occurrence of Microplastics Across Matrices. *Appl. Spectrosc.* **2020**, *74* (9), 1099–1125.

(23) Cowger, W.; Booth, A. M.; Hamilton, B. M.; Thaysen, C.; Primpke, S.; Munno, K.; Lusher, A. L.; Dehaut, A.; Vaz, V. P.; Liboiron, M.; Devriese, L. I.; Hermabessiere, L.; Rochman, C.; Athey, S. N.; Lynch, J. M.; De Frond, H.; Gray, A.; Jones, O. A. H.; Brander, S.; Steele, C.; Moore, S.; Sanchez, A.; Nel, H. Reporting Guidelines to Increase the Reproducibility and Comparability of Research on Microplastics. *Appl. Spectrosc.* **2020**, *74* (9), 1066–1077.

(24) Joint Committee for Guides in Metrology. *Guide to the Expression of Uncertainty in Measurement — Part 1: Introduction*; Bureau International des Poids et Mesures, 2023.

(25) Brandt, J.; Fischer, F.; Kanaki, E.; Enders, K.; Labrenz, M.; Fischer, D. Assessment of Subsampling Strategies in Microspectroscopy of Environmental Microplastic Samples. *Front. Environ. Sci.* **2021**, *8*, No. 579676.

(26) Thaysen, C.; Munno, K.; Hermabessiere, L.; Rochman, C. M. Towards Raman Automation for Microplastics: Developing Strategies for Particle Adhesion and Filter Subsampling. *Appl. Spectrosc.* **2020**, *74* (9), 976–988.

(27) Leeson, P. T. Rational Choice, Round Robin, and Rebellion: An Institutional Solution to the Problems of Revolution. *J. Econ. Behav. Organ.* **2010**, *73* (3), 297–307.

(28) Pierson, R. H.; Fay, E. A. Guidelines for Interlaboratory Testing Programs. *Anal. Chem.* **1959**, *31* (12), 25A–49A.

(29) Kanaki, E.; Fischer, F.; Brandt, J.; Fischer, D. *A Filtration Apparatus for the Analysis of Microplastics*; Zenodo 2024.

(30) Käßler, A.; Windrich, F.; Löder, M. G. J.; Malanin, M.; Fischer, D.; Labrenz, M.; Eichhorn, K. J.; Voit, B. Identification of Microplastics by FTIR and Raman Microscopy: A Novel Silicon Filter Substrate Opens the Important Spectral Range below 1300 cm^{-1} for FTIR Transmission Measurements. *Anal. Bioanal. Chem.* **2015**, *407* (22), 6791–6801.

(31) Brandt, J.; Bittrich, L.; Fischer, F.; Kanaki, E.; Tagg, A.; Lenz, R.; Labrenz, M.; Brandes, E.; Fischer, D.; Eichhorn, K.-J. High-Throughput Analyses of Microplastic Samples Using Fourier Transform Infrared and Raman Spectrometry. *Appl. Spectrosc.* **2020**, *74* (9), 1185–1197.

(32) Hufnagel, B.; Stibi, M.; Martirosyan, H.; Wilczek, U.; Möller, J. N.; Löder, M. G. J.; Laforsch, C.; Lohninger, H. Computer-Assisted Analysis of Microplastics in Environmental Samples Based on μFTIR Imaging in Combination with Machine Learning. *Environ. Sci. Technol. Lett.* **2022**, *9* (1), 90–95.

(33) Welch, W. J. Construction of Permutation Tests. *J. Am. Stat. Assoc.* **1990**, *85* (411), 693–698.

(34) Lenz, R.; Enders, K.; Vizsolyi, É. C.; Schumacher, M.; Lötsch, J.; Löder, M. G. J.; Eder, G.; Voronko, Y.; Andrade-Garda, J. M.; Muniategui-Lorenzo, S. N.; Laforsch, C.; Fischer, D.; Labrenz, M. *Data and Supplementary Files of the Publication: "What Goes Around Should Not Move Around: Immobilizing Microplastics as a New Approach for Analytical Ring Trials"*, Zenodo 2024.

(35) Primpke, S.; Fischer, M.; Lorenz, C.; Gerdt, G.; Scholz-Böttcher, B. M. Comparison of Pyrolysis Gas Chromatography/Mass

Spectrometry and Hyperspectral FTIR Imaging Spectroscopy for the Analysis of Microplastics. *Anal. Bioanal. Chem.* **2020**, *412*, 8283–8298.

(36) Primpke, S.; Fischer, M.; Lorenz, C.; Gerdts, G.; Scholz-Böttcher, B. Quantifying Microplastics in Complex Environmental Samples: Py-Gc/Ms vs. Hyperspectral Ftir – Potential and Limitations. In *30th International Meeting on Organic Geochemistry (IMOG 2021)*; European Association of Geoscientists & Engineers: Online, 2021; pp 1–2.

Supporting Information

for the Paper

“What Goes Around Should Not Move Around: Immobilizing Microplastics as a New Approach for Analytical Ring Trials”

Robin Lenz^{1,2,✉}, Kristina Enders^{1,2}, Eva Cseperke Vizsolyi³, Mareike Schumacher¹, Julia Lötsch¹, Martin Löder³, Gabriele Eder⁴, Yuliya Voronko⁴, José Manuel Andrade-Garda⁵, Soledad Muniategui-Lorenzo⁵, Christian Laforsch³, Dieter Fischer^{1,✉} and Matthias Labrenz^{2,✉}

¹ Leibniz Institute of Polymer Research Dresden, 01069 Dresden, Germany

² Leibniz Institute for Baltic Sea Research Warnemünde, 18119 Rostock, Germany

³ University of Bayreuth, 95440 Bayreuth, Germany

⁴ Österreichisches Forschungsinstitut für Chemie und Technik, 1030 Wien, Austria

⁵ University of A Coruña, 15071 A Coruña, Spain

✉ Correspondence: Robin Lenz <robin.lenz@ipfdd.de>, Dieter Fischer <fisch@ipfdd.de>, Matthias Labrenz <matthias.labrenz@io-warnemuende.de>

Contents

SI1:	3
Preparation of particle suspensions P1 – P3 for the parallel ILC	3
Preparation of media for the immobilised MP samples S1 – S3 for serial ILCs	4
SI2: Approaches for measurement target area definition	5
SI3: Custom filter holder and transportation box	6
SI4.1: Absolute particle counts	7
SI4.2: Extended plot: relative standard deviations	8
SI5: Potassium silicate – spectroscopic effects	8
SI6: Perspective of mass-spectroscopic techniques	11
References	12

Summary:

Number of pages:	12
Number of figures:	7
Number of tables:	0

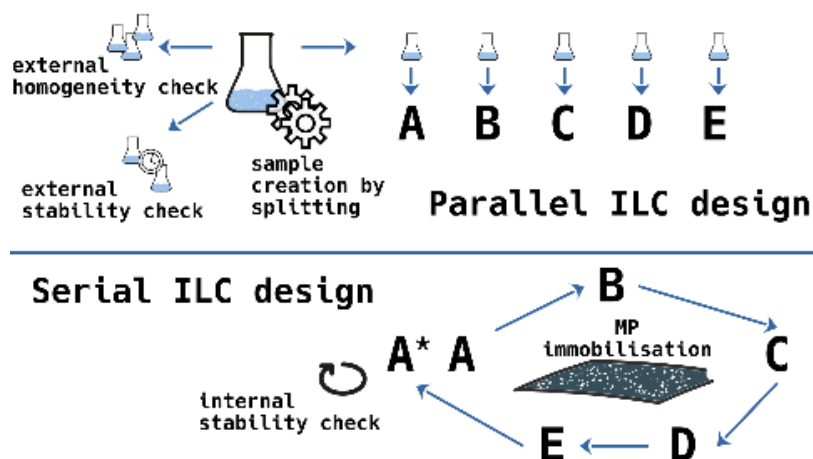


Table-of-Contents Graphic | A parallel and a serial ILC design with participating laboratories A - E. In a parallel ILC (upper part), a separate sample specimen is prepared for each participant, with additional ones held back for homogeneity and stability controls. Specifically for microparticulate analytes like microplastics (MP), the homogeneity of the measurand between sample specimen cannot be guaranteed or controlled. In a serial ILC (lower part), only one sample exists which is measured in turns by all participants, with host participant A repeating their measurement (here A*) to evaluate sample stability. This requires the preparation of a permanently immobilised sample. For its production we propose a filtration-immobilisation technique using potassium silicate as an inorganic adhesive. After particles are applied to the filter substrate as aqueous suspension, the curing of the adhesive arrests them in position by water-insoluble bonding to the substrate. Transported in suitable containers, these samples can be passed around the consortium of participants without compromising their integrity, allowing them to be measured repeatedly using different techniques chosen by the participants.

SI1:

Preparation of particle suspensions P1 – P3 for the parallel ILC

An aqueous solution of 0.005% (v/v) TritonX-100 (Merck KGaA) surfactant was prepared and filtered through 0.2 μm cellulose acetate filters to avoid microplastics (MP) contamination. 1 mg of each polymer (measured by an XPR6U microscale, Mettler Toledo, Switzerland) was added to 500 mL of the surfactant solution and homogenised in an ultrasonic bath. The particle suspension was filtered onto a 2 μm stainless steel filter (Spörl KG, Germany) and the bottle was rinsed out to avoid the loss of particles sticking to the inner walls. The filtrate, containing the particle fraction below 2 μm , was discarded. During filtration, care was taken to ensure a homogenous distribution of the particles on the filter. The sample was then halved using an in-house made sample dividing device, which is able to support the filter from below while covering one half of the filter (see Figure SI1). With this tool, it is possible to wash off the uncovered half of the filter into a glass beaker with 500 mL of the MP-free surfactant solution. The technique was developed to provide a more homogenous splitting compared to pipetting the suspension, where MP can attach to the pipette tips inside and outside, and where inhomogeneities of the polymer distributions may arise due to different material densities, sizes and shapes. We note that the use of this specific tool may still have had an influence on the resulting MP content of the splits obtained. However, the same would be true if any other splitting technique was chosen. In parallel ILCs, the uncertainties of sample production will always propagate to the final results (as we illustrate in Figure 1).

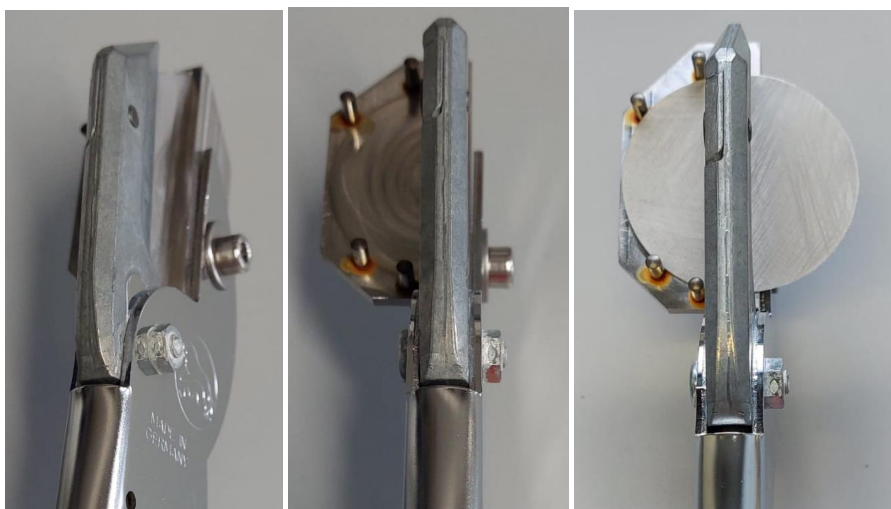


Figure SI1 | Modified pliers used as a sample splitting device. The right image shows how a 47 mm diameter stainless steel mesh filter is inserted. The device supports one half of the filter, blocking one half by a separating wall while particles on the other half of the filter can be rinsed off freely.

The procedure of filtration and splitting was conducted five times consecutively, in order to yield suspensions, where the particle concentration was in an acceptable range. The suspensions were then transferred into glass Erlenmeyer flasks and closed with glass stoppers using metal clamps to secure the suspensions during transport. The participants were advised to filter the sample specimens onto a spectroscopic substrate of their choice: either Si porous wafer filters or alumina membranes were used.

Preparation of media for the immobilised MP samples S1 – S3 for serial ILCs

For immobilisation, we used a technical grade potassium silicate solution ($K_2SiO_3 \cdot n H_2O$, also known as “water glass”, 1.25 g cm^{-1} , Baufan Bauchemie Leipzig GmbH) as inorganic adhesive bonding agent, which is non-toxic, readily available and inexpensive. When exposed to air, the water evaporates from the aqueous potassium silicate solution, which then silicifies by absorbing CO_2 . We use this effect to form polymeric silica structures on the contact surfaces between the MP particles and the filter substrate. This eliminates the need for organic polymer-based adhesives, which have been used to immobilise MP particles but introduce interfering bands¹. Therefore, we avoid that polymer-based adhesive bands overlay the MP spectra obtained for particle identification. Based on preliminary tests with potassium silicate concentrations of 10%, 20% and 30% (v/v), it was found that 10% gave the best trade-off between filterability, immobilisation capabilities, layer thickness and pot life. Higher concentrations led to increased amounts of residual adhesive on the immobilised particles, which disturbs in particular FTIR transmission measurements. An attempt to create K_2SiO_3 -based immobilisation by spin-coating¹ did not produce satisfactory results here because of uneven wafer surface wetting and crack formation during curing.

For samples S1 and S2, an adhesive stock solution was prepared by mixing 10 mL of a potassium silicate solution with 90 mL MP-free H_2O at room temperature in a glass Erlenmeyer flask with glass stopper. The solution was then filtered through $1 \mu\text{m}$ Si filters. The filtrate was used as the MP-free suspension and adhesion medium thereafter. A total mass of 1.52 mg of a powder mix of approximately equal bulk volumes of the five polymers (LDPE, PA12, PET, PP, PS) was added to the prepared medium. The closed flask with the suspension was submitted to an ultrasonic bath (10 min, USC600TH, VWR, 45 kHz, 120 W) for particle dispersion and then held on top of a high frequency excentrical shaker for homogenisation while volumes were being extracted for filtration using 1 mL Pasteur glass pipettes.

For samples S3, the same adhesion medium was used, however, without added MP particles.

SI2: Approaches for measurement target area definition

1. For sample S1, participants were given a step-by-step guideline to find the specific area based on a macroscopically clearly visible feature on the filter surface (Figure 2a in the main text). The rectangular area dimensions were 2.2 by 2.0 mm.
2. For sample S2, four target areas were created using an engraving laser. Through the engraving process, we produced a grid of four independent measurement areas (A1 - A4, 2 by 2 mm each) separated by a frame where the laser had burnt off the top layer including the MP particles, the adhesive and approximately 3 μm of the Si filter material. Scanning electron microscopy (SEM) images were obtained on a Zeiss Ultra Plus SEM at 3 kV after sputtering 3 nm platinum on a replicate of S2 which was not used for the spectroscopic measurements (Figure 2b in the main text).

The engraving was conducted using the following equipment and settings:

Instrument: Rofin Combiline Advanced WT
Laser source: Rofin Powerline F20 Varia
Wave length: 1064 nm

Process parameters for used in the engraving of sample S2:

Track width: 0,015mm
Laser power: 0.8W
Frequency: 20000Hz
Speed: 50mm/s
Pulse width: 4ns
Defocussing: 0%

Exemplary CAD files are provided as part of the data deposit².

3. On the Al_2O_3 filters (samples S3), before particle immobilisation, a boundary was drawn manually with a thin black marker pen, the inside of which was the intended measurement target area (shown in Figure 2c in the main text). Although irregular, these manually defined measurement areas were approximately rectangular with dimensions of 1.9 by 1.8 mm and 1.8 by 1.6 mm for S3.1 and S3.2, respectively.

SI3: Custom filter holder and transportation box

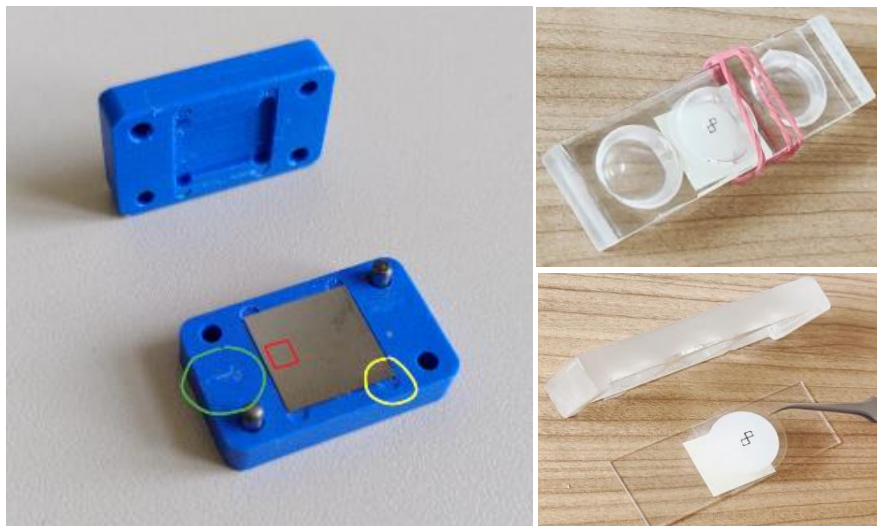


Figure SI3 | Custom-made Si filter holders for sample transport. Left: blue PTFE containers used for sample S1 and S2 consist of two parts that can be plugged together. During shipping the holder was tightly wrapped in adhesive tape to ensure that the sample remained in place. The engraved arrow on one side of the bottom part (green circle) indicates where the measurement area should be located (red square). This measure keeps the measurement area out of the filter support area where friction can affect the sample. There are also milled pockets in the corners for gentle handling of the filter with tweezers (yellow circle). Right upper: Sample S3 was transported in a glass sandwich with a microscopy slide as the bottom and a thicker circular concave cavity glass cover. When closed the slide slips in place into the recess of the cover and was secured with rubber bands. Right lower: After opening, the alumina filter was moved by tweezers on the outer support ring. The hand-drawn measurement area markings are visible.

The consortium consisted of participants from three countries (Austria, Germany, Spain). Immobilised samples of the two different substrates (Si and alumina) investigated here for use in serial ILCs were prepared by two different groups at different institutes. This includes the development of the transport solutions, which therefore also differ significantly. While the Si filters were shipped in a blue PTFE box custom-made by a scientific mechanical workshop, the alumina filters were secured for transport using only off-the-shelf laboratory glassware (Figure SI3).

SI4.1: Absolute particle counts

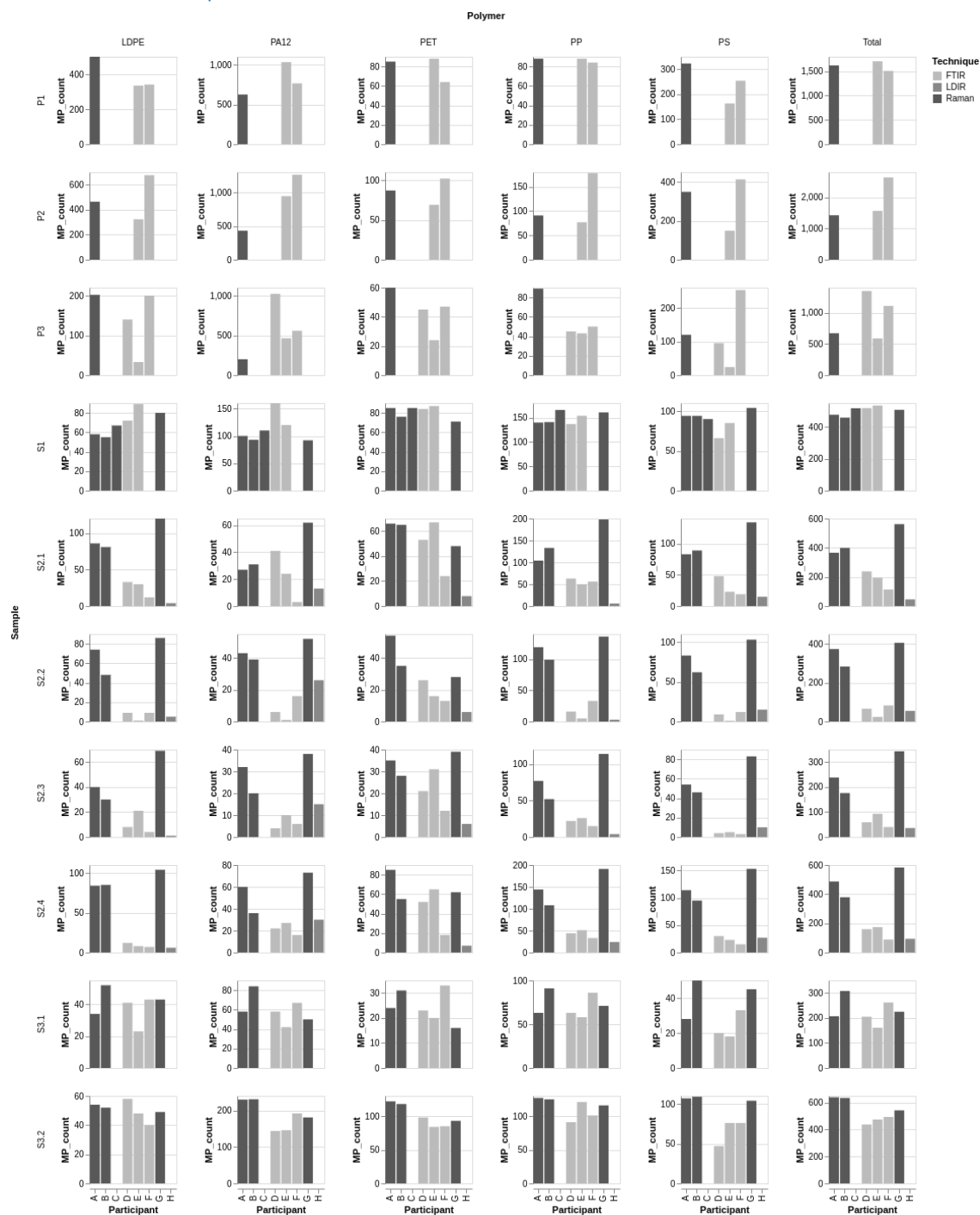


Figure SI4.1 | Counts reported by the participants, after harmonisation of common measured area and particle sizes (i.e. Raman $\geq 10 \mu\text{m}$). Bars are missing where samples were not measured or results not reported.

SI4.2: Extended plot: relative standard deviations

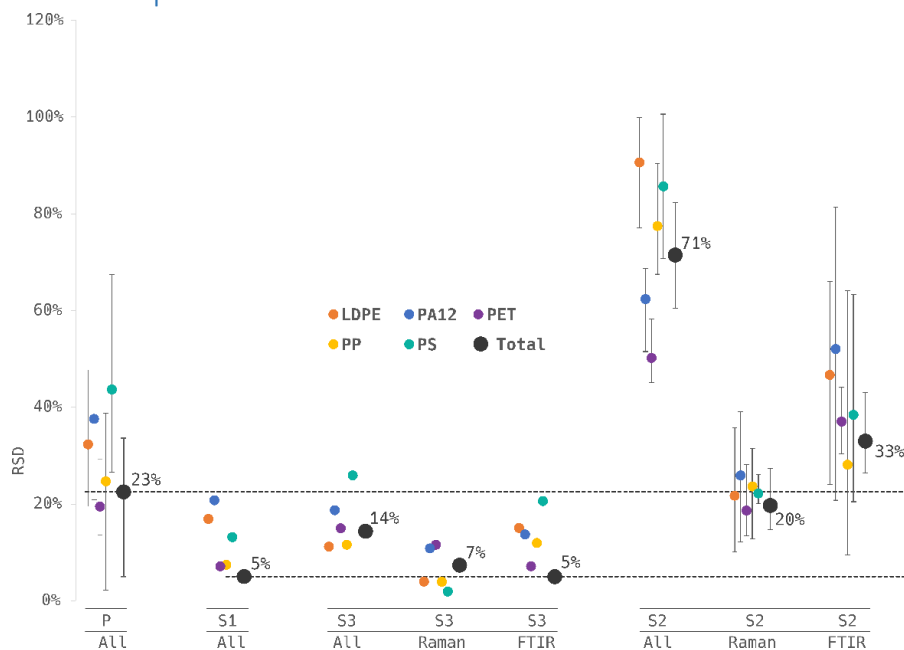


Figure SI4.2 | RSD among participants for the different ILC samples including sample S2. The greater RSD in S2 is explained by the surplus of potassium silicate adhesive remaining in the smaller pores and the resulting interference, which negatively affect IR-based techniques. LDIR (participant H) is only represented in the “All” category of S2. Whiskers show the extents to the minimum and maximum of the unpooled RSD values.

SI5: Potassium silicate – spectroscopic effects

Excess amounts of potassium silicate negatively impact the signal to noise ratio of FTIR and LDIR measurements (as has been observed on the smaller-pore sized filters S2 and partly S3). In Raman spectra it can exhibit bands around 545 and 1030 cm^{-1} (Figure S5.1), however, we observed no negative impact in the spectra acquired on the surfaces of the measured polymer types. For reference, potassium silicate spectra were recorded and are provided with the deposited data².

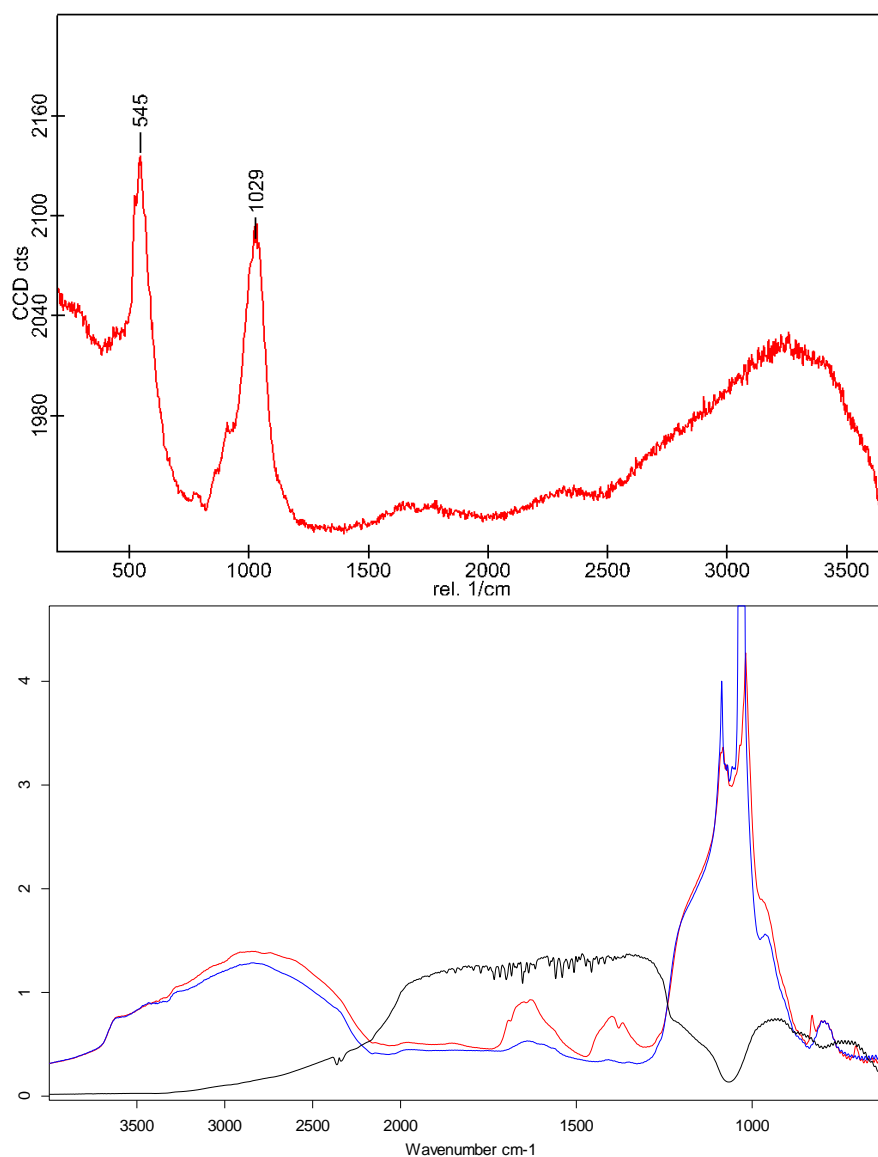


Figure S15.1 | Raman and FTIR spectra of the polymerised potassium silicate, used as an inorganic adhesive for particle immobilisations. Water glass solution (Baufan Bauchemie Leipzig GmbH) was dripped onto an ethanol-cleaned Si wafer and allowed to dry. Upper: Raman spectrum, measurement conditions: 532 nm, 20 x, 50 accumulation, 0.5 s, 5 mW. Lower: FTIR spectra: in black shows the single-channel transmission spectrum of the Si filter without potassium silicate (used as background for the other two spectra), red and blue show absorption spectra of the silica-laden filter at locations with and without excess crusts, respectively. FTIR microscope Bruker Hyperion 2000, coupled to Vertex 70, 4000 – 600 cm^{-1} , HgCdTe detector, resolution 4 cm^{-1} , 100 scans per acquisition.

A deliberately exploited effect of the filtration immobilisation on the 10 μm pore size Si filter is the optimal distribution of particles on the substrate. Smaller particles predominantly come to rest on top of single pore cavities. This provides a nearly regular particle pattern which ensures that high particle

S9

numbers can be measured in a small area. Larger particles are irregularly interspaced between or on top the grid-like smaller particles, leading to realistic scenarios of tightly aligned or overlaid particles. An example of a region of sample S1 illustrates this distribution (Figure S5.2).

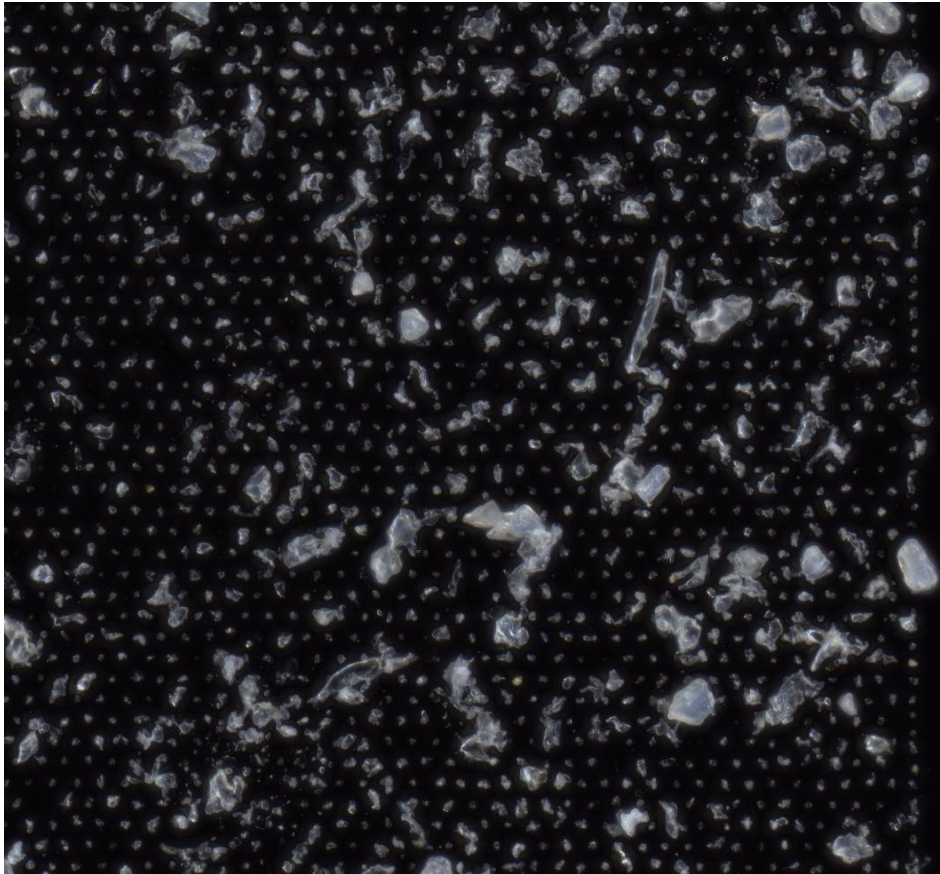


Figure S15.2 | Measurement area of sample S1. The arrangement of particles is a result of the immobilisation filtration principle. Particles close to the pore size ($10\ \mu\text{m}$) assemble in a grid like pattern on top of the pore cavities.

SI6: Perspective of mass-spectroscopic techniques

While we did not employ Pyrolysis-Gas Chromatography/Mass Spectrometry (Py-GC-MS) in this study, it is worth discussing its value, as it emerged as a valuable complementary technique for the analysis of MP³⁻⁵. Given an adequate pre-concentration of MP, so that the total mass of each polymer in a sample exceeds the respective limits of quantification, this technique is particularly useful for measuring small MP and nanoplastics embedded in complex matrices³, such as soils and sediments, where traditional spectroscopic methods may face limitations.

Incorporating Py-GC-MS data would enable valuable comparative measurements between particle- and mass-based techniques. For instance, Raman spectroscopy, as employed by the participants in our ILCs, not only identifies polymer types but also provides high-resolution microscopic images that allow for particle size estimation in three dimensions. This capability enables the conversion of the obtained MP particle number to an estimated mass, which could be compared to Py-GC-MS results. Similar comparisons between FTIR and Py-GC-MS have been conducted^{6,7}.

However, Py-GC-MS is a destructive method which conflicts with the concept of a serial ILC that relies on a single sample being passed around among participants. One potential solution could be to include one Py-GC-MS participant as the last in the sequence of the ILC. This approach would allow for the comparison of mass-based and particle-based techniques, but it comes with the drawback that the host participant would not be able to repeat their measurement after the ILC for stability control.









Additionally, the sample could not be preserved for possible future re-consultations. Therefore, in scenarios of mixed ILCs, including participants using mass- as well as particle-based techniques, a parallel design might still be preferable.

References

1. Lenz, R. *et al.* Measuring impacts of microplastic treatments via image recognition on immobilised particles below 100 µm. *Microplastics Nanoplastics* **1**, 12 (2021).
2. Lenz, R. *et al.* Data and supplementary files of the publication: "What Goes Around Should Not Move Around: Immobilizing Microplastics as a New Approach for Analytical Ring Trials".
<https://doi.org/10.5281/zenodo.10791088> (2024).
3. Fischer, M. & Scholz-Böttcher, B. M. Microplastics analysis in environmental samples – recent pyrolysis-gas chromatography-mass spectrometry method improvements to increase the reliability of mass-related data. *Anal. Methods* **11**, 2489–2497 (2019).
4. Ivleva, N. P. Chemical Analysis of Microplastics and Nanoplastics: Challenges, Advanced Methods, and Perspectives. *Chem. Rev.* **121**, 11886–11936 (2021).
5. Scholz-Böttcher, B. M. Mass-based methods for the analysis of micro- and nanoplastics. *Wiley Anal. Sci. Mag.* (2023) doi:10.1002/was.00050419.
6. Primpke, S., Fischer, M., Lorenz, C., Gerdts, G. & Scholz-Böttcher, B. M. Comparison of pyrolysis gas chromatography/mass spectrometry and hyperspectral FTIR imaging spectroscopy for the analysis of microplastics. *Anal. Bioanal. Chem.* 1–16 (2020) doi:10.1007/s00216-020-02979-w.
7. Primpke, S., Fischer, M., Lorenz, C., Gerdts, G. & Scholz-Boettcher, B. Quantifying Microplastics in Complex Environmental Samples: Py-Gc/Ms vs. Hyperspectral Ftir – Potential and Limitations. in *30th International Meeting on Organic Geochemistry (IMOG 2021)* 1–2 (European Association of Geoscientists & Engineers, Online, 2021). doi:10.3997/2214-4609.202134253.

Article

A Public Database for Microplastics in the Environment

Natalja Čerkasova ^{1,2,*} , Kristina Enders ^{3,4} , Robin Lenz ^{3,4} , Sonja Oberbeckmann ⁴ , Josef Brandt ⁵ , Dieter Fischer ³, Franziska Fischer ³ , Matthias Labrenz ⁴  and Gerald Schernewski ^{1,4,*} 

¹ Marine Research Institute, Klaipeda University, Universiteto ave. 17, LT-92294 Klaipėda, Lithuania

² Texas A&M AgriLife Research, 720 E Blackland Rd, Temple, TX 76502, USA

³ Leibniz Institute of Polymer Research Dresden; Hohe Straße 6, D-01069 Dresden, Germany

⁴ Leibniz-Institute for Baltic Sea Research, Seestrasse 15, D-18119 Rostock, Germany

⁵ Department of Marine Sciences, University of Gothenburg, Box 461, SE-405 30 Göteborg, Sweden

* Correspondence: natalja.cerkasova@ku.lt (N.Č.); gerald.schernewski@io-warnemuende.de (G.S.)

Abstract: During recent years plastics became one of the focuses of EU policy. A harmonisation and comparability of microplastics monitoring results across Europe is needed. The complexity of microplastic data makes it necessary to develop a specific, tailor-made database rather than adapting and modifying one of the existing databases. To meet this demand, we present a publicly accessible, flexible, and extendable structured relational database for particle-based microplastic data. The developed relational database is adaptive and meets the specific demands of microplastics, e.g., a large variety of sampling, processing and analytical methods, many types of plastics, and a very wide size spectrum ranging from micrometres to millimetres. In this paper we discuss the development of the database, data entry specifics, sample analysis methods, microplastics data manipulation and quality assurance, and database integration and accessibility.

Keywords: microplastic data; database; marine; particles; EU policies; Marine Strategy Framework Directive



Citation: Čerkasova, N.; Enders, K.; Lenz, R.; Oberbeckmann, S.; Brandt, J.; Fischer, D.; Fischer, F.; Labrenz, M.; Schernewski, G. A Public Database for Microplastics in the Environment. *Microplastics* **2023**, *2*, 132–146. <https://doi.org/10.3390/microplastics2010010>

Academic Editors: Nicolas Kalogerakis and Tony Robert Walker

Received: 30 December 2022

Revised: 15 January 2023

Accepted: 7 February 2023

Published: 15 February 2023



Copyright: © 2023 by the authors. Licensee MDPI, Basel, Switzerland. This article is an open access article distributed under the terms and conditions of the Creative Commons Attribution (CC BY) license (<https://creativecommons.org/licenses/by/4.0/>).

1. Introduction

Environmental policy in European countries is driven by ambitious European Union (EU) legislation, which has affects beyond the EU member states. Some major EU policy fields are the marine and coastal environment, nature and biodiversity, and water. The water policy aims at protecting the European Union's water resources and ecosystems and ensuring access to clean drinking and bathing water. This includes specific policies, e.g., on marine, surface, bathing and drinking water, floods, nitrate pollution, groundwater, urban wastewater, water reuse, water scarcity, and droughts. Most environmental policies are implemented though legally binding directives. These directives are accompanied by implementation guidelines that regulate, for example, monitoring, methodological standards, quality thresholds, and environmental quality assessment. A consequence of EU environmental policy implementation is the collection of enormous amounts of heterogeneous environmental data.

The need to deal with this data initiated the development of the EU Shared Environmental Information System (SEIS). It was established to improve the collection, exchange, and use of environmental data and information across Europe [1]. The SEIS serves as an umbrella for specific data platforms such as the Marine Information System for Europe (WISE-Marine) and regional sea platforms, e.g., for the North Sea (OSPAR), or the Baltic Sea (HELCOM). WISE-Marine and the regional platforms directly support European environmental policies' implementation. These international approaches are complemented by national environmental data platforms, for example, in Germany the Marine Data Infrastructure Germany (MDI:DE).

The general marine data management in Europe consists of three major elements: SeaDataNet, EMODnet, and Copernicus CMEMS. SeaDataNet is a distributed marine data

infrastructure for diverse in situ data sets. EMODnet is using available data for preparing multi-resolution maps of all European seas, and Copernicus is the earth observation program and offers information services mainly based on satellite data.

It is obvious that the large amount of heterogeneous data, multiple platforms that depend on data-exchange, and a wide range of potential data uses require rules that ensure data quality and accessibility. These rules are provided by the EU INSPIRE Directive. An important aspect is that INSPIRE contains guidelines on metadata documentation based on EN ISO 19115 and EN ISO 19119. Metadata provide the required background information about data. Metadata descriptions are a prerequisite so that data, physically stored in a database, can be found and used by others.

During recent years, plastics became one focus of EU policy. In 2018, the EU adopted the plastics strategy (EC COM/2018/028, 2018) with the aim to protect the environment and reduce marine litter. It is part of the circular economy action plan, revised in 2020, and builds on existing measures to reduce plastic waste. In the marine environment this is complemented by the EU Marine Strategy Framework Directive (MSFD 2008/56/EC). The MSFD has the aim to protect and achieve a good environmental status (GES) in marine ecosystems. The GES is assessed on the basis of eleven descriptors and marine litter is one of them, which aims to ensure that properties and quantities of marine litter do not cause harm to the coastal and marine environment. As a consequence, the state-of-pollution of the marine environment has to be assessed, environmental targets and associated indicators have to be developed, major emission sources have to be identified and quantified, and effective measures leading to reductions in marine litter pollution have to be tested. One focus is on trends in the amount, distribution, and composition of microplastics. This has caused a wide range of scientific and monitoring activities during the last decade and the need to establish joint databases that follow FAIR (Findable, Accessible, Interoperable, and Reusable) data principles [2].

A first European litter database, linked to EMODnet, exists [3]. It focuses on macro-litter, the size fraction above 25 mm, found at beaches using the 100 m monitoring method [4]. A recent review shows that the database suffers from many data weaknesses, for example, spatiotemporal heterogeneity, inconsistencies in the different litter identification lists, and variability in the survey protocols and data sources. The conclusion is that a harmonisation and comparability of results across Europe are still needed. For microplastics, a comparable database does not exist yet, but there are several lessons learned from the macro-litter beach database. A public microplastic database should be available at an early stage of monitoring. It needs to be flexible and adaptive and must meet the specific demands of microplastics, e.g., a large variety of sampling, processing and analytical methods, many types of plastics or a very wide size spectrum ranging from micrometres to five millimetres. The complexity of microplastic data makes it necessary to develop a specific, tailor-made database rather than adapting and modifying one of the existing marine databases. This means that the new database needs to be visible for and integrated into existing database structures.

To meet this demand, we present a publicly accessible, flexible, and extendable structured database (DB) for particle-based microplastic data, that meets the FAIR data principles, takes into account the INSPIRE metadata requirements, and is linked to and harvested by other databases.

2. Materials and Methods

2.1. Basic Requirements and Background

The database was developed to meet the data storage and reporting requirements of two international projects with focus on coastal and marine microplastics in the Baltic Sea region, namely Bonus MicroPoll (<https://www.io-warnemuende.de/project/192/micropoll.html>, accessed on 12 December 2022) and MicroCatch (<https://www.io-warnemuende.de/microcatch-home.html>, accessed on 12 December 2022). Database requirements were that relevant sample parameters had to be efficiently (i.e., no data loss, consistency, simplicity)

communicated between the entities. It had to be possible to reconstruct each individual microplastic particle's history from sampling to final analysis. This was the key for ascertaining data quality in terms of good scientific practice. It had to be possible for sample recruiters to share sample locations, sample type, sampling method, and time. Contact details of the responsible persons of each sub-task had to be taken into account. Important information concerning the sample purification, such as treated sample amount, blanks (contamination control), purification methods, and date had to be represented. Among relevant parameters of microplastic analysis were, e.g., polymer type, size, particle shape, colour, analysis method, the fraction analysed (if a purified sample was split), and blanks.

All the above information and additional required details were implemented into the Marine Plastic Database (MPDB) design and optimised over several years with respect to scientific accuracy, relevance, clarity, and consistency of terms and information within and across database tables. In particular, the two latter requirements were driven by the goal to make the MPDB publicly available. Therefore, we aimed at reducing the information to a minimum that is mandatory for marine plastic-monitoring in the environment. At the same time, it was important to keep flexibility with respect to the large variability of different sample requirements (e.g., concerning purification or analysis methods). The database had to take into consideration that microplastic monitoring involves different actors across various stages with different tasks, such as sample collection, sample purification, and spectroscopic analysis.

2.2. Types of Data

Quantitative microplastic (MP) data is typically either mass- or particle-based, both methods having their own advantages and limitations. Eventually, the targeted polymer types and size ranges, and the foremost research question determines the analytical method of choice.

Mass-based data, as for example from pyrolysis gas chromatography mass spectrometry (Py-GC-MS), usually necessitates less sample purification and hence accelerates data generation. Losses caused during pre-treatment, which particularly affect the small size classes, become obsolete and make this analysis especially advantageous for target particles in the sub-micrometre range. Limitations arise on the detection of multiple polymer types, as interferences can occur [5] that involve increasing resources and efforts when aiming at a large coverage of materials addressed by the umbrella term “microplastics”. Microplastic particles' polymer types that appear in low amounts are prone to fall below the limit of detection if they belong to a rarely occurring type, or if the particles are so small that they, although being numerous, do not provide enough mass [6,7]. In any case, the main disadvantage is that only the mass of the MP polymer type is obtained and there is no information on particle sizes and their distribution.

Any research question that requires a higher resolution of particle size, examples are the determination of transport patterns, normalisation of biofilm coverage, or the encounter rates of potentially affected organisms necessary for a respective risk assessment, will demand or consider particle-based data acquisition. Particle-based analysis is usually performed using μ -Raman- or Fourier-Transform-Infrared-Microspectroscopy (FTIR) with the ability to detect very low numbers of polymer particles. The methods are either done in imaging or particle measurement mode. Imaging entails scanning the entire filter area and acquiring spectra at every pixel. After spectra evaluation, adjacent pixels with the same chemical classification are grouped as particles [8,9]. In particle measurement, at first an optical image of the filter is acquired, from which the location of the individual particles is determined, together with information about size, shape, and colour or texture. Only then are the spectra acquired at the locations where particles were found [10,11].

2.3. Morphological Properties of Microplastic Particles

The minimum size of particles to be detected depends on the spectroscopy technique used (FTIR: approx. 10–15 μm , Raman: approx. 1 μm). Which technique is used also de-

depends on the sensitivity of the analysis towards certain substances [12]. Spectra quality, and thus, method reliability can be impacted by fouling of particles or fluorescent components (in case of Raman).

Using the particle-based approach, concentrations are typically reported as MP counts per unit environmental matrix (e.g., kg^{-1} , or m^{-3}). In addition, other particle characteristics, such as shape properties or colour can be determined on a per-particle basis.

The particle count concentrations themselves are, however, of limited usefulness when being reported without substantial context. As an example, estimates of how many trillion “pieces” of MP are polluting the ocean, are readily incorporated and circulated by various media [13,14]. It is questionable if actual informative content about the pollution’s extent can be conveyed in this manner, or rather, if a broader public attraction is intended simply by the magnitude of an unimaginable high number. Representations of particle sizes (e.g., as individual particle properties or continuous distributions [15]) and study design details (e.g., applied mesh sizes) are examples of such augmenting data that should preferably be communicated alongside MP concentrations. The same is true for comparative data on natural particles where applicable (e.g., as proxy for the hydrodynamic regime in sediment MP studies [16]). An appropriate database structure for particle-based MP pollution data should therefore provide the possibility to map all relevant morphological data which is then available for any future assessment. From simple to sophisticated, such morphological properties (“morphologicals” hereafter) may include size class [16,17], longest size dimension, [18] or multiple size dimensions, area [19,20], circumference, or shape related aspects, such as sphericity, convexity, eccentricity, right up to fully 2D or 3D descriptions of the irregular particles (e.g., as point meshes). Referenced studies in the above list give examples from the scientific literature that utilised the respective morphological features to describe their identified particles. The more sophisticated morphological features may have higher demands for the analytical process, but they give the resulting data set a higher diagnostic quality for describing the interactions the identified particles may invoke in the environment. Although not trivial, particle mass estimates may be inferred if the reported particle morphological data are of sufficient detail, i.e., at least a proper shape classification and maximum extents in 3 dimensions. This allows to link the realms of particle- and mass-based analyses, which would be highly beneficial to the field of MP research. In contrast, inferring morphological data from destructive mass-based analytics is unfeasible.

Fortunately, for the choice of appropriate morphological features, it is not necessary to start ab initio, as much knowledge can be transferred from other particle-based research fields, such as from sedimentology, with a great repertoire on various size characteristics of sediment grains [16,20,21].

2.4. Software and Tools

Prerequisite for a database is that it contains a structured set of data, meaning that data should be organised using formal design and modelling techniques. Structured data, which usually reside in relational databases, provide benefits, including but not limited to data integrity and independence from applications or programs, increased consistency, decreased updating errors, improved data access to users, and data security. This ensures that the research data meet the FAIR principles—findable, accessible, interoperable, and reusable. It is worth noting that the mentioned advantages entail additional expenses such as the time and intellectual requirements to design a complex database, possible software and hardware costs, and costs for training the personnel to use and administrate, as well as maintain the database.

An SQL (structured query language) database can be effectively set up to represent multiple levels of abstractions. It is a collection of highly structured tables, wherein each row reflects a data entity, and every column defines a specific information field. Relational databases are built using the structured query language to create, store, update, and retrieve data.

The MySQL™ software delivers a very fast, multithreaded, multi-user, and robust SQL database server [22], hence was considered to be a perfect tool for the development of the MP database. The MySQL software is Dual Licensed; in this study the MySQL as an Open-Source product under the terms of the GNU General Public License (<https://www.fsf.org/licenses/>, accessed on 10 December 2022) was used. Depending on user preferences and requirements, other tools were in use as well, such as the HeidiSQL, [23] MySQL Workbench (<https://www.mysql.com/products/workbench/>, accessed on 10 December 2022), and certain Python libraries (mysql.connector [24]) for automated access to the DB. Any relational database management system (RDBMS) can be used to access the database, as long as it uses SQL as its standard database language. The database server is hosted by the Leibniz Institute for Baltic Sea Research Warnemünde-IOW, which allows usage by registered users. As in any database management system (DBMS), users may perform tasks which correspond to their rights, granted by the administrator: view, edit, delete, etc. The possible database usage possibilities are explained in MySQL documentation (available at <https://dev.mysql.com/doc/>, accessed on 10 December 2022), and many tutorials and videos present online [25].

2.5. Database Development

The database development process was conducted following a classical waterfall model [26], with iterative process revision (Figure 1). Firstly, specific needs for data were identified, followed by determination of data types. The first step was carried out mainly by the environmental scientists, who oversaw collecting or analysing samples; judging from their experience, these users could immediately identify what data should be collected, whether it is possible to collect all the data (obligatory fields in the database), which data is optional or incidental (optional fields), and what could be further used in later research (quantification of entries). This step was followed by a conceptual model development, which established connections between possible tables and entities. The conceptualisation was completed with tight communication between the team members, who oversaw sampling and analysis, and those responsible for the MPDB technical implementation (database developer). Where one could identify the relationships between data, the other could comment on the possibility of implementing such a relationship and to assure database structure logic.

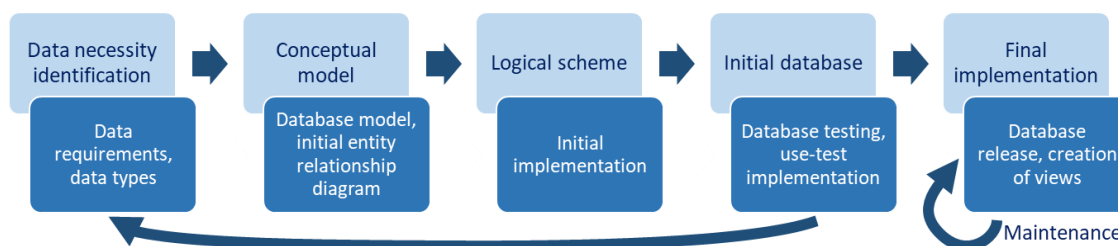


Figure 1. Marine Plastic Database development process stages.

Further steps (logical schema, initial and final implementation) were completed by the developer, based on the possible use-case scenarios, provided by the MPDB users. Currently the database is in its finalised stage, with maintenance and the support to create custom database views on demand. Database views are pre-established query commands, which are kept in the database dictionary to generate a certain preview of structured data, possibly combining entries from multiple tables or other views, performing certain calculations, or simplifying multiple tables to a single table, which can then be used for further data analysis. The use of such views greatly facilitates data extraction for specific repetitive evaluation tasks.

The MPDB development stages 1 to 4 (see Figure 1) were revisited several times, as some requirements and improvement suggestions were received after the initial test-

ing of the database, which in turn assured a reliable product that suits the users and stakeholder needs.

2.6. Data Entry

The most efficient method of data entry depends on the type of data, its amount, and the frequency with which it accrues. Some data entries are best entered manually, e.g., to populate the 'contributors' table (a contributor is a person who is working with the samples or analysis), or some categories, such as the 'colour' or the 'shape' (we use the term "auxiliary" tables, when describing such entity properties). Such tables are usually referred to as pre-populated categories. For bulk data entry, however, a manual approach would be counter-productive and undermine the development of the relational database in the first place. Instead, the database ought to be populated wherever possible with bulk entries using queries, spreadsheets (comma-separated values (CSV) sheets), any structured text document, as well as using fully- or semi-automated scripts.

Data entry for the 'samples' table were most useful in the form of SQL 'insert' queries which pulled a prepared CSV file into the table. The creation of data describing samples typically involves highly manual tasks, such as insertion of information from handwritten field work logbooks. Most researchers will prefer a simple spreadsheet application for this work. In such a case, a simple export of the DB table into a CSV file format may be utilised and further used as a template where the new data can be appended. This ensures that the later CSV upload to the DB can be completed by a standard SQL script without errors or data incompatibilities in a semi-automated way.

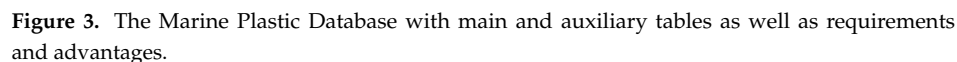
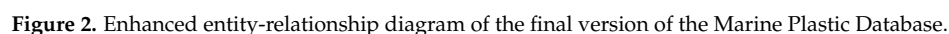
The tables containing actual analytical result data (such as 'particles' or 'analysis') receive the highest number of entries (as there may be hundreds or thousands of MP particles per sample) and are therefore impractical to be populated by manual data entry or individual CSV files. For this purpose, a Python software package was developed which performs an automated particle measurement and data evaluation and entry [27]. Using the mysql.connector Python library [24] allowed streamlining the necessary data compilation, conversion, and SQL insertion to reduce manual effort to a minimum. The custom-made graphical user interface (GUI) allowed reviewing summarised and categorised particle information and uploading the results of hundreds of particles in less than a minute.

3. Results

3.1. Database Structure

The final structure of the MPDB is presented in an enhanced entity-relationship (EER) database diagram which represents requirements and complexities of the developed database (Figure 2). There are 14 auxiliary tables, 3 main, and 2 junction tables. The data in the auxiliary tables have to be entered only once or updated very rarely, i.e., if new contributors (a person who is working with the samples or analysis) are engaged in the procedure, then their information should be entered once. Every contribution (sample or analysis) will be automatically assigned to that person with a unique ID. Hence, the information is stored once and is referenced via a foreign key attribute.

The three main tables of the database are: samples, analysis, and particles (see also Figure 3). Any sample may be analysed via various methods and yield many particles. For instance, a certain sample was treated with several different purification methods, all of which had to be registered in the database. Similarly, a certain particle could be measured with both methods, FTIR and Raman, yielding individual results that should all be included in the MPDB. Hence, the standard relational database rule of one-to-one or one-to-many relationship is not sufficient; a many-to-many connection had to be established. This is achieved via the two associative or junction tables: 'sample2methods' and 'particles2analysis'. The connections are stored in these junction tables via the copies of the primary keys of joining tables (Figure 2).



Lab blanks represent potential contamination introduced during analysis preparation and spectroscopic measurement (FTIR or Raman microspectroscopy) of a sample, which is a critical step for introducing contaminations. There is one corresponding lab blank for each environmental sample. Process blanks cover the sample type-specific treatment pipeline [28], where a group of process blanks typically represent potential contamination

from the purification procedures of all environmental samples treated alike during a certain time period.

Based on the 'Is_blank' flag, and the entries for 'Process_blank' and 'Lab_blank' an extraction of either type of samples (environmental sample, process blank, lab blank) can be achieved easily by querying the wanted sequence. Particles found in a blank may be used to adjust the particle numbers of their corresponding environmental samples. A recommendation of how to implement a blank correction in the particle domain is given in Section 3.4. A recent review on blank procedures [29] evaluates several further options.

3.2. Data Extraction and Example Queries

Database data retrieval for further analysis is usually done via the data export of views. Database users may use the existing views or ask the administrator to create views based on their description.

3.2.1. Data Filtering Scenario

Some data may need only a simple filtering from one specific table. A simple data filter example may be as follows:

"every sample, from the MicroCatch project from compartment "water" from location between 12.17–12.2 and 53.95–55.0 (lat, long) in the year 2018".

The SQL query snippet for the example is:

```
SELECT * FROM 'samples'
WHERE
samples.Project = 'MicroCatch' AND
samples.Compartment = 'water' AND
year(samples.Date) = 2018 AND
samples.GPS_LON >= 12.17 AND samples.GPS_LON <= 12.2 AND
samples.GPS_LAT >= 53.95 AND samples.GPS_LAT <= 55.0;
```

3.2.2. Data Retrieval from Two Tables Scenario

When extraction of data from multiple tables is needed, the best solution is to create a new joint table, which is called a View, where all the related data entries are linked. After this, the new table can be filtered as in the data filtering scenario. An example for this scenario can be a modified query, as follows:

"every particle, from location between 12.17–12.2 and 53.95–55.0 (Lat, long) in 2018, with a size fraction of 11–100 µm".

Creation of view:

```
CREATE VIEW 'particles_v_samples' AS
SELECT p.'Sample', s.'Date', s.'GPS_LON', s.'GPS_LAT', p.'Size_fraction'
FROM 'particles' AS p
INNER JOIN 'samples' AS s
ON p.'Sample' = s.'Sample_name';
```

Filtering the view:

```
SELECT * FROM micropoll.particles_v_samples
WHERE
year(particles_v_samples.year) = 2018 AND
particles_v_samples.GPS_LON >= 12.17 AND particles_v_samples.GPS_LON <= 12.2 AND
particles_v_samples.GPS_LAT >= 53.95 AND particles_v_samples.GPS_LAT <= 59.0 AND
particles_v_samples.Size_fraction = '11-100';
```

3.2.3. Data Extraction to a Local File Scenario

The data may be extracted to a spreadsheet or other formats for further analysis. Extraction requires either the usage of DBMS tools (like the export tools available from MySQL workbench, or HeidiSQL), or the direct application of SQL commands:

```
INTO OUTFILE 'D:\full_path\samples_table.csv'
```

FIELDS TERMINATED BY ','
 ENCLOSED BY ''''
 LINES TERMINATED BY '\n';

The provided examples present only a fraction of the user possibilities and may be modified, i.e., to include only unique values of entries, or additional fields or filters. As the stored data has a spatial locator (X and Y coordinates), one can, for example, utilise the functionality of various GIS tools and plugins to plot and represent the data on maps.

3.3. Data Quality Assurance—Dealing with Different Particles

Microplastics—being particulate pollutants that are typically investigated individually for properties such as material, colour, shape, or size—generate data on a per particle basis (at least for quantitative particle-based studies). For statistical analysis, interpretation and dissemination to the general public and stakeholders, data are typically transferred to aggregated information, e.g., counts of particles or averages of sizes, which are reported per sample, or time, or region. This section aims to elucidate the importance of a transparent handling and dissemination of the raw particle data as a means for better data compatibility and re-usability among MP studies. The understanding of particle-based vs. aggregated data is crucial to be able to perform data operations, such as correcting for self-contamination (blank correction) or limit of detection (to be implemented for removal of singular erroneous or misfit results) as explained in the examples below.

Conceptually, we distinguish between data in the “sample domain” (sampling meta-data such as sample quantity, location, dates) as opposed to the “particle domain” (individual properties of each particle). Particle domain data (PDD) can be used to generate sample domain data (SDD) by aggregation. Sums, means, or other descriptive statistics of PDD from a particular sample or sample group may be aggregated to yield the respective SDD. SDD, in turn, cannot be decomposed into the underlying PDD because the information on individual particles is lost in aggregation.

Figure 4 illustrates the distinct representations of data that are handled by the MPDB: in PDD the base of a single entry is an individual particle and it holds particle property data; whereas in SDD the base is a sample, which has sample metadata and aggregated particle data. The phenotyping procedure (PhT) is used to conduct operations on PDD and translate them into SDD.

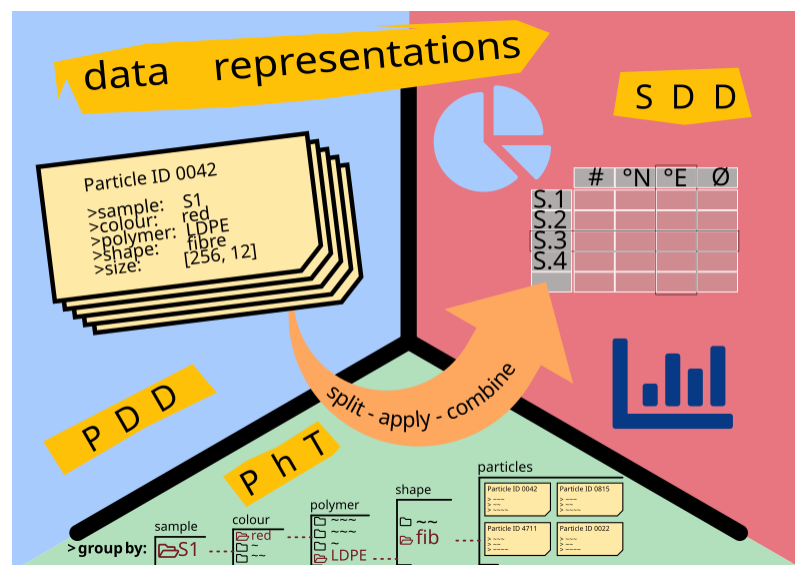


Figure 4. The distinct representations of data that are handled by the MPDB and the algorithms we use are illustrated in this info graphic.

To elaborate the implications of the distinction of SDD and PDD, let us consider the concentration of MP of a sample. In SDD this would be a number of MP per reference quantity of the environmental matrix (e.g., 100 m^{-3} or 23 kg^{-1}). Here, each MP within that number is considered equal, as there are no individual particles regarded by SDD, only their sum. If the underlying raw data (PDD) would only consist of identical particles, a value correction would seem intuitively feasible by a simple subtraction of the required amount. However, MP samples usually do not consist of a number of homogeneous MP particles, but for example, of a red PET fibre and a transparent PE fragment, which can only provide information on possible sample contamination of their kind and not of MP in general. The blank correction must, therefore, be done in PDD, where each particle is *not* equal. In PDD, a subtraction in a mathematical sense is, however, not possible, as each datum represents an individual, not an aggregation. Instead, an elimination of individuals can be an approach to facilitate the correction.

In case of negligible contamination, this theoretical excursion into particle identity should be of little relevance for reported MP data. However, experience shows that (1) contamination is an issue of concern, especially for studies working with small MP, and (2) not seldomly, MP data sets are on the brink of statistical exploitability due to low numbers of the costly to identify specimens, therefore data handling and sanitation procedures are to be chosen carefully.

The here described implications of working with particle data versus aggregated data does not only apply to MP research. Approaches of particle-based data conversion are, for example, discussed in polydisperse systems modelling [28].

3.4. Data Sanitation-Phenotyping and Blank Subtraction

As stated above, the omnipresence of MP easily leads to self-contamination of MP samples, which necessitates blank sample corrections. As the raw data of particle-based MP studies is represented in PDD, a number of individual particles needs to be selected for being regarded as introduced by the sampling and lab procedures, and therefore rejected from final results. The decision of which particle needs to be eliminated must be based on a set of rules. Naturally, there will be no perfect correspondent among the individuals, so the rules need to be designed to find the best matching pair of a blank and an environmental MP particle. Although we know what particles were present in the environmental and respective blank samples, the result will differ depending on the selected elimination rules and methods. To facilitate a matching procedure between ‘non-equal’ particles, we propose a phenotyping procedure that aggregates all relevant categorical particle properties and uses size as single continuous measure for discrimination. A phenotype is a group of particles that share the same values for ‘sample’, ‘colour’, ‘shape’, and ‘polymer type’. It is recommended to unify the categories of colour and shape into few, unambiguous clusters, i.e., red, green, blue, other, or fibre, non-fibre. More detailed specifications of phenotypes come along with a higher uncertainty (e.g., due to differences in illumination or particle shape recognition), especially when working with small MP. Particle size may be converted into a single measure, if not already so, i.e., in some cases we receive a major and a minor length for each particle (first and second dimension), where we take the geometric mean of the two as it is more area-preserving than the arithmetic mean. Phenotyping provides groups of particles which are both SDD (number of particles of phenotype X per sample Y) as well as PDD (the actual particle data in each phenotype group including the single measure size attribute).

It now becomes possible to conduct a blank correction process in PDD by identifying the corresponding blank for the sample in question and consecutively matching the phenotypes present in both. Particle elimination may then be conducted by matching and removing the nearest sized sample particle for each blank particle one by one. In a case where multiple (process-) blanks were taken to cover the same work process they would be, together as a group, valid for all samples prepared by that process. Consequently, for a certain phenotype, the average number of particles per blank is equal to its expected value

of contamination from the work processes covered by the blanks. However, averaging is a SDD operation and cannot be easily performed in PDD. Therefore, we recommend the following procedure/algorithm:

- After phenotyping (as described above) the lists of particles are—for each phenotype separately—concatenated from all blanks;
- The combined list is sorted by size;
- It then needs to be shortlisted to only yield the number of particles required by the SDD average (hence, total number of particles of the respective phenotype in all blanks divided by the number of blanks and rounded to the next integer);
- To achieve minimal size distribution deformation, the particles would best be selected beginning from the median of the sorted combined list and selecting every n -th element towards smaller and larger sizes alternately until k particles are selected, with n being the number of blanks and k the respective phenotype's SDD average;
- The shortlisted group of particles may be used further for the actual blank subtraction procedure on the sample particles in the same way as if there was only one relevant blank available.

Rounding, stereotyping particles into phenotypes, and the use of a unified size measure are assimilations that unavoidably introduce distortions, leading to an apparent, systematic error in the results. After all, every particle is *not* equal.

3.5. Data Manipulation and Quality Assurance

Depending on the analysis setup, it may be adequate to eliminate rarely occurring outliers from the data set, such as unlikely polymer types, which may otherwise elicit wrong-headed conclusions. For example, it might be decided that for a particle phenotype that occurs only once in the entire data set or in a sample, there is not enough analytical support that this is a valid particle, and it should thus be excluded as an outlier. This concept is also known as limit of detection and limit of quantification and applied in many other analytical research branches [30–32] in order to increase the soundness of a particular dataset. In MP analysis, such rare occurrences may be caused by poor signal-to-noise spectra, cosmic ray artefacts in Raman spectra, or unsystematic human error, which may justify setting a limit of detection.

However, sample size, reference library size, number of blanks, and whether it is applied on sample or data set level, are just a few factors that influence the outcome of such limit determination. This is mainly due to the statistics of small numbers, which MP data scientists are faced with. Where total MP numbers are low, the ultimate probability for certain particle (pheno-)types to appear is accordingly low. In such cases, data become less robust by eliminating phenotypes below the limit of detection, hence one might conclude that 'every particle counts'. Nevertheless, an initial data quality check is recommended to identify instances of rarely occurring phenotypes, as they can lead to the detection of erroneous data entries.

3.6. Database Integration and Accessibility

An important aspect is the MPDB connection to existing international database structures. A prerequisite to comply with FAIR principles is a description of the data available in the database: the metadata. MPDB is hosted by the Leibniz Institute for Baltic Sea Research (IOW) and stored on a server under the micropoll.io-warnemuende.de domain, and the metadata are available at <http://micropoll.io-warnemuende.de/iow-metadata.xml>, accessed on 20 December 2022. The MPDB metadata are stored on a central meta-database at IOW, IOWMETA. IOWMETA transfers this meta-information to national German databases and major international databases. This ensures knowledge about the existence of MPDB and its content (Figure 5).

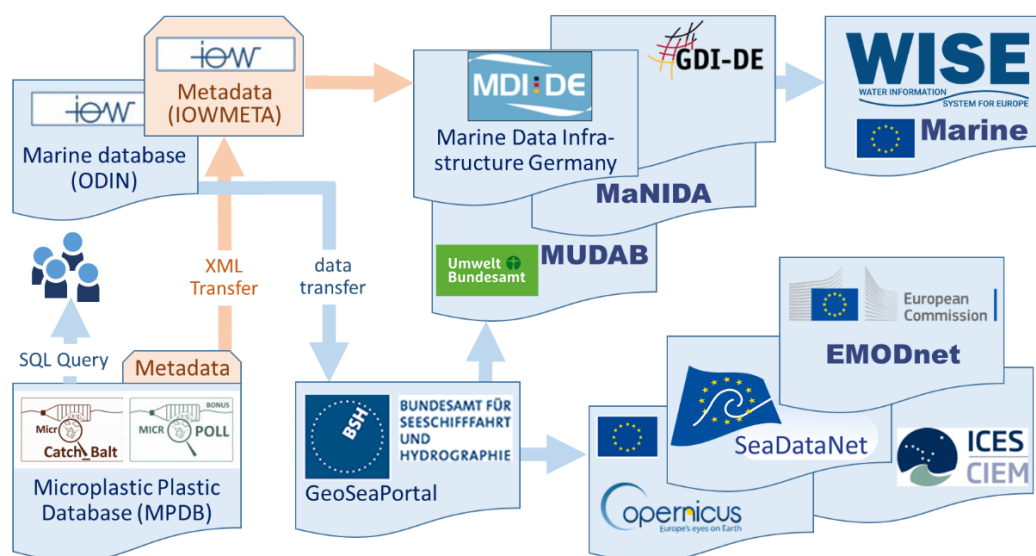


Figure 5. Integration of the microplastic database into national German and international database structures.

The second important aspect is access to the data. Presently, potential users may request MPDB access via e-mail to the main author. The potential database users are encouraged to familiarise themselves with the database documentation (Supplementary Materials).

4. Discussion

We provide the first elaborated MP-related database and aim at contributing towards a universal data repository. SQL-supporting DBMS tools provide flexible data entry and storage possibilities with many applications in various fields. The development and maintenance of such a database requires significant knowledge and resources that are hardly always available. One solution is the use of already established and tested database models. This can be achieved by replicating the DB structure from the EER diagrams (Figure 2) or directly via the provided SQL ‘create...’ statements (see Data availability statement below). The MPDB structure can be used for developing new, modified data repositories. The database re-installation and maintenance can be handled by IT departments of other research facilities or can be outsourced to such service providers. This has been done with respect to the Leibniz Institute of Polymer Research Dresden who uses and further develops an independent version of the database with a focus on microplastic in food. Alternatively, the presented MPDB version, which is hosted by the Leibniz Institute for Baltic Sea Research, can be used and further developed on request. This solution ensures that the database content is visible for other databases, through the metadata data information, and the content accessible on request.

Environmental sciences benefit from open-access data, developed and stored in structured relational databases. Taking into account that almost any sampling and analysis campaigns are costly, comparable data repositories with transparent metadata and structure are of importance for the scientific community and stakeholders.

Knowledge on emission, transport, and behaviour of microplastic in the environment presently largely results from calculations and modelling studies. Examples for the Baltic Sea are the approaches by Osinski [33], Piehl [34], or Schernewski [35,36]. A major shortcoming is the lacking result validation with microplastic field data. The MPDB and its content is a major step to overcome this weakness. The usage of structured databases ensures access to reliable data. Invalid, incomplete, or faulty data entries are detected, removed, or clarified either in the data entry phase (i.e., data with missing required fields

is not allowed in the database), or data usage (i.e., the retrieval of data, which is not related to a specific attribute will not appear in the generated view).

5. Conclusions and Outlook

The Marine Plastic Database meets all technical requirements with respect to data storage and documentation, but access to data requires expert knowledge. For end-users or stakeholders (non-researchers/scientists) the MPDB is presently not user-friendly. Several possible solutions might be examined to shape the data for easy interpretation. This process would involve two stages: (1) developing use-case scenarios for data entry/viewing/presentation, and (2) development of a front-end application or solution. Possible stakeholder use-case scenarios might be the preview of abundance of MP in their region or area of interest, prevailing MP types and their sources (media), etc. The front-end implementation solution examples would be to create an online platform for MPDB data filtering and preview, or a standalone tool (an application), developed solely for the user. To achieve this, one would require further development (web or application), extra tools and services (i.e., a server with management software). All these solutions can be explored in future uses of the MPDB. We welcome the usage of the database and are open for a collaboration aiming at an improved user-friendliness.

Supplementary Materials: The following supporting information can be downloaded at http://micropoll.io-warnemuende.de/Guideline_for_usage_of_Microplastic_Database.pdf: Guideline for Usage of Microplastic Database.

Author Contributions: Conceptualisation, database development, and writing, N.Č.; DB structure conceptualisation, support of database development, writing, visualisations, and editing, K.E., R.L., J.B., D.F., and F.F.; writing and complementary visualisation, G.S.; editing, project administration and funding acquisition, S.O. and M.L. All authors have read and agreed to the published version of the manuscript.

Funding: This research was supported by project BONUS MICROPOLL project supported by BONUS (Article 185), funded jointly by the European Union and national funding agencies (the German Federal Ministry of Education and Research (BMBF, 03F0775A;) as well as project MicroCatch_Balt (BMBF, 03F0788A)).

Institutional Review Board Statement: Not applicable.

Informed Consent Statement: Not applicable.

Data Availability Statement: Data are available in a publicly accessible repository. The data presented in this study are openly available in a repository at Zenodo [37]. The data contain an SQL database export, which can be used to create the MPDB discussed in this article.

Conflicts of Interest: The authors declare no conflict of interest.

Abbreviations

DB—database; EER—enhanced entity-relationship; FAIR—findable, accessible, interoperable, and reusable; FTIR—Fourier-Transform-Infrared-Microspectroscopy; MP—microplastic; MPDB—Marine Plastic Database; PDD—particle domain data; SDD—sample domain data; SQL—structured query language.

References

1. European Commission. *Shared Environmental Information System (SEIS)*; European Commission: Brussels, Belgium, 2020; Available online: https://www.eea.europa.eu/ds_resolveuid/FWIZEG45MT (accessed on 29 December 2022).
2. Wilkinson, M.D.; Dumontier, M.; Aalbersberg, I.J.; Appleton, G.; Axton, M.; Baak, A.; Blomberg, N.; Boiten, J.-W.; da Silva Santos, L.B.; Bourne, P.E.; et al. The FAIR Guiding Principles for Scientific Data Management and Stewardship. *Sci. Data* **2016**, *3*, 160018. [CrossRef]

3. Addamo, A.M.; Brosich, A.; Chaves Montero, M.M.; Giorgetti, A.; Hanke, G.; Molina Jack, M.E.; Vinci, M. *Marine Litter Database Lessons Learned in Compiling the First Pan-European Beach Litter Database*; Publication Office of the European Union: Luxembourg, 2018; ISBN 9789279978661. [CrossRef]
4. European Commission. *MSDF Guidance on Monitoring Marine Litter*; Publications Office of the European Union: Luxembourg, 2013; ISBN 9789279978661. Available online: <https://mcc.jrc.ec.europa.eu/documents/201702074014.pdf> (accessed on 29 December 2022).
5. Rauert, C.; Pan, Y.; Okoffo, E.D.; O'Brien, J.W.; Thomas, K.V. Extraction and Pyrolysis-GC-MS Analysis of Polyethylene in Samples with Medium to High Lipid Content. *J. Environ. Expo. Assess.* **2022**, *1*, 13. [CrossRef]
6. Fischer, M.; Scholz-Böttcher, B.M. Microplastics Analysis in Environmental Samples—Recent Pyrolysis-Gas Chromatography-Mass Spectrometry Method Improvements to Increase the Reliability of Mass-Related Data. *Anal. Methods* **2019**, *11*, 2489–2497. [CrossRef]
7. Hermabessiere, L.; Himber, C.; Boricaud, B.; Kazour, M.; Amara, R.; Cassone, A.-L.; Laurentie, M.; Paul-Pont, I.; Soudant, P.; Dehaut, A. Optimization, Performance, and Application of a Pyrolysis-GC/MS Method for the Identification of Microplastics. *Anal. Bioanal. Chem.* **2018**, *410*, 6663–6676. [CrossRef] [PubMed]
8. Primpke, S.; Lorenz, C.; Rascher-Friesenhausen, R.; Gerdt, G. An Automated Approach for Microplastics Analysis Using Focal Plane Array (FPA) FTIR Microscopy and Image Analysis. *Anal. Methods* **2017**, *9*, 1499–1511. [CrossRef]
9. Primpke, S.; Dias, P.A.; Gerdt, G. Automated Identification and Quantification of Microfibres and Microplastics. *Anal. Methods* **2019**, *11*, 2138–2147. [CrossRef]
10. Anger, P.M.; von der Esch, E.; Baumann, T.; Elsner, M.; Niessner, R.; Ivleva, N.P. Raman Microspectroscopy as a Tool for Microplastic Particle Analysis. *TrAC Trends Anal. Chem.* **2018**, *109*, 214–226. [CrossRef]
11. Brandt, J.; Bittrich, L.; Fischer, F.; Kanaki, E.; Tagg, A.; Lenz, R.; Labrenz, M.; Brandes, E.; Fischer, D.; Eichhorn, K.-J. High-Throughput Analyses of Microplastic Samples Using Fourier Transform Infrared and Raman Spectrometry. *Appl. Spectrosc.* **2020**, *74*, 1185–1197. [CrossRef]
12. Käßler, A.; Fischer, D.; Oberbeckmann, S.; Schernewski, G.; Labrenz, M.; Eichhorn, K.-J.; Voit, B. Analysis of Environmental Microplastics by Vibrational Microspectroscopy: FTIR, Raman or Both? *Anal. Bioanal. Chem.* **2016**, *408*, 8377–8391. [CrossRef] [PubMed]
13. Georgiou, A. Microplastics in the Ocean May Be Vastly Underestimated, with up to 125 Trillion Particles Floating Around, Study Says. Available online: <https://www.newsweek.com/microplastics-ocean-vastly-underestimated-125-trillion-particles-floating-around-1505404> (accessed on 29 December 2022).
14. Simon Matt Who's to Blame for Plastic Microfiber Pollution? | WIRED. Available online: <https://www.wired.com/story/whos-to-blame-for-plastic-microfiber-pollution/> (accessed on 29 December 2022).
15. Kooi, M.; Koelmans, A.A. Simplifying Microplastic via Continuous Probability Distributions for Size, Shape, and Density. *Environ. Sci. Technol. Lett.* **2019**, *6*, 551–557. [CrossRef]
16. Enders, K.; Käßler, A.; Biniash, O.; Feldens, P.; Stollberg, N.; Lange, X.; Fischer, D.; Eichhorn, K.J.; Pollehne, F.; Oberbeckmann, S.; et al. Tracing Microplastics in Aquatic Environments Based on Sediment Analogies. *Sci. Rep.* **2019**, *9*, 1–15. [CrossRef] [PubMed]
17. Bergmann, M.; Wirzberger, V.; Krumpfen, T.; Lorenz, C.; Primpke, S.; Tekman, M.B.; Gerdt, G. High Quantities of Microplastic in Arctic Deep-Sea Sediments from the HAUSGARTEN Observatory. *Environ. Sci. Technol.* **2017**, *51*, 11000–11010. [CrossRef] [PubMed]
18. Enders, K.; Lenz, R.; Stedmon, C.A.; Nielsen, T.G. Abundance, Size and Polymer Composition of Marine Microplastics $\geq 10\mu\text{m}$ in the Atlantic Ocean and Their Modelled Vertical Distribution. *Mar. Pollut. Bull.* **2015**, *100*, 70–81. [CrossRef] [PubMed]
19. Frère, L.; Paul-Pont, I.; Moreau, J.; Soudant, P.; Lambert, C.; Huvet, A.; Rinnert, E. A Semi-Automated Raman Micro-Spectroscopy Method for Morphological and Chemical Characterizations of Microplastic Litter. *Mar. Pollut. Bull.* **2016**, *113*, 461–468. [CrossRef]
20. Vianello, A.; Jensen, R.L.; Liu, L.; Vollertsen, J. Simulating Human Exposure to Indoor Airborne Microplastics Using a Breathing Thermal Manikin. *Sci. Rep.* **2019**, *9*, 8670. [CrossRef]
21. Altuhafi, F.; O'Sullivan, C.; Cavarretta, I. Analysis of an Image-Based Method to Quantify the Size and Shape of Sand Particles. *J. Geotech. Geoenvironmental Eng.* **2013**, *139*, 1290–1307. [CrossRef]
22. MySQL::MySQL Installer Release Notes. Available online: <https://dev.mysql.com/doc/relnotes/mysql-installer/en/> (accessed on 29 December 2022).
23. Becker Ansgar HeidiSQL Technical Help Document. Available online: <https://www.heidisql.com/help.php#credits> (accessed on 29 December 2022).
24. Mysql-Connector-Python-PyPI. Available online: <https://pypi.org/project/mysql-connector-python/> (accessed on 29 December 2022).
25. MySQL Team: MySQL Workbench Manual. Available online: <https://dev.mysql.com/doc/workbench/en/> (accessed on 29 December 2022).
26. Wescon, I. Managing the Development of Large Software Systems. In Proceedings of the 9th International Conference on Software Engineering, Monterey, CA, USA, 30 March–2 April 1987; IEEE Computer Society Press: Washington, DC, USA, 1987; pp. 328–338.
27. Čerkasova, N.; Enders, K.; Lenz, R.; Brandt, J.; Fischer, F. Guideline for Usage of Microplastic Database. 2020. Available online: http://micropoll.io-warnemuende.de/Guideline_for_usage_of_Microplastic_Database.pdf (accessed on 29 December 2022).

28. Enders, K.; Lenz, R.; Ivar do Sul, J.A.; Tagg, A.S.; Labrenz, M. When Every Particle Matters: A QuEChERS Approach to Extract Microplastics from Environmental Samples. *MethodsX* **2020**, *7*, 100784. [\[CrossRef\]](#)
29. Dawson, A.L.; Santana, M.F.M.; Nelis, J.L.D.; Motti, C.A. Taking Control of Microplastics Data: A Comparison of Control and Blank Data Correction Methods. *J. Hazard. Mater.* **2023**, *443*, 130218. [\[CrossRef\]](#)
30. Lux, L.; Phal, Y.; Hsieh, P.-H.; Bhargava, R. On the Limit of Detection in Infrared Spectroscopic Imaging. *Appl. Spectrosc.* **2022**, *76*, 105–117. [\[CrossRef\]](#)
31. Klymus, K.E.; Merkes, C.M.; Allison, M.J.; Goldberg, C.S.; Helbing, C.C.; Hunter, M.E.; Jackson, C.A.; Lance, R.F.; Mangan, A.M.; Monroe, E.M.; et al. Reporting the Limits of Detection and Quantification for Environmental DNA Assays. *Environ. DNA* **2020**, *2*, 271–282. [\[CrossRef\]](#)
32. Saadati, N.; Abdullah, M.P.; Zakaria, Z.; Sany, S.B.T.; Rezayi, M.; Hassonizadeh, H. Limit of Detection and Limit of Quantification Development Procedures for Organochlorine Pesticides Analysis in Water and Sediment Matrices. *Chem. Cent. J.* **2013**, *7*, 63. [\[CrossRef\]](#) [\[PubMed\]](#)
33. Osinski, R.D.; Enders, K.; Gräwe, U.; Klingbeil, K.; Radtke, H. Model Uncertainties of a Storm and Their Influence on Microplastics and Sediment Transport in the Baltic Sea. *Ocean Sci.* **2020**, *16*, 1491–1507. [\[CrossRef\]](#)
34. Piehl, S.; Hauk, R.; Robbe, E.; Richter, B.; Kachholz, F.; Schilling, J.; Lenz, R.; Fischer, D.; Fischer, F.; Labrenz, M.; et al. Combined Approaches to Predict Microplastic Emissions Within an Urbanized Estuary (Warnow, Southwestern Baltic Sea). *Front. Environ. Sci.* **2021**, *9*, 616765. [\[CrossRef\]](#)
35. Schernewski, G.; Radtke, H.; Hauk, R.; Baresel, C.; Olshammar, M.; Osinski, R.; Oberbeckmann, S. Transport and Behavior of Microplastics Emissions from Urban Sources in the Baltic Sea. *Front. Environ. Sci.* **2020**, *8*, 579361. [\[CrossRef\]](#)
36. Schernewski, G.; Radtke, H.; Hauk, R.; Baresel, C.; Olshammar, M.; Oberbeckmann, S. Urban Microplastics Emissions: Effectiveness of Retention Measures and Consequences for the Baltic Sea. *Front. Mar. Sci.* **2021**, *8*, 594415. [\[CrossRef\]](#)
37. Čerkasova, N.; Enders, K.; Lenz, R.; Brandt, J.; Fischer, F. MPDB: Marine Plastics DataBase. Available online: <https://zenodo.org/record/7495007> (accessed on 30 December 2022).

Disclaimer/Publisher's Note: The statements, opinions and data contained in all publications are solely those of the individual author(s) and contributor(s) and not of MDPI and/or the editor(s). MDPI and/or the editor(s) disclaim responsibility for any injury to people or property resulting from any ideas, methods, instructions or products referred to in the content.

Guideline for usage of Microplastic Database

The database (DB) is used to commonly collect data on microplastics (MP) from the projects BONUS MICROPOLL (BONUS) and MicroCatch_Balt (BMBF). The purpose of this guideline is to ensure that a new user has the required understanding of how to enter, extract and interpret data.

Please carefully read the following sections in order to understand how the database is designed and how it should be used. **It is absolutely critical that the data within the database is entered, extracted and interpreted in a consistent manner.** If not, the extraction of information from the database can yield wrong information that lead to wrong interpretation of any kind of results.

Whenever in doubt, contact the following people:

Natalja Čerkasova	KU	DB creation and maintenance	natalja.cerkasova@apc.ku.lt
Kristina Enders	IOW	Sampling, processing	kristina.enders@io-warnemuende.de
Robin Lenz	IOW	Sampling, processing	robin.lenz@io-warnemuende.de
Josef Brandt	IPF	Analysis	brandt@ipfdd.de
Franziska Fischer	IPF	Analysis	fischer-franziska@ipfdd.de

Table of Contents

Guideline for usage of Microplastic Database	1
DB structure	2
Main tables.....	2
Auxiliary tables.....	3
Linking tables	3
Data entry	4
Upload of a sample	4
Upload of a particle	9
Data retrieval	11
Extraction from a single table (example).....	11
Extraction from multiple tables (example).....	12
Data interpretation	13
Additional information	15

DB structure

The DB consists of tables where data is entered (Figure 1). Each table has got defined columns, which tell what data can be entered (e.g. “size”), if applicable what unit is expected (part of the name, e.g. “ μm ”) and which data type the entry requires (e.g. “float”). An entry in a table means a line filled with coherent information about one object.

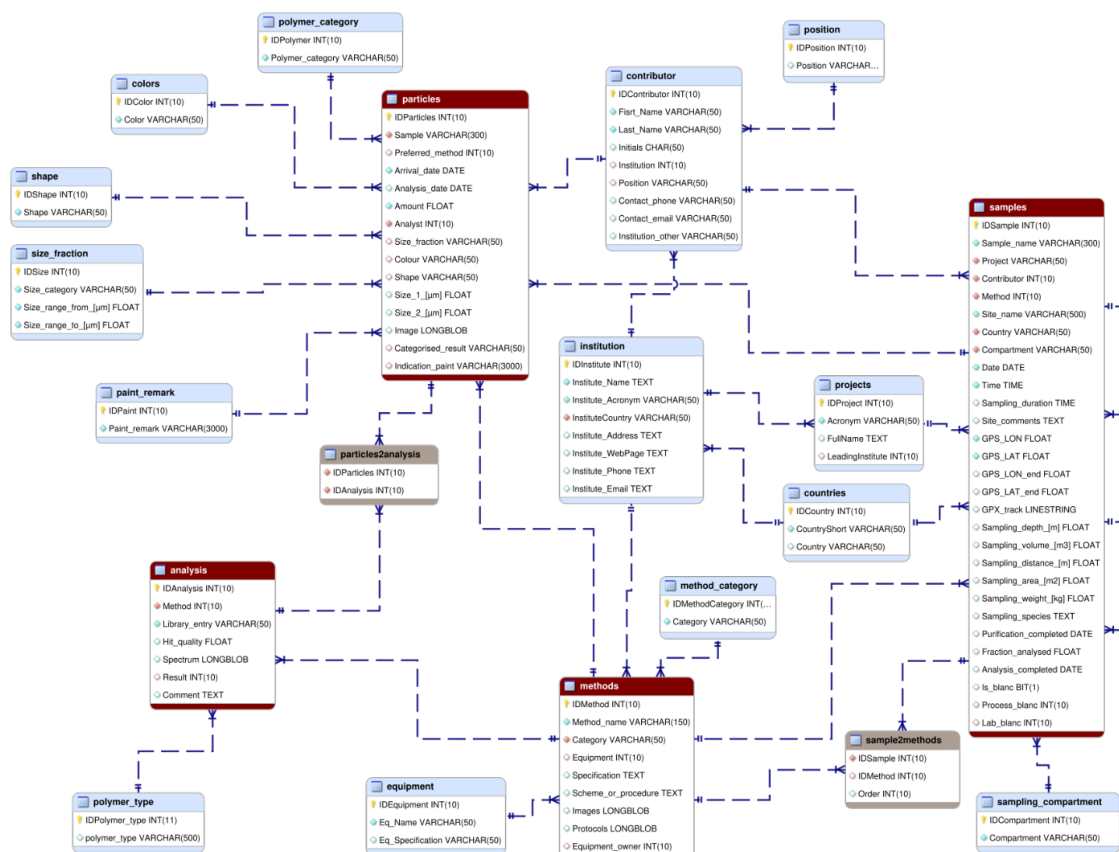


Figure 1: MP-database structure

For simplicity, the tables can be grouped into 3 categories: main, auxiliary and linking tables.

Main tables

→ contain the actual data about MP a user typically would like to do research on. They inherit a lot of attributes from the auxiliary tables (see below).

- **Samples**
 - each entry describes properties of one sample (e.g. sediment taken at a specific time and location)
 - for information on the “Upload of a sample” (page 4) and specifications of this table see the respective section
- **Methods**

- every method, from sampling, processing and pre-analysis treatment to final particle identification is listed here
- this avoids inflating the tables “samples”, “particles” and “analysis” with repetitive entries of methodological details
- all relevant information has to be listed (e.g. mesh sizes, laser wave lengths, chemicals used, etc.)
- files (sketches, photographs and detailed protocols) can be included
- **Particles**
 - an entry in this table stands for one analysed suspected plastic item
 - if a sample was analysed and no plastic was found the *Particles* table should receive only one entry containing the link to the sample ID, the arrival and analysis date (and no actual results)
 - the column “categorised_result” contains a decision for what polymer type and group the particle is made of based on the analytical results
- **Analysis**
 - each entry details the specific analytical results of a successful attempt to identify the polymer type of a particle

Auxiliary tables

→ Many of them are simple lists that provide predefined entries for certain columns of the main tables

- “shape”
- “colour”
- “polymer_category”
- ...

→ Some of these tables also provide additional information on the entered object to better describe it

- “contributors” is a list of people that is used to link entries from “methods” or “samples” to the responsible person. Besides the name it provides various contact information.
- “projects” lists projects (currently just BONUS MICROPOLL and MicroCatch_Balt), along with their leading institutes
- “institutes” provides names, locations and contact information of involved institutes
- ...

Linking tables

→ are used in places where it is necessary that it is possible that several entries in one table can be linked to several entries of another table

- “samples2methods”: any method can be used by many samples but also every sample is treated by several methods (e.g. sampling method and purification method)
- “particles2analysis”: every particle can have several analytical results (e.g. multiple measurements or complementary analyses on different instruments)

Data entry

Data entry tools

Entries to the DB can be made manually or, as in most cases, for multiple entries an entire data set can be uploaded to the DB. One option to prepare a data set for a group of samples is to set up a spreadsheet (Excel or Calc) and save it to comma separated file (.csv).

It is advisable to download the current version of the target table in the database as a csv file. This file can then be used to insert the new data entries in order to ensure the correct formatting and column structure. The csv containing the new entries can then be merged into the DB table by use of a MySQL management software (e.g. free tools, like the HeidiSQL, MySQL Workbench; or commercial software like Navicat for MySQL, etc.) or available MySQL interface for programming languages (e.g. R, Python). An example of how to include new data entries via csv import in HeidiSQL is given at the end of this section.

Another way is to open the current version of a DB table using the Microsoft Excel add-on “MySQL for Excel” where entries can be added manually or by pasting new content and committing the changes when done. An explanation video can be found at: https://drive.google.com/open?id=1hdwP6AmJ1AAYQ-JbPyR0Sf7XGZGH_I5Z

Data entry tables and fields

Several fields are **mandatory** for an entry to be accepted by the DB, others do only apply to certain sample or particle types and are therefore optional. Generally, this information can be found in the DB table information in a column typically named “Nullable” or “Allow Null” (NO – mandatory, YES – optional) and is also described in Figure 1.

You do not have access to all tables. Especially *auxilliary tables*, e.g. holding data about possible colours or shapes, are fixed. If you wish to have more entries there, please consider the absolute need for such additions (discuss this in a group with your colleagues and consider how much this will benefit your data representation accuracy) and contact Natalja to add them. The current entries in the *auxilliary tables* have seen much scrutiny, so we feel that some additions are not required.

Data backup/ Accidental manipulation of data

Generally, try to avoid changing data entered by others. However, if you accidentally manipulated or deleted data or notice any other kind of mistake, please contact the responsible person and the DB creator (Natalja) for clarification. A backup of the DB is made every week, in accordance with the data management plan.

Upload of a sample

A sample contains all information regarding the sampling and pre-treatment procedure and is required to add analysed MP particles. Each particle is assigned to a sample, so without having the sample in the DB, no particles can be entered. **Make sure sample data is entered at the latest when samples are transferred to the analyst.**

Please agree with all people involved on suitable and consistent naming conventions and clarify WHO is supposed to upload a sample. There were cases, in which samples were added twice – once in regular

spelling, once in all lowerCase letters. Such duplicates are very hard to identify and can lead to serious errors. **Make sure each sample is present in the DB exactly once!**

The database is structured to distinguish blank samples from environmental samples. **Blanks are critical to assess the reliability of any final analysis.** We consider two different types of blank samples: Process_blanks and Lab_blanks. Process_blanks are samples of MP-free milliQ water that were treated identically to an actual environment sample (including workup-procedures). They indicate any contaminations coming from sample workup. Lab_blanks, on the other hand, are MP-free milliQ-samples that were created in the analysis lab and can indicate contaminations coming from the analysis lab environment.

The database stores ALL FOUND MP PARTICLES. So, to get a particle report of a certain environmental samples, one has to retrieve all particles of the sample of interest, but also check the corresponding blanks. Ideally, the blanks only contain negligible amounts of MP particles. If, however, in rare cases there was a contamination, the blanks will indicate these and show, for instance, 200 PE particles. Consequently, any PE content of the corresponding environmental sample is highly questionable and should probably be discarded.

To add a sample, you have to add an entry within the samples-table in the DB. For the samples table the following information is required for each entry (mandatory \diamond optional):

mandatory attributes:

- **IDSample:** ID automatically generated by the DB
- **Sample_name:** What name describes the sample best? → uniqueness and consistency!
- **Project:** To which project does the sample belong (project financing the campaign)? → choose ID of linked entry in the *projects* table!
- **Contributor:** Who is responsible for the sample? This is the person who sampled and/or processed the sample and is thus in charge of the quality of the data entry. This person has to agree on the usage of the data and results by other DB users. → choose ID of linked entry in the *contributors* table!
- **Site_name:** Where was the sample acquired? → If you got replicate samples, the site_name is the same for all. The replicates should be distinguishable by the sample_name
- **Country:** In which country the sample was taken? → choose abbreviation of linked entry from the *countries* table!
- **Compartment:** Which environmental compartment / matrix is sampled (e.g., biota, beach, soil)? → choose ID of linked entry of the *sampling_compartments* table!
- **Date:** What date the sample was taken?
- **Time:** What time the sample was taken? → Accuracy limit: min. 1 hour, if possible
- **GPS_LON:** geodetic longitudinal coordinates in decimal degrees → Accuracy limit: 4 decimal places, positive numbers are east, negative numbers are west

- **GPS_LAT:** geodetic latitudinal coordinates in decimal degrees → Accuracy limit: 4 decimal places, positive numbers are north, negative numbers are south

optional attributes:

- **Sampling_duration:** How long did the sampling take? → Required for samples listed under the compartment “water”, possibly “waste water” and “biota”
- **Sample_comments:** Are there any additional information that could influence during sampling that could influence the result? Alternatively, the field can also be used to inform the analyst on the existence of sample splits, by the analyst to inform about additional information retrieved during analyses (e.g. internal standard particles) and other information important for the specific small set.
- **GPS_LON_end:** In case of transects being sampled: What is the longitudinal coordinate endpoint in decimal degrees → Accuracy limit: 4 decimal places, positive numbers are east, negative numbers are west, required for e.g. Manta net sampling
- **GPS_LAT_end:** In case of transects being sampled: What is the latitudinal coordinate endpoint in decimal degrees → Accuracy limit: 4 decimal places, positive numbers are north, negative numbers are south, required for e.g. Manta net sampling
- **Sampling_depth_[m]:** In which depth layer the sample was taken? → In case of water, biota and sediment samples = water depth; soil and beach samples: depth from surface, if not surface
- **Sampling volume_[m3]:** What is the volume of the matrix sampled? → Required for samples listed under the compartment “water”, possibly “waste water” and “biota”
- **Sampling_weight_[kg]: What is the weight of your sample?** → only required for samples listed under the compartment “biota”, “sediment”, “soil”, possibly “beach”. Apart from “biota” it always refers to the dry weight
- **Sampling_species: Which organism (biota) has been sampled?** → only required for samples listed under the compartment “biota”
- **Purification_completed:** What date the purification/pre-treatment is completed, and the sample is ready to be transferred to the analyst?
- **Fraction_analysed:** If only a certain percentage of the sample was analysed (e.g., due to too high particle numbers), indicate the fraction. Example: 50 % sample translates to fraction of 0.5.
- **Analysis_completed:** Date of the finished analysis, i.e., date of upload to database
- **Is_blank:** Enter a 0 (=False), if the sample is an environmental sample. Enter a 1 (=True), if the sample is a blank sample.
- **Process_blank:** If the sample is an environmental sample, indicate the sample index of the corresponding process_blank sample (if existing).
- **Lab_blank:** If the sample is an environmental sample or a process blank, indicate the sample index of the corresponding lab_blank sample (if existing).

Connect sample to all relevant methods:

To understandably track the history of each sample, please use the **sample2methods** table to explain what methods were applied in what order.

Example: Your sample is already entered and has the sample-index 125. The sample was sampled with the “Rocket sampling” method, underwent a “Density Separation” and was digested with H2O2. Go to the **methods** table and find out the indices of the used methods. Then go to the **samples2methods** table and add the following entries:

IDSample	IDMethod	Order
125	8	1
125	12	2
125	13	3

Final upload procedure on example of HeidiSQL

To download the current samples table in HeidiSQL open the table (just click on it) and activate the data pane. Then go to “Tools” > “Export grid rows”. A dialogue window pops up. Chose a path where to save the file and CSV as output format. Click ok.

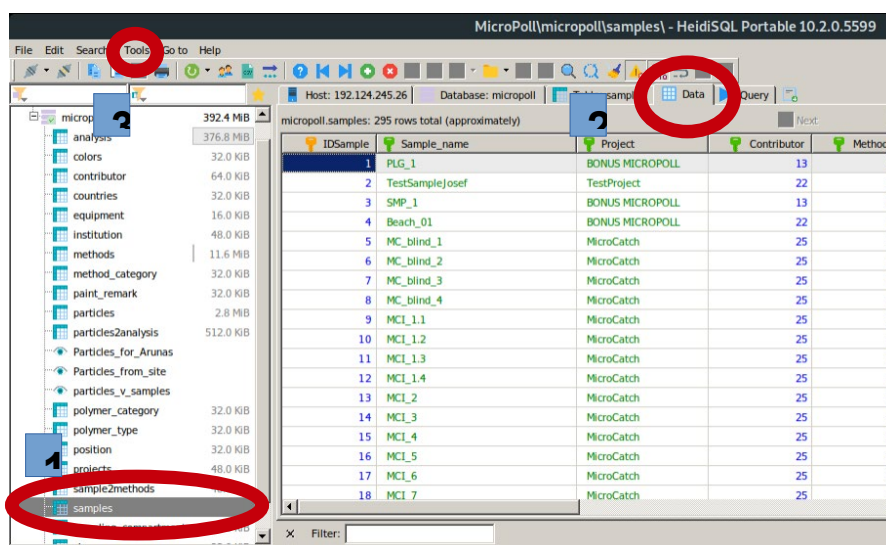


Figure 2: HeidiSQL user interface

You can then go to the downloaded file and open it for example in MS Excel or LibreOffice Calc. Replace the existing data entries with your new entries but don't change the column structure. For empty fields enter NULL, which will indicate for the DB that no entry has to be made there (beware: this is not possible for mandatory fields).

It is advisable to delete the column “IDSample” to have it set automatically by HeidiSQL when the data is uploaded.

When the new data has been formatted and inserted + saved into the previously downloaded csv snapshot of the samples table, the new csv file is ready to be uploaded.

Open HeidiSQL and log on to your account, got to **Tools > Import CSV file...**

A dialogue will open where you specify the path to your csv file. Set all options as shown in the screenshot below. Remove the check mark in front of “IDSample” if you have deleted this column as advised. Then click on import.

Figure 3: HeidiSQL Data import user interface

Go back to the data view of the samples table and press F5 to refresh. If the import worked your data entries from the CSV file will now be visible at the bottom of the table and should have received automatically generated entries in the “IDSample” field.

Upload of a particle

Uploading a particle is closely related to uploading an analysis. The concept is, that the **particle table** holds any “coarse” information, such as the size and a categorized-result (polyolefin, polyester, epoxy resin). This info is sufficient for any modelling purposes, but some analysts would like to have more detailed info about the exact measurement conditions and results.

At this point, the **analysis table** comes into play. It holds exact details of an analysis (i.e., exact assignment, method used, spectrum). The following figure illustrates the concept. Thereby, each particle can be linked to any number of individual analyses. The link is realized by using the **particles2analysis table**.

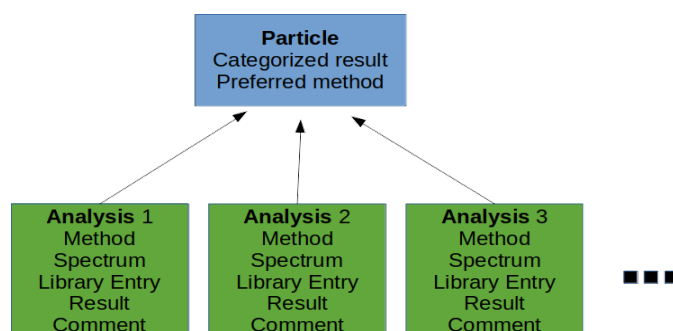


Figure 4: Particles and analysis data structure diagram

Let's go step-by-step and start with the **particle table**:

- **IDParticles:** Id of the new particle, will be automatically generated by the DB
- **Sample:** Name of the sample the particle belongs to.
- **Preferred_method:** Index of the analysis method that yields the final result. If only one analysis was done, its method is automatically the preferred one. → Chose index from **methods table**.
- **Arrival_date:** When did the particle arrive for analysis?
- **Analysis_date:** When was the analysis finished (i.e., uploaded to the DB)?
- **Amount:** If you have two particles that are identical **in every aspect**, you just need to upload it once and indicate the number of identical particles here.
- **Analyst:** Who did the analysis? → choose Index from **contributor table**.
- **Size-fraction:** To what size-fraction does the particle belong? → choose category text from **size_fraction table**.
- **Shape:** How would you describe the particle's shape? → Choose category text from **shape table**.
- **Size_1_[μ m]** and **Size_2_[μ m]:** Long and short size of the particle, respectively. Given in μ m.
- **Image:** If you have an image of the particle, you can upload it here.

- **Categorised_result:** Choose text from **polymer_category table**. Two entries there are worth explaining: “Unknown” means that you can see/feel that it is a plastic particle, but don’t have the possibility to analyze it more in detail. “Uncertain” means that you have analyses at hand with **ambiguous** results.
- **Indication_paint:** Used to indicate, whether the particle is likely to originate from paint applications. → Choose text from **paint_remark table**.

Let’s come to the **analysis table**. Please create for each particle *at least* one analysis entry.

- **IDAnalysis:** Unique id, will be created automatically by the DB.
- **Method:** Method index of the used analysis technique → Choose from **method table**.
- **Library_entry:** free text of whatever your spectra library reported
- **Hit_quality (optional):** Hit quality of the database search
- **Spectrum (optional):** Upload the corresponding spectrum
- **Result (optional):** Index of the polymer result → Choose from **polymer_type table**
- **Comment (optional):** Free text of anything you want us to know about the analysis.

Finally, you have to define what analysis/analyses belong to what particle. This is done analogously to the methods-to-sample-assignment, but now we use the **particles2analysis** table.

Example: You entered a particle, which got assigned the id 324. Then you entered two analyses, which received the ids 640 and 641. Go to the **particle2analysis** table and enter:

IDParticles	IDAnalysis
324	640
324	641

Data retrieval

When extracting data from the DB the responsible person shown in the field “**contributor**” should be contacted **to verify the results and to give permission** on its usage. This person will be able to forward you to others who were involved in the result generation and might be of help.

In the following two examples are described on how to extract data from the DB yourself. If you encounter problems, every partner (for internal usage) can make a request to the DB creator to provide certain views/scenarios which will contain the requested type of data.

Extraction from a single table (example)

Scenario: I need every sample, from the MicroCatch project from compartment “water” from location between 12.17 – 12.2 and 53.95 – 55.0 (Lat, long) in year 2018.

Explanation: when extracting data from single table you only need to “SELECT” the data. After the “SELECT” based on certain criteria, the user may specify where to store the data and in what format.

Base syntax: SELECT * FROM tableName WHERE condition;

Example:

```
SELECT * FROM `samples`  
WHERE  
  samples.Project = 'MicroCatch' AND  
  samples.Compartment = 'water' AND  
  year(samples.Date) = 2018 AND  
  samples.GPS_LON >= 12.17 AND samples.GPS_LON <= 12.2 AND  
  samples.GPS_LAT >= 53.95 AND samples.GPS_LAT <= 55.0;
```

Note: every query ends with a semicolon (;)

Export everything to csv: either by using the export tool in HeidiSQL (tools -> Export grid rows); or by executing a statement (for this, delete the last semicolon and update the query as follows):

```
INTO OUTFILE 'D:\full_path\samples_table.csv'  
FIELDS TERMINATED BY ','  
ENCLOSED BY '"'  
LINES TERMINATED BY '\n';
```

Note: keep in mind that different separators are used to indicate a table (` `) and an entry (` `).

Extraction from multiple tables (example)

Scenario: I need every particle, from location between 12.17 – 12.2 and 53.95 – 55.0 (Lat, long) in year 2018, with a size fraction of 11-100 micro-meters.

Explanation: when extracting data from multiple tables you need to create a new joint table, which is called a View, where all the related data entries are linked. After this, the new table can be filtered as in example 1.

Step 1. CREATE VIEW NewName AS SELECT ColumnName FROM tableName INNER JOIN tables

Example:

```
CREATE VIEW `particles_v_samples` AS  
SELECT p.`Sample`,s.`Date`, s.`GPS_LON`, s.`GPS_LAT`,p.`Size_fraction`  
FROM `particles` AS p
```

```
INNER JOIN `samples` AS s
ON p.`Sample` = s.`Sample_name`;
```

Step 2. Filter the new view table as you see fit (like in example 1)

```
SELECT * FROM micropoll.particles_v_samples
WHERE
year(particles_v_samples.year) = 2018 AND
particles_v_samples.GPS_LON >= 12.17 AND particles_v_samples.GPS_LON <=
24.2 AND
particles_v_samples.GPS_LAT >= 53.95 AND particles_v_samples.GPS_LAT <=
59.0 AND
particles_v_samples.Size_fraction = '11 - 100';
```

Step 3. Follow the instructions on data export, described previously in this document.

Scenario II: All particles, type of polymer, size, all locations in the compartment water. I also need to know the number of plastic particles per sample and sample volume.

Example

Step1:

```
CREATE VIEW `particles_v_samples_volume` AS
SELECT p.`Sample`, p.`Amount`, p.`Categorised_result`, p.`Size_fraction`,
s.`GPS_LON`, s.`GPS_LAT`, s.`Compartment`, s.`Sampling_volume_[m3]`, s.`Sam-
pling_weight_[kg]`
FROM `particles` AS p
INNER JOIN `samples` AS s
ON p.`Sample` = s.`Sample_name`;
```

Step2: Filter the new view table as you see fit (like in example 1)

```
SELECT * FROM particles_v_samples_volume
WHERE
particles_v_samples_volume.Compartment = `water`;
```

Step 3. Follow the instructions on data export, described previously in this document.

Data interpretation

Handling of blanks:

As already mentioned in the section about sample-upload, the handling of blanks is critical for ensuring validity and reliability of the entered data.

We agreed on uploading ALL MP-PARTICLES to the DB that we find in the respective samples. So, any particles that are most likely contaminations by any of the used methods, will be present in the DB as well. Consequently, when retrieving particle data of a particular sample you have to retrieve the particle data of the corresponding blanks as well and check for possible MP-contaminations.

The reason behind our considerations is, that the decision whether to include any particles that might be due to contaminations, is a very delicate one.

Example:

Your sample of interest has 40 PE particles, the corresponding blank shows:

- (a) 0 PE particles. → Great, no questions here!
- (b) 30-50 PE particles. → You most likely consider neglecting the PE particles.
- (c) 5-10 PE particles. → You probably consider subtracting the number of PE particles. Or you keep the number? Or you neglect all?

As you can see, case (c) can lead to different opinions in how to treat the conflict. Unfortunately, we don't have any reliable data at the moment to tell if case (c) occurs rarely or frequently. Hence, we decided on including *all data* in the first place to be able to decide on a more profound database later on.

Please communicate with persons connected to a certain sample if you have any doubts in how to handle the information from the corresponding blank samples.

There exists two kind of blanks (or also called blinds)

- analytical laboratory blanks
 - there exists one blank per sample analysed with μ Raman and / or μ FTIR
 - it represents potential contamination introduced during the filtration of the purified sample onto the spectroscopic substrate and during spectroscopic measurements
 - can be seen as a control where detected MP particle counts should be close to zero
- process blanks
 - one or several process blanks show the expectable contamination for a larger group of samples (typically all samples processed in that way)
 - represent sampling and purification steps of a sample as close as possible without containing actual sample material
 - moderate MP particle counts are expected here and define the lower detection limits

Recommendation for blank data implementation – Concept of MP phenotypes

After extraction of a data set (e.g. all MP particles found in one sample) a list of frequencies of each MP phenotype should be made.

Definition: MP phenotype is used here as a unique combination of the entries of polymer type (depending on your needs either categorised results or specific polymer match)

Table 1: Example of an MP phenotype frequency list

Phenotype			Frequency
Green	Polyamide	Fibre	19
White	ABS	Flake	44
Blue	Polyurethane	Foam	62
etc.	etc.	etc.	...

In the same way MP phenotype frequencies are determined for the corresponding lab and process blanks.

To yield MP data corrected for the respective detection limits, the frequencies of each phenotype of the process blanks are subtracted from those of the sample. Furthermore, we recommend to remove any particle counts with phenotype frequencies < 2 , to avoid inclusion of potential measurement errors (a MP rarely comes alone). If there is significant contamination present in the corresponding lab blank a subtraction may be done in the same way as for the process blanks.

Finally it is important to report the corrected number of particles found in a sample as a concentration, e.g. MP counts per unit sample. This could be per volume, weight, area, individual, or other depending on the kind of sampling compartment (you can find the needed information in the sample table in the respective columns, e.g. Sampling_volume, Sampling_weight, etc). Also verify in the database whether the whole sample has been processed and analysed or if subsampling or partial analysis has been applied and correct the numbers accordingly. (take a look at the “fraction_analysed” field of the samples table).

Two notes on sizes

1. In addition splitting of the total sample, there may be cases where the samples was size fractioned on spectroscopic filters of different pore sizes (e.g. a 10 μm filter and a 50 μm filter) and only the larger fraction was analysed due to time restraints. In this case, the listed particles may still include MP $< 50 \mu\text{m}$, which however should be omitted, as is it only by chance whether an individual particle came to rest on the 50 μm filter or went through to the 10 μm filter. It is, however still important that those particles are listed in the DB, in case the 10 μm fraction gets analysed later to have a more comprehensive dataset.
2. The database is intended to be used for particle based MP analysis. Reported data (i.e. numerical MP concentrations) are nearly useless without a detailed analysis of sizes. For samples analysed by microspectroscopy two size dimensions are reported (shorted and longer axes of a fitted ellipse around the pixels of the particle). Only reporting the size range of MP your study focusses on is not sufficient for a scientific evaluation of the pollution problem. As a minimum a size spectrum

histogram should be presented with the numerical concentrations. An approximation of volume (from sizes values) or mass concentrations (from sizes and polymer density) can be calculated.

You may contact the responsible person of a sample to verify your data analysis or if in doubt about anything concerning the sample.

Additional information

Use of the database for internals: When using other project contributors data – please get in-touch with the responsible person and confirm that he/she allows you to use the data. Always acknowledge the persons behind the work and respect your colleagues!

Use of the database for externals: The meta-data is visible for other DB that are connected with our BONUS MICROPOLL DB. The actual data can be requested by them. This request must be answered/allowed by the responsible person that is the author of the respective data.

RESEARCH ARTICLE

Open Access

Measuring impacts of microplastic treatments via image recognition on immobilised particles below 100 µm



Robin Lenz^{1*} , Kristina Enders¹, Franziska Fischer², Josef Brandt³, Dieter Fischer² and Matthias Labrenz^{1*}

Abstract

The treatment of samples for microplastic (MP) analysis requires purification steps that sufficiently reduce the non-MP content while preserving the targeted particles integrity. Besides their macromolecular structure this also encompasses their in situ numbers and sizes. However, any step of sample manipulation will come at a cost: particle loss, fragmentation, coagulation or degradation may lead to distorted results, predominantly in the smaller fraction of the MP size range. Therefore, the evaluation of MP resistivity against applied methods such as chemical digestions is a vital criterion for obtaining meaningful results on MP content of a sample. We developed a framework to test the applicability of MP purification methods and apply it to four protocols commonly used to prepare environmental samples for MP particle identification. The approach was designed for MP particles being too small to be handled manually (i.e. 10–70 µm). The evaluation consists of a two-tiered assay: a simple particle suspension approach is used to confirm a post-treatment qualitative recognisability of the target polymers by the analysis method of choice (here Raman and FTIR). In a following quantitative part, immobilised particles are used to evaluate the preservation of particle numbers and areas after the treatment on an individual particle level. A Python image analysis package was written that identifies, matches and measures particles on pairs of pre- and post-treatment images, and is available as open source software. Our results show that the chemical digestions using hydrogen peroxide, cooled Fenton's and a combined alkaline / oxidative treatment using potassium hydroxide and sodium hypochlorite are suitable methods for preparing MP samples for a microspectroscopic analyses. Also acidic sodium polytungstate solution used for MP density separations and a pentane based protocol for lipid removal were found applicable for small sized MP. Certain degradative effects were found when acrylonitrile butadiene styrene is exposed to acidic treatments, as well as for MP from acrylate and epoxy based paint resins in strong oxidative regimes. Several paint resins tested here were spectroscopically not identifiable by polymer attributed bands even before treatment, indicating that these materials might slip through analyses of environmental samples and consequently being underreported. We conclude that evaluating chemical treatment procedures on MP < 100 µm is feasible, despite limitations of the current methodology which we discuss. Our results provide more certainty on the tested methods for MP studies specifically targeting small sizes and should be extended for more protocols used in MP laboratory practises.

Keywords: Microplastics, Purification, Digestion, Qualitative, Quantitative, Resistivity, Method evaluation, Validation, Image recognition

* Correspondence: robin.lenz@io-warnemuende.de; matthias.labrenz@io-warnemuende.de

¹Leibniz Institute for Baltic Sea Research Warnemünde, Seestraße 15, 18119 Rostock, Germany

Full list of author information is available at the end of the article



© The Author(s). 2021 **Open Access** This article is licensed under a Creative Commons Attribution 4.0 International License, which permits use, sharing, adaptation, distribution and reproduction in any medium or format, as long as you give appropriate credit to the original author(s) and the source, provide a link to the Creative Commons licence, and indicate if changes were made. The images or other third party material in this article are included in the article's Creative Commons licence, unless indicated otherwise in a credit line to the material. If material is not included in the article's Creative Commons licence and your intended use is not permitted by statutory regulation or exceeds the permitted use, you will need to obtain permission directly from the copyright holder. To view a copy of this licence, visit <http://creativecommons.org/licenses/by/4.0/>.

Introduction

Microplastic (MP) purification techniques were developed by a number of studies in order to facilitate measurements of abundance of this inhomogeneous group of environmental contaminants [1–12] and reviews of recent developments are available [13–18]. Within MP, practically any synthetic polymeric material can be of interest, among others classical thermoplastics, varieties of elastomers as well as paint resins. The challenge has been to extract all relevant particles from the large diversity of sample matrices.

Depending on the system studied these matrices typically consist to large degrees of inorganic fractions like minerals from sediments and soils [19], and organic content such as detritus, tissue or microbial films, particularly confounding spectroscopic analysis [20]. The contained MP loads often range in the ppm to ppt (w/w, [21]). Physical density and chemical inertness to certain degradative agents are the two most harnessed properties of MP to facilitate a separation from the respective sample matrix. However, both of these principles involve deficiencies contributing to uncertainties in the resulting numbers or masses of MP obtained through the subsequent analysis of the treated samples.

For density separation, hydrodynamic problems occur that can hinder the intended particle advection. These include flocculation or coagulation of targeted and non-targeted particles altering the apparent density [22] as well as forces such as turbulence and adhesion [23] counteracting the — with decreasing particle size diminishing — impact of buoyancy. Also mechanical action involved in any extraction technique can contribute to errors for instance if samples are incompletely transferred between vessels or particles are altered through activities such as shaking, grinding, stirring or ultrasonication [24]. In chemical digestion processes loss of relevant particles can occur through unwanted chemical interactions of certain MP species with the applied digestant such as oxidation, hydrolytic polymer chain cleavage, or bleaching.

Purification steps aiming at the removal of non-targeted material through dissolution involve chemicals that exhibit degradative effects on these materials while — in the optimal case — leaving the present MP unimpacted. Based on the high chemical diversity of both, the material group of plastics and the unwanted constituents, the selection of suitable protocols for purification are a critical and difficult task. This includes the rigorous testing of the MP particles resistivity to a method in question. A broad range of plastic polymer types needs to be examined, as their large chemical diversity provides a variety of possibilities for chemical degradation. The size range of particles being tested needs to match the lower sizes of MP targeted by the planned

environmental studies aiming to apply the respective protocol. Existing method development and validation studies often tested against larger MP or macroplastic items [1, 25, 26], which allows relatively simple experimental designs. The resistance of larger plastic objects (e.g. millimetre sized pellets) against a digestive reagent is, however, no sufficient cause to assume that this would be equally the case for MP orders of magnitude smaller. Hence, MP particles in the lower μm size are of paramount importance in method validation tests, which was also emphasised by another recent study [12]. There are reasons to attest them a higher vulnerability to chemical degradation than larger particles, due to their increased surface to volume ratio, resulting in a higher number of exposed polymer backbones, functional groups and chain ends. Furthermore, the polymer matrices of MP particles in the lower micrometre scale are not necessarily homogenous, even when coming from the same origin. In the environment, weathering may reach individual particles differently and therefore produce varieties of particles differing in mean molecular weight and prevalent functional groups as well as end groups. The shares of crystalline and amorphous domains (i.e. regions of different chain folding and conformation) are related to vulnerability to degradation [27] and the typical domain size depends on the molecular weight of the chain fragment [28]. In semi-crystalline polymers the sizes, numbers and shapes of MP formed in fragmentation of degrading macroplastics depend on their crystalline morphology [29]. Varying additive content also influences certain polymer properties like mechanical strength or oxidative resistance [30].

Aim and scope

The scope of the present study is to evaluate the resistance of MP against chosen chemical agents on the example of treatment protocols previously recommended for purification of MP samples (as summarised by Enders et al. [31]). As stated above, there is already an extensive knowledge base in the literature on a variety of treatment methods, although rather heterogeneous. There is a knowledge gap, however, for resistivity of particles in the lower μm sizes, including a lack of methods for manipulations and measurements on an individual particle basis and simultaneously in large numbers. The endpoint of evaluation hereby should be the qualitative and quantitative detectability of the treated MP by microspectroscopic analyses and microscopic imaging. Our contribution is to study the impact of protocols including oxidative, alkaline, acidic and organic solvent based chemicals. They are tested on 19 polymer types (including 5 synthetic paint resins) in the size range of 10 to 70 μm (Table 1). Our primary objective is to enable method testing for particles below 100 μm , which

Table 1 Specifications of test MP particles, ^a rosin may not be regarded as a polymeric resin matrix, but was included as it is a common ingredient in self-eroding antifouling coatings of ships, and may therefore be a relevant type of environmental paint flakes

Group	Sample Name	Long Name	Origin (product name and manufacturer)	Colour	Density
Commodity Plastics	ABS	acrylonitrile butadiene styrene	Terluran GP-22, Ineos Styrolution	white	1.04
	EVA	ethylene vinyl acetate	Escorene Ultra FL 00328, Exxon Mobil	white	0.951
	HDPE	high density polyethylene	HDPE HTA 108, Exxon Mobil	white	0.961
	LDPE	low density polyethylene	LDPE LD 100.BW, Exxon Mobil	white	0.923
	PA6	polyamide 6	Ultramid B40, BASF	white	1.14
	PA6.6	polyamide 6.6	Ultramid A34 01, BASF	white	1.13
	PA12	polyamide 12	Vestamid L1600, Evonik	white	1.01
	PC	polycarbonate	Lexan 121R, Sabic	white	1.2
	PET	polyethylene terephthalate	ES306030/1 powder, Goodfellow	white	1.3–1.4
	PMMA	polymethyl methacrylate	Plexiglas 8N, Evonik	white	1.19
	PP	polypropylene	Moplen HP400R, LyondellBasell	white	0.9
	PS	polystyrene	Polystyrol 143 E, BASF	white	1.043
	PVC	polyvinylchloride	EVIPOL SH6830, Globichem	white	~ 1.4
	TPU	thermoplastic polyurethane	Elastollan C85A10, BASF	white	1.19
Paint resins	rosin ^a	maritime antifouling rosin resin	Hempel's Classic 76110, Hempel	red	n/a
	acrylate	general purpose primer acrylic resin	b1, J.W. Ostendorf	white	n/a
	PU	anticorrosive polyurethane resin	Temadur SC 533, Tikkurila Oyj	black	n/a
	epoxy	maritime anticorrosive epoxy resin	Hempadur 45148, Hempel	red	n/a
	alkyd	maritime primer alkyd resin	Hempel's Underwater Primer 26030, Hempel	grey	n/a

cannot easily be handled or manipulated due to their small size. A description of where the scope of this study has its boundaries is detailed further in the SI (S1).

We evaluate polymer resistivity to each protocol based on the following two questions:

- Qualitative: Are there diminishing effects on the spectroscopic recognisability of the polymer?
- Quantitative: Are sizes or particle numbers significantly altered?

Besides the reporting of the tested resistivities, this study commits to the principles of the open science approach, wherefore underlying data and procedures, including all implementations of algorithms that were developed in this study, are made publicly available.

Comparison of our concept to other approaches in current literature

Several studies reported polymer resistivity based on particle recoveries in spiked real matter matrices (e.g. sediments [10], soil and sludge [32, 33], or biota [10, 11]). This allows combining the evaluation of the efficacy of a digestion (matrix reduction) and the possible effect on the MP particles. However, also interactions between the matrix and MP particles may occur and can obfuscate the effects of the treatment itself on the polymers.

While this may be regarded as being more realistic with respect to an actual environmental MP purification, it is less comparable and generalisable. The influence of matrix parameters (e.g. grain size, material composition) and the interaction with the spiked MP particles (coagulation, grinding, etc.) during purification treatments are not yet well understood [31]. When the focus is primarily on effects of the treatment on the polymer, the combination of digestion efficiency and polymer resistivity tests is not compulsory to yield insight into effects individual treatments may have on certain polymer particles. We chose to operate in a matrix-free environment, as to gain primary insight into the genuine reagents-particles-interactions, but acknowledge that these treatments would only practically be used in the presence of a matrix, that must be reduced, as this is the primary goal of these treatments. Hence, our assessments can be valuable basis for future matrix-specific treatment validations, which are an important and logical next step.

Evaluation tests could be done without a matrix solely by applying the treatment to a particle suspension. The post-treatment state may then be measured by solid state technique, e.g. microscopic imaging after an additional filtration step, or by liquid phase techniques such as Beckman-Coulter-Counters, flow-cytometry, laser diffraction or dynamic image analysis. Each of these techniques will have their own advantages and limitations,

but commonly, it can be said that the experimental setup and conduction would be comparably simple, as the techniques are well established, and large particle amounts could be measured (for microscopic imaging with the constraint of required filter area and measuring time). It is however not possible to relate the post-treatment measurements directly to the pre-treatment state of the same particle. When measuring effects on median particle sizes or similar properties, this is of little relevance when the particle number is large enough to yield meaningful statistical aggregates. Particle counts and their treatment-induced changes, are, however, not readily inferred from suspended bulk measurements. Furthermore, approaches working with mobile particles are prone to errors owed to the manual handling of the particles (e.g. filtration, rinsing), which are difficult to account for when working with small MP. Here lies the prospect of the technique used in the present study, where MP particles are immobilised on a plane surface, and microscopic measurements of individual particles can be linked between pre- and post-treatment conditions.

General background on the experimental model design

To evaluate the applicability of MP treatment protocols, we expose the test material of irregularly shaped MP particles to the chemicals and physical conditions of the respective protocol (Fig. 1). Before and after exposure we take the measurements on those particles as detailed below.

In a typical MP particle-based analysis the particle material is first qualitatively determined (e.g. spectroscopically, to decide acceptance or rejection as MP) and, second, for confirmed MP further properties are obtained optically (e.g. size, colour, shape). For our method validation concept, we formalised those distinct categories of measurements as two separate experimental approaches that are each optimised for their respective requirements.

Using qualitative measurements, i.e. Raman and Fourier transform infrared (FTIR) spectra, we need to determine whether a reagent has reacted with a polymer to a degree that it would no longer be recognised as what it is by means of its spectroscopic signal. To obtain this information it is not necessary to handle individual particles, which is difficult and time demanding in the targeted size range. Instead, here it is sufficient to work with bulk particle suspensions. An approximate amount of test particles is added to the liquid reagent and removed after the treatment period is over. A complete recovery of particles is not necessary. Spectra can then be acquired on any of the recovered particles. However, qualitative measurements alone are insufficient to evaluate a protocol's applicability. We need to assume that fractions of particles could be destroyed by the treatment, while others persisted and could be measured.

Quantitative measurements allow us to make a statement on whether and to which degree particles have been lost or deformed during the treatment. Due to the chosen size range individual handling of particles (e.g. by

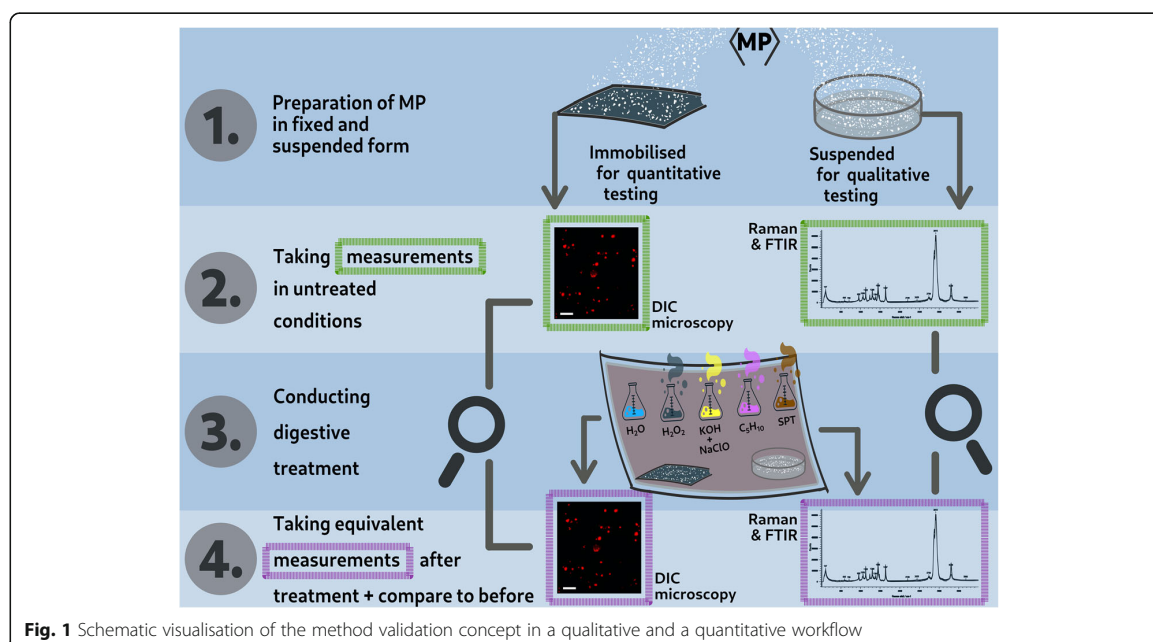


Fig. 1 Schematic visualisation of the method validation concept in a qualitative and a quantitative workflow

tweezers) for transfer or counting, is no suitable approach here. At the same time, large numbers of particles should be processed to allow for a robust statistical analysis of the measurements. The here presented approach is based on immobilising the MP particles on a silicon wafer coated with a thin film of epoxy resin. This method allows us to compare pre- and post-measurements on an individual particle basis which enables a more granular analysis, e.g. with respect to differences across the particle size spectrum. A microscopic image of a defined region of the wafer serves as the pre-treatment data point and is compared to an image of the exact same region after the treatment has been conducted.

It should be noted here that this combination of a qualitative and quantitative approach will not be able to pick up qualitative-only effects (i.e. chemical alterations not leading to effects on the quantitative particle properties), that do not occur in all particles of a polymer in a specific treatment, but rather only a hypothetical minority with certain characteristics. By the nature of the particles used herein - all being produced in the same manner from pristine raw materials - such deviant behaviours are not assumed to be occurring relevant numbers. It would be, however, a question worth investigating for future studies aiming at particle stability during treatments with a more detailed focus on exact particle properties, such as very narrow size and shape ranges, or specific surface properties.

Methods

Preparation of polymer test materials

For the group of commodity plastics pre-production polymer pellets were cryo-milled and sieved to yield particles of the targeted size range. The raw materials of

each polymer type (see Table 1), were individually submitted to cryogenic ball milling (Retsch CryoMill, 50 ml grinding jar, 25 mm ball, 5–6 g raw material, pre-cooling: 10 min at 5 Hz, 6 grinding cycles consisting of 2 min milling at 35 Hz and 2 min cooling at 5 Hz). The fraction that was used in the following procedures consisted of particles that passed a 71 µm, but were retained on a 10 µm stainless steel analytical sieve (Topas GmbH). The group of paint resin polymers was obtained from commercial consumer or industrial products of common outdoor appliances or maritime paints, which were tempered as recommended by the manufacturers and squeegeed in customary manner. Films were left to cure and later ground and sieved as described above by cryo-milling.

Treatment specifications

The specifications were adapted from the original protocol references and are detailed in Table 2. All treatment solutions were filtrated at 1.5 µm prior to application (vacuum filtration in glass bottles, Whatman 943-AH glass filter membranes) and 3–5 ml of the respective reagent were added to ensure that all MP particles were wetted.

In contrast to all other treatments, the H₂O₂ treatments were not consistent between the qualitative and the quantitative analyses. Qualitatively we tested Fenton's catalysed H₂O₂ digestions (cooled and uncooled), as well as a non-catalysed 2 weeks long exposure. The quantitative approach did not include Fenton's catalysed reactions. The strongly exothermic progression of Fenton's reactions were regarded as a practically not feasible application for the particle immobilisations: strong heat and foam formation would hinder an equal exposure of all particles on a wafer. Also the 2 weeks long exposure

Table 2 Short specifications and protocol references to the tested treatments

Treatment name	Specifications	Protocol Reference
Water (negative control)	ultra-purified water, 24 h, RT	–
H ₂ O ₂ Fenton's (Fe) uncooled ^a	30% H ₂ O ₂ + catalyst (6.67 mg ml ^{−1} of Fe(II)SO ₄ , pH 4), ca. 10 min, max. 85 °C (measured after 5 min)	[2]
H ₂ O ₂ Fenton's (Fe) cooled ^a	30% H ₂ O ₂ + catalyst (6.67 mg ml ^{−1} of Fe(II)SO ₄ , pH 4), 24 h, 20–30 °C (on ice, measured after 5 min)	[2]
H ₂ O ₂ LT ^a	30% H ₂ O ₂ , non-catalysed, 14 days, RT	[31]
H ₂ O ₂ ^b	30% H ₂ O ₂ , non-catalysed, 24 h, RT	[31]
KOH + NaClO	per 1 L: 700 ml H ₂ O, 150 ml NaClO 14% active chlorine and 150 ml saturated KOH (1120 g L ^{−1}), 5 h, RT	[1]
Pentane (C ₅ H ₁₀)	15 min in an immiscible water - ethanol (pH 3) - pentane mixture (5:1:1), shaken 3 times, 30–35 °C	[31]
SPT	Sodium polytungstate solution 1800 kg m ^{−3} , acidified with HCl (pH 3), 24 h, RT	[31]
HCl (positive control) ^b	one wafer with PA6, only for image processing algorithm calibration: 10% HCl, 20 min, RT, to fully dissolve MP	–

RT room temperature, LT Long term

^a only in qualitative part, ^b only in quantitative part

to non-catalysed H_2O_2 was replaced by a 24 h period, as it was uncertain whether the epoxy adhesive layer would withstand the 2 weeks exposure to a degree necessary to uphold its function of immobilising the particles. For many MP sample purifications scenarios this still resembles a typical application duration, i.e. for water samples [31]. The longer treatment in the qualitative part could be regarded to cover any effects that would also occur in the 24 h quantitative measurements, but not necessarily vice versa. This should be kept in mind when drawing detailed conclusions from the here presented data on the specific treatment protocols.

Qualitative analysis

Preparation and spectra acquisition

Prior to treatment, FTIR and Raman spectra were obtained on the milled test-MP particles as a spectroscopic reference. Approximately 5 mg of each of these particles were submitted to the respective treatments (Table 2). After the treatment procedure was completed, the particles were retained in a wet filtration on a vacuum filtration device with a stainless steel sieve of 10 μm nominal pore size (Spörl KG). On the filter, the particles were thoroughly rinsed with MP-free H_2O (prepared according to Enders et al. [31]) before few particles were manually transferred to a Si wafer as a plane spectroscopic substrate. Post-treatment spectroscopy was conducted using ATR-FTIR (PerkinElmer Spotlight 400, spectral resolution: 4 cm^{-1} , 32 scans, or Bruker ATR microscope Hyperion 2000 with 20x ATR objective, coupled to Bruker FTIR spectrometer Vertex 70, spectral resolution: 4 cm^{-1} , 100 scans) and Raman microscopy (Renishaw, inVia Qontor, laser: 532 nm, 100 accumulations, 0.5 s per scan, magnification: 50x, laser power: 60 μW - 4 mW). The settings used for each instrument were manually chosen to provide a sufficient spectroscopic data quality that allowed for the intended analyses and conclusions to be drawn. Which spectra were measured on which instrument and settings may be inferred from the deposited spectra data set [34], where the name of the spectrometer is given for each spectrum measured. For each treatment and polymer, three different MP particles were spectroscopically analysed as replicates as a minimum.

Data analysis

To compare and evaluate the Raman spectra, all replicates of one treatment and a representative spectrum of the untreated material (reference) were plotted together using the Renishaw WiRE 5.2 software. Changes, such as baseline shifts or the occurrence of new peaks were noted. For spectra with newly emerged peaks, a library search was conducted using the WITec TrueMatch 5.2 software. We searched the range of 200 to 4000 cm^{-1}

after a shape background subtraction was applied (subtract shape size: 200). The hit quality index (HQI) was then calculated as the Pearson Correlation Coefficient of the non-derivative spectra. The commercially available ST Japan Raman libraries for pristine polymer references were used. For the FTIR spectra, reference and treatment-specific spectra were plotted in the same way using either the Perkin Elmer Spectrum software or the Bruker OPUS (v7.5) software and changes were noted. Manual spectra evaluation was used to detect any changes in molecular vibration frequencies and to suggest their origin. For example, the emergence of new IR bands in the range of 1580–1600 cm^{-1} and 1350–1380 cm^{-1} indicates generation of a carboxylic acid salt as a result of polymer oxidation. The FTIR spectroscopic evaluations included also the calculation of HQIs, which were performed to assist in the manual spectra evaluation, but were deliberately not used as the sole decision criterion. Their calculation was conducted in the Bruker OPUS software using the proprietary Euclidean-distance-based HQI algorithm and the following list of libraries: ATR-LIB-COMplete Vol 1–3 (ST Japan), Hummel Industrial Polymers (Chemical Concepts), Hummel (Bruker), MERCK (Bruker), Polymer library (Bruker), General library IR (Bruker) and a custom library of self-measured common polymer types.

To classify changes in the spectroscopic signals, we assigned each treated polymer to one of four categories (Table 3). The decision on a category was derived as the result of the manual spectra evaluation as described above. Where replicates exhibited different changes in spectra, the decision was based on what the majority of replicates indicated. We defined the categories with the goal to differentiate the spectra into groups of similar chances for successful spectroscopic polymer recognition. Similar categorisation approaches have been taken by other MP treatment validation studies [1, 14]. Category “x” was assigned when an evaluation could not be conducted, because, independent of treatment, no exploitable spectral bands spawned from the respective polymer with the respective spectroscopic technique.

When identifying environmental MP spectroscopically, usually semi-automated library searches are used instead of manual spectra evaluations. For a subset of the polymer types, we reported Raman HQI values of the highest correct polymer type match and compared deviations between the reference HQI (untreated polymer) and HQI of treated replicates with our manual category assignments.

Quantitative analysis

Based on the qualitative test and previously published resistance studies, a set of polymers and treatments was selected for further quantitative analysis. The decision to

Table 3 Categories used to evaluate the impact of a treatment on the spectroscopic recognisability of the treated polymers.Exemplary spectra for each category can be found at the given page numbers in the respective data deposits: ^aRaman+FTIR_commodityPolymers.pdf, ^b Raman+FTIR_paintResins.pdf

Category	Definition	Consequences	Example Spectra Raman	Example Spectra FTIR
0	no relevant changes, spectra identical within natural background noise levels	polymer recognition unhindered	p. 77 in [34] ^a	p. 156 in [34] ^a
1	changes in non-band spectral properties, i.e. baseline slope or elevation, fluorescence	polymer recognition unhindered, changes do not mask polymer bands	p. 44 in [34] ^a	n/a
2	emergence of new bands or individual band intensities increased due to polymer degradation processes (e.g. oxidation)	polymer recognition largely unhindered, changes do not mask polymer bands	p. 23 in [34] ^b	p. 11 in [34] ^a
3	removal or strong alteration of polymer specific bands	polymer recognition is hindered	p. 20 in [34] ^b	n/a
x	no polymer specific spectrum measurable independent of treatment	no evaluation possible	p. 31 in [34] ^b	p. 41 in [34] ^b

not analyse all polymers that were included in the qualitative part was due to the limited analytical capacities. Of chemically similar polymer types only one representative was used (polyethylenes and polyamides). In the group of paint resins, we limited the selection to the acrylate and epoxy based products, of which we got usable results in the qualitative part of the study.

Preparation of particle immobilisations

For the quantitative analysis particles were immobilised on silicon wafers with a thin epoxy resin layer as an adhesive (see Fig. 2). Rectangular pieces, ca. 1–2 cm², 700 µm thick, were cut from the silicon wafer material and initially cleaned by being immersed and rotated for at least 10 min in piranha solution (H₂SO₄ 60% and H₂O₂ 30% mixed in a 1:1 ratio just before the wafers were added). The cleaned wafers were coated with a layer of epoxy resin (L20 + EPH 161 thinned with acetone, 100:25:25 weighed ratio, Hexion). The resin has a drip time of 90 min. A single wafer piece was mounted on a spin coater chuck and

spun at 7500 rpm for approximately 20 s (Polos BL MCD, APT GmbH, Germany). The film thickness was determined via z-axis differences for focus on the wafer surface versus focus on the film surface using the same instrument and settings as described below (Image acquisition and reagent application). On eight random locations the mean thickness was 4.25 µm with a standard deviation of 1.98. After a short curing interval of approximately 2 min, the test-MP of one polymer type were applied to the glue surface by trickling them through a stainless steel mesh (100 µm pore size, held approximately 5 cm above the wafer) with help of a metal spatula. The particles came to rest on the still adhesive resin layer and the wafer was left at 40 °C to fully cure overnight. For each treatment, one wafer per polymer was prepared in this way. During spin coating and particle application the wafers were only handled inside a ventilated cabinet and were placed in closed-lid transparent polystyrene boxes for transport and curing, as to prevent unintended dust particle settling.

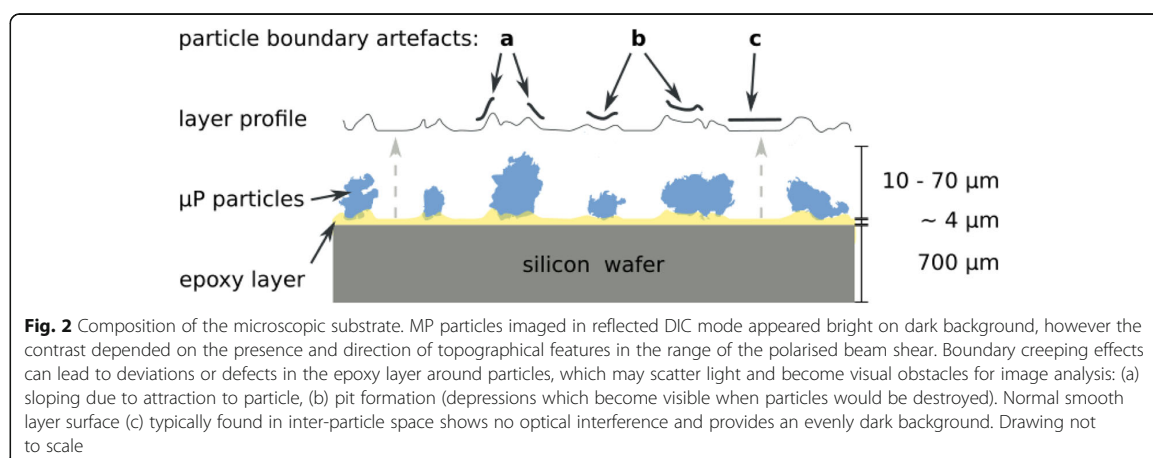


Image acquisition and reagent application

Optical microscopic images were acquired with a Zeiss Axio Imager.Z2m digital microscope on a defined region of each coated wafer (prior to treatment) after they had been rinsed with ultra-purified H₂O and dried with nitrogen purge gas to remove any loose particles or dust. Each wafer was then exposed to one of the treatment reagents (see Table 2) and rinsed again with ultra-purified H₂O to remove any residual chemical reagents. A post-treatment image was then obtained from the same area on the wafer as for the pre-treatment image. All images were taken using the Zeiss Zen software v2.7, a 20 x objective in reflected light differential interference contrast (DIC) mode. DIC was chosen as it gave the largest contrast difference between particles and background, when compared with other techniques (bright field and dark field). The resulting image signal-to-noise ratio depended however strongly on the polymer type, limiting the applicability of this technique for some polymers (i.e. PVC and PMMA, see also section Methodological caveats for an evaluation of diagnostic limitations). Images were acquired as tiling mosaics with a fixed zero overlap stitching. It was necessary to postprocess the images manually. For pairs of corresponding pre- and post-treatment images areas of visual artefacts (e.g. air entrainment on wafer borders) were cropped simultaneously (Fig. 3 shows the differences between original and

processed images). Differing light conditions in the original images were accounted for by histogram adaptation (conducted equally for pre- and post-image pairs). The images used for analysis were in 8-bit tiff format with a pixel resolution of 0.72 $\mu\text{m px}^{-1}$.

Image analysis

Particle identification algorithm The analysis routine for the DIC images was written in python and is available for use and contribution under GNU GPL v3.0 at: https://github.com/robna/ImmobileParticles_MatchAndAnalyse, and as a static citable version [35]. A number of open source python libraries were used, most notably: Altair [36] which builds on the declarative visualisation grammar Vega-Lite [37], pandas [38, 39], statsmodels [40], OpenCV [41] and SKimage [42]. The routine consists of a three-step procedure (Table 4).

First, a particle recognition routine identifies particles on both the pre- and the post-treatment image. Their coordinates are used to align the images, i.e., to remove any image tilt and offset. From the aligned images, for each particle in the pre-treatment image the corresponding particle in the post-treatment image is identified (if present). This particle matching allows determining and comparing particle statistics, such as size or brightness, before and after the treatment on a per-particle basis.

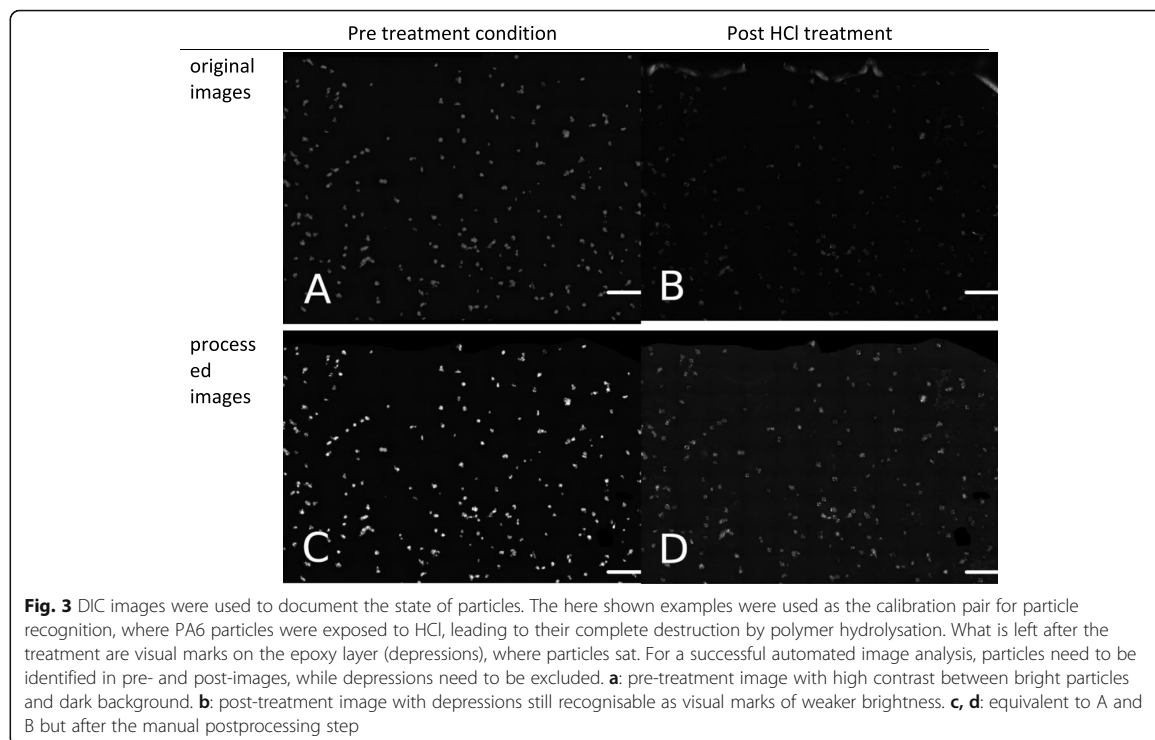
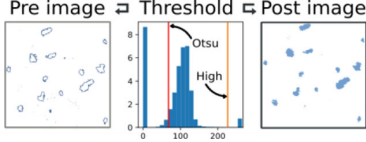
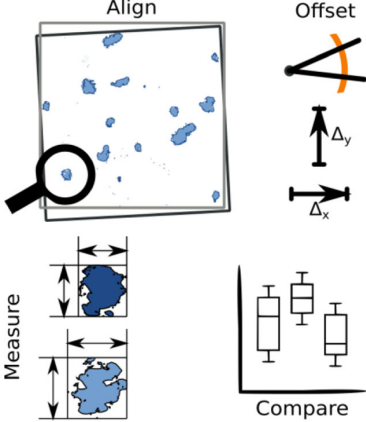
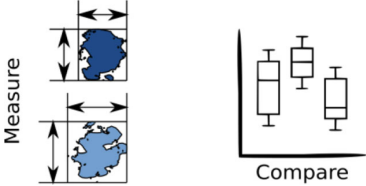


Table 4 Steps of the image analysis. More detailed documentation of the applied algorithms is provided along with the source code https://github.com/robna/ImmobileParticles_MatchAndAnalyse

Initial particle detection		<ul style="list-style-type: none"> particles get separated from background by thresholding with hysteresis [43] <ul style="list-style-type: none"> a lower threshold is calculated using Otsu's method [44], which selects full particle areas areas are accepted as particles if > 10% of their pixels also exceed a higher threshold fixed at 75% maximum brightness
Finding corresponding particles		<ul style="list-style-type: none"> image registration: pre- and post-images get aligned <ul style="list-style-type: none"> particles found in pre- image are matched to equivalent particles in post-image if present
Obtaining particle properties		<ul style="list-style-type: none"> matched particles get measured on pre- / post-images measurements are used to compute change rates of properties

Using a positive control for calibration of particle detection

The task of the automated image analysis is to discriminate particles from background and match corresponding particles in pre- and post-treatment images. In case a treatment would have destroyed particles, marks in the resin layer are expected to remain visible in the post-treatment image (e.g. a depression where the particle was sitting) and could potentially be falsely classified as a particle. Hence, the detection method has to be capable of distinguishing depressions from actual particles as well. For this purpose, as a positive control, we used one additional wafer with PA6 particles. This wafer was submerged in hydrochloric acid (37%) for 20 min at room temperature (which was shown to completely dissolve PA6, [14]). Pre- and post-imaging, as well as any rinsing steps were conducted as described above. The images that were obtained of this wafer are shown below (Fig. 3). They also serve as a general example of the type of image material that the quantitative part of this study is based on.

The destruction of the particles was confirmed by Raman microscopy (Renishaw, inVia Qontor, laser: 532 nm). Twenty randomly selected depressions in the epoxy layer were analysed, where no distinct PA6 spectrum was present in 17 out of 20 cases (85.0%). In places where PA6 attributed bands could still be detected, a visual microscopic inspection revealed that particle structures were no longer clearly recognisable, indicating that only residues of the PA material were left. This shows that the HCl treated PA6 wafer can be regarded as a

suitable positive control where $\geq 85\%$ of particles were effectively removed and can be used for calibration of the particle detection algorithm. Translated to a non-embedded particle system (e.g. suspensions) where particles would be exposed to the digestant from all sides, this is likely to be a complete particle loss.

The calibration of the particle detection algorithm was conducted on several parameters, most notably the upper brightness threshold, the tolerated displacement and particle size limits. For various combinations of values of these parameters, the resulting particle numbers detected in the pre- and post-treatment images of the positive control wafer were compared with the goal of identifying the parameter set that produced the lowest false positive and false negative errors. Because particles were intentionally destroyed on this wafer, false positives are equivalent to features being recognised on the post-treatment image, while false negatives correspond to particles remaining undetected on the pre-treatment image, despite being obviously present to a human observer. This optimised parameter set was then used for the particle detection in all other images and can be viewed in the source code.

The calibrated image analysis resulted in a particle count reduction of 85.2% ($n_{\text{matched}}/n_{\text{pre}} = 30/203$), which corresponds to the visually and Raman spectroscopically determined particle loss of 85%. In the 30 remaining particles the average area was reduced by 86.3% ($A_{\text{post, matched}}/A_{\text{pre, matched}} = 320/2332 \mu\text{m}^2$, compare Fig. 6). For this fraction it remains unclear whether the particles had

been destroyed incompletely (thus, identified correctly), or misidentified as false positives, despite having been removed. This can occur due to the misidentification of depressions with bright embedded air bubbles or optical artefacts (e.g. bright halos appearing around depressions, see also Fig. 3 bottom images), which could not be avoided. This sets a measurement uncertainty, and if any of the tested treatments would have caused an equivalent reduction in particles, it should ultimately be interpreted as a complete destruction.

Data analysis

As the number of particles per imaged wafer was not constant, measured values of counts and particle area are reported as relative changes. In counts (n) they are calculated from the number of particles in a pre-treatment image which could be matched to a particle present in the corresponding post-treatment image in relation to the total pre-treatment particle count. A relative particle loss $L_{rel.}$ is calculated according to Eq. 1, ranging from 0.0 (all particles were matched) to 1.0 (all lost). Particle areas were aggregated as the mean area per matched particle \bar{a} in both, pre- and post-treatment images, whereof relative changes $C_{rel.}$ were calculated (Eq. 2).

$$L_{rel.}(n) = 1 - \frac{n_m}{n_{pre}} \quad (1)$$

$$C_{rel.}(\bar{a}) = \frac{\bar{a}_{post}}{\bar{a}_{pre}} - 1 \quad (2)$$

Where

n_{pre} = number of particles in pre-treatment images.

n_m = number of particles that could be matched between pre- and post-treatment images. Indices for a alike.

Statistics Influences of non-treatment factors, such as varying contrast and image quality as well as available particle number on a wafer, appeared to have confounding effects on the successful particle recognition and matching. These factors were formalised as n_{pre} being the total particle count that could be identified on a particular wafer before treatment exposure on the one hand, and a range of image histogram obtained variables (Table 5), on the other.

Generalised linear model (GLM) residual analyses were used to estimate and remove these impact of the confounding factors. For an application-oriented introduction and references for further reading on GLMs, we recommend the website of the statistical package statsmodels [45], which was used here for the model calculations. The models followed the form of Eq. 3, with X being an $i \times j$ matrix of the linearly combined independent explanatory variables (predictor terms), y being the dependent response variable and $g(\cdot)$ some function of the conditional expectation of the response, that links it to the linear term of p predictors multiplied with individual coefficients β_j .

$$g(E(y = y_i | X = x_i)) = \sum_{j=0}^p \beta_j \cdot x_{ij} \quad (3)$$

For particle count losses, the binomial distributions for particles matched (successes) and lost (failure) were used as the dependent variable. The model was fitted to the predictor terms using a logistic link function (as given in

Table 5 Image quality related attributes tested as explanatory confounding factors in the statistical modelling applied to the quantitative particle data. Lo = lower threshold as calculated by the particle hysteresis detection algorithm. ^a chosen as suitable for modelling of influences on particle count loss, ^b chosen as suitable for modelling of influences on particle area change, ^c used for calculation of the background distortion index (BDI)

Name	Description	Mathematical Expression
pre_histBGpeak	pre-treatment image background brightness	grey value at the local histogram maximum between but not including 0 and Lo
pre_histFGpeak	pre-treatment image foreground brightness	grey value at the local histogram maximum between but not including Lo and 255
post_histBGpeak	post-treatment image background brightness	grey value at the local histogram maximum between but not including 0 and Lo
post_histFGpeak	post-treatment image foreground brightness	grey value at the local histogram maximum between but not including Lo and 255
pre_histDelta ^a	contrast spreading between the image background and foreground prior to treatment	$\text{pre_histFGpeak} - \text{pre_histBGpeak}$
histBGpeakSum ^c	combined background brightnesses	$\text{pre_histBGpeak} + \text{post_histBGpeak}$
histBGpeakDist ^{b, c}	mismatch between pre- and post-treatment background brightness	$ \text{pre_histBGpeak} - \text{post_histBGpeak} $

Eq. 4, with π_i being the probability of a single success, which is equivalent to the predicted response \hat{y}). For particle areas the absolute mean of area changes of each wafer was modelled using an identity link of the mean μ (Eq. 5) assuming a *Gamma* distribution.

$$g(\pi_i) = \ln \left(\frac{\pi_i}{1-\pi_i} \right) = \ln \left(\frac{\hat{y}_{i,n_{matched}}}{\hat{y}_{i,n_{lost}}} \right) \quad (4)$$

$$g(\mu) = \mu \quad (5)$$

The model was optimised by systematically varying the type and number of employed predictors, whereby the final set was chosen according to the significance of the obtained coefficients, the models deviance and general logic explainability of the ensemble. For both models (count loss and area change) n_{pre} was chosen as one predictor. A second predictor was chosen from the set of image quality related attributes and is indicated with asterisks in Table 5.

The resulting model setups are shown in pseudo-formula notation in Eq. 6 and Eq. 7 for the count loss and area change GLM respectively.

$$particle_counts[successes, failures] \sim \beta_0 + \beta_1 n_{pre} + \beta_2 pre_histDelta \quad (6)$$

$$area_change \sim \beta_0 + \beta_1 n_{pre} + \beta_2 histBGpeakDist \quad (7)$$

The predicted response was then taken as the portion of particle loss caused by the confounders, whereas the responses standard residuals were regarded as the remaining unexplained, hence treatment-attributed portion of the effect. Only where the residuals exceeded the 95% prediction interval of the water fitted response, effects were interpreted as significant.

Besides for the GLM models the image quality predictors (Table 5) were also used to calculate a generic index (background distortion index, BDI, see Eq. 8) providing a rough estimation of contrast problems due to the image background brightness level. The index number is higher for image pairs of worse quality. It was used for illustration purposes and to determine a limit of which images are not of acceptable quality and need to be excluded from analysis. The two coefficients α and γ were empirically found by optimising an ordinary least squares regression of relative particle losses against BDI. The calculated BDIs were normalised to range from 0 to 100, in order to be independent of the average image brightness. A BDI of 0 corresponds to the best and 100 to the worst image quality present.

$$BDI = \alpha \text{ histBGpeakSum} + \gamma \text{ histBGpeakDist} \quad (8)$$

with $\alpha = 2$, and $\gamma = 9$.

Using negative controls for method uncertainty estimations As a negative control, one wafer per polymer type was exposed to ultra-purified water (see Table 2). The GLMs were trained using an iteratively reweighted least squares algorithm [46] on the set of the negative control samples (see SI (S2) for details).

Results and discussion

Qualitative analysis

Commodity polymers

Overall, none of the post-treatment polymer spectra, both in FTIR and Raman, showed substantial spectral band changes that would hinder recognition (Fig. 4, Commodity polymers). However, minor alterations were detected in several cases, which are further detailed below.

Using Raman, increased fluorescence or baseline shifting (category 1 changes) were the most frequently seen effects, but did not hinder a successful recognition of the MP's polymer type. Only for PVC in the H_2O_2 Fe uncooled treatment clear degradation effects on the polymer basis became visible in multiple measured replicate spectra. Two peaks around 1124 and 1511 cm^{-1} ($C=C$ double bonds) strongly increased, which are a direct result of the dehydrochlorination reaction due to thermo-oxidative processes [47]. It is noteworthy that these degradation processes appear to affect individual PVC particles differently, as we see from the varying spectral characteristics between the replicate measurements (see also deposited spectroscopic data at <https://doi.org/10.5281/zenodo.4568683> [34]) and also from varying degrees of visual yellowing from white over beige to yellowish brown across particles.

In 10 out of the 125 Raman measurements multiple new peaks appeared which could not be attributed to specific functional group frequencies and were therefore not regarded as a polymer related change (these cases are indicated by * in Fig. 4, compare annotated deposited spectra [34]). These peaks were treatment and polymer unspecific and most frequently appeared in the water control. This lead to the suspicion that the water, used to rinse after the treatment, introduced the impurities. Switching to ultra-purified water for the remaining tests (i.e. H_2O_2 LT, Pentane, SPT) completely prevented these unknown peaks. They do not carry exploitable information for the question of polymer recognisability and their emphasis in Fig. 4 merely serves the purpose of clarity when comparing the here presented results to the original spectra provided in the deposited spectra [34].

In FTIR, the polymer basis was always clearly identifiable. We detected, however, minor polymer degradation processes in the H_2O_2 LT treatment. This concerned ABS, PC, PMMA, PP, PVC, TPU where new bands could be assigned to carboxylic acids which may have

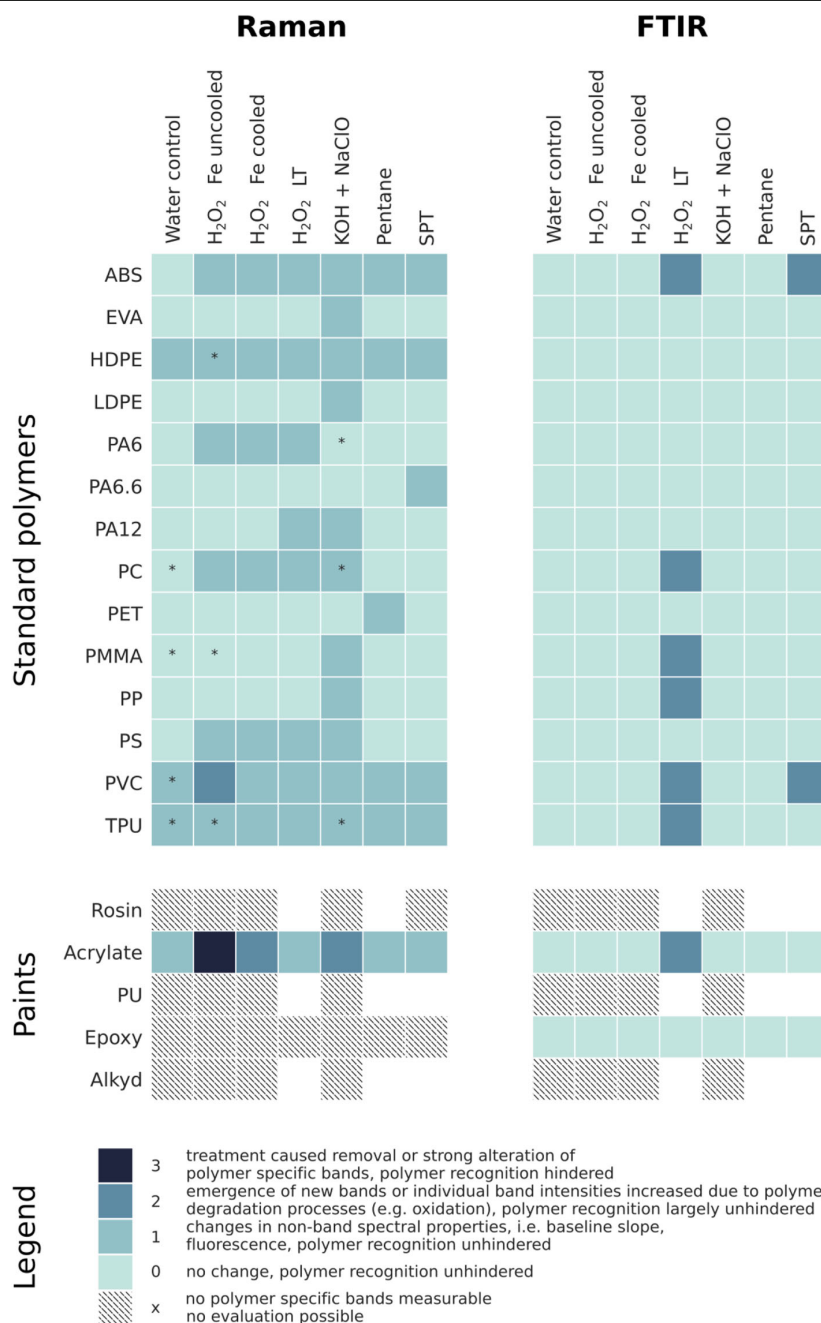


Fig. 4 Spectral changes expressed as categories as they were assigned by manually comparing the post-treatment spectra to the pre-treatment references. Asterisks (*) indicate spectra with newly evolved bands which, however, could be traced back to inorganic impurities originating from the rising water (not used in category assignment). White tiles indicate data not available (measurements were not taken due to expected unexploitable spectra, as other measurements of the same polymers indicated)

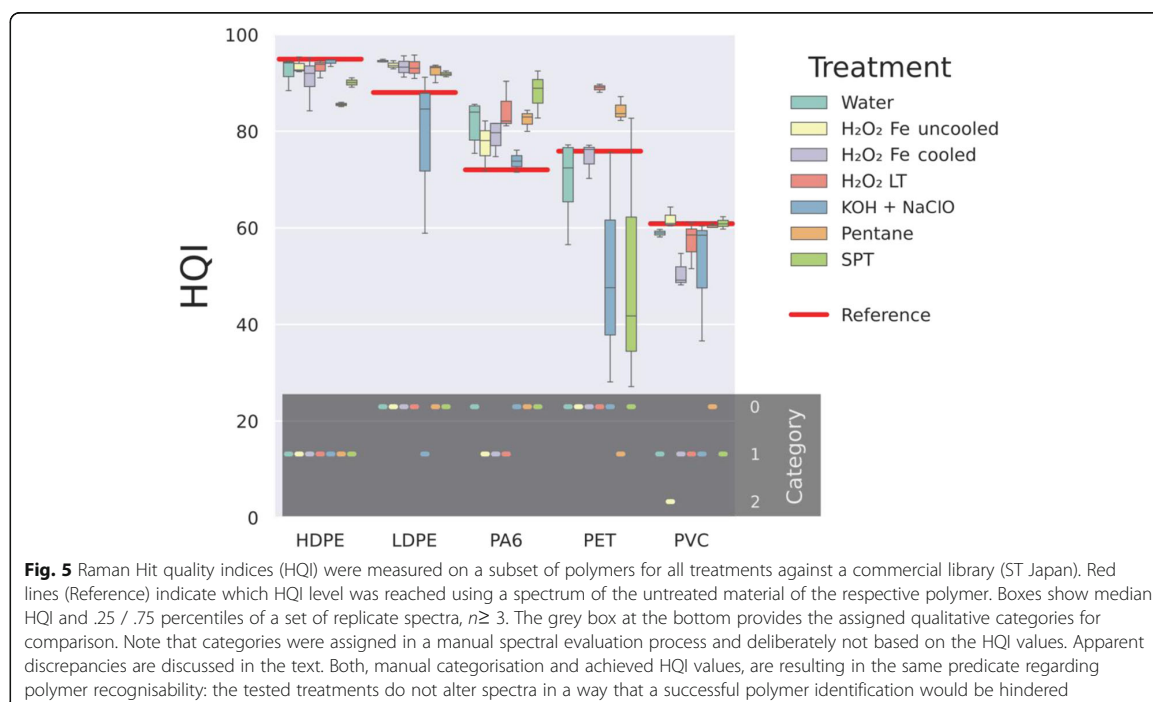
resulted from oxidising polymer chain ends. In the SPT treatment, similar oxidations were observed for ABS and PVC. The corresponding Raman spectra, however, did not systematically indicate these changes. This is plausible as FTIR is sensitive to polar organic groups, such as $C=O$ and its variations (e.g. esters, anhydrides, amides, imides), while Raman is less sensitive to these.

It appears that for FTIR category 2 changes occur rather treatment-specific, whereas for Raman spectra no treatment-specific impacts were seen. Instead, several cases of category 1 effects appeared in a rather polymer-specific manner. Although category 1 effects were also found in the water control of HDPE and TPU, it is noticeably the actual treatments that got assigned to this category.

As Fig. 5 shows, the HQI of the treated samples lie in the range of the untreated reference for most tested polymer types. For some treatments, the HQI range of the replicates varied more than for others. In the case of LDPE, the HQI distribution reflects the assignment of the categories (compare Fig. 4). That is, the KOH + NaClO treatment introduced category 1 changes, while no significant changes occurred in the other treatments. Only for KOH + NaClO, the HQI drops to around 90–59 for the different replicate

spectra. Similarly, the correct material type was found amongst the first ten hits in the library search, except two single replicates of a polymer-treatment-combination. One pentane-treated HDPE was identified as aliphatic fatty acid or alcohol. This is, from our experience, a frequently occurring problem in Raman spectroscopy. This and the fact that it only happened for one in three replicates should not lead to classifying the pentane treatment as harmful for this polymer type. The second not correctly identified spectrum resulted from a KOH + NaClO-treated PET replicate. Here, the occurrence of the inorganic contaminant calcium carbonate led to extra bands that prevented a semi-automated polymer identification. Overall, this confirms the assumption that none of the treatments induced changes that prevented the identification by a manually supervised spectral library search, as it is common in microplastics research. The result of a HQI based polymer attribution depends, however, on the available references, the applied algorithm and search parameters. It is not generalisable between studies and laboratories and therefore not used as a systematic evaluation criterion here.

In summary, our qualitative results indicate that, regarding the spectroscopic recognisability of MP



particles of any of the tested commodity polymers, all of the tested treatments are safe to apply, when the chosen analysis technique is either FTIR or Raman spectroscopy. However, effects on the treated polymers spectra, that were less critical to polymer recognition (i.e. category 1, Table 3), occurred frequently. Raman baseline shifts can be caused by heating of the sample during measurement [48]. Fluorescence mainly originates from sample characteristics, but background conditions such as ambient lighting, can play a role as well [49]. Both effects are too unspecific to be assigned to a polymer degradation process. Changes in the ATR-FTIR baseline can occur due to multiple changes in the optical path, e.g. the contact between the sample and the ATR crystal. They reflect physical rather than chemical changes, and again, are not fit to indicate a change in the polymer composition.

Paint resins

Out of the five paints, in all but one (acrylate) the polymer resin was not identifiable, already in the pre-treatment Raman spectra. In the KOH + NaClO as well as in the H₂O₂ Fe cooled treatment acrylate showed effects of degradation, however, was still recognisable. After the uncooled H₂O₂ Fe treatment, however, the polymer related bands were not found any longer, making an identification impossible. All other four paint spectra were substantially masked by fluorescence in both pre- and post-treatment spectra. In some cases, pigments (inorganic bands) dominated the spectra. One black (PU) and one grey paint (alkyd) showed an additional band which is indicative for black carbon (1343 cm⁻¹ and 1581 cm⁻¹, [47]). But as black carbon can stem from various sources in environmental samples, without any signal of the polymer bases the Raman spectra of these paint resins are unspecific and an identification by an automated detection procedure is not possible. As a result, no conclusions can be drawn concerning effects of the tested treatments on the polymer bases and associated processes of polymer degradation based on Raman spectroscopy.

The polymeric binders were clearly detectable for acrylate and epoxy based paints using FTIR spectroscopy. In these paints none of the treatments lead to a change in spectral quality, except the H₂O₂ LT treatment, which introduced carboxylic acid salt signatures around 1600, 1350 and 789 cm⁻¹ in acrylic paint, indicating polymer oxidation processes. While for PU based paint no exploitable spectral properties could be found in neither pre- nor post-treatment spectra, the paints based on rosin and alkyd exhibited some weaker bands that could be attributed to the organic binder matrix by an experienced spectroscopist,

however not with sufficient confidence. Hence, we note that only the epoxy and the acrylic paint can be regarded as reliably identifiable by their polymer FTIR bands and are thus useful for evaluating the treatments effects on polymer recognisability. Chemical treatment-caused spectral changes i.e. bands weakening or disappearing were found in acrylic paint for H₂O₂ (Fe + LT) and SPT treatments. This did, however, not hinder the recognition of the polymeric binder as only inorganic components were affected indicating mineral depletion (CaCO₃). Thus, no restricting categories were assigned based on this observation (Fig. 4).

Comparing Raman and FTIR spectra of paints, overall masking was weaker in the FTIR spectra. Where peak changes were present, they were dominantly caused by pigments or other fillers, for both techniques. Only for acrylic paint the strong thermo-oxidative regime of high temperature Fenton's catalysed H₂O₂ treatment made an unambiguous spectral recognition impossible in Raman, however not in FTIR.

In paints based on rosin, polyurethane and alkyd the detection of binder matrix bands was not possible already on the untreated material (at least not to a degree of certainty that would allow the identification if the material was unknown). Thus, degradative effects of the treatments cannot be studied with the here applied techniques. Our conclusions are limited to the observation that in general a reliable detection of paint flakes of these resins using spectroscopic identification is not guaranteed. In contrast to commodity plastics, paint resins are typically composed of high amounts of non-polymeric constituents and only a smaller portion of the polymer itself. Accordingly, it is questionable whether paint resins can be exhaustively and reliably identified in environmental systems using spectroscopic methods [20, 50]. The chemical bonds of many inorganic and organic pigments and other paint constituents are strong Raman scatterers, which renders them well detectable in Raman spectra (also better than with FTIR). On the downside they frequently mask the weaker bands of the polymeric binder due to their strong intensities or additional fluorescence. Large reference libraries containing spectra of large varieties of paint composites preferably from different manufacturers might be able to detect paint flake MP based on their (pigment dominated) fingerprint. This approach has also been taken by other studies [13, 51]. Most pigments are, however, not solely applied in synthetic polymers but in a large diversity of technical applications, which is why an indirect identification of MP via those pigments cannot be done in a systematic way. Furthermore, due to the large variety in different paint compositions, an automatic detection is limited unless the particular paint product is available in the spectral library.

Quantitative analysis

Particle property comparisons

As for the qualitative data, a high level overview on the quantitative data can be gained from the heat maps that summarise the relative changes that we could attribute to the treatments (Fig. 6). Noticeable are elevated values present in various polymers exposed to the H_2O_2 treatment. Further, for ABS, PC and epoxy based paint there are higher values found across treatments.

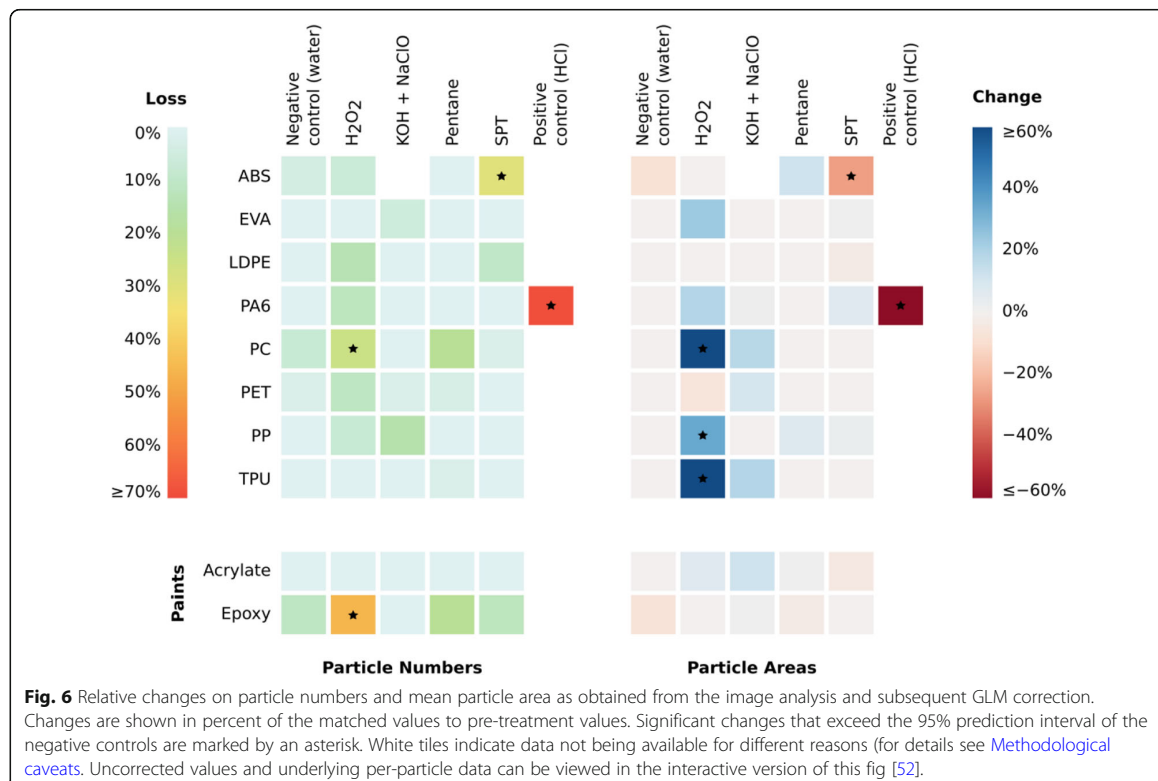
To enable a deeper insight into the quantitative dataset, we provide an interactive version of the heat map figures (Fig. 6), augmented with plots of individual particle data showing detailed and aggregated differences between pre- and post-treatment images. It may also be used to understand the necessity and effect of the GLM corrections that were applied to the data. The interactive figure may be downloaded from: <https://doi.org/10.5281/zenodo.4568524> [52].

Particle counts From the GLM corrected data, it can be seen that the majority of polymer treatment combinations did not show any loss significantly different from the negative control. Exceptions are the SPT treated ABS (30%) and the H_2O_2 treatments of epoxy based paint and PC (46% and 25%, respectively). For these three polymers also the

corresponding water treatments show particle losses higher than any of the other polymers. This indicates that for images of these polymers not all of the confounding effects could be removed by the GLM correction, and the actual treatment caused changes must be lower.

For the H_2O_2 treated epoxy paint particles we conclude that the relative loss in the GLM corrected data is indeed indicative of an actual treatment caused effect. Influences of confounding factors were comparably low for this image pair ($n_{pre} = 212$, $BDI = 0$). The modal value of particle brightness is reduced in the post-treatment image ($pre_histFGpeak = 183$ and $post_histFGpeak = 103$ out of maximum of 255, respectively, see Table 5 for explanations), indicating a possible material erosion, which could not be explained by other factors. This is further substantiated by looking at individual particles in a pre-post-comparison, where dark indentations or holes become visible, in places where the particle surface or boundary were priorly intact (Fig. 7).

It is known that certain polyepoxides are susceptible towards peroxides, in fact, this is utilised in certain technical applications. One study used 24% and 50% H_2O_2 to superficially degrade epoxy resins and expose embedded fibres in a fibre reinforced polymer (FRP) [53]. For the recycling of carbon fibres from FRPs, acetic acid (30%) was



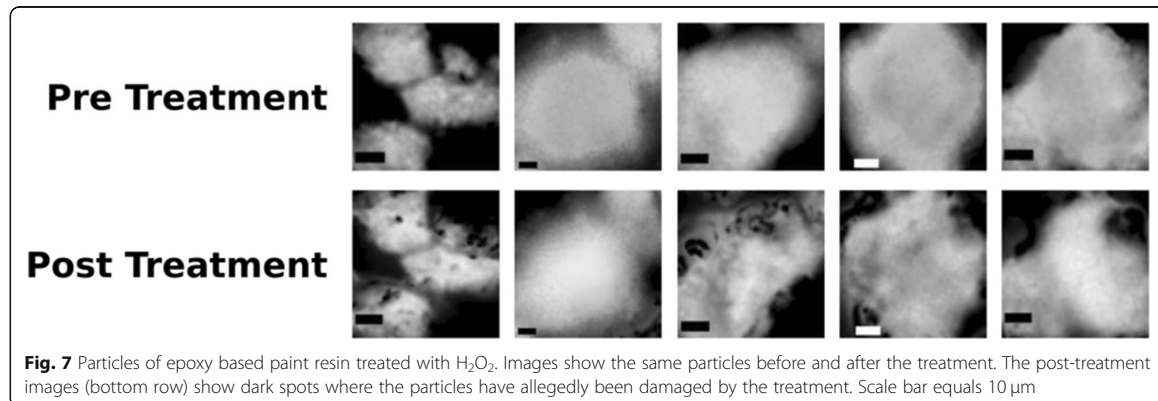


Fig. 7 Particles of epoxy based paint resin treated with H_2O_2 . Images show the same particles before and after the treatment. The post-treatment images (bottom row) show dark spots where the particles have allegedly been damaged by the treatment. Scale bar equals $10\ \mu\text{m}$

deemed effective for an epoxide matrix decomposition in an overnight treatment [54]. When epoxy resin particles are targeted within environmental MP studies and peroxide digestion protocols are applied, we recommend for future studies to note that numbers are likely underrepresenting the actual environmental load for these polymers. In our data the corrected particle loss exceeded that of the epoxy water digestion by 35 percentage points. Hence, it can be assumed, that a reported concentration of epoxy MP particles in a certain environment are only covering approximately 65% of the total load present, at least for particles in the here studied size range.

The effect of H_2O_2 could also be seen on the epoxy layer that we used to immobilise the particle on the Si wafers. Increased brightness and haziness of the image background was apparent especially around the wafer edges, which made more encroachments by manual image postprocessing necessary in those wafers. Small defects in the layer were promoted to brighter visual appearances after the treatment that could lead to false positive detections, while increased brightness in the near field surrounding of particles, is likely a contributor to the observed particle area growth that was observed in several H_2O_2 treated polymers. These effects on the layer show that with the epoxy resin used here, we have not yet found the optimal immobilisation adhesive for the purpose of the study. We argue though, that the effects do not constitute a failure of the immobilisation technique, as we know from the positive control wafer (PA6 treated with HCl) the detailed visual characteristics of spots where particles got removed from the layer. Such appearances were not what we could typically observe in the images of H_2O_2 treated wafers, instead, the image objects at places where particles were expected generally resembled what particles looked like in the other treatments (including the negative control water treatment). This is yet not sufficient evidence to fully exclude that a loosening of particles may have occurred in some places due to the layer being affected, but it shows the this was not predominant process. Hence we conclude: the spin-

coated epoxy layer did resist our H_2O_2 treatment at least to a degree that particles could be held in place and measured after the treatment. It could be further improved by finding an adhesive composition that does not show any visual nor integrity-related impacts from any of the tested treatments. Experiences and advice from our adhesive layer development phase are detailed in the SI (S3).

The wafer of H_2O_2 treated PC suffered the problem of having a low total particle number ($n_{pre} = 26$), which could not be entirely alleviated by the applied GLM correction. The particle brightness was not reduced on this wafer after the treatment ($pre_$ and $post_histFGpeak$ were at 88 and 89, respectively), suggesting that there was no treatment caused effect acting on all particles collectively. Instead the loss was driven by only six particles that could not be matched between the images. The low n_{pre} is thus regarded here as the main reason for the resulting significant loss.

The loss of particles from the SPT treated ABS wafer should only with certain reservations be seen as an indicator of particle degradation, as the image quality was on the brink of our exclusion level ($BDI = 26$). We interpret the observed losses as partly treatment caused and discuss this interpretation below (Comparison of qualitative and quantitative results).

Most prominent, but also expected, is the loss of nearly all particles in the positive control wafer (HCl on PA6), where 69% of pre-treatment particles could no longer be confirmed to be present post treatment (85%, without GLM correction, see also Using a positive control for calibration of particle detection).

Particle areas In contrast to particle counts, changes of particle area were recorded to differ in negative (area decrease) as well as positive (area increase) direction. The largest decrease of particle area can be seen in the positive control, however, also the SPT treated ABS was recorded with a significant area reduction of 30%. But as noted above, one should take this result with caution,

due to the low image quality of this wafer. Several polymers treated with H_2O_2 revealed significant area increases post treatment (PP, TPU and PC with a 34%, 60% and 220% average increase, respectively). The extreme increase in particle area of PC was mostly caused by two outliers where in the pre-treatment image the particle was only partly detected by the thresholding algorithm. An increase in area or particle volume would not hinder a MP detection, however, it may lead to a distorted representation of particle sizes.

For the H_2O_2 treated epoxy paint particles, where we described a significant particle loss above, we do not see a change in area for the remaining matched particles. The formation of dark holes in particles (Fig. 7) is not represented in the post-treatment area measurements, because particles are identified as closed shapes by the detection algorithm.

Methodological caveats

The here presented technique for quantitative MP treatment evaluation was limited in two ways. Limitations were caused either by effects of a specific treatment on the adhering epoxy layer, or, by polymer specific characteristics which impeded a contrast rich DIC imaging.

The KOH + NaClO treatment disrupted the adhesion between the spin coated layer and the underlying Si wafer, which lead to a partial or complete detachment of the epoxy film and wrinkling artefacts on the images in several cases. The film itself did not seem to be degraded or otherwise affected as microscopic imaging could confirm that the epoxy matrix and attached MP particles were visually intact. However, the correct placement for a post-treatment imaging was disturbed and the layers were partially outside of the microscope's focal plane, which resulted in darker areas that could no longer be recognised by the particle detection. This affected especially the KOH + NaClO treated wafers of PP and PET, where such areas needed be mutually excluded from the pre- and post-treatment images in the manual image postprocessing. The H_2O_2 treatment had a different effect on the epoxy layer, however without affecting the image quality to an extent where the image analysis would be impeded. The wafers treated with H_2O_2 were showing varying degrees of obliqueness in the otherwise clear epoxy layer, indicating a surface affect or softening of the layer. The resulting implications are discussed in the above section.

For PVC, PMMA, PS and, to a lesser degree, ABS the chosen microscopy mode (reflected DIC) was not able to generate images that have a good particle to background contrast. The image postprocessing did increase the particle brightness for the particle detection algorithm but at the cost of a proportionally gained brightness of the image background. For reasons unbeknown to us, the

surface topography of MP particles of these polymers did not create an optical path length difference that would allow for contrast rich DIC images. The size range of the particles of these polymers was not different than for the other polymers and further investigations beyond the scope of the study would be necessary to clarify whether this is indeed due to polymer specific optical characteristics or rather special interactions between the particles and the uncured epoxy layer at the time of application. Unless a solution is found to create particles and immobilisations of these four polymers that yield a sufficient contrast, the more suitable approach would be applying a different microscopic technique. Possible candidates are discussed in the SI (S3).

With the current state of the experimental approach, the polymers of PVC, PS and PMMA, could not be included in the analysis, due to the above-mentioned reasons. PMMA and PVC were excluded due to low image qualities. Of the ABS wafers only the KOH + NaClO treated sample had image qualities that resulted in a BDI exceeding the set cut-off of 27. For PS, however, the BDI was not able to ascertain that the image quality was unsuitable for an analysis, because the image defects in PS were slightly different than in PVC and PMMA. While the latter showed a general and evenly low contrast between particles and background, PS had mostly a stronger contrast but included many optical artefacts (i.e. bright ring-like halos around particles). It was attempted in image postprocessing to remove the artefacts manually, however, the PS images could not be improved sufficiently. Images of PVC and PS can be viewed in the deposited imaging dataset at <https://doi.org/10.5281/zenodo.4568488> [55] as an example of the contrast problems.

The above discussed caveats currently pose certain limitations in terms of applicability, explanatory power and required work effort. The true value, however, is present here as the possibility of the immobilisation approach to study effects on individual particles simultaneously on large particle numbers in the smaller MP size ranges. How this compares to other concepts is discussed below in the section [Comparison of experimental concepts](#). Additionally, in the SI we describe more detailed the lessons learned and attempts to further methodological improvements for interested readers (S3).

Comparison of qualitative and quantitative results

While the quantitative particle data provides insights in the particle-based alterations of a treatment, it does not convey whether these can be recorded by the chosen analysis technique (here Raman and FTIR spectroscopy). As an example, particles might still be present after a treatment, but changes on the surface of the particles or the polymer matrix might render them undetectable.

The other way round - a polymer type is recognised post treatment but the quantitative measurements reveal particle losses or area changes - is also a possible scenario. In fact, the epoxy based paint resin in our data is an example, where we observed a significant particle loss after a 24 h H_2O_2 exposure, while FTIR recorded no changes to the polymer spectrum even after a prolonged 2 weeks' exposure or the uncooled Fenton's with its $80 + ^\circ\text{C}$ temperatures. The two-tiered approach, providing qualitative and quantitative data on the same polymer treatment model systems, therefore allows for a higher certainty on the applicability of the tested treatments. For a comprehensive evaluation both aspects are of importance.

A related study also reported qualitative (spectroscopic) and quantitative (recovery of spiked particles) data [11]. They noted a qualitative change on H_2O_2 treated PVC (see also below section for further details: Comparison of our results to current literature), however could not confirm that the described polymer degradation would manifest in the quantitative measurements.

In our data, SPT treated ABS that was indicating negative changes in particle numbers in the quantitative result, also showed alterations in the spectra of FTIR (assigned category 2, emergence of new bands or band intensities altered), and Raman (category 1, baseline drift). The treatment with SPT resembles a density separation where HCl is used to acidify the solution to pH 3, in order to prevent sodium poly tungstate precipitation [31]. We know that ABS is attacked by acidic digestions [1], however, this was only shown for highly concentrated and strongly oxidative acids (HNO_3 69% and HClO_4 70%), neither of which applies to the here deployed solution. As it was demonstrated there, the acidic treatment lead to a bloating and bubbling dissolution of the macroplastic piece that was tested [1]. The present results indicate an area reduction of those particles that were found again after the treatment. A testable conjecture beyond the scope of this study, is that a count and area decrease was detectable - despite working under a much weaker acidic environment - because of the small size range of particles that were used here, and which potentially are more easily damaged by acids.

Comparison of our results to current literature

To our knowledge, polymer chemical resistance tests in qualitative and quantitative manner have not yet been performed on such small MP particles. Partly related studies reported recovery rates of $> 90\%$ of spiked particles using fluorescence-labelled microspheres $\leq 30 \mu\text{m}$ as representatives of small MP for a novel magnetic separation [12] and in a density separation and digestions [10]. Working with aliquoted pipetting of bulk particle suspensions, they noted that

direct comparisons of the same particles' pre- and post-treatment counts was infeasible in this size range [12]. Generally, our overall finding, that, with respect to spectroscopic recognisability, no considerable changes to the polymeric bands were caused by the tested treatments on $\text{MP} < 70 \mu\text{m}$, is in agreement with other studies which used larger MP particles. One study tested the same $\text{KOH} + \text{NaClO}$ protocol on a similar set of 12 commodity polymers ($\geq 5 \text{ mm}$) and performed Raman spectroscopy on pre- and post-treatment particles, finding no relevant changes on the polymer matrix [1]. Dehaut et al. [5] applied a KOH protocol without an additional oxidiser, also reporting no effect on Raman spectra even at $60 ^\circ\text{C}$ in all 11 polymers that were comparable between their and our study. Similarly, Hurley et al. [25] found no significant spectral changes applying a Fenton's protocol (cooled, $< 40 ^\circ\text{C}$) to a set of 8 different commodity polymers ($\sim 3 \text{ mm}$) using FTIR.

In our Raman measurements, the only polymer degradative effect was observed in PVC, where the formation of $\text{C}=\text{C}$ double bonds (caused by dehydrochlorination) occurred only in the uncooled H_2O_2 Fe treatment ($> 80 ^\circ\text{C}$, 10 min) as a direct consequence of thermo-oxidative processes on the polymer matrix (as we also observed in an early study [47]). Likewise, Raman spectra measured by Karami et al. [11] on PVC particles treated with $50 ^\circ\text{C}$ H_2O_2 were described as being diminished in the $\text{C}-\text{Cl}$ stretching band, which would be indicative of the same dehydrochlorination process that we observed. But, as mentioned above, PVC exposed to $60 ^\circ\text{C}$ in a KOH based treatment (10%, 24 h) exhibited no effect on Raman spectra [5], albeit the presence of a hydrolytic and thermo-oxidative pressure. The difference lies apparently in the stronger oxidising potential of the H_2O_2 , that induces detectable - but non-critical - polymer degradation of PVC. It should be noted though, that the occurrence of PVC thermo-oxidative degradation depends on the specific PVC material and its added stabilisers. It is plausible that for other PVC compositions this effect may be induced alone by temperature rises above $60 ^\circ\text{C}$.

In general, negative impacts of elevated temperatures during treatments have also been demonstrated by various studies. For instance, increased mass loss for PA in H_2O_2 (among other treatments), was reported for temperatures between 60 and $70 ^\circ\text{C}$ [14] and for $> 70 ^\circ\text{C}$ [25]. In our qualitative analysis PA did not show signs of degradation, however, we cannot infer whether particle losses or area changes may have resulted from these treatments, as no treatments involving elevated temperatures were part of our quantitative analysis. Yet, the non-catalysed H_2O_2 treatment (room temperature) resulted in no change of PA6 particle numbers or areas.

For the pentane treatment [31] we could now demonstrate polymer resistivity among our test series. The protocol, which involves a weakly acidic digestant (ethanol acidified to pH 3 using acetic acid is added to the sample before pentane), had no impact on the spectra of any of the tested polymers, hence also not on the polyamides, known to be susceptible to acidic degradation. PA6 particles, which we tested quantitatively, suffered no detectable impact by the pentane treatment in particle numbers or areas. Similarly, the acidic SPT was not affecting particle numbers or sizes, except for ABS, where a minor degradative effect could not be excluded, based on our data.

It was reported that PA6.6 melted when applying H_2O_2 at 70 °C and a significant weight and size loss was measured [25]. In our uncooled catalysed H_2O_2 treatment (reaching up to 85 °C for the 10 min treatment duration) PA 6 showed a yellowing effect despite not showing significant quantifiable losses in size or area. Potentially, the temperature exposure in our treatment was not long enough to melt the polymer compared to their exposure time (12 h).

Studies exist that found degradative effects of alkaline protocols on PET [5, 14, 25], however also other factors such as elevated temperatures were involved in some of these cases. Our qualitative results of the protocol using $\text{KOH} + \text{NaClO}$ do not show signs of degradation of PET in FTIR or Raman spectra; neither do we see a significant particle loss or area change in the quantitative data. The quantitative are, however, of lower confidence, as these samples were affected by the $\text{KOH} + \text{NaClO}$ induced displacement of the epoxy layer, complicating image analyses.

Comparison of experimental concepts

To our knowledge, working with particles immobilised by adhesives to obtain quantitative measurements has not been performed so far. A related approach was developed recently for measuring PS nanoplastic spheres, where etched cavities in Si wafers were serving as a nanofabricated grid [56]. Particles placed in suspension on the cavity array were assembling by capillary forces and thus temporarily arrested for subsequent material and size determination using Raman spectroscopy. Alternative approaches to microscopy have been applied to determine size changes, such as laser sizing [57]. However, when measuring in wet dispersion problems can arise for polymers with a lower density than water as a sufficient particle dispersion can be challenging to achieve. Absolute particle counts cannot be determined using this technology and problems can arise if post-treatment particle numbers fall below the measurement limit of the specific laser sizer [57]. Also Coulter counters or flow cytometry, might be suitable techniques for

these kind of measurements. Usually applied for counting plankton or cells, they allow simultaneous count and size measurements. A disadvantage, however, is the necessity for a filtration step to purify the particles for a post-treatment measurement. Finally, direct microscopic imaging of filtered bulk particle suspensions before and after a treatment could be a viable approach as well. However, like all methods using mobile particles entails the problem, that count data is difficult to obtain for small-sized MP. Particles can get lost in transfer steps and effects like breaking apart, aggregation, handling loss or real treatment-caused degradation are difficult to disentangle. This has been observed by others as well. Thiele et al. [13] used MP particles < 600 μm (that could still be manually handled) for spiking and recovery tests in a treatment evaluation and reported issues with particle loss in transfer steps that needed to be mathematically accounted for. With an immobile particle approach these problems do not arise.

Conclusion

We identified the need in the scientific community for a method to evaluate the impact of treatment procedures on MP particles that are smaller than what can be easily be handled manually, e.g. using fine-tipped tweezers. Studies which aim at identifying MP in the lower μm sizes rely on the certainty that the investigated MP particles are not destroyed by the chosen sample purification protocol.

In summary, we could show that conducting treatment evaluations with immobilised MP particles in the lower micrometre sizes is possible and has a range of advantages. From a theoretical perspective this could be readily adapted for even smaller MP and nanoplastics. In contrast to mobile particle approaches, particle properties changing due to a treatment can be studied here on individual particle level.

For the first time it was possible to demonstrate for MP as small as 10 μm , that purification methods, which are already routinely used, do not substantially alter the spectroscopic detectability, nor quantitative properties for many of the most common polymer types. Our results substantiate the validity of applications that extract particles in this size range by those methods. It turned out that polymer resins used as binders in synthetic paints are distinct from MP derived from commodity plastics. In chemical treatments they were more easily taking damage and their spectroscopic recognisability was severely limited independent of treatment. A tentative conclusion hereof is that numbers of paint flakes, found in environmental samples, are likely to be underestimated compared to other MP species.

We recommend that future studies take up the approach – and lessons learned – for qualitative and quantitative evaluations on immobilised MP, to yield further certainty of applicability of their respective methodological setups.

Abbreviations

MP: Microplastic(s); BDI: Background distortion index; DIC: Differential interference contrast microscopy; FRP: Fibre reinforced polymer(s); FTIR: Fourier transform infrared spectroscopy; GLM: Generalised linear model(s); HQI: Hit quality index; Lo: Lower threshold; LT: Long term; RT: Room temperature; SI: Supplementary information; SPT: Sodium polytungstate

Supplementary Information

The online version contains supplementary material available at <https://doi.org/10.1186/s43591-021-00012-0>.

Additional file 1.

Acknowledgements

For helpful comments and expertise, we thank Klaus-Jochen Eichhorn, Mikhail Malanin and Lars Bittrich. Support in laboratory work was kindly provided by Elisavet Kanaki, Pia Ullischberger, Anne Rödiger, Piotr Jachimowicz, Julia Muche and Juliana Ivar do Sul.

Authors' contributions

RL, KE, DF and ML developed the idea for this research; RL, KE, and FF contributed the conception and design of the work; RL, KE and FF conducted the acquisition, analysis and interpretation of data; RL and JB created new software used in the work; JB provided code revision; RL, KE and FF have drafted the manuscript; JB, DF and ML substantively revised it. The authors read and approved the final manuscript.

Funding

Funding of this study was received from the project MicroCatch_Balt (German Federal Ministry of Education and Research (BMBF), grant number 03F0788A) and the BONUS project Micropoll (funded jointly by the European Union and the BMBF, grant number 03F0775A). Open Access funding enabled and organized by Projekt DEAL.

Availability of data and materials

- The source code of the image and statistical analysis and visualisation is available as a static archive on Zenodo [35] with the identifier <https://doi.org/10.5281/zenodo.4592319> and as a repository on Github at https://github.com/robna/ImmobileParticles_MatchAndAnalyse
- The interactive figure that was used for the exploration and analysis of the quantitative dataset of this study is available on Zenodo [52] with the identifier <https://doi.org/10.5281/zenodo.4568524>
- DIC microscopy data that support the quantitative findings of this study are available on Zenodo [55] with the identifier <https://doi.org/10.5281/zenodo.4568488>. This includes all pre- and post-treatment images after manual processing and downscaling (as used in the analysis). Original raw imaging data is not provided there due to large file size (> 1 TB), but are available upon reasonable request from the authors.
- The Raman and FTIR spectroscopy data that support the qualitative findings of this study are available on Zenodo [34] with the identifier <https://doi.org/10.5281/zenodo.4568683>.

Declaration

Competing interests

The authors declare that they have no competing interests.

Author details

¹Leibniz Institute for Baltic Sea Research Warnemünde, Seestraße 15, 18119 Rostock, Germany. ²Leibniz Institute of Polymer Research Dresden, Hohe Straße 6, 01069 Dresden, Germany. ³University of Gothenburg, Department of Marine Sciences, Kristineberg 566, S-45178 Fiskebäckskil, Sweden.

Received: 15 March 2021 Accepted: 17 June 2021

Published online: 18 July 2021

References

1. Enders K, Lenz R, Beer S, Stedmon CA. Extraction of microplastic from biota: recommended acidic digestion destroys common plastic polymers. *ICES J Mar Sci*. 2017;74(1):326–31. <https://doi.org/10.1093/icesjms/fsw173>.
2. Tagg AS, Harrison JP, Ju-Nam Y, Sapp M, Bradley EL, Sinclair CJ, et al. Fentons reagent for the rapid and efficient isolation of microplastics from wastewater. *Chem Commun*. 2017;53(2):372–5. <https://doi.org/10.1039/c6cc08798a>.
3. Löder MGJ, Imhof HK, Ladehoff M, Lösche LA, Lorenz C, Mintenig S, et al. Enzymatic purification of microplastics in environmental samples. *Environ Sci Technol*. 2017;51(24):14283–92. <https://doi.org/10.1021/acs.est.7b03055>.
4. Kühn S, van Werven B, van Oyen A, Meijboom A, Rebolledo ELB, van Franeker JA. The use of potassium hydroxide (KOH) solution as a suitable approach to isolate plastics ingested by marine organisms. *Mar Pollut Bull*. 2017;115(1–2):86–90. <https://doi.org/10.1016/j.marpolbul.2016.11.034>.
5. Dehaut A, Cassone A-L, Frère L, Hermabessiere L, Himber C, Rinnert E, et al. Microplastics in seafood: benchmark protocol for their extraction and characterization. *Environ Pollut*. 2016;215:223–33. <https://doi.org/10.1016/j.envpol.2016.05.018>.
6. Avio CG, Gorbi S, Regoli F. Experimental development of a new protocol for extraction and characterization of microplastics in fish tissues: first observations in commercial species from Adriatic Sea. *Mar Environ Res*. 2015;111:18–26. <https://doi.org/10.1016/j.marenvres.2015.06.014>.
7. Nuelle M-T, Dekiff JH, Remy D, Fries E. A new analytical approach for monitoring microplastics in marine sediments. *Environ Pollut*. 2014;184:161–9. <https://doi.org/10.1016/j.envpol.2013.07.027>.
8. Mathalon A, Hill P. Microplastic fibers in the intertidal ecosystem surrounding Halifax Harbor, Nova Scotia. *Mar Pollut Bull*. 2014;81(1):69–79. <https://doi.org/10.1016/j.marpolbul.2014.02.018>.
9. Cole M, Webb H, Lindeque PK, Fileman ES, Halsband C, Galloway TS. Isolation of microplastics in biota-rich seawater samples and marine organisms. *Sci Rep*. 2014;4(1). <https://doi.org/10.1038/srep04528>.
10. Claessens M, Cauwenberghe LV, Vandegehuchte MB, Janssen CR. New techniques for the detection of microplastics in sediments and field collected organisms. *Mar Pollut Bull*. 2013;70(1–2):227–33. <https://doi.org/10.1016/j.marpolbul.2013.03.009>.
11. Karami A, Golieskardi A, Choo CK, Romano N, Ho YB, Salamatinia B. A high-performance protocol for extraction of microplastics in fish. *Sci Total Environ*. 2017;578:485–94. <https://doi.org/10.1016/j.scitotenv.2016.10.213>.
12. Grbic J, Nguyen B, Guo E, You JB, Sinton D, Rochman CM. Magnetic extraction of microplastics from environmental samples. *Environ Sci Technol Lett*. 2019;6(2):68–72. <https://doi.org/10.1021/acs.estlett.8b00671>.
13. Thiele CJ, Hudson MD, Russell AE. Evaluation of existing methods to extract microplastics from bivalve tissue: adapted KOH digestion protocol improves filtration at single-digit pore size. *Mar Pollut Bull*. 2019;142:384–93. <https://doi.org/10.1016/j.marpolbul.2019.03.003>.
14. Pfeiffer F, Fischer EK. Various digestion protocols within microplastic sample processing evaluating the resistance of different synthetic polymers and the efficiency of biogenic organic matter destruction. *Front Environ Sci*. 2020;8. <https://doi.org/10.3389/fenvs.2020.572424>.
15. Lusher AL, Welden NA, Sobral P, Cole M. Sampling, isolating and identifying microplastics ingested by fish and invertebrates. *Anal Methods*. 2017;9(9):1346–60. <https://doi.org/10.1039/c6ay02415g>.
16. Vandermeersch G, Cauwenberghe LV, Janssen CR, Marques A, Granby K, Fait G, et al. A critical view on microplastic quantification in aquatic organisms. *Environ Res*. 2015;143(Pt B):46–55. <https://doi.org/10.1016/j.envres.2015.07.016>.
17. Bläsing M, Amelung W. Plastics in soil: analytical methods and possible sources. *Sci Total Environ*. 2018;612:422–35. <https://doi.org/10.1016/j.scitotenv.2017.08.086>.
18. Quinn B, Murphy F, Ewins C. Validation of density separation for the rapid recovery of microplastics from sediment. *Anal Methods*. 2017;9(9):1491–8. <https://doi.org/10.1039/c6ay02542k>.
19. Elert AM, Becker R, Duemichen E, Eisentraut P, Falkenhagen J, Sturm H, et al. Comparison of different methods for MP detection: what can we learn from them, and why asking the right question before measurements matters? *Environ Pollut*. 2017;231(Pt 2):1256–64. <https://doi.org/10.1016/j.envpol.2017.08.074>.

20. K  ppler A, Fischer D, Oberbeckmann S, Schernewski G, Labrenz M, Eichhorn K-J, et al. Analysis of environmental microplastics by vibrational microspectroscopy: FTIR, Raman or both? *Anal Bioanal Chem*. 2016;408(29): 8377–91. <https://doi.org/10.1007/s00216-016-9956-3>.
21. Fischer M, Scholz-B  ttcher BM. Microplastics analysis in environmental samples recent pyrolysis-gas chromatography-mass spectrometry method improvements to increase the reliability of mass-related data. *Anal Methods*. 2019;11(18):2489–97. <https://doi.org/10.1039/c9ay00600a>.
22. Zobkov MB, Esiukova EE. Evaluation of the Munich plastic sediment separator efficiency in extraction of microplastics from natural marine bottom sediments. *Limnol Oceanogr Methods*. 2017;15(11):967–78. <https://doi.org/10.1002/lom3.10217>.
23. Enders K, Lenz R, Stedmon CA, Nielsen TG. Abundance, size and polymer composition of marine microplastics $\geq 10 \mu\text{m}$ in the Atlantic Ocean and their modelled vertical distribution. *Mar Pollut Bull*. 2015;100:70–81. <https://doi.org/10.1016/j.marpolbul.2015.09.027>.
24. L  der MGJ, Gerdt G. Methodology Used for the Detection and Identification of Microplastics—A Critical Appraisal. In: Bergmann M, Gutow L, Klages M. (eds) *Marine Anthropogenic Litter*. Cham: Springer; 2015. https://doi.org/10.1007/978-3-319-16510-3_8.
25. Hurley RR, Lusher AL, Olsen M, Nizzetto L. Validation of a method for extracting microplastics from complex, organic-rich, environmental matrices. *Environ Sci Technol*. 2018;52(13):7409–17. <https://doi.org/10.1021/acs.est.8b01517>.
26. Budimir S, Set  l   O, Lehtiniemi M. Effective and easy to use extraction method shows low numbers of microplastics in offshore planktivorous fish from the northern Baltic Sea. *Mar Pollut Bull*. 2018;127:586–92. <https://doi.org/10.1016/j.marpolbul.2017.12.054>.
27. Julienne F, Delorme N, Lagarde F. From macroplastics to microplastics: role of water in the fragmentation of polyethylene. *Chemosphere*. 2019;236: 124409. <https://doi.org/10.1016/j.chemosphere.2019.124409>.
28. Allegra G, Famulari A. Chain statistics in polyethylene crystallization. *Polymer*. 2009;50(8):1819–29. <https://doi.org/10.1016/j.polymer.2009.01.063>.
29. Julienne F, Lagarde F, Delorme N. Influence of the crystalline structure on the fragmentation of weathered polyolefines. *Polym Degrad Stabil*. 2019; 170:109012. <https://doi.org/10.1016/j.polymdegradstab.2019.109012>.
30. Ober CK, M  llen K. Introduction applications of polymers. In: Matyjaszewski K, M  ller M. (eds) *Polymer science: a comprehensive reference*: Elsevier; 2012. p. 1–8. <https://doi.org/10.1016/B978-0-444-53349-4.00199-0>.
31. Enders K, Lenz R, do Sul JAI, Tagg AS, Labrenz M. When every particle matters: a QuEChERS approach to extract microplastics from environmental samples. *MethodsX*. 2020;7:100784. <https://doi.org/10.1016/j.mex.2020.100784>.
32. Wang Z, Taylor SE, Sharma P, Flury M. Poor extraction efficiencies of polystyrene nano- and microplastics from biosolids and soil. *PLoS One*. 2018;13(11):e0208009. <https://doi.org/10.1371/journal.pone.0208009>.
33. Lares M, Ncibi MC, Sillanp    M, Sillanp    M. Intercomparison study on commonly used methods to determine microplastics in wastewater and sludge samples. *Environ Sci Pollut R*. 2019;26(12):12109–22. <https://doi.org/10.1007/s11356-019-04584-6>.
34. Lenz R, Enders K, Fischer F, Brandt J, Fischer D, Labrenz M. Raman and FTIR spectra used in: Lenz et al. 2021, "Measuring impacts of microplastic treatments via image recognition on immobilised particles below 100 μm "; 2021. <https://doi.org/10.5281/zenodo.4568683>.
35. Lenz R, Enders K, Fischer F, Brandt J, Fischer D, Labrenz M. *ImmobilisedParticles_MatchAndAnalyse*: Python code used for analysis of image data in Lenz et al. 2021, "Measuring impacts of microplastic treatments via image recognition on immobilised particles below 100 μm "; 2021. <https://doi.org/10.5281/zenodo.4592319>.
36. VanderPlas J, Granger B, Heer J, Moritz D, Wongsuphasawat K, Satyanarayan A, et al. *Altair: interactive statistical visualizations for Python*. J OSS. 2018; 3(32):1057. <https://doi.org/10.21105/joss.01057>.
37. Satyanarayan A, Moritz D, Wongsuphasawat K, Heer J. Vega-lite: a grammar of interactive graphics. *IEEE Trans Visual Comp Graphics (Proc InfoVis)*. 2017; 23(1):341–50. <https://doi.org/10.1109/tvcg.2016.2599030>.
38. The pandas development team. *Pandas-dev/pandas: pandas*; 2020. <https://doi.org/10.5281/zenodo.3509134>.
39. McKinney W. Data structures for statistical computing in Python. In: van der WS, Jarrod M, editors. *Proceedings of the 9th Python in Science Conference*; 2010. p. 56–61.
40. Seabold S, Perktold J. *Statsmodels: econometric and statistical modeling with Python*. In: 9th python in science conference; 2010.
41. Bradski G. The OpenCV library. *Dr Dobb's J Software Tools*. 2000;25:120–5.
42. Van Der WS, Sch  nberger JL, Nunez-Iglesias J, Boulogne F, Warner JD, Yager N, et al. *scikit-image: Image processing in Python*. *PeerJ*. 2014;2:e453. <https://doi.org/10.7717/peerj.453>.
43. Canny J. A computational approach to edge detection. *IEEE T Pattern Anal*. 1986;PAMI-8(6):679–98. <https://doi.org/10.1109/tpami.1986.4767851>.
44. Otsu N. A threshold selection method from gray-level histograms. *IEEE Trans Syst Man Cybern*. 1979;9(1):62–6. <https://doi.org/10.1109/tsmc.1979.4310076>.
45. Statsmodels Contributors. 2021. *Statsmodels.org*. <https://www.statsmodels.org/stable/glm.html>. Accessed 29 Jan 2021.
46. Green PJ. Iteratively reweighted least squares for maximum likelihood estimation, and some robust and resistant alternatives. *J R Stat Soc Ser B Methodol*. 1984;46(2):149–70. <https://doi.org/10.1111/j.2517-6161.1984.tb01288.x>.
47. Lenz R, Enders K, Stedmon CA, Mackenzie DMA, Nielsen TG. A critical assessment of visual identification of marine microplastic using Raman spectroscopy for analysis improvement. *Mar Pollut Bull*. 2015;100(1):82–91. <https://doi.org/10.1016/j.marpolbul.2015.09.026>.
48. Zouboulis E, Renusch D, Grimsditch M. Advantages of ultraviolet Raman scattering for high temperature investigations. *Appl Phys Lett*. 1998;72(1):1–3. <https://doi.org/10.1063/1.121437>.
49. Butler HJ, Ashton L, Bird B, Cinque G, Curtis K, Dorney J, et al. Using Raman spectroscopy to characterize biological materials. *Nat Protoc*. 2016;11(4): 664–87. <https://doi.org/10.1038/nprot.2016.036>.
50. Imhof HK, Laforsch C, Wiesheu AC, Schmid J, Anger PM, Niessner R, et al. Pigments and plastic in limnetic ecosystems: a qualitative and quantitative study on microparticles of different size classes. *Water Res*. 2016;98:64–74. <https://doi.org/10.1016/j.watres.2016.03.015>.
51. Piehl S, Hauk R, Robbe E, Richter B, Kachholz F, Schilling J, et al. Combined approaches to predict microplastic emissions within an urbanized estuary (Warnow, southwestern Baltic Sea). *Front Environ Sci*. 2021;9. <https://doi.org/10.3389/fenvs.2021.616765>.
52. Lenz R, Enders K, Fischer F, Brandt J, Fischer D, Labrenz M. Interactive figure for exploration and analysis of the quantitative image data set in Lenz et al. 2021, "Measuring impacts of microplastic treatments via image recognition on immobilised particles below 100 μm "; 2021. <https://doi.org/10.5281/zenodo.4568524>.
53. de Sousa Menezes M, Queiroz EC, Soares PV, Faria-e-Silva AL, Soares CJ, Martins LRM. Fiber post etching with hydrogen peroxide: effect of concentration and application time. *J Endod*. 2011;37(3):398–402. <https://doi.org/10.1016/j.joen.2010.11.037>.
54. Navarro CA, Kedzie EA, Ma Y, Michael KH, Nutt SR, Williams TJ. Mechanism and catalysis of oxidative degradation of fiber-reinforced epoxy composites. *Top Catal*. 2018;61(7–8):704–9. <https://doi.org/10.1007/s11244-018-0917-2>.
55. Lenz R, Enders K, Fischer F, Brandt J, Fischer D, Labrenz M. DIC microscopy images used in: Lenz et al. 2021, "Measuring impacts of microplastic treatments via image recognition on immobilised particles below 100 μm "; 2021. <https://doi.org/10.5281/zenodo.4568488>.
56. Valsesia A, Quarato M, Ponti J, Fumagalli F, Gilliland D, Colpo P. Combining microcavity size selection with Raman microscopy for the characterization of nanoplastics in complex matrices. *Sci Rep*. 2021;11(1):362. <https://doi.org/10.1038/s41598-020-79714-z>.
57. Al-Azzawi MSM, Kefer S, Wei  er J, Reichel J, Schwaller C, Glas K, et al. Validation of sample preparation methods for microplastic analysis in wastewater matrices reproducibility and standardization. *Water*. 2020;12(9): 2445. <https://doi.org/10.3390/w12092445>.

Publisher's Note

Springer Nature remains neutral with regard to jurisdictional claims in published maps and institutional affiliations.

Supplementary Information — Measuring impacts of microplastic treatments via image recognition on immobilised particles below 100 μm ,

Robin Lenz^{1,*} Kristina Enders¹ Franziska Fischer²
Josef Brandt³ Dieter Fischer² Matthias Labrenz^{1,*}

¹ Leibniz Institute for Baltic Sea Research Warnemünde (Seestraße 15, 18119 Rostock, Germany)

² Leibniz Institute for Polymer Research (Hohe Straße 6, 01069 Dresden, Germany)

³ University of Gothenburg, Department of Marine Sciences (Kristineberg 566, S-45178 Fiskebäckskil, Sweden)

* Correspondence: Robin Lenz <robin.lenz@io-warnemuende.de>¹, Matthias Labrenz <matthias.labrenz@io-warnemuende.de>²

S1 - Limits of the scope and methodological practicality of this study

To allow for controlled testing conditions, several deviations from environmental sample conditions were accepted:

- test material was produced from non-environmentally exposed plastics and polymer degradation products can be assumed to be absent in the untreated sample material
- natural fragmentation was simulated only by mechanical forces (cryo-milling), neglecting that UV light and thermal degradation and leaching of additives could alter μP formed under environmental conditions
- as polymer source materials for cryo-milling, uncoloured virgin plastics (pellets, powder) were chosen to keep the additive content as low as possible
- environmental non- μP matrix constituents (i.e. biofilms, minerals) were not present in our samples

It has to be noted that in environmental samples the above mentioned aspects may be different, leading to aggravated analysis conditions and differing results of confirmed μP .

¹mailto:robin.lenz@io-warnemuende.de

²mailto:matthias.labrenz@io-warnemuende.de

The development of a new purification protocol also requires the demonstration of success of the non-target matter removal, i.e. organics or mineral debris. The sample has to be brought to a degree of purity that is sufficient for the reliable identification of the μP present in a sample. The removal efficacy for the herein tested treatments has been demonstrated in the original studies [1, 2, 3, see also tbl. 2 in the main manuscript]. As we followed these tested protocols, further efficacy testing is not part of this study.

In the quantitative part, the numbers of immobilised particles available for an analysis (n_{pre}) ranged from 20 (TPU, H_2O_2) to 479 (PA6, water). The reason for this variability is that the density of particles that fell on the wafers could only be partially controlled due to the way of how they were manually scattered. The correlation between n_{pre} and the measured effects can be seen in fig. 1, where also a dependence on image quality (expressed as BDI) becomes visible. This observation gave the impetus, to calculate the portion of particle losses and area changes that were not attributable to the effects of a treatment. The GLM residual analysis was the chosen procedure to eliminate these portions from the results. Furthermore a cut-off at $\text{BDI} = 27$ was used to exclude images that were of abnormally bad quality.

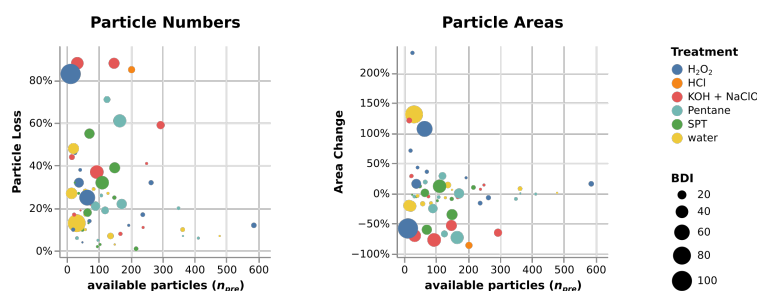


Figure 1: Low particle numbers available for image analysis (n_{pre} and elevated BDI are correlated with higher relative particle losses and higher absolute relative area changes in the non-GLM-corrected data. Data points include all imaged polymer types (in the interactive version of the figure the distribution of individual polymers can be viewed).

S2 - Additional information on the statistics of the quantitative approach: Negative controls (water digested samples) for GLM model creation

The negative control wafers had relative particle losses ranging from 3% to 29% and mean particle area changes from -17% to +14% in the uncorrected data. Causes for these effects were found to be related to low image contrast and total number of particle (n_{pre}) available for analysis. For both, area changes

and count loss the GLM fitted to the ensemble of all water wafers, explains the influence of either of the two confounding factors. The optimised model predictor coefficients and p values are summarised in tbl. 1. More detailed model fit results and pearson residual plots can be seen in the respective plots below. The enclosing prediction intervals provide a measure of the method intrinsic variability.

Table 1: Summarised model fit parameters for detecting confounder caused effects in particle loss and area change.

	Predictor term	Coefficient	p Value
particle loss GLM	Intercept	0.6701	0.0901
	n_{pre}	-0.0025	0.0000
	image quality (pre_histDelta)	-0.0230	0.0000
area change GLM	Intercept	0.0820	0.0010
	n_{pre}	-0.0001	0.0066
	image quality (histBGpeakDist)	0.0164	0.0355

With the GLM corrected data only the treatment attributable effects are exhibited. Most of the water treatments were corrected to 0% change, with exceptions being epoxy based paint (11%), PET (2%), PC (8%) and ABS (4%) for particle count losses and epoxy based paint (-7%) and ABS (-8%) for area changes.

Based on the water GLMs, the predicted standard residuals for all wafers are reported as the corrected values in fig. 7 in the main manuscript. Values are regarded as significantly different from the control where they exceed the upper bound 95% prediction interval of the fitted water values. This is the case for the positive control (HCl on PA6), H_2O_2 on PC and epoxy based paint and SPT on ABS.

Raw output of the statsmodels package <https://statsmodels.org/> [4], that was used for the creation of the two GLMs and representative controls plots (figs. 2, 3) are provided below.

```

Generalized linear model of particle count losses
=====
Model:          GLM                AIC:          90.9404
Link Function:   logit              BIC:          6.3998
Dependent Variable: ['failure', 'success'] Log-Likelihood: -
42.470
Date:           2021-01-31 12:06      LL-Null:      -
75.831
No. Observations: 13                Deviance:     32.049
Df Model:       2                    Pearson chi2:  31.4
Df Residuals:   10                   Scale:       1.0000
Method:         IRLS

```

	Coef.	Std.Err.	z	P> z	[0.025	0.975]
Intercept	0.6701	0.3953	1.6950	0.0901	-0.1047	1.4449
pre_count	-0.0025	0.0004	-5.5977	0.0000	-0.0034	-
0.0016						
pre_histDelta	-0.0230	0.0046	-5.0200	0.0000	-0.0320	-
0.0140						

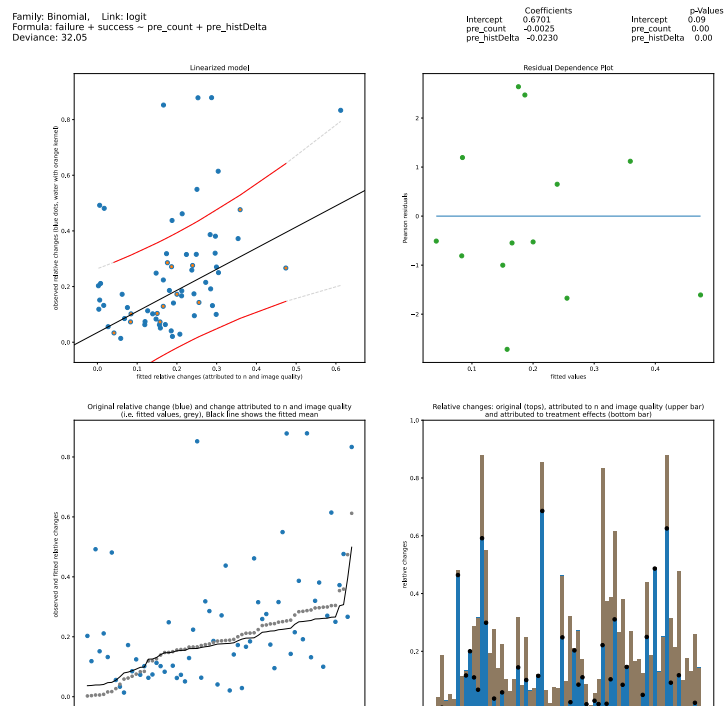


Figure 2: Data of quantitative count losses (fitted and original) in different representations. Detailed contents of the subplot are explained in the plot and axes titles.

Generalized linear model of particle area changes

Model:	GLM	AIC:	-20.8417
Link Function:	identity	BIC:	-8.6266
Dependent Variable:	area_change	Log-Likelihood:	13.421
Date:	2021-01-31 12:18	LL-Null:	-2.6605

No. Observations:	13	Deviance:	17.023			
Df Model:	2	Pearson chi2:	5.07			
Df Residuals:	10	Scale:	0.50728			
Method:	IRLS					

	Coef.	Std.Err.	z	P> z	[0.025	0.975]

Intercept	0.0820	0.0249	3.2967	0.0010	0.0332	0.1307
pre_count	-0.0001	0.0001	-2.7148	0.0066	-0.0003	-0.0000
histBGpeakDist	0.0164	0.0078	2.1025	0.0355	0.0011	0.0318

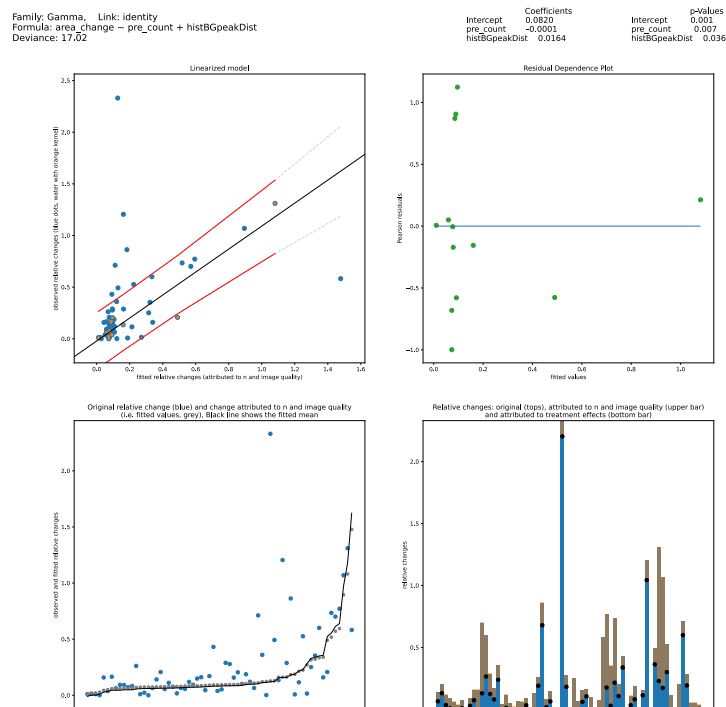


Figure 3: Data of quantitative area changes (fitted and original) in different representations. Detailed contents of the subplot are explained in the plot and axes titles.

S3 - Practical recommendations for future studies and developments of the quantitative evaluation method

Our quantitative approach (using immobilised, epoxy-glued particles) came along with certain drawbacks as we already detailed in the section “Methodological caveats” in the main manuscript. Several limitations may, however, be circumvented by further developments of the methodology. The epoxy layer was not ideally resistant towards all tested treatments. Other adhesive or arrestive layers were tested in the development phase. Sodium silicate (“water glass”), in particular, was considered as a low viscosity spinnable inorganic glue, but first trials did not yield satisfactory results, as the spin coated layers showed microscopic crack formations while curing, which would be hindering for the imaging of particles. Other inorganic cement-like adhesives were considered, however, not tested due to their coarse granular texture. Potential size changes in the z-dimension could not be detected with the 2D aerial view images. Using a different microscopic technique such as scanning electron microscopy, might enable a more in-depth size change analysis. When working with dyed particles is an option, also bright-field microscopy could be used. Disturbance by visual image artefacts are likely less prominent, eliminating the need for manual image postprocessing, and simplifying the particle detection. Also the polymer-dependent contrast issues could be circumvented in this way. A thinner and plainer adhesive layer would be beneficial for measurements on the smallest particles and could reduce the entrainment of reflective air bubbles. The prevention of dust or other micro debris would improve the image analysis, with fewer defects present in the layer. As we observed a distortion of results for samples with a small particle number, it is advisable to control the particle n on the imaged area to be at or above a recommended n of 200 particles.

We described and demonstrated the quantitative and qualitative measurements of treatment-induced particle effects as two separate experimental approaches. This serves merely the cause that there might be cases where they may be applied alone (e.g. only the qualitative evaluation, when particle quantification is not intended, such as in mass based microplastic studies). When both are parts are intended, however, they could as well be combined, i.e. the qualitative measurements of material recognisability could be performed on the immobilised particles prepared for the quantitative measurements.

References

1. Enders K, Lenz R, Beer S, Stedmon CA (2017) Extraction of microplastic from biota: Recommended acidic digestion destroys common plastic polymers. ICES J Mar Sci 74:326–331. <https://doi.org/10.1093/icesjms/fsw173>
2. Tagg AS, Harrison JP, Ju-Nam Y, Sapp M, Bradley EL, Sinclair CJ, Ojeda JJ (2017) Fentons reagent for the rapid and efficient isolation of microplastics from wastewater. Chem Commun 53:372–375. <https://doi.org/10.1039/c6cc08798a>

3. Enders K, Lenz R, Sul JAI do, Tagg AS, Labrenz M (2020) When every particle matters: A QuEChERS approach to extract microplastics from environmental samples. *MethodsX* 7:100784. <https://doi.org/10.1016/j.mex.2020.100784>
4. Seabold S, Perktold J (2010) statsmodels: Econometric and statistical modeling with Python. In: 9th python in science conference



Assessment of Subsampling Strategies in Microspectroscopy of Environmental Microplastic Samples

Josef Brandt^{1,2*}, Franziska Fischer¹, Elisavet Kanaki¹, Kristina Enders³, Matthias Labrenz³ and Dieter Fischer^{1*}

¹Leibniz-Institut für Polymerforschung Dresden e. V., Dresden, Germany, ²Department of Marine Sciences, University of Gothenburg, Gothenburg, Sweden, ³Leibniz Institute for Baltic Sea Research Warnemünde (IOW), Rostock, Germany

OPEN ACCESS

Edited by:

Andrew Turner,
University of Plymouth,
United Kingdom

Reviewed by:

Claudia Lorenz,
Aalborg University, Denmark
Joana Correia Prata,
University of Aveiro, Portugal

*Correspondence:

Josef Brandt
josef.brandt@gu.se
Dieter Fischer
fisch@ipfdd.de

Specialty section:

This article was submitted to
Toxicology, Pollution and
the Environment,
a section of the journal
Frontiers in Environmental Science

Received: 03 July 2020

Accepted: 15 December 2020

Published: 27 January 2021

Citation:

Brandt J, Fischer F, Kanaki E,
Enders K, Labrenz M and Fischer D
(2021) Assessment of Subsampling
Strategies in Microspectroscopy of
Environmental Microplastic Samples.
Front. Environ. Sci. 8:579676.
doi: 10.3389/fenvs.2020.579676

The analysis of environmental occurrence of microplastic (MP) particles has gained notable attention within the past decade. An effective risk assessment of MP litter requires elucidating sources of MP particles, their pathways of distribution and, ultimately, sinks. Therefore, sampling has to be done in high frequency, both spatially and temporally, resulting in a high number of samples to analyze. Microspectroscopy techniques, such as FTIR imaging or Raman particle measurements allow an accurate analysis of MP particles regarding their chemical classification and size. However, these methods are time-consuming, which gives motivation to establish subsampling protocols that require measuring less particles, while still obtaining reliable results. The challenge regarding the subsampling of environmental MP samples lies in the heterogeneity of MP types and the relatively low numbers of target particles. Herein, we present a comprehensive assessment of different proposed subsampling methods on a selection of real-world samples from different environmental compartments. The methods are analyzed and compared with respect to resulting MP count errors, which eventually allows giving recommendations for staying within acceptable error margins. Our results are based on measurements with Raman microspectroscopy, but are applicable to any other analysis technique. We show that the subsampling-errors are mainly due to statistical counting errors (i.e., extrapolation from low numbers) and only in edge cases additionally impacted by inhomogeneous distribution of particles on the filters. Keeping the subsampling-errors low can mainly be realized by increasing the fraction of MP particles in the samples.

Keywords: microplastics, subsampling, microspectroscopy, Raman, Fourier-Transform infrared

INTRODUCTION

The occurrence of microplastic (MP) particles in environmental compartments has gained notable interest in both scientific and mainstream media, a trend that is predicted to increase in the coming years (Halden 2015). A major cause of concern related to plastic materials is its accumulation potential due to their high persistence in the environment, while production rates further increase and concomitantly the plastic waste (Jambeck et al., 2015; Brandon et al., 2019; Borrelle et al., 2020). Assessments of the abundance of MP particles in various kinds of samples can be found throughout the literature e.g., in water (Lenz and Labrenz 2018; Liu et al., 2019; Karlsson et al., 2020), sediment or

soil (Claessens et al., 2013; Vianello et al., 2013; Bergmann et al., 2017; Enders et al., 2019), wastewater treatment plants (Tagg et al., 2015; Murphy et al., 2016) as well as biota (Lusher et al., 2017). Understanding sources, pathways and sinks of MP particles is key to understand how to effectively limit further spreading of this pollutant (Halle et al., 2016; Geyer et al., 2017; Siegfried et al., 2017). Therefore, large numbers of environmental samples have to be analyzed quantitatively, as not only the *spatial* but also the *temporal* occurrence of MP particles at a given location is of high relevance. Methods suitable for comprehensive monitoring studies need to be fast, quantitative and automated to deal with the high number of samples to process.

The currently used analytical tools can be sorted into two categories: mass and particle-based methods. Mass based methods are pyrolysis gas chromatography and mass spectrometry (Py-GC-MS) (Fischer and Scholz-Böttcher, 2019; Logemann et al., 2018; Dierkes et al., 2019) or thermoextraction and desorption coupled with gas chromatography-mass spectrometry (TED-GC-MS) (Fischer and Scholz-Böttcher, 2019; Dümichen et al., 2014; Dümichen et al., 2015; Dümichen et al., 2017). Their main advantages are short analysis times and straightforward application. Also challenging environmental samples can be processed in few hours (Fischer and Scholz-Böttcher, 2019; Dümichen et al., 2017), with only relatively little sample preparation. The better the removal of organic matter, however, the more robust the analysis results will be, as organic compounds can hamper the correct data interpretation (Primpke et al., 2020a). As a drawback, only the integral mass fraction of polymer within the sample is obtained, without giving details on particle numbers or size distribution. Furthermore, the techniques are destructive, which makes it impossible to reuse the samples after measurement. Particle-based methods, such as spectroscopic imaging by Fourier-Transform infrared (FTIR) spectroscopy (Löder et al., 2015; Käßler et al., 2016; Primpke et al., 2017; Primpke et al., 2019) or microspectroscopic particle measurement using FTIR (Browne et al., 2010; Vianello et al., 2013; Löder et al., 2015; Tagg et al., 2015; Wagner et al., 2017; Käßler et al., 2018; Poulain et al., 2019) or Raman (Lenz et al., 2015; Käßler et al., 2016; Anger et al., 2018; Schymanski et al., 2018), register size, morphology and chemical classification of each particle (mass fractions can be estimated by applying volume estimates and bulk density values (Simon et al., 2018)). Particles >500 µm are often picked and investigated manually. For particles <500 µm, a purified particle dispersion (i.e., after removal of non-MP particles) is typically filtered onto a suitable filter substrate and then subjected to either imaging or individual particle measurement. The imaging approach entails scanning the entire filter area without a-priori knowledge about particle locations. Each spectrum at each measured pixel is evaluated and particle information is obtained by grouping together adjacent pixels with identical spectral classification (Primpke et al., 2017; Primpke et al., 2019; Primpke et al., 2020b). The particle measurement approach is done in two passes. First, an optical image is acquired with a light microscope (LM) to identify particles. Then, spectra are only

acquired where particles were detected. **Figure 1** illustrates both approaches graphically.

Both methods are inherently slower than the mass-based techniques and require elaborate sample purification steps to remove non-plastic particles (Enders et al., 2020). Increasing the fraction of MP particles per sample allows for a faster and more reliable analysis, as less particles have to be processed and overloaded filters are avoided, which can lead to erroneous results. The currently used microspectroscopic techniques cannot compete with mass-based techniques regarding their sample throughput rates. However, to assess the potential toxicological impacts on both biota and humans, knowledge about MP particle size distribution and numbers is critical (Masó et al., 2003; Zettler et al., 2013). Hence, microspectroscopic methods for MP analysis are of high current relevance and the acceleration of sample throughput rates is one of the major challenges.

One approach to speed up imaging and particle measurements is to measure only a certain fraction of any sample and to extrapolate the obtained results. This can be achieved in two ways: i) Subsampling before filtration: only a fraction of the entire sample is filtered onto the sample substrate which will be completely measured. This method requires very careful homogenization of the sample to avoid extrapolation errors. For homogenization, different densities and the fast sedimentation of the particles in aqueous suspensions pose challenges. The success of this splitting before filtration is largely influenced by the method and splitting tools applied. ii) Subsampling during analysis: The entire sample is filtered on one or multiple filters, but only a fraction of each filter is measured. This method circumvents the challenges of prior homogenization and sample splitting, but requires a robust strategy to select which areas or particles to measure. The main statistical problems therein arise from both, the inhomogeneous distribution of the particles on the filter and the low numbers of MP particles, of typically around 1%. The present study focuses on pathway ii) i.e., the statistical subsampling of particles that are already on the filter substrate. The results are applicable to any MP sampling technique probing particles spatially distributed on a filter substrate, irrespective of the exact measurement technique. However, we do not strive to determine hard numbers for potential speed gains, as these are highly dependent on the actually used method and measurement requirements. Speed optimization of each analysis technique is an important, yet difficult endeavor requiring careful balancing the runtime with result quality, which is highly specific for the respective methods.

Subsampling on a Substrate: Challenges

Filtering particles from an environmental sample onto a microscopy filter does not lead to a homogeneous distribution of particles on the filter area. Comprehensive guidelines explain the challenges and recommend strategies for successful filtrations. (Merck, 2018). The stream of water is usually not of a constant flow-rate, leading to different forces on the particles on the filter throughout the filtration process. Air bubbles can be present that

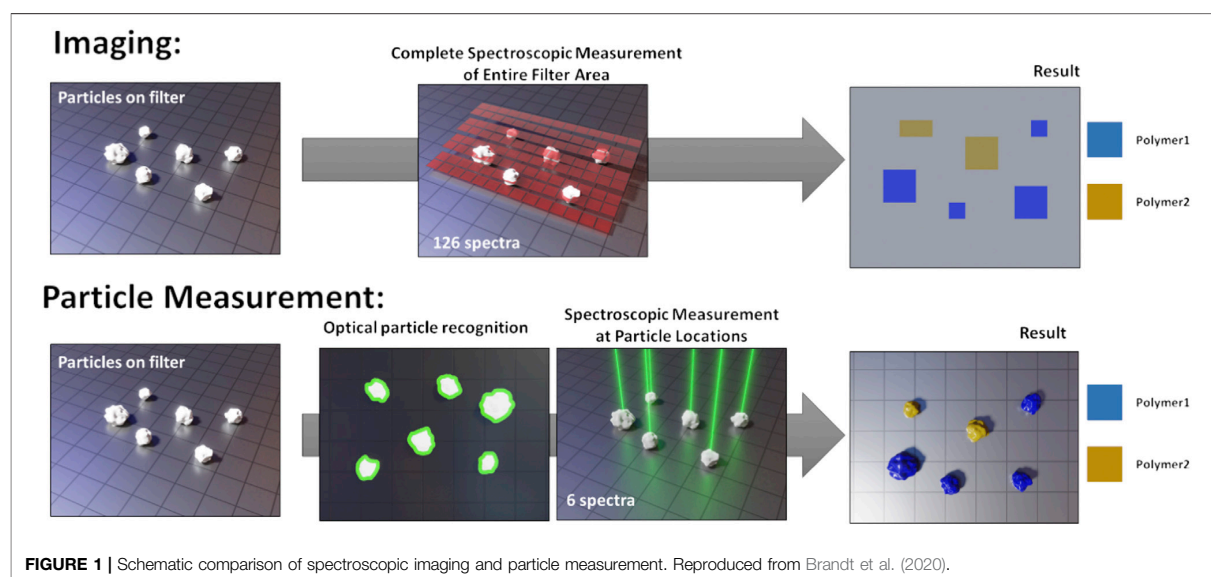
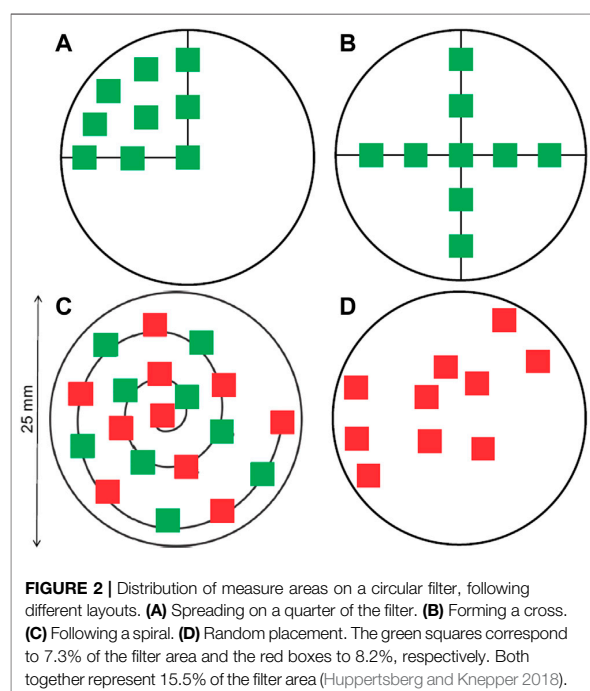


FIGURE 1 | Schematic comparison of spectroscopic imaging and particle measurement. Reproduced from Brandt et al. (2020).



introduce additional unpredictable forces. Often, the particle concentration on the filter follows a gradient with low concentrations around the filter center and higher concentrations closer to the filter perimeter (Thaysen et al., 2020). To minimize coagulation of particles on the filter, the flow rate can be reduced or tangential flow filtration can be performed (Buffle and Leppard 1995).

Further inhomogeneity is introduced by the nature of the environmental particles. Depending on the sample origin (e.g., rainwater or wastewater treatment sludge) and given the large range of MP types itself, the samples contain a broad variety of particles different in size, density and shape; properties that have a significant influence on particle distribution dynamics. In addition, particles that tend to aggregate easily clump together and can even incorporate particles of other types. The low fraction of MP particles per sample can lead to low statistical robustness of any deduced conclusions (Anger et al., 2018; Karlsson et al., 2020). All such factors make the selection of a representative subset an especially challenging task and have to be considered during the assessment.

Proposed Subsampling Strategies

The strategies proposed to select a representative subset during analysis can be sorted into two categories, corresponding to two different workflows.

The first category, the “area selection strategy,” does not need any *a priori* knowledge and distributes a number of box-shaped areas to measure over the entire filter area. It is mostly suitable for imaging protocols. Different layouts for distributing the measuring boxes can be considered to account for the inhomogeneous distribution of particles on the filter, such as a cross or a spiral layout (refer to Figure 2). (Huppertsberg and Knepper, 2018). The number and size of the boxes can be adjusted to cover a desired fraction of the filter. After the spectroscopic measurements within the box areas, the result is then extrapolated according to the fraction of filter area covered by the boxes. It is theoretically possible to design area-based subsampling approaches that do not rely on placing rectangular boxes, for instance dividing the filter in cake-piece shaped sections. Such a section accounts for a radial inhomogeneity by covering central and peripheral area of the filter. Their

TABLE 1 | Summary of origin of analyzed samples (WWTP = wastewater treatment plant).

Compartment	Origin	Number of samples
Rainwater	Weser catchment area, Germany	5
Riverine surface water	Warnow catchment area, Germany	6
Riverine sediment or beach sand	Schlei river, Germany, Baltic Sea beaches in Germany, Denmark, Sweden	10
Wastewater sludge	Municipal WWTP designed for 50,000 inhabitants, Germany	6

practical application could be limited, however, as most FTIR- or Raman-software packages are restricted to the selection of rectangular areas for measurement. The viability of the different layouts will be assessed practically later in this manuscript.

The second category, the “particle selection strategy,” requires some *a priori* knowledge that is gained from first acquiring an overview optical image from the entire filter using a light microscope (LM). That image can be used to determine the number and location of each particle or even characterize the particles further regarding their size, shape and color (thereby decreasing the uncertainty about the particle location) and the actual fraction of particles measured can be adjusted more precisely. If further information per particle is derived, more sophisticated chemometric methods for finding representative subsamples can be engaged (Chaudhuri, 1994; Daszykowski et al., 2002; Rodionova and Pomerantsev, 2008).

It is also possible to combine both approaches. Imhof et al., for instance, chose to manually identify particles larger than 500 μm and to automatically measure all smaller particles based on an “area selection strategy,” measuring approx. 1.6% of the filter area (Imhof et al., 2016).

Different subsampling strategies are currently in use that usually measure about 1–10% of the filter area. Their use is in most cases justified by hypothetical considerations, but practical validations of the subsampling strategies are scarce. A recent study by Mintenig et al. assessed the subsampling and errors of riverine water samples and concluded that at least 50% filter coverage is needed for robust particle counts, which is substantially higher than most studies aim for (Mintenig et al., 2020).

With this publication, we revisited 27 MP samples from different environmental compartments that were measured by Raman microspectroscopy, without using any subsampling method. The GEPARD software was used for particle detection and automated Raman measurement, an appropriate tool to reduce analysis time and remove operator-bias (Brandt et al., 2020). As a side effect, all information about the filtered sample (e.g., particle count, coordinates, sizes and spectral identification) is stored in particle datasets. These datasets are used to re-evaluate the sample by simulating a measurement using a dedicated subsampling strategy and determining the subsampled result. Comparing subsampled to original result allowed us to draw quantitative conclusions about the statistical robustness and usability of the investigated subsampling strategies.

MATERIALS AND METHODS

Sample Details and Filtration

27 fully analyzed samples from different environmental compartments were the basis for our analysis (Table 1). The samples underwent purification procedures identical to established schemes as presented by Enders et al. (Enders et al., 2020), a study which presents a flow chart of detailed protocols for the different sample conditions. Reproducibility of the applied purification methods is thereby ensured. An exception to the above are the rainwater samples that underwent a combination of oxidation with Fenton's reagent, enzymatic digestion and density separation using ZnCl_2 (Löder et al., 2017). The final filtration was done using a tailor-made glass filtration device. After cleaning all glass parts with 3% H_2O_2 and sonication in MilliQ water (3×10 min, renewal of the MilliQ water after each 10 min interval), 10×10 mm silicon filters with 10 or 50 μm holes were inserted into the filtration device using red PTFE filter holders that also act as seals. During filtration, the flow rate of the water is observed to avoid overloading of the filters. The filtration is done in a laminar flow box (Telstar Aeolus V) to avoid contamination from air-borne particles. Full details about used filters and the filtration setup are already published and can be found elsewhere (Käppler et al., 2015; Brandt et al., 2020). Without prior homogenization, each sample was filtered onto several filters. Only one of these filters per sample was used in the following analyses, so the particle numbers and MP content are not representative for the actual environmental sample. Therefore, further information on the sample origin and the sampling is neglected. The analyzed samples counted between 1,500 and 33,000 particles per filter. In the following, both “sample” and “filter” refer to the single filter representing each environmental sample.

Particle Measurements

Full details about the measurement workflow using the GEPARD software are reported in a separate publication (Brandt et al., 2020); only a short summary is given here.

LM images were acquired directly in the Raman microscope (WITec® alpha 300R), which is also used for the spectroscopic measurements using a 532 nm laser and a 600 L/mm spectroscopic grating. The optical LM images were acquired in dark-field at adjustable focus heights, which allows constructing an image of optimal depth-of-field for both, small and large, particles. A watershed-based image segmentation algorithm was used to localize particles and determine their boundaries. Raman spectra were collected for each particle (typical conditions: 0.5 s

integration time, five accumulations) and the TrueMatch® software (WITec®) was used for spectral evaluation. The results from spectra database matching were combined with the particle information from the particle recognition step to obtain complete information about particle type and size distributions.

Data Processing

The datasets generated by the GEPARD software contain all information about particle location, contour and chemical classification. This readily allows revisiting the datasets and selecting particles from the entirety of the particle list according to any desired subsampling strategy. The code for all calculations is realized in form of a *Python* script, the full source code can be found on <https://gitlab.ipfdd.de/Brandt/subsampling>.

To assess the performance of any considered subsampling model it is necessary to derive quantitative measures of its performance. We calculated the *subsampling-error* according to **Equation 1**. A subsampling model was applied to each fully measured dataset and the subsampled count of MP particles determined (SI chapter “Application of Subsampling Methods”). To estimate the total MP particle count, the subsampled count was extrapolated by dividing by the subsampling fraction. That estimated MP particle count was then divided by the original MP particle count.

$$\text{subsamplingError} = \frac{\text{mpCount}_{\text{subsampled}} / \text{fraction}}{\text{mpCount}_{\text{original}}} \cdot 100\% \quad (1)$$

To reduce statistical deviations, each filter was processed 10 times. For each iteration, the filter was rotated about 36° around the filter center and then the subsampling is repeated. This increases the number of performed tests by 10-fold and reduces noise in the results, making data interpretation more robust.

Implemented Subsampling Methods

Hereafter, we describe the implemented subsampling methods. The first two followed the particle selection strategy, *i.e.*, rely on knowledge about particle location, and the remaining methods follow the area selection strategy, *i.e.*, they represent different approaches for placing rectangular areas (boxes) for conducting measurements. To test practically relevant fractions, we tested fractions from 2 to 90% in terms of particle count fractions, and from 2% to the maximum achievable fraction in terms of filter area coverage for the individual box selection methods.

Random Particle Subsampling

The method is based on a prior particle recognition step. Out of the list of detected particles, a given number is selected on a completely random basis to represent the desired fraction of particles measured.

SizeBin Particle Subsampling

The concept is the same as in the random particle subsampling with additional accounting for size distribution bias to reduce the uncertainty related to low number size fractions (as usually the

TABLE 2 | Highest achievable filter coverage for the implemented patterns. By its pattern, the cross layout is only feasible with five or 9 boxes (3 or five boxes across, respectively). The other patterns were arbitrarily set to have either 5, 10 or 20 boxes.

Number of boxes	Cross	Spiral	Random	Random quarter
5	54%	26%	46%	21%
9	38%	n.a.	n.a.	n.a.
10	n.a.	29%	47%	17%
20	n.a.	25%	43%	14%

case for larger particles). Therefore, the detected particles are first grouped into size bins. The chosen size limits in between the bins are 5 µm, 10 µm, 20 µm, 50 µm, 100 µm, 200 µm, and 500 µm. After sorting the particles into the bins, a certain number of particles is randomly drawn from each bin so that the measured fraction of particles is equal for all bins. At least one particle is taken from each bin (given, that the bin is not empty). For example, when 10% of all particles have to be measured, the algorithm will select 5 particles out of a bin with 50 particles, 20 out of a bin with 200 particles and 1 out of a bin with only 4 particles.

Box Selection Subsampling

Four different layouts were implemented for placing measuring boxes on the circular filter:

- Cross layout with either 3 or 5 boxes across, respectively (**Figure 2B**)
- Spiral layout with 5, 10 or 20 boxes. The first box is located in the center and the last one touches the perimeter of the filter area. (**Figure 2C**).
- Random layout with 5, 10 or 20 boxes. The boxes are placed randomly on the filter area. Given this random character, the highest achievable fractions can vary slightly, also depending on how many tries the algorithm was allowed to perform to find a valid solution. The implemented algorithm sets the random number generator to a fixed seed prior to calculation to yield the same random pattern for each run (**Figure 2D**).
- Random layout on a quarter of the filter with 5, 10 or 20 boxes. Same as iii), but box placement is restricted to only a quarter of the filter (**Figure 2A**).

In all box selection approaches, the size of the (square) boxes is adjusted so that the desired fraction of filter area is covered, without having the individual boxes overlap or range over the filter perimeter. The maximum achievable fraction of filter to be covered is summarized in **Table 2** (More details about box placement and the link to the code for interactive visualization can be found in SI chapter 1).

Figure 3 shows a graphic user interface (gui) to visualize the implemented methods on real samples, measured by GEPARD. All the subsampling methods in **Figure 3** are configured to select 10% of the sample *i.e.*, 10% of the particles are measured by the “random” and the “size bin” selection, whereas 10% of the filter area is covered by the respective box selection methods. The gui

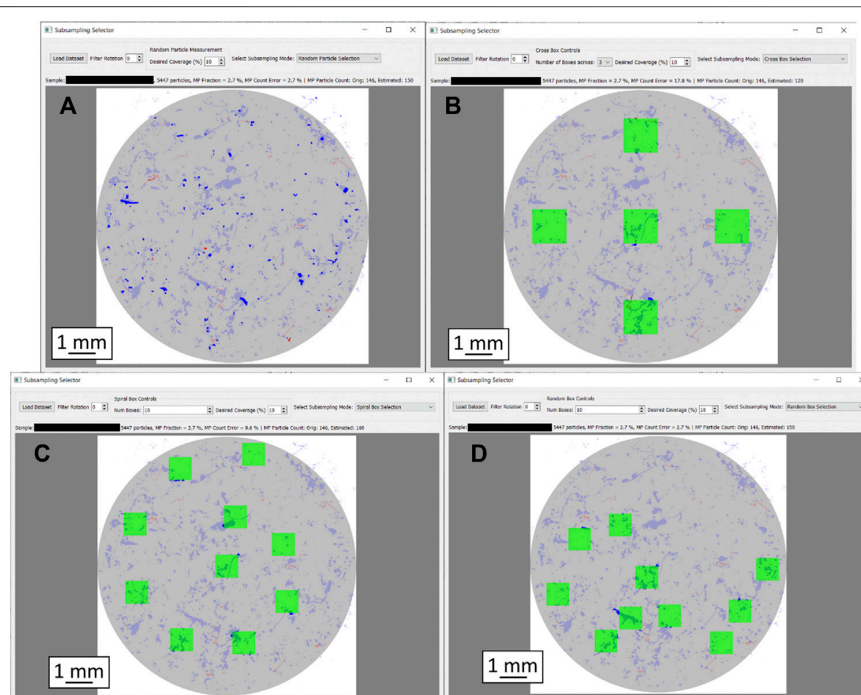


FIGURE 3 | Graphic representation of the particle distribution heterogeneity as well as different subsampling approaches with 10% filter coverage each. Filter diameter is 10 mm in each case. **(A):** Random subsampling, **(B):** Box selection, cross layout, **(C):** Box selection, spiral layout, **(D):** Box selection, random layout. MP particles are shown in red, others in blue. Particles missed by the respective subsampling method are displayed in pale colors; only the particles in strong colors were captured.

allows adjusting the measured fraction of each method, as well as the number of boxes for the box sampling methods. Furthermore, the loaded sample can be rotated about a given angle. A text box above the filter scheme summarizes sample details (particle count, MP percentage) and displays the results from the respective subsampling method.

RESULTS AND DISCUSSION

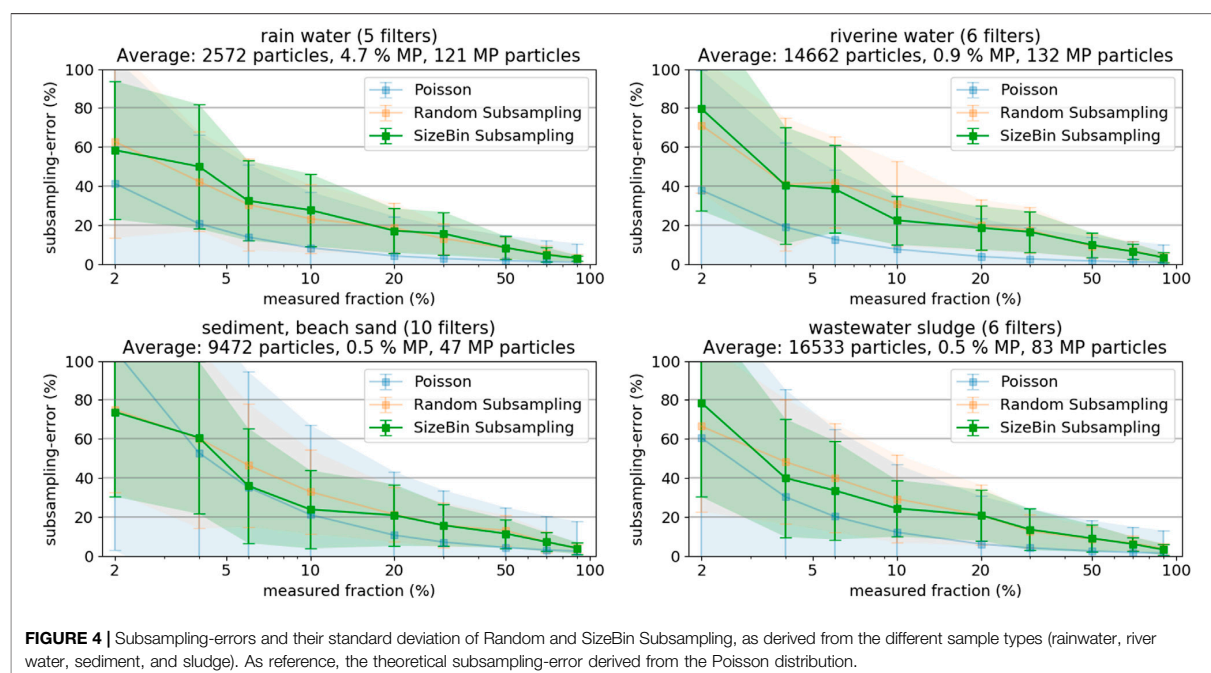
Particle-Based Subsampling

At first, we investigated the subsampling-error (%) as a function of the measured fraction of particles (%) for the four respective sample categories (**Figure 4**), see SI chapter “Selected Images of Filters” for example images. We chose grouping the samples by their environmental origin because a sample’s origin is always known. Sorting samples into categories allows deduction of parameters influencing subsampling efficiency and, vice versa, allows estimating subsampling efficiency if a sample’s category was known. Hence, any correlation between environmental compartment and subsampling performance would allow for a better planning of the subsampling strategy without any further sample characterization. The averaged particle numbers per filter are given in the plot titles for each category, as well as the average MP percentage within these particles. Each data point in **Figure 4**

represents the average over all filters from the respective group of sample types (number of filters is given in plot title), where each filter was evaluated 10 times. The resulting subsampling-error exponentially decreases with increasing measured fraction and approaches 0 at 100% (note the logarithmic x-axis in **Figure 4**). Comparing the two different particle based subsampling methods shows that sorting particles into size bins (**Figure 4**, green) or not (**Figure 4**, orange) does not seem to have a systematic advantage across sample types.

The results illustrate that measuring only small filter fractions (both in terms of particle count or covered filter area) can lead to large counting errors. Measuring less than 5% of the entire particle population leads to errors exceeding 50%. Even worse, also the error margins increase with decreasing fraction measured in the plots in **Figure 4**. For example, at 5% measured fraction, the subsampling-error could be 20% or 80%. This large range of potential errors of a particular filter demonstrates that measuring such small fractions does not allow a sensible extrapolation of MP occurrences.

Comparing the results from the different compartments shows that the subsampling-errors are generally lower when the sample has more particles (i.e., higher number of particles is measured at a given fraction) or the sample has a higher content of MP particles. Especially the MP content is critical: The high MP content of the rainwater samples compensates the low particle



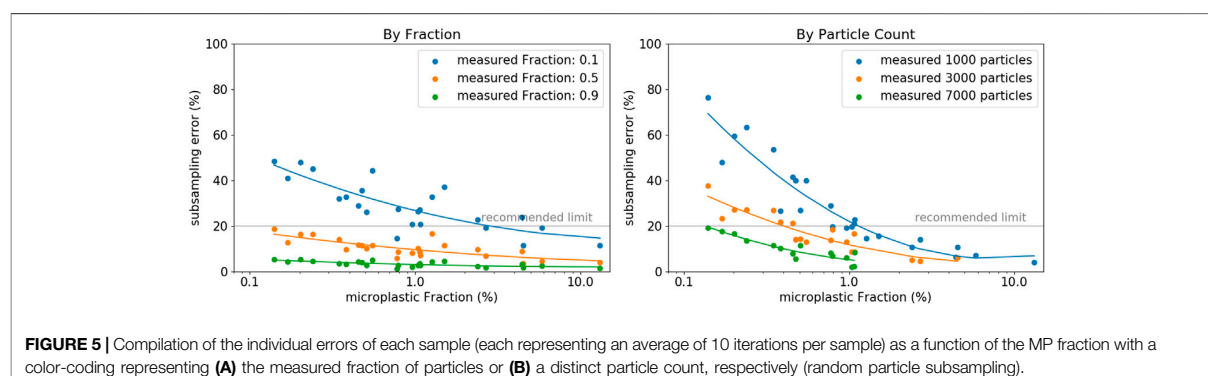
count (at 10%, only about 300 particles are measured!) and the subsampling-errors are comparable to the sludge samples with a substantially higher particle count (at 10%, about 1,700 particles have to be measured) but low MP content.

Reliably predicting magnitude and standard deviation of the subsampling-error is a complicated task. Anger et al. used the normal distribution to estimate the number of particles to achieve a certain error, but applying the formula requires knowing MP fraction and the prediction interval (Anger et al., 2018). Karlsson et al. used the Poisson distribution to model the probability density functions of MP occurrence observations (Karlsson et al., 2020). The Poisson distribution is better suitable for smaller sample sizes and, for application to the present study results, only requires an estimate of the MP fraction (mean equals variance in the Poisson distribution). **Figure 4** also shows the theoretically expected errors and error margins for the Poisson distribution, assuming the average MP count indicated in the plot titles. The agreement of theoretical and experimental subsampling-errors is good for the samples from sediment and beach sand, having the lowest absolute number of MP particles. However, the Poisson distribution more and more underestimates the subsampling-error with increasing number of MP particles. A more in-depth statistical discussion of the topic should be the scope of a separate study.

The estimation of the present MP content on a particular filter is difficult, but vital for the determination of the minimum subsampling fraction to measure. Based on the diverse set of different sample types and applying the random particle subsampling, we found, that if we accept a maximum subsampling-error of 20%, the minimum fraction of particles to measure is either 50% of all particles, or a total of 7,000

particles (**Figure 5**). These thresholds are valid even for MP fractions approaching as low values as 0.1%. Note, the set of filters herein analyzed was characterized with relatively low total particle counts (maximum of 33,000), which hinders applying our findings to larger filters with substantially higher particle counts. These results furthermore show decreasing subsampling-errors with increasing MP content. This, in turn, highlights the tremendous importance of effective sample purification measures to increase the MP fraction. As a result, not only analysis times shorten by reducing the total number of particles to consider, but also the extrapolation of results becomes more reliable when applying subsampling methods.

Measuring at least 5,000 particles per filter might be a realistic target for scientific purposes, but might also be impractical for monitoring applications with substantially higher sample counts. Measurement times can vary greatly depending on the exact parameters for optical scan and spectroscopic measurement. Our Raman microspectroscopy approach would require approximately 6 to 8 h for such a measurement, including optical scan (1–3 h), particle detection (several minutes) and spectroscopic measurement (approximately 5 h, a more comprehensive review of commonly used analysis times for Raman microspectroscopy is given by Anger et al. (2018)). The particle-based methods allow exploiting information from the optical microscope image to decrease the subsampling-errors at very low measured fractions. The image of the filter not only allows to precisely count and locate the particles, but also to analyze each particle in terms of its characteristics regarding shape, color, size and texture. A classifier that allows distinguishing MP from non-MP particles (with a certain level of confidence) based on these characteristics can be trained by



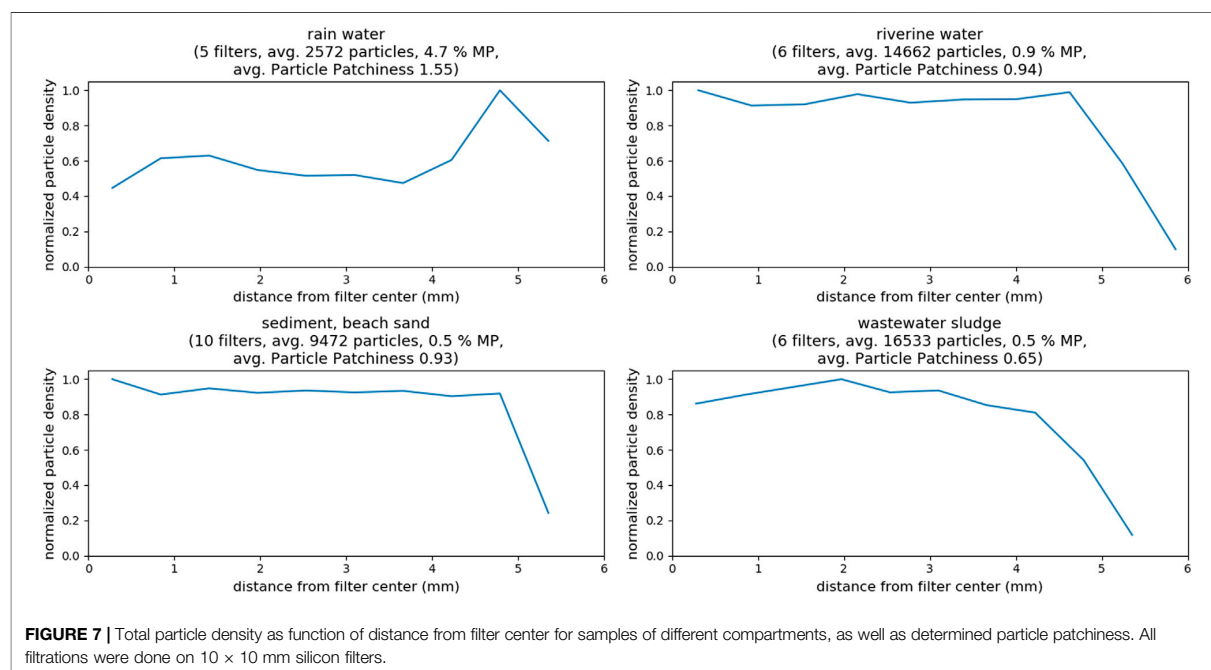
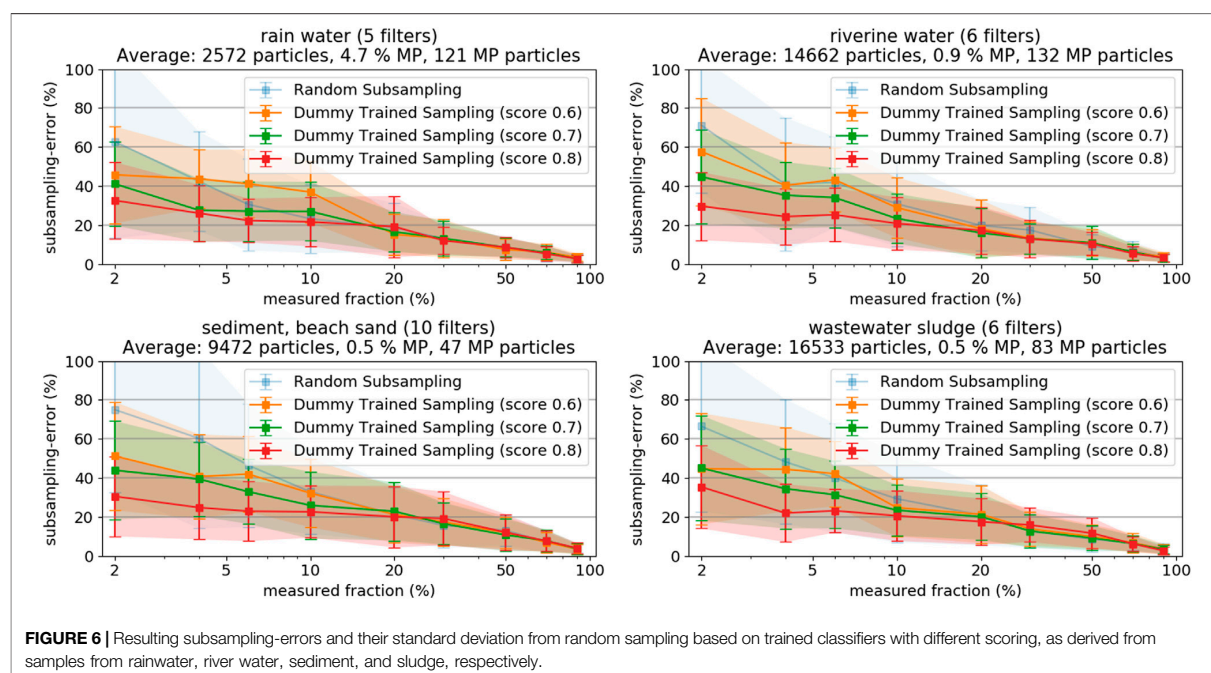
running a feature extraction on a large number of particles of known type (i.e., MP and non-MP, respectively). This “artificial” up-concentration of MP particles post purification reduces the error-margins in subsampling and is especially useful when only low percentages of particles can be measured. Procedures for the classification of particles from microscopy can be found throughout literature and give valuable information about what kind of particle features to exploit (Xu et al., 1997; Xu et al., 2018; Peng and Kirk, 1998). Developing a machine-learning model for effective MP classification from microscopy images goes beyond the scope of this manuscript, due to the complexity of such an endeavor, especially due to the low content of MP particles i.e., the highly imbalanced datasets (Batista et al., 2004; Wei and Dunbrack 2013). Instead, we decided to assess the final reduction in subsampling-errors, given a classifier with a certain accuracy score would exist. That helps deciding on whether to actually start the efforts of developing a real classifier. As our datasets were already fully analyzed, a dummy classifier can be readily set up yielding any desired score from 0.5 (i.e., no actual knowledge, sampling is completely random) to 1.0 (i.e., perfect classifier). Three dummy classifiers with scores of 0.6, 0.7, and 0.8 were tested, respectively. The concept is to use the classifier to extract a subsample of all particles, which will have a higher MP fraction than the original set of particles. As discussed above, a higher fraction of MP has the highest potential to increase subsampling accuracy. Then, the desired number of particles is chosen on a random base from the subset with increased MP fraction. Details about the dummy classifier and the exact calculations can be found in SI chapter “Details on Trained Random Particle Subsampling”. **Figure 6** shows the results of the three classifiers, as compared to the purely random particle subsampling.

The subsampling-errors at low measured fractions decrease significantly when the score of the used classifier increases. The results clearly show that the application of a classifier substantially decreases the very high subsampling-errors below 10% measured fraction, even if their classification score is not higher than 0.6 to 0.8. The effect gets less pronounced at higher measured fractions wherefore it is most sensible to apply the methods if the measured fractions are lower than 10%. It is important to keep in mind that the final particle assignment is done according to the results of the spectroscopy measurement, regardless of the used classifier’s initial guess. Subsampling based on a classifier, however, complicates the

step of extrapolation as the sample measured is no longer a random representative of the statistical universe of the filter. Refer to SI chapter 5 for more details on the calculations. The obtained findings are good reason for engaging in development of a real classifier suitable for MP classification on LM images. However, also other techniques, such as particle staining with fluorescent dyes, could be exploited for an according pre-selection of a subset with increased MP content (Shim et al., 2016).

Box-Based Subsampling

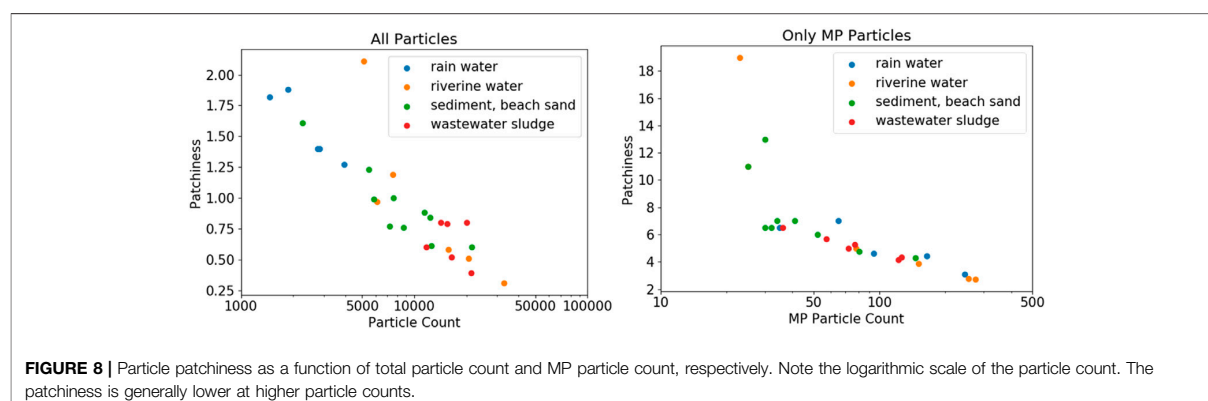
A closer investigation on distribution of the particles on the filters is necessary before reviewing the box-based subsampling method. The patchy and inhomogeneous distribution of the particles on the filter exemplifies the difficulty to design a pattern for a box selection subsampling (**Figure 3**, MP particles in red, others in blue). Analyzing the impact of particle distribution heterogeneity on the subsampling-error of the box-placement methods requires quantification of the heterogeneity, which is a difficult endeavor. Comparable literature studies are scarce but, fortunately, a recent study investigated the distribution of particles on filters (Thaysen et al., 2020). However, only examples from artificially produced model samples were included. They proposed plotting particle count as a function of particle distance to filter center to observe particle distribution patterns. They exhibited “starburst” particle distributions with highest particle density around the filter center. To compare our results of real environmental samples to their results we did the same calculations for filters from different environmental compartments. However, we converted “particle count” into “particle density”. Particle density is obtained by dividing particle count by the area of the filter section that is represented by the respective distances (intuitively, the section from 1 to 2 mm away from filter center is smaller than the section from 4 to 5 mm). Thereby, the differences in area of the filter sections is taken into account and patterns emerge more clearly (the original plots with particle count as function of distance from filter center (i.e., without correction for filter increasing area of filter sections) can be found in supporting information **Supplementary Figure S1**). However, the distance from the filter center distribution alone does not fully capture particle distribution inhomogeneity. For instance, the method would be insensitive to particles distributed only on one half, or quarter, of the filter. To overcome this potential error we developed and



implemented an orthogonal approach to calculate the “average particle patchiness” value. The approach entails dividing the filter area in cells (e.g., 50 × 50), and calculating the number of particles in each cell. The average particle patchiness is then obtained by dividing standard deviation of the particle number per cell by its

mean value. **Supplementary Figure S2** in the SI shows example images of filters with low, medium and high particle patchiness and the respective (increasing) values.

In **Figure 7**, the filters are grouped again according to their environmental origin. Again, knowing if there was any



correlation between particle distribution homogeneity and sample compartment would be useful (see SI chapter “Selected Images of Filters” for example images). In case of the rainwater filters, particle density on the filters peaks at around 5 mm, indicating a ring formation of particles at the perimeter of the filter (refer to **Supplementary Figure S3**); inhomogeneous particle distribution is also indicated by the high patchiness value of about 1.5. The samples from all other compartments show a similar pattern with almost constant particle density from center to the border of the filter, where particle density eventually decreases (refer to **Supplementary Figures 4 - 6**). The analyzed examples did not reveal any “starburst” pattern as to be expected from model samples (Thaysen et al., 2020), but drawing any conclusions is difficult, without taking into account details about sample workup and filtration procedures (Merck, 2018). Conversely, observing the averaged particle counts and the corresponding patchiness values indicates a correlation. Higher overall particle counts lead to a more homogeneous distribution of the particles on the filter. In fact, the observed patchiness of all investigated samples correlates well with the particle count, as shown in the left panel of **Figure 8**. It is important not to misunderstand that finding! The goal should not be to maximize the absolute particle count, but to increase the number of MP particles on a filter. The right panel of **Figure 8** shows that the correlation between patchiness and particle count is the same if only MP particles on the filter are considered. The trend is the same, although the absolute values of the patchiness increase substantially. Refer to **Supplementary Figure S2** in the SI for a visualization of different levels of patchiness.

Reviewing the subsampling-errors of the box subsampling methods, our investigations showed that the obtained subsampling-errors are very similar for the individual layouts when applied to the filters grouped according to their environmental origin (refer to **Supplementary Figure S7–Supplementary Figure S10**). The number of boxes to create the individual layouts does not seem to have a notable effect, although the cross layout shows slightly lower errors when using five, instead of three boxes across. Only in case of the rainwater samples with low particle counts and inhomogeneous particle distribution (resulting in many empty spaces on the filter i.e., high patchiness), the errors from box measurement subsampling exceed the errors from the random particle

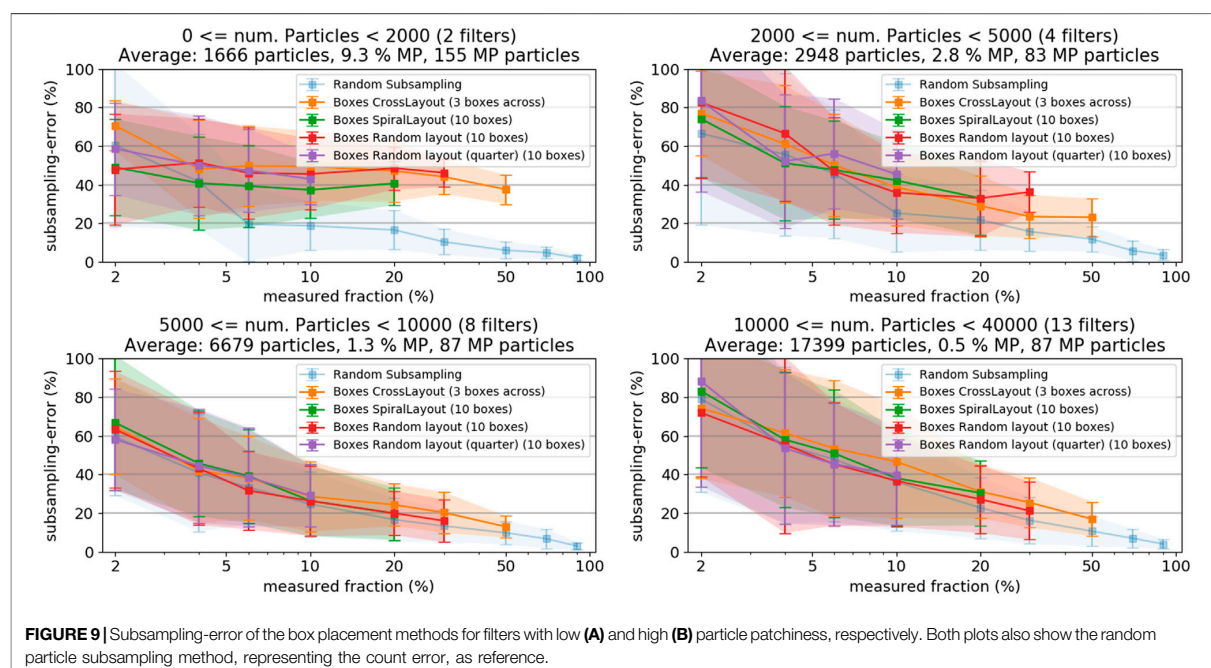
subsampling. Otherwise, the observed subsampling is dominated by the counting error, rather than an additional error resulting from inhomogeneous particle distribution.

Figure 9 shows the subsampling-error of the box-placement methods when sorting the filters into categories with different particle counts. Including the random particle subsampling-error, which is not affected by particle patchiness, allows distinguishing the pure counting error from errors resulting from inhomogeneous particle distribution on the filter. In case of very low particle numbers (≤ 2000) the subsampling-error from the box-based methods is substantially higher than for the random particle subsampling, which indicates an additional contribution of particle distribution inhomogeneity to the subsampling-error. At higher particle counts, the subsampling-errors from random particle subsampling and the box-placement methods come closer together, indicating a decreasing influence of the particle distribution inhomogeneity. At around 5,000 particles (corresponding to a patchiness of approximately 1.0, see **Figure 8**) the box-based sampling methods do not perform worse than the random particle subsampling.

In order to keep the subsampling-error and its deviation within one sigma below a 20% error margin, the covered area of the filter should be at least 50%. A 50% filter area coverage could only be fully realized with the cross layout with three boxes across and, near enough, the random box layout (with 47% coverage at 10 boxes, **Table 2**). In contrast to the particle-based subsampling, the box placement methods do not bear opportunities for exploiting machine-learning methods to increase accuracy at low measured fractions.

Counting all MP vs. Counting Particular MP Types

To simplify the quantitative assessment, herein only the integral MP particle numbers were considered without discrimination into different polymer types or morphological features. Most studies, however, require information of MP species such as chemical classification, color, size and shape. There are no standard categorization methods in place as it depends on the research question and the precise analytical tasks chosen. However, the issue shall be addressed with some general reflections.



Our study demonstrated the occurrence of high subsampling-errors and high error margins when measuring low fractions of particles on a filter. As a differentiation of different particle types would decrease the individual particle numbers, the subsampling-errors would increase accordingly. In other words, if particle types have to be distinguished, the overall number of particles to measure has to be increased. Thus, predicting which MP particle classes are present in a sample results in even larger uncertainties than estimating the integral MP content. A general recommendation about required particle numbers cannot be reliably given for such cases. A practical approach should entail measuring a certain fraction of all particles, counting the particles in all categories of interest and deciding if more particles need to be measured. As a consequence, already reducing the initial sample volumes prior to the purification steps can limit the final robustness of the results i.e., when yielding to small numbers of the target particles. Treated sample volumes should therefore be generously calculated. Karlsson et al. discussed how many particles have to be measured for having a statistically robust number (Karlsson et al., 2020). Their study concluded a reasonable number would be of about 30 particles per class. This is in agreement with the results of our analysis that revealed an error of about 20% (Figure 4) when having measured about 30 MP particles. Nevertheless, exceptions have to be made for “very rare” categories.

CONCLUSION AND OUTLOOK

Spectroscopic particle measurements are of high importance when it comes to MP analysis in environmental samples but need to be sped up to be established as monitoring tools. We

compared the performance of different subsampling approaches, based on two different method categories: 1) particle-based methods and 2) measure box placement methods on 27 environmental samples from different compartments, such as rainwater, river water, sediment and wastewater sludge.

The results can be summarized in three general findings. First, none of the tested subsampling methods was identified to clearly outperform the others. The dependency of the subsampling-errors on the fraction measured was very similar for all methods; differences could only be seen in edge scenarios, as for instance in the case of filters with relatively low particle counts and inhomogeneous particle distribution on the filter. There, the particle-based subsampling proved to be more accurate than the box-based methods. In the majority of samples however, the observed subsampling-error was due to the counting error (i.e., extrapolating from a low number of measured particles) and particle distribution inhomogeneity is negligible.

Second, the magnitude of the averaged subsampling-error easily exceeded 50% if only 5% or less of the filter was measured. More critically, the standard deviation of the subsampling-error strongly increases when decreasing the measured fraction. If reliable particle counts with an error of less than 20% are required, the measured fraction should be at least 50% or, in the case of particle-based subsampling, at least 7,000 particles. However, if exact counts of particular types of MP particles are of interest, the measured fraction would have to be increased even further, thus reducing the time saving from the subsampling. It might be advisable to measure the entire filter in these cases.

Third, the best way to increase accuracy at low particle counts is to increase the fraction of MP particles in the sample. This can be done by further optimization of sample preprocessing steps or by

implementing methods to identify possible MP particles prior to spectroscopic measurement (by specifically trained classification models or fluorescent staining). That finding seems trivial, but is important to keep in mind when designing workflows for workup and analysis of certain sample types. If only qualitative results are required (i.e., are MP particles present or not), higher error margins can be tolerated. Vice versa, if robust particle numbers are required, sample preprocessing should be optimized or, if not possible, higher fractions of the sample have to be measured.

To increase the validity of the herein gathered results to a larger diversity of filters, especially with higher particle counts, we encourage scientists in the field to critically reassess their measurements similarly as described here. Deeper statistical considerations would be beneficial for underpinning the observed effects.

The decision on the most appropriate subsampling strategy for a fast and proper quantification of specific objects from different environmental compartments is important for several scientific disciplines, going far beyond microplastic research. Only one example would be the microscopic quantification of specific prokaryotic groups via phylogenetic staining of cells e.g., by Fluorescence *in situ* hybridization (FISH). Therefore, we also understand this study as a general stimulus for a more extensive and interdisciplinary research on statistically relevant counting of small and less abundant objects in the environment.

DATA AVAILABILITY STATEMENT

The datasets and calculations presented in this study can be found in online repositories. The repositories can be found under: <https://gitlab.ipfdd.de/Brandt/subsampling>.

REFERENCES

- Anger, P. M., Esch, E., Baumann, T., Elsner, M., Niessner, R., Ivleva, N. P., et al. (2018). Raman microspectroscopy as a tool for microplastic particle analysis. *TrAC Trends Anal. Chem.* 109, 214–226. doi:10.1016/j.trac.2018.10.010
- Batista, G. E. A. P. A., Prati, R. C., and Monard, M. C. (2004). A study of the behavior of several methods for balancing machine learning training data. *ACM SIGKDD Explor. Newsl.* 6, 20–29. doi:10.1145/1007730.1007735
- Bergmann, M., Wirzberger, V., Krumpfen, T., Lorenz, C., Primpke, S., Tekman, M. B., et al. (2017). High quantities of microplastic in arctic deep-sea sediments from the HAUSGARTEN observatory. *Environ. Sci. Technol.* 51, 11000–11010. doi:10.1021/acs.est.7b03331
- Borrelle, S. B., Ringma, J., Law, K. L., Monnahan, C. C., Lebreton, L., McGivern, A., et al. (2020). Predicted growth in plastic waste exceeds efforts to mitigate plastic pollution. *Science*. 369: 1515–1518. doi:10.1126/science.aba3656
- Brandon, J. A., Jones, W., and Ohman, M. D. (2019). Multidecadal increase in plastic particles in coastal ocean sediments. *Sci. Adv.* 5, eaax0587. doi:10.1126/sciadv.aax0587
- Brandt, J., Bittrich, L., Fischer, F., Kanaki, E., Tagg, A., Lenz, R., et al. (2020). High-throughput analyses of microplastic samples using fourier transform infrared and Raman spectrometry. *Appl. Spectrosc.* 74 (9), 1185–1197. doi:10.1177/0003702820932926
- Browne, M. A., Galloway, T. S., and Thompson, R. C. (2010). Spatial patterns of plastic debris along estuarine shorelines. *Environ. Sci. Technol.* 44, 3404–3409. doi:10.1021/es903784e
- Buffle, J., and Leppard, G. G. (1995). Characterization of aquatic colloids and macromolecules. 2. Key role of physical structures on analytical results. *Environ. Sci. Technol.* 29, 2176–2184. doi:10.1021/es00009a005

AUTHOR CONTRIBUTIONS

All authors listed have made a substantial, direct, and intellectual contribution to the work and approved it for publication.

FUNDING

This research was funded by the projects MicroCatch_Balt (03F0788A), PLASTRAT (02WPL1446 I) and PLAWES (03F0789A) supported by the Federal Ministry of Education and Research (BMBF Germany) and the BONUS MICROPOLL project supported by BONUS (Art 185), funded jointly by the European Union and BMBF (03F0775A).

ACKNOWLEDGMENTS

We thank Robin Lenz, Dr. Alexander Tagg and Juliana Ivar do Sul (IOW), Dr. Sarmite Kernchen, Dr. Martin Löder, and Prof. Christian Laforsch (University of Bayreuth), as well as Annett Mundane, Natalie Wick, and Prof. Christian Schaum (Universität der Bundeswehr München) for obtaining, treating and providing the samples.

SUPPLEMENTARY MATERIAL

The Supplementary Material for this article can be found online at: <https://www.frontiersin.org/articles/10.3389/fenvs.2020.579676/full#supplementary-material>.

- Chaudhuri, B. B. (1994). How to choose a representative subset from a set of data in multi-dimensional space. *Pattern Recogn. Lett.* 15, 893–899. doi:10.1016/0167-8655(94)90151-1
- Claessens, M., Van Cauwenberghe, L., Vandegehuchte, M. B., and Janssen, C. R. (2013). New techniques for the detection of microplastics in sediments and field collected organisms. *Mar. Pollut. Bull.* 70, 227–233. doi:10.1016/j.marpolbul.2013.03.009
- Daszykowski, M., Walczak, B., and Massart, D. L. (2002). Representative subset selection. *Anal. Chim. Acta.* 468, 91–103. doi:10.1016/S0003-2670(02)00651-7
- Dierkes, G., Lauschke, T., Becher, S., Schumacher, H., Földi, C., and Ternes, T. (2019). Quantification of microplastics in environmental samples via pressurized liquid extraction and pyrolysis-gas chromatography. *Anal. Bioanal. Chem.* 411, 6959–6968. doi:10.1007/s00216-019-02066-9
- Duemichen, E., Braun, U., Senz, R., Fabian, G., and Sturm, H. (2014). Assessment of a new method for the analysis of decomposition gases of polymers by a combining thermogravimetric solid-phase extraction and thermal desorption gas chromatography mass spectrometry. *J. Chromatogr. A.* 1354, 117–128. doi:10.1016/j.chroma.2014.05.057
- Dümichen, E., Barthel, A.-K., Braun, U., Bannick, C. G., Brand, K., Jekel, M., et al. (2015). Analysis of polyethylene microplastics in environmental samples, using a thermal decomposition method. *Water Res.* 85, 451–457. doi:10.1016/j.watres.2015.09.002
- Dümichen, E., Eisentraut, P., Bannick, C. G., Barthel, A.-K., Senz, R., Brau, U., et al. (2017). Fast identification of microplastics in complex environmental samples by a thermal degradation method. *Chemosphere.* 174, 572–584. doi:10.1016/j.chemosphere.2017.02.010
- Enders, K., Käßler, A., Biniash, O., Feldens, P., Stollberg, N., Lange, X., et al. (2019). Tracing microplastics in aquatic environments based on sediment analogies. *Sci. Rep.* 9, 15207. doi:10.1038/s41598-019-50508-2

- Enders, K., Lenz, R., Ivar do Sul, J. A., Tagg, A. S., and Labrenz, M. (2020). When every particle matters: a QuEChERS approach to extract microplastics from environmental samples. *Methods*. 7, 100784. doi:10.1016/j.mex.2020.100784
- Fischer, M., and Scholz-Böttcher, B. M. (2019). Microplastics analysis in environmental samples-recent pyrolysis-gas chromatography-mass spectrometry method improvements to increase the reliability of mass-related data. *Anal. Methods*. 11: 2489–2497. doi:10.1039/C9AY00600A
- Geyer, R., Jambeck, J. R., and Law, K. L. (2017). Production, use, and fate of all plastics ever made. *Sci. Adv.* 3, e1700782. doi:10.1126/sciadv.1700782
- Halden, R. U. (2015). Epistemology of contaminants of emerging concern and literature meta-analysis. *J. Hazard Mater.* 282, 2–9. doi:10.1016/j.jhazmat.2014.08.074
- Halle, A. T., Ladirat, L., Gendre, X., Goudouneche, D., Pusineri, C., Routaboul, C., et al. (2016). Understanding the fragmentation pattern of marine plastic debris. *Environ. Sci. Technol.* 50, 5668–5675. doi:10.1021/acs.est.6b00594
- Logemann, J., Oveland, E., Bjoroy, Ø., Peters, W., Cojocariu, C., and Kögel, T. (2018). “Pyrolysis-GC-Orbitrap MS-a powerful analytical tool for identification and quantification of microplastics in a biological matrix”. (2018), application note 10643.
- Huppertsberg, S., and Knepper, T. P. (2018). Instrumental analysis of microplastics-benefits and challenges. *Anal. Bioanal. Chem.* 410, 6343–6352. doi:10.1007/s00216-018-1210-8
- Imhof, H. K., Laforsch, C., Wiesheu, A. C., Schmid, J., Anger, P. M., Niessner, R., et al. (2016). Pigments and plastic in limnetic ecosystems: a qualitative and quantitative study on microparticles of different size classes. *Water Res.* 98, 64–74. doi:10.1016/j.watres.2016.03.015
- Jambeck, J. R., Geyer, R., Wilcox, C., Siegler, T. R., Perryman, M., Andrady, A., et al. (2015). Marine pollution. Plastic waste inputs from land into the ocean. *Science*. 347, 768–771. doi:10.1126/science.1260352
- Käppler, A., Fischer, D., Oberbeckmann, S., Schernewsk, G., Labrenz, M., Eichhorn, K.-J., et al. (2016). Analysis of environmental microplastics by vibrational microspectroscopy: FTIR, Raman or both? *Anal. Bioanal. Chem.* 408, 8377–8391. doi:10.1007/s00216-016-9956-3
- Käppler, A., Fischer, M., Scholz-Böttcher, B. M., Oberbeckmann, S., Labrenz, M., Fischer, D., et al. (2018). Comparison of μ -ATR-FTIR spectroscopy and py-GCMS as identification tools for microplastic particles and fibers isolated from river sediments. *Anal. Bioanal. Chem.* 410, 5313–5327. doi:10.1007/s00216-018-1185-5
- Käppler, A., Windrich, F., Löder, M. G. J., Malanin, M., Fischer, D., Labrenz, M., et al. (2015). Identification of microplastics by FTIR and Raman microscopy: a novel silicon filter substrate opens the important spectral range below 1300 cm^{-1} for FTIR transmission measurements. *Anal. Bioanal. Chem.* 407, 6791–6801. doi:10.1007/s00216-015-8850-8
- Karlsson, T. M., Kärrman, A., Rotander, A., and Hasselöv, M. (2020). Comparison between manta trawl and *in situ* pump filtration methods, and guidance for visual identification of microplastics in surface waters. *Environ. Sci. Pollut. Res. Int.* 27, 5559–5571. doi:10.1007/s11356-019-07274-5
- Lenz, R., Enders, K., Stedmon, C. A., Mackenzie, D. M., and Nielsen, T. G. (2015). A critical assessment of visual identification of marine microplastic using Raman spectroscopy for analysis improvement. *Mar. Pollut. Bull.* 100, 82–91. doi:10.1016/j.marpolbul.2015.09.026
- Lenz, R., and Labrenz, M. (2018). Small microplastic sampling in water: development of an encapsulated filtration device. *Water*. 10, 1055. doi:10.3390/w10081055
- Liu, F., Olesen, K. B., Borregaard, A. R., and Vollertsen, J. (2019). Microplastics in urban and highway stormwater retention ponds. *Sci. Total Environ.* 671, 992–1000. doi:10.1016/j.scitotenv.2019.03.416
- Löder, M. G. J., Imhof, H. K., Ladehoff, M., Löschel, L. A., Lorenz, C., Mintenig, S., et al. (2017). Enzymatic purification of microplastics in environmental samples. *Environ. Sci. Technol.* 51, 14283–14292. doi:10.1021/acs.est.7b03055
- Löder, M. G. J., Kuczera, M., Mintenig, S., Lorenz, C., and Gerdt, G. (2015). Focal plane array detector-based micro-Fourier-transform infrared imaging for the analysis of microplastics in environmental samples. *Environ. Chem.* 12, 563–581. doi:10.1071/en14205
- Lusher, A. L., Welden, N. A., Sobral, P., and Cole, M. (2017). Sampling, isolating and identifying microplastics ingested by fish and invertebrates. *Anal. Methods*. 9, 1346–1360. doi:10.1039/c6ay02415g
- Masó, M., Garcés, E., Pagès, F., and Camp, J. (2003). Drifting plastic debris as a potential vector for dispersing Harmful Algal Bloom (HAB) species. *Sci. Mar.* 67, 107–111. doi:10.3989/scimar.2003.67n1107
- Merck (2018). *AD030 Air and fluid particle monitoring guide*, Darmstadt, Germany: MerckKGaA.
- Mintenig, S. M., Kooi, M., Erich, M. W., Primpke, S., Redondo-Hasselerharm, P. E., Dekker, S. C., et al. (2020). A systems approach to understand microplastic occurrence and variability in Dutch riverine surface waters. *Water Res.* 176, 115723. doi:10.1016/j.watres.2020.115723
- Murphy, F., Ewins, C., Carbonnier, F., and Quinn, B. (2016). Wastewater Treatment Works (WwTW) as a source of microplastics in the aquatic environment. *Environ. Sci. Technol.* 50, 5800–5808. doi:10.1021/acs.est.5b05416
- Peng, Z., and Kirk, T. B. (1998). Automatic wear-particle classification using neural networks. *Tribol. Lett.* 5, 249–257. doi:10.1023/A:1019126732337
- Poulain, M., Mercier, M. J., Brach, L., Martignac, M., Routaboul, C., Perez, E., et al. (2019). Small microplastics as a main contributor to plastic mass balance in the North Atlantic subtropical Gyre. *Environ. Sci. Technol.* 53, 1157–1164. doi:10.1021/acs.est.8b05458
- Primpke, S., Christiansen, S. H., Cowger, W., Frond, H. D., Deshpande, A., Fischer, M., et al. (2020a). Critical assessment of analytical methods for the harmonized and cost-efficient analysis of microplastics. *Appl. Spectrosc.* 74, 1012–1047. doi:10.1177/0003702820921465
- Primpke, S., Cross, R. K., Mintenig, S. M., Simon, M., Vianello, A., Gerdt, G., et al. (2020b). Toward the systematic identification of microplastics in the environment: evaluation of a new Independent software tool (siMPle) for spectroscopic analysis. *Appl. Spectrosc.* 74 (9), 1127–1138. doi:10.1177/0003702820917760
- Primpke, S., Dias, P. A., and Gerdt, G. (2019). Automated identification and quantification of microfibrils and microplastics. *Anal. Methods*. 11, 2138–2147. doi:10.1039/C9AY00126C
- Primpke, S., Lorenz, C., Rascher-Friesenhausen, R., and Gerdt, G. (2017). An automated approach for microplastics analysis using focal plane array (FPA) FTIR microscopy and image analysis. *Anal. Methods*. 9, 1499–1511. doi:10.1039/c6ay02476a
- Rodionova, O. Y., and Pomerantsev, A. L. (2008). Subset selection strategy. *J. Chemom.* 22, 674–685. doi:10.1002/cem.1103
- Schymanski, D., Goldbeck, C., Humpf, H. U., and Fürst, P. (2018). Analysis of microplastics in water by micro-Raman spectroscopy: release of plastic particles from different packaging into mineral water. *Water Res.* 129, 154–162. doi:10.1016/j.watres.2017.11.011
- Shim, W. J., Song, Y. K., Hong, S. H., and Jang, M. (2016). Identification and quantification of microplastics using Nile Red staining. *Mar. Pollut. Bull.* 113, 469–476. doi:10.1016/j.marpolbul.2016.10.049
- Siegfried, M., Koelmans, A. A., Besseling, E., and Kroeze, C. (2017). Export of microplastics from land to sea. A modelling approach. *Water Res.* 127, 249–257. doi:10.1016/j.watres.2017.10.011
- Simon, M., van Alst, N., and Vollertsen, J. (2018). Quantification of microplastic mass and removal rates at wastewater treatment plants applying Focal Plane Array (FPA)-based Fourier Transform Infrared (FT-IR) imaging. *Water Res.* 142, 1–9. doi:10.1016/j.watres.2018.05.019
- Tagg, A. S., Sapp, M., Harrison, J. P., and Ojeda, J. J. (2015). Identification and quantification of microplastics in wastewater using focal plane array-based reflectance micro-FT-IR imaging. *Anal. Chem.* 87, 6032–6040. doi:10.1021/acs.analchem.5b00495
- Thaysen, C., Munno, K., Hermabessiere, L., and Rochman, C. (2020). EXPRESS: toward Raman automation for microplastics: developing strategies for particle adhesion and filter subsampling. *Appl. Spectrosc.* 74, 0003702820922900. doi:10.1177/0003702820922900
- Vianello, A., Boldrin, A., Guerriero, P., Moschino, V., Rella, R., Sturaro, A., et al. (2013). Microplastic particles in sediments of Lagoon of Venice, Italy: first observations on occurrence, spatial patterns and identification. *Estuar. Coast. Shelf Sci.* 130, 54–61. doi:10.1016/j.ecss.2013.03.022
- Wagner, J., Wang, Z. M., Ghosal, S., Rochman, C., Gassel, M., and Wall, S. (2017). Novel method for the extraction and identification of microplastics in ocean trawl and fish gut matrices. *Anal. Methods*. 9, 1479–1490. doi:10.1039/C6AY02396G

- Wei, Q., and Dunbrack, R. L. (2013). The role of balanced training and testing data sets for binary classifiers in bioinformatics. *PLoS One*. 8, e67863. doi:10.1371/journal.pone.0067863
- Xu, B., Wen, G., Zhang, Z., and Chen, F. (2018). Wear particle classification using genetic programming evolved features. *Lubric. Sci.* 30, 229–246. 10.1002/lis.1411
- Xu, K., Luxmoore, A. R., and Deravi, F. (1997). Comparison of shape features for the classification of wear particles. *Eng. Appl. Artif. Intell.* 10, 485–493. doi:10.1016/S0952-1976(97)00017-1
- Zettler, E. R., Mincer, T. J., and Amaral-Zettler, L. A. (2013). Life in the “plastisphere”: microbial communities on plastic marine debris. *Environ. Sci. Technol.* 47, 7137–7146. doi:10.1021/es401288x

Conflict of Interest: The authors declare that there the research was conducted in the absence of any commercial or financial relationships that could be construed as a potential conflict of interest.

Copyright © 2021 Brandt, Fischer, Kanaki, Enders, Labrenz and Fischer. This is an open-access article distributed under the terms of the Creative Commons Attribution License (CC BY). The use, distribution or reproduction in other forums is permitted, provided the original author(s) and the copyright owner(s) are credited and that the original publication in this journal is cited, in accordance with accepted academic practice. No use, distribution or reproduction is permitted which does not comply with these terms.

Supplementary Material

Assessment of Subsampling Strategies in Microspectroscopy of Environmental Microplastic Samples

**Josef Brandt^{1,2*}, Franziska Fischer¹, Elisavet Kanaki¹, Kristina Enders³,
Matthias Labrenz³, Dieter Fischer^{1*}**

¹Leibniz-Institut für Polymerforschung Dresden e.V., Hohe Straße 6, D-01069 Dresden, Germany

² University of Gothenburg, Department of Marine Sciences, Kristineberg 566, S-45178
Fiskebäckskil, Sweden

³Leibniz Institute for Baltic Sea Research Warnemünde (IOW), Seestraße 15, D-18119, Rostock,
Germany

1 Application of Subsampling Methods

The dataset objects created by the GEPARD measurements hold (amongst others) a list of all particles measured. Each particle is registered with (amongst others) its contour data, long and short size, and the spectral assignment. The contour data is given as a numerical array storing the pixel coordinates of all contour pixels.

A list containing the particles matching the respective subsampling criteria is derived from the list of all measured particles. In case of the random particle sampling, the `random.sample` method from Python's `random` library is used to derive the desired number of elements from the original particle list in a random fashion. In case of the sizebin subsampling, the particles are first sorted into sub-lists according to their size and the desired bins. Then, from each sub-list the desired fraction of particles is drawn using again the `random.sample` method. As an example, let's consider a desired fraction of 10 % and five bins with the following numbers of particles: 0, 3, 20, 45, 100. Then, the algorithm would choose the following numbers of sub particles randomly from the bins: 0, 1, 2, 5, 10. According to the fraction, the second bin with only 3 particles would result in no particle at all. But since there were particles in the bin, at least one is always taken.

In case of the box placement methods, the procedure is as follows. Each box placement method creates a list of measuring boxes, according to filter dimensions, desired covered fraction of filter and number of boxes. (For details on how to derive the measure box locations, the reader is referred to the Python code in the gitlab repository: <https://gitlab.ipfdd.de/Brandt/subsampling> The individual classes for the subsampling approaches can be found in the `geometricMethods.py` file.) To derive the list of subsampled particles, a loop through all original particles is required. In each step, the contour data of the respective particle is compared with the coordinates of the measure boxes. If the contour overlaps with one of the measure boxes, it is considered to be captured by the subsampling method and added to the list of subsampled particles.

After having derived the list of subsampled particles, the number of MP particle in each list is determined according the scheme presented in the following chapter. The ratio of MP count in original particle list and subsampled particle list then represents the subsampling error.

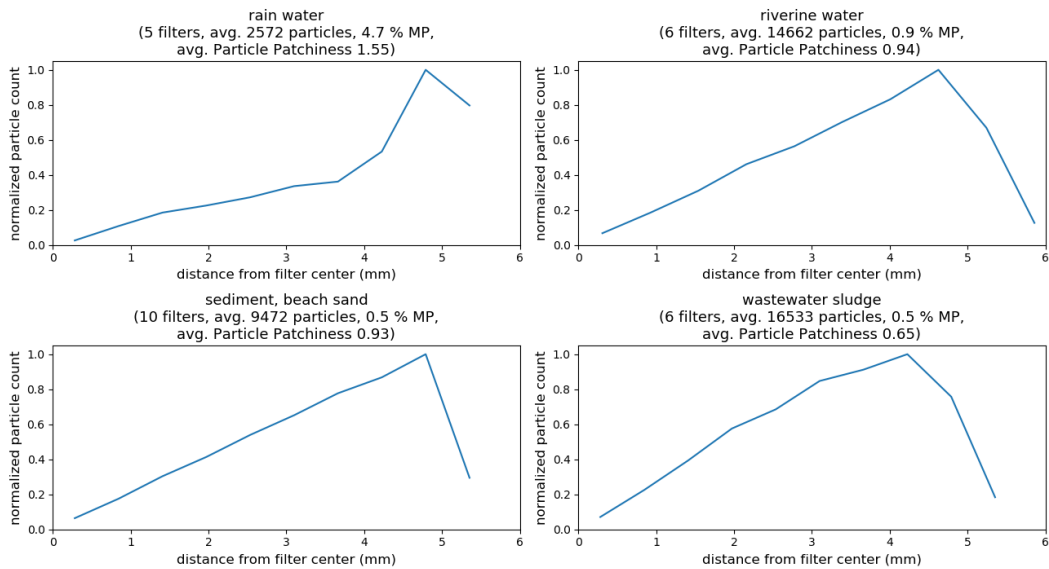
2 Determination of MP particle count

All particles with classifications listed below are considered MP particles:

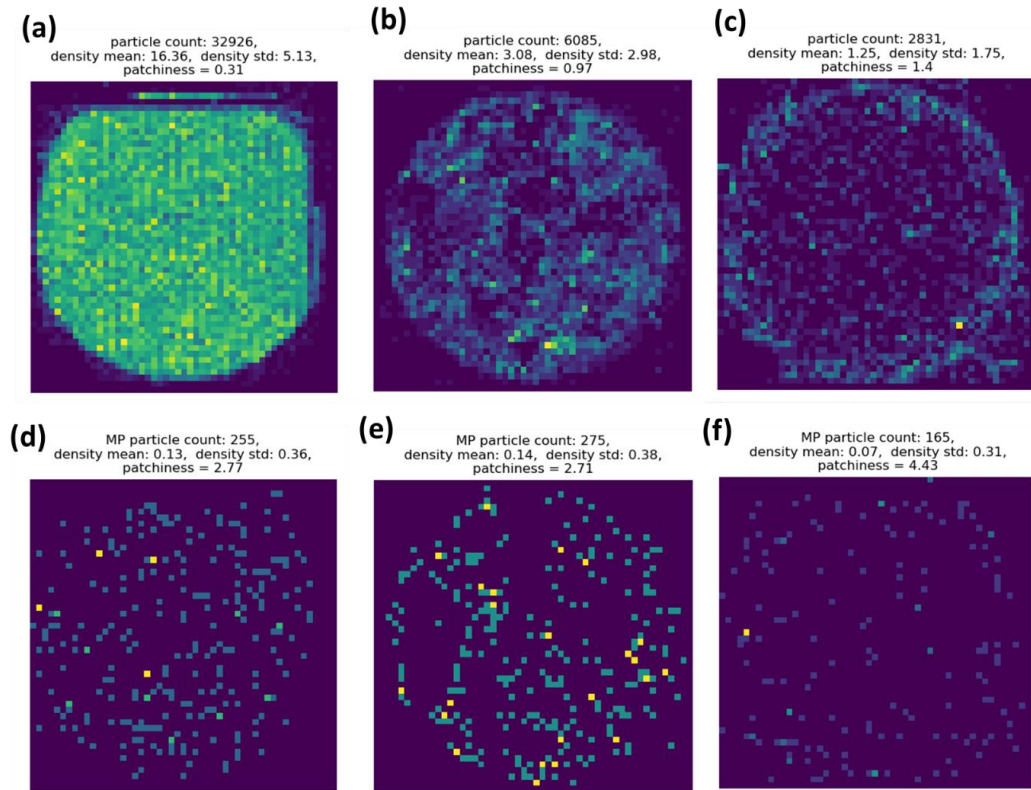
- Isoprene rubber
- Polybutylene terephthalate
- Polyphthalamide
- Poly(tetrafluoroethylene)
- Polyoxymethylene
- Pigment Violet 23
- Polyamide 6
- Poly(methyl methacrylate)
- Ethylen-propylen-dien-Copolymer
- Polylactide
- Thermoplastisches Polyurethan
- Polystyrene
- Pigment Yellow 17 based
- Epoxy + Pigment Blue 15 + Pigment Yellow 180
- Polyethylene + Pigment Blue 15
- Silicone-rubber
- Poly(vinyl chloride)
- Pigment Violet 37
- Pigment Blue 15 + Pigment Yellow 17
- Silicone-rubber+Pigment Red 254
- Polypropylene + Pigment Yellow 17
- Pigment Red 101
- Poly(ethylene terephthalate)
- Polyethylene
- Poly(ethylene terephthalate)
- Ethylen-Vinylacetat-Copolymer
- Pigment Blue 15
- Pigment Blue 15+TiO₂
- Pigment Yellow 184
- Poly (methyl methacrylate)
- Polypropylene + Pigment Blue 15
- Polyethylene + Pigment Red 221
- Acrylnitril-Butadien-Styrol-Copolymer
- Polypropylene

Particles being classified as pigments were also counted as MP particles. Although the actual polymer spectrum might not be visible in the Raman spectrum due to the high Raman activity of the pigment, it is very likely that the matrix is.

3 Quantification of particle heterogeneity on filter

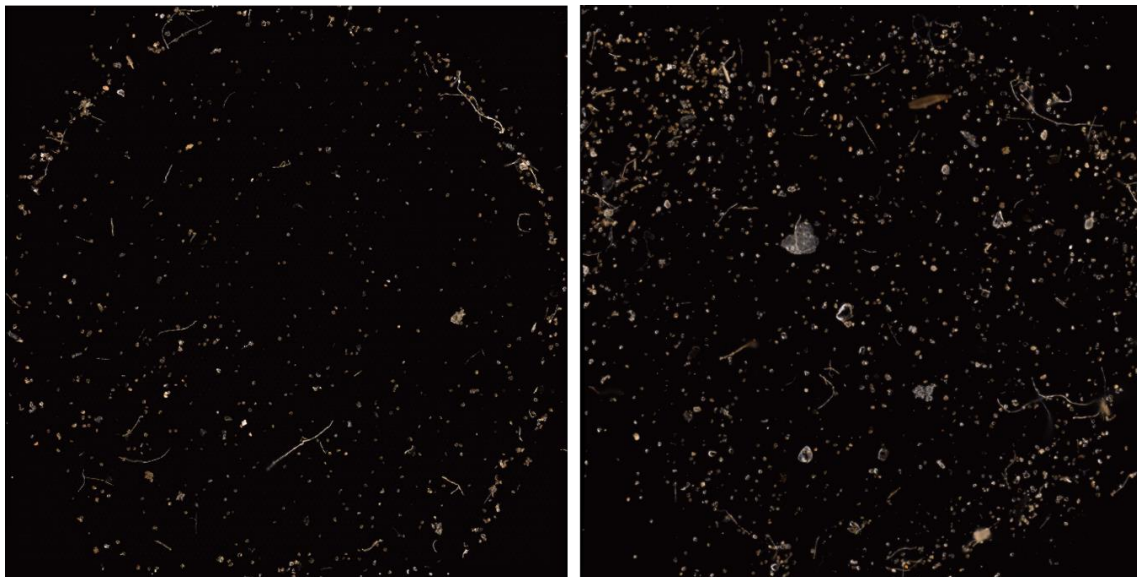


Supplementary Figure 1: Particle heterogeneity in terms of distance of particles to filter center, without correcting for the fact that ring segment area increases with increasing distance from the filter center.

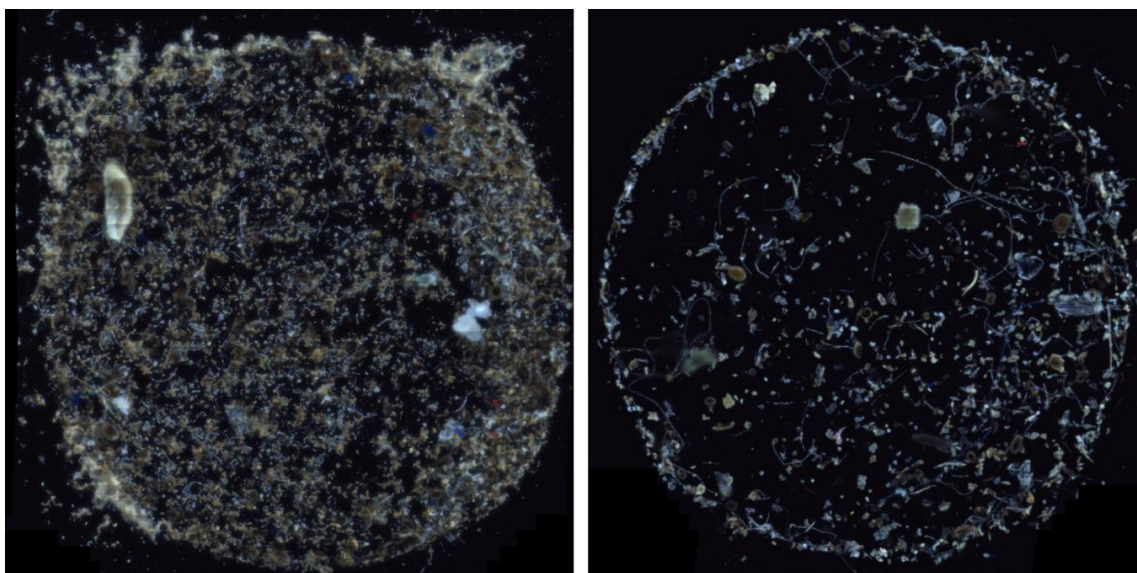


Supplementary Figure 2: Visualization of particle patchiness of filters with different particle counts. From (a) to (c): All particles on the filter are counted, patchiness increases from (a) to (c). Panels (d) to (f) show the same three filters, but only MP particles are counted.

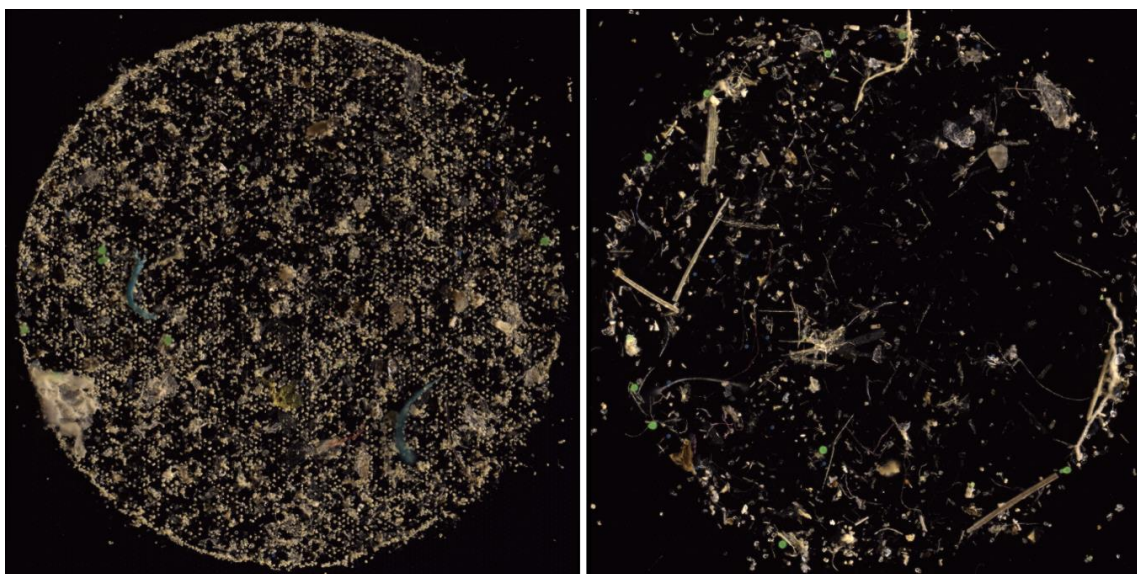
4 Selected Images of Filters



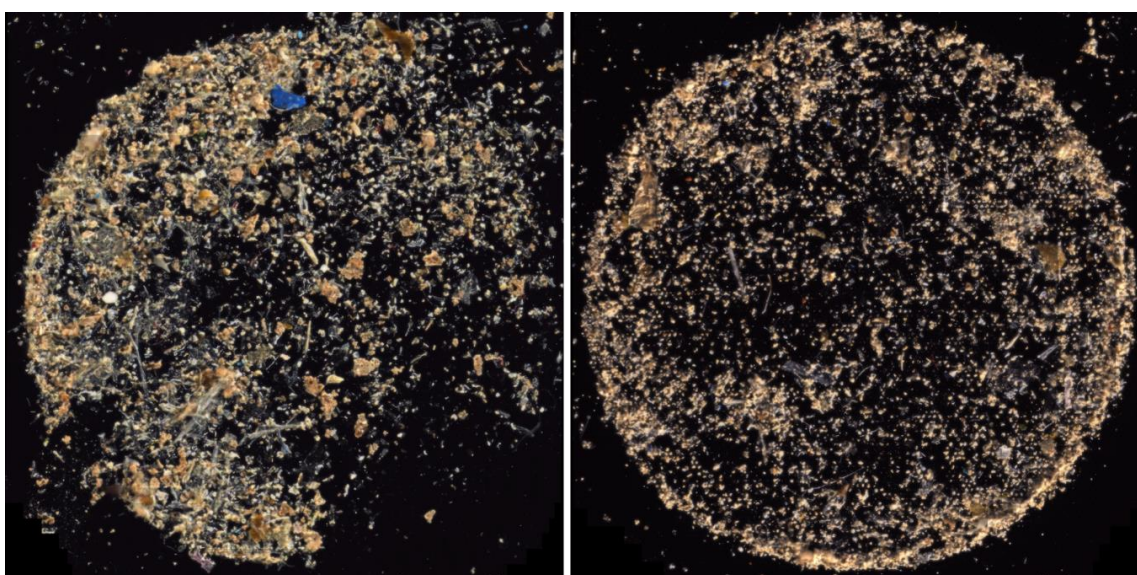
Supplementary Figure 3: Two examples of filters from rainwater. Acquired in dark-field at 20x magnification on the WITec alpha 300R.



Supplementary Figure 4: Two examples of filters with particles from riverine water. Acquired in dark-field at 20x magnification on the WITec alpha 300R.



Supplementary Figure 5: Two examples of filters with particles from sediment. Acquired in dark-field at 20x magnification on the WITec alpha 300R.



Supplementary Figure 6: Two examples of filters with particles from wastewater sludge. Acquired in dark-field at 20x magnification on the WITec alpha 300R.

5 Details on Trained Random Particle Subsampling

The application of the trained sampling using the dummy classifier works as follows. First, the classifier is applied to the full list of particles to find all particles that it would classify as microplastic. In that case, only a binary decision is made – MP or non MP. The repository contains attempts for classifiers extracting a set of features from the contour data and the respective particle images; the code can be found in the `classification.py` file within the `chemometrics` directory.

To produce a list of predicted MP particles with a desired prediction score, the dummy classifier works as follows:

```
For each original particle:
    predictedAssignment = non-MP
    if is_MP_particle(original particle):
        if randomNumber <= desiredScore:
            predictedAssignment = MP
    else:
        if randomNumber > desiredScore:
            predictedAssignment = MP
```

For each particle, the predicted assignment is first set to “non-MP” and a random number between 0.0 and 1.0 is drawn. If the particle was an MP particle and the random number is smaller than or equal to the desired score, the particle’s predicted assignment will be MP. Otherwise it remains predicted as “non-MP” and is a false negative. If the particle is a non-MP particle and the random number is greater than the desired score, the particle’s predicted assignment is set to “MP”, which corresponds to a false positive.

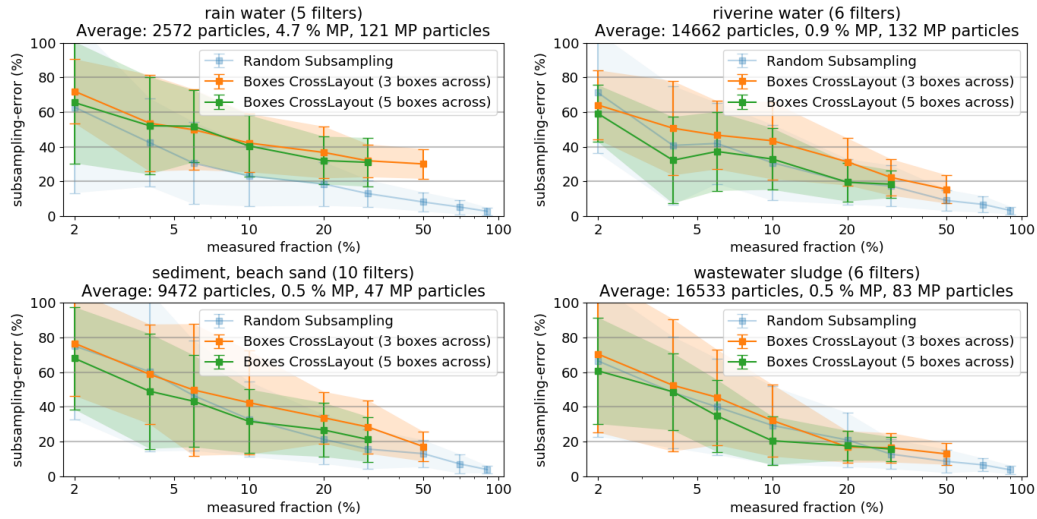
The classifier predicts a list of assignments (MP or non-MP) for all particles in the sample, which is used to create a new set of particles with an MP fraction being larger than in the original set of particles. If the desired fraction of particles to measure is $\leq 5\%$, only the predicted MP particles are put in that newly created particle set. When the fraction is between 5 and 15 %, the number of predicted non-MP particles is gradually increased from 0 % (at 5 % measured fraction) to 100 % (at 15 % measured fraction). Including an increasing number of predicted non-MP particles into the set with increasing measured fraction is necessary to also have the chance to measure false negative classified MP particles.

The desired number of particles (*i.e.*, 100, if 10 % of originally 1000 particles are to be measured) is then drawn from this newly created list of particles instead of from the original particle list. The factor used to extrapolate the found particle numbers to the original dataset is determined by:

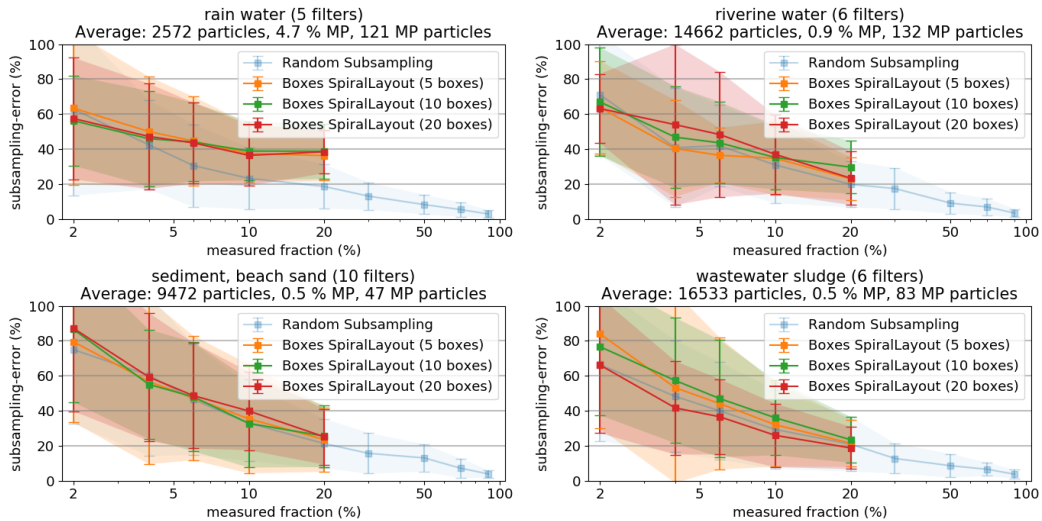
$$\text{Extrapolation Factor} = \frac{1}{\text{desiredFraction} * \frac{\text{numOriginalParticles}}{\text{numPredictedParticles}}}$$

, where *desiredFraction* is the fraction of particles to measure, *numOrigParticles* the number of particles in the original particle list and *numPredictedParticles* the number of particles in the particle list that was created using the classifier.

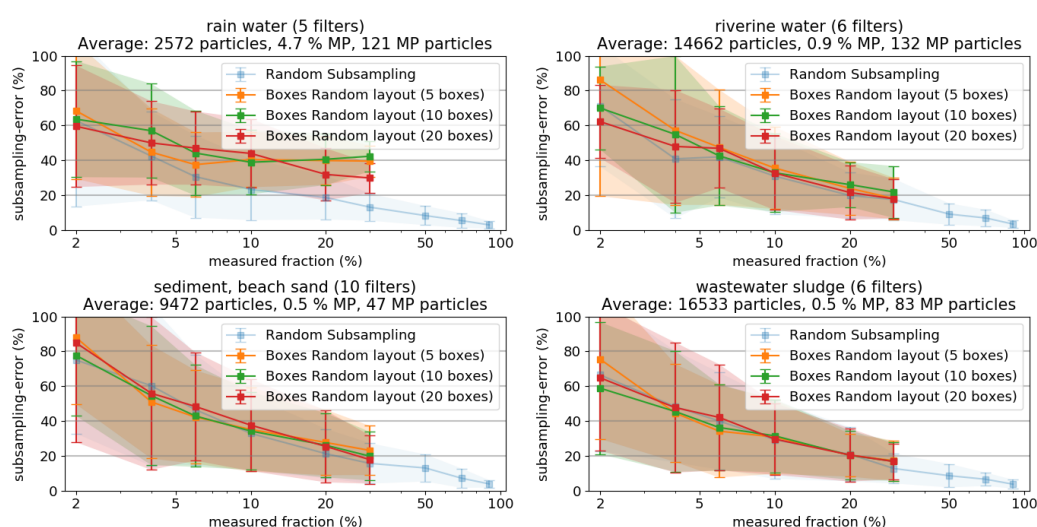
6 MP Error plots for box placement methods



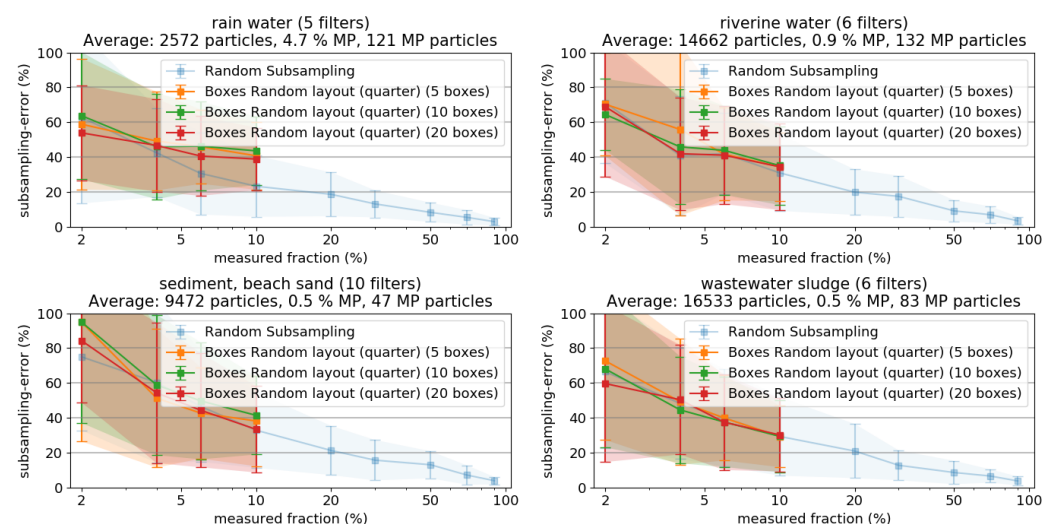
Supplementary Figure 7: Resulting subsampling errors and their standard deviation from box-based subsampling using the cross layout, as derived from samples from rainwater, river water, sediment and sludge, respectively.



Supplementary Figure 8: Resulting subsampling errors and their standard deviation from box-based subsampling using the spiral layout, as derived from samples from rainwater, river water, sediment and sludge, respectively.



Supplementary Figure 9: Resulting subsampling errors and their standard deviation from box-based subsampling using the random layout, as derived from samples from rainwater, river water, sediment and sludge, respectively.



Supplementary Figure 10: Resulting subsampling errors and their standard deviation from box-based subsampling using the random layout on a quarter of the filter, as derived from samples from rainwater, river water, sediment and sludge, respectively.



Model uncertainties of a storm and their influence on microplastics and sediment transport in the Baltic Sea

Robert Daniel Osinski, Kristina Enders, Ulf Gräwe, Knut Klingbeil, and Hagen Radtke

Leibniz Institute for Baltic Sea Research Warnemünde, Seestrasse 15, 18119 Rostock, Germany

Correspondence: Hagen Radtke (hagen.radtke@io-warnemuende.de)

Received: 6 April 2020 – Discussion started: 30 April 2020

Revised: 11 September 2020 – Accepted: 21 October 2020 – Published: 3 December 2020

Abstract. Microplastics (MPs) are omnipresent in the aquatic environment where they pose a risk to ecosystem health and functioning. However, little is known about the concentration and transport patterns of this particulate contaminant. Measurement campaigns remain expensive, and assessments of regional MP distributions need to rely on a limited number of samples. Thus, the prediction of potential MP sink regions in the sea would be beneficial for a better estimation of MP concentration levels and a better sampling design. Based on a sediment transport model, this study investigates the transport of different MP model particles, polyethylene-terephthalate (PET) and polyvinyl chloride (PVC) particles with simplified spherical sizes of 10 and 330 μm , under storm conditions. A storm event was chosen because extreme wave heights cause intense sediment erosion down to depths that are otherwise unaffected; therefore, these events are critical for determining accumulation regions. The calculation of metocean parameters for such extreme weather events is subject to uncertainties. These uncertainties originate from the imperfect knowledge of the initial conditions and lateral boundary conditions for regional models, which are necessary to be able to run a numerical model. Processes, which can be resolved by the model, are limited by the model's resolution. For the processes for which the model resolution is too coarse, parameterizations are used. This leads to additional uncertainty based on the model physics. This sensitivity study targets the propagation of uncertainty from the atmospheric conditions to MP erosion and deposition, on the basis of freely available models and data. We find that atmospheric conditions have a strong impact on the quantity of eroded and deposited material. Thus, even if the settling and resuspension properties of MP were known, a quantitative transport estimation by

ocean models would still show considerable uncertainty due to the imperfect knowledge of atmospheric conditions. The uncertainty in the transport depends on the particle size and density, as transport of the larger and denser plastic particles only takes place under storm conditions. Less uncertainty exists in the location of erosional and depositional areas, which seems to be mainly influenced by the bathymetry. We conclude that while quantitative model predictions of sedimentary MP concentrations in marine sediments are hampered by the uncertainty in the wind fields during storms, models can be a valuable tool to select sampling locations for sedimentary MP concentrations to support their empirical quantification. The purpose of this study is to support the strategic planning of measurement campaigns, as the model predictions can be used to identify regions with larger net deposition after a specific storm event.

1 Introduction

The presence of MP particles has been proven in a variety of different ecosystems (e.g. Huerta Lwanga et al., 2016; Andrady, 2011). MPs constitute potential transport vectors for toxic substances, both substituted chemicals during production and adsorbed environmental pollutants, which can be assimilated by aquatic organisms (Besseling et al., 2019). The pollution of the environment with these synthetic particles, which are foreign and incompatible with natural cycles, is happening at an unprecedented rate and contributes to the degradation of ecosystem services worldwide (Watkins et al., 2017). The relevance of these particulate pollutants for specific ecosystems cannot, however, be assessed when

drivers of their distribution are not understood and their current stocks remain unknown.

Currently, MP data collection from various environmental compartments is expensive and time-consuming; consequently, only small data sets are presently achievable. Here, numerical models, which are known and vigorously applied in sediment transport studies (e.g. Sassi et al., 2015), can help to complement sparse measurements. For this purpose, an initial data set is necessary to calibrate and validate the numerical models. The initial model set-up can be applied as a support tool for measurement campaign planning, as it can help identify regions in which net deposition can be expected. This is the major purpose of this study.

Plastic denotes a wide range of different polymer types with different density ranges. Among the most widely produced (PlasticsEurope, 2019) are polyvinyl chloride (PVC), which has a density of 1275 kg m^{-3} , and polyethylene-terephthalate (PET), which has a density of 1400 kg m^{-3} (Andrady and Neal, 2009); these two plastics were used as model particles in the present study.

During cyclone “Xaver” in October 2017, mean horizontal bottom water currents exceeded 0.5 m s^{-1} , e.g. in the Arkona Basin (Bunke et al., 2019). We expect that significant transport and sorting of larger and denser plastic particles only takes place under such storm conditions. This assumption is justified in this study by a 1 month model run including storm and calm conditions. The interest of this study is the identification of potential areas of accumulation of MP particles to support the planning of measurement campaigns by identifying potential areas of interest, because we assume that a stock of high-density plastic particles exists in Baltic Sea sediments.

Extreme events have a strong impact on particle transport (e.g. Bartholomä et al., 2009). The idea that storm events determine the relocation of settled MP is supported by existing knowledge from the amber hunting community. It has been observed that beach combing and jewellery hunting for amber only becomes profitable after strong wave and ocean current activity. Amber is a naturally occurring polymer with a density range between 1050 and 1150 kg m^{-3} (similar to MP) and is especially abundant in the Baltic Sea. It was produced a long time ago by the resin of trees and now forms a standing stock on the Baltic Sea seafloor. Amber was also taken into account in laboratory measurements by Shields (1936), who found that the initiation of motion of amber can be described by the Shields curve and is comparable to that of sediments.

Chubarenko and Stepanova (2017) compared the transport behaviour of amber with that of MPs and found dimensionless critical bottom shear stresses close to that represented by the Shields curve. They also found a variation depending on the plastic type and shape. Therefore, the Shields curve was adapted to calculate the critical shear stress.

A sediment transport model is applied in this study to simulate the transport of MP as suspended matter with sizes of the order of sand particles. Certain factors cannot be ac-

counted for, such as the plastic type and shape, which can influence the critical bottom shear stress (Chubarenko and Stepanova, 2017; Enders et al., 2019) and the settling velocity of particles (Khatmullina and Isachenko, 2017). Based on laboratory measurements using MPs down to 0.4 mm in size, Waldschläger and Schüttrumpf (2019) calculated a sinking formula depending on the particle shape. For simplicity, the standard Stokes formula (Stokes, 1851) for spherical particles is used here.

Although the critical bottom shear stress and the settling velocity are assumed to strongly impact the uncertainty in the transport behaviour, this initial study focuses on a quantification of the metocean uncertainty in the transport behaviour. There are several other approaches to estimate the transport of MPs (e.g. Ballent et al., 2013; Bagaev et al., 2017). These models are based on deterministic metocean products and metocean models. Our objective is instead to assess whether the relocation of MP particles during a single storm event is quantitatively predictable, or whether it is too sensitive to the meteorological uncertainties to allow for a sufficiently precise model estimation. If this uncertainty is too large, even precise knowledge of a particle’s sinking and erosion properties would not allow for an estimation of its transport.

A well-known method to quantify sensitivity to uncertainties in numerical models is the use of an ensemble approach. Ensemble forecasts have been used in operational weather prediction for more than 25 years (Buizza, 2018) and have also been successfully applied in different areas, such as aviation (e.g. Osinski and Bouttier, 2018), the energy sector (e.g. Taylor and Buizza, 2003), or hydrology (e.g. Pappenberger et al., 2008). An application of ensemble forecasts to quantify the uncertainty in the morphological impact of storms was proposed by Baart et al. (2011). Osinski et al. (2016) applied a windstorm tracking algorithm to the operational ensemble forecasts of the European Centre for Medium-Range Weather Forecasts (ECMWF) and demonstrated strong variation in the track as well as in the damage potential of the different realizations of historical storm events in the ensemble members. This range of uncertainty should also be reflected in the uncertainty in the transport of suspended matter. An ensemble of 30 members, produced by a mesoscale atmospheric model in non-hydrostatic mode, is applied in the presented study to estimate these uncertainties in the transport behaviour of MPs.

Existing studies on the transport of MPs in the marine environment are mainly based on a particle tracking approach (e.g. Jalón-Rojas et al., 2019b; Liubartseva et al., 2018). Jalón-Rojas et al. (2019a) showed the importance of applying a 3-D model to estimate MP transport. This is the case in this study, and an Eulerian approach was applied in our model, i.e. MP is stored as a concentration in grid cells and a bottom reservoir.

2 Data and models

For our assessment, we applied a four-step model chain, as illustrated in Fig. 1. Firstly, ensemble data based on stochastic perturbations were produced with the WRF-ARW (Weather Research and Forecasting Model in the Advanced Research WRF variant) atmospheric model to account for uncertainties in the representation of storm events. Secondly, the atmospheric fields were passed to the WAVEWATCH III® wind wave model. Thirdly, atmospheric and wave ensemble data were then applied to drive the GETM (General Estuarine Transport Model) regional ocean model. Finally, a transport module in GETM simulated the transport of PET and PVC with particle sizes of 10 and 330 μm . The WRF-ARW atmospheric model was applied here to produce an ensemble hindcast of a storm surge event in the Baltic Sea and to provide the necessary forcing fields for the wave and the ocean model. The simulation period covered 1–4 January 2019. This includes the storm Alfrida (the reader is referred to the ECMWF Severe Event Catalogue: <https://confluence.ecmwf.int/pages/viewpage.action?pageId=129123779>, last access: 2 April 2020) which moved across southern Sweden and especially hit the island of Gotland, where wind speeds of 27.5 m s^{-1} (10 Bft) were reached (The Local, 2019). Storms of this strength occur approximately two to three times per year in the Baltic Sea, although at different locations. WAVEWATCH III® was used to produce ensemble hindcasts of wave parameters based on the WRF-ARW output. GETM was driven by the ensemble hindcasts of the corresponding atmospheric and wave parameters from the unperturbed and perturbed model runs.

2.1 The WRF-ARW atmospheric model

Version 4.1.1 of the WRF-ARW atmospheric mesoscale model (<https://github.com/wrf-model/WRF/releases>, last access: 14 March 2020) (Skamarock et al., 2019) was used in this study for ensemble hindcasting. A region slightly larger than the Baltic Sea was used with a horizontal resolution of about 0.063° , and output was written every 5 min. Vertically, 89 pressure levels were applied up to 50 hPa, corresponding to levels 2 to 90 in the ERA5 reanalysis (Copernicus Climate Change Service, C3S). Initial and lateral boundary conditions originated from the ERA5 reanalysis. Osinski and Radtke (2020) tested different ensemble generation strategies with WRF-ARW driven by ERA5 and compared the outcome with the uncertainty measure provided by the ERA5 reanalysis. As demonstrated in Osinski and Radtke (2020), stochastic perturbations, namely stochastically perturbed parameterization tendencies (SPPT; Buizza et al., 1999) and stochastic kinetic energy backscatter (SKEB; Shutts, 2005), were used here to produce a small ensemble of 30 members to study the impact of the uncertainty in the atmospheric forcing on the transport patterns, which includes random perturbations of the lateral boundary conditions (Skamarock et al., 2019).

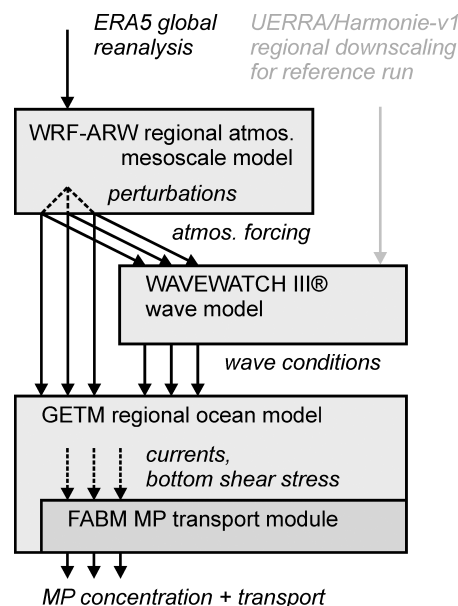


Figure 1. Schematic overview of the model chain used in this study.

Instead of validating the atmospheric data against observations, the wind data were validated indirectly by the wave model output. A visual comparison of the WRF-ARW wind fields against UERRA/HARMONIE-v1 and ERA5 data can be found in Osinski and Radtke (2020).

Sources of uncertainty in atmospheric model predictions originate from the initial conditions and from the model physics; for a regional model, they also originate from lateral boundary conditions. Osinski and Radtke (2020) compared different ensemble generation methods and proposed the use of the ERA5 data from the Ensemble of Data Assimilations as initial conditions to allow for a spread from the start of the simulation. The initial conditions in the presented study are based on the high-resolution ERA5 reanalysis, and the model approach includes perturbations of the model physics and the lateral boundary conditions. In contrast, the desired spread needs to develop in the model ensemble in the method chosen here. We selected this method to keep our results comparable with a potential future application in forecast mode. While we ran the model for a storm event in the past, the same could be done for a predicted storm, possibly based on a deterministic forecast product.

2.2 The WAVEWATCH III® wind wave model

Wave-induced bottom shear stress is an important driver for the resuspension of bottom sediments and, potentially, of high-density MPs on the seafloor, as investigated in this study. To be able to prescribe wave parameters at high spatial and temporal resolution, the WAVE-

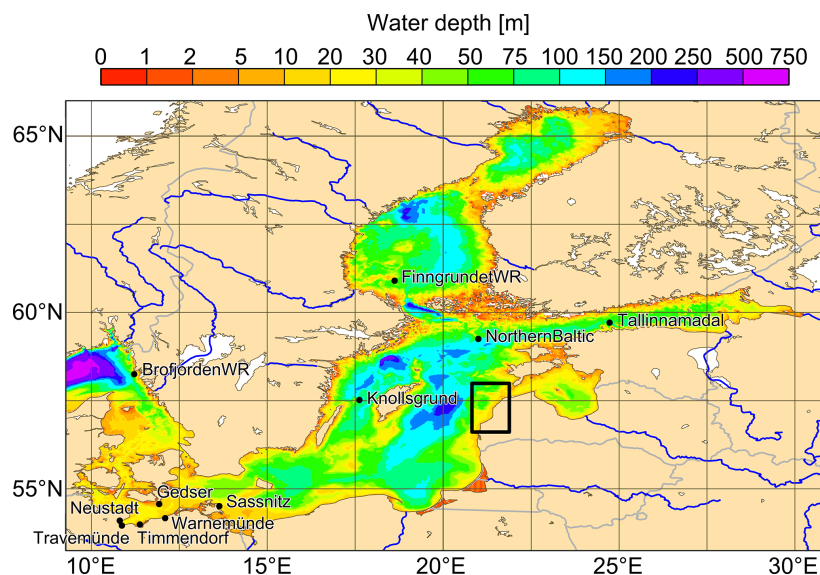


Figure 2. Bathymetry [m] of the 1 nautical mile WAVEWATCH III[®] set-up. Black dots show stations for the validation of water level and significant wave height. The black rectangle shows the subregion for plots of the transport simulation results.

WATCH III v6.07[®] (<https://github.com/NOAA-EMC/WW3> third-generation spectral wind wave model, last access: 14 March 2020) (Tolman, 1991; The WAVEWATCH III[®] Development Group (WW3DG), 2019) was applied in a three-level one-way nested configuration. The model domain with the highest resolution is based on the same grid as in the GETM model (Gräwe et al., 2019). Dissipation and wind input were based on the formulation of Ardhuin et al. (2010), and the SHOWEX bottom friction scheme was applied following Ardhuin et al. (2003). For the latter, a map of the D50 (median diameter of the particle size distribution) sediment grain size was prescribed based on the European Marine Observation and Data Network (EMODnet; <http://www.emodnet-geology.eu/>, last access: 14 March 2020) data. The wave spectrum was discretized in the same way as in the ERA5 reanalysis: 24 directions starting at 7.5° with a 15° direction increment, and 30 frequencies starting at 0.03453 Hz geometrically distributed with a step of 1.1. A set-up with a 0.1° resolution covering the North Sea and a small part of the eastern Atlantic Ocean was used to produce boundary conditions for the Baltic Sea set-up at the border with the North Sea. The 0.1° model was nested into a set-up for the Atlantic Ocean with a 0.5° resolution. The GEBCO_2014 Grid, version 20150318 (<http://www.gebco.net>, last access: 14 March 2020), was used as bathymetry for the Atlantic and North Sea set-ups. The Baltic Sea set-up had a resolution of 1 nautical mile with a bathymetry based on the work of Seifert et al. (2001). The 0.5° set-up is driven by ERA5 winds and the ERA5 sea ice cover fraction. For the 0.1° set-up, UERRA/HARMONIE-

v1 (Ridal et al., 2017) winds and the ERA5 sea ice cover fraction were used because of their higher spatial resolution. The Baltic Sea set-up was driven by two data sets: the UERRA/HARMONIE-v1 wind for a reference simulation, and the wind produced with the WRF-ARW wind ensemble for the MP ensemble simulations. Sea ice was taken from the Ostia reanalysis (<http://marine.copernicus.eu/services-portfolio/>, last access: 29 November 2020). An obstruction grid based on the GSHHS (Global Self-consistent, Hierarchical, High-resolution Shorelines) (Wessel and Smith, 1996) coastline data set has been generated with the Gridgen software (<https://github.com/NOAA-EMC/gridgen>, last access: 14 March 2020) to take unresolved orography into account.

Observation data from buoys available from the Copernicus Marine Environment Monitoring Service (<http://marine.copernicus.eu/services-portfolio/access-to-products/>, last access: 14 March 2020) (CMEMS) were used for validation and calibration. A comparison with station data in Fig. 3 shows good agreement in the significant wave height as well as verification scores over January 2019 (Table 1). The spread in the ensemble is visible at all stations and is expected to provoke differences in the bottom shear stress, leading to differences in the resuspension.

Waves affect the seafloor until a water depth of about half the wave length. The dominant wavelength in the Baltic Sea is between 20 and 70 m and can reach up to 130 m (Kriaučiūnienė et al., 1961).

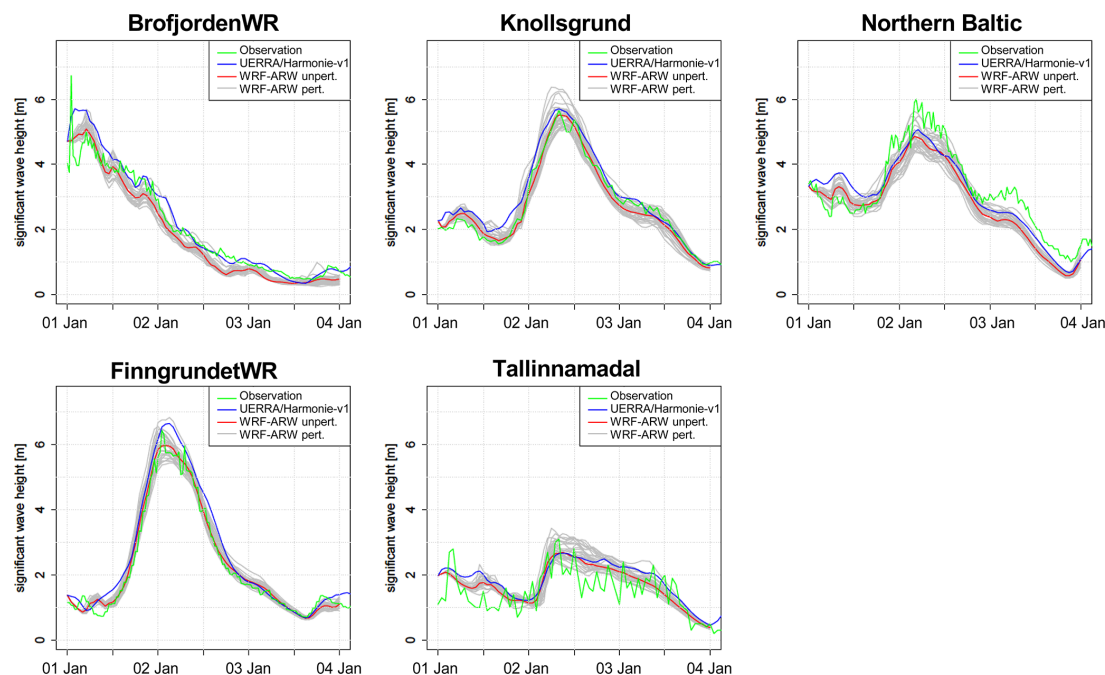


Figure 3. Significant wave height at five stations from the 1 nautical mile WAVEWATCH III[®] model run. Wind data are from UERRA/HARMONIE-v1, WRF-ARW is unperturbed, and the 30 WRF-ARW members are generated with stochastic perturbations.

Table 1. Verification scores – root mean square error (RMSE), scatter index (SI, Zambresky, 1989), and correlation (COR) – for significant wave height simulated by WAVEWATCH III[®] driven by UERRA/HARMONIE-v1 for January 2019.

Station	Bias [m]	RMSE	SI [%]	COR
BrofjordenWR	0.08	0.26	22.64	0.96
Knollsgrund	−0.02	0.20	15.25	0.98
Northern Baltic	−0.11	0.29	18.33	0.96
FinngrundetWR	0.01	0.24	18.05	0.98
Tallinnamadal	0.22	0.41	61.75	0.85

2.3 The GETM regional ocean model

GETM (General Estuarine Transport Model; Burchard and Bolding, 2002; Hofmeister et al., 2010; Klingbeil and Burchard, 2013) is an ocean model specifically designed for the coastal ocean (see review by Klingbeil et al., 2018). In the present study, GETM was applied to the Baltic Sea with the model set-up of Gräwe et al. (2019), on the same 1 nautical mile grid as the innermost WAVEWATCH III[®] nest. The model domain is shown in Fig. 2. The original set-up was extended by coupling it to FABM (Framework for Aquatic Biogeochemical Models; Bruggeman and Bolding, 2014) in order to consider sediment and MP. For an accurate 3-D transport of these quantities, GETM provides high-order advec-

tion schemes with reduced spurious mixing (Klingbeil et al., 2014), a state-of-the-art second-moment turbulence closure for vertical mixing from GOTM (General Ocean Turbulence Model; Burchard et al., 1999; Umlauf and Burchard, 2005), and flow-dependent lateral mixing (Smagorinsky, 1963). Numerical mixing leads to an unrealistically high diffusion of transported concentrations, reducing the peak concentrations and overestimating the area in which tracers spread. The accuracy of the model is further increased by adaptive vertical coordinates that guarantee an optimal vertical mesh aligned to the dynamic boundary layers and to the stratified interior (Gräwe et al., 2015). Air–sea fluxes were calculated from the meteorological data provided by the atmospheric model according to the bulk formulas of Kondo (1975). Based on the data provided by the wave model, GETM calculated the mean and maximum combined wave- and current-induced bed stress during a wave cycle. The latter was used in FABM for the erosion of sediment and MPs from the bottom pool (see Sect. 2.4). A realistic initial state as the starting condition for the hydrodynamical model was obtained by prolonging the simulations from Gräwe et al. (2019) with the UERRA/HARMONIE-v1 atmospheric data set. Further details about open boundary conditions and river discharge can be found in Gräwe et al. (2019).

A detailed validation of the model set-up can be found in Gräwe et al. (2019) and Radtke et al. (submitted). For demonstration purposes, only the spread in sea sur-

face elevation due to the different atmospheric forcing sets is shown here (Fig. 4). A verification of the water level at different stations from EMODnet (<https://www.emodnet-physics.eu/>, last access: 14 March 2020) showed satisfactory performance for both forcing data sets (WRF-ARW and UERRA/HARMONIE-v1). A large spread is also visible in the water level, especially at the peak of the surge.

The ensemble generation in the GETM model in this study is only based on the ensemble hindcasts of the atmospheric and wave parameters driving the model runs. Brankart et al. (2015) showed that stochastic perturbations in the ocean model are also important for uncertainty estimation. The uncertainty in the ocean currents could therefore be underestimated.

2.4 Microplastic representation

In GETM and FABM, sediment and MPs are represented as Eulerian concentration fields. GETM simulated the 3-D transport of the pelagic concentrations, whereas the FABM model calculated the interaction with the corresponding bottom pools due to erosion and deposition and provided settling velocities to GETM. In FABM, a model for non-cohesive sediments (see Sassi et al., 2015) was used to calculate erosion, settling, and deposition of both sediment and MPs. The different transport was caused by the lower densities of MPs, which exceed that of the ambient water, i.e. we only considered sinking particles. This study focuses on model MPs with the sizes and densities reported by Stuparu et al. (2015): 10 and 330 μm for both PVC with a density of 1275 kg m^{-3} and PET with a density of 1400 kg m^{-3} . To study the impact of density and particle size on the uncertainty in the transport, additional densities of 1100, 1200, and 1300 kg m^{-3} and particle sizes of 200, 250, 300, and 350 μm were tested. As our main aim is to support measurement campaigns and larger particles are easier to sample, we focus our attention on particles above 300 μm .

The simulations in this study started from homogenous bottom pools of 1 kg m^{-2} as a purely hypothetical reference value as well as zero suspended material in the water column. Rivers and open boundaries were assumed to not import material into the model domain. MP transport in the model is affected by wave activity and different types of currents. Tidal currents are represented, but they only play a role in the Danish straits, as the interior of the Baltic Sea is non-tidal. Turbidity currents cannot be represented in our model, as the concentration of suspended matter has no influence on seawater density in the model. Thermohaline circulation, in contrast, is fully taken into account.

3 Results and discussion

3.1 MP relocation and its uncertainty

After a 2 d storm surge event, a rearrangement of particles could be observed in the model with some locations dominated by erosion and others by deposition. This can be seen by the change in the amount of MP stored in the bottom pool (PET and PVC with a diameter of 330 μm). To demonstrate the range of uncertainty in the transported amount of MP, two different grid cells in the Gotland Basin were selected (Fig. 5): 57.69° N, 21.35° E (Fig. 6a–b) as a net erosion location, and 57.66° N, 21.32° E (Fig. 6c–d) as a net deposition location. Relative to the initial concentration, net erosion varied between 39 % and 72 % for PVC and between 16 % and 45 % for PET. Net accumulation varied between –13 % and 38 % for PVC and between 22 % and 34 % for PET. Thus, for PVC in the deposition grid cell (Fig. 6c), weak erosion is visible in some ensemble members, whereas the majority of the ensemble members show net deposition at this location. For the denser PET, the uncertainty range is smaller than for PVC, implying that its transport is less sensitive to uncertainties in the wind fields and more predictable. Still, the transported amount, even in this particle class, varies by around a factor of 2 between realizations, showing that a realistic quantitative estimation of MP transport is impossible in ocean circulation models, even if the precise sinking, settling, and resuspension properties of the MP particles were perfectly known.

3.2 Erosion and deposition areas

Now we consider the spatial patterns where erosion and sedimentation take place. The spatial pattern in four selected ensemble members and the deterministic runs is shown in Fig. 7. We chose four members with a considerable spread in the simulated wave height (Fig. 7g). The overall spatial pattern is very similar between the different realizations. The main impact of the metocean uncertainty lies in the amount of the transported material. The perturbations of the atmospheric model also produce deviations in the track of the storm between ensemble members, which impacts the direction of ocean waves and currents and, in turn, the direction in which the bottom shear stresses are directed. These findings indicate that the bathymetry has a predominant impact on the region where erosion and deposition take place, as the locations are insensitive to changes in the track of the storm. For this specific storm surge event and selected region, net deposition took place on the south-western sides of ridges, and net erosion took place on the north-eastern sides. Model MP with a diameter of 330 μm in deeper regions, below 50 m, was completely unaffected. It is well known that water depth plays a major role in sediment erosion by waves, as deep-water waves (with wavelengths much shorter than the water depth) show an exponential attenuation in their velocity am-

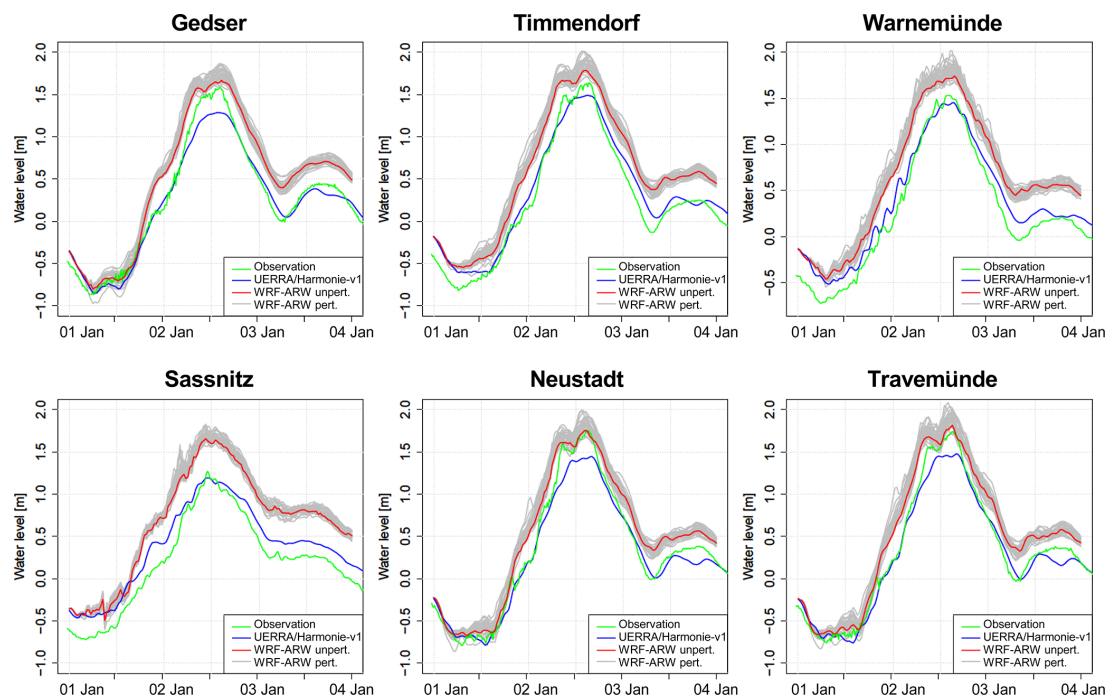


Figure 4. Water level at six stations with the 1 nautical mile GETM model; atmospheric data from UERRA/HARMONIE-v1, WRF-ARW is unperturbed, and the 30 WRF-ARW members are generated with stochastic perturbations.

plitude with depth (e.g. Kundu and Cohen, 2001). Our findings suggest that this causes stability in the spatial patterns of MP transport against changes in the wind forcing and makes the areas where erosion and deposition take place during a specific storm event predictable.

The uncertainty ranges of the spatial pattern of the model results were further investigated by means of the ensemble statistics composed of the mean, minimum, and maximum of each individual grid cell of all ensemble members (Fig. 8). The net effect – whether the location was characterized by deposition or erosion – appeared largely consistent for the entire uncertainty range. Only a few locations showed deviations from this finding where some ensemble members shifted between weak erosional and depositional net effects. The larger extent of the erosional areas was due to more severe representations of the storm event in some ensemble members. Overall, these findings suggest stability in spatial patterns of MP transport against changes in the wind forcing. Areas of erosion and deposition during a specific storm event are predictable.

3.3 Effect of particle size on transport uncertainty

Next, we investigate the effect of particle size on the uncertainty in the transport by reducing the size of the particles to $10\ \mu\text{m}$. The small PET particles show a net erosion across almost the whole model domain due to slower reset-

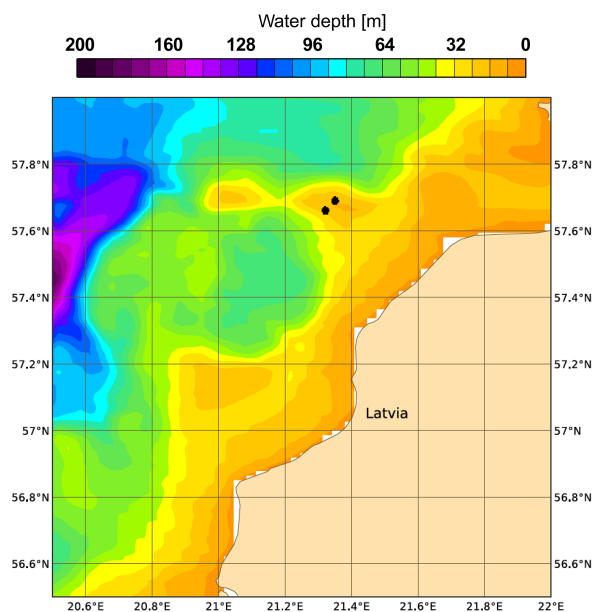


Figure 5. Bathymetry [m] of the subregion for which the model results are presented. Black dots indicate the locations of two selected grid cells for later reference.

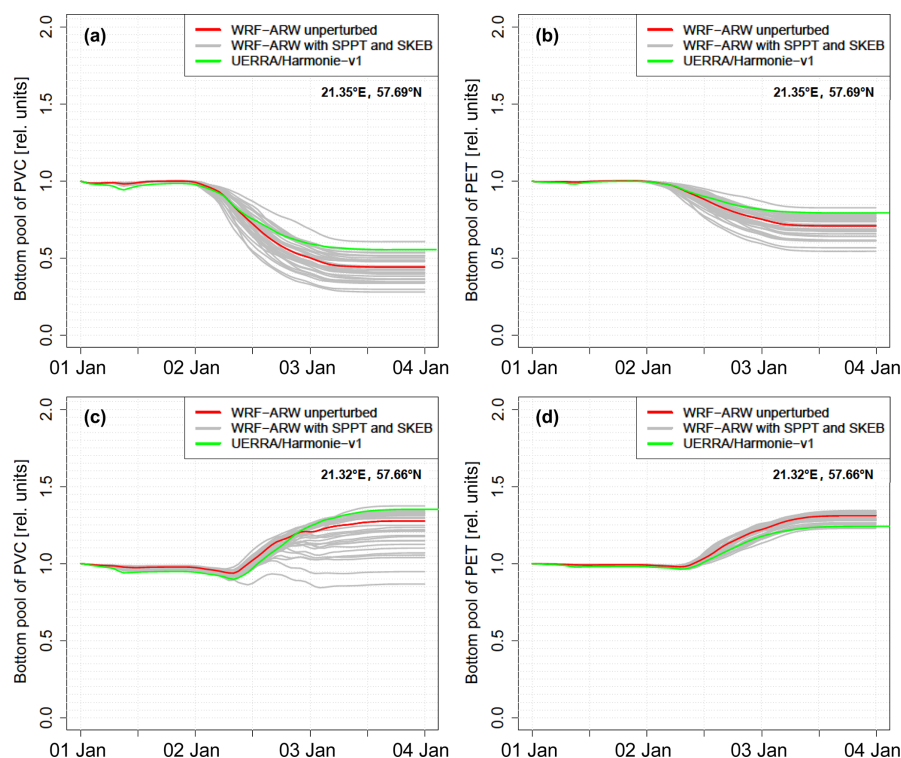


Figure 6. Changing bottom concentration of PVC (a, c) and PET (b, d) particles with a 330 µm diameter in the two grid cells indicated in Fig. 5, relative to the initial concentration. The different curves show 30 perturbed runs and 1 unperturbed run with WRF atmospheric forcing and another simulation with UERRA/HARMONIE-v1 forcing. Panels (a) and (b) show a grid cell predominated by processes of net erosion, whereas panels (c) and (d) show a cell with net sedimentation.

tlement. That is, they are still found in the water column up to 1.5 d after the storm (at the end of the simulation). This partly explains the large difference between the ensemble minimum and maximum (Fig. 9b, c): When sedimentation takes longer, quantitative differences in erosion strength will result in larger transport deviations, as the material can be advected further. This finding is also supported by theory on sediment transport: smaller particles (if unconsolidated) are suspended under lower shear stress levels and also require calmer metocean conditions to deposit. Thus, the uncertainty in MP transport appears to strongly depend on the particle diameter and density.

To find out whether this is a systematic effect, the uncertainties in the amount of transported material dependent on the particle properties size and density were investigated in more detail. These relationships were studied based on sensitivity runs with 30 ensemble members for (1) PVC with grain sizes of 200, 250, 300, and 350 µm as well as (2) 330 µm MP with different densities of 1100, 1200, 1300, and 1400 kg m⁻³ (Fig. 10a, b). The seafloor concentrations at the end of the model run deviate between the ensemble members. Relative deviations from the ensemble mean were cal-

culated. Figure 10c and d show that the relative uncertainty increases with decreasing density and/or particle diameter, with the exception of the 1100 µm MP class, which shows a smaller uncertainty as it is almost completely resuspended at the chosen location. We conclude that the uncertainty in the amount of transported material on the seafloor at a specific time depends strongly on the properties of the transported material. Thus, the application of an ensemble approach (using more than one model realization to predict transport pathways) is especially important if finer and lighter material is to be represented in future model applications.

3.4 Pathways of atmospheric uncertainty propagation

In the following, the mechanism by which the atmospheric uncertainty affects the MP transport is identified. In our model, this can be caused (a) by influencing the wave height, which changes the bottom shear stress and, therefore, MP mobilization, or (b) by directly affecting the ocean circulation through factors such as momentum input, thereby influencing both mobilization and transport. We focused on these two major pathways and attempted to distinguish their influence. The possibility of interlinkage by wave–current in-

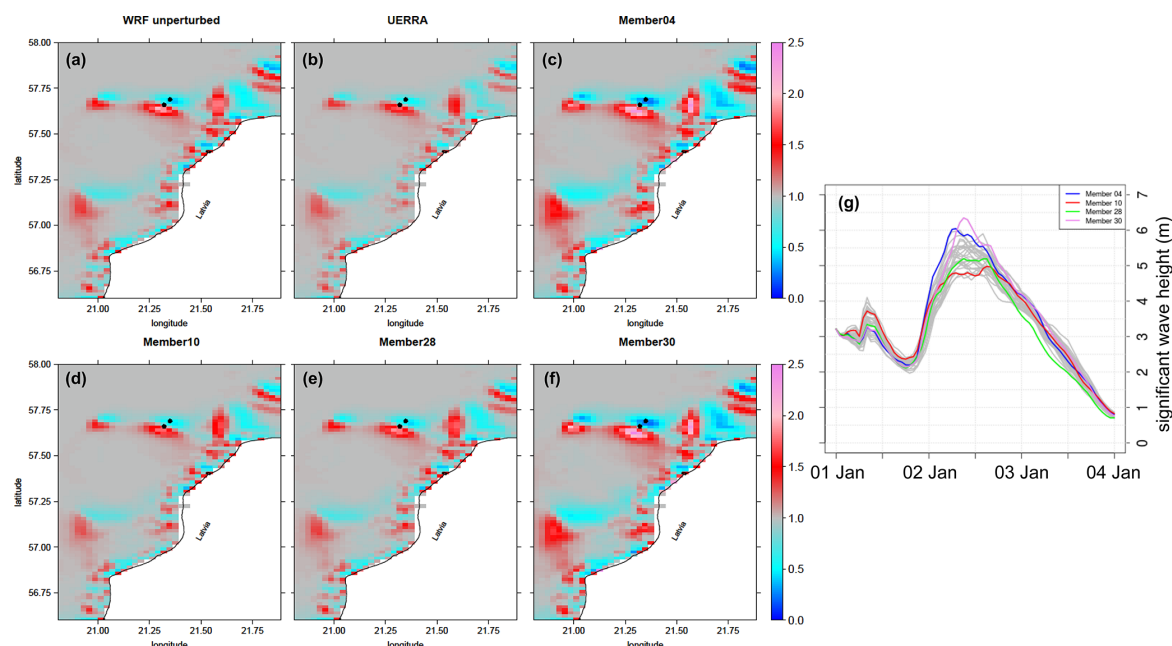


Figure 7. Seabed concentration of PVC with a 330 µm diameter on 3 January 2019 at 12:00 UTC, i.e. after the storm surge event in the model, relative to the homogenous initial concentration. Individual panels show the unperturbed WRF run (a), the model driven by UERRA/HARMONIE-v1 (b), and four selected WRF ensemble members (c–f). Dots show the locations of the grid cells selected in Fig. 6. (g) Time series of the significant wave height [m] at the position of the dot in the other figures with net erosion.

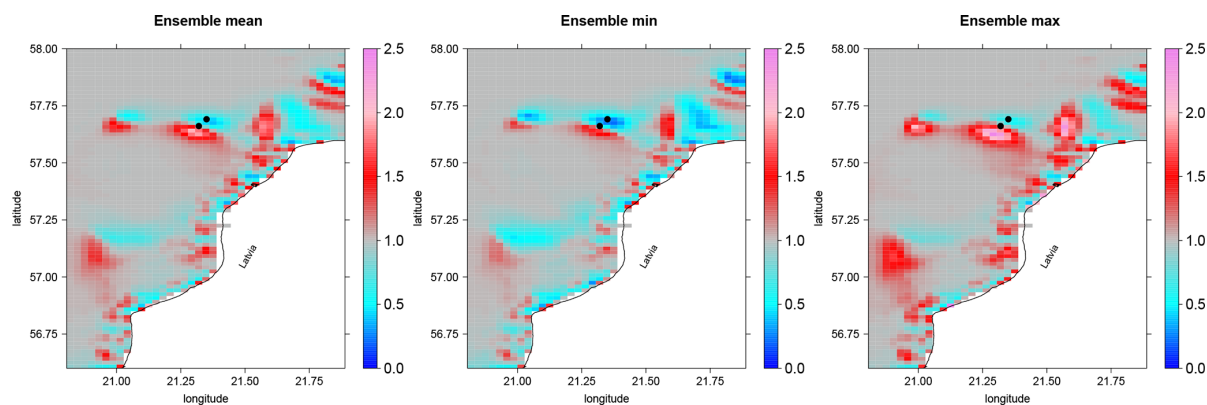


Figure 8. Ensemble mean, minimum, and maximum of the seabed concentration of PVC with a 330 µm diameter on 3 January 2019 at 12:00 UTC, i.e. after the storm surge event in the model, relative to the homogenous initial concentration. Dots show the locations of the grid cells selected in Fig. 6.

teraction is neglected in the present model cascade. To estimate the respective uncertainties of MP transport of the two above-mentioned pathways, an ensemble driven with the wave data from the unperturbed WRF-ARW run with the perturbed WRF-ARW atmospheric forcing and vice versa (with perturbed wave data and unperturbed atmospheric data) has been conducted. By comparing (Fig. 11) the outcome with

the original ensemble, where both perturbed atmospheric and wave data were used, it can be seen that the impact of the wave field depends on the properties of the transported material. The lighter or smaller the MP, the more important the impact of the wave uncertainty on the amount of transported material. For denser and larger MP, the uncertainty in the di-

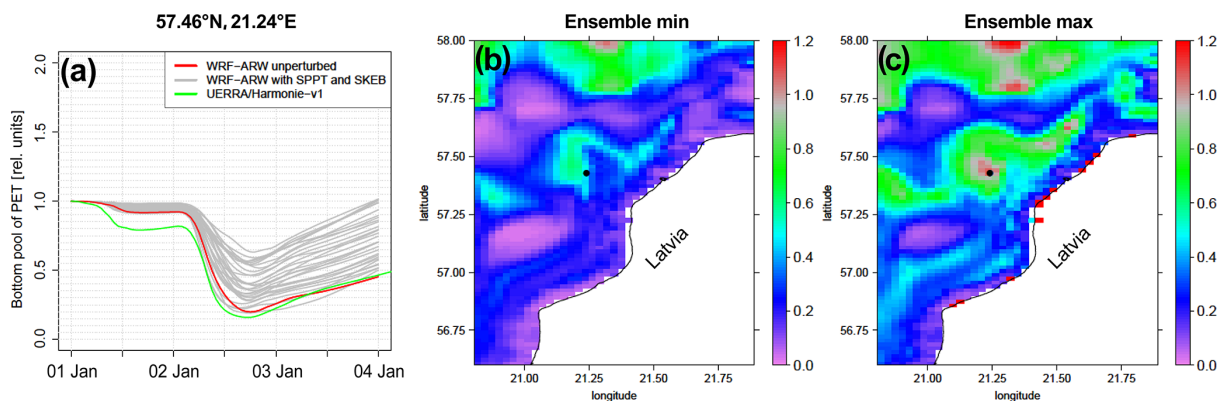


Figure 9. (a) Change in the seafloor concentration of PET particles with a 10 μm diameter in one selected grid cell in 30 perturbed runs and 1 unperturbed run with WRF forcing and 1 run with UERRA/HARMONIE-v1 forcing. (b) Ensemble minimum and (c) ensemble maximum on 4 January 2019 at 00:00 UTC (at the end of the simulation). All concentrations are relative to the homogenous initial concentration. The black dots show the locations for the time series plots.

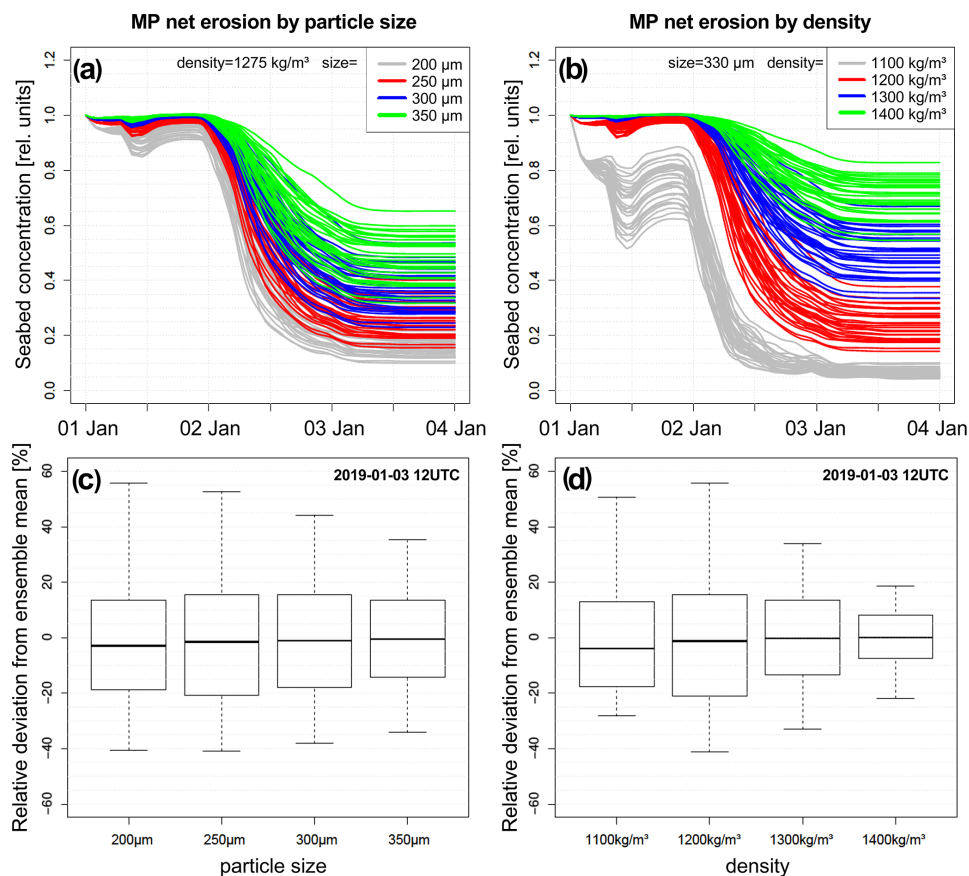


Figure 10. Time series of 30 ensemble members at 57.69° N, 21.35° E for (a) different MP sizes and (b) different MP densities. (c, d) Box-and-whisker plots show the uncertainty in the concentration of material on the seabed, expressed as a relative deviation of the individual ensemble members from the ensemble mean.

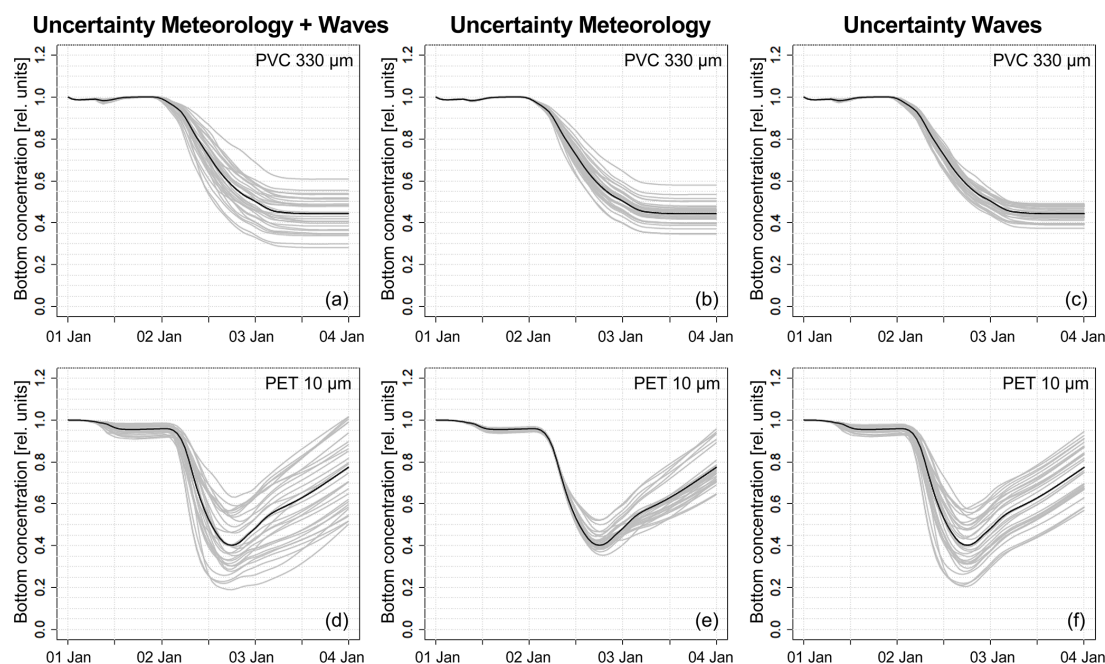


Figure 11. Spread of runs with varying atmospheric forcing and/or varying wave forcing for PVC with a 330 μm diameter (**a**, **b**, **c**) and PET with a 10 μm diameter (**d**, **e**, **f**), for the bottom concentration at 57.69° N, 21.35° E (see Fig. 9) relative to the initial value.

rect effect of atmospheric uncertainty on hydrodynamics is predominant.

3.5 Importance of storms for MP transport

Higher-density MPs of about 300 μm diameter were only transported under severe storm conditions, as demonstrated in Fig. 12. The continuation of the simulation for the rest of January 2019 caused almost no further erosion or deposition. This confirms the assumption regarding the importance of extreme events for MP transport, which complicates its direct empirical determination. Budget methods will be required to empirically determine quantities of transported MP. A budget method relates (a) the input and (b) the output of a quantity to (c) changes in its mass, e.g. inside an area of interest. If two of the three values are known, the third one can be determined. That is, transport rates might be more reliably derived from observed amounts before and after storm events than by multiplying abundances of suspended MP by instantaneous volume transports, both of which might show strong temporal variation during extreme weather conditions.

3.6 Similarities between MP and sediment transport

The finding that spatial patterns of MP can be reliably predicted by ocean models, while the quantitative estimation of MP is prone to considerable uncertainties shows that additional approaches are required for a more reliable estima-

tion of large-scale MP concentration levels. Here, the recently found MP–sediment proxy postulated by Enders et al. (2019), which is based on correlations between certain high-density polymer size fractions ($> 1000 \text{ kg m}^{-3}$, $> 500 \mu\text{m}$) and sediment grain size fractions, would be an achievable method. Estimations of MP levels can be based on a relatively small in situ data set and extrapolated to larger spatial scales by using the MP–sediment correlates. Lower densities of MP ($1000\text{--}1600 \text{ kg m}^{-3}$) compared with sediments (quartz: 2650 kg m^{-3}) are offset by a larger size. This relationship was explained by comparable threshold bed shear stresses (and thus erosion rates) between these size fractions, which appeared to be the predominant mechanism determining the sorting in the described study area (Warnow Estuary, Baltic Sea, Germany; Enders et al., 2019). Although the MP size ranges covered in the present study were below those investigated by Enders et al. (2019), it is assumed that similar patterns can be found for smaller size ranges. Indeed, in the present study, after the storm surge event, model PVC with a diameter of 330 μm co-occurred with 64 μm sediment grains, as apparent by the high correlation coefficient shown in Fig. 13. This correlation is found to be largely explained by similar erosion rates (Fig. 12b), whereas bottom concentrations, predominantly determined by deposition, are also influenced by the settling velocity of particles and, thus, differ slightly (higher amounts of PVC). Therefore, it is expected that areas largely influenced by the settling of MP show a

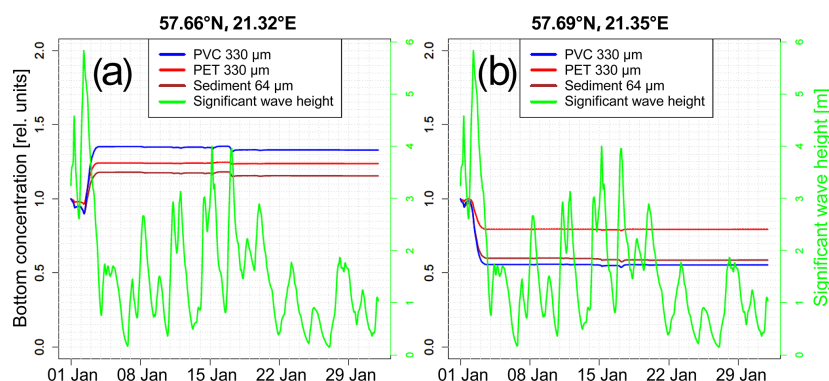


Figure 12. Evolution of the amount of PET and PVC with a 330 µm diameter and sediment with a 64 µm diameter on the seafloor during January 2019, starting from initial amount of 1 kg m^{-2} , at two grid cells, (a) with net deposition and (b) with net erosion.

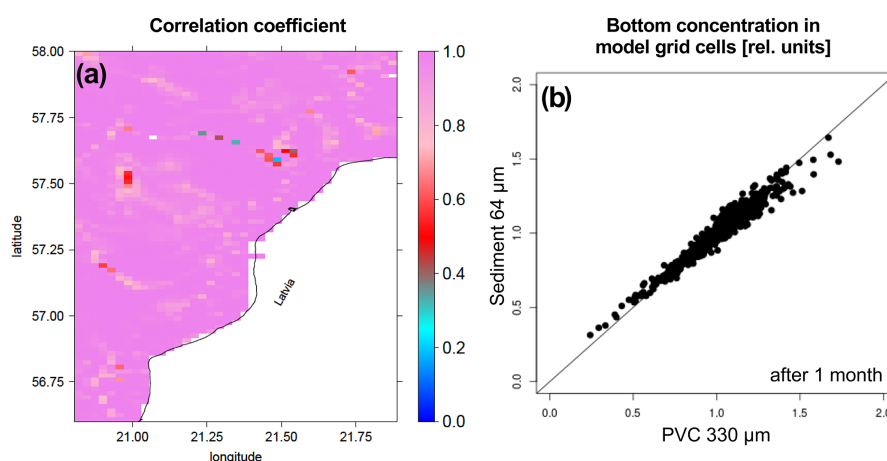


Figure 13. (a) Pearson correlation between the time series of bottom concentrations of PVC with a 330 µm diameter and sediment with a 64 µm diameter for January 2019. (b) Scatter plot of bottom concentrations after the 1-month simulation. Concentrations are given relative to the homogenous initial concentration.

larger difference in the expected MP–sediment size relation than described by the current MP–sediment proxy. For instance, larger (and/or heavier) MP particles than 330 µm PVC (such as PET) would be closer to the deposition rate of sediment grains of 64 µm (Fig. 12a). Existing maps of sediment substrate type, which typically differentiate between median grain sizes above and below 63 µm (e.g. EMODnet, 2020), may therefore also provide information about the MP concentrations to be expected. However, as this investigation is purely based on our model results with the above-mentioned uncertainties, in situ measurements are inevitable to further research the influences on this MP–sediment proxy.

4 Conclusions

A storm surge event in the Baltic Sea in January 2019 has been hindcast by a four-step probabilistic model chain started from an homogeneous initial MP distribution. The model validation showed a good performance for water level and significant wave height compared with different station data.

A strong variation in the amount of transported MP between ensemble members was found. This illustrates that quantitative modelling of MP transport during storm events already exhibits substantial uncertainty due to uncertainties in meteorological forcing fields (e.g. wind speeds). A test with different particle sizes and densities showed a dependence of the uncertainty in the transport on the particle properties. The impact of the metocean uncertainty on sediment and MP transport increases with decreasing particle density and/or size.

The spatial distribution pattern where material was eroded or accumulated in the model runs was stable against the atmospheric perturbations, illustrating the capability of a numerical model to identify regions of interest where seafloor sampling of MP concentrations is promising.

The demonstrated procedure could also be applied in forecast mode, by exchanging the ERA5 reanalysis data used in this study for data such as the freely available GFS forecasts (https://www.emc.ncep.noaa.gov/emc/pages/numerical_forecast_systems/gfs.php, last access: 14 March 2020). As a synoptic-scale winter storm event can be well predicted at medium-range timescales (3–5 d), this would allow for the production of ensemble simulations of MP transport a couple of days in advance in order to identify sampling regions, as a strategic support tool for measurement campaigns. The impact of the uncertainty from the lack of knowledge on settling velocities and critical bottom shear stresses would then have to be taken into account. One idea to reduce the necessary computational resources is a clustering of the atmospheric ensemble data and driving the rest of the model chain (wave and ocean model) with a reduced set of representative ensemble members.

As a consequence of the insensitivity of the location of erosional and depositional areas to the uncertainty in the metocean forcing and a substantially smaller transport during moderate conditions, this study indicates that it would, in principle, be possible to construct a map of the spatial distribution of high-density MP particles in the Baltic Sea using long model runs containing several storm events. Differences between storm events might be larger than the uncertainty in a single event. To get a more general picture of erosional and depositional regions in the Baltic Sea, other storm events with different tracks also have to be taken into account.

The demonstrated ensemble approach can also be useful for other applications, such as implementation in the maritime transport sector. After a strong storm event, it could help to predict whether it would still be possible for large vessels to enter a harbour or whether the morphodynamic changes are so strong that dredging would be necessary.

Appendix A: Mathematical description of the particle sinking and erosion model

Sinking velocity of the particles is initially calculated using the Stokes formula:

$$w_{\text{Stokes}} = \frac{gD^2}{18\nu} \frac{\rho_p - \rho_w}{\rho_w}, \quad (\text{A1})$$

where g is the gravitational acceleration, D is the particle diameter, ν is the kinematic viscosity of water, and ρ_p and ρ_w are the densities of the particle and the water respectively. To correct for larger particles whose sinking velocity would be overestimated by the Stokes formula, a Newtonian correction is applied by an iterative algorithm:

- a Reynolds number is calculated as $Re = 0.64w_{\text{sink}}D/\nu$;
- a relative drag coefficient is derived from this Reynolds number as $C_D = 18.5/Re^{0.6}$ following Perry and Chilton, as cited by Khalaf (2009);
- the updated velocity is calculated as $w_{\text{sink}} = \sqrt{\frac{4gD}{3C_D} \frac{\rho_p - \rho_w}{\rho_w}}$, which can be understood as a weighted geometric mean between the two velocities w_{Stokes} and ν/D .

This correction makes large particles sink slower than the Stokes formula suggests. However, we also erroneously applied the correction to the small particles where it resulted in an undesired upward correction. This has no effect on particle erosion, but it accelerates redeposition, which may even lead to an underestimation of the influence of meteorological uncertainty for the small particles in our study.

Erosion takes place when the actual shear stress exceeds the critical shear stress. To determine the critical shear stress, we follow the Shields curve, using the version that was corrected by Soulsby (1997). First, we calculate the dimensionless particle diameter D_* , which relates the particle diameter D to a viscosity-determined length scale, following Rijn (1984):

$$D_* = \sqrt{3} \frac{g}{\nu^2} \frac{\rho_p - \rho_w}{\rho_w} D, \quad (\text{A2})$$

where ν is the kinematic viscosity of water, ρ_p is the particle density, and ρ_w is the water density. Then, we calculate the critical Shields parameter for non-cohesive grains, θ_{cr} (also dimensionless), following Soulsby (1997) as cited by Ziervogel and Bohling (2003):

$$\theta_{\text{cr}} = \frac{0.3}{1 + 1.2D_*} + 0.055 \cdot (1 - e^{-0.02D_*}). \quad (\text{A3})$$

The critical shear stress can then be calculated as

$$\tau_{\text{cr}} = D(\rho_p - \rho_w)\theta_{\text{cr}}. \quad (\text{A4})$$

Table A1. Sinking velocities and critical shear stress in the model at 10 °C.

Diameter (μm)	Density (kg m^{-3})	Sinking velocity (mm s^{-1})	Critical shear stress (N m^{-2})
10	1275	0.15	0.006210895
330	1275	8.14	0.045142586
10	1400	0.20	0.009277999
330	1400	10.98	0.062337737

The actual shear stress is calculated from the wave-induced and the current-induced shear stress, τ_w and τ_c respectively. The current-induced shear stress itself, however, is also modified by the wave field, as it changes the bottom drag coefficient according to the DATA2 formula given by Soulsby (1997):

$$\tau_m = \left(1 + 1.2 \left(\frac{\tau_w}{\tau_c + \tau_w}\right)^{3.2}\right) \tau_c, \quad (\text{A5})$$

where τ_c is the shear stress induced by the current in the absence of waves. The shear stresses induced by currents and waves are combined depending on the angle α between currents and waves:

$$\tau^2 = \tau_w^2 + \tau_m^2 + 2\tau_w\tau_m\cos(\alpha). \quad (\text{A6})$$

If the actual shear stress exceeds the critical one, the deposited material becomes resuspended with first-order kinetics, i.e. proportional to its mass in the sediment pool.

The actual values for sinking velocities and critical stresses depend on temperature, as it influences sea water viscosity. Values for 10 °C are presented in Table A1.

Code and data availability. The WRF source code is available from <https://github.com/wrf-model/WRF/releases> (University Corporation for Atmospheric Research, 2020), WAVEWATCH III® is available from <https://github.com/NOAA-EMC/WW3> (NOAA Environmental Modeling Center, 2020), and the GETM code is available from <https://getm.io-warnemuende.de> (Klingbeil, 2020). ERA5 and the UERRA/HARMONIE-v1 reanalysis can be retrieved from the Climate Data Store at <https://cds.climate.copernicus.eu> (Copernicus, 2020).

Sample availability. The demonstrated model results can be obtained upon request from the corresponding author.

Author contributions. RO developed the concept of the ensemble approach, set up the wave and atmospheric model, and carried out the model runs. KE planned the sediment–MP proxy study. UG and KK created the ocean model set-up and provided technical assistance. HR planned the MP transport study and provided assistance with the ocean model set-up. All authors contributed to writing the paper.

Competing interests. The authors declare that they have no conflict of interest.

Acknowledgements. This study was financed by the BONUS MICROPOLL project; BONUS MICROPOLL received funding from BONUS (article 185), which was jointly funded by the EU and Baltic Sea national funding institutions. Knut Klingbeil acknowledges sub-project M5 “Reducing spurious diapycnal mixing in ocean models” of the Collaborative Research Centre TRR 181 “Energy Transfers in Atmosphere and Ocean” (project no. 274762653), funded by the German Research Foundation (DFG). The simulations run in this study consumed computing resources at the North German Supercomputing Alliance (HLRN). Observational data originate from the EU Copernicus Marine Environment Monitoring Service. The simulations in this study were generated using Copernicus Climate Change Service information (2018/2019). The research and work leading to the UERRA data set used in this work has received funding from the European Union Seventh Framework Programme (FP7/2007–2013; under grant agreement no. 607193). We would like to thank the WRF and WAVEWATCH III® developers for providing their models via GitHub, the editor Erik van Sebille, and the two reviewers Andrei Bagaev and Florian Pohl.

Financial support. This study was financed by the BONUS MICROPOLL project.

The publication of this article was funded by the Open Access Publishing Fund of the Leibniz Association.

Review statement. This paper was edited by Erik van Sebille and reviewed by Andrei Bagaev and Florian Pohl.

References

- Andrady, A. L.: Microplastics in the marine environment, *Mar. Pollut. Bull.*, 62, 1596–1605, 2011.
- Andrady, A. L. and Neal, M. A.: Applications and societal benefits of plastics., *Philos. T. R. Soc. Lon. B*, 64, 1977–84, 2009.
- Ardhuin, F., Herbers, T. H. C., O’Reilly, W., and Jessen, P.: Swell Transformation across the Continental Shelf. Part I: Attenuation and Directional Broadening, *J. Phys. Oceanogr.*, 33, 1921, [https://doi.org/10.1175/1520-0485\(2003\)033<1921:STATCS>2.0.CO;2](https://doi.org/10.1175/1520-0485(2003)033<1921:STATCS>2.0.CO;2), 2003.
- Ardhuin, F., Rogers, E., Babanin, A. V., Filipot, J.-F., Magne, R., Roland, A., van der Westhuysen, A., Queffelecoul, P., Lefevre, J.-M., Aouf, L., and Collard, F.: Semiempirical Dissipation Source Functions for Ocean Waves. Part I: Definition, Calibration, and Validation, *J. Phys. Oceanogr.*, 40, 1917–1941, <https://doi.org/10.1175/2010JPO4324.1>, 2010.
- Baart, F., van Gelder, P. H. A. J. M., and van Koningsveld, M.: Confidence in real-time forecasting of morphological storm impacts, *J. Coastal Res.*, 64, 1835–1839, 2011.
- Bagaev, A., Mizyuk, A., Khatmullina, L., Isachenko, I., and Chubarenko, I.: Anthropogenic fibres in the Baltic Sea water column: Field data, laboratory and numerical testing of their motion, *Sci. Total Environ.*, 599/600, 560–571, <https://doi.org/10.1016/j.scitotenv.2017.04.185>, 2017.
- Ballent, A., Pando, S., Purser, A., Juliano, M. F., and Thomsen, L.: Modelled transport of benthic marine microplastic pollution in the Nazaré Canyon, *Biogeosciences*, 10, 7957–7970, <https://doi.org/10.5194/bg-10-7957-2013>, 2013.
- Bartholomä, A., Kubicki, A., Badewien, T. H., and Flemming, B. W.: Suspended sediment transport in the German Wadden Sea—seasonal variations and extreme events, *Ocean Dynam.*, 59, 213–225, <https://doi.org/10.1007/s10236-009-0193-6>, 2009.
- Besseling, E., Redondo-Hasselerharm, P., Foekema, E. M., and Koelmans, A. A.: Quantifying ecological risks of aquatic micro- and nanoplastic, *Crit. Rev. Env. Sci. Tec.*, 49, 32–80, <https://doi.org/10.1080/10643389.2018.1531688>, 2019.
- Brankart, J.-M., Candille, G., Garnier, F., Calone, C., Melet, A., Bouttier, P.-A., Brasseur, P., and Verron, J.: A generic approach to explicit simulation of uncertainty in the NEMO ocean model, *Geosci. Model Dev.*, 8, 1285–1297, <https://doi.org/10.5194/gmd-8-1285-2015>, 2015.
- Bruggeman, J. and Bolding, K.: A general framework for aquatic biogeochemical models, *Environ. Modell. Softw.*, 61, 249–265, <https://doi.org/10.1016/j.envsoft.2014.04.002>, 2014.
- Buizza, R.: Introduction to the special issue on “25 years of ensemble forecasting”, *Q. J. Roy. Meteor. Soc.*, 145 (Suppl. 1), 1–11, <https://doi.org/10.1002/qj.3370>, 2018.
- Buizza, R., Milleer, M., and Palmer, T. N.: Stochastic representation of model uncertainties in the ECMWF ensemble prediction system, *Q. J. Roy. Meteor. Soc.*, 125, 2887–2908, <https://doi.org/10.1002/qj.49712556006>, 1999.
- Bunke, D., Leippe, T., Moros, M., Morys, C., Tauber, F., Virtasalo, J. J., Forster, S., and Arz, H. W.: Natural and Anthropogenic Sediment Mixing Processes in the South-Western Baltic Sea, *Front. Mar. Sci.*, 6, 677, <https://doi.org/10.3389/fmars.2019.00677>, 2019.
- Burchard, H. and Bolding, K.: GETM – a General Estuarine Transport Model, Scientific Documentation, Tech. Rep. EUR 20253 EN, JRC23237, European Commission, 155 pp., 2002.

- Burchard, H., Bolding, K., and Villarreal, M. R.: GOTM – a General Ocean Turbulence Model. Theory, implementation and test cases, Tech. Rep. EUR 18745 EN, European Commission, 103 pp., 1999.
- Chubarenko, I. and Stepanova, N.: Microplastics in sea coastal zone: Lessons learned from the Baltic amber, *Environ. Pollut.*, 224, 243–254, <https://doi.org/10.1016/j.envpol.2017.01.085>, 2017.
- Copernicus Climate Change Service (C3S): ERA5: Fifth generation of ECMWF atmospheric reanalyses of the global climate, Copernicus Climate Change Service Climate Data Store (CDS), available at: <https://cds.climate.copernicus.eu/cdsapp#!/home> (last access: 26 March 2019), 2017.
- Copernicus: Climate Data Store, available at: <https://cds.climate.copernicus.eu>, last access: 30 November 2020.
- EMODnet: Map viewer Geology – seabed substrate, available at: https://www.emodnet-geology.eu/map-viewer/?p=seabed_substrate (last access: 30 November 2020), 2020.
- Enders, K., K  ppler, A., Bini  sch, O., Feldens, P., Stollberg, N., Lange, X., Fischer, D., Eichhorn, K.-J., Pollehne, F., Oberbeckmann, S., and Labrenz, M.: Tracing microplastics in aquatic environments based on sediment analogies, *Sci. Rep.-UK*, 9, 15207, <https://doi.org/10.1038/s41598-019-50508-2>, 2019.
- Gr  we, U., Holtermann, P. L., Klingbeil, K., and Burchard, H.: Advantages of vertically adaptive coordinates in numerical models of stratified shelf seas, *Ocean Model.*, 92, 56–68, <https://doi.org/10.1016/j.ocemod.2015.05.008>, 2015.
- Gr  we, U., Klingbeil, K., Kelln, J., and Dangendorf, S.: Decomposing Mean Sea Level Rise in a Semi-Enclosed Basin, the Baltic Sea, *J. Climate*, 32, 3089–3108, <https://doi.org/10.1175/JCLI-D-18-0174.1>, 2019.
- Hofmeister, R., Burchard, H., and Beckers, J.-M.: Non-uniform adaptive vertical grids for 3D numerical ocean models, *Ocean Model.*, 33, 70–86, <https://doi.org/10.1016/j.ocemod.2009.12.003>, 2010.
- Huerta Lwanga, E., Gertsen, H., Gooren, H., Peters, P., Sal  nki, T., van der Ploeg, M., Besseling, E., Koelmans, A. A., and Geissen, V.: Microplastics in the Terrestrial Ecosystem: Implications for Lumbricus terrestris (Oligochaeta, Lumbricidae), *Environ. Sci. Technol.*, 50, 2685–2691, <https://doi.org/10.1021/acs.est.5b05478>, 2016.
- Jal  n-Rojas, I., Wang, X.-H., and Fredj, E.: Technical note: On the importance of a three-dimensional approach for modelling the transport of neustic microplastics, *Ocean Sci.*, 15, 717–724, <https://doi.org/10.5194/os-15-717-2019>, 2019a.
- Jal  n-Rojas, I., Wang, X. H., and Fredj, E.: A 3D numerical model to Track Marine Plastic Debris (TrackMPD): Sensitivity of microplastic trajectories and fates to particle dynamical properties and physical processes, *Mar. Pollut. Bull.*, 141, 256–272, 2019b.
- Khalaf, H. K.: The theoretical investigation of drag coefficient and settling velocity correlations, PhD thesis, Nahrain University, Nahrain, Iraq, 138 pp., 2009.
- Khatmullina, L. and Isachenko, I.: Settling velocity of microplastic particles of regular shapes, *Mar. Pollut. Bull.*, 114, 871–880, <https://doi.org/10.1016/j.marpolbul.2016.11.024>, 2017.
- Klingbeil, K.: GETM & Co., available at: <https://getm.io-warmemuende.de> (last accessed: 30 November 2020), 2020.
- Klingbeil, K. and Burchard, H.: Implementation of a direct nonhydrostatic pressure gradient discretisation into a layered ocean model, *Ocean Model.*, 65, 64–77, <https://doi.org/10.1016/j.ocemod.2013.02.002>, 2013.
- Klingbeil, K., Mohammadi-Aragh, M., Gr  we, U., and Burchard, H.: Quantification of spurious dissipation and mixing – Discrete Variance Decay in a Finite-Volume framework, *Ocean Model.*, 81, 49–64, <https://doi.org/10.1016/j.ocemod.2014.06.001>, 2014.
- Klingbeil, K., Lemari  , F., Debreu, L., and Burchard, H.: The numerics of hydrostatic structured-grid coastal ocean models: state of the art and future perspectives, *Ocean Model.*, 125, 80–105, <https://doi.org/10.1016/j.ocemod.2018.01.007>, 2018.
- Kondo, J.: Air-sea bulk transfer coefficients in diabatic conditions, *Bound.-Lay. Meteorol.*, 9, 91–112, <https://doi.org/10.1007/BF00232256>, 1975.
- Kriauci  nien  , J., Gailiusis, B., and Kovalenkovi  n  , M.: Peculiarities of sea wave propagation in the Klaip  da Strait, Lithuania, available at: <http://citeseerx.ist.psu.edu/viewdoc/download;jsessionid=D6B2487835980E6828B2FD6D4D63DB9D?doi=10.1.1.133.7480&rep=rep1&type=pdf> (last access: 30 November 2020), 1961.
- Kundu, P. K. and Cohen, I. M.: Fluid Mechanics, Academic Press, San Diego, USA, 2001.
- Liubartseva, S., Coppini, G., Lecci, R., and Clementi, E.: Tracking plastics in the Mediterranean: 2D Lagrangian model, *Mar. Pollut. Bull.*, 129, 151–162, <https://doi.org/10.1016/j.marpolbul.2018.02.019>, 2018.
- NOAA Environmental Modeling Center (EMC): WW3, GitHub repository, available at: <https://github.com/NOAA-EMC/WW3>, last accessed: 30 November 2020.
- Osinski, R. and Bouttier, F.: Short-range probabilistic forecasting of convective risks for aviation based on a lagged-average-forecast ensemble approach, *Meteorol. Appl.*, 25, 105–118, <https://doi.org/10.1002/met.1674>, 2018.
- Osinski, R. D. and Radtke, H.: Ensemble hindcasting of wind and wave conditions with WRF and WAVEWATCH III^{  } driven by ERA5, *Ocean Sci.*, 16, 355–371, <https://doi.org/10.5194/os-16-355-2020>, 2020.
- Osinski, R., Lorenz, P., Kruschke, T., Voigt, M., Ulbrich, U., Leckebusch, G. C., Faust, E., Hofherr, T., and Majewski, D.: An approach to build an event set of European windstorms based on ECMWF EPS, *Nat. Hazards Earth Syst. Sci.*, 16, 255–268, <https://doi.org/10.5194/nhess-16-255-2016>, 2016.
- Pappenberger, F., Bartholmes, J., Thielen, J., Cloke, H. L., Buizza, R., and de Roo, A.: New dimensions in early flood warning across the globe using grand-ensemble weather predictions, *Geophys. Res. Lett.*, 35, L10404, <https://doi.org/10.1029/2008GL033837>, 2008.
- PlasticsEurope: Plastics – the Facts 2019, Tech. rep., PlasticsEurope Deutschland e. V., available at: https://www.plasticseurope.org/application/files/6015/7908/8734/Plastics_the_facts_2019.pdf (last access: 30 November 2020), 2019.
- Radtke, H., Brunnabend, S.-E., Gr  we, U., and Meier, H. E. M.: Investigating interdecadal salinity changes in the Baltic Sea in a 1850–2008 hindcast simulation, *Clim. Past*, 16, 1617–1642, <https://doi.org/10.5194/cp-16-1617-2020>, 2020.
- Ridal, M., Olsson, E., Uden, P., Zimmermann, K., and Ohlsson, A.: Uncertainties in Ensembles of Regional Re-Analyses – Deliverable D2.7 HARMONIE reanalysis report of results

- and dataset, available at: <http://www.uerra.eu/component/dpattachments/?task=attachment.download&id=296> (last access: 30 November 2020), 2017.
- Rijn, L. C. V.: Sediment transport, part II: suspended load transport, *J. Hydraul. Eng.*, 110, 1613–1641, 1984.
- Sassi, M., Duran-Matute, M., van Kessel, T., and Gerkema, T.: Variability of residual fluxes of suspended sediment in a multiple tidal-inlet system: the Dutch Wadden Sea, *Ocean Dynam.*, 65, 1321–1333, <https://doi.org/10.1007/s10236-015-0866-2>, 2015.
- Seifert, T., Tauber, F., and Kayser, B.: A high resolution spherical grid topography of the Baltic Sea, 2nd Edn., Baltic Sea Science Congress, Stockholm, Sweden, 25–29 November 2001, 147, 2001.
- Shields, A. R.: Application of similarity principles and turbulence research to bed-load movement, <https://authors.library.caltech.edu/25992/1/Sheilds.pdf> (last access: 30 November 2020), translated by: Ott, W. P. and van Uchelen, J. C., 1936.
- Shutts, G.: A kinetic energy backscatter algorithm for use in ensemble prediction systems, *Q. J. Roy. Meteor. Soc.*, 131, 3079–3102, <https://doi.org/10.1256/qj.04.106>, 2005.
- Skamarock, W. C., Klemp, J. B., Dudhia, J., Gill, D. O., Liu, Z., Berner, J., Wang, W., Powers, J. G., Duda, M. G., Barker, D., and Yu Huang, X.: A Description of the Advanced Research WRF Model Version 4, Tech. rep., NCAR/TN-556+STR, National Center for Atmospheric Research, Boulder, Colorado, USA, 162 pp., 2019.
- Smagorinsky, J.: General Circulation Experiments with the Primitive Equations, *Mon. Weather Rev.*, 91, 99–164, 1963.
- Soulsby, R.: Dynamics of Marine Sands, Thomas Telford Publishing, London, UK, 1997.
- Stokes, G. G.: On the Effect of the Internal Friction of Fluids on the Motion of Pendulums, *Transactions of the Cambridge Philosophical Society*, 9, 8–106, 1851.
- Stuparu, D., der Meulen, M. V., Kleissen, F., Vethaak, D., and el Serafy, G.: Developing a transport model for plastic distribution in the North Sea, 36th IAHR World Congress, The Hague, The Netherlands, 28 June–3 July 2015, available at: <https://research.vu.nl/en/publications/developing-a-transport-model-for-plastic-distribution-in-the-nort> (last access: 30 November 2020), 2015.
- Taylor, J. W. and Buizza, R.: Using weather ensemble predictions in electricity demand forecasting, *Int. J. Forecasting*, 19, 57–70, [https://doi.org/10.1016/S0169-2070\(01\)00123-6](https://doi.org/10.1016/S0169-2070(01)00123-6), 2003.
- The Local: Thousands without power and traffic disrupted as 2019's first storm hits Sweden, available at: <https://www.thelocal.se/20190102/> (last access: 30 November 2020), 2019.
- The WAVEWATCH III Development Group (WW3DG): User manual and system documentation of WAVEWATCH III version 6.07. Tech. Note 333, NOAA/NWS/NCEP/MMAB, College Park, MD, USA, 465 pp. + Appendices, available at: <https://raw.githubusercontent.com/wiki/NOAA-EMC/WW3/files/manual.pdf> (30 November 2020), 2019.
- Tolman, H. L.: A Third-Generation Model for Wind Waves on Slowly Varying, Unsteady, and Inhomogeneous Depths and Currents, *J. Phys. Oceanogr.*, 21, 782–797, [https://doi.org/10.1175/1520-0485\(1991\)021<0782:ATGMFW>2.0.CO;2](https://doi.org/10.1175/1520-0485(1991)021<0782:ATGMFW>2.0.CO;2), 1991.
- Umlauf, L. and Burchard, H.: Second-order turbulence closure models for geophysical boundary layers. A review of recent work, *Cont. Shelf Res.*, 25, 795–827, <https://doi.org/10.1016/j.csr.2004.08.004>, 2005.
- University Corporation for Atmospheric Research (UCAR): WRF, GitHub repository, available at: <https://github.com/wrf-model/WRF/releases>, last access: 30 November 2020.
- Waldschläger, K. and Schüttrumpf, H.: Effects of Particle Properties on the Settling and Rise Velocities of Microplastics in Freshwater under Laboratory Conditions, *Environ. Sci. Tech.*, 53, 1958–1966, <https://doi.org/10.1021/acs.est.8b06794>, 2019.
- Watkins, E., ten Brink, P., Sirini Withana, M. K., Daniela Russi, K. M., Schweitzer, J.-P., and Gitti, G.: The socio-economic impacts of marine litter, including the costs of policy inaction and action, in: *Handbook on the Economics and Management of Sustainable Oceans*, edited by: Nunes, P. A., Svensson, L. E., and Markandya, A., Edward Elgar Publishing, Cheltenham, UK, 296–319, 2017.
- Wessel, P. and Smith, W. H. F.: A global, self-consistent, hierarchical, high-resolution shoreline database, *J. Geophys. Res.-Sol. Ea.*, 101, 8741–8743, <https://doi.org/10.1029/96JB00104>, 1996.
- Zambresky, L.: A verification study of the global WAM model December 1987– November 1988, available at: <https://www.ecmwf.int/node/13201> (last access: 30 November 2020), 1989.
- Ziervogel, K. and Bohling, B.: Sedimentological parameters and erosion behaviour of submarine coastal sediments in the south-western Baltic Sea, *Geo-Mar. Lett.*, 23, 43–52, <https://doi.org/10.1007/s00367-003-0123-4>, 2003.



Evaluation of Electrostatic Separation of Microplastics From Mineral-Rich Environmental Samples

Kristina Enders*, Alexander S. Tagg and Matthias Labrenz*

Environmental Microbiology Working Group, Leibniz Institute for Baltic Sea Research Warnemünde, Rostock, Germany

OPEN ACCESS

Edited by:

João P. G. L. Frias,
Galway-Mayo Institute of Technology,
Ireland

Reviewed by:

Venkatramanan Senapathi,
Ton Duc Thang University, Vietnam
An Liu,
Shenzhen University, China

*Correspondence:

Kristina Enders
kristina.enders@io-warnemuende.de
Matthias Labrenz
matthias.labrenz
@io-warnemuende.de

Specialty section:

This article was submitted to
Toxicology, Pollution and the
Environment,
a section of the journal
Frontiers in Environmental Science

Received: 07 April 2020

Accepted: 29 June 2020

Published: 17 July 2020

Citation:

Enders K, Tagg AS and Labrenz M
(2020) Evaluation of Electrostatic
Separation of Microplastics From
Mineral-Rich Environmental Samples.
Front. Environ. Sci. 8:112.
doi: 10.3389/fenvs.2020.00112

Reliable, easy, cost-effective and reproducible ways of extracting microplastics (MP) from environmental samples remain important requirements for MP research. In this context, electrostatic separation is a new proposition, especially for extracting MP from mineral-rich samples and large sample volumes. However, there is little research evaluating the reliability of the technique. This study has evaluated the effectiveness of the Corona-Walzen-Scheider (KWS) system; a small-scale version of larger machines designed to sort recycling materials. Recovery rates of a variety of sizes of MP, spiked in beach sediments, were found to be highly dependent on the MP size. MP ≥ 2 mm achieved 99 – 100% recovery (with the exception of fibers: $\sim 80\%$), MP of 63–450 μm achieved ~ 60 –95% recovery and MP of 20 μm achieved $\sim 45\%$ recovery. For particle-based analysis, additional density separation is still inevitable for the analysis of small MP after KWS separation and further reduces the overall recovery rates. Mass reduction rates of beach and commercial reference sand greatly differed, 93 and 17%, respectively. Mineral analysis using SEM-EDX suggested that lower reduction rates found in commercial sand was due to high presence of small (<50 μm) calcite particles. Tests based on environmental soil samples revealed comparatively low mass reduction rates ($\sim 1\%$), suggesting that KWS treatment was inefficient for soils due to high levels of fine particulates. Sieving to remove fine particles improved mass reduction, though only to $\sim 15\%$. To specifically test for influence of fine particulates, recovery rates were determined for sand samples spiked with a defined amount of silicate dust, resulting in a reduction of certain MP recovery rates, especially medium-sized (450 μm) MP. Conclusively, several key influential parameters were identified, such as mineral composition and grain size, that can negatively effect sediment mass reduction as well as MP recovery rates. Given the variability in recovery rates, the use of internal standards is recommended when using the KWS, particularly for smaller MP (<500 μm). For large-volume (beach) sand samples, where interest is mainly in MP > 450 μm , electrostatic separation is a reliable and fast approach for MP extraction from the environment.

Keywords: electroseparation, method test, protocol, anthropogenic litter, plastic, monitoring, reference material

INTRODUCTION

Current limitations in the field of microplastics (MP) extraction from complex matrices foster the development of, and search for, new approaches. Electrostatic separation is one of the techniques that has recently been proposed by Felsing et al. (2018) for MP purification of different sample matrices, ranging from beach sand to more complex matrices like freshwater suspended particulate

matter and freshwater sediments. In their study, a set of six different commodity polymers were tested at four different size ranges (2–5 mm, 0.63–2 mm, 200–630 μm and 63–200 μm) using a Korona-Walzen-Scheider (KWS-XS, Hamos GmbH) and yielded recovery rates of 90–100%.

The intended effect of electrostatic separation is to selectively separate non-MP particulates from MP particles, thereby reducing the non-MP particulate portion. This reduces the amount of material submitted to the subsequent steps and hence allows for preparation of larger initial sample volumes. The subsequent treatment of the electrostatically reduced sample is completed with already-established methods (e.g., density separation and digestion).

Density separation alone is the most widely used reduction method of the inorganic fraction. By using a variety of different density salt solutions (e.g., ZnCl_2 , NaI, sodium polytungstate) it can reduce bulk particulate material in many samples (Hidalgo-Ruz et al., 2012). However, there is a general lack of efficient separation procedures targeting large sample volumes of several kilos which is often needed when dealing with relatively low MP numbers in order to increase statistical robustness. The Munich Plastic Sediment Separator has been designed to density separate larger volumes, though, it appears to be a rather labor-intensive method (Imhof et al., 2012). Electrostatic separation is not as exhaustive as density separation in eliminating the entire mineral fraction ($99.98 \pm 0.03\%$, Enders et al., 2020), although approximately 98% mass could be reduced in previous tests in just 5 h (Felsing et al., 2018). However, due to deviating objectives a direct comparison to other established methods is difficult (though respective reviews exist, see Stock et al., 2019). Most other purification techniques where chemicals (acidic or basic) or mechanical forces (e.g., stirring during density separation) are involved require elaborate testing of MP resistivity (Lenz et al., 2020). Electrostatic separation can be considered a very gently treatment and such tests can be omitted as no effect on the MP integrity is to be expected.

The working principle of electrostatic separation using the KWS is based on the different electrical conductivity of the sample particulates, with mineral particulates being generally more conductive than plastics. As water content fundamentally changes the electrostatic behavior of particles, an initial (freeze) drying step is needed. The dried sample is then entered at the sample-entry funnel of the instrument and transported by a vibrating conveyor plate toward the Corona electrode system. For better visualization of this process, see the KWS-XS schematic in the supporting information (**Supplementary Information, Figure S1**). The particles become charged in a high-voltage electrical field (max. 35 kV, DC) between the grounded drum and an above-mounted rake-shaped electrode. More conductive mineral particles discharge quicker and jump off the drum with the diving flap guiding them into the “sediment container.” Less conductive plastics discharge slower and remain adhered to the rotating drum and only detach later into a separate collection container (the herein named “plastic container”). All particles that remained adhering to the drum are mechanically removed by a scraping plate, which lets them fall into the plastic container as well. By recycling the

content of the plastic container into the top (i.e., repeated runs), the mineral fraction is further reduced and MP are further refined. According to the prior study, three repetitions were found to be most efficient. As the working principle is already thoroughly explained by Felsing et al. (2018), in the following, the focus is concentrated only on the additional findings of this method e.g., concerning influential factors on the recovery rates as well as on the working steps necessary to allow a replication of the method.

Based on the results by Felsing et al. (2018), the aim of the present study was the validation of the instrument-functionality for current sample matrices and the determination of their standard error to be reported in future studies. The main scope was to use electrostatic separation for beach samples, as they (by experience) often require relatively large initial volumes (up to several kilos) to reach statistically robust MP numbers. Beach sediments are usually on the less complex end (low in organics, relatively homogeneous grain size distribution) of possible environmental matrix compositions and reached highest enrichment rates in the prior study mentioned above. However, more complex matrices (freshwater suspended particulate matter) also appeared to reach reasonable recovery rates and mass reductions. This is why we also report observations on the extraction efficiency of soil samples, a matrix which typically challenges other methods due to their complex compositions (rich in organics, heterogeneous grain size distribution, high levels of aggregation; Möller et al., 2020).

The extraction efficiency was evaluated based on three requirements:

- a reasonable mass reduction of the initial sample mass that allows for a subsequent quick and easy density separation in a separation funnel [as presented in Enders et al. (2020)]
- reasonable and reproducible (i.e., consistent) recovery rates of MP
- low influence of matrix-related variables (i.e., grain size, mineral composition) on recovery rates and mass reduction

As the prior study showed no differences in recovery rates between polymer types, the present study focuses only on different particle sizes with a broader overall size range from 20 μm to 4 mm, as well as with finer steps between each size range compared to prior tests (Felsing et al., 2018).

MATERIALS AND METHODS

Test Material

Recovery rates were determined using the same model of electrostatic separator (2nd prototype, KWS-XS, Hamos GmbH) as presented in Felsing et al. (2018). Sets of different recovery-test MP of various sizes, polymers and shapes (**Table 1** and **Supplementary Information, Figure S2**) were prepared and the test sediment samples spiked. The smaller the particles, the higher the number of spiked test MP due to the expected lower recovery rates. Spiked MP

TABLE 1 | Set of spiked MP of various size (longest dimension), color, polymer type and shape.

Number added	Size	Color	Polymer	Shape
20, 40	4 mm	black	PA66 (Polyamide)	pellet
20, 40	2 mm	white	HDPE (High-density Polyethylene)	pellet
20	2 mm	green	PE	fiber
20, 40	450 μm	red	PA6	pellet
60 - 80	125–150 μm	green (fluorescent)	PE	sphere
60 - 220	63–74 μm	blue (fluorescent)	PE	sphere
20 - 201	20–27 μm	green (fluorescent)	PE	Sphere

An image of the listed particles can be found in the **Supplementary Information, Figure S2**. Added numbers of spiked MP varied (see 1st column).

were counted visually ($\geq 450 \mu\text{m}$) aided with a binocular microscope (Zeiss Stemi 2000) and an ultraviolet light source (Tattu U2, 395 nm) where necessary ($\leq 150 \mu\text{m}$, fluorescent microspheres, Cospheric LLC).

Test samples were composed of either:

(a) 100 g (d/w) beach sand from the Baltic Sea (Warnemünde beach, 0–2 cm surface, $d_{50} = 319 \mu\text{m}$, 197–530 μm [10, 90 th percentiles], **Supplementary Information, Figure S3A**)

(b) 100 g (d/w) commercial sand (Aquarienkies, Rosnerski Quarz Verpackungswerk, $d_{50} = 310 \mu\text{m}$, 193–512 μm [10, 90th percentiles], **Supplementary Information, Figure S3B**)

(c) 100 g (d/w) sand as described in (a) added with 30 g micro glass beads with a size range of 40–70 μm (Strahlgut, Samore GmbH)

(d) 500 g w/w (~ 440 g d/w) agricultural soils (0–30 cm surface mixed-core soil, from two test fields, one with 10 tons ha^{-1} of sludge from a waste water treatment plant previously applied in 2014, the other without sludge).

Preparation

Test samples (a)–(c) were baked for 5 h at 500°C to eliminate any MP contamination present in the sample which would potentially hinder a quick determination of the recovery rates. The soil samples (d) were not baked but freeze dried (according to Enders et al., 2020) as both the organic fraction was intended to be preserved and the determination and thus conservation of environmental MP was targeted in addition to the recovery rates of the spiked MP standards.

The test sediments were added together with the spiked MP into the entry-funnel at the top of the KWS and a test run started according to the attached protocol (**Supplementary Information, Text S1**). The procedures described here were written based on the steps reported by Felsing et al. (2018) and experiences made by the authors of this study. For example, run repetitions were set to five (instead of three) in order to increase the mass reduction. Subsequently, a small-scale density separation was performed according to Enders et al. (2020) to allow unhindered identification of the spiked test-MP. A schematic overview of the separation steps can also be found in Felsing et al. (2018, **Figure 3**).

Optimal Instrument Settings

At first, optimal instrument settings had to be identified to perform recovery tests. Those initial tests were performed using the test MP between 4 mm and $450 \mu\text{m}$ in size (**Table 1**), as they could be quickly visually identified without performing a subsequent density separation. For beach sands (a, c) two different high voltages (20 kV, 22 kV) were tested and the full set of MP recovery rates and mass reduction determined. The voltage optimum was found to be at 22 kV. While higher voltages generally improved the separation efficiency, when further increased (up to 25 kV), smaller particles were strongly dissipated and scattered in an uncontrollable manner. The drum speed was set relatively slow, 5 rpm (4%), as otherwise centrifugal forces and particle-particle interactions prevented independent separation of particles. To ensure the maintenance of a mono-layer of sample material on the drum, the terminal vibration strength of the conveyor plate was set between 60 and 120 rpm (1–2%). Initially, higher vibration strength might be needed as it depends on the sample weight on the conveyor plate which has to be transported. Depending on the sample type, drum speed and vibration strength can be changed but must be configured to ensure mono-layering of particulate matter on the drum. The sample-entry funnel on top of the KWS comes with a relatively large output opening (12 cm), which caused large variations of sample weight present on the conveyor plate and thus a lot of manual adjustment of the required vibration intensity to achieve a mono-layer (as a function of the sample being processed). Since, in this original design, failure in properly adjusting the vibration strength during sample-processing could influence the results (by impacting drum mono-layering), the funnel was modified with additional tapering using an adjustable stainless steel plate. The new opening can be adjusted to approximately 5–10 mm (**Supplementary Information, Figure S1**). It is further noted that the original particle shield (Polyvinyl chloride) above the vibration plate and drum, built to reduce the loss of particles to the KWS interior, was unmounted due to several reasons. These are: (1) Both sand and MP particles were found adhering to the shield surface and were thus lost from the sample; (2) The PVC shield constitutes a potential source of plastic contamination, and (3) It hindered control of mono-layering. Given these benefits, it is not expected that the shield removal negatively effects results. As an additional modification, a hardboard sheet was added above the sediment container to reduced the loss of sediment to the KWS interior (**Supplementary Information, Figure S1**). The metal dividing flap that determines the boundary between sediment and plastic container was set to an angle of 19.5° , the optimally determined position where maximum sediment would be separated without any large MP falsely entering the sediment container (standard procedures and parameters in **Supplementary Information, Text S1, Figure S4**).

Mineral and Grain Size Classification

SEM-EDX analyses were completed at the IOW by the authors using a Zeiss Merlin VP Compact Scanning Electron Microscope (SEM) combined with an Oxford X-Max 80 energy-dispersive

x-ray (EDX) spectrometer to analyse mineral content of two exemplary sand samples (software: Oxford AZtec 3.3). Samples were vacuum sputter-coated with elemental carbon to provide good electrical conductivity (Cressington Carbon Coater 108carbon/A, TESCAN GmbH, 10 nm layer thickness). Measurements were taken with an aperture of 30 μm , a working distance of 8.5 mm and a kV of 15.00 using Inca feature 5:04 software. An upper limit of 1000 features (i.e., particulates) were measured per sample. Mineral classification was applied according to the in-house-developed Baltic Sea Standard. Homogenized and freeze dried subsamples were grain size analyzed in two replicates using the laser-sizer Mastersizer 3000 by Malvern (10 s ultrasound applied).

RESULTS

Recovery Rates

Across the different types of sand sediment matrices (a–c), MP recovery rates decreased with MP size (**Figure 1**, data in **Supplementary Information Table S1**). The standard deviation increased for smaller MP as well as fibers.

For beach sand (a), the MP recovery rates decreased from 100 to 10% median recovery, including losses generated during density separation (**Figure 1**, red box plots; **Supplementary Information Tables S1A–D**). The recovery rates presented here were determined after the density separation, a necessary procedural step, as otherwise remaining sediment particles hindered a direct analysis, especially of the particles $\leq 150 \mu\text{m}$. To determine KWS specific recovery rates, the recovery rates of the density separation only were determined separately and subtracted from the total (**Figure 1**, opaque bars; **Supplementary Information Table S1L–M**), resulting in a corrected recovery rate declining from 100 to 45% with size. There was no difference in recovery rates between the two different voltages (20 and 22 kV), thus recovery rates were averaged (**Supplementary Information Tables S1A–D**).

Median recovery rates for the commercial sand (b) were slightly lower compared to the beach sands (**Figure 1**, turquoise box plots; **Supplementary Information Tables S1E–G**), with the exception that the recovery rates of the smallest spiked MP (20–27 μm) were significantly higher (t -test, $p = 0.03$).

The presence of the fine (40–70 μm) glass beads (c) resembling fine sediment grains or, more generally, dust, partly distorted the previously described recovery-rate pattern for beach sand sediments (**Figure 1**, dark blue box plots; **Supplementary Information Tables S1H–K**). While the large particles ($> 2 \text{ mm}$) were unaffected, the recovery rate of the intermediate size class (450 μm) was significantly reduced (t -test, $p = 0.04$) by nearly 40%. Spiked MP (125–150 and 63–75 μm) closer to the size spectrum of the added dust particles showed a slightly increased recovery rate compared to the previous test without additional dust. It seems reasonable to assume that the added dust particles cannot sufficiently adhere to MP particles of similar size and thus do not negatively affect the recovery rate. However, larger MP which can be sufficiently surface-coated by dust can obtain a higher net-conductivity and enter the sediment container more

frequently. This negative effect on the intermediate size class seems to amplify when using glass beads as sole sample matrix (one observation only; **Supplementary Information Table S1O**).

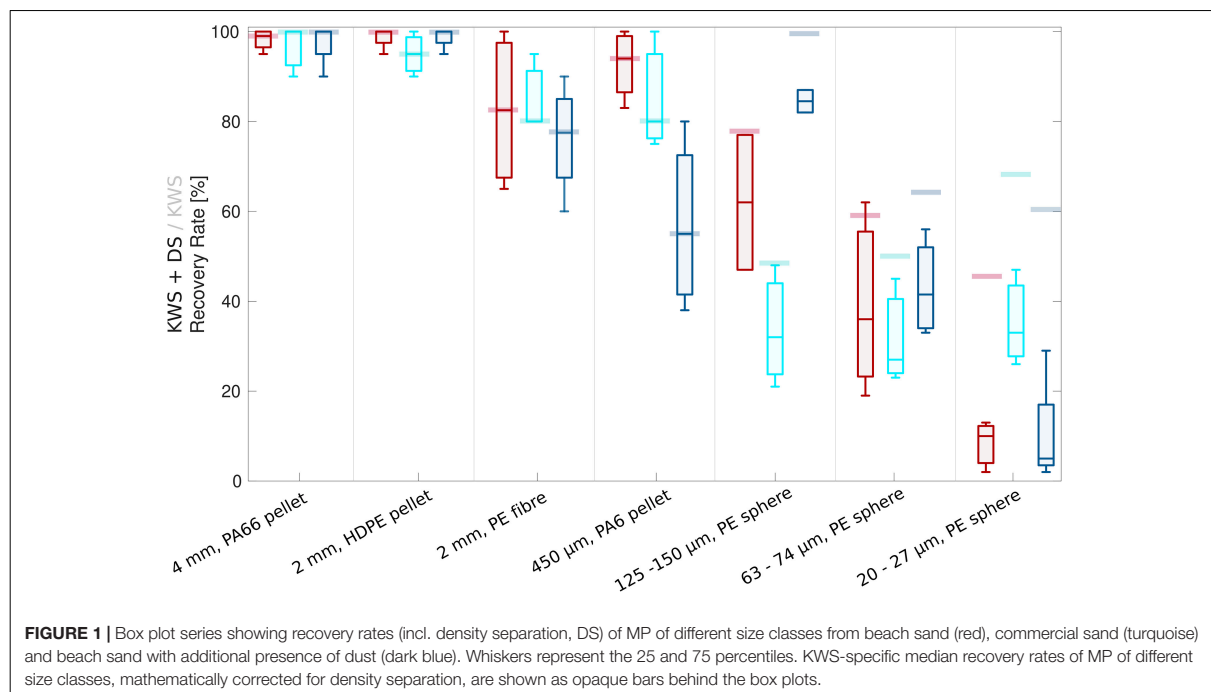
Mass Reduction

The main reason of applying the KWS is the selective MP refinement by reduction of the mineral mass fraction. In case no considerable mass-reduction is achieved for a specific sample, electrostatic separation would simply constitute an increase in methodological efforts and resources (as well as an extra step for possible contamination and loss of particles), without any prominent benefit. Therefore, besides MP recovery rates, the mass reduction is the ultimate measure of treatment effectiveness.

The mass reduction of beach sand was influenced by the voltage applied and resulted in 74% at 20 kV and 93% at 22 kV. Comparable numbers were acquired with dust added, 70% at 20 kV and 94% at 22 kV. Thus, a higher voltage generally increases the mass reduction. However, as already mentioned in the above section “Optimal instrument settings,” a further increase strongly affected the smaller particles that scattered in an uncontrollable manner.

The effectiveness of the method in terms of mass reduction for the commercial sand was substantially lower compared to the beach sand, resulting in a 17% average (at 22 kV), MP recovery rates were within the same ranges. The lower mass reduction, and thus a larger remaining volume, of the commercial sand probably explains the higher recovery rates of the smallest spiked MP, which appear not to be actively separated. An increase in voltage (to 25 kV) did not have a measurable effect on the mass reduction of commercial sand, as the majority of the material remained adhered to the drum before being collected into the plastic container by the scraping plate. As the grain size distribution of both sand types (a, b) were very similar, likely mineral compositions (e.g., mineral specific electrical conductivity) plays a larger role.

The mass reduction can also be influenced by the angle of the dividing flap between the sediment and plastic containers. The larger the angle, the more of the mineral fraction will be separated (and ultimately eliminated). However, over-increasing the flap angle comes at the cost of MP recovery rates, as certain (particularly large) MP will start to be eliminated from the sample if the angle is too extreme. As stated above, an optimum angle was determined to be 19.5°; the highest angle where no large MP were lost to the sediment container (runs: $n = 3$). It has been observed that an initially higher angle (starting at 28°) lead to an increased loss of MP, particularly the 4 mm black pellets and the 2 mm fibers (up to 10%), to the sediment container. The rounded morphology of these MP occasionally initiated rolling movement on the drum which, combined with drum-centrifugal force, likely explains the higher trajectory and loss to the sediment container of these MP. For the sands used in this study, a higher flap angle of 28° did not further increase mass reduction rates. It was observed that the eventual non-separated sediment fraction was adhering to the drum, indicating that further increase of the angle would have a negligible effect. While initial instrument settings, such as the angle of the dividing flap or high voltage, can influence the separation efficiency, the



determining factor for the final mass reduction seems to depend on sediment composition.

Sediment Composition

It was not initially clear why beach and commercial sand had different mass reduction rates, since they are expected to be compositionally similar (i.e., mainly quartz(SiO_2)-based). However, given there was a clear difference in mass reduction, and that the two sands had a different visual appearance (beach sand brown in color while commercial sand was white, **Supplementary Information, Figure S3**), it was necessary to further analyse the mineral composition of the sediment to better understand if, and how, mineral composition influences reduction rates. SEM-EDX spectroscopy was applied to the two sand samples. It was apparent that the commercial sand contained higher levels (50.5%) of small ($<50\ \mu\text{m}$) calcite particles in comparison to beach sand (23.5%). A visual demonstration of this difference can be seen in **Figure 2**. Aside from this, the elemental analysis showed slightly lower levels of certain metal elements (e.g., aluminum, potassium and magnesium) in the commercial sand.

From the obtained data we can only presume that either the actual mineral composition differences lead to changes in the material conductivity and thus different electrostatic separabilities. Or, that the compositional differences lead to distinct hygroscopic properties that entail varying material humidities at the time of separation. The latter may be tested in a humidity controlled environment, which is, however, beyond the scope of this study.

Soils

Initially, soil samples (d) achieved $\sim 1\%$ visually estimated reduction after two runs. This ineffectiveness of the KWS was postulated to be due to the high levels of silt and clay particulates present in soils (especially agricultural soils). Therefore, dry-sieving to remove the $<100\ \mu\text{m}$ quotient was applied (according to Enders et al., 2020). After a further six runs of the sieved sample, the mass was reduced overall by $\sim 15\%$ (total eight runs taking $\sim 7\ \text{h}$ per 500g w/w sample, not including reductions of the sieved-out fraction). This indicates that removal of the dust-sized quotient of the soil samples improved the performance considerably (from ~ 1 to $\sim 15\%$ reduction); however, this reduction rate was far below that observed for beach sand. Due to such a comparatively poor reduction, it was considered redundant to test recovery rates for KWS treatment of soil. This is because to enable MP analysis, other methods, such as sieving, and multiple cycles of density separation and H_2O_2 digestion were required. This makes KWS-specific recovery rates difficult to accurately determine, and ultimately without value, given the lack of usefulness of the KWS approach for these samples going forward.

DISCUSSION

Influential Factors

Microplastics recovery rates for different mineral-rich samples using the KWS scaled with MP size, with generally the highest rates achieved for the largest particles. In consequence, a general standard error for overall MP recovery using the KWS is not

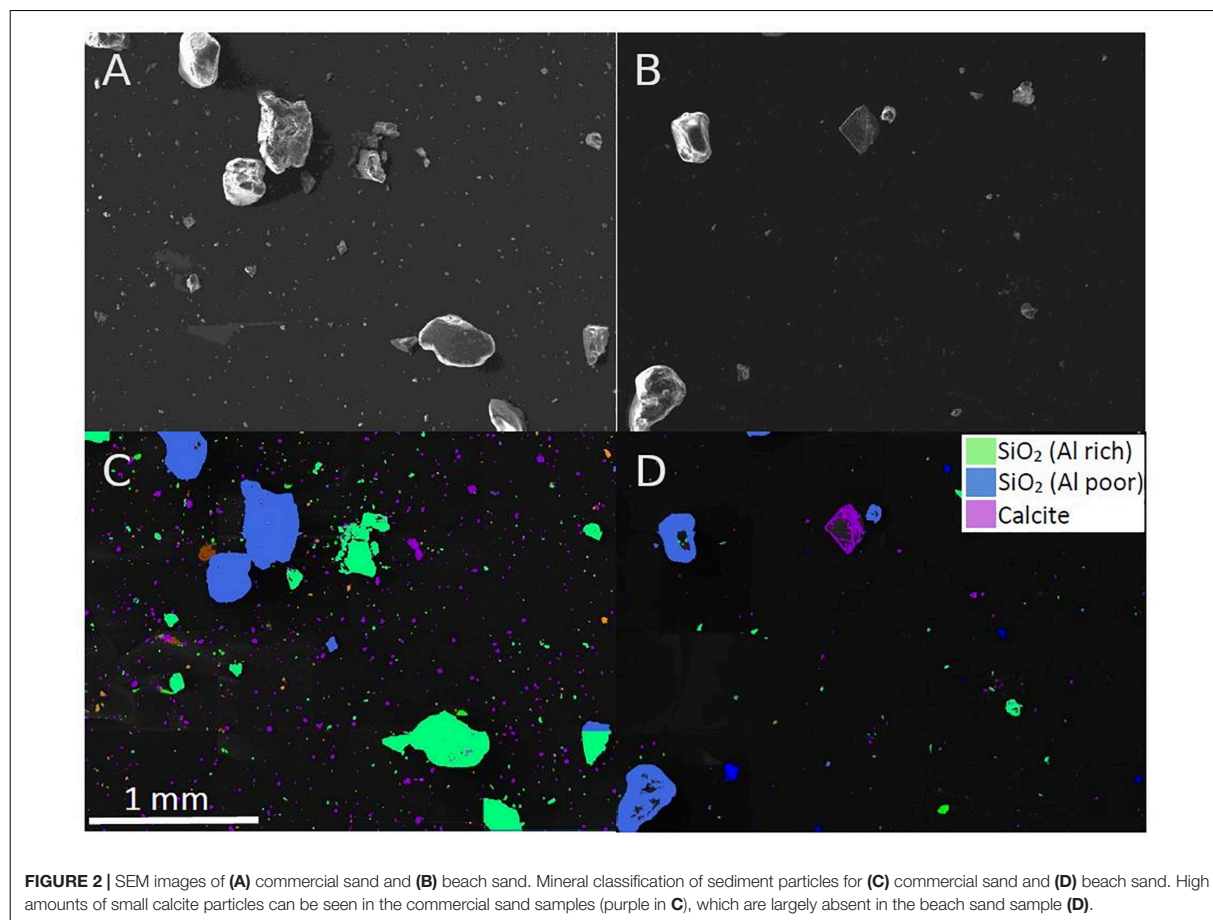


FIGURE 2 | SEM images of (A) commercial sand and (B) beach sand. Mineral classification of sediment particles for (C) commercial sand and (D) beach sand. High amounts of small calcite particles can be seen in the commercial sand samples (purple in C), which are largely absent in the beach sand sample (D).

useful and thus not determined, suggesting to report a standard error per size range (see Figure 1).

The results demonstrated that, aside from customisable instrument settings, many factors concerning the composition of the sediment matrix can potentially influence MP recovery rates obtained by electrostatic separation. While some of these factors can be easily adjusted, such as sample condition e.g., humidity by prior freeze-drying, factors determining sample composition are more complex to control for. Among those are grain size distribution (especially with respect to the smaller “dust” fraction), mineral composition as well as organic matter content (potentially causing aggregation). This study showed that increased presence of dust of one specific grain size strongly influenced the recovery rate of certain MP sizes. An explanation for this effect could be an increased surface-coating of MP by smaller silicate particles causing a higher net-conductivity and increased loss to the sediment container. SEM-EDX analysis suggested that presumably the high presence of calcite dust (as seen in the commercial sand, Figure 2) or lower presence of metal-rich minerals reduced sediment reduction rates, lowering the usefulness of the approach. It is, however, still unclear which dust sizes or mineral compositions have the greatest impact on

size-dependent recovery rates and mass reduction rates. The amount of dust likely negatively scales with the specific recovery rates, as observed when using the dust particles as the sole sample matrix. In contrast to the freshly produced and clean test MP, environmental MP are usually coated with organics and fine dust. Therefore, the actual recovery rates for environmental MP are likely below those presented here.

Soil observation results also suggest that high presence of fine particulates and the presence of agglomerates (as typical for soils) in samples limits KWS applicability. As the primary purpose of implementing electrostatic separation is for the bulk reduction of sample volume, it turned out that KWS treatment, even with a large amount of fine particles being removed by dry-sieving, enabled only a reduction of the original volume of ~15%. Taken into account that the time taken to perform this reduction was 7 h, the value of the applied method was low for our purpose. Indeed, even after sieving and KWS treatment, an advanced density separation was still required to process the samples. Methods for the refinement of MP in environmental samples benefit from having the least steps necessary, given the problems of particle loss and contamination (Dehaut et al., 2019; Enders et al., 2020). As such, the method applied to soils within this study

offers limited promise. However, it should be considered that dry-sieving does not completely remove dust, as conglomerates of fine material and those adhering to larger particles may not pass through the sieve. Wet-sieving (performed before freeze-drying), which uses water to carry material through the sieve, is likely to be more efficient at dust-removal. However, it is unknown how much of a pronounced difference this might have on KWS reduction rates on agricultural soils. Given issues surrounding agglomeration of particulates in soils, reduction rates are still anticipated to be well below those of sand, and progressing directly to a larger-scale density separation is likely to produce better results than wet-sieving combined with KWS.

The material requirements reported by the manufacturer of the KWS (hamos GmbH) are in line with our findings in view of a conservative perspective. The company recommends sizes of 2–12 mm for plastic separation and $>100\text{ }\mu\text{m}$ for mineral separation. Ideally, the material is dust-free and completely disintegrated (no composites/agglomerates).

Other Limitations

As already mentioned the KWS has originally been developed for large-scale recycling material separation, focusing on plastic particles of several millimeters to centimeters (Tilmatine et al., 2009; hamos GmbH, 2020). Although the KWS-XS has been downscaled in size which allows an application of smaller samples in a usual scientific lab, certain limitations derive from the design of the instrument and related physics of particles. The KWS has a relatively closed outer hull which prevents contamination from outside. However, when working with particles down to the smaller micrometers in size, the arrangement of the functional inner parts would obviously require a more closed system of higher precision, with less surfaces and corners causing potential particle losses. It has frequently been observed that larger particles, especially fibers and smaller MP, repeatedly remained adhered to the drum as a result of not being dislodged by the scraping plate which is installed to provoke particles, still adhered once passing the sediment (waste) container, to fall into the plastic container. The scraping plate also unintentionally collects particles on the rear side over time, and requires manual opening and scraping to ensure all relevant particles are collected in the MP container. This process is, however, less effective the smaller the MP. In the case of soil samples, clay presence was so high that, given the inefficiency of the scraping plate at consistently removing small particles, after a number of runs the drum was permanently coated in fine particulates. This made mono-layering highly challenging and probably contributed to the lower mass reduction rates. In general, the large surface areas inside the KWS offer small particles plenty of space to stick to due to electrostatic forces of attraction. This effect can be observed after sample runs that contained relatively small grain sizes, after which all surfaces gathered dust. Accordingly, cleaning between sample runs is exhaustive. A size measurement of the dust collected on the inner surfaces of the KWS after a beach sand separation showed an average size of $54\text{ }\mu\text{m}$, ranging from 33 to $79\text{ }\mu\text{m}$ as the 10 and 90th percentiles, respectively. Occasionally, larger MP ($>450\text{ }\mu\text{m}$) fell to the bottom of the instrument, outside the remit of the collection containers.

The MP container collecting the refined material has to be thoroughly rinsed and the rinse water collected following sample transferral to the density separation (or any other desired next experimental step). In some cases, more than 50% of the spiked MP $<150\text{ }\mu\text{m}$ were found in this rinsate (and included in the results).

Scope of Application

The results of the present study showed that a reduction of MP recovery rates correlated with size, with the smallest fraction (20–27 μm) achieving consistently less than 20% recovery (incl. KWS and density separation) for sands that were sufficiently reduced in mass. In contrast, Felsing et al. (2018) found as high as 100% for all MP size fractions tested, from their largest (2–5 mm) to their lowest size fraction (63–200 μm), in both quartz and beach sand. Although this is a much larger and broader range size category than in the present study, the most comparable size class to their smallest size fraction is 63–74 μm , which achieved less than 60% for beach and commercial sands, when corrected for the density separation (for best comparability as Felsing et al. (2018) counted recovery rates without density separation).

Instrument settings were overall comparable between the two studies. Although drum speed and vibration of the conveyor plate were slightly faster in the prior study, as long as the mono-layering is ensured, no influence on the recovery rate is expected. The angle of the metal flap divider between the collection containers was also in a similar range (20°) in the Felsing et al. (2018) study (Kochleus, 2020). However, in the present study, it has been shown that, rather than the instrument settings, sample matrix variance influences the mass reduction to the greatest degree, as demonstrated by SEM analysis of the two sand samples as well as the ineffectiveness of KWS treatment on the soil samples.

A difference between the designs of the two studies concerns the shape of the spiked MP used. Whereas the prior paper used MP with a flake-like (flat) morphology, the present study used mainly pellet or round MP. Flat particles have a larger surface area-volume ratio which presumably better-adhere to the drum, whereas round MP, due to the relatively small contact area compared to mass, are more likely to fall from the drum prematurely if the electrostatic force is insufficient compared to gravity acting upon the particle. As mentioned above, this fall-off effect was observed especially for the larger MP ($>2\text{ mm}$). However, it is unlikely that shape significantly affects the recovery of the smaller MP. The small MP fraction reported by Felsing et al. (2018) describes particles within a comparatively larger size range (e.g., 63–200 μm) and the actual size distribution of particles within that range is unknown. This makes it difficult to compare to the finer small-MP size ranges used in the present study (125–150, 63–74, and 20–27 μm). The MP sample number was lower in the previous study ($n = 10$), compared to the present study ($n > 20$), for the individual spiked MP which increases the risk of statistical outliers.

However, an important factor to consider when comparing studies testing electrostatic separation is that we now know that mineral composition plays an important role. SEM analysis of the two sand samples within the current study showed that

TABLE 2 | Summary of advantages and limitations of electrostatic separation (using the KWS) for MP purification from sediments.

Advantages	Limitations
<ul style="list-style-type: none"> • relatively fast and easy method • reduction of a potentially large sediment fraction • no polymer resistivity tests needed due to non-destructive separation mechanism • generally good recovery rates for large MP 	<ul style="list-style-type: none"> • additional (established) treatment steps needed if a particle-based analysis is targeted • mass reduction depends on multiple matrix-related factors which can negatively impact the efficiency: (1) mineral composition, presence of less conductive or less hygroscopic minerals; (2) grain size, presence of fine sediment (<100 μm) • decreasing MP recovery rates with smaller MP sizes • fine sediments (<100 μm) can reduce MP recovery rates • improvements on the instrument design needed

Findings are elaborated in more detail above.

both the size and composition of particulate matter can have a marked difference on mass reduction. Therefore, comparing reduction or recovery rates between samples where mineral composition is unknown is a challenge. Yet, the difference in results between the two studies are so pronounced that, even with a difference in mineral composition, it is likely that more unknown factors are in play.

Microplastics samples treated with electrostatic separation require further subsequent treatment steps such as density separation and digestion. Ultimately, the recovery rates of the respective procedural steps add up. The sum of all this can be quite considerable for some size classes, as shown with the example of combined electrostatic and density separation (**Figure 1**, box plots). The more methodological handling steps, the more errors occur and it is generally recommended to keep the individual treatment pipeline as short and simple (but robust) as possible. Therefore, it has to be evaluated case by case, whether the requirements shown in the present paper fit both the sample type and the research question. Less complex sediment matrices with expectantly low MP content that statistically require larger initial sample volumes (>1 kg) may justify such a first volume reduction step. In any case, the additional financial investment, as well as per-sample time and effort related to electrostatic separation has to be taken into account. A simple density separation (hand-shaking) in a separation funnel is efficient to up to ~50 g of sediment (lower for organic-rich samples). For samples up to 500 g (or even up to 1 kg if the sample is split), a density separation, combined with advanced stirring, such as the spiral sediment conveyor (Enders et al., 2020) is most-likely more efficient and robust for a greater range of research questions. However, samples significantly larger than this can make density separation too challenging as a first step. In these cases, the KWS approach could be used to reduce the starting volume, especially for sand samples. However, given the variance in recovery rates due to MP size and sample composition, the use of internal standards is highly beneficial, especially for the smallest sizes targeted (something typically determined by analysis limitations).

MP that are highly unusual (so as not to be confused with real environmental MP) and easy to distinguish (i.e., brightly colored) are most recommended. UV-fluorescent MP are highly beneficial for this purpose.

Despite the above, open questions still remain from the current state of knowledge, and of particular concern are the recovery rates of environmental (degraded) MP and the influence of MP shape. Larger systematic tests would be needed to better understand these questions, as well as to quantify the impact of the identified key influential parameters of the sediment matrix. As a concise summary of the above findings, advantages and limitations of electrostatic separation (using the KWS) for MP purification from sediments are listed in **Table 2**.

CONCLUSION

Based on the presented results, the application of the KWS for MP purification can be recommended for sediments of relatively large grain sizes (above 100 μm), in absence of dust and for large MP sizes between 0.5 and 5 mm, especially where large sample volumes (>1 kg) are desired. It should be tested in advance whether the mass reduction of the targeted matrix achieves the required volume for further processing, given that although mineral composition has shown to be of influence, the extent of this influence is unknown. The use of internal standards is highly recommended, especially for small MP, as recovery rates vary with MP size as well as sediment composition.

DATA AVAILABILITY STATEMENT

All datasets presented in this study are included in the article/**Supplementary Material**.

AUTHOR CONTRIBUTIONS

KE and ML: study design. KE: data acquisition and analysis (KWS). AT: data acquisition and analysis (SEM). KE and AT: writing—original draft. ML: writing—review and editing, supervision, and project administration. KE: visualization of KWS. AT: visualization (SEM). All authors contributed to the article and approved the submitted version.

FUNDING

This work resulted from the BONUS MICROPOLL project supported by BONUS (Art 185), funded jointly by the European Union and Federal Ministry of Education and Research (BMBF) (03F0775A), and the BMBF project MicroCatch_Balt (03F0788A).

ACKNOWLEDGMENTS

We would like to thank Sascha Plewe for his contributions to the SEM and EDX analyses and Friederike Stock,

Christian Kochleus and Stefanie Felsing for knowledge exchange on the KWS. We also thank Juliana Ivar do Sul, Friederike Uchtmann and other research assistants for support during lab work and Robin Lenz for helpful comments.

REFERENCES

- Dehaut, A., Hermabessiere, L., and Duflos, G. (2019). Current frontiers and recommendations for the study of microplastics in seafood. *TrAC Trends Anal. Chem.* 116, 346–359. doi: 10.1016/j.trac.2018.11.011
- Enders, K., Lenz, R., Ivar do Sul, J. A., Tagg, A. S., and Labrenz, M. (2020). When every particle matters: a QuEChERS approach to extract microplastics from environmental samples. *MethodsX* 7:100784. doi: 10.1016/j.mex.2020.100784
- Felsing, S., Kochleus, C., Buchinger, S., Brennholt, N., Stock, F., and Reifferscheid, G. (2018). A new approach in separating microplastics from environmental samples based on their electrostatic behavior. *Environ. Pollut.* 234, 20–28. doi: 10.1016/j.envpol.2017.11.013
- hamos GmbH (2020). *Recycling- and Separation Technology [WWW Document]. Electrostatic Separators*. Available at <https://www.hamos.com/products/electrostatic-separators,35,eng> (accessed February 18, 2020).
- Hidalgo-Ruz, V., Gutow, L., Thompson, R. C., and Thiel, M. (2012). Microplastics in the marine environment: a review of the methods used for identification and quantification. *Environ. Sci. Technol.* 46, 3060–3075. doi: 10.1021/es2031505
- Imhof, H. K., Schmid, J., Niessner, R., Ivleva, N. P., and Laforsch, C. (2012). A novel, highly efficient method for the separation and quantification of plastic particles in sediments of aquatic environments. *Limnol. Oceanogr. Methods* 10, 524–537. doi: 10.4319/lom.2012.10.524
- Kochleus, C. (2020). *Personal Communication*. Koblenz: German Federal Institute of Hydrology.

SUPPLEMENTARY MATERIAL

The Supplementary Material for this article can be found online at: <https://www.frontiersin.org/articles/10.3389/fenvs.2020.00112/full#supplementary-material>

- Lenz, R., et al. (2020). A universal concept for microplastic resistance assays. *Front. Environ. Sci.* (in press).
- Möller, J. N., Löder, M. G. J., and Laforsch, C. (2020). Finding microplastics in soils: a review of analytical methods. *Environ. Sci. Technol.* 54, 2078–2090. doi: 10.1021/acs.est.9b04618
- Stock, F., Kochleus, C., Bänsch-Baltruschat, B., Brennholt, N., and Reifferscheid, G. (2019). Sampling techniques and preparation methods for microplastic analyses in the aquatic environment – A review. *TrAC Trends Anal. Chem.* 113, 84–92. doi: 10.1016/j.trac.2019.01.014
- Tilmatine, A., Medles, K., Bendimerad, S. E., Boukholda, F., and Dascalescu, L. (2009). Electrostatic separators of particles: application to plastic/metal, metal/metal and plastic/plastic mixtures. *Waste Manag.* 29, 228–232. doi: 10.1016/j.wasman.2008.06.008

Conflict of Interest: The authors declare that the research was conducted in the absence of any commercial or financial relationships that could be construed as a potential conflict of interest.

Copyright © 2020 Enders, Tagg and Labrenz. This is an open-access article distributed under the terms of the Creative Commons Attribution License (CC BY). The use, distribution or reproduction in other forums is permitted, provided the original author(s) and the copyright owner(s) are credited and that the original publication in this journal is cited, in accordance with accepted academic practice. No use, distribution or reproduction is permitted which does not comply with these terms.

Supplementary information (SI)

Title: Evaluation of Electrostatic Separation of Microplastics from Mineral-Rich Environmental Samples

Authors: Kristina Enders, Alexander S. Tagg, Matthias Labrenz

Text S1: Protocol

Instrument: 2nd prototype of the electrostatic separator (Korona Walzen Scheider (KWS), hamos GmbH). Schematic of the design is presented in Fig. S1.

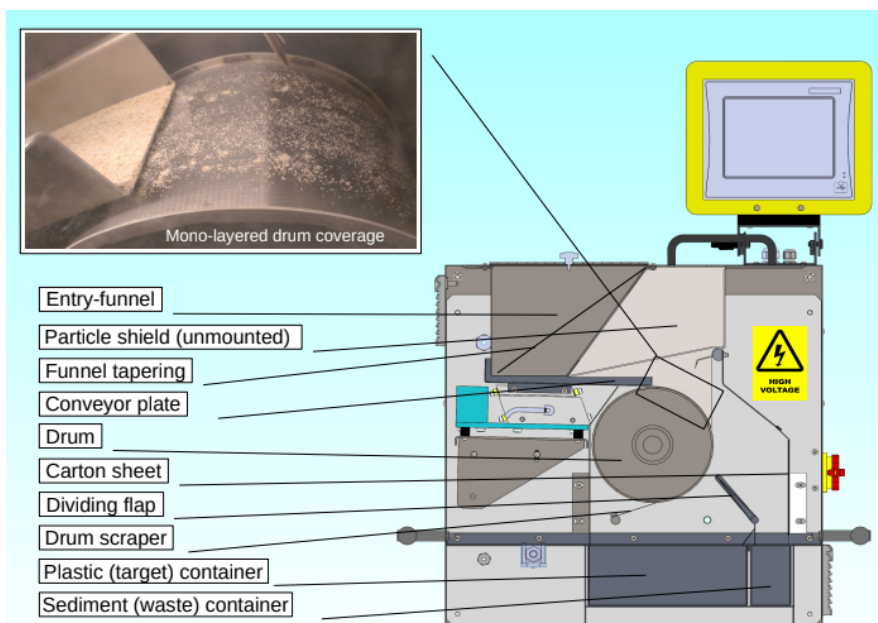


Fig. S1: KWS descriptive schematic with labels of key components; Top-left corner: Presentation of mono-layering of sediment necessary for proper functionality. KWS Scheme modified from hamos GmbH.

Test sediment samples and spiked microplastics (MP): as reported in associated paper section Methods and Materials – Test material: (a) – (d) and Table 1.

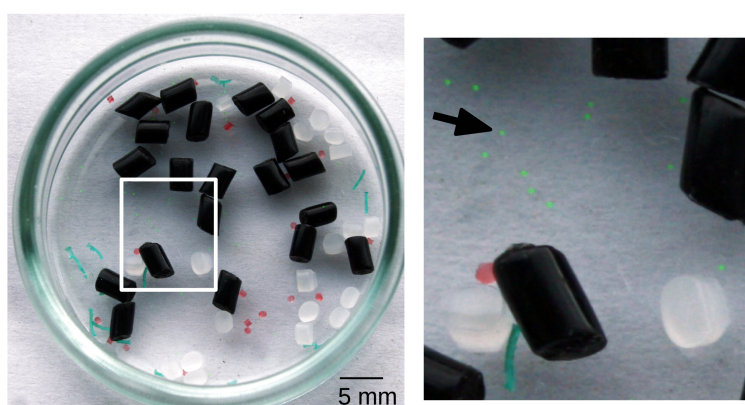


Fig. S2: Spiked MP as listed in Table 1 in the associated paper. The two smallest size groups of MP are not visible by eye, however have an appearance alike the green fluorescent spheres of 125 – 150 μm in size as shown in the close up (white rectangle, black arrow).

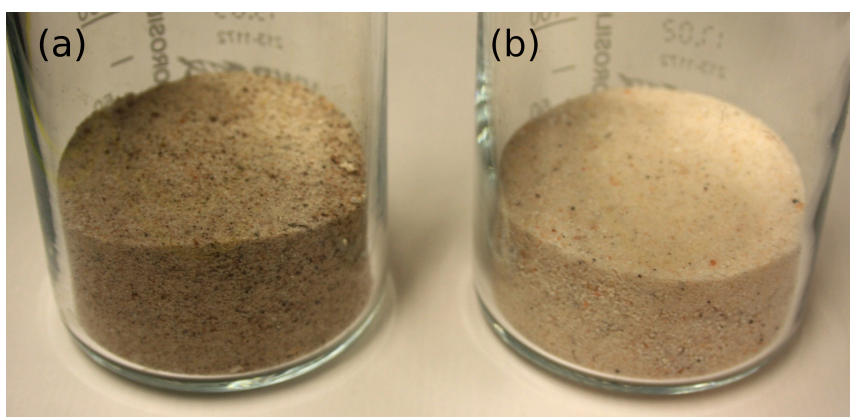


Fig. S3: Sample matrices (a) beach sand and (b) quartz sand.

Procedure

1. **Cleaning:** KWS has to be thoroughly cleaned between samples to prevent cross-contamination. In case the KWS was not used (and thus automatically cleaned), start an 'empty' run with higher drum rotations and vibration values (approx. 20%). After that, vacuum-clean the conveyor plate, funnel, etc.. Wash the MP collection container with microplastic free (MPF) water and dry. See a descriptive figure of the KWS above (Fig. S1). Empty the sediment collection container into a waste container.

2. **Insert:** Boot up KWS control screen. Insert half of the previously freeze-dried sample (as e.g. shown in Fig. S3) into the entry-funnel. Then add the prepared internal standard (spiked MP, Table 1, Fig. S2) from the glass petri dish directly into the funnel by rinsing it with remaining sediment sample (at least three times). Note the Internal Standard numbers.

3. **Run:** Turn on illumination, voltage (1.), drum (2.) and vibration (3.) of the KWS according to the following **Standard parameters** (see Fig. S4 for an image of the KWS screen displaying the settings) :

High voltage: **22 kV**
 Vibration: **~1 % (final) - ~13 % (initially)**
 Drum: **4 %**
 Position flap: **19.5°**

The vibration should be adjusted so that particle coverage on the drum is mono-layered, see Fig. S1, to guarantee optimal separation results. For large sample volumes where the funnel is initially filled with sediment the vibration should be set to ~ 13% (by experience, adjust depending on coverage on the drum). Mind that the entry-funnel should not be in contact with the vibration plate as vibration may then be dampened.

4. **Repeat:** When no remaining sample material is on the conveyor plate (or the drum begins to be multi-layered) pause the KWS and add the content of the target (plastic) container again to the funnel. When pausing/ stopping a run, power off components in the following order: vibration, drum, voltage. Carefully move the sediment in one corner of the target container (e.g. by knocking) and slowly (avoiding formation of dust) re-insert sample into the entry-funnel and start a new run. In the case of the funnel becoming clogged before being noticed, leading to the sample passing through the KWS without proper separation, re-add the content in the sediment container to the entry-funnel. Given the possibility of such cases, it is advantageous to empty the sediment container following a well-controlled run to avoid having to re-include previously separated sediment volume. Repeat run 4 times (5 runs total).

5. **Finish:** Following the final run, turn off the voltage and increase the vibration again (> 20 %) in order to 'flush' all remaining particles into the containers. Flip the drum scraper (copper plate) in order to empty the trapped sediment into the MP container.

6. **Transfer:** Weigh both the content of the left and right container to determine the total mass reduction. Transfer the content of the MP container into the density separation device and perform a density separation (here according to Enders et al., 2020). Subsequently, determine spiked MP numbers under a binocular microscope (florescent particles with help of a UV lamp). Rinse the left container with MPF water and filter onto a 10 µm filter, count any remaining MP and add to numbers previously-counted following density separation. It can help to remove the smaller MP particles when counting with a wet needle from the filter to avoid double-counts. Check all surfaces of larger particles.



Fig. S4: KWS display showing the standard settings of the test runs.

Table S1: KWS recovery rate data [%] (A – K) for the differently-sized MP that the test sediment samples were spiked with. Recovery rates for the density separation alone are presented (L - N). Median and percentiles are calculated for dust and non-dust beach sand samples, commercial sand and density separation only. Below are the mass reduction rates for the individual tests and their averages.

	Recovery rates [%]																								Med -ian	Dust only
	(a) Beach sand (kV)	(a) Beach sand (20 kV)	(a) Beach sand (22 kV)	Med -ian	Perce- ntiles [25, 75]	DS corr. ect.	b) Commercial sand (22 kV)	Med -ian	Perce- ntiles [25, 75]	DS corr. ect.	(c) Beach sand + dust (20 kV)	(c) Beach sand + dust (22 kV)	Med -ian	Perce- ntiles [25, 75]	DS corr. ect.	Density separation	L	M	N	O						
	A	B	C	D			E	F	G			H	I	J	K											
Spiked MP																										
4 mm, PA66 pellet	98	100	95	100	99	[97, 100]	99	100	100	90	100	[95, 100]	100	100	100	100	90	100	[98, 100]	100	100	100	100	100	95	
2 mm, HDPE pellet	100	100	100	95	100	[99, 100]	100	100	95	90	95	[93, 98]	95	100	95	100	100	100	[99, 100]	100	95	100	100	100	93	
2 mm, PE fibre	95	100	70	65	83	[69, 96]	83	95	80	80	80	[80, 88]	80	90	75	80	60	78	[71, 83]	78	90	100	100	100	100	
450 µm, PA6 pellet	98	83	100	90	94	[88, 98]	94	100	80	75	80	[78, 90]	80	38	45	65	80	55	[43, 69]	55	100	90	100	100	25	
125 – 150 µm, PE sphere	n.d.	n.d.	77	47	62	[55, 70]	78	48	32	21	32	[27, 40]	48	n.d.	n.d.	87	82	85	[84, 86]	100	97	82	84	84	n.d.	
63 – 74 µm, PE sphere	19	62	n.d.	36	36	[28, 49]	59	27	45	23	27	[25, 36]	49	33	35	57	49	42	[35, 51]	64	67	85	78	78	67	
20 – 27 µm, PE sphere	2	10	n.d.	13	10	[6, 12]	45	26	47	33	33	[30, 40]	68	2	5	5	29	5	[4, 11]	60	65	81	63	65	0	
Mass reduction [%]	76.4	71.2	91.6	94.0				9.8	18.1	22.9				79.1	61.6	92.6	95.5									
	73.8		92.8							16.9				70.4		94.0										



Contents lists available at ScienceDirect

MethodsX

journal homepage: www.elsevier.com/locate/mex

Method Article

When every particle matters: A QuEChERS approach to extract microplastics from environmental samples



Kristina Enders*, Robin Lenz, Juliana A. Ivar do Sul,
Alexander S. Tagg, Matthias Labrenz

Leibniz Institute for Baltic Sea Research, Seestraße 15, 18119 Rostock, Germany

A B S T R A C T

The identification of microplastics (MP), especially small (<500 µm) MP, using automated surface-chemistry approaches requires the best possible reduction of natural particles whilst preserving the integrity of the targeted synthetic polymers particles. In general, both natural and synthetic particles can be highly diverse physically and chemically and MP extraction, particularly from complex matrices such as sediments, sludge and soils, requires efficient method pipelines. Our paper presents a universal framework of modular protocols (presented in a decision tree) that fulfil predefined user requirements (QuEChERS: Quick, Easy, Cheap, Effective, Rugged, Safe) as well as providing best practises for reasonable MP working conditions within a standard laboratory. New procedures and technical innovations for density separation of particle-rich matrices are presented, such as a spiral conveyor developed and validated for MP recovery. In sharing such best-practice protocols, we aim to help in the push towards MP quantification method standardisation.

- Publication of protocols of an entire MP extraction (10 µm – 5 mm) pipeline for particle-based analysis of various environmental matrices
- Modularity: Optimised quantitative sample preparation adapted to particle sizes and sample matrices
- New protocols and technical innovations (e.g. spiral conveyor) optimise MP extraction

© 2020 Published by Elsevier B.V. This is an open access article under the CC BY-NC-ND license (<http://creativecommons.org/licenses/by-nc-nd/4.0/>).

Abbreviations: QuEChERS, Quick, Easy, Cheap, Effective, Rugged, Safe; MP, microplastics; µFTIR, micro Fourier transform infrared; ATR, attenuated total reflection; MPF, microplastic free; SPT, sodium polytungstate; QA, quality assurance; QC, quality control; PTFE, polytetrafluoroethylene; UR, user requirements; SR, system requirements; TS, technical solution; SI, supplementary information; MQ (water), MilliQ (water)/ ultrapure water; SOPs, standard operation procedures.

* Corresponding author.

E-mail addresses: kristina.enders@io-warnemuende.de (K. Enders), robin.lenz@io-warnemuende.de (R. Lenz), juliana.ivardosul@io-warnemuende.de (J.A. Ivar do Sul), alexander.tagg@io-warnemuende.de (A.S. Tagg), matthias.labrenz@io-warnemuende.de (M. Labrenz).

<http://dx.doi.org/10.1016/j.mex.2020.100784>

2215-0161/© 2020 Published by Elsevier B.V. This is an open access article under the CC BY-NC-ND license (<http://creativecommons.org/licenses/by-nc-nd/4.0/>).

ARTICLE INFO

Method name: A QuEChERS approach to extract microplastics from environmental samples

Keywords: Sequential protocol, Purification technique, Chemical digestion, Handbook for laboratory work, Manual for good practices on microplastic extraction, Contamination prevention, Recovery rates, Wastewater, Particle-rich

Article history: Accepted 30 December 2019; Available online 15 January 2020

Specification Table

Subject Area:	Environmental Science
More specific subject area:	Microplastic pollution
Method name:	A QuEChERS approach to extract microplastics from environmental samples
Name and reference of original method:	<ul style="list-style-type: none"> - Sieving: Moore, C.J., Moore, S.L., Weisberg, S.B., Lattin, G.L., Zellers, A.F.A comparison of neustonic plastic and zooplankton abundance in southern California's coastal waters. Mar. Pollut. Bull. 2002, 44, 1035–1038 [27] - Density separation: Thompson, R.C., Olsen, Y., Mitchell, R.P., Davis, A., Rowland, S.J., John, A.W.G., McGonigle, D., Russell, A.E., 2004. Lost at sea: Where is all the plastic? Science 304, 838. doi: https://doi.org/10.1126/science.1094559 [28] - Chemical digestion (H₂O₂): Liebezeit, G. Dubaish, F. 2012. Microplastics in beaches of the East Frisian islands Spiekeroog and Kachelotplate. Bull. Environ. Contam. Toxicol. 89, 213–217 [26] - (KOH/NaOCl): Enders, K., Lenz, R., Beer, S., Stedmon, C.A., 2017. Extraction of microplastic from biota: Recommended acidic digestion destroys common plastic polymers. ICES Journal of Marine Science 74, 326–331. https://doi.org/10.1093/icesjms/fsw173 [12]
Resource availability:	<p>Solutions/liquids/reagents</p> <ul style="list-style-type: none"> • Sodium polytungstate (SPT) solution, density 1800 kg m⁻³ (CAS Number 12141-67-2, TC-Tungsten Compunds) • Sodium polytungstate, crystalline (CAS Number 12141-67-2, TC-Tungsten Compunds) • 30% Hydrogen peroxide (CAS Number 7722-84, Carl Roth) • 30% Hydrochloric acid (CAS Number 7647-01-0, Merck) • Potassium hydroxide pellets (CAS Number 1310-58-3, Roth) • Sodium hypochlorite solution, 14% active chlorine (CAS Number 7681-52-9, VWR) • Acetic acid 100% (CAS Number 64-19-7, VWR) • Ethanol 99% (CAS Number 64-17-5, VWR) • Pentane (CAS Number 109-66-0, VWR) • Tween80 (CAS Number 9005-65-6, Merck) <p>Lab equipment</p> <p><i>Devices</i></p> <ul style="list-style-type: none"> • Laminar flow bench, “Clean bench” (S2020 1.8, Thermo Scientific) • Pump (Model 412721, Welch) • Freeze dryer (Delta 1-24 LSCplus, Christ) • Water purification system (Milli-Q Reference A+with Q-POD dispenser, Merck Millipore) • Sieve shaker (AS200 control, Retsch) • Stereoscope microscope (Stema 2000, Carl Zeiss) • Ultrasonic bath (Sonorex Super, Bandelin) • Muffle oven (L15/11/B170, Nabatherm GmbH) • Freezer (−20 °C) • Fridge (4 °C) • Fine particulate air filter (Vita Shield IPS, Philips) • pH meter (WTW Ingold, Mettler Toledo) • Analytical balance (EMB 2000-2, Kern) • Stain steel filtration device for tap water filtration (01WTGD05, Wolftechnik Filter-systeme GmbH & Co) equipped with stainless steel stand and handle (custom-made: IOW workshop) • Electrical overhead stirrer (Heidolph, RZR 1) <p><i>Appliances</i></p> <ul style="list-style-type: none"> • All-Glass Vacuum-filter device (ø 47 mm, metal clamp; Sartorius stedium GmbH) • Large stainless steel sieves (ø 20 cm, different mesh sizes; Retsch) • Small stainless steel sieves (ø 47 mm, different mesh sizes; VWR)

- Separation funnels, 250 ml (Squibb, Lenz Laborglas GmbH)
- Separation funnel with extra wide opening (50 mm) and valve outlet (10 mm), 500 ml, 1000 ml, (Squibb, custom-made: Hellbach Glasbläserei)
- Stainless steel (ø 20 mm) and brass (ø 35 mm) spiral conveyors (custom-made: IOW workshop)
- Stainless steel filter (ø 47 mm, 10 µm; Spörl KG)
- Stainless steel filter (200 µm; F. Carl Schröter)
- Glass fibre filter (ø 47 mm; Whatman 934-AH)
- Glass syringes (variable volumes (i.e. 20 ml, 50 ml); FORTUNA® OPTIMA®)
- Glass beakers (VWR, variable volumes i.e. 250 ml, 600 ml, 1 l)
- Glass Erlenmeyer flasks with ground glass lid and metal clamp (50 ml, 100 ml; Labsolute)
- Ceramic bowls (varying sizes, Jizerská porcelánka s.r.o.)
- Aluminium foil (30 µm thickness; Roth)
- Stainless steel tweezers (Dumont)/spoons/spatulas
- Glass Petri dishes (VWR)
- Microscopic glass slides (VWR)
- Fluorescent Green Polyethylene Microspheres (UVPMP-BG-1.025 125-150 µm, Cosphe-ric)

Method details

Protocols background

Microplastics (MP) are particulate synthetic polymerised hydrocarbons which are foreign to natural cycles and act as persistent pollutants if occurrent in the environment. It is to be expected that globally rising production volumes induce rinsing levels of this environmental pollutant if the development of waste management systems do not keep pace and non-circular economic practices persist. Commonly reported sizes of MP range between 1 µm to 5 mm. In contrast to many other environmental pollutants (e.g. heavy metals, pesticides), MP act as dispersed or suspended solid particles and their number and size determine distribution patterns and possible encounter and interaction rates with biota. Therefore, reliable techniques determining numbers and sizes of MP in various environmental matrices are greatly needed.

MP research has intensified considerably since being first scientifically described. Sampling, extraction and analysis methods have been developed and improved continuously to reach higher accuracies. However, the extraction of especially small MP (<500 µm) from various environmental matrices remains very time consuming and a general lack of standards persists. Especially particle-rich matrices such as sediments, sludge and soils require more efficient MP extraction pipelines. Ongoing developmental processes in this research field (see recent review by Zarfl [1]) produce a large variety of protocols which usually depend on the conditions and resources of the laboratories, as well as the sample type and research questions involved. There are numerous scientific publications on MP extraction of a specific sample matrix [2–5], which can be disadvantageous, both in terms of additional costs and required expertise when diversifying the MP extraction work between several sample types.

Objectives

We present a comprehensive compilation of both modified and new methods for MP purification, organised into individual methodological modules designed to be adaptable to the sample type proposed for analysis, and flexible enough to be implemented in a general-purpose research laboratory. Although an optimal working condition for MP sample treatment would require a purpose-built clean lab facility (see SI.1 for further information), the de facto condition for many researchers is to work in a standard laboratory, often used by several other research disciplines simultaneously. Yet some adaptations to a general lab are highly encouraged, the most important of which is the installation of a laminar flow bench to be used exclusively as an MPF zone for all steps involving work on open MP samples. Within the proposed protocol modules are also novel technical steps to further

improve both accuracy and efficiency of MP purification. This is especially important given the increasing shift from visual analysis of large MP only towards a focus on the full spectrum of MP size and type using highly-precise, automated, particle-based analysis approaches. Therefore, the overarching aim of this paper is to enable and encourage an adoption of MP-suitable working conditions. To pursue this goal, the following objectives are satisfied:

- a set of coordinated protocols and devices are presented
- a technical solution to density separations is demonstrated that addresses shortcomings of existing methods
- advice is given to the reader on how to construct a full workflow from the provided protocols, which is adapted to the specific sample properties

Analytical requirements: when every particle counts

The endpoint of automated particle-based analyses, i.e. via micro Fourier transform infrared (μ FTIR) or Raman spectroscopy, is the quantification of MP particles based on their chemical compositions or fingerprints without prior visual inspection. Independent of the sample type, the analysis time is mainly dependent on the final number of particles that has to be measured. Thus, when extracting MP from environmental samples, the overarching goal is the best possible reduction of natural particles while preserving the targeted synthetic polymers in numbers, sizes, shapes as well as their chemical composition. The final particle number also greatly depends on the particle size limit. While a common definition of the lower MP size is not yet established, the presented protocols are designed and applied for MP of 10 μ m to 5 mm. It should be noted, that MP cover a size range differing up to 500-fold. An analysis attempt in one go would lead to restricted efficiency and quality in the analysis, i.e. by larger particles eclipsing smaller ones. We suggest several options to size-fractionate large, manually handleable particles from smaller MP and prepare them for single particle analysis, e.g. attenuated total reflection (ATR) FTIR (personal communication with Fischer) [6].

All the methods proposed here have been developed with the “QuEChERS” (quick, easy, cheap, effective, rugged and safe) approach in mind [7,8], and are presented in a way reminiscent of systems engineering [9,10]. Fig. 1 visually demonstrates how these approaches have been applied to the presented MP methodology; giving users the methods to achieve their desired goals whilst meeting QuEChERS standards.

In order to analyse a variety of sample matrices, which can differ markedly in composition (i.e. water vs soil), different methodological steps may be needed. By segmenting the methods into modules, certain procedures can be included or omitted as required by the sample type in question, greatly increasing the flexibility of the proposed methods. In order to ascertain which modules should be combined and in what order for a given sample matrix, a decision tree is an ideal way to guide a user to what specific methods they require.

The protocol tree: a decision tree for the protocol modules

We used a decision tree to visualise the complete workflow of connectible protocol modules (see section Protocol modules m0–m6), referred to as the protocol tree (Fig. 2).

How to use the protocol tree and modules?

The sample matrix and the numbers and the sizes of targeted MP determine the route through the tree. They define the optimal protocol pipeline along the tree structure adapted for a given individual case. Essential advancements of the presented methods originate from newly developed equipment applied in the protocols and are described in the respective section (New Equipment). All other materials needed are listed in the beginning of the paper. General MP laboratory procedures, including the cleaning of equipment and laboratory, MPF-filtration of solutions, etc. are described in the general module (m0). Further general measures of quality assurance and control (QA/QC) are described in the

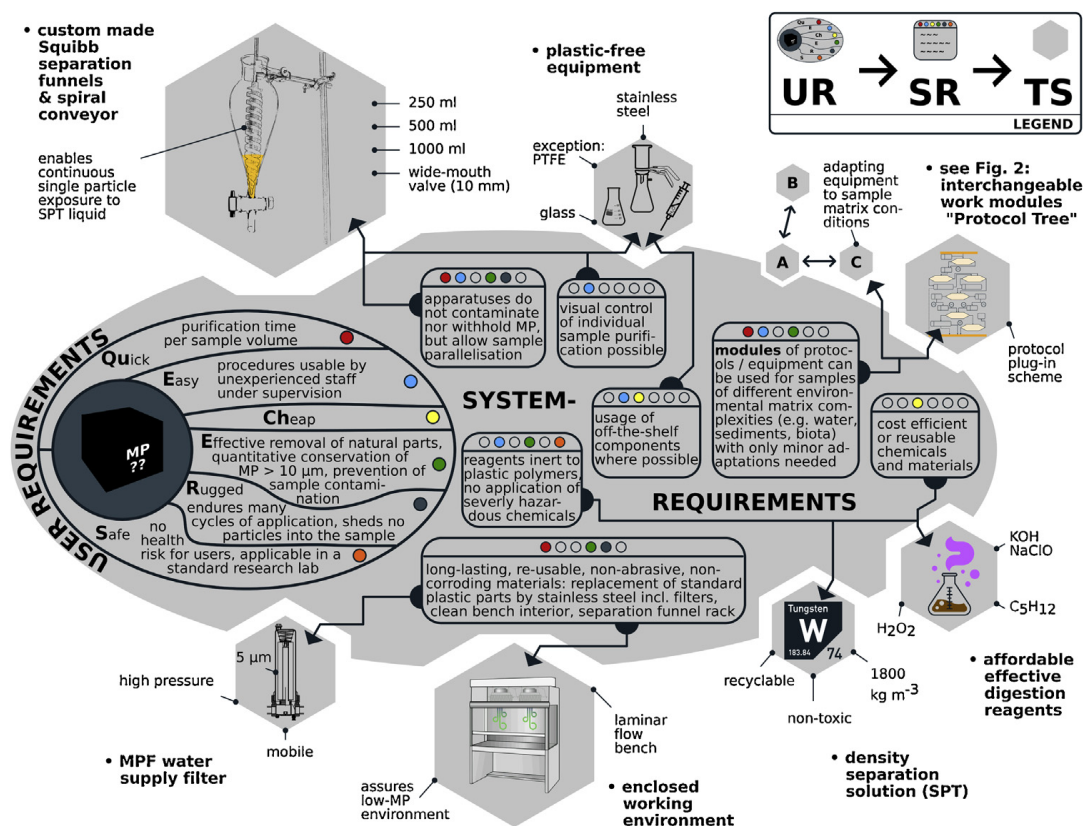


Fig. 1. The scheme detailing the three main components of a system engineering approach is meant to be read from the kernel (the "black box") of a yet to be analysed MP sample. Under the overall goal of enabling a sample to be submitted for efficient microspectroscopic particle identification, the main objectives are the near-complete reduction of natural substances and the preservation of the contained MP. Users requirements (UR, placed around the kernel) formulate typical considerations of MP researchers working under these objectives. They are summarised here by the targets of a QuEChERS approach. One or more UR define a system requirement (SR, in rounded boxes) that specifies what a solution must provide in order to achieve the UR targets. The coloured circles indicate which SR are derived from which UR. Finally, the approach culminates in technical specifications (TS) that satisfy the previously defined requirements. Part of the solutions are the equipment (chemicals,

respective SI section (SI.2). To cover the diversity of samples in volume and composition some protocol modules contain different optional paths to follow, indicated by an arrow (➡).

Modularity and variations due to sample composition

The two widely used techniques to extract MP for a particle-based analysis are a separation by particle density (MP typically range from 900 to 1600 kg m⁻³) which primarily eliminates the mineral fraction (e.g. quartz, $\rho = 2650$ kg m⁻³), and chemical destruction i.e. digestion of particulate organic matter (see e.g. review by [11]). Covering the entire range of possible sample matrices (conceivably substances like honey, household dust, food waste, construction rubble, etc.) would make the decision tree increasingly complex. The focus of the presented protocol workflows is on environmental samples, such as water, soils, sludge, sediments and biota. Biota, for instance, comprise a large range of different biogenic material compositions (chitin, keratin, lipids, etc.) ranging from small zooplankton to stomach contents of birds, some of which may require a repetition or skipping of modules. In most of these cases a freeze drying step may be omitted if the dry weight is not required. Besides, freeze drying facilitates the following digestion step by breaking up cell walls (i.e. in samples rich in plant-based material). In case of a sample being largely made of animal tissue, this time-consuming step may be left out and still yields readily digestible samples. Also, a density separation module might not

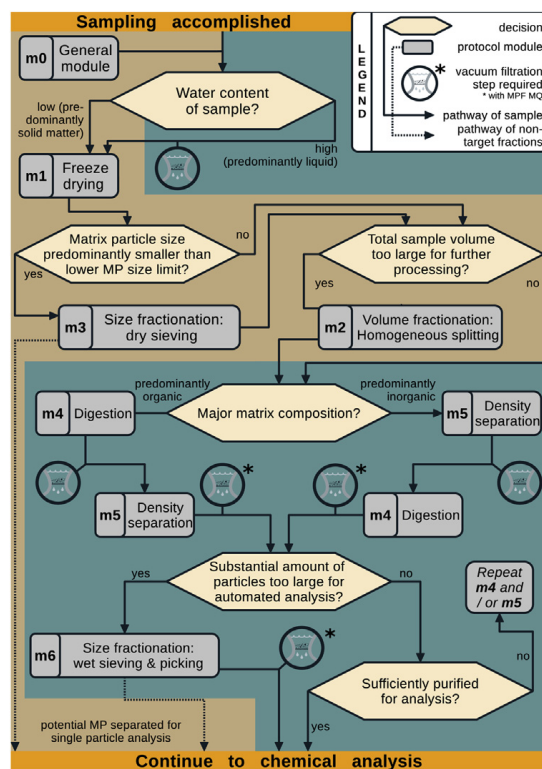


Fig. 2. The decision tree comprises the procedural steps involved in the preprocessing of environmental samples for later particle-based MP chemical analysis. The decision tree starts after accomplished sampling with the sample being transferred from the sampling device, if applicable. It consists of a number of protocol modules equipped with indices (m0–m6) each of them referring to the detailed protocols. The digestion module m4 is further subdivided by specific treatments in a scheme below. These protocol modules are linked through various decisional paths that have to be taken for a complete pretreatment. The background colours indicate whether the sample is in dry (brown) or wet (blue) condition. Vacuum-filtration often finalises wet modules and is included in the respective protocol modules. As filtration is an important intermediate step, it is indicated by a respective symbol (close up of a filter unit, see legend).

be necessary, if only negligible amounts of dense non-MP particles remain after digestion. Generally, fewer treatment modules, hence less sample manipulation, is preferential when dealing with potentially small numbers of MP. The required minimum particle size determines parts of the procedural details (e.g. m3 or m6) to assure that also the smallest targeted MP can be reliably quantified.

Digestion modules (m4.1–m4.3) more often necessitate a case-by-case adaptation and are therefore a good example of methodological variation based on sample type. While a purely oxidative treatment with hydrogen peroxide can successfully be applied for purification of water or sediment samples (m4.1), it often fails to degrade animal tissues in reasonable time [2]. A combined alkaline-oxidative treatment based on diluted potassium hydroxide and sodium hypochlorite [12,13] serves as a more appropriate choice for many biota samples (m4.2). The high fat, oil or wax content that can be present in biota samples can in principal be broken up by simple alkaline hydrolysis. However, this process may require longer reaction times or higher temperatures than what is desirable for MP purifications. Therefore, remaining lipid constituents are recommended here to be removed by an additional *n*-pentane based washing module instead (m4.3). In contrast to the other digestion and density separation modules, the application of a *n*-pentane based treatment has not yet been described for MP sample purification. The effectiveness of the proposed method in terms of achieving better spectral qualities in Raman or μ FTIR analysis is promising for sample matrices where lipids could not be sufficiently removed by the other protocols. Apart from biota samples, the application of the *n*-pentane treatment was preliminarily tested for primary sludge samples from waste water treatments plants that contain potentially high levels of fats

and oils, partly due to artificial substitution. This is especially challenging during MP extraction as fats and oils enclose sample material and this way reduce the effectiveness of the other treatments. A proposed digestion pipeline for these specific sample matrices is a treatment with n-pentane enclosed by repeated hydrogen peroxide digestions. However, the n-pentane module is presented here as a preliminary method, as its inertness to targeted polymers is currently being evaluated (R. Lenz, unpublished data). The general principle is based on classic organic chemistry procedures to dissolve or extract emulsified or deposited lipids from a sample and was applied before in a similar manner e.g. in infant milk fat extraction protocols [14,15]. Fischer and Scholz-Böttcher, 2017 [16] used petroleum ether to prepare greasy fish stomach samples for a mass-based MP analysis (Pyrolysis-Gas Chromatography - Mass-Spectrometry). Compared to n-pentane, use of petroleum can reduce operating costs but has higher health risk due to its hexane contents. The lipid removal potential and resistance of polymers can be expected to be comparable between the two chemicals. The following section presents all protocol modules that build the protocol tree.

Protocol modules

m0 – General module

► Irrespective of the protocol pathway selected it is recommended to read the general module as a prerequisite for many other modules as it covers overarching procedural steps when working with MP. It only contains procedures that are specific for the here applied protocols and materials and/or are not yet exhaustively covered in the MP literature and/or are not standard laboratory routines.¹

Clean bench SOPs: Ensure to keep all surfaces in the laminar flow bench MPF and ready to use. Solely use tissues made of non-disintegrating natural fibres. All water used to clean surfaces should be MPF water. Before use, make sure to rinse all materials with MPF water or muffle at 500 °C. Before muffling, cover with aluminium foil and open again only inside the clean bench to avoid contamination. All sample containers should be rinsed with MPF water when entering the clean bench coming from non-MPF conditions (such as field sampling or cold storage). Additionally, vessels like beakers or Erlenmeyer flasks which hold samples inside the bench are to be thoroughly rinsed with MPF water or MPF MQ before being poured into a filtration or another container. This is important, as a complete separation of droplets from the inner and outer walls cannot be guaranteed during pouring and rinsing procedures. Contamination should also be prevented by entering the bench with arms and hands when working in it. Always wear a 100% cotton lab coat and nitrile gloves kept over the lab coat sleeves to protect the skin and avoid contamination by synthetic clothes. Before entering always use abundant MPF water to wash your hands/gloves.

Cleaning fine stainless steel filters (e.g. 10 µm): After usage, rinse all stainless steel filters with MPF water from the tap to remove coarse dirt. Put the filters in a glass beaker, fill with MPF water and cover with aluminium foil (at all times). Apply repetitive ultrasonic bath sessions with changing power values (50–100%).² Recommended are 10 min at 35 kHz and 225 W (for a volume of the ultrasonic bath of 18.7 l). In the initial session, diluted H₂O₂ can be added if the filters contain organic matter. Alternatively few drops of MPF Tween80 can be added. Rinse the beaker and filters and renew the MPF water in between subsequent baths to make sure that all particles are removed from the both the filters and the residual water. It is advisable to apply a minimum of 3 repetitions. However, if the water in the beaker remains cloudy or hazy after sonification the procedure should be repeated. After the final treatment, discard the water from the beaker, rinse and fill up with fresh MPF water. At this point, the MPF filters are ready to be used. Keep them inside the bench in a beaker. Just before use, rinse again with MPF water using tweezers and a syringe.

¹ Note: This document does not include a complete health and safety evaluation of the laboratory procedures. Please carry out a risk assessment for all field and lab work activities and adhere to the health and safety guidelines at your institute or organisation.

² It was observed that changing the power resulted in a more efficient removal of matter.


MPF solutions: It is essential when working with MP to ensure that all solutions which get in contact with the sample and/or are used in the clean bench are MPF. Use a vacuum filtration system to filter all solutions (apart from tap water, see tap water filter in the SI.3). Use a filter below your minimum size threshold to ensure a complete removal, e.g. the presented protocols predominantly use 10 μm as the minimum size threshold, a 1.5 μm glass fibre filter (cleaned beforehand³) is used for the last filtration. Make sure that the solutions are filtered in pre-cleaned MPF glass bottles and are covered with aluminium foil inside the bench. Appropriate labelling of samples and solutions is part of standard laboratory routines. During MP-extraction it can help to consistently label all the MPF solutions accordingly with “MPF”. Inside the clean bench, keep one glass syringe for each specific solution in use and avoid cross-over.


SPTrecovery: The SPT solution can be used for many density separation cycles either by recycling at the manufacturer (if available) or by vacuum filtration in the laboratory. After usage of the SPT solution leave it to settle in a collection flask (>24 h). Pour the supernatant into a separate collection flask. As soon as stirred up particles appear, leave the remaining solution to completely settle again for later recovery. Check pH of recovered SPT before use and adjust to pH 3 if necessary by adding droplets of HCl (10%). Check the density by weighing a defined volume (e.g. 100 ml) and adjust to 1800 kg m^{-3} by dissolving the required amount of crystalline SPT salt in the recovered solution. Vacuum-filter the SPT solution onto a MPF glass fibre filter as explained in the MPF solution section above. In case of high particle content, a pre-filtration on a filter with larger pore sizes (e.g. on 10 μm stainless steel filters) may be applied beforehand to expedite the process. Reconfirm pH and density again after filtration.

Explanatory remarks

► **Starting condition:** Any sampling equipment or specific pretreatment step, such as the removal of sample material from a given sampling device, must be completed beforehand. The assumed sample condition for the following protocols begins with the sample material in a dedicated vessel (e.g. glass beaker).

► **Finishing condition:** The aspiration of a complete pipeline is to bring an environmental MP sample from any possible compartment to an acceptable condition for particle-based chemical analysis. The presented protocols assume that there is a temporal or spatial discontinuity between the sample purification and the analysis, which is why treatments end with readily purified MP particles suspended in MPF MQ water, stored in a sealed MPF glass container (e.g. Erlenmeyer flasks with ground glass joint). This specific procedure is described in detail below (Final Filtration) and is to be conducted at the end of a protocol pipeline. As it would be repetitive to include them in every respective section they are stated here as a general instruction. In case the sample will be submitted to chemical analysis instantly within the same lab, the finalising filtration may be conducted directly onto the desired analysis substrate.

 **Filtration:** Vacuum-filtration often finalises wet modules and is described in detail in the respective protocol modules. The symbol is to be found in the protocol tree (Fig. 2). Additional ultrasonification: Depending on filter pore size and sample composition, removing the sample particles from the filter by rinsing may be non-exhaustive⁴. In such cases the filter should be additionally cleaned in an ultrasonic bath for minimum 2 minutes and residues added to the sample⁵. Check if additional ultrasonification is needed to remove all sample particles from the filter.

 **Final Filtration:** The “Final Filtration” symbol is included as an optional path in the respective protocol modules where applicable. This is your last step before chemical analysis. Flush your filtering sample again using MPF MQ water to remove all solutes from the sample⁶ (it is marked in the protocol

³ To MPF-clean glass-fibre filters, transfer them to a clean petri dish and cover it with aluminium foil. Bake all filters at 500 °C for 5 h. Only remove the filters from the petri dish inside the bench.

⁴ Check filter after rinsing step under a binocular microscope for remaining material.

⁵ The use (or avoidance) of an ultra-sonification should be conducted in a systematic way within one study.

⁶ Remaining solutes can influence spectroscopic results.

tree with the filtration symbol and an asterisk). At the end of a filtration the filter is removed from the apparatus using tweezers.

➡ If you see >3 MP particles too large for microspectroscopic analysis, apply the module “Size-fractionation: wet sieving & picking” (m6).

Then rinse off the remaining sample particles from the filter into the same final Erlenmeyer flask using MPF MQ water. Place the filter in a clean beaker and cover it with MPF MQ water and sonicate for 2 min to remove all particles from the filter. Then rinse the filter off and add the residues into the same Erlenmeyer flask that contains the bulk of the sample. Close with glass stopper and secure with metal clip. Once the filter is cleaned without residues it can be removed. The sample should be stored in a fridge (4 °C).⁷

m1 – Freeze-drying

► Freeze drying is usually performed for one or several of the following three reasons: a) reduction of water in the sample and breakage of particle conglomerates (resulting in a “fluffy” texture) to allow unrestricted performance of the next processing steps (e.g. digestion or density separation), b) determination of the dry weight and c) breakage of cell walls and membranes during the freezing step to increase later digestion efficiency.

1. **Filter:** If the sample is predominantly liquid, filter it in the vacuum filtration set up on a stainless steel filter of the lowest size threshold (e.g. 10 µm). Replace filters if clogged. Make sure to properly rinse all walls, including the sample vessel and the vacuum filtration funnel that the sample was in contact with. Depending on the sample matrix, it may be appropriate to use a diluted detergent solution (e.g. Tween80) to remove sample adherences from the glass ware. Collect all filters (containing sample material) in a glass beaker and add the sample rinsate of the filtration funnels. Cover with aluminium foil.

2. **Freeze:** Freeze the sample at –20 °C (~24 h).⁸

3. **Cover:** Cover sample with an air-permeable MPF membrane with a mesh size smaller than that of the lowest detection size (dust-free tissue paper is ideal for most applications). Fix coverings firmly in place (elastic bands are appropriate). It is recommended to perform the uncovered part near an air filtration device or within an MPF clean bench to avoid contamination.

4. **Freeze-dry:** Freeze-dry the sample according to machine manufacturer’s guidelines until the sample is completely dry.

5. **Weigh:** If the sample is not further split, the dry weight is now to be determined.

m2 – Volume-fractionation (homogeneous splitting)

► Depending on the initial sample volume, a volume fractionation can be necessary to reduce the amount of sample that is treated, or split into several sub-fractions (e.g., for method comparison purposes). If this step is used as sub-sampling (i.e. not all split parts are to be further processed) an effective homogenisation of the sample is most critical for a successful volume fractionation.

1. **Mix:** For freeze-dried samples, shake the sample with the lid closed for minimum 2 min. Then wait until all particles settled. Open the lid and mix the sample with a clean MPF long metal spoon for further minimum 2 min⁹ within the MPF clean bench or, if not possible, near an air filtration device. If mixing in the available sample container is restricted, transfer the sample to a MPF-cleaned bowl (i.e. ceramic or stainless steel) and proceed with the homogenisation process.

2. **Split:** Transfer the required sample (dry) weight directly into a separate glass beaker, tarred on a scale. If required, several replicate sub-fractions can be obtained in this way.

⁷ Cooling the extracted MP sample prevents new biofilms to establish, which would hamper spectroscopic analysis.

⁸ If the sample is in a glass container, there is a risk of the glassware breaking as a function of the increasing volume. Placing the sample at a <45° angle can improve matters as this increases the expandable surface area. However, the use of non-breakable MPF containers, such as stainless steel or aluminium, is an ideal alternative for large water volumes.

⁹ Mixing times need to be adjusted depending on sample volume and container.

m3 – Size-fractionation (dry sieving)

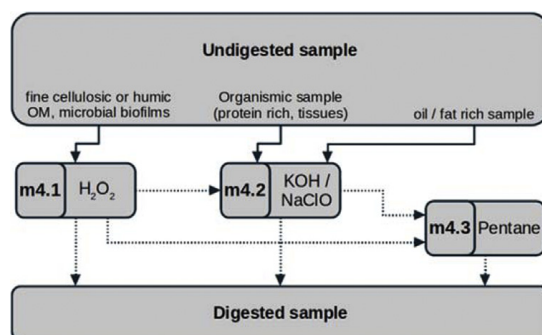
► To further ease processing and analysis of samples where the predominant particle size is substantially smaller than the lower MP size limit, the sample volume can be reduced by sifting out a lower particle size fraction by dry sieving. In principle, this method can also be applied to compartmentalise the sample into a variety of sample fractions of differing particle size, e.g., for differing analytical approaches (visual, surface chemistry, chromatography).¹⁰

1. Prepare: Select sieve sizes appropriate to the size-fractions desired and form a stack. Use a close-fitting stainless steel lid, alternatively thick aluminium foil, to cover the sieve(s) from the top and the bottom. Then slowly add the sample (ideally freeze-dried) to the top sieve, in an MPF clean bench or near an air filtration device. Close the sieve stack making sure there are no gaps where sample material may escape (or contaminated air may enter).

2. Sieve: Secure sieve stack in shaker. The amplitude and time can be adjusted according to how easily the sample sieves. We suggest, however, to start with lower amplitudes and shake times and document progress. Two rounds of 5–10 min at 0.75–1.5 mm amplitudes have been found to be sufficient for a variety of soil samples.

m4 – Digestion

► Chemical digestion is a major step to reduce the organic matter content of a sample. A set of different digestion sub-modules are provided that are to be applied for different sample matrices (see scheme below).¹¹



m4.1 – Hydrogen peroxide (H₂O₂) digestion

► Hydrogen peroxide (H₂O₂) at 30% is a strong oxidizer. Typically, it is the primary choice for digesting water, sediment, soil, waste water and sludge samples. However, in certain cases the sample matrix might contain substances that are highly resistant to the treatment in which cases other subsequent digestion steps may be added.

1. Add: Depending on the nature of the sample, i.e. organic matter content and presence of iron ions, the reaction after the addition of H₂O₂ can be very energetic (bubble formation and temperature rise). Because of that, it has to be added very carefully and in small amounts. With a glass syringe, add up to 5 ml of H₂O₂ to the sample. For unknown sample matrix even smaller amounts (~2 ml) should be added initially and observed.¹² To anticipate heat generation or an overflow event, the beaker can be

¹⁰ Dry sieving should only be applied if unavoidable as it comes at the risk of losing small particles either during the transfer processes or due to adherence on larger particle surfaces. If applied, use it consistently for the entire data set.

¹¹ None of the chemicals proposed here are listed under “severely hazardous” (class 3) in the water hazard class (German Water Hazard Classification).

¹² Bubbles indicate that the oxidation of the organic matter started (CO₂ is formed as a result of the chemical reaction between H₂O₂ and organic C). Bubble formation can be delayed by several minutes to hours after addition.

kept in a second MPF container (e.g. larger beaker or ceramic bowl) with cold MPF water to avoid temperature rise to more than 40 °C. When working in a fume hood without appropriate MPF conditions an aluminium foil lid should cover the sample at all times and only shortly opened to insert the tip of the glass syringe.

2. **Proceed:** Add more H_2O_2 with a syringe until it completely covers the whole sample. Shake the sample and rinse the walls with H_2O_2 to allow all particles to be in contact with the digestion solution. The beaker should be kept closed in a fume hood for minimum 24 h. Generally, additional H_2O_2 should be added or replaced (filter sample and add new H_2O_2) for as long as the digestion process continues or organic matter remains visible.¹³

► If the sample remains with large indigestible non-MP debris manually pick each item, rinse off adherent smaller particles into the sample and discard. It is recommended to cut very large pieces (e.g. blades of grass, leaves, braches) into smaller ones to allow a more efficient disintegration of biofilms and particle conglomerates during the digestion process.

3. **Filter:** To end the digestion, filter the digested sample in the vacuum filtration set up on a stainless steel filter of the lowest size threshold (e.g. 10 μm). Carefully rinse the stainless steel filter that remained in H_2O_2 from the previous filtration step from all sides using MPF water, hold it with tweezers and/or a gloved hand. Replace filters if clogged. Once the filter is cleaned without residues it can be removed. Make sure to properly rinse all walls, including the beaker and the vacuum filtration funnel that the sample was in contact with. Depending on the sample matrix, it may be appropriate to use a diluted detergent solution (e.g. Tween80) to remove sample adherences from the glassware.



m4.2 – Potassium hydroxide (KOH) digestion

► This protocol module may be applied for samples high in protein content like animal tissue (e.g. stomach analysis). It can also be applied for environmental samples with a challenging matrix composition, that do not sufficiently digest in H_2O_2 .

1. **Prepare:** A saturated KOH stock solution is prepared by dissolving 1120 g/l of dry KOH salt (pellets) in water inside a tightly-closed glass bottle. Shake well until complete dissolution. Beware of heat generation, it may be advisable to reduce the temperature with a water bath. The digestion solution is prepared according to the below recipe:

Per 1 l of digestion solution to add to a glass bottle: 700 ml of water (tap water or MilliQ)
ml NaClO (14% active chlorine)
ml KOH stock solution

After adding the active chlorine, re-seal the bottle and shake well for homogenisation. The ready digestion solution can now be MPF filtered (see General Module m0).

2. **Digest:** Add 5 ml of MPF-filtered digestion solution per gram wet-weight of sample¹⁴ into the sample vessel, however at least so much that the sample is completely covered with solution. Shake gently to allow the solution to reach all parts of the sample. Leave for 5 h incubation at room temperature.

3. **Filter:** To stop the digestion, filter the digested sample in the vacuum filtration set up on a stainless steel filter of the lowest size threshold (e.g. 10 μm). Carefully rinse the stainless steel filter(s) that remained in the digestive solution from the previous filtration step from all sides using MPF water, hold it by tweezers and/or gloved hand. Replace filters if clogged. Once the filter is cleaned without residues it can be removed. Make sure to properly rinse all walls, including the beaker and the vacuum filtration funnel that the sample was in contact with. Depending on the sample matrix, it may

¹³ This recommendation aims to provide H_2O_2 in excess to the available digestible OM.

¹⁴ To estimate the required amount of digestion solution measure the wet weight of the samples.

be appropriate to use a diluted detergent solution (e.g. Tween80) to remove sample adherences from the glass ware.



m4.3 – n-Pentane (C_5H_{12}) digestion

► Oil and fat constituents in sample matrices can sometimes remain in the digested sample and hinder a successful spectroscopic analysis.¹⁵ Possible use-cases of n-pentane¹⁶ include digested animal tissues (e.g. in fish stomach analysis) post-KOH digestion and primary sludge samples from waste water treatment facilities post- H_2O_2 digestion. The procedure requires extended times with the sample exposed to air and should therefore be conducted inside the MPF clean bench. Check if your work safety regulations require wearing a gas mask (filter type “AX”).

1. **Solubilise:** As a precondition, the digested sample should be contained in a tightly sealed vessel (e.g. Erlenmeyer flasks with ground glass joint) and must be suspended in MPF water or MPF MQ. To better solubilise the fatty constituents, hold the sample in a 35 °C water bath during the procedure. Wait for the sample to warm up to approx. 35 °C, then add 10 ml of the acidified ethanol (pH ~ 3.0, acidified with acidic acid) per 50 ml of sample. Close and shake the sample for 1 min. Place in the warm water bath again.

2. **Wash:** When the ethanol is fully mixed in the sample continue by adding 10 ml of n-pentane per 50 ml of sample. Close the lid tightly and shake for 2 min. Stop shaking and open the flask periodically to release pressure.¹⁷ Return the sample to the warm water bath and allow the phases to separate for 5 min, with a loosely-closed lid.

3. **Remove:** Remove the pentane phase from the top of the sample using a glass pipette.¹⁸ Stop just before the pentane layer disappears to avoid sucking the sample.¹⁹ Repeat the above steps a further two times.

4. **Filter:** To remove any remaining dissolved fats and pentane continue with a vacuum filtration. Filter the sample in the vacuum filtration set up onto a stainless steel filter of the lowest size threshold (e.g. 10 µm). Make sure to properly rinse all walls, including the Erlenmeyer flask and the vacuum filtration funnel that the sample was in contact with. Check if additional ultasonification is needed to remove all sample particles from the filter (see Filtration above). Once the filter is cleaned without residues it can be removed. Make sure to properly rinse all walls, including the beaker and the vacuum filtration funnel that the sample was in contact with. Depending on the sample matrix, it may be appropriate to use a diluted detergent solution (e.g. Tween80) to remove sample adherences from the glass ware.



m5 – Density separation

► Density separation is a major step to reduce the inorganic matter content of a sample.

¹⁵ Droplets of fat or oily remains may or may not be visible, but fatty acids, their salts or alcohol combinations can be identified by spectroscopic analysis if present in the sample.

¹⁶ Based on theoretical chemical considerations, it is not expected that the protocol could impact the integrity, numbers or spectral recognisability of common plastic polymers. However, a detailed test on actual MP is yet to be completed.

¹⁷ Pentane has a boiling point of 36 °C, pressure may build up in the tightly closed containers.

¹⁸ The pentane phase should not contain any MP due to a lower density (630 kg m^{-3}) than that of plastics and low surface tension. This was checked by observing the behaviour of standard fluorescent PE spheres mixed in a water/pentane dispersion.

¹⁹ Low density MP particles might float directly in the phase boundary.

1. **Transfer:** Choose a separation funnel of appropriate volume.²⁰ Transfer the sample (dry or suspended in SPT) from a beaker or filter to the separation funnel.

➡ **Size fractionation:** If the sample contains particles >5 mm or larger than the outlet valve, manually pick (if just very few larger particles) or sieve the sample during transfer to prevent blockage in the outlet valve or during the stirring of the sample. Sieving: Place a glass or metal funnel²¹ in the top of the separation funnel with a small sieve (e.g. 4 mm pore size) inside and pass the entire sample (preferably dry) through with help of a metal spatula. Thoroughly rinse the large particles that remained on the sieve with SPT to rinse all adhering smaller particles into the sample. Optionally, retained particles can also be transferred to a beaker with a few droplets of H₂O₂ and SPT to ensure a complete detachment of adhering particles. The detachment process might take some minutes. The rinsate is then added to the separation funnel.

Fill approximately 10% of the separation funnel (valve closed!) with MPF SPT (1800 kg m⁻³).

Add a first fraction of the sample (maximum up to 5 cm high from the lower tip of the separation funnel) and shake thoroughly to ensure that all particles in the lowest tip of the separation funnel are coated by the SPT solution. Then gently swing/shake the separation funnel inclining it ~45°.

➡ If the sample does not contain more than approximately 5 g of solids (e.g. water samples) repeat gentle swinging of the separation funnel every 15 min during the first hour to resuspend the settled material and disintegrate agglomerates.

➡ If the sample does not allow for digestion before density separation, add a few droplets of H₂O₂ solution during the shaking process to initiate the disintegration of particle conglomerates, wait for the reaction to proceed.²²

2. **Upwell:** If the sample material exceeds a volume where shaking of the separation funnel becomes insufficient in freeing possible overlays of particles (as often the case for sediment and soil samples) continue with the following steps. Firstly, prefill a part of the required SPT solution into the separation funnel followed by a small amount of the sample material. Subsequently add the remaining sample material and SPT solution. Top up with a minimum of 5 cm SPT solution to form the separation phase. Thoroughly rinse all equipment that was in contact with the sample material with SPT, such as the beaker, funnel and sieve and add it to the separation funnel. Insert the spiral conveyor to the sample and mount it to the electrical overhead stirrer. Centre and place it as low as possible but make sure it does not touch the walls of the separation funnel. Run it at relatively low speed (~35–60 rpm) for approximately 2 h. The time needed to allow sufficient reshuffling of the material depends on sample composition, amount and dimensions of the separation funnel and spiral conveyor.²³ After conveying, stop the spiral conveyor and thoroughly rinse adhering material into the separation funnel with ample MPF SPT while slowly lifting it out of the separation funnel. Release the lower tip (approximately 3 cm) of the separation funnel into a beaker and re-add to the separation solution.²⁴

²⁰ Maximum filling level of the separation funnels should not exceed 2/3 of the total volume. If samples with high matter content (e.g. sediment, soils, etc.) are treated and the application of the spiral conveyor is needed, use the appropriate separation funnels equipped with a wider neck and wider outlet valve (see section: Modified separation funnels – a versatile application for particle-rich samples).

²¹ The here-presented set up also allows for sieving without a funnel, as the neck of the separation funnel fits the size of the small sieves applied. However, using a funnel potentially prevents loss of material.

²² Be careful when adding H₂O₂ to the density separation. Always add only a few droplets to prevent the risk of strong foam formation and loss of sample material. Consider that the addition of H₂O₂ dilutes the density of the solution, therefore adjust or use an initially higher density.

²³ The time reported here is based on sufficient extraction results based on test MP particles (125–150 µm) in very fine sediments (40–70 µm) in a 500 ml separation funnel (see section: Conical spiral conveyor – a gentle way to separate particles). Larger volumes or more complex sample compositions may require longer time. If in doubt, test the specific sediment matrix with recovery particles.

²⁴ In order to recover potential MP that have become trapped close to the outlet of the separation funnel.

3. Wait: Rinse the inner walls of the separation funnel to ensure that all particles are in the separation solution. Leave it to separate for 1.1 h per 1 cm rising distance in the fluid separation phase.²⁵

4. Divide: Slowly (no stirring up of particles) release the sedimented fraction into a MPF beaker placed below the separation funnel and shut the valve securely before any surface floating particles could be flushed out.

5. Repeat (*X_{DS}): Depending on the sediment composition (especially fine/organic rich samples) the density separation (DS) cycle has to be repeated (X_{DS} times) to reach a higher purification efficiency. Therefore, refill some MPF SPT, shake and leave it again to settle for 15 h. After this, evaluate whether you need to repeat again. As a rule, apply as many separation cycles until no further material has settled.

6. Filter: When the separation is finished, rinse the supernatant upside down from the separation funnel into the vacuum filtration apparatus equipped with a stainless steel filter of the lowest size threshold (e.g. 10 µm). Replace filters if clogged. Recover the undiluted SPT solution by transferring it from the filtration apparatus to a dedicated SPT recovery container (see General module m0). Then continue to thoroughly rinse the content of the separation funnel (incl. walls and glass stopper if used) into the vacuum filtration funnel using MPF water and a syringe. Take care not to lose any droplet or particle. Rinse all walls of the top part of the vacuum filter apparatus. Once the filter is cleaned without residues it can be removed. Depending on the sample matrix, it may be appropriate to use a diluted detergent solution (e.g. Tween80) to remove sample adherences from the glass ware.



m6 – Size-fractionation (wet sieving or visual sorting)

► Samples which remain relatively rich in larger particles (>500 µm) even after passing the treatment pipeline should be size-compartmentalised to ease later chemical analysis.

► The sorting and picking process should always be conducted in a very conservative manner, meaning that only particles with clear indications of natural origin may be discarded and any other particle is to be picked and retained for analysis. This is important to minimise researcher bias. Whether to use 0.5 or 1 mm as a cut-off size should be decided according to the following criteria table:

	Situations suggesting a cut-off size of 0.5 mm	1 mm
Experience level of the separator	High: picking of 500 µm particles in a conservative manner is only possible with an experienced eye and hand	Low: only for particles larger 1 mm, can an inexperienced user conduct a conservative separation after a basic introduction
Number of particles in 500–1000 µm and >1000 µm size range	Particles potentially disturbing the microspectroscopic analysis are numerous in the 0.5–1 mm range	Particles potentially disturbing the microspectroscopic analysis are predominantly in the >1 mm range
Size cut-off predefined by sampling technique	Lower than 300 µm (e.g. sediment samples, flow-through filtration water samples)	300 µm and larger (e.g. Manta samples)

It should be noted that a 500 µm cut-off size should preferably be used in all cases where possible and meaningful, as it will be more beneficial to ease and expedite the microspectroscopic analysis of the remaining small fraction.

²⁵ The required rising time (waiting time) is calculated based on a spherical 10 µm particle of a density of 1.7 g cm⁻³ that travels a certain distance measured between the bottom to the top of the separation phase in SPT of 1.8 g cm⁻³ (Stokes law). Example: For a distance of 13.5 cm (maximum height experienced by the authors) this particle needs 13.7 h to rise to the top (1.1 h for 1 cm).

► Depending on the number of particles, a case by case decision needs to be taken whether wet sieving is applied before visual sorting. In general, when more than 10 particles are above the chosen upper size limit for microspectroscopic analysis, it is advisable to first wet sieve the particles according to the below steps:

Optional wet sieving prior to visual sorting and picking

1. **Set up:** Prepare a filtration set-up as usual (e.g. 10 or 200 μm filter depending on minimum size limit) and place an additional 1 mm²⁶ stainless steel sieve into the vacuum filtration apparatus.

2. **Rinse:** Turn on the vacuum pump and transfer the sample by using ample MPF water, rinse the sample container and the filtrate thoroughly.²⁷ Finish this step by rising the sample and all relevant walls with MPF MQ water.

3. **Conserve:** Stop the pump and place the 1 mm filter into a petri dish and observed it under a binocular microscope. Particles on the smaller filter (e.g. 200 μm) are filled (back) into the Erlenmeyer beakers by using MPF MQ water.

Visual sorting and picking

1. **Sort on sieve:** If applicable, firstly check the larger (i.e. $>0.5\text{ mm}$ or $>1\text{ mm}$) fraction on the sieve (or on the original vacuum filter, if no wet sieving was applied) for prominent plastic suspects,²⁸ separate them using fine tweezers and rinse off potentially adhering smaller particles with MPF MQ above the sample. Sandwich the separated particle between two MPF microscopy glass slides using tweezers. These “sandwiches” can then be closed with two small stripes of paper tape and labelled with a running number (e.g.: [station name]_[sample number/ ID]_[consecutive number of the plastic suspect (starting with 001)]). It is advisable to mark the location of the particle in the sandwich by circling it with a permanent marker on the outside.

► If the possibility exists, particles may be directly transferred to the analysis stage of an ATR-FTIR instead of “sandwiching”.

2. **Sort in petri dish:** When further picking on the sieve is limited (due to the dark background and/or a high number of particles overlaying each other) rinse the sieve content into a petri dish using MPF MQ²⁹ water and continue picking all MP suspects. Ensure to assess all particles, so none remain on the filter.

3. **Creation of particle groups:** In case of a high number ($>>40$) of particles of identical morphological characteristics (i.e. colour, size class and surface structure) only transfer a subsample of 40 particles into individual sandwiches, labelled with an additional consecutive index number (e.g.: [. . .].[1–40]). Count all other particles of the same kind (e.g. using a click counter) and place together into an additional glass slide sandwich or petri dish, name accordingly (e.g.: [. . .].rest:[remaining total particle number]).³⁰

²⁶ The pore size of the filter used here is 1 mm, which is based on the experiences made by the authors especially when treating Manta net samples. However, this needs to be evaluated case by case and filters can be changed or substituted with additional filters depending on the specific sample compositions.

²⁷ The step of flushing and rinsing the filters/sieves used to perform size-compartmentalisation of the sample must be executed exhaustively in order to prevent smaller particles remaining within the larger size fractions as they may otherwise be lost for analysis.

²⁸ The pre-analysis of plastic suspects should be executed in a conservative manner, which increases the number of false-positives, however, this also prevents false-negative particles and thus the loss of particles. False-positives will be identified and eliminated in the later chemical analysis.

²⁹ MPF MQ is recommended here, to dilute and wash out solutes in and on the picked particles, as they are subjected to spectroscopic analysis thereafter.

³⁰ Based on the subsample of 40 particles which undergo chemical analysis, the remaining particles will be extrapolated for plastic/non-plastic origin, as well as polymer type distribution. If the analysed fraction of particles is too diverse, a larger subsample can be compiled.

New equipment

Within the postulated protocols, the required work effort is reduced and extraction efficiency is increased by the conception and application of new equipment. The technical advancements are explained and validated in the following section. Minor accessory equipment, namely simple and mobile tap water filters is presented in the SI.3, Fig. SI.1 which provides ample MPF water supply in the laboratory and thus contribute to QA measures.

Modified separation funnels – a versatile application for particle-rich samples

The application of glass separation funnels for density separation was applied previously [17–19]. They exhibit many advantages as such that they fulfil all relevant system requirements previously defined (Figs. 1 and 3). Firstly, glass allows for visual control of the status and quality of the separation process. Secondly, by having a steep sloping wall, the Squibb-form separation funnels was chosen in order to prevent particle adherence to walls when rising while still having an acceptable volumetric capacity that allow handling in standard laminar flow benches. Furthermore, separation funnels are off-the-shelf, long-lasting products of little cost. The previous problem of only fitting small amounts of sample material [19,20] is overcome by using the newly developed conical spiral conveyor, presented in the respective section below, which allows for efficient MP extraction despite an enormous overlay of particles. Some modifications on the separation funnels were required for matter-rich samples, for instance, to overcome the problem of clogging [17] when using very fine or very coarse materials. Standard outlet valves of all separation funnels, especially those intended for particle-rich samples, were replaced by larger ones (\varnothing 10 mm) to ease the release of sedimented particles. To satisfy the non-contaminating system requirement, plastic handles and nuts were replaced by stainless steel parts. Furthermore, a widening of the standard neck size (\varnothing 25 mm) was necessary to allow the installation of the larger spiral conveyor (\varnothing 35 mm, Fig. 3). We decided that 50 mm was the optimum size as this also fits the sieves potentially used for particle fractionation (m5). While custom equipment can be costly, these adaptations typically come at a low cost and constitute a one-time investment, fulfilling QuEChERS requirements (Fig. 1). All customisations of glass ware can be provided by a glass blower. Protocol modularity can limit costs, simplify the procedures and equalise extraction effectiveness when working with various sample matrices. Hence, the modular use of equipment is of advantage and is implemented by the universal application of the separation funnels for samples from water, sediments, beaches, soils, waste water, etc.

Conical spiral conveyor – a gentle way to separate particles

During density separation, it has to be ensured that particles get in contact with the liquid phase of the density separation solution in order to prevent trapping of particles by overlaying material. Different approaches were applied in previous studies, such as shaking or stirring the sample (e.g. [4,13]). However, shaking (by hand or machine) is efficient only on relatively small sample amounts and stirring blades, such as those implemented in the MicroPlastic Sediment Separator (MPSS; [4]), are prone to disintegrate MP particles by grinding sample matter directly against a hard (i.e. stainless steel) surface and thus falsify results [21]. To increase the extraction efficiency of MP from particle-rich samples whilst overcoming these potential limitations, we developed a custom-made spiral conveyor that allows for gentle and sufficient separation of the particles (Fig. 3A). Instead of uncontrolled mixing, particles from the bottom of the separation vessel are gently transported upwards and released in a fountain-like manner to the liquid separation phase above. Once freely suspended, particles can separate based on their physical features and either float to the top, stay in suspension or settle again to the sedimented solid phase. A side effect of the gentle movement is the disintegration of material conglomerates which contributes to an efficient separation process. The conical shape reduces the bottom-facing area of the rotating spiral conveyor to just a fine tip. Compared to other stirring procedures described in the literature which use flat rotor blades or rods (e.g. Imhof, 2012 [4]) this is an important improvement, as it minimises the area and thus the possibility of grinding and squeezing particles between the rotating element and the vessel walls.

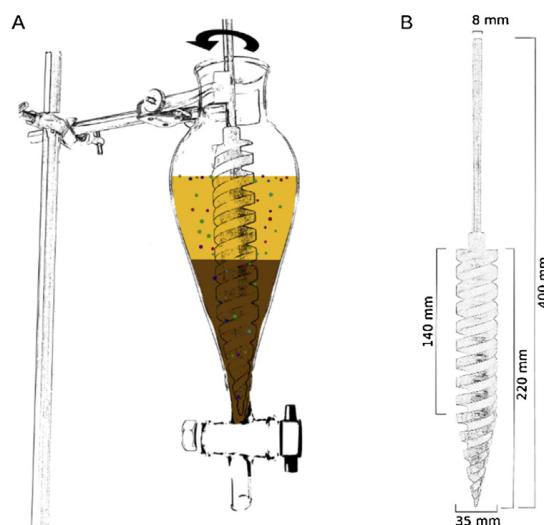


Fig. 3. A) Sketch showing the custom-made conical spiral conveyor, which improves the extraction efficiency of MP in a density separation despite being buried by particulate matter. The spiral conveyor is operated within a separation funnel (Squibb form). The particles of the sample are transported upwards and released in a fountain-like manner into the density separation solution above, where they can freely separate. A video (picture sequence over 2 hours) visualising the efficiency of the density separation process by means of the conical spiral conveyor is provided as supplementary material to the paper. Approximately 0.5 g of test MP i.e. fluorescent green polyethylene microspheres ($125\text{--}150\text{ }\mu\text{m}$, $\rho = 1025\text{ kg m}^{-3}$) were added initially in the lower part of the sediment fraction (glass particles, $40\text{--}70\text{ }\mu\text{m}$). SPT ($\rho = 1800\text{ kg m}^{-3}$) is added as the density separation solution. When starting the spiral conveyor, it can be observed that the test MP are being transported upwards and partially rise to the top. Some test MP cannot be freed in the first cycle and are covered again by sediments. After several cycles (after $\sim 2\text{ h}$) all particles are extracted and float on the top of the density solution (supernatant). B) The technical drawing of the large spiral conveyor ($\varnothing 35\text{ mm}$) with details on the physical dimensions. Other sizes can be up or down-scaled accordingly.

The principal functioning of the spiral conveyor is based on the widely-used industrial screw conveyors. In the lower 80 mm, the spiral conveyor fits the conical shape of the Squibb form separation funnels with a 5 mm wide gap in between. As different sample volumes are required depending on the sample type and research question, two different conveyor sizes were built that allow sufficient mobilisation of the particle phase. The smaller one ($\varnothing 20\text{ mm}$) is designed for the application in 250 ml separation funnels, the larger one ($\varnothing 35\text{ mm}$) for 500–1000 ml separation funnels. The spatial dimensions of the larger spiral conveyor are given in Fig. 3B. Other sizes could be simply scaled up or down or adapted to other types of separation vessels. It is important to note, that the screw conveyor part is designed to protrude into the separation solution above the sedimented particles for an efficient separation process to work. The shaft fits into a drill chuck of a typical electrical overhead stirrer for quick (dis)mounting. Due to the corrosive nature of most separation media, stainless steel is considered the optimal material. In the case of the larger conveyor, brass was used due to limitations of the available lathe machine. The presented set up for particle-rich matrices has a volumetric capacity of up to 1 l, appropriated to fit approximately 500 ml of particulate matter. By experience, this is a reasonable amount to achieve robust MP numbers. This volumetric capacities compares to other methods like the elutriation approach [22], though requiring less space and less steps involved in the separation process to reach reasonable extraction efficiencies. There are few, such as the MPSS, that have a larger sample capacity ($\sim 6\text{ kg}$, [4]), however, most other separators hold substantially smaller volumes [17,20].

Method validations and comparison

Recovery and reduction rates

A first semi-quantitative validation test was given by the video sequence shown above (link, Fig. 3A) demonstrating the efficiency of the density separation process by means of the conical spiral conveyor. Additionally, we performed recovery tests as a measure of extraction efficiency of the entire MP

extraction procedure based on beach sediment samples ($n = 7$, $d_{50} \sim 300 \mu\text{m}$). The recovery tests followed the respective pathway through the protocol tree including the operation of the spiral conveyor to separate particle-rich matrices. Test particles were visually identified using a microscope by their specific morphological characteristics. Polyamide particles (PA-6) of $450 \mu\text{m}$ ($n = 20$) in size were used and resulted in recovery rate of $95 \pm 6\%$. This value is within the higher margin of other available recovery rates of other MP extraction methods, e.g. modified decanting, elutriation, MP sediment separator, sequential density extraction, oil extraction (see Table 1 in [17] or [19,23] for comparison). However, recovery rates are known to decrease with MP size [20] and most studies lack sufficient tests [24], especially in the size range below $300 \mu\text{m}$ (longest dimension). We determined the recovery rate of smaller MP using PE fluorescent particles of $125\text{--}150 \mu\text{m}$ ($n = 60\text{--}80$) in size resulting in $78 \pm 6\%$. In this size class, however, reasonable comparisons to other studies are difficult as insufficient data is available. Not all study designs in the available literature (keyword search Web of Science: microplastics, recovery, sediment/soil/sludge) were technically able to extract the full range of polymer types (e.g. $\rho = 900\text{--}1400 \text{ kg m}^{-3}$). Of those that were, only very few studies tested the distinct size range of small MP from real, particle-rich environmental matrices (e.g. soils, sediments, sludge), whilst applying particle-based analytics and reporting sufficient information on the recovery test to allow a comparison. For instance, Imhof et al. [4] and Claessens et al. [22] tested particles between $40\text{--}309 \mu\text{m}$ and $\sim 250 \mu\text{m}$ respectively, resulting in a recovery rate above 95%. However, a comparison of our recovery rates to the two mentioned is in question for several reasons. These studies used sediments that underwent several cleaning steps (sequential density separation, elutriation) before performing recovery tests which ultimately results in a test matrix of very low conglomeration potential and thus not a realistic sample matrix. It is expected that several factors such as the sediment composition, i.e. grain size and/or organic matter content influence the extraction efficiency, potentially to a significant degree. This is a current knowledge gap that needs to be investigated in detail in a separate study. Further, when testing such small MP it is important to ensure that the size remained unchanged after the treatment as some techniques are prone to disintegrate MP [21] and thus potentially falsely increase the MP number. This remained unclear in some cases [4]. Hengstmann et al. [25] performed tests in a comparable size range ($63\text{--}200 \mu\text{m}$) to our study acquiring smaller recovery rates of $66 \pm 17\%$. However, they used MP test particles with a higher density which often show reduced recovery rates compared to lighter once. Inconsistencies between recovery test designs exist as some studies tested the entire MP extraction pipeline (present, [23]), while others determined the recovery rates of the separation step solely [4,25]. The latter is likely to achieve higher values. The use of large MP size class ranges (e.g. $100\text{--}500 \mu\text{m}$, [20]) without determining the size distribution (e.g. median, mean value) complicates a comparison to more narrow size ranges, such as those used in the present study, as the size-dependency of extraction efficiency remains disregarded. For a reasonable comparison of extraction methods, standards on the test material and procedure are needed. To date, a comparison of recovery rates of small MP ($<500 \mu\text{m}$) between different studies is not reliable due to the listed reasons.

Another measure of method validation is the mass reduction, i.e. the weight difference between the initial and treated dry weight sample. The mass reduction of exemplary sediment samples, ranging from beach sand (low in organics, coarse sediment) to estuary sediments (high in organics, fine sediment) was $99.98 \pm 0.03\%$ ($n = 6$) on average (SI.4, Table SI.1). Neither the initial sample mass nor the different sample matrix complexities could entirely account for the variability in the amount of material left in a sample after treatment. It can be assumed that the final number of particles also depends on the instruments and procedures used as well as on the operator.

Process time

While selecting the best methodological steps is critical for final accuracy of results, improvements must also be time-efficient. The time consuming nature of MP extraction was often reported in the past (e.g. Zarfl, 2019 [1]), however, without documentation of the concrete time measurements [24]. We report estimated procedural time for exemplary protocol pipelines, conducted by an experienced person, for better comparability of methods and planning of treatment procedures (SI.5, Table SI.2).

This paper presents a compilation of all methods necessary to fully process any given environmental sample ready for automated surface chemistry analysis. These methods are presented in a modular way which can be adapted to what a special sample requires. New equipment has also

been described which, combined with the presented methods, significantly improve the methods for extracting both large (>0.5 mm) and small (<0.5 mm) MP from environmental samples.

Funding

This work resulted from the BONUS MICROPOLL project supported by BONUS (Art 185), funded jointly by the European Union and Federal Ministry of Education and Research (BMBF) (03F0775A), the BMBF project MicroCatch_Balt (03F0788A) and the BMBF project PLASTRAT (02WPL1446 J).

Acknowledgements

We thank the IOW workshop for the construction of the spiral conveyor and the clean bench setup, and Dr. Klaus-Jochen Eichhorn (Leibniz-Institute for Polymer Research), as well as Jakob Strand (Aarhus University) for the helpful advice on the development of the pentane protocol for improved spectroscopic analysis. Thanks also to Franziska Fischer and Dieter Fischer for their assistance in method validation.

Declaration of Competing Interest

The authors declare that there are no conflicts of interest.

Appendix A. Supplementary data

Supplementary material related to this article can be found, in the online version, at doi:<https://doi.org/10.1016/j.mex.2020.100784>.

References

- [1] C. Zarfl, Promising techniques and open challenges for microplastic identification and quantification in environmental matrices, *Anal. Bioanal. Chem.* 411 (2019) 3743–3756, doi:<http://dx.doi.org/10.1007/s00216-019-01763-9>.
- [2] M. Cole, H. Webb, P.K. Lindeque, E.S. Fileman, C. Halsband, T.S. Galloway, Isolation of microplastics in biota-rich seawater samples and marine organisms, *Sci. Rep.* 4 (2014) 4528, doi:<http://dx.doi.org/10.1038/srep04528>.
- [3] A. Dehaut, L. Hermabessiere, G. Duflos, Current frontiers and recommendations for the study of microplastics in seafood, *TrAC Trends Anal. Chem.* 116 (2019) 346–359, doi:<http://dx.doi.org/10.1016/j.trac.2018.11.011>.
- [4] H.K. Imhof, J. Schmid, R. Niessner, N.P. Ivleva, C. Laforsch, A novel, highly efficient method for the separation and quantification of plastic particles in sediments of aquatic environments, *Limnol. Oceanogr. Methods* 10 (2012) 524–537, doi:<http://dx.doi.org/10.4319/lom.2012.10.524>.
- [5] A.L. Lusher, N.A. Welden, P. Sobral, M. Cole, Sampling, isolating and identifying microplastics ingested by fish and invertebrates, *Anal. Methods* 9 (2017) 1346–1360, doi:<http://dx.doi.org/10.1039/C6AY02415G>.
- [6] D. Fischer, Personal Communication, Leibniz-Institute for Polymer Research (IPFDD), 2019.
- [7] D.B. Alcântara, T.S.M. Fernandes, H.O. Nascimento, A.F. Lopes, M.G.G. Menezes, A.C.A. Lima, T.V. Carvalho, P. Grinberg, M.A.L. Milhome, A.H.B. Oliveira, H. Becker, G.J. Zocolo, R.F. Nascimento, Diagnostic detection systems and QuEChERS methods for multiclass pesticide analyses in different types of fruits: an overview from the last decade, *Food Chem.* 298 (2019) 124958, doi:<http://dx.doi.org/10.1016/j.foodchem.2019.124958>.
- [8] M. Anastassiades, S.J. Lehotay, D. Štajnbaher, F.J. Schenck, Fast and Easy Multiresidue Method Employing Acetonitrile Extraction/Partitioning and “Dispersive Solid-Phase Extraction” for the Determination of Pesticide Residues in Produce 21, (2003) .
- [9] D.M. Buede, W.D. Miller, *The Engineering Design of Systems: Models and Methods*, Wiley Series in Systems Engineering and Management, Wiley, 2016.
- [10] R. Marshall, P.G. Leaney, A systems engineering approach to product modularity, *Proc. Inst. Mech. Eng. Part B: J. Eng. Manuf.* 213 (1999) 847–851, doi:<http://dx.doi.org/10.1243/0954405991517272>.
- [11] V. Hidalgo-Ruz, L. Gutow, R.C. Thompson, M. Thiel, Microplastics in the marine environment: a review of the methods used for identification and quantification, *Environ. Sci. Technol.* 46 (2012) 3060–3075, doi:<http://dx.doi.org/10.1021/es2031505>.
- [12] K. Enders, R. Lenz, S. Beer, C.A. Stedmon, Extraction of microplastic from biota: recommended acidic digestion destroys common plastic polymers, *ICES J. Mar. Sci.* 74 (2017) 326–331, doi:<http://dx.doi.org/10.1093/icesjms/fsw173>.
- [13] J. Strand, Z. Tairova, Microplastic Particles in North Sea Sediments (No. No. 178), Aarhus University, DCE – Danish Centre for Environment and Energy, 2015.
- [14] S. Albalá-Hurtado, L.E. Pascual-Sastre, M.C. Vidal-Carou, A. Mariné-Font, J. Permanyer-Fàbregas, Comparison of two fat extraction methods in powdered infant milks, *J. Food Compos. Anal.* 12 (1999) 333–337, doi:<http://dx.doi.org/10.1006/jfca.1999.0837>.
- [15] A. Dieffenbacher, B. Lüthi, Die Direkte Kolorimetrische Bestimmung der Peroxidzahl (POZ) in Milchprodukten, *Mitteilungen aus dem Gebiete der Lebensmitteluntersuchung und Hygiene* 77 (1986) 544–553.

- [16] M. Fischer, B.M. Scholz-Böttcher, Simultaneous trace identification and quantification of common types of microplastics in environmental samples by pyrolysis-gas chromatography-mass spectrometry, *Environ Sci Technol.* 51 (9) (2017) 5052–5060, doi:http://dx.doi.org/10.1021/acs.est.6b06362.
- [17] R.L. Coppock, M. Cole, P.K. Lindeque, A.M. Queirós, T.S. Galloway, A small-scale, portable method for extracting microplastics from marine sediments, *Environ. Pollut.* 230 (2017) 829–837, doi:http://dx.doi.org/10.1016/j.envpol.2017.07.017.
- [18] E. Fries, J.H. Dekiff, J. Willmeyer, M.-T. Nuelle, M. Ebert, D. Remy, Identification of polymer types and additives in marine microplastic particles using pyrolysis-GC/MS and scanning electron microscopy, *Environ. Sci. Process. Impacts* 15 (2013) 1949–1956, doi:http://dx.doi.org/10.1039/c3em00214d.
- [19] T. Mani, S. Frehland, A. Kalberer, P. Burkhardt-Holm, Using castor oil to separate microplastics from four different environmental matrices, *Anal. Methods* 11 (2019) 1788–1794, doi:http://dx.doi.org/10.1039/C8AY02559B.
- [20] R. Nakajima, M. Tsuchiya, D.J. Lindsay, T. Kitahashi, K. Fujikura, T. Fukushima, A new small device made of glass for separating microplastics from marine and freshwater sediments, *PeerJ* 7 (2019) e7915, doi:http://dx.doi.org/10.7717/peerj.7915.
- [21] M.B. Zobkov, E.E. Esiukova, Evaluation of the Munich Plastic Sediment Separator efficiency in extraction of microplastics from natural marine bottom sediments, *Limnol. Oceanogr. Methods* 15 (2017) 967–978, doi:http://dx.doi.org/10.1002/lom3.10217.
- [22] M. Claessens, L. Van Cauwenberghe, M.B. Vandegehuchte, C.R. Janssen, New techniques for the detection of microplastics in sediments and field collected organisms, *Mar. Pollut. Bull.* 70 (2013) 227–233, doi:http://dx.doi.org/10.1016/j.marpolbul.2013.03.009.
- [23] R.R. Hurley, A.L. Lusher, M. Olsen, L. Nizzetto, Validation of a method for extracting microplastics from complex, organic-rich, environmental matrices, *Environ. Sci. Technol.* 52 (2018) 7409–7417, doi:http://dx.doi.org/10.1021/acs.est.8b01517.
- [24] M.E. Miller, F.J. Kroon, C.A. Motti, Recovering microplastics from marine samples: a review of current practices, *Mar. Pollut. Bull.* 123 (2017) 6–18, doi:http://dx.doi.org/10.1016/j.marpolbul.2017.08.058.
- [25] E. Hengstmann, M. Tamminga, C. vom Bruch, E.K. Fischer, Microplastic in beach sediments of the Isle of Rügen (Baltic Sea)—implementing a novel glass elutriation column, *Mar. Pollut. Bull.* 126 (2018) 263–274, doi:http://dx.doi.org/10.1016/j.marpolbul.2017.11.010.
- [26] G. Liebezeit, F. Dubaish, Microplastics in beaches of the East Frisian islands Spiekeroog and Kachelotplate, *Bull. Environ. Contam. Toxicol.* 89 (2012) 213–217, doi:http://dx.doi.org/10.1007/s00128-012-0642-7.
- [27] C.J. Moore, S.L. Moore, S.B. Weisberg, G.L. Lattin, A.F. Zellers, A comparison of neustonic plastic and zooplankton abundance in southern California's coastal waters, *Mar. Pollut. Bull.* 44 (2002) 1035–1038, doi:http://dx.doi.org/10.1016/S0025-326X(02)00150-9.
- [28] R.C. Thompson, Y. Olsen, R.P. Mitchell, A. Davis, S.J. Rowland, A.W.G. John, D. McGonigle, A.E. Russell, Lost at sea: where is all the plastic? *Science* 304 (2004) 838, doi:http://dx.doi.org/10.1126/science.1094559.

SI Supplementary information

Title: *When every particle matters: a QuEChERS approach to extract microplastics from environmental samples*

Authors: Kristina Enders, Robin Lenz, Juliana A. Ivar do Sul, Alexander S. Tagg and Matthias Labrenz

SI.1 – Starting principles and a purpose-built MP laboratory

Our own observations and published literature (e.g. reviewed in Dehaut et al. (2019) or Zarfl (2019)) agree that sample contamination is the crux of environmental MP research, especially when small MP sizes are targeted (i.e. < 500 µm). The omnipresence of plastic materials in a standard laboratory, but also in clothing, airborne dust and laboratory equipment enables the abrasion and intrusion of contaminating MP into the samples. Also other non-plastic particles such as hair or skin ablation, cotton fragments or wear of glass or metal parts can contribute to the pool of contaminating particles. Together they have negative impacts on MP detection limits and analysis time.

Optimal working conditions for MP sample treatment are not easily, nor cheaply established in typical research laboratory environment. The following list can be seen as an inexhaustible collection of the most impactful infrastructural adaptations of a purpose-built MP lab:

- dedicated clean room facility with no avoidable plastic devices (especially mechanical parts)
- fine particulate filters on any supplies of air, gases, water
- non-circulating laminar flow bench connected to lab air exhaust
- supply of external vacuum to avoid pump operation inside the clean room
- unavoidable plastic parts all made of the same (non-abrasive) non-target polymer (e.g. PTFE)
- wet lab capabilities (floor drain, large washing / rinsing area)
- muffle oven with exhaust system connection for pyrolysis of contaminating MP
- water ultra-purification system with a plastic-free dispenser unit
- working surfaces and equipment made of hard and smooth materials, e.g. polished stainless steel and borosilicate glass.

SI.2 – QA / QC measures

Precautions have to be taken at every protocol step to mitigate MP contamination, for example, from the laboratory air, tap water or the chemicals required for processing. A range of good practices on MP extraction is suggested by MP researchers working on diverse topics (e.g. Dehaut et al., 2019), and we also strongly encourage these measures to be a routine for MP studies. Firstly, a clean bench was installed in the lab creating a microplastic free (MPF) environment where samples can be safely manipulated and are protected from airborne MP, especially fibres. The clean-bench was set up with an assembly for the parallel mounting of separation funnels (up to 16) for a more efficient density separation. The installation of the clean bench per se is not enough. It is necessary to clean and rinse all the materials that eventually enter the clean bench (see also Specifications table and General module m0 in the associated paper). To minimise and monitor levels of fibres and other MP particles in laboratory air, an air filter equipped with a fine particulate sensor was installed allowing researchers to take decisions on whether to close the clean bench in a specific event (e.g. doors or windows of the lab being opened, cleaning of lab surfaces). All above measures aim to assure that quality standards required for particle-based MP analyses are met. However, those measures can only minimise and not eliminate particle loss or contamination. Quality control measures of regular parallel blind samples (negatives) and artificially spiked recovery samples (positives) further help to reify both what fraction of the environmental MP pool can be accounted for by a particular study as well as how large the error margins are likely to be.

SI.3 Simple and mobile tap water filters

In many cleaning and/or sample handling steps in our protocols, flushing, resuspending or soaking is necessary. Here the usage of filtered (for the minimum MP size range of interest, i.e. > 10 µm) normal tap water has many objective advantages, i.e. being quick, rugged and effective. This can be achieved by equipping an existing water tap with a filtration unit that only allows passage for particulates substantially smaller than the lower detection size limit. Depending on available funds and required amount of water, this may be constructed out of standard sanitary metal fittings with the insertion of a fine-meshed stainless steel sieve disk or as a larger compounded filtration device like a stainless steel cartridge filter (Figure SI.1). In any case, it is important that the non-targeted plastic polymers are used in or past the filter. Besides the supply of particle free water, a tap water MPF-filtration setup provides the advantage of a high pressure rinsing possibility for cleaning procedures of glassware.



Figure SI.1: Demonstration of two quickly-constructed and mobile tap water filtration devices for the provision of ample MPF water as required for many tasks in a MP laboratory. (A) A stainless steel cartridge filter is used (pore size below the minimum MP size limit, here: 5 μm) and is portable by means of a custom-built stand with a handle. The water is delivered through a standard PVC water hose and dispensed after passing the filtration device either directly through the nozzle or by use of a hose piece of a non-target material (e.g. silicone rubber or PTFE, if they are excluded during analysis). (B) A much simpler version can be built from sanitary pipe fittings, where a hand-cut circle of stainless steel mesh can be inserted and is held in place by screwing the pieces together (arrow). It can then be mounted to the water tap directly or through a short hose piece. The drawback of the much smaller filter is that it will clog much earlier.

SI.4 Process time


Depending on the sample type, hence the pathway taken through the decision tree, time estimates vary. The total time period needed for a sample treatment is usually in the region of 6 – 17 days, however, as up to 8 samples can be treated in parallel, one has to calculate with approximately 1 – 3 days per sample on average. The largest time fraction is due to waiting / processing time. Thus, the actual working time for a person per sample amounts to roughly 2 h or up to 12 – 19 h for 8 samples in parallel, depending on sample composition (see example 1 and 2 in Table SI.1). Not included are laboratory preparation time and cleaning (see m0 in associated paper). Some samples require less predictable procedural measures, e.g. the manual elimination of large organic matter fraction or the visual pre-analysis of large MP fraction, which essentially scales with the amount of total material in the sample (see example 3 in Table SI.1).

Table SI.1: Exemplary sample treatments i.e. pathways through the protocol tree were selected to calculate total treatment times. The actual working time that a person needs to spend on the preparation is given in black, the additional waiting time (due to machine or chemical process times) is given in red. Estimated times were calculated based on the minimum time needed for each step by an experienced person. Not included are the duration needed for preparation of MPF solutions, cleaning of equipment, note taking, etc. The abbreviation X_{DS} describes the number (X) of density separation (DS) cycles.

#1	Particle-rich sample, predominantly inorganic (e.g. sediments)	#2	Particle-poor sample, predominantly organic (e.g. water, small MP)	#3	Particle-poor sample, pre-dominantly organic (Manta net water, large MP)
Freeze-drying	10 min + 84 h	Filtration	20 min + 1 h	Filtration	20 min
Splitting (Homogenisation + Split/ weighing)	6 min (5 min, 1 min)	Freeze-drying	10 min + 84 h	Freeze-drying	10 min + 84 h
Density separation (Transfer, shaking, wet sieving, stirrer installation, X_{DS} * DS cycles, filtration)	50 min + 15 h * X_{DS} (5 min, 5 min, 10 min, 5 min, 10 min * X_{DS} , 15 min)	H₂O₂ Digestion (Refill * $X_{H_2O_2}$, Filtration)	16 min + 24 h * $X_{H_2O_2}$ (1 min * $X_{H_2O_2}$, 15 min)	H₂O₂ Digestion (Cut, Pick and rinse large organic matter pieces, Fill Filtration)	36 - 86 min + 24 h (10 min, 10 - 60 min, 1 min, 15 min)
H₂O₂ Digestion (Transfer, Refill * $X_{H_2O_2}$, Filtration, Final Transfer)	26 min + 24 h * $X_{H_2O_2}$ (5 min, 1 min * $X_{H_2O_2}$, 10 min, 10 min)	Density separation (Transfer, shaking, X_{DS} * DS cycles, filtration, Final Transfer)	43 min + 15 h * X_{DS} (1 min, 12 min, 10 min * X_{DS} , 10 min, 10 min)	Density separation (Transfer, shaking, DS cycle, filtration, Final Transfer)	43 min + 15 h (1 min, 12 min, 10 min, 10 min, 10 min)
Total_{min} ($X_{DS}=1$, $X_{H_2O_2}=1$; coarse sediments, low in organic matter)	92 min + 123 h ~ 6 d (if based on a 8 h working day)	Total_{min} ($X_{DS}=1$, $X_{H_2O_2}=1$)	89 min + 124 h ~ 6 d (if based on a 8 h working day)	Visual sorting > 1 mm particles	30 min – 40 h (depending on particle amounts)
Total_{max} ($X_{DS}=5$, $X_{H_2O_2}=10$)	141 min + 399 h ~ 17 d (if based on a 8 h working day)	Total_{max} ($X_{DS}=2$, $X_{H_2O_2}=3$)	101 min + 187 h ~ 6 d (if based on a 8 h working day)	Total_{min} ($X_{DS}=1$, $X_{H_2O_2}=1$)	139 – 2559 min + 133 h ~ 6 -11 d (if based on a 8 h working day)
Total_{min/ parallel} (up to 8 samples treated in parallel)	736 min + 123 h ~ 6 d (if based on a 8 h working day)	Total_{min/ parallel} (up to 8 samples treated in parallel)	712 min + 124 h ~ 6 d (if based on a 8 h working day)	Total_{min/ parallel} (up to 8 samples treated in parallel)	1112 – 20472 min + 133 h ~ 6 -20 d (if based on a 8 h working day)
Total_{max/ parallel} (up to 8 samples treated in parallel)	1128 min + 399 h ~ 17 d (if based on a 8 h working day)	Total_{max/ parallel} (up to 8 samples treated in parallel)	808 min + 187 h ~ 8 d (if based on a 8 h working day)		

OPEN

Tracing microplastics in aquatic environments based on sediment analogies

Kristina Enders¹, Andrea K  ppler², Oliver Bini  sch¹, Peter Feldens¹, Nicole Stollberg¹, Xaver Lange¹, Dieter Fischer², Klaus-Jochen Eichhorn², Falk Pollehne¹, Sonja Oberbeckmann¹ ¹ & Matthias Labrenz^{1*}

Microplastics (MP) data collection from the aquatic environment is a challenging endeavour that sets apparent limitations to regional and global MP quantification. Expensive data collection causes small sample sizes and oftentimes existing data sets are compared without accounting for natural variability due to hydrodynamic processes governing the distribution of particles. In Warnow estuarine sediments (Germany) we found significant correlations between high-density polymer size fractions ($\geq 500 \mu\text{m}$) and sediment grain size. Among potential predictor variables (source and environmental terms) sediment grain size was the critical proxy for MP abundance. The MP sediment relationship can be explained by the force necessary to start particle transport: at the same level of fluid motion, transported sediment grains and MP particles are offset in size by one to two orders of magnitude. Determining grain-size corrected MP abundances by fractionated granulometric normalisation is recommended as a basis for future MP projections and identification of sinks and sources.

The majority of the plastic that reaches aquatic environment originates from land-based sources¹ and is thought to eventually reach the sea via streams and rivers, with sea basins as an ultimate sink for particles^{2,3}. This concept is widely accepted in scientific literature and leads to the preclusion of microplastics (MP) deposition and temporary or long-term storage in rivers and coastal environments and thus potentially results in an underestimation of the total plastic removal. Recent studies (e.g.^{4,5}) showed the potential of freshwater systems to retain a substantial fraction of MP. As deposition is the dominant sink for MP in aquatic environments^{6,7} it is important that the controlling mechanisms are studied and understood^{8–10}.

A valid estimation of the actual plastic load in sediments is currently prevented due to the lack of data analysis standards that account for natural variability and the generally low sample densities. The observation that small scale spatial variations in MP abundance can exceed those across larger spatial scales¹⁰ indicates that local hydrodynamic conditions that influence particle motion have to first be taken into account before valid comparisons across temporal and spatial scales can be made. Being part of the general pool of suspended solids within a specific hydrodynamic regime, the distribution dynamics of MP – likewise all natural particulate matter – can be obtained from the physics of particle motion. With decreasing sediment grain sizes the threshold for the initiation of particle motion decreases¹¹. Thus, the sediment grain size distribution is mainly determined by the hydrodynamic (turbulence) regime; for non-cohesive particles, fine-grained sediments are found in low-energy environments, coarser sediments in high-energy environments¹². Accordingly, a relationship between organic (particulate) matter and sediment grain size has often been described¹³.

Hereby, MP correlations to ubiquitous and natural particles, such as organic matter or siliclastic sediments could be useful tools to infer MP contamination levels. In other contaminant studies granulometric and geochemical normalisation approaches are standard¹². Herein, normalisation is defined as a mathematical procedure to adjust MP abundance values for the influence of the natural variability in sediment granulometry induced by the energetic condition of the environment. Comprehensive surveys continue to be expensive due to the wide variety of synthetic polymer composites collected under the umbrella term ‘microplastics’ requiring extensive sample preparation measures. The development of proxies for MP data would allow for sensible extrapolations to

¹Leibniz Institute for Baltic Sea Research Warnem  nde (IOW), Seestra  e 15, 18119, Rostock, DE, Germany. ²Leibniz Institute for Polymer Research Dresden (IPF), Hohe Str. 6, 01069, Dresden, DE, Germany. *email: matthias.labrenz@io-warnemuende.de

larger spatial scales which is ultimately necessary for a quantification of the MP contamination in aquatic systems across the world.

Only relatively few studies have systematically examined sedimented MP in relation to environmental conditions that influence particle transport. Conclusions on whether or not MP abundance varies with sediment composition, such as grain size or organic matter content, were vastly diverging. Whereas Strand *et al.*, Maes *et al.* and Vianello *et al.*^{14–16} found indications for the existence of such a relationship, others^{9,17–22} could not confirm it. Such controversy in the literature exemplifies the existing knowledge gaps for a potential MP - sediment relationship. In this study, it is hypothesised that MP distribution patterns can be approximated by patterns of sedimentary composition. This relationship is investigated in sediments of an estuary that receives freshwater from the Warnow river in Germany and flows to the Baltic Sea. The selected site is representative of a large sediment grain size distribution and composition and an expectantly significant exposure to MP contamination due to intensive anthropogenic usage (urban, industrial).

The overall aim of this study is to establish the basis for a proxy for rational MP distribution maps which account for heterogeneous sedimentary environments. At first a conventional documentation of MP abundances and composition and a characterisation of MP intrinsic physical properties with respect to spatial distribution is provided for the area studied. In order to explore the parameters that determine the distribution of MP in the Warnow estuary generalised linear models (GLM) were developed. This multiple regression analysis was performed on a large set of potential MP sources (e.g. population density, marinas, etc.) and environmental parameters (e.g. sediment grain size, depth, etc.). Major factors were then analysed in detail. As a result the principal part of the study focuses on the MP-Sediment relationship. A correlation analysis is performed between MP fractions, defined by physical properties, and sediment grain size fractions. The empirically derived relationships are evaluated based on fundamental sediment transport concepts (critical shear stress¹¹). Limitations of the analysis are being discussed. For validation of the results with respect to the hydrodynamic conditions in the Warnow estuary shear stress data was retrieved from an established hydrodynamic coastal ocean model²³. By compiling available MP data sets from the literature that provide sediment grain size parameters, major influential factors on the quality of the MP - sediment relationship were identified. Exemplary offshore data (deep basins from the Baltic Sea) is provided for comparison based on the presented integrated normalisation approach. Additional one-year sediment trap samples complemented the analysis in order to improve our understanding of long-distance MP transport and sea-based sources. Finally, land-based point sources and recommendations and prospect of the granulometric normalisation approach of MP data is summarised.

Results and Discussion

Initial analysis. *MP abundance and composition in the Warnow estuary.* Total MP (TMP) abundances along the river bed were highest in the upper part of the estuary and then steadily decreased downstream towards the mouth of the river (Fig. 1A). Abundances appear to range over two orders of magnitude and assigned to three different areas. The upper Warnow estuary (S1–S7) showed a median TMP abundance of 93 [46–100] kg^{−1} dry weight (DW), with one station standing out with higher relative MP numbers of 346 kg^{−1} DW (S5). The Baltic Sea opening had comparatively low abundances of 2[2–2] kg^{−1} DW (S8, S9), whereas the Alter Strom (adjacent side arm of the Warnow estuary) revealed highest levels of 379 ± 28 kg^{−1} DW (n = 3, S10) (Fig. 1A) of the area studied.

MP were categorised based on polymer types and morphology. That is, ordinary polymers (Fig. 1A, blue bars) including those of higher density (HD) and those of lower density (LD) than water ($\rho_{\text{Warnow}} = 1.00\text{--}1.01\text{ g cm}^{-3}$), paint resins (Fig. 1A, red bars) and micro polystyrene (PS) beads (Fig. 1A, white bars). Most of these PS beads were spectroscopically identified as a variety of ion exchange polymers and dominated TMP by 58% in the estuary. Specifications of the identified PS beads are provided in the supplementary information (SI), Fig. S1. In total, paint and ordinary polymers were equally common across the sample set. A more detailed description for the composition and distribution of each MP category is provided in the SI, Text S1.

Fractionation of MP species based on physical properties. The diversity of plastic compositions brings with it a variety of properties that influence particle transport hampering the prediction of TMP distribution based on one single proxy. In order to identify MP distribution patterns within the present hydrological environment MP were grouped according to the most determining intrinsic variables with regard to particle transport behaviour: size, density and shape^{11,24}.

Size: In the estuary, the size distribution appeared to be dependant on density with significant differences between HD and LD polymers (SI, Fig. S2A). HD polymers increased in numbers with smaller sizes, following a power law regression scaling with an exponent of -3.88 (Spearman: $r_s = -1$, $p = 0.08$). Whereas, LD polymers remained at a constant low level without variations in size. As an exception, one sample is positioned in a side arm (Alter Strom) of the Warnow estuary which connect at the estuary mouth. Here, both LD and HD polymers show a decrease in abundance below 1000 μm (SI, Fig. S2B).

Density: Spectroscopically identified polymer types were used to infer typical density ranges. Ordinary polymers composed the group of polyolefines, including polypropylene (PP) and polyethylene (PE), acetates, including copolymeric polyvinylacetate and ethylvinylacetate (PVAc/EVA), polystyrenes (PS), polyamides (PA), acrylates, including polymethylmethacrylate (PMMA) and polyacrylonitrile (PAN), and polyvinylchlorides (PVC). These polymers span a large range of typical densities from 0.89–1.41 g cm^{−3}²⁵, summarised in²⁶. Excluded from this analysis were polytetrafluorethylene (PTFE) and polyethylene terephthalate (PET), as they appeared in contamination controls (SI, Text S2). Based on a report from the EPA²⁷ we calculated that paint resins possess an average density of approximately 1.6 g cm^{−3}. PS beads were density categorised according to their basis polymer PS (see SI, Text S1).

HD polymers were more than twice as abundant as LD polymers within the ordinary polymer category along the estuary. By density, paint and PS beads were also assigned to the category of HD polymers which resulted in

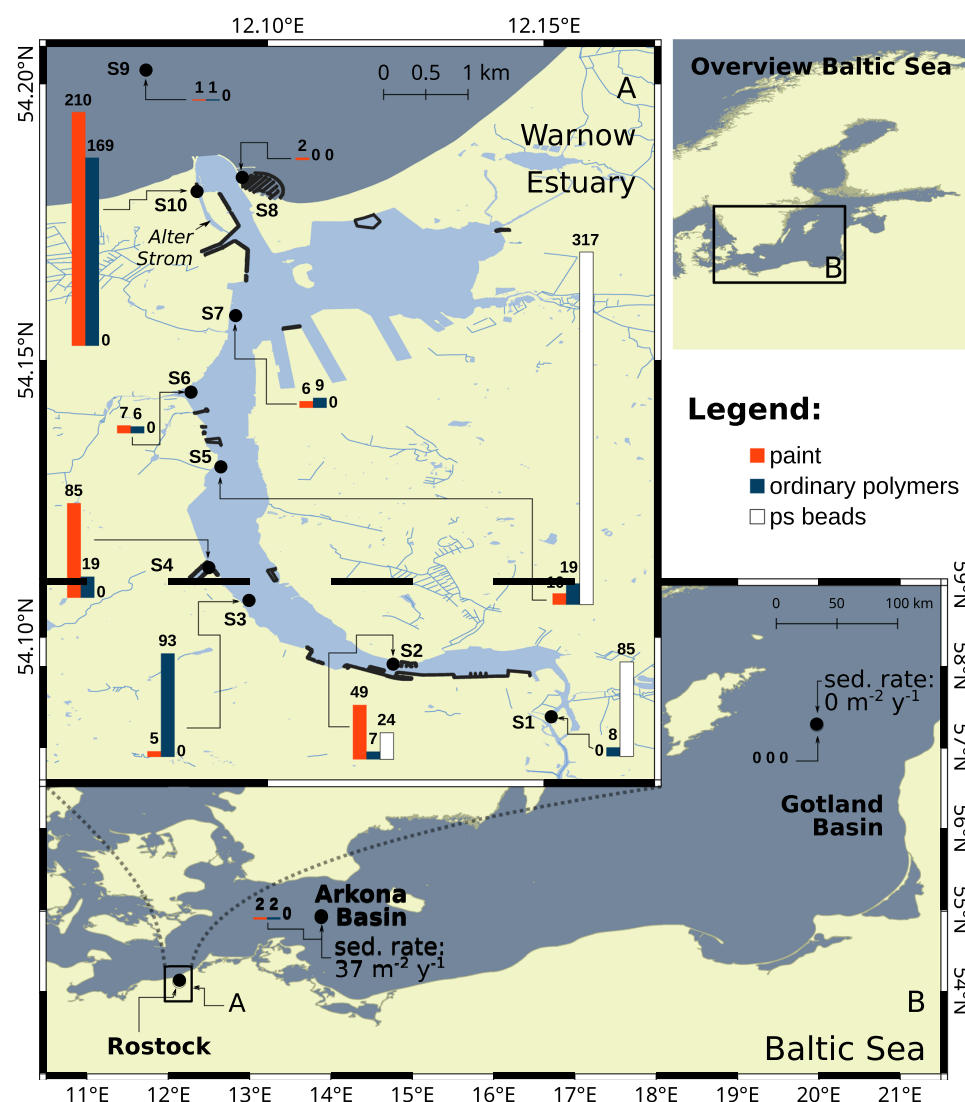


Figure 1. MP abundance maps of all sediment samples taken: (A) the Warnow estuary and (B) Arkona and Gotland basins in the Baltic Sea (referred section: MP contamination levels comparison to Baltic Sea basins). Sedimentation rates derived from sediment trap sampling in the two basins are displayed next to the stations. Blue bars indicate the occurrence of ordinary polymers, red bars paint resins and white bars PS beads. Respective abundances [kg^{-1} DW] are shown above the bars. Representative replicates ($n = 3$) were available for station S2 and S10 amounting to $78 \pm 10 \text{ kg}^{-1}$ DW and $379 \pm 28 \text{ kg}^{-1}$ DW, respectively. Possible deviations when adding up polymer type-specific abundances can arise due to rounding differences. Marinas and harbours are shown as black shapes. Sampling stations are highlighted as black circles along with the respective station number. Presented maps are projected in a geodetic system WGS 84 (EPSG:4326) and were created in QGIS⁶² using OpenStreetMaps (OSM) data⁶⁴.

a percentage contribution of approximately 90% and 95% within the overall data set and Warnow estuary (excl. Alter Strom), respectively. The plastic composition is, thus, clearly dominated by HD polymers (Fig. 2A). In the Alter Strom sediments, LD polymers were more abundant, with 23%. Otherwise, the overall polymeric distribution largely coincided with those found in the estuary.

The critical shear stress, calculated for the Warnow estuary stations (simulated maximum over one year, see section Hydrodynamic model), is introduced as an important measure of the energetic environment (Fig. 2B)¹¹. Generally, the larger the shear stress forces on the sediment bed the larger the proportion of HD polymers ($r = 0.73$, $p = 0.04$) relative to LD polymers ($\text{HD} = \text{TMP} - \text{LD}$). The significance level of this correlation rose ($r = 0.82$, $p = 0.01$) when excluding HD fibres, hence only HD particulate polymers were considered (Fig. 2B).

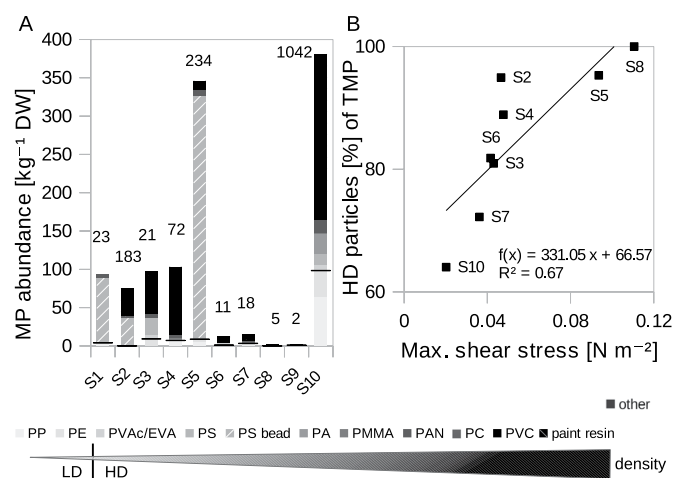


Figure 2. MP distribution by polymer type with distinct given densities and their dependency of shear stress. (A) MP distribution with numbers n above the bars. Grey scaling indicates the corresponding given densities of the polymers, increasing from light to dark ($0.89\text{--}1.6\text{ g cm}^{-3}$). The black line indicates the transition from LD to HD polymers determined by the density of water ($\sim 1\text{ g cm}^{-3}$). The polymeric category “other” consists of a variety of different HD polymers and consequently displayed separately from the grey scale. (B) HD particles (= TMP - LD - HD fibres) percentage of all polymers as a function of simulated maximum shear stress in the Warnow estuary. Two stations were excluded from the correlation for reasons of missing coverage by the hydrodynamic model (S1) or low sample size (S9).

The influence of shape is addressed in the following paragraph. Conclusively, hydrodynamic conditions appear to be an important influential factor on the selection of different polymer types i.e. densities.

Shape: Shape categories were split into fibres and particles, the latter of which was dominated by irregular fragments and spheres. Fibrous MP were usually composed of PAN, PA and PP and remained at a rather low level in the estuarine transect. In the Alter Strom, fibres reached abundances of $84 \pm 45\text{ kg}^{-1}\text{ DW}$, roughly equalling particulate ordinary polymers. Although most fibres by density can be related to the HD polymer fraction (64%, overall), their rather dispersed distribution pattern aligned much better with that of non-fibrous LD polymers ($r = 0.99$, $p < 0.001$).

Exploration of determining parameters for MP distribution. GLMs were developed to explore which parameters - potential sources and/or environmental factors - can explain MP distribution patterns in the Warnow estuary. The abundance of each MP category, paint resins, ordinary polymers, PS beads (restricted to ion exchangers) as well as TMP was analysed separately in order to find type specific emitters. Tested potential source terms were: distance to closest waste water treatment plant (WWTP), marina, recycling station, mixed water and rain water sewers as well as population density, number of tourism activity points, industrial areas and metal companies in 1000 m radius. Environmental parameters included physical parameters such as salinity, depth and maximum shear stress. Further, different types of natural (particulate) matter such as organic matter (total organic carbon (TOC) $\times 2.22$), TOC/N, sediment grain size ($< 63\text{ }\mu\text{m}$) and CaCO_3 were tested to evaluate their potential usage as proxies. This is based on the assumption that various types of particulate matter and MP are similarly influenced by the present hydrodynamic conditions. A table including values of explanatory variables with units, parameter definition and references of data acquisition is included in the SI, Table S3.

Explanatory variables (unstandardised) represent an estimation of parameter influence in original units and are given in descending order of importance. This is evaluated by the change of several statistical parameters such as decrease of deviance, Akaike information criterion (AIC), increase in coefficient of determination r^2 , level of significance, t-values and residual analysis. All predictor terms that composed the final models attained a level of significance of $p < 0.05$. Further GLM specifications and residual analysis are provided in the Materials and Methods section and SI, Fig. S3A–C. Best model fits for the individual MP categories are composed as follows:

$$\log(\widehat{\text{paint resin}}) = 2.352 + 0.032 \text{ Grain Size } (< 63\text{ }\mu\text{m}) - 0.003 \text{ Distance Marina} \quad (1)$$

with $r^2 = 0.97$, a residual deviance of 54 with 7 degrees of freedom and Chi-squared vs. constant model: 725, $p < 0.001$. The strongest impact ($r^2 = 0.84$, $p < 0.001$) on the model for paint resins (Eq. (1)) had the term sediment grain size ($< 63\text{ }\mu\text{m}$). Additionally, the distance to marinas (and harbours), one potential source term, showed significant impact. In other words, the MP composition of stations close to marinas and harbours were dominated by paint resins. This significant correlation is even supported when it is used as the only predictor (Fig. 3A, Spearman: $r_s = -0.7$, $p = 0.03$). Industrial areas, including metal and ship constructing sectors also fit paint resin distribution, however, had to be excluded due to model overfitting.

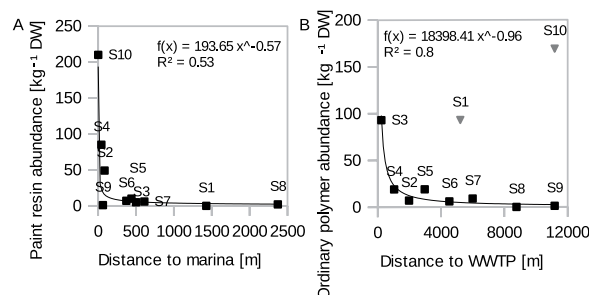


Figure 3. Relationship of MP and major identified sources: (A) between paint resin abundance and distance to marinas per station ($n = 10$) and (B) ordinary polymers to distance to WWTP per station ($n = 8$). The outliers S10 and S1 (grey triangles) would decrease the regression fit r^2 to 0.09 and were consequently excluded from the analysis.

$$\log(\text{ord. polymer}) = 0.505 + 0.0452 \text{ Grain Size } (<63 \mu\text{m}) + 0.0249 \text{ Org. Matter} \quad (2)$$

with $r^2 = 0.77$, a residual deviance of 199.1 with 7 degrees of freedom and Chi-squared vs. constant model: 431, $p < 0.001$. Apart from sediment grain size distribution, organic matter had an explanatory power for ordinary polymers (Eq. (2)). A reason for this could be the overlap in density ranges, contrarily to the heavier paint resins. Initially, the distance to the WWTP was the most significant source term for local ordinary polymer abundance. However, the occurrence of two outliers and consequent model overfitting excluded this term from the final model. When excluding the outliers the model fit improved ($r^2 = 0.92$, among other parameters of evaluation) now containing both grain size ($<63 \mu\text{m}$) and distance to WWTP as significant explanatory variables. This indicates that distance to WWTP ascribes a type specific emitter. The linear regression between ordinary polymers and the distance to WWTP is presented separately (Spearman: $r_s = -0.84$, $p = 0.01$, Fig. 3B). It is noted that PS beads from station S1 were added to the pool of ordinary polymers as they were not identified as ion exchangers (Fig. S1) and likely originate from different sources. They were not explained by the distance to the WWTP either (see outlier S1, Fig. 3B) and possibly diverge due to the increased distance of S1 upstream of the WWTP. Station S10 is furthest away from the WWTP and situated in a sheltered side arm of the Warnow wherefore additional source terms or deviating hydrodynamic conditions could explain the divergence from the regression fit.

Available source terms could not explain the distribution pattern of ion exchanger beads. This may be due to the versatile applicability of these beads. At the same time they could originate from a specific point emitter which might not be covered by the identified industrial activities used for the parameterisation.

$$\log(\text{TMP}) = -0.4207 + 0.0826 \text{ Grain Size } (<63 \mu\text{m}) + 0.056 \text{ CaCO}_3 - 0.0002 \text{ Distance WWTP} \quad (3)$$

with $r^2 = 0.99$, a residual deviance of 20.7 with 6 degrees of freedom and a Chi-squared vs. constant model: 1280, $p < 0.001$. TMP distribution (3) was best explained ($r^2 = 0.58$) by the fine fraction of sediments ($<63 \mu\text{m}$). The correlation with CaCO_3 is introduced based on a cooccurrence with ion exchangers. Apart from a possible correlation in transport behaviour with CaCO_3 (if e.g. from fragmented mussel shells), it could also be indicative of the composition of the ion exchanger polymers or related application processes (i.e. decalcification) which would lead to increased CaCO_3 levels. Regarding the small set of data points statistical robustness and causality of this correlation is not clear. If ion exchangers were excluded from TMP the relative importance of sediment grain size increased ($r^2 = 0.95$).

Conclusively, the MP composition found in the Warnow sediments can be explained by both the co-occurrence of natural (particulate) matter and potential source terms. Local occurrences of paint resins and HD ordinary polymers could, in turn be used as specific source indicators. Diffuse sources were generally difficult to fit as the impact is more dispersed and indiscernible from unexplained statistical deviations or unexplored source terms. A higher resolution and larger sample size could likely result in higher model accuracy. Independent of the MP categories, sediment grain size ($<63 \mu\text{m}$) appeared as the most prominent explanatory parameter. This suggests, that both materials are similarly influenced by present hydrodynamic conditions. Lower energetic environments would have the capacity to trap more MP of averagely smaller sizes compared to higher energetic environments. The selected fine sediment fraction ($<63 \mu\text{m}$) is the most widespread granulomeric normaliser of contaminants in use. This specific size threshold is principally based on physical properties (point at equal particle bond - weight ratio) and a measure of the clay fraction characterised by a high binding capacity and coating formation e.g. with organic matter (reviewed in¹²). However, the variable nature of grain size spectra is reduced to only one parameter at the expense of accuracy. Therefore sediment grain size should undergo a more detailed evaluation with respect to their potential usage as a proxy for MP contamination levels.

MP - Sediment relationship. *Field data.* A correlation analysis of the empirically derived MP, fractionated by the afore described physical properties and distinct sediment grain size fractions revealed strong

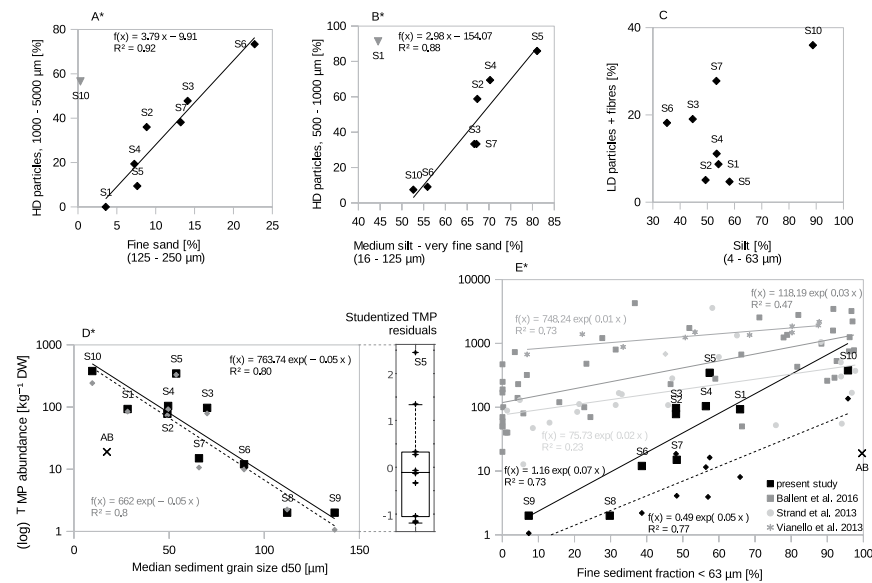


Figure 4. Relationships between MP and sediment distribution patterns. (A–C) Correlation analysis of specific MP and sediment grain size fractions in relative abundances. The inclusion of the outliers (shown as grey triangles) S10 and S1, would unduly influence the regression fit (decrease of r^2 to 0.31 and 0.07, respectively) and were consequently excluded from the analysis. (D) Correlation of TMP (log transformed, black squares) and HD polymers (grey diamonds with dashed line) as absolute values with median grain size (d50). (D, insert) Residual analysis of TMP values normalised by the median grain size (d50). Individual studentised residuals are shown as pluses non of which is deemed a clear outlier. (E) Fine sediment fraction (<63 μm) against TMP abundance (log transformed, black squares). Y-axis label is shared with (D). Graphs in different shades of grey present an assemblage of available study sites^{9,14,16} showing comparable relationships. Small black diamonds with the dashed line represent LD polymers and fibres. For later reference, in both (D) and (E), the respective position of the Baltic Sea sample, Arkona Basin (AB, d50 = 17.3 ± 1.7 μm, <63 μm = 99.6 ± 0.4%, n = 4³⁶), is marked as a cross. The Gotland Basin with comparable sediment grain size features (GB, <63 μm = 95.7 ± 3.5%, n = 3⁶⁵) does not display in the log rendering as MP numbers equal zero. The used grain size data for the two Baltic Sea sediment samples showed neglectable variation across our sampling region^{36,65}. Significant correlations are marked with asterisks. All data displayed on a log scale are based on log transformed regression coefficients.

correlations for HD particulate polymers (Fig. 4A,B). Station S8 and S9 were excluded as MP numbers were too low to calculate statistically robust percentage values of the respective MP fractions. HD particulate MP of sizes between 1000 and 5000 μm correlated with the fraction of fine sand (125–250 μm) with high significance ($r = 0.96$, $p < 0.001$, Fig. 4A). Likewise, HD particulate MP of 500 to 1000 μm significantly correlated ($r = 0.94$, $p = 0.002$, Fig. 4B) with a grain size range between medium silt to very fine sand (16–125 μm). The performed correlation analysis was based on grain size fractions classified by Udden and Wentworth²⁸ and those that yielded most significant fits are presented. LD particulate polymers and fibres showed no clear correlation with either of these fractions. As mentioned before, the spatial distribution of LD polymers and HD fibres of the studied size range equalled each other. The best fit of this MP category was found with silt, although not significant (4–63 μm, $r = 0.51$, $p = 0.2$, Fig. 4C). Instead, a significant correlation was found between LD particles in combination with all fibres and the fine sediment fraction of <63 μm ($r = 0.88$, $p = 0.002$, dashed line in Fig. 4E).

The median grain size (d50) highly correlated with TMP abundance ($r = -0.9$, $p < 0.001$); the finer the sediment, the more abundant TMP (Fig. 4D). The correlation was determined by the preponderance of HD particulate polymers ($r = -0.9$, $p < 0.001$, Fig. 4D, grey diamonds). The sedimentary fine-grained fraction (<63 μm) correlated with TMP ($r = 0.86$, $p = 0.001$, Fig. 4E), as also demonstrated by the high predictive power in Eqs. (1)–(3) of the GLM. No correlation was found between organic matter (total organic carbon, TOC) and TMP (S1, Fig. S4).

Theoretical validation. The transport behaviour of MP and non-cohesive sediment particles is controlled by their respective densities, shapes and grain sizes. Assuming a flat seafloor and spherical particles, the threshold bed shear stress τ_{cr} required to initiate movement on a sediment or MP particle can be calculated¹¹:

$$\tau_{cr} = \Theta_{cr} g (\rho_{sp} - \rho) d \quad (4)$$

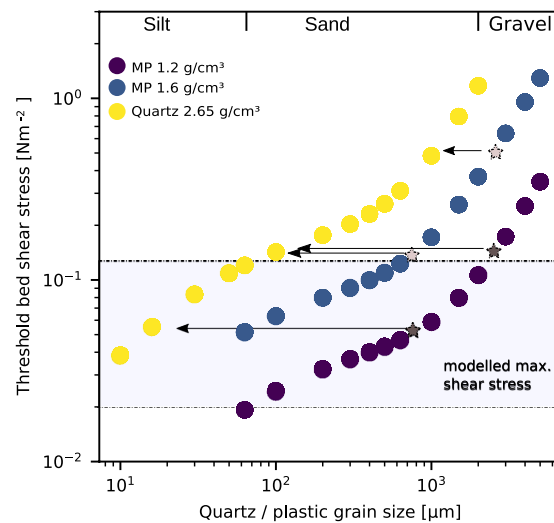


Figure 5. Threshold bed shear stress of quartz and plastic, HD ordinary polymers (average density 1.2 g cm^{-3}) and paint resins (average density of 1.6 g cm^{-3}) respectively. Stars and arrows indicate the equivalent quartz sediment grain and MP size (diameter) that is mobilised when subjected to the same bed shear stress. Stars are placed at the mean MP size fraction, 2500 and $750 \mu\text{m}$, derived from the empiric analysis (Fig. 4A,B). The area between the dashed lines indicates the simulated maximum shear stress range (S2–S10) in the Warnow area based on a one-year average (see Hydrodynamic Model under the Materials and Methods section).

Here, τ_{cr} is the bed shear stress [Nm^{-2}] exerted on the bottom at the initiation of movement that depends on the current velocity profile, water depth, water density and particle grain size, g is the acceleration due to gravity [m s^{-2}], ρ is the density of water [kg m^{-3}], $\rho_{s/p}$ is the density of quartz (2.65 g cm^{-3}) and plastic (assumed with 1.2 and 1.6 g cm^{-3}), respectively, d is the grain diameter [m]. Θ_{cr} is the threshold Shields parameter, describing the equilibrium of force exerted on a particle by water movement and the counteracting force due to the particle weight. It is estimated from the Shields curve following Soulsby¹¹. The density ratio $\rho_{s/p}/\rho$ may be directly important in controlling the threshold of motion, invalidating the above approximation of Θ_{cr} that was developed for density values of quartz grains. Such effects were measured for the case of large density differences (e.g. for different atmospheric pressures). However, for transport in water no impact of changing density ratios between 1.2 and 3 g cm^{-3} to the threshold of motion initiation have been reported²⁹.

The results of the threshold bed shear stress calculation for particles of different grain size and density are shown in Fig. 5. The results show a non-linear relationship for the initiation of motion for quartz and MP particles of the same diameter. For large MP particles ($2500 \mu\text{m}$ as an average) of a high density (1.6 g cm^{-3}), an initiation of motion comparable to quartz grains of $1000 \mu\text{m}$ can be expected, while large HD MP particles of a lower density (1.2 g cm^{-3}) would initiate transport with the fine sand fraction. Smaller MP particles ($750 \mu\text{m}$ as an average) of higher density initiate movement with quartz grains of the very fine sand fraction, while those of lower density mobilise with the medium silt fraction. Generally, the size difference between quartz and MP particles, mobilised under the same bed shear stress, decreases with increasing grain size and decreasing density difference.

The theoretical approximations are in general agreement with the empirical results, within the available accuracy limits discussed below. The analysed HD MP and sediment fractions show a shift in grain size by approximately one to two orders of magnitude. While effects of shape on particle movement were sparsely considered and a better distinction of MP grain sizes is required, the agreement of theoretical and available field data indicates that the observed particle size difference is the fundamental feature of HD MP dynamic. A better validation of the MP sediment relationship would require a higher resolution of MP size intervals. However, much higher MP abundances per sample are then required. Simulated shear stress data (see Hydrodynamic model) was retrieved to validate whether thresholds are sufficient to initiate motion of the particles measured. The transport of MP during average environmental conditions at the Warnow stations is limited (0.003 N m^{-2}). The maximum bed shear stresses for a one-year modelling run (2014) were found to range between 0.02 – 0.11 N m^{-2} between stations, indicating that less dense or smaller HD particles are mobilised. Thus the bulk of MP transport in the Warnow estuary is likely to occur during extreme events causing increased bed shear stress. For LD MP, a comparison with established sediment dynamic models is not possible. While a correlation between LD polymers and sediment coarser than medium silt may have been not found due to the low number of LD particles in the sample distribution, no correlation is expected. LD polymers would initially stay afloat and thus have fundamentally different transport mechanics compared to sediment particles. LD may settle when influenced by external factors such as attach-detach cycles of biota³⁰. This points towards a hydrodynamic relationship with fine-grained sedimentary components of a higher cohesive capacity i.e. sedimentation as a result of aggregation or flocculation, indicated by a significant correlation between LD and the fine sediment fraction ($r = 0.77$, $p = 0.02$, when all fibres included: $r = 0.88$, $p = 0.002$). Such a transport mechanism is supported by previous studies that found a

TMP-TOC relationship^{14,31} for data sets dominated by sizes below the minimum size class analysed in the present study. This indicates that a correlation exists between TOC and TMP < 500 μm .

Summarising, a fractionated granulometric normalisation based on mathematical correlations between the abundance of specific MP categories (defined by size, density and shape) and the reference sediment grain size fraction to eliminate hydrodynamic variability is the more accurate approach to account for different MP compositions within data sets. The application of single hydrodynamic parameters (e.g. d50, < 63 μm) for a granulometric normalisation is recommended as an approximation of MP abundances in case no further fractionation is possible. HD particulate MP > 500 μm were best explained by the d50, based on the underlying direct size fractionated correlations (Fig. 4A,B). LD and fibrous MP (and supposedly TMP < 500 μm) were better explained by the < 63 μm fine fraction. On the one hand, the application of LD MP and thus TMP abundances for the d50 normalisation within the studied size limits is questionable due to the absence of a clear correlation with a sediment grain size fraction (Fig. 4C) and median sediment grain size ($r = -0.64$, $p = 0.06$, when all fibres included: $r = -0.79$, $p = 0.01$). On the other hand, the shown correlation between the < 63 μm fraction and TMP (or HD particles only: $r = 0.86$, $p = 0.002$) is likely to be based on a cross-correlation between < 63 μm and d50. A single accurate proxy is thus difficult to obtain for the entire MP pool (~10 μm –5 mm, 0.89–1.6 g cm⁻³) and requires a selection tailored to the composition of the MP data set under investigation.

Residual analysis and MP re-assessment. TMP abundances as a function of sediment composition, such as median grain size, could explain a large degree of variability within the data set (decrease of mean squared error from 3.7 to 0.8, TMP log transformed). A residual analysis of the grain sized normalised TMP abundance values and the determined regression (base)line showed an independent distribution without any clear outliers (below ± 3), although station S5 is close to this threshold (Fig. 4D, insert). Generally, such residual analysis can reveal stations that currently function as a sink or source (positioned below or above the regression line) to the investigated system at the time of measurement. In theory, granulometric normalised MP abundances would approach an optimum of zero residual deviance in a hydrological system of sufficient connectivity and steady state. Conclusively, granulometric normalisation of MP data is of importance when assessing MP abundances because site-specific differences were largely explained by grain size differences. Lacking this, variations might be misinterpreted as source load differences and hot spot areas. Concerning the fractionated granulometric normalisation approach it was observed that at stations with a low grain size, such as in S1 and S10, the exerted shear stress might be too low to transport certain size specific MP that entered locally. This could be the reason why these stations appeared as outliers in the size fractionated correlation analysis (Fig. 4A,B, respectively). This phenomenon of very fine grained areas hence low shear stress levels could represent a potential limitation in the MP projection based on shear stress correlates and needs further investigation, e.g. concerning the influence of sinking velocity.

Implementation. *Study site cross - comparison reveals essential parameters.* The data of other study sites confirms the general relationship between MP and sediments as compiled and presented in Fig. 4E^{9,14,16}. However, a comparison of MP contamination levels between different study sites is difficult due to a) different sampling and analysis techniques and b) often insufficient consideration of the hydrodynamic environment.

The MP - sediment relationship depends on the respective MP input level and spatio-temporal connectivity of the available sampling stations. A larger sample area coverage can cause a less prominent correlation such as in Strand *et al.* and Ballent *et al.*^{9,14}. Similarly, less significant fits can occur when temporal connectivity is not fully guaranteed. Highest correlations were consequently achieved by Vianello *et al.*¹⁶ and the present study, both based on small scale well-connected sampling areas and periods. Deviations in the course of the shown graphs (4E) can occur due to different analytical preparation steps applied. A table comparing the displayed studies in different systemic parameters is provided in the SI, Table S1. Varying MP size thresholds as well as different density separation thresholds were applied during MP isolation by these studies. If the mentioned systemic differences were resolved an accurate comparison of the (normalised) MP contamination level between sites could be made. An additional common constraint of studies that reported the absence of a relationship between MP and sediments, is a missing coverage of large variability ranges of sediment grain sizes^{17,18} or complete exclusion of the fine fraction¹⁷, partly owed to a low sample sizes. A sample coverage spanning a sufficient range of grain sizes, representative for the region of interest, is thus essential to determine the MP contamination level in sediments. The sedimentary environment in which MP resided in the Warnow estuary spanned a reasonable diversity of sediment types, from clayey silt and very silty sandy mud to slightly silty sand (classified according to Flemming³²) with a d50 range across 100 μm . Some of the above referenced studies did not verify MP suspects via spectroscopic or other chemical test measures (SI, Table S1) which allows no unambiguous and thus sound identification and quantification, especially in the small size range³³.

MP contamination level comparison to Baltic Sea basins. Two Baltic Sea basin sediment samples were analysed and grain-size normalised to be compared to the MP contamination levels found in the Warnow estuary. These samples, together with sediment trap samples, revealed valuable information on the connectivity of the two systems in terms of MP bed load transport and major transport pathways to this environment.

No plastics within the analysed size range were found in the sediment trap samples from the Gotland basin over the entire period of nearly 10 months (excluding 9 PET fibres counted as contamination suspects, see Text S1). In the Arkona basin samples, a cumulative number of 12 ordinary polymers, all of which were fibrous, and 7 paint resins were identified (Fig. 6). Assuming a constant intra-annual MP sedimentation rate, this amounts to 0.1 m⁻² d⁻¹, which sums up to 37 m⁻² per year (Fig. 1B). The maximum entry within a sampling interval of 10 days amounted to 3 MP. There were slightly more MP during the late summer and autumn months which generally coincides with a higher sedimentation rate of natural particles (Fig. 6B). However, differences between

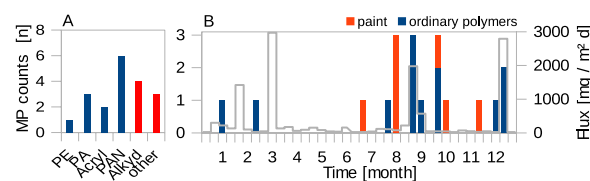


Figure 6. Ordinary polymer (blue) and paint resin (red) distribution found in the Arkona basin sediment trap samples. **(A)** cumulative and **(B)** over time. **(B)** Numbers on the x-axis represent the time in months over the sampling year from December 2012 until January 2014. The grey line illustrates the sediment flux (<400 μm). Ordinary polymers are all of a fibrous nature.

time intervals were marginal due to the small sample size and could well derive from increased local MP input, as, for instance, from maritime activities. The observation is made that paint resins in contrast to ordinary polymers descend independent from the natural particle flux, indicating a sea-based origin independent from natural particle transport routes. Sedimentation rates were based on the <400 μm fraction, which is used as a proxy for the total material flux.

The polymer composition in the Arkona basin sediment trap sample showed that only approximately 5% of MP (i.e. one PE fibre) belonged to the group of LD polymers (Fig. 6A); a percentage comparable to the Warnow estuary. One paint resin and one PA fibre could be identified in the Arkona basin sediments, being equivalent to 5 kg^{-1} DW (Fig. 1B) and largely match the polymer composition found in the water column. Also MP abundances between the two interlinked compartments show reasonable consistency as discussed in a hypothetical comparison as follows. Reported mean sedimentation rates in the Arkona Basin of 3 $\text{mm m}^{-2} \text{y}^{-1}$ ³⁴ imply that the taken sediment sample comprises layers equivalent to the last 33 years. Based on the MP sedimentation rate from sediment trap sampling, 1233 MP m^{-2} could have sedimented during this time period based on current MP sedimentation rates. An extrapolation of the MP abundances found in the Arkona sediment sample of 5 kg^{-1} DW equal 222 MP m^{-2} . Based on knowledge from sediment records, it seems reasonable to assume that current MP sedimentation rates rose with production volumes during the last decades³⁵. Then, the cumulative number of sedimented MP would be about half of that currently measured and, thus, lied within the same order of magnitude.

The calculation of MP sedimentation rates in the sea basins paired with the time integrated abundances found in the sediment below indicate a direct link between water column borne and benthic MP in this region. This would imply that a majority of the local MP burial originated from vertical deposition of particles rather than horizontal near-bottom transport, suggesting a sea-based origin or long distance transport of particles in suspension. The comparison of the MP abundances found in the Baltic Sea basins normalised to grain size (Fig. 4D,E, crosses) showed a contamination level of one to two orders of magnitude below that of the estuary. Under the restriction of the low sample size, these comparative data points shall exemplify the impact of the granulometric normalisation on the interpretation of MP contamination levels (methods identical). Otherwise, it would have been within the same range of that of the estuary. A larger data set (across a larger grain size range) is nevertheless needed to draw a grain size corrected MP contamination curve and thus determine the contamination level of the Baltic Sea region.

MP sinks: Sorting of particles in suspension along their deposition velocities is ultimately influenced by the environment's turbulence level. With a diminishing level of turbulence along a depth gradient from coastal environments, the deep sea basins are expectantly a sink for very fine sediments (<63 μm) and thus MP that correlate with that fraction (fibres, LD polymers and MP <500 μm). This is in coherence with our findings of a predominance of fibres and generally very small numbers of MP > 500 μm in the basins. The absence of HD ordinary particles, suggests no significant long distance transport to the sea basins but their sedimentation closer to the source. Paint resins with a higher relative threshold bed shear stress and sinking velocity as well as their sedimentation decoupled from natural particle flux suggests a sea-based entry. That fibres can reach the Baltic Sea basins from land-based sources was recently demonstrated in a modelling study⁷. Our finding, that fibres dominated sea basin sediments, echo the MP composition found by another study³, (paint resins excluded). The function of low energetic environments as a sink for smaller MP (<500 μm) and its scale should be focused on in future studies. Particles of sizes where density-determined advection becomes negligible compared to turbulence-driven diffusion are considered equally distributed throughout the sea²⁶. Then other mechanisms gain influence: conglomeration of suspended material rises the particles deposition velocity and consolidation and cohesion of deposited material increases the threshold shear stress necessary to initiate motion. Once deposited, (Baltic) sea basins foster an ultimate burial of MP, due to the relatively low resuspension probability. In the Baltic, only rare inflow events of dense, saline North Sea water or strong cyclonic winds could temporarily resuspend MP³⁶.

Backtracking point sources. A large-scale correlation between population density and MP along river shores was recently demonstrated³⁷. In the present study, sediment samples were taken in a relatively dense spatial resolution, which allowed to reveal direct sink source relationships. As a result, major point sources were backtracked to the WWTP and harbour areas.

Despite the generally high filtering efficiency of MP by WWTPs, absolute release numbers were found to be significant³⁸. The relatively high threshold shear stress required to transport paint resins explains their most significant source backtracking curve within the data set (Fig. 3A). The occurrence of paint resins coincides with previously documented elevated heavy metal burdens of copper, cadmium and lead in the estuary³⁹.

Cross-correlations with other emitters of heavy metals are possible. However, heavy metal leaching from the paint matrix and their function as transport vehicle of contaminants to the environment is unquestioned⁴⁰. Copper, for instance, is an active ingredient in most antifoulant paints and a chromophore complex constituent of many blue and green pigments⁴¹, reaching highest concentrations compared to other heavy metals.

The found micro PS beads are likely to be emitted by nearby industries, as a contribution of this sector has been shown to exist^{9,42}. In the present study, parameterisation and thus allocation to the industrial sector were, however, complicated due to the broad application possibilities of these products. PS ion exchangers are being used for water purification, desalinisation, softening, demineralisation and micro-fouling control and are used predominantly in metal or pharmaceutical sectors. It is especially due to the above mentioned industrial sectors that billions of m³ of untreated waste water enter the aquatic environment annually in Germany⁴³. In an Austrian case study⁴⁴, the generous thresholds that are set for industrial MP discharges were criticised. Similar 'spherules' in water samples were identified along the Rhine river which occurred at very high frequencies (overall average of 60%), especially in areas of high industrial density⁴². Proportions (58% overall), morphology (opaque, 300–1000 µm in size), their polymeric assignment to cross-linked PS and the proximity to industrial areas compare with our findings in Warnow estuarine sediments. Their apparent presence in both compartments, the sediments and the water surface, might be explained by the inclusion of gas bubbles within the spherules as occasionally observed by the mentioned study⁴². Ageing effects, described for ion exchangers as the oxidative breakage of cross-linkers past water uptake, can also cause swelling and softening⁴⁵. The general dominance of the PS based ion exchanger beads shows that they constitute a so far largely ignored MP species of potentially very large quantities in urban waters.

Conclusions and Prospects of Granulometric Normalisation

Particles, whether they are of clastic sediment or synthetic polymeric nature are principally governed by the same environmental laws. The presented direct correlations in transport - deposition behaviour between the two materials can be used as a foundation for an improved estimation and projection of the MP distribution in sediments confirming our initial hypothesis. Fractionated granulometric normalisation based on mathematical correlations between specific MP categories and the reference sediment grain size fraction to eliminate hydrodynamic variability is highly recommended. This has implications on the interpretation of former study results, concluding that without correction for variability of natural particle composition in consequence of hydrodynamic differences, rational comparison of MP abundances between samples is impeded. We propose this as a basis for the prediction of MP distribution from small precursory MP deposition data sets by using spatial sediment grain size data along with data on local sources. Considerations on spatio-temporal connectivity of the system studied and heterogeneity of the sedimentary matrix are pivotal for a sound and comprehensive assessment. Resolving the physical fate of MP in the aquatic environment can be approached by building upon the extensive knowledge of sediment transport mechanisms. Using sediment grain size as a proxy, identification of pathways, sinks and sources of MP on a regional and potentially global scale are achievable objectives. Changing anthropogenic influences, over space and time, can subsequently be determined, which is of direct importance when applied as a stratigraphic indicator of the anthropocene⁴⁶. In a nutshell, a close look at sediment distribution maps is of importance prior to sampling as well as during data interpretation when assessing an area's MP contamination level.

The developed MP-sediment relationship should be understood as a first approximation derived from field data. The basic calculations of sediment and MP dynamics and the comparison to normalised data of previously published data supports the idea of a general applicability of the fractionated granulometric normalisation. However, further validation and extension by larger data sets covering larger MP size ranges, analysing the influence of shape in more detail and testing the relationships found in areas with similar as well as deviating hydrodynamic conditions, such as fluvial and marine, are needed. In areas where other mechanisms determine particle sorting (i.e. sinking velocity), correlations might deviate. It is questionable whether beaches and shorelines reflect the same direct linkage between MP and sediment grain size^{8,47}. The more complex distribution behaviour of LD polymers should be a future research focus to complete our understanding of MP transport and deposition patterns.

Materials and Methods

Sample collection. *Warnow estuary.* Sediment sampling in the Warnow estuary followed a transect, from past the sluice gate (S1) in the centre of the city Rostock, downstream to approximately 2 km past the estuary where it discharges into the Baltic Sea (S8, S9). A total of 9 stations were sampled along the lower Warnow, plus one station (S10) in the adjacent side arm Alter Strom connected via the Baltic Sea. In close intervals of 0.8 to 5 km, sampling was conducted from aboard a boat by deploying a Van-Veen grab (which covers an area of 0.04 m² and has a maximum capacity of 5 l). Wet weights ranged from 1550 to 2700 g. At two stations a total of three replicates were taken and analysed exemplary to evaluate local variability. The sampled sediment was then transferred into a 1.5 l glass jar with the use of a metal bowl and spoon, which were thoroughly rinsed with micro-filtrated water (MilliQ) beforehand. The samples were stored in a dark room at a temperature of 4 °C until processing.

Arkona and Gotland basin. Sediment trap sampling: Sediment trap sampling was part of a larger benthic-pelagic monitoring program and comprised two series, one in the Arkona, the other in the Gotland basin, with individual sampling intervals (1–20) of 10 and 14 days, respectively (location information: SI, Table S2). The round and funnel-shaped inlet of the sediment traps spans 80 cm in diameter, covering an area of 0.503 m². The sediment trap content was collected in a 400 ml PE vessels and subsequently sieved, as only the fraction >500 µm was investigated for this study. The remains were fixed in formaldehyde and kept in 20 ml glass vessels.

Sediment sampling: Sediment samples at the two Baltic Sea stations (same locations as sediment traps) were taken with a box corer during the Poseidon cruise 488 in 2015. The box corer covers an area of 15 × 15 cm and

a sampling depth of 10 cm was attempted. 1 kg wet weight from each location, comprising 500 g of two separate samples, taken in parallel, was the basis for later analysis.

Sample preparation. *Sediment samples.* DW analysis was conducted by determining the weight differences of a defined amount of homogenised wet sediment subsample between pre- and post-drying in a drying closet, at 60 °C for 48 h, until no further weight reduction was measurable. Wet sediment samples were density separated using a MicroPlastic Sediment Separator (MPSS, Hydro-Bios). The instrument is entirely made of stainless steel and glass, except for EPDM o-rings and PTFE hoses and sealings. The MPSS has a documented recovery rate of 100% in the analysed size class. A detailed description of the MPSS⁴⁸ and appropriate protocols⁴⁹ are published.

In this study we used sodium polytungstate (TC-Tungsten Compounds) at a density of approximately 1.8 g cm^{-3} as a density separation solution. A methodological remark on the recommended density separation threshold that includes paint resins is available in the SI, Text S3. Each sediment sample was added to 4 l of prefiltered sodium polytungstate in the MPSS with a metal spoon. By means of a vacuum pump, the density solution was transferred from a stainless steel barrel to the sediment container, passing two prefilters of 10 and $5 \mu\text{m}$. A rotor (20 rpm) at the bottom of the container stirs the sample to free potential MP and pass them into the conical stand pipe and then into the dividing chamber for final separation. Larger floating pieces ($>1 \text{ cm}$) such as shells or pieces of wood were removed (rinsing ensured no MP loss) as they can cause clogging of the dividing chamber. In order to avoid precipitation reactions, causing the clogging of filters and leakage, the pH had to be kept at an optimum of 3 to 3.4. This was achieved by adding prefiltered 37% hydrochloric acid after each passage when the solution had been in contact with the sediment at higher pH. Density was checked regularly and readjusted if necessary. The separation process lasted 24 h while the MPSS hull was occasionally knocked, to limit the possibility of MP adhering to the walls. Following this, the separation chamber was closed and dismantled and the supernatant transferred into a beaker glass. The remaining residues in the separation chamber were rinsed with MilliQ into a second glass beaker. After each sample run, the sodium polytungstate was filtered through a $15 \mu\text{m}$ mesh back into the storage barrel. The liquids were collected to be recycled by the producer. Prior to each new sample treatment, a cleaning sequence guaranteed a contamination free MPSS. For general contamination prevention measures and control testing, see SI, Text S2.

Since this study intended to examine the larger fraction of MP, the supernatant was passed through a stainless steel sieve with apertures of $500 \mu\text{m}$. Samples not directly analysed, were stored in beakers filled with MilliQ and covered with aluminum foil. The sample was subsequently pre-analysed under the microscope (Zeiss Stemi 200, magnification: 6.5 to $50\times$) in a custom-built Bogorov chamber ($20 \times 20 \text{ cm}$). MP suspects were manually isolated according to defined visual criteria^{50,51}. These suspects were then placed between two glass slides, which were then kept bound together with parafilm, pending spectroscopic analysis. The sieve was thoroughly scanned for potential MP remains.

After density separation, some of the samples (S1, S2, S3, S8, S9) underwent further treatment in order to reduce organic material content and ease subsequent visual and spectral analysis. An array of treatments with SDS, enzymes, sodium hydroxide (NaOH), hydrogen chloride (HCl) or a repeated density separation were applied depending on the degree of biogenic or silicate debris⁵². All applied chemicals are known to be non-destructive to MP⁵³.

Sediment trap samples. Some of the Gotland samples (1–2, 3–4, 7–9, 10–12, 13–15, 16–17) were pooled because of their low sample volume. In total, 49 subsamples were taken. Sediment trap samples were transferred to glass petri dishes and examined for MP by means of a binocular microscope (Zeiss Stemi 2000, 6.5–8x magnification, $50\times$ for a detailed study of the particle morphology) from top to bottom in horizontal lines. This was then repeated up to three times in different orientations of the petri dish. In case of large volumes, the sample was subdivided. By means of fine tweezers with $0.05 \times 0.01 \text{ mm}$ tips, isolated MP were transferred in 1.5 ml PE Eppendorf-tubes previously filled with $700 \mu\text{l}$ sample water. As the removal of biofilms and other material is generally recommended to ensure best possible spectra quality during FTIR and Raman spectroscopy^{33,54}, the isolated MP suspects underwent a 72 h purification treatment by adding $750 \mu\text{l}$ of 30% hydrogen peroxide (H_2O_2) solution. Both efficiency and resistance by plastic of the oxidising agent is known from other studies⁵⁵. Temperature rise of the exothermic reaction was ensured to be minimal⁵⁶. Via bottle top filtration, the samples were transferred onto PC filters of $3 \mu\text{m}$ pore size (47 mm in diameter) which were then separated using filter paper stored in petri dishes until further analysis. MP suspects were photo-documented in a second binocular run (Zeiss Discovery V.8 Stereo with camera module AxioCam ICc 3, Software Axio Vision, 16–128x magnification), and pregrouped into plastic or unknowns. Subsequent spectroscopic analysis would correct for false positive misidentifications.

Chemical characterisation via μ -ATR-FTIR and Raman-spectroscopy. All MP suspects were analysed via micro-attenuated total reflection - Fourier transform infrared spectroscopy (μ -ATR-FTIR) as single point measurements. A Bruker Vertex 70 FTIR- spectrometer coupled with a Bruker Hyperion 2000 FTIR-microscope equipped with a 20x ATR objective with a germanium crystal and a Mercury Cadmium Telluride single element detector was used. Measurements were taken with a resolution of 4 cm^{-1} in a wavenumber range of $4000\text{--}600 \text{ cm}^{-1}$ with 100 scans per sample. The contact area of the germanium crystal approximates $25 \times 25 \mu\text{m}$. The FTIR detector requires liquid nitrogen for cooling and this must be filled 30 minutes before operation and repeated every 5–6 hours. Background spectra were regularly measured against air with the same setting as described above. Appropriated signal-to-noise ratios required a close contact between the ATR crystal tip and MP suspect situated on the glass slide. Between measurements the ATR crystal was cleaned with ethanol to avoid cross-contamination.

The software Opus 7.5 (Bruker Optics) was used for spectral measurement, processing and evaluation. Multiple reference libraries were indexed: ATR-FTIR Library complete Volume 1–3, Hummel Industrial Polymers Vol. 1–3, Bruker Optics, as well as internal IPF libraries. Plastic-positive spectra as well as some exemplary non-plastic spectra were archived and are available upon request. For items yielding insufficient spectral quality (about 5–10% of the samples) complementary measurements were either taken via Raman-microspectroscopy or were excluded. Single point measurements by Raman-microspectroscopy were performed as described in K  ppler *et al.*⁵⁴.

Morphological characterisation. Potential MP items were categorised according to shape, colour and size. MP length were digitally measured via GIMP (version 2.8.16) across their longest dimension and categorised into 500–1000–2000–5000, >5000 μm intervals. In case of repeatedly occurring identical items, a subset was measured spectroscopically.

Geological and chemical analysis. Grain size distribution was analysed in two sample replicates with the laser-sizer CILAS 1180 with ultrasound applied. For station S5–S8, grain size data is based on only one measurement due to problems during sample splitting, which could not guarantee grain size independent separation. Prior to analysis, the samples were homogenised. A 30% H_2O_2 pretreatment ensured organic matter-free material. Organic and inorganic carbon, nitrogen and CaCO_3 determination was conducted on lyophilised sample material using elemental analysers multi-EA 2000 (Analytik Jena) and EA 1110 CHN (CE-instruments). These granulometrical methods are well established in geological studies⁵⁷.

Hydrodynamic model. For data retrieval of simulated shear stress values from the Warnow estuary model simulations were carried out with the help of the three-dimensional coastal ocean model GETM (General Estuarine Transport Model⁵⁸). It calculates time series of salinity, temperature and current velocity among others, on a high-resolution grid with 20 m horizontal resolution. As GETM has been successfully applied in numerous studies (e.g. in⁵⁹), particularly in the Warnow estuary^{23,60,61}, only very fundamental information on the model is provided. For more detail the reader is referred to the previously mentioned publications. Here, the same underlying model configuration has been used with a state-of-the-art turbulence closure scheme GOTM (General Ocean Turbulence Model) and a second-order advection scheme (SUPERBEE) to reduce numerical diffusion and fully conserve mass, energy and momentum. Meteorological forcing is calculated from output of the German Weather Service Local Model (DWD-LM) with a horizontal resolution of 7 km. Sea level, temperature and salinity at the open boundary are generated by larger scale outer models of the western Baltic Sea (see⁵⁹ for details) and time series of Warnow river discharge are provided by the Federal Maritime and Hydrography agency. The barotropic processes are captured in terms of sea level with a root mean square error of 0.08 m and bottom temperature is reproduced with a r.m.s.e. of 0.82 $^{\circ}\text{C}$.

Statistical analysis. Regional abundances are presented as median value with the 25 and 75-percentiles [0.25–0.75] due to non-normality. Replicated samples are presented as mean \pm standard deviation (SD). Two-tailed Pearson correlation coefficient r was used to test for the degree of association in case of linear relationships; otherwise Spearman's rank r_s is mentioned when applied. In figures containing regression analysis the coefficient of determination r^2 is given as a measure of Goodness-of-fit (least square) together with the fitted equation. Outliers were based on studentized residuals with the threshold at ± 3 .

As the MP abundance data μ_i [kg^{-1} DW] analysed with the GLMs was both not normally distributed and integer based, the poisson link function was chosen:

$$\log(\hat{\mu}_i) = \beta_0 + \beta_1 x_{i,1} + \beta_2 x_{i,2} + \dots + \beta_k x_{i,k}, i = 1, \dots, 10 \quad (5)$$

After a first preselection, a set of k predictor variables x_i were tested. Unstandardised β coefficients were calculated to estimate parameter influence. Both backward and forward simplification approaches were applied to achieve best model fit. Whether to include or remove a term was evaluated by means of the AIC, deviance and the significance of the standardised regression coefficients ($p < 0.05$). Overfitting was addressed by using the adjusted r^2 . Exploratory data analysis (EDA) assisted the decision process to, for instance, avoid collinearity among variables which would reduce statistical power. Collinearity was resolved either by using a combination of the two variables for logical relationships or exclusion of one of them. Model validation was conducted via residual analysis, visualised in the probability plot of the Pearson residuals for standard normal distribution and the plot of residuals vs. fitted values. The GLM was built in matlab (version 2017b).

Geospatial analysis. Source related predictor variables mentioned above were generated using the nearest neighbour analysis and intersection geoprocessing tool in QGIS⁶² using the UTM-33N (EPSG:7417) projection. Data from potential diffuse sources were determined within a buffer zone of 1000 m (radius) which was a trade-off between the catchment zone and practicality, as this avoided overlapping of influence zones. Point sources were measured as distances. Diffuse sources were counted within a 1000 m radius. Parameterisation was based on a qualitative assessment of the present estuary with regards to potential MP emitting sources, as they are generally widely discussed in the literature⁶³. This was assisted by EDA. It is noted that the data set may not be complete and data retrieval is dependent on both the type of reference and the method of choice. A transfer of the model to other locations would possibly require incorporation of additional parameters of relevance and/or to dispense with others.

Received: 5 December 2018; Accepted: 15 September 2019;

Published online: 23 October 2019

References

- Andrady, A. L. Microplastics in the marine environment. *Mar. pollution bulletin* **62**, 1596–605, <http://www.ncbi.nlm.nih.gov/pubmed/21742351>, <https://doi.org/10.1016/j.marpolbul.2011.05.030> (2011).
- Lebreton, L. C. *et al.* River plastic emissions to the world's oceans. *Nat. Commun.* **8**, 1–10, <https://doi.org/10.1038/ncomms15611> (2017).
- Woodall, L. C. *et al.* The deep sea is a major sink for microplastic debris. *Royal Soc. Open Sci.* **1**, <http://rsos.royalsocietypublishing.org/content/1/4/140317.abstract>, <https://doi.org/10.1098/rsos.140317> (2014).
- Besseling, E., Quik, J. T., Sun, M. & Koelmans, A. A. Fate of nano- and microplastic in freshwater systems: A modeling study. *Environ. Pollut.* **220**, 540–548 Besseling, E., Quik, J. T. K., Sun, M., & K., <https://doi.org/10.1016/j.envpol.2016.10.001> (2017).
- Hurley, R., Woodward, J. & Rothwell, J. J. Microplastic contamination of river beds significantly reduced by catchment-wide flooding. *Nat. Geosci.* **11**, 251–257, <https://doi.org/10.1038/s41561-018-0080-1> (2018).
- Goldberg, E. D. Plasticizing the seafloor: An overview. *Environ. Technol. (United Kingdom)* **18**, 195–201, <https://doi.org/10.1080/09593331808616527> (1997).
- Bagaev, A., Mizyuk, A., Khatmullina, L., Isachenko, I. & Chubarenko, I. Anthropogenic fibres in the Baltic Sea water column: Field data, laboratory and numerical testing of their motion. *Sci. Total. Environ.* **599–600**, 560–571, <https://doi.org/10.1016/j.scitotenv.2017.04.185> (2017).
- Browne, M. A., Galloway, T. S. & Thompson, R. C. Spatial patterns of plastic debris along Estuarine shorelines. *Environ. science & technology* **44**, 3404–9, <http://www.ncbi.nlm.nih.gov/pubmed/20377170>, <https://doi.org/10.1021/es903784e> (2010).
- Ballent, A., Corcoran, P. L., Madden, O., Helm, P. A. & Longstaffe, F. J. Sources and sinks of microplastics in Canadian Lake Ontario nearshore, tributary and beach sediments. *Mar. Pollut. Bull.* **110**, 383–395, <https://doi.org/10.1016/j.marpolbul.2016.06.037> (2016).
- Martin, J., Lusher, A., Thompson, R. C. & Morley, A. The Deposition and Accumulation of Microplastics in Marine Sediments and Bottom Water from the Irish Continental Shelf. *Sci. Reports* **7**, 1–9, <https://doi.org/10.1038/s41598-017-11079-2> (2017).
- Soulsby, R. *Dynamics of marine sands: a manual for practical applications* (Thomas Telford, London, 1997).
- Kersten, M. & Smedes, F. Normalization procedures for sediment contaminants in spatial and temporal trend monitoring. *J. Environ. Monit.* **4**, 109–115, <https://doi.org/10.1039/b108102k> (2002).
- Leipe, T. *et al.* Particulate organic carbon (POC) in surface sediments of the Baltic Sea. *Geo-Marine Lett.* **31**, 175–188, <https://doi.org/10.1007/s00367-010-0223-x> (2011).
- Strand, J., Lassen, P., Shashoua, Y., Andersen, J. H. *Microplastic particles in sediments from Danish waters* (2013).
- Maes, T. *et al.* Below the surface: Twenty-five years of seafloor litter monitoring in coastal seas of North West Europe (1992–2017). *Sci. Total. Environ.* **630**, 790–798, <https://doi.org/10.1016/j.scitotenv.2018.02.245> (2018).
- Vianello, A. *et al.* Microplastic particles in sediments of Lagoon of Venice, Italy: First observations on occurrence, spatial patterns and identification. *Estuarine, Coast. Shelf Sci.* **130**, 54–61, <http://linkinghub.elsevier.com/retrieve/pii/S0272771413001480>, <https://doi.org/10.1016/j.ecss.2013.03.022> (2013).
- Alomar, C., Estarellas, F. & Deudero, S. Microplastics in the Mediterranean Sea: Deposition in coastal shallow sediments, spatial variation and preferential grain size. *Mar. Environ. Res.* **115**, 1–10, <https://doi.org/10.1016/j.marenvres.2016.01.005> (2016).
- Renzi, M. *et al.* Is the microplastic selective according to the habitat? Records in amphioxus sands, Mäerl bed habitats and Cymodocea nodosa habitats. *Mar. Pollut. Bull.* **130**, 179–183 www.sciencedirect.com/science?_ob=GatewayURL&{_}origin=IIRSSSEARCH&{_}method=citationSearch&{_}piikey=S0025326X18301644&{_}version=1&md5=38bc8ff4bfd78997c0a654c46c228bd4, <https://doi.org/10.1016/j.marpolbul.2018.03.019> (2018).
- Blašković, A., Fastelli, P., Čizmek, H., Guerranti, C. & Renzi, M. Plastic litter in sediments from the Croatian marine protected area of the natural park of Telašćica bay (Adriatic Sea). *Mar. Pollut. Bull.* **114**, 583–586, <https://doi.org/10.1016/j.marpolbul.2016.09.018> (2017).
- Fastelli, P. *et al.* Plastic litter in sediments from a marine area likely to become protected (Aeolian Archipelago's islands, Tyrrhenian sea). *Mar. Pollut. Bull.* **113**, 526–529, <https://doi.org/10.1016/j.marpolbul.2016.08.054> (2016).
- Romeo, T. *et al.* Environmental quality assessment of Grand Harbour (Valletta, Maltese Islands): a case study of a busy harbour in the Central Mediterranean Sea. *Environ. Monit. Assess.* **187**, <https://doi.org/10.1007/s10661-015-4950-3> (2015).
- Peng, G. *et al.* Microplastics in sediments of the Changjiang Estuary, China. *Environ. Pollut.* **225**, 283–290, <https://doi.org/10.1016/j.envpol.2016.12.064> (2017).
- Lange, X. *The impact of wind forcing on estuarine circulation*, PhD thesis. Ph.D. thesis (2019).
- Kowalski, N., Reichardt, A. M. & Wanek, J. J. Sinking rates of microplastics and potential implications of their alteration by physical, biological, and chemical factors. *Mar. Pollut. Bull.* **109**, 310–319, <https://doi.org/10.1016/j.marpolbul.2016.05.064> (2016).
- Stuart, B. H. *Polymer Analysis* (Sydney, 2002).
- Enders, K., Lenz, R., Stedmon, C. A. & Nielsen, T. G. Abundance, size and polymer composition of marine microplastics 10 mm in the Atlantic Ocean and their modelled vertical distribution. *Mar. Pollut. Bull.* **100**, 70–81, <http://linkinghub.elsevier.com/retrieve/pii/S0025326X15300370>, <https://doi.org/10.1016/j.marpolbul.2015.09.027> (2015).
- Epa. (Reformatted 1/95). In *Ap-42*, vol. 81, 4–7 (1981).
- Wentworth, C. K. A Scale of Grade and Class Terms for Clastic Sediments. *The J. Geol.* **30**, 377–392, [10.1086/622910](https://doi.org/10.1086/622910). 846 (1922).
- Iversen, J., Greeley, R., Marshall, J. & Pollack, J. Aeolian saltation threshold: the effect of density ratio. *Sedimentol.* **699–706**, <https://doi.org/10.1111/j.1365-3091.1987.tb00795.x> (1987).
- Morét-Ferguson, S. *et al.* The size, mass, and composition of plastic debris in the western North Atlantic Ocean. *Mar. pollution bulletin* **60**, 1873–8, <http://www.ncbi.nlm.nih.gov/pubmed/20709339>, <https://doi.org/10.1016/j.marpolbul.2010.07.020> (2010).
- Maes, T. *et al.* Microplastics Baseline Surveys at the Water Surface and in Sediments of the North-East Atlantic. *Front. Mar. Sci.* **4**, 1–13, <https://doi.org/10.3389/fmars.2017.00135> (2017).
- Flemming, B. W. A revised textural classification of gravel-free muddy sediments on the basis of ternary diagrams. *Cont. Shelf Res.* **20**, 1125–1137, [https://doi.org/10.1016/S0278-4343\(00\)00015-7](https://doi.org/10.1016/S0278-4343(00)00015-7) (2000).
- Lenz, R., Enders, K., Stedmon, C. A., MacKenzie, D. M. & Nielsen, T. G. A critical assessment of visual identification of marine microplastic using Raman spectroscopy for analysis improvement. *Mar. Pollut. Bull.* **100**, 82–91 <http://linkinghub.elsevier.com/retrieve/pii/S0025326X15300424>, <https://doi.org/10.1016/j.marpolbul.2015.09.026> (2015).
- Feistel, R., Nausch, G. & Wasmund, N. State and Evolution of the Baltic Sea, 1952–2005: A Detailed 50-Year Survey of Meteorology and Climate, Physics, Chemistry, Biology, and Marine Environment. In Feistel, R., Nausch, G. & Wasmund, N. (eds) *State and Evolution of the Baltic Sea, 1952–2005: A Detailed 50-Year Survey of Meteorology and Climate, Physics, Chemistry, Biology, and Marine Environment*, 1–703, [10.1002/9780470283134](https://doi.org/10.1002/9780470283134) (2008).
- Turner, S., Horton, A. A., Rose, N. L. & Hall, C. A temporal sediment record of microplastics in an urban lake, London, UK. *J. Paleolimnol.* **61**, 449–462, <https://doi.org/10.1007/s10933-019-00071-7> (2019).
- Bunke, D. Sediment mixing processes and accumulation patterns in the south-western Baltic Sea, PhD thesis, University of Greifswald (2017).
- Klein, S., Worch, E. & Knepper, T. P. Occurrence and spatial distribution of microplastics in river shore sediments of the rhine-main area in Germany. *Environ. Sci. Technol.* **49**, 6070–6076, <https://doi.org/10.1021/acs.est.5b00492> (2015).
- Mintenig, S. M., Int-Veen, I., Löder, M. G., Primpke, S. & Gerdts, G. Identification of microplastic in effluents of waste water treatment plants using focal plane array-based micro-Fourier-transform infrared imaging. *Water Res.* **108**, 365–372, <https://doi.org/10.1016/j.watres.2016.11.015> (2017).

39. LUNG Mecklenburg Vorpommern. Marine Daten-Infrastruktur <http://www.fis-wasser-mv.de/mdi-de/portal> (2017).
40. Turner, A. Marine pollution from antifouling paint particles. *Mar. Pollut. Bull.* **60**, 159–171, <https://doi.org/10.1016/j.marpolbul.2009.12.004> (2010).
41. Imhof, H. K. *et al.* Pigments and plastic in limnetic ecosystems: A qualitative and quantitative study on microparticles of different size classes. *Water Res.* **98**, 64–74, <https://doi.org/10.1016/j.watres.2016.03.015> (2016).
42. Mani, T., Hauk, A., Walter, U. & Burkhardt-Holm, P. Microplastics profile along the Rhine River. *Sci. Reports* **5**, 17988 <http://www.nature.com/articles/srep17988>, <https://doi.org/10.1038/srep17988> (2015).
43. Destatis, S. B. Nichtöffentliche Wasserversorgung und nichtöffentliche Abwasserentsorgung - Fachserie 19 Reihe 2.2–2013. Tech. Rep. 2.2, https://www.destatis.de/DE/Publikationen/Thematisch/UmweltstatistischeErhebungen/Wasserwirtschaft/WasserAbwasserNichtoeffentlich2190220139004.pdf?__blob=publicationFile (2016).
44. Lechner, A. & Ramler, D. The discharge of certain amounts of industrial microplastic from a production plant into the River Danube is permitted by the Austrian legislation. *Environ. Pollut.* **200**, 159–160, <http://linkinghub.elsevier.com/retrieve/pii/S0269749115000949> <http://www.ncbi.nlm.nih.gov/pubmed/25734504>, <https://doi.org/10.1016/j.envpol.2015.02.019> (2015).
45. Michaud, C. The role of Crosslinking in Ion Exchange Resins. *Water Cond. & Purif.* (2011).
46. Zalasiewicz, J. *et al.* The geological cycle of plastics and their use as a stratigraphic indicator of the Anthropocene. *Anthropocene* **13**, 4–17, <https://doi.org/10.1016/j.ancene.2016.01.002> (2016).
47. Chubarenko, I. P., Esiukova, E. E., Bagaev, A. V., Bagaeva, M. A. & Grave, A. N. Three-dimensional distribution of anthropogenic microparticles in the body of sandy beaches. *Sci. Total. Environ.* **628–629**, 1340–1351, <https://doi.org/10.1016/j.scitotenv.2018.02.167> (2018).
48. Imhof, H. K., Schmid, J., Niessner, R., Ivleva, N. P. & Laforsch, C. A novel, highly efficient method for the separation and quantification of plastic particles in sediments of aquatic environments. *Limnol. Oceanogr. Methods* **10**, 524–537, <https://doi.org/10.4319/lom.2012.10.524> (2012).
49. Lorenz, C. Detection of microplastics in marine sediments of the German Coast via FT-IR spectroscopy, [http://rosdok.uni-rostock.de/resolve/id/rosdok\[thesis\]0000000017..10.1002/ejoc.201200111](http://rosdok.uni-rostock.de/resolve/id/rosdok[thesis]0000000017..10.1002/ejoc.201200111). arXiv:1011.1669v3 (2014).
50. Norén, F. Small plastic particles in Coastal Swedish waters, <http://www.kimointernational.org/WebData/Files/SmallplasticparticlesinSwedishWestCoastWaters.pdf> (2007).
51. Enders, K. & Lenz, R. How to Find the Small Plastic in the Big Sea - The Identification and Characterisation of Microplastic 10 m from the Atlantic Ocean (Master Thesis) (2015).
52. Löder, M. G. *et al.* Enzymatic Purification of Microplastics in Environmental Samples. *Environ. Sci. Technol.* **51**, 14283–14292, <https://doi.org/10.1021/acs.est.7b03055> (2017).
53. Cole, M. *et al.* Isolation of microplastics in biota-rich seawater samples and marine organisms. *Sci. reports* **4**, 4528, <http://www.ncbi.nlm.nih.gov/pubmed/24681661>, <https://doi.org/10.1038/srep04528> (2014).
54. Käßler, A. *et al.* Analysis of environmental microplastics by vibrational microspectroscopy: FTIR, Raman or both? *Anal. Bioanal. Chem.* **408**, 8377–8391, <https://doi.org/10.1007/s00216-016-9956-3> (2016).
55. Tagg, A. S., Sapp, M., Harrison, J. P. & Ojeda, J. J. Identification and Quantification of Microplastics in Wastewater Using Focal Plane Array-Based Reflectance Micro-FT-IR Imaging. *Anal. Chem.* **87**, 6032–6040, <https://doi.org/10.1021/acs.analchem.5b00495>. arXiv:0711.2730v2 (2015).
56. Munno, K., Helm, P. A., Jackson, D. A., Rochman, C. & Sims, A. *Impacts of Temperature and Selected Chemical Digestion Methods on Microplastic Particles*. **37**, 91–98, <https://doi.org/10.1002/etc.3935> (2018).
57. Leipe, T. *et al.* Regional distribution patterns of chemical parameters in surface sediments of the south-western Baltic Sea and their possible causes. *Geo-Marine Lett.* **37**, 593–606, <https://doi.org/10.1007/s00367-017-0514-6> (2017).
58. Burchard, H., Bolding, K. & Villarreal, M. R. Three-dimensional modelling of estuarine turbidity maxima in a tidal estuary. *Ocean. Dyn.* **54**, 250–265, <https://doi.org/10.1007/s10236-003-0073-4> (2004).
59. Gräwe, U., Naumann, M., Mohrholz, V. & Burchard, H. Anatomizing one of the largest saltwater inflows into the Baltic Sea in December 2014. *J. Geophys. Res. Ocean.* **120**, 7676–7697, <https://doi.org/10.1002/2015JC011269> (2015).
60. Buer, A.-L. *et al.* Long term development of Bathing Water Quality at the German Baltic coast: spatial patterns, problems and model simulations. *Mar. Pollut. Bull.* **135**, 1055–1066, <http://www.sciencedirect.com/science/article/pii/S0025326X18306180>, <https://doi.org/10.1016/j.marpolbul.2018.08.048> (2018).
61. Jurasinski, G. *et al.* Understanding the Coastal Ecocline: Assessing Sea–Land Interactions at Non-tidal, Low-Lying Coasts Through Interdisciplinary Research. *Front. Mar. Sci.* **5**, 1–22, <https://doi.org/10.3389/fmars.2018.00342> (2018).
62. QGIS Development Team. QGIS Geographic Information System (version 2.18.13), <http://qgis.osgeo.org> (2018).
63. Sundt, P., Schulze, P.-E. & Syversen, F. *Sources of microplastic- pollution to the marine environment Project report DOI M-321|2015* (2014).
64. OpenStreetMap contributors. OSM, <https://www.openstreetmap.org> (2017).
65. Hille, S. New aspects of sediment accumulation and reflux of nutrients in the Eastern Gotland Basin (Baltic Sea) and its impact on nutrient cycling. **120** (2005).

Acknowledgements

We thank Regina Hansen for help on the sediment trap sampling, Thomas Leipe, Ines Scherff and Mischa Schönke for access and assistance on the geological analysis, Alexander Hentzsch for the installation of the MPSS, Rica Wegener and Franziska Klaeger for assistance during laboratory work, Luis H. B. Alves for knowledge exchange on GLMs, the IOW workshop team for technical support, Alexander Tagg and Colin A. Stedmon for language editing, Robin Lenz, Hans Burchard and Helge Arz for valuable comments. This work resulted from the MikrOMIK project funded by the Leibniz Association (SAW-2014-IOW-2), the BONUS MICROPOLL project supported by BONUS (Art 185), funded jointly by the European Union and Federal Ministry of Education and Research (BMBF) (03F0775A) and the BMBF project MicroCatch_Balt (03F0788A).

Author contributions

Conceptualization: K.E. and M.L.; Sampling and Preparation: O.B., N.S., F.P. and S.O.; Chemical Analysis: K.E., A.K., O.B., D.F. and K.-J.E.; Theoretical Validation: K.E., P.F. and X.L.; Formal Analysis: K.E.; Data Curation: K.E.; Writing—Original Draft: K.E.; Writing—Review and Editing: A.K., O.B., N.S., P.F., X.L.; K.-J.E., F.P., S.O. and M.L.; Visualization: K.E. and P.F.; Supervision: M.L.; Project Administration: M.L.; Funding Acquisition and Resources: S.O., M.L.

Competing interests

The authors declare no competing interests.

Additional information

Supplementary information is available for this paper at <https://doi.org/10.1038/s41598-019-50508-2>.

Correspondence and requests for materials should be addressed to M.L.

Reprints and permissions information is available at www.nature.com/reprints.

Publisher's note Springer Nature remains neutral with regard to jurisdictional claims in published maps and institutional affiliations.



Open Access This article is licensed under a Creative Commons Attribution 4.0 International License, which permits use, sharing, adaptation, distribution and reproduction in any medium or format, as long as you give appropriate credit to the original author(s) and the source, provide a link to the Creative Commons license, and indicate if changes were made. The images or other third party material in this article are included in the article's Creative Commons license, unless indicated otherwise in a credit line to the material. If material is not included in the article's Creative Commons license and your intended use is not permitted by statutory regulation or exceeds the permitted use, you will need to obtain permission directly from the copyright holder. To view a copy of this license, visit <http://creativecommons.org/licenses/by/4.0/>.

© The Author(s) 2019

Supporting Information (SI)

Tracing microplastics in aquatic environments based on sediment analogies

Kristina Enders, Andrea K  ppler, Oliver Biniasch, Peter Feldens, Nicole Stollberg, Xaver Lange, Dieter Fischer, Klaus-Jochen Eichhorn, Falk Pollehne, Sonja Oberbeckmann and Matthias Labrenz

Files in this SI Appendix: Text S1 to S3, Figures S1 to S4, Tables S1 to S3

Text S1. Composition and distribution of MP categories

Paint resins. Paint resin distribution was subject to great fluctuations and local hotspots appear with highest abundances in the Alter Strom of $210 \pm 69 \text{ kg}^{-1} \text{ DW}$. The background level of paint outside the hotspot areas can be described as relatively constant and ranges between 0 to $10 \text{ kg}^{-1} \text{ DW}$. Paint resins were grouped according to most frequently appearing categories. Alkyd resin (which incorporates acrylic resins as they are often applied in combination and also exhibit spectral similarities) comprising 90% of all measured paint resin particles, was by far the most dominating category. Polyurethane (PU) resin was a separate group with a percentage frequency of 2%. PU-alkyd combinations (urethanised alkyds) were common and classified as alkyd. With 6%, epoxy resins were the second most common group. Slightly less than 2% could not be clearly assigned to any of the above. However, spectral bands showing indications of paint resin origin and the presence of typical morphological features were deemed sufficient criteria to include these particles as paint resins.

PS beads. PS beads appeared in a very patchy distribution pattern, only at station S1, S2 and S5 ranging from 24 ± 21 to $317 \text{ kg}^{-1} \text{ DW}$. For some PS beads found at station S2, very high spectral quality with correlation scores between 80% and 97% enabled a precise allocation as either sodium polystyrene sulfonate (SPSS) or calcium polystyrene sulfonate (CPSS), both being ionomers. This revealed their identity as ion exchangers. For these PS beads, a colour gradient from transparent to orange to brownish to black and sizes approximating 500 to $900 \mu\text{m}$ were detected. Station S1 solely contained opaque non-transparent beads that matched with pure PS within a slightly broader size range of 500 to $1100 \mu\text{m}$. A mixture of both types along with polystyrene divinylbenzene (PS-DVB) occurred very abundantly, with $317 \text{ kg}^{-1} \text{ DW}$ recorded at station S5 (Fig S1). Due to the high numbers of PS beads and the occurrence of spectral masking, only subsets were spectroscopically examined (N_{spectra} , see Fig. S1). Others were identified based on identical morphological features wherefore relative abundances of the PS bead species were not ascertainable. In some cases, clear identification was limited either due to the masking by foreign spectra of water or other inorganic residues. It is not unusual that ion exchangers have a high moisture retention⁴⁸, which might explain this spectral overlay as well as the different degrees of softness found. Depending on the manufacturer and age the crosslinkage and water load of the ion exchangers can vary vastly and as a result its density. Therefore an accurate specification of the density cannot be made. Since the basis polymer is PS, they were categorised accordingly. This assumption is acceptable as for the latter correlation analysis no differentiation between the different HD polymers was made.

Ordinary polymers. Ordinary polymers were most abundant at station S3, approximately 200 m downriver past the wastewater treatment plant (WWTP), amounting to $93 \text{ kg}^{-1} \text{ DW}$. Also, the two stations S4 and S5 reached elevated numbers in both particles and fibres of $19 \text{ kg}^{-1} \text{ DW}$ and 9 to $10 \text{ kg}^{-1} \text{ DW}$, respectively, compared to all other Warnow samples. In contrast to LD, HD ordinary polymer numbers dropped quickly after station S3. Apart from this elevated region, numbers of ordinary polymers remained relatively low between 4 to $9 \text{ kg}^{-1} \text{ DW}$ within the estuarine transect and only $1 \text{ kg}^{-1} \text{ DW}$ within the Baltic Sea opening past the estuary (S8, S9). Fibres found in the Arkona basin fibres by polymer composition showed indication of maritime sources: PA, the material most fishing ropes and nets are made of. Included in this group is the high tech fabric poly paraphenylene terephthalamide (aka Kevlar) which finds many applications in the marine sector due to its thermal and fire resistance and lightweight strength. Further, acrylates (acryl) for fishing ropes and PAN primarily found as copolymer also has various marine applications (sails, fishing rods).

Text S2. Contamination control

Results. Controls taken alongside the sediment trap samples only contained cellulose fibres (resulting from a heavy usage of paper towels in the laboratory) and no plastic polymers. Additionally, the sediment trap control bottle from the field contained no plastic in the analysed size fraction, giving an indication of a contaminant-free work flow. By contrast, the sediment sample control representing the MPSS passage revealed three blue fibres comprised of polyesters (PET). PET fibre abundances found in the Warnow sample set correlate significantly with overall fibre abundances ($r = 0.71$, $p = 0.02$) suggesting that contamination of these PET fibres is marginal, as an otherwise randomised or constant background value is expected. Moreover, the likelihood to find PET fibres among sediment-related samples is generally rather high, as it is a HD polymer (1.37 g cm^{-3}) and among the major polymer types produced⁶⁶. Furthermore, their coinciding appearance with other fibres, especially at S5 with high PET numbers of $15 \text{ kg}^{-1} \text{ DW}$, as well as highest values in the Alter Strom, indicate a rather low contamination level. The widespread occurrence of PET in the sample set, conversely, usually within the same colour regime (transparent- blue - black) can be interpreted as an indicator of contamination. As the limited number of controls do not allow for a quantitative assessment of

contamination, a conservative interpretation requires an entire exclusion of PET fibres from the final results. This includes the data from the sediment trap samples as the surrounding conditions (operators, laboratory facility) did not change and air-born sources are most probable. Although the purification process of the sediment trap samples included less intensive chemical treatment, PET appeared frequently across the samples sets, with more than half (Akrona basin, $n_{PET\ fibre} = 17$) or all (Gotland basin, $n_{PET\ fibre} = 9$) of the polymers identified being assigned to this polymer type.

A second polymer type was eliminated from the results retrospectively; PTFE. This is because the conclusion must be drawn that these MP originate from the treatment within the MPSS, as several parts, such as within the separation chamber and the outlet valve, are made from this polymer. We observed that, without exception, all PTFE particles found have the same appearance (transparent-whitish, within the same size class, morphologically similar). The low but non-correlated and yet widespread occurrence throughout the sediment samples (including Arkona basin sediment sample) and absence in the sediment trap samples which did not undergo the MPSS treatment strengthens an MPSS-associated PTFE contamination. The pH adjustment of the sodium polytungstate solution was done in a Schott flask with a PTFE screw cap which was subsequently refilled into the MPSS. Abrasion of PTFE particles is possible. Although, the sodium polytungstate solution has a lower density than average PTFE ($2.1 - 2.3\text{ g cm}^{-3}$), surface tension effects could lead to the flotation, and consequent retrieval, of these small particles⁶⁷.

Contamination prevention and controls - Methods. To comply with requirements of quality assurance, both the application of control samples and best practice contamination prevention measures throughout both lab and field work were ensured. A cellulosic laboratory coat and nitrile gloves were worn at all times. Prior to use, all instruments and vials were sanitised with tap water and rinsed with deionised and micro-filtrated water (MilliQ, $0.2\ \mu\text{m}$). Where possible prefiltered 70% ethanol was used for decreasing the water drops surface tension in which plastic particles or fibers potentially could remain. Sieves were additionally ultra sonicated (up to three times for 10 minutes). Frequently used metal and glassware were flamed. Filtration measures were undertaken within a laminar flow chamber in order to avoid air-born contamination. During microscopy, petri dishes were kept closed and the Bogorov chamber was covered with aluminum foil while awaiting further analysis.

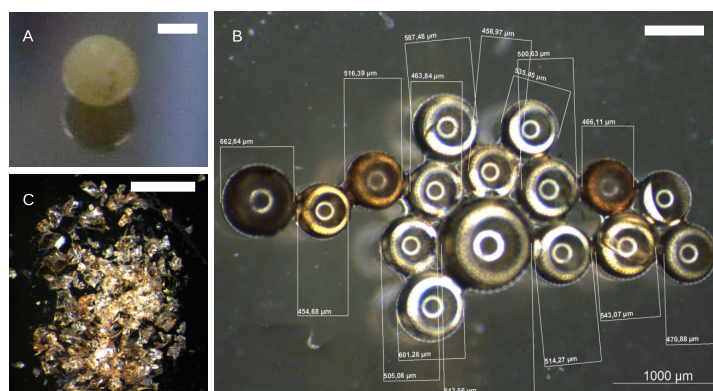
The sodium polytungstate solution was recycled each time by filtration through a $15\ \mu\text{m}$ gaze, ensuring that the density separation solution was free of contamination within the detection limit. Given the used separation density, fluoropolymeric compounds such as polytetrafluorethylen (PTFE, 2.2 g cm^{-3}) is not accounted for as the density would need to be increased significantly. The application of PTFEs as coatings of containers, hoses and sealings, bears the potential for unknown systematic contamination, as was the case in the present study. There are multiple reasons for excluding PTFE from particle-based study designs. Production volumes are proportionally low and PTFE MP probably enters the environment preferentially in the lower micrometer or nanometer size range since it has become highly relevant as nano-coatings⁶⁸. The omnipresence of perfluorochemicals (PFCs) in nature along with the ecotoxicological risk have been studied extensively. Specific mass-based detection methods of PFCs already exist⁶⁹.

In general the use of plastic items was avoided where possible. Restrictions are to be noted during sediment trap sampling, as the aperture is partly made out of plastic or coated with paint. The contamination risk for particles $> 500\ \mu\text{m}$ is, however, calculable as MP collection bottles closed underwater and were not opened until analysis. It is expected that any system-caused MP contamination would be identifiable by a correspondence between the characteristics of any used and found particles or a repetitive occurrence of the same kind of particles throughout the sample set.

Control steps accounting for contamination during the processing procedures were taken according to the same procedures as the sediment samples or sediment trap samples were processed. In parallel to the sediment samples ($n_{\text{Warnow}} = 14$; $n_{\text{Arkona+Gotland}} = 2$), a total of three controls, where two were covering the MPSS treatment and another one the exposure time during the visual identification process in the Bogorov chamber, were acquired. The degree of contamination during the sediment trap sample processing ($n_{\text{Arkona+Gotland}} = 2$ with 18 - 20 subsamples each) was evaluated by means of three controls in total. One separate collection bottle in the sediment trap set-up accounted for possible contamination during this part of the field sampling process. The bottle was filled with MilliQ water while sampling time and bottle lid opening and closing movements resembled the actual sampling. In this way, potential abrasion from the bottles entirely comprised of PE would be detected.

Text S3. Methodological remark on density separation threshold

The crux of MP field studies is the missing standardisation of MP isolation techniques. Density separation is most commonly used, however, setups greatly vary and the critical density is often below that of many HD polymers which prevents a detailed distribution analysis of the full spectrum of synthetic polymers⁷⁰. The authors consider a density separation threshold of 1.8 g cm^{-3} as scientifically reasonable, as it includes the full spectrum of commonly excepted plastic polymers. It also accounts for the majority of dried paint resins²⁹, which were calculated to possess an average specific gravity of approximately 1.6 g cm^{-3} . The chemical composition of paint resins: polymer base resin, pigments and additives, resembles that of commodity plastics with a larger proportion of heavy pigments. Due to the higher loads of heavy metals, the inclusion of paint resins into MP studies is highly relevant, particularly from an ecotoxicological perspective⁴⁴.



Station	Polymer type	Size [μm]	Colour	Abundance [kg^{-1} DW]	N_{spectra}	N_{total}	Fig.
S1	PS	500-1100	opaque, non-transparent	85	8	21	A
S2	SPSS, CPSS	500 - 900	transparent - orange – brown - black	24 ± 21	15	54	B
S5	SPSS, PS, PS-DVB	all above	all above	317	9	214	A, B

Fig. S1. Specifications on the identified group of PS beads, displayed via a selection of images (A-C) and details per station in the table beneath. A - opaque PS bead, B - ion exchanger beads based on sulfonated PS in different variations in size and colour, C - disintegration of ion exchanger bead into particles of $< 50 \mu\text{m}$ caused by the exertion of pressure of the ATR-FTIR crystal. This was likely fostered by physical degradation of ion exchangers for instance by oxidation⁴⁸. Scale bars equal $500 \mu\text{m}$.

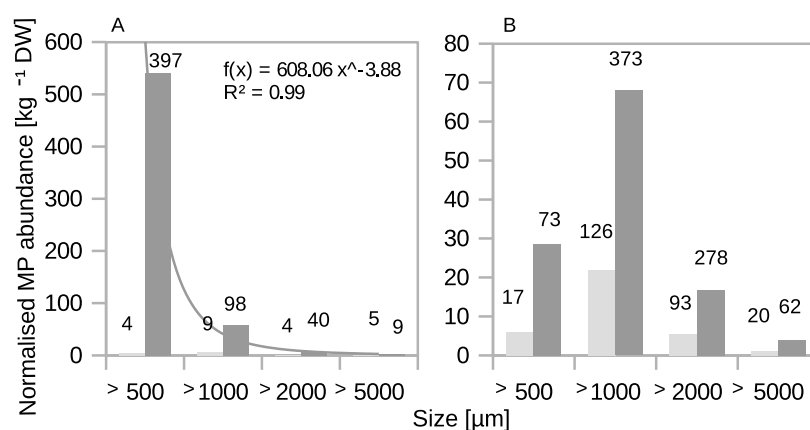
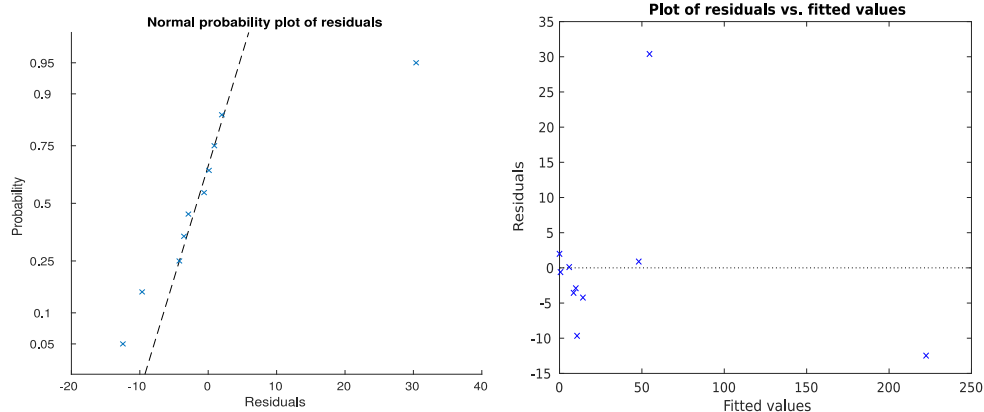
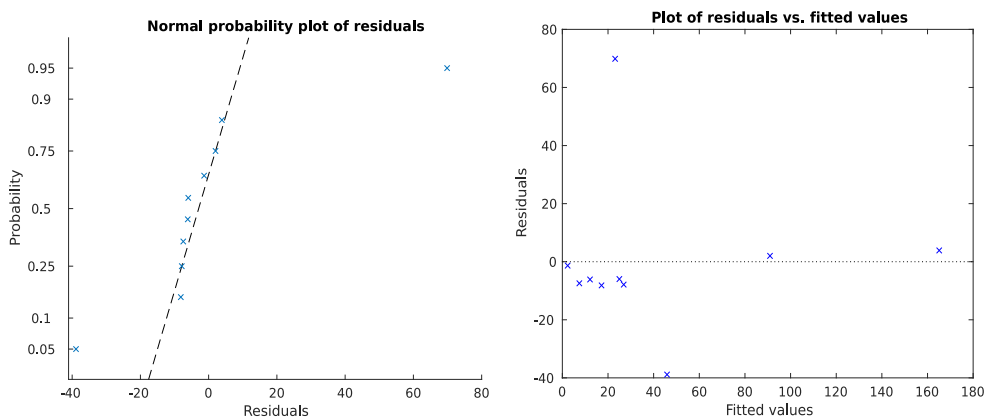


Fig. S2. Normalised size distribution of HD (dark grey) and LD polymers (light grey) in (A) the Warnow estuary and (B) the Alter Strom. Absolute number counts n of measured MP are shown above the bars.

A Paint resins



B Ordinary polymers



C TMP

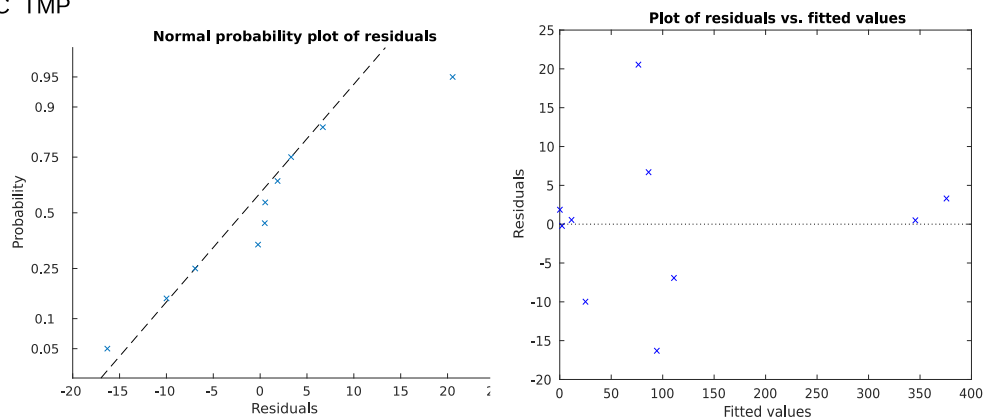


Fig. S3. Plots showing the equality of residual variances and normality of residuals of (A) paint resins, (B) ordinary polymers and (C) TMP. Residual analysis ensured that GLM assumptions of homoscedasticity and normality hold.

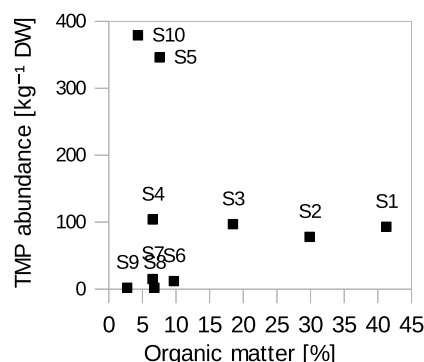


Fig. S4. Organic matter against TMP abundance.

Table 1. Comparison of systemic parameters of MP studies providing data on sediment grain size distribution. For "n.a." no or imprecise data was available. Significant correlations are marked with asterisks. No correlations are marked with minus with the suspected reasons in italic type. More studies provided data showing no or very weak correlations^{19–21}, however, study design and thus reasons for a low fit were comparable to the two listed. Note that correlation coefficients (*r*) were calculated based on log transformed MP data, as shown in Fig. 4E.

	Strand2013 ¹⁴	Vianello2013 ¹⁶	Ballent2016 ⁹	present	Alomar2016 ¹⁷	Renzi2018 ¹⁸
Min. Size [μ m]	38	32	63	500	63	400
Location	Baltic, North Sea, DK	Lagoon of Venice, IT	Lake Ontario, CA	Warnow estuary, DE	Mallorca, ES	Adriatic Sea, IT
Compartment	coastal, marine	coastal	limnic	coastal	coastal	coastal, marine
Polymer analysis	partly	yes	yes	yes	<i>no</i>	<i>no</i>
Max. density [g cm^{-3}]	1.2	1.2	1.5	1.8	n.a.	1.2
Number of samples	22	10	50	10	6	7
Sediment analysis technique	sieve&weigh	sieve&weigh	sieve&weigh	Laser-diffraction	sieve&weigh	sieve&weigh
Spatial connectivity	low	high	medium	high	medium	high
Temporal connectivity	n.a.	high	low	high	medium	high
Sediment variation	high	high	high	high	<i>low</i>	<i>low</i>
r	0.48*	0.86*	0.68*	0.86*	-	-
p-value	0.02	0.001	< 0.001	0.001	-	-

Table 2. Specification on sampling stations in the Baltic Sea, both sediment as well as sediment trap samples.

Sediment samples	Date of sampling	Latitude	Longitude	Depth [m]
Arkona basin	02/09/2015	54.914 N	13.838 E	45
Gotland basin	22/08/2015	57.307 N	20.077 E	248
Sediment trap samples				
Arkona basin	12/2012-01/2014	54.884 N	13.862 E	35
Gotland basin	02/2013-11/2013	57.305 N	20.077 E	196

Table 3. Predictor variables, potential MP source terms and environmental parameters, for GLM test including measurements, parameter definition, tools used and references of data acquirement per station (St.).

St.	dist_WWT	dist_recyc	dist_marina	pop_density	num_tourism	dist_rain	dist_mixed	num_metal	num_ind	OM [%]	TOC/N	CaCO ₃	grain size	depth	max_shear	SAL
[m]	[m]	[m]	[m]	_1000m [#]	[#]	water[m]	water[m]	_1000m[#]	_1000m[#]		[%]	[%]	<63µm[%]	[m]	stress[Nm ⁻²]	[PSU]
S1	5220	2240	1428	10961	75	223	2700	1	0	41.3	14.3	8.7	65.9	1.5	-	1
S2	1980	2440	85	17298	109	97	233	4	0	29.9	14.3	11.8	48.1	2.5	0.047	2
S3	230	2240	501	851	8	203	459	5	6	18.5	14.3	14.8	48.1	1.5	0.043	3
S4	1040	1480	43	478	9	395	1247	7	15	6.5	9.9	12.2	56.4	7.0	0.048	4
S5	2970	480	440	468	6	320	3169	6	3	7.6	9.5	38.0	57.4	1.6	0.094	4
S6	4530	2050	372	9700	33	683	4710	1	0	9.7	11.3	10.3	38.7	1.2	0.042	6
S7	6000	3560	610	1217	4	116	6192	0	3	6.1	10.1	15.3	48.3	6.5	0.036	10
S8	8770	8720	2373	0	0	2372	11500	0	0	6.2	9.0	9.3	29.8	3.5	0.111	12
S9	11180	7340	63	1826	11	301	9400	0	0	0.5	8.2	1.5	7.3	4.0	0.032	12
S10	11180	7000	1	5838	121	150	9400	1	0	10.8	8.8	12.2	95.8	3.5	0.02	11
definition	Distance to the nearest WWTP within the water layer	Distance to the nearest recycling station following water paths	Distance to the nearest point of the nearest marina within the water layer	Cumulative population density of the statistical blocks that are within the 1000m radius of the station	Cumulative number of typical touristic activity points defined by number of restaurants, bars, cafes, beer gardens, fast food restaurants hotels, parks, zoos, picnic sites, viewpoints, museums, tourist information points, guest houses, caravan sites, coffee shops, artworks.	Distance to nearest rain water drainage point, including second order streams	Distance to nearest rain water drainage point, including second order streams	Number of metal industry/companies within a 1000m radius	Number of industrial sectors within a 1000m radius	TOC=TC-TIC, organic matter (OM) = TOC * 2.22, averaged from two sample replicates	TOC divided by Total Nitrogen, averaged from two sample replicates	Calcium carbonate	Measured < 1mm, siliclastic sediments	Water depth	maximum shear stress over one year model run (2014)	min. salinity depth averaged, Dec 2005
tools	Measure line, QGIS	Measure line, QGIS	NNJoin plugin (Nearest Neighbor Analysis), Measure line, QGIS	Geoprocessing tool-buffer and Intersection, QGIS	Data management Tools-Merge vector layers, Geoprocessing tool-buffer and Intersection, QGIS	NNJoin plugin, QGIS	NNJoin plugin, Measure line, QGIS	google maps measuring tool, search for 'metal'	Geo processing tool-buffer and Intersection, QGIS	see Geological and chemical analysis				In-situ measured	modelled in matlab	estimate
original data reference	open street maps	Abfall-wirtschaft, Abfall-entsorgungsanlagen, Recyclinganlagen, www.umweltkarten.mv-regierung.de (2017)	www.opendata-hro.de/dataset/statistische bloecke (2017); Population densities from Kommunale Statistikstelle, Rostock	Data from 'Quick OSM' QGIS plugin ^{24,25} , Based on Top3 local tourist activities, Tourismuskonzeption 2022	Coordinates of inlets and max. discharge volume: Eu-ra-Wasser-Nord GmbH	Coordinates of inlets and max. discharge volume: Eu-ra-Wasser-Nord GmbH	google maps	Data from 'Quick OSM' QGIS plugin	see section Hydro-dynamic model	Das Ost-seemod-ell der BAW Technische Dokumentation, 2015						

Original Article

Extraction of microplastic from biota: recommended acidic digestion destroys common plastic polymers

Kristina Enders^{1,*}, Robin Lenz¹, Sabrina Beer² and Colin A. Stedmon¹

¹National Institute of Aquatic Resources, Technical University of Denmark, DTU, Kavalergården 6, Charlottenlund 2920, Denmark

²Copenhagen University, Nørregade 10, København 1165, Denmark

*Corresponding author: tel: +4591940467; e-mail: kren@aqu.dtu.dk

Enders, K., Lenz, R., Beer, S. and Stedmon, C. A. Extraction of microplastic from biota: recommended acidic digestion destroys common plastic polymers. – ICES Journal of Marine Science, 74: 326–331.

Received 1 April 2016; revised 6 September 2016; accepted 7 September 2016; advance access publication 26 October 2016.

The chemical digestion of tissue from marine biota for microplastic analysis is currently conducted following a variety of protocols published in scientific literature. Often there is a lack of information on whether and to which degree the applied chemicals are destructive to microplastic particles of various polymer types. In the present study we report that a digestion protocol recently recommended by ICES using nitric and perchloric acid has strong detrimental effects on several common plastic polymers, in particular polyamide and polyurethane and to a lesser degree acrylonitrile butadiene styrene, polymethyl methacrylate and polyvinylchloride. Raman spectroscopic measurements revealed changes in peak occurrence and intensity for several polymers that did not otherwise show visual macroscopic changes. We developed and tested an alkaline digestion protocol in order to preserve small microplastic particles while removing organic tissue material. We recommend this method for the development of guidelines for plastic microplastic monitoring in biota.

Keywords: digestion, method development, microplastic, stomach samples.

Introduction

Plastic is accumulating in the oceans (Eriksen *et al.*, 2014) where as a result of exposure to various environmental stressors (e.g. Ultra Violet light and abrasion), it breaks down to ever-smaller fragments resulting in microplastic. Plastic of all sizes is of potential harm to marine life overlapping with the feeding size spectrum of a wide range of organisms (Enders and Lenz, 2015). The quantification of microplastic in the stomachs of various biota is central to assessing the impact and extent of plastic pollution and to determining its pathways through food webs and sinks (Setälä *et al.*, 2014). The development of techniques to isolate and characterize microplastic is, however, still in progress and methodologies across different studies are barely standardized. The monitoring of plastics in fish has been integrated into the European Union Marine Strategy Framework Directive (Galgani *et al.*, 2013) and Oslo-Paris Commission (OSPAR) guidelines. OSPAR has requested a common monitoring protocol for plastic particles in fish stomachs, which was provided through a special advice report (ICES, 2015).

Before microplastic distribution and impacts can be systematically assessed standardized sampling and laboratory techniques are required. A major challenge is the removal of organic matter that is often associated with microplastic particles. This can be both detrital organic matter or in the form of tissue or secretion in the case of samples from living biota. Due to the hydrophobic nature of many plastics organic matter in environmental samples will aggregate on its surfaces to form biofilms. Before microplastic can be characterized, either visually or spectroscopically, the organic matrix must be removed. Various approaches have been developed including: enzymes (Cole *et al.*, 2014); bases such as sodium hydroxide (NaOH; Claessens *et al.*, 2013; Cole *et al.*, 2014) or potassium hydroxide (KOH; Foekema *et al.*, 2013); alkaline cleaning agents (Strand and Tairova, 2015); concentrated acids such as nitric acid or hydrochloric acid (HNO₃, HCl; Claessens *et al.*, 2013), or perchloric acid (HClO₄; Zoeter Vanpoucke, 2015); oxidants such as hydrogen peroxide (H₂O₂; Nuelle *et al.*, 2014); or other bleaching agents such as sodium hypochlorite (NaClO; Sørensen *et al.*, 2013).

Table 1. Description of the four digestions solutions tested.

Acid mix (ICES)	4:1 (v/v) HNO ₃ 69% (AnalR, VWR International S.A.S.) + HClO ₄ 70% (Rectapur, VWR International S.A.S.), procedure: Addition of 5 ml/g and digestion for 5 hours and subsequent heating in a laboratory oven for 10 min in 80 °C.
KOH	Solution of KOH pellets (Emsure, Merck) in microfiltrated H ₂ O 1120 g/L, procedure: refer to "Methods" section.
NaClO	NaClO solution, 14% active chlorine (VWR International S.A.S.), procedure: refer to "Methods" section.
Industrial CIP agent	VIP 1 (Novadan Aps, Kolding, Denmark), ready solution containing ~3% Potassium hydroxide, ~1% Potassium triphosphate, ~1% Potassium silicate, and ~7% Sodium hypochlorite, procedure: refer to "Methods" section.

A preliminary protocol for the digestion of organic matter in conjunction with microplastic isolation and sample preparation has been issued by ICES. The procedure recommends the usage of a mixture of HNO₃:HClO₄ (4:1) as digestive agents (ICES, 2015) and had the goal of contributing towards the standardization of current methods. During preparations for national monitoring activities for microplastics in fish stomachs (Lenz *et al.*, 2016) it was decided to follow the ICES recommendations as they aim to harmonize microplastic protocols. During the course of the sample preparations we found indications that the recommended acid combinations had severe effects on a range of common polymers. An assessment of the suitability of the different digestion chemicals used for microplastic isolation was therefore initiated. In this study, we report the results of tests run on a set of 21 common plastic polymers that underwent the tissue digestion treatment following the ICES protocol. For comparison parallel digestions with KOH, NaClO, and a commercially available alkaline cleaning agent were also carried out.

Methods

Plastic resistance to test chemicals

Polymer samples were chosen from a selection of consumer plastic items of which the material or recycling label was visible. Several pieces of roughly 0.5 × 1 cm in size but with varying thicknesses (~1 mm) were cut and transferred into a separate 8 ml laboratory glass vials with a black butyl/PTFE screw top lid. Further effort to standardize the plastic samples was hindered by the variable properties of the materials such as densities, pliability, and structure (e.g. compact, expanded, or fibrous). A 5-ml aliquot of digestion reagent was added to each vial and the vials were stored upright and unshaken during the testing period. Four different digestion solutions were compared: the recommended acid mix (ICES, 2015); a KOH solution; a NaClO solution; and a commercially available industrial cleaning-in-place (CIP) agent (Table 1). The effects of the different treatments were documented photographically before the addition of chemicals and after 30 min, 1 h, and 5 h. Following this treatment period at room temperature all samples were exposed to 80 °C for 20 min, while still submerged in the digesting agent, as recommended in the ICES advice guidelines (ICES, 2015) and observed changes were documented in the same manner. In the case of the ICES treatment an extra image series was recorded after 10 h to better screen for subtle changes. Observed effects were categorized by severity into four levels (Table 2).

Raman micro-spectrometry

In order to better evaluate weak chemical changes on the outer matrix of the polymer a selection of samples was measured with Raman micro-spectroscopy after the digestive treatments (5 h

Table 2. Definition of the four different impact levels that the outcome of the digestions was classified into.

Level of impact	Description
L1	Initial visually recognizable changes (colour, surface morphology)
L2	Morphological changes and early stages of dissolution
L3	Strong morphological disintegration and change of bulk structure
L4	Complete dissolution or disintegration

plus 20 min at 80 °C). The spectra were compared with a spectral library of the same polymers in original condition.

Testing tissue digestion effectiveness

A comparison study was conducted in order to test for digestion effectiveness of fish stomachs among the treatments with: (i) KOH, (ii) NaClO; (iii) KOH and NaClO in combination; and (iv) VIP1. VIP1 is a ready-made solution which contains both KOH (3%) and NaClO (7%) as the main ingredients. This is also the reason for selecting to test each individually for their digestive power first and then later in combination. The cod stomachs tested in this study were caught in the Baltic Sea (Lenz *et al.*, 2016) and weighed between 8 and 22 g. For each gram of tissue, 5 ml test solution (i–iv) was added to the sample respectively contained in a laboratory glass bottles. All treatments were first subjected to a 15 min ultrasonic bath followed by two hours of thorough shaking. The most effective digestion solution was then further diluted to find an optimum i.e. most economical concentration.

Results

ICES acid mix treatment

Examples of the observations from the ICES exposure are shown in Figures 1–4 and are summarized in Table 3. More comprehensive photographic documentation is presented in the [Supplementary Material S1](#). The strongest effects were observed for polyamide (PA), polyurethane (PU), and a black tire rubber elastomer, all of which were completely dissolved by the acidic treatment. In the case of PA6 the complete dissolution (L4) was observed within seconds to minutes after submersion in the acid mix. Other structurally affected polymers were acrylonitrile butadiene styrene (ABS), polymethyl methacrylate (PMMA), and polyvinyl chloride (PVC). The latter being affected in moderation, mainly colour leaching and softening (L2–L3). The structure of polymer samples of polycarbonate (PC), expanded and solid polystyrene (EPS, PS) and polyethylene terephthalate (PET) was only slightly affected resulting in staining or colour loss (L1). No effects were observed for polypropylene (PP), high- and low-density polyethylene (HDPE, LDPE), ethylene-vinyl acetate (EVA), and polytetrafluoroethylene

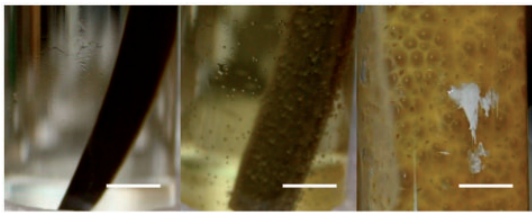


Figure 1. ABS bloating by acidic treatment after 5 h (left), 10 h (middle), and additional heating to 80 °C (right). Scale bar = 0.5 cm. Note: The white spot is a reflection on the glass vial. The entire picture series can be found under [Supplementary Material S1](#).

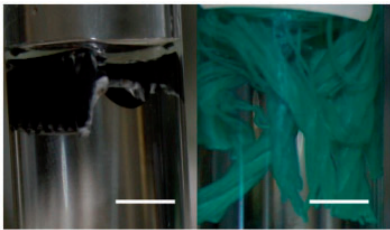


Figure 2. No observable changes after acidic treatment of polyolefins (PP left, HDPE right). Scale bar = 0.5 cm.

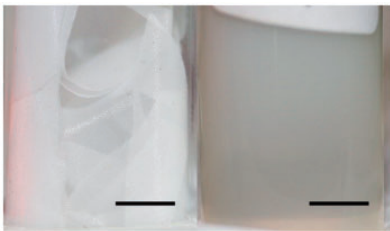


Figure 3. PA-6 before (left) and after first contact with acidic treatment. Scale bar = 0.5 cm.

(PTFE). Heating to 80 °C after the digestion period was found to have an exacerbating effect on the polymer destruction in all cases where an initial effect was observed. Raman micro-spectroscopy measurements were performed on all polymer samples, which did not show severe visible changes after the acid mixture treatment. The spectra revealed that apart from ABS ([Supplementary Material S2](#)) all remaining polymers had spectra similar to that of the original polymers although some showed signs of degradation or peak shifts ([Table 4](#)).

Alkaline treatments

All tested polymers were unaffected by the alkaline treatments according to the defined levels ([Table 2](#)) during both the individual and combined reagent treatments. The characteristics of acquired Raman spectra, however, differed between treatments ([Table 4](#)). Minimal changes were seen for the 30% dilution 1:1 combined KOH:NaClO solution which was the found optimized protocol.

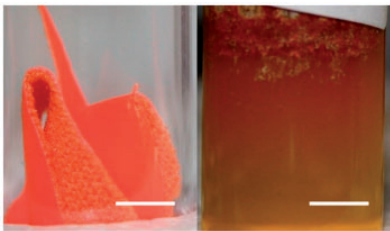


Figure 4. PU before (left) and after 5 h of acidic treatment. Scale bar = 0.5 cm.

Table 3. Tested polymer types in the acid test treatment with observed impact levels corresponding to the classification in [Table 2](#).

	0.5 h	1 h	5 h	10 h	80 °C	No change
PP						x
LDPE						x
HDPE						x
PS					L1	
EPS					L1	
ABS		L1	L2		L3	
PU	L2	L3	L4			
PA 1	L4					
PA 2	L2		L3			
EVA						x
PET			L1			
PC	L1					
Nitrile	L1		L3	L4		
PVC 1			L1		L2	
PVC 2			L1		L2	
PVC 3						x
PMMA		L2	L3			
PTFE (Teflon)						x
RE 1- Rubber elastomer	L3	L4				
RE 2- Rubber elastomer	L2	L3			L4	
RE 3- Rubber elastomer	L1	L2	L3		L4	

Results are shown for different digestion time incubations at room temperature and for an additional 20 minutes at 80 °C. The final column indicates polymers where no change was evident.

The polymer samples treated with pure and saturated KOH solutions exhibited larger spectral deviations and lower quality spectra ([Table 4](#), [Supplementary Material S2](#)). Despite these alterations to the Raman spectra as a result of the digestions all polymer types could still be recognized by comparison with the library of clean spectra from the untreated polymers.

Testing tissue digestion effectiveness

[Table 5](#) shows that among all chemicals tested KOH in combination with NaClO had the most satisfactory effect, dissolving sample tissue completely. Either KOH or NaClO alone were not as effective. The VIP1 treatment was nearly comparable although some mucoid sediment remained undissolved. The KOH:NaClO mixture was then tested in three different proportions (IIIa, IIIb, IIIc) of which IIIc (1:1) was found to be optimal. Higher

Table 4. Evaluation of Raman spectra changes after chemical treatments with the acid mix, saturated KOH and KOH:NaClO 30% solution
Colour legend:

	Recognizable, largely identical		
	Recognizable, with noted peak changes if applicable		
	Not recognizable		
	n/a: not measured		
	Acid mixture	KOH, saturated solution	30% KOH: NaClO
PP			
LDPE			
HDPE			
PS	slightly noisy, florescence		
EPS	n/a	n/a	
ABS	not recognizable, change in peak positions and fluorescence. 1605 cm ⁻¹ peak remains	higher noise level than in spectrum of untreated ABS	higher noise level than in spectrum of untreated ABS
PA	n/a	missing peak at 147 cm ⁻¹	peak at 147 cm ⁻¹ weakened
PET		peak at 3080 cm ⁻¹ and 861 cm ⁻¹ enhanced, new peaks at 1418 cm ⁻¹ and 1132 cm ⁻¹	
PC		new peak at 1065 cm ⁻¹	
PVC	fluorescence, weaker main peaks at 704 and 637 cm ⁻¹ indicating degradation processes	weaker main peaks at 704 and 637 cm ⁻¹ indicating degradation processes	
PMMA	new peak at 1054 and 1308 cm ⁻¹	new peak at 1070 cm ⁻¹	
PTFE	n/a	n/a	

The spectra measured are presented in the [Supplementary Materials](#). Grey shadings symbolize the degree of spectral matching compared to spectra of the untreated clean polymer.

Table 5. Descriptive test results for digestion effectiveness of KOH (I), NaClO (II), KOH: NaClO (III), and VIP1 (IV).

	Treatment	Post treatment
I	100% KOH	Layer of black/brown slime afloat, no big pieces remain.
IIa	30% NaClO	Milky solution, fish stomach still floating as one piece.
IIb	100% NaClO	Only half of mixture added because of very strong foam formation, risk of spillage
III	1:1 (KOH:NaClO)	Sample tissue completely dissolved
IVa	30% VIP1	Sample mostly dissolved, slimy sediment remaining.
IVb	100% VIP1	Sample dissolved better, less slimy sediment remaining.

a and b indicate when different concentrations were applied. The most effective treatment is highlighted in bold.

Table 6. Results of testing different proportions of KOH:NaClO as a digestion reagent.

	Treatment	Post treatment
IIIa	2:1 (KOH:NaClO)	Numerous small items afloat: undigested stomach content, many of visible biological origin (food items).
IIIb	1:2 (KOH:NaClO)	Foam formation (minimized by cooling glass bottle in cold water), few small pieces (food remaining)
IIIc	1:1 (KOH:NaClO)	Foam formation (slightly less than above). Sample tissue completely dissolved

The most effective one is marked in bold.

proportions of NaClO caused foam formation, while lower NaClO concentrations reduced the digestion effectiveness (Table 6). Finally a diluted version (30%) of the 1:1 KOH:NaClO mixture was tested and found to still be capable of full digestion and offer a more economical working reagent.

Discussion and recommendations

The tests performed here were carried out on macroscopic plastic fragments and one can assume that the detrimental effects documented for the ICES treatment are likely more severe for

microplastics due to the comparatively larger surface area and more fragile nature. This is particular relevant for studies investigating microplastic below 300 µm in size. Raman spectroscopic results revealed that several of the treatments had negative effects on the quality of the spectra obtained and therefore could potentially influence the spectral matching of environmental samples to pure polymer spectra. In particular, the spectra of ABS were greatly influenced.

Several of the other tested polymers lost dyes when exposed to the acid mix treatment. Although this was classified only as low

impact level L1, this increases the likelihood that discoloured microplastics of the concerned polymers are overlooked during visual analyses. The fact that marine microplastics are usually exposed to environmental weathering for extended periods before eventual sampling and isolation (in contrast to the new polymers used in this study) may result in the digestion having more adverse effects than documented here. Environmental weathering from UV degradation is already known to impair microplastic identification (Lenz *et al.*, 2015).

Various studies have already applied the recommended acid mixture (De Witte *et al.*, 2014; Vandermeersch *et al.*, 2015; Zoeter Vanpoucke, 2015) or nitric acid alone (Van Cauwenberghe and Janssen 2014) and are therefore likely to systematically underestimate microplastic abundance and documented polymer diversity. Therefore abundances based on the use of the ICES protocol (ICES, 2015) should be interpreted as a conservative estimate with some bias with respect to polymer detection. The results of this study show the importance of conducting chemical resistance tests prior to a wide application of any microplastic sample digestion protocols and further study on other spectroscopic techniques is warranted.

Another study (Strand and Tairova, 2015) successfully used VIP1 for sediment and tissue digestion purposes. The main digestive ingredients in VIP1 are the same as in the KOH-NaClO-mixture and in order to test the VIP1 solution a small quantity of the same batch that the authors originally work with was obtained (J. Strand and Z. Tairova, pers. comm.). Hence, VIP1 used in the present study was already several months old and has been opened before which makes it likely that active chlorine has deteriorated to some extent. This would mean that the effectiveness was limited and perhaps better results can be obtained when using a fresh VIP1 solution. However, its widespread availability to the scientific community is limited and its actual composition is unknown and this makes it an inappropriate choice for a community-standardized method. The results presented here suggest that due to the widespread availability and effective digestion ability the usage of a 30% KOH:NaClO mixture is the most appropriate and we recommend it therefore as a fast, inexpensive and effective digestion method. For 1 L of reagent 150 ml of saturated KOH solution (1120 g/L) and 150 ml NaClO solution (14% active chlorine) is mixed into 700 ml micro-filtrated water. Although not tested in this study it is likely that this solution is similarly appropriate to remove biofilms, algae, flocculated organic particles and other protein and lipid rich materials of biological origin. The success of the reagent combination also aligns with findings by Strand and Tairova (2015) and Cole *et al.* (2014) which suggest that the KOH and NaClO are useful as active compounds in digestion protocols for sediment and tissue microplastic samples, as well as biota-rich sea water samples.

The alkaline treatments, both KOH and the optimized 30% KOH:NaClO solution did not impair the identification of the tested polymers by Raman micro-spectrometry. Occurring chemical alterations produced minor peak changes in spectra or elevated background noise levels which however did not mask the original polymer signal. We therefore argue that the presented solution can also be applied for the analysis of small microplastic particles (<300 µm). We recommend it being further compared with enzymatic digestion protocols under aspects of economy, digestion effectiveness and plastic resistance. Having evidenced the complete dissolution of sample tissue in reasonable work time while not impairing the integrity of the most common plastic

polymer groups, we argue for the described method being considered in international guidelines targeting the standardization of protocols.

Supplementary data

Supplementary material is available at the ICESJMS online version of the article.

Acknowledgements

We thank Jakob Strand for valuable input on digestive solutions.

Funding

This study received funding from the Danish Nature Agency (Naturstyrelsen).

References

- Claessens, M., Van Cauwenberghe, L., Vandegehuchte, M. B., Janssen, C. R. 2013. New techniques for the detection of microplastics in sediments and field collected organisms. *Marine Pollution Bulletin*, 70: 227–233. <http://www.ncbi.nlm.nih.gov/pubmed/23601693> (last accessed 20 January 2014).
- Cole, M., Webb, H., Lindeque, P. K., Fileman, E.S., Halsband, C., and Galloway, T. S. 2014. Isolation of microplastics in biota-rich seawater samples and marine organisms. *Scientific Reports*, 4: 4528. <http://www.ncbi.nlm.nih.gov/pubmed/24681661> (last accessed 1 April 2014).
- De Witte, B., Devriese, L., BeKaert, K., Hoffman, S., Vandermeersch, G., Cooreman, K., and Robbens, J. 2014. Quality assessment of the blue mussel (*Mytilus edulis*): comparison between commercial and wild types. *Marine Pollution Bulletin* 85: p146–155. <http://linkinghub.elsevier.com/retrieve/pii/S0025326X14003671>.
- Enders, K., and Lenz, R. 2015. How to find the small plastic in the big sea - the identification and characterisation of microplastic ≥10 µm from the Atlantic Ocean (Master Thesis). DTU Aqua. <http://findit.dtu.dk/en/catalog/2292736934>.
- Eriksen, M., Lebreton, L. C., Carson, H. S., Thiel, M., Moore, C. J., Borerro, J. C., Galgani, F., *et al.* 2014. Plastic Pollution in the World's Oceans: More than 5 Trillion Plastic Pieces Weighing over 250,000 Tons Afloat at Sea H. G. Dam, ed. *PLoS One*, 9: e111913. <http://dx.plos.org/10.1371/journal.pone.0111913> (last accessed 10 December 2014).
- Foekema, E. M., De Gruijter, C., Mergia, M. T., van Franeker, J. A., Murk, A. J., and Koelmans, A. A. 2013. Plastic in north sea fish. *Environmental Science and Technology*, 47: 8818–8824. <http://www.ncbi.nlm.nih.gov/pubmed/23777286>.
- Galgani, F., Hanke, G., Werner, S., Oosterbaan, L., Nilsson, P., Fleet, D., Kinsey, S., *et al.*, 2013. Guidance on Monitoring of Marine Litter in European Seas Contact information.
- ICES. 2015. ICES Special Request Advice Northeast Atlantic and Arctic Ocean. OSPAR request on development of a common monitoring protocol for plastic particles in fish stomachs and selected shellfish on the basis of existing fish disease surveys. IICES Advice 2015, Book 1 (June), 1–6.
- Lenz, R., Enders, K., Stedmon, C. A., Mackenzie, D. M., Nielsen, T. G. 2015. A critical assessment of visual identification of marine microplastic using Raman spectroscopy for analysis improvement. *Marine Pollution Bulletin*, 100: 82–91. <http://dx.doi.org/10.1016/j.marpolbul.2015.09.026>.
- Lenz, R., Enders, K., Beer, S., Sørensen, T. K., Stedmon, C. 2016. Analysis of microplastic in the stomachs of herring and cod from the North Sea and Baltic Sea. *Naturstyrelsen*. <http://naturstyrelsen.dk/publikationer/2016/apr/analyse-af-mikroplast-i-torske-og-sildemaver>.
- Nuelle, M. T., Dekiff, J. H., Remy, D., and Fries, E. 2014. A new analytical approach for monitoring microplastics in marine sediments. *Environmental Pollution (Barking, Essex: 1987)*, 184: 161–169. <http://www.ncbi.nlm.nih.gov/pubmed/24051349> (last accessed 21 January 2014).

- Setälä, O., Fleming-Lehtinen, V., and Lehtiniemi, M. 2014. Ingestion and transfer of microplastics in the planktonic food web. *Environmental Pollution* (Barking, Essex: 1987), 185: 77–83. <http://www.ncbi.nlm.nih.gov/pubmed/24220023> (last accessed 21 January 2014).
- Sørensen, T. K., Stedmon, C. A., Enders, K., Henriksen, O. 2013. Analyse af marint affald i sild og hvilling fra det nordlige Storebælt.
- Strand, J., and Tairova, Z. 2015. Microplastic particles in North Sea sediments. <http://dce2.au.dk/pub/SR178.pdf>.
- Van Cauwenberghe, L., and Janssen, C. R. 2014. Microplastics in bivalves cultured for human consumption. *Environmental Pollution* (Barking, Essex: 1987), 193: 65–70. Available at: <http://www.sciencedirect.com/science/article/pii/S0269749114002425>.
- Vandermeersch, G., Van Cauwenberghe, L., Janssen, C. R., Marques, A., Granby, K., Fait, G., Kotterman, M. J. *et al.* 2015. A critical view on microplastic quantification in aquatic organisms *Environment Research*, 143: 46–55.
- Zoeter Vanpoucke, M. 2015. Impact of microplastic uptake: contamination in sprat and microplastic-mediated uptake of PAHs by European shore crab. Master thesis. Institute for Agricultural and Fisheries Research (ILVO), Ghent.

Handling editor: Howard Browman

Supporting online material to:

Extraction of Microplastic from Biota: recommended acidic digestion destroys common plastic polymers

Kristina Enders^a, Robin Lenz^a, Sabrina Beer^b, Colin Stedmon^a

Authors' affiliation:

^a National Institute of Aquatic Resources, Technical University of Denmark, DTU, Kavalergården 6, 2920 Charlottenlund, Denmark

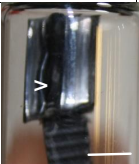




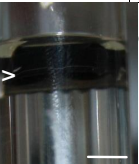

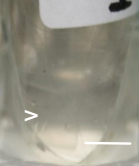
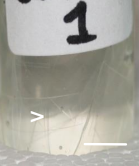
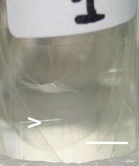
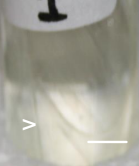
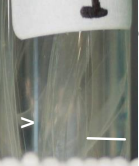
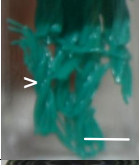




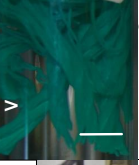

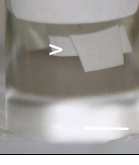
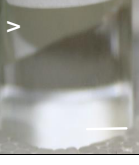

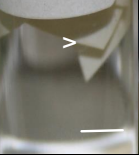
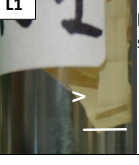
^b Copenhagen University, Nørregade 10, 1165 København, Denmark


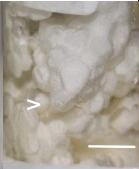
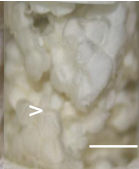
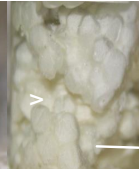
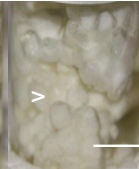
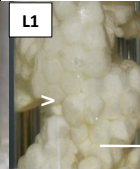
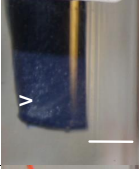
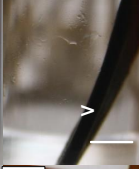
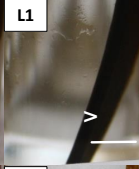
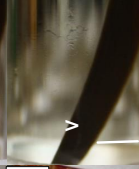
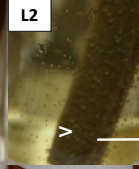
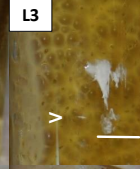
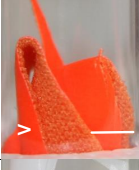

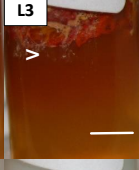
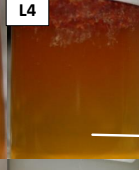
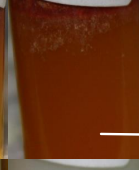


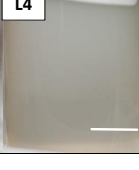

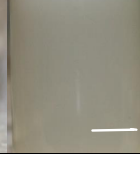
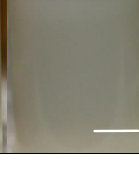
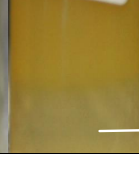
Contents


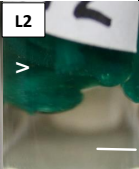

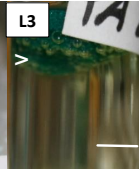
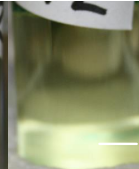
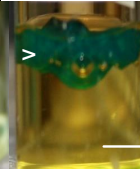
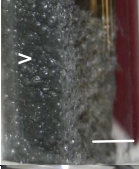
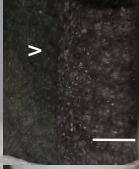
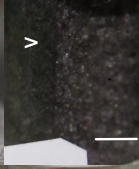


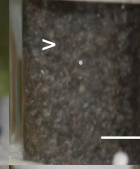
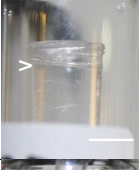
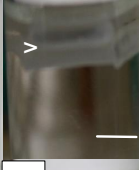
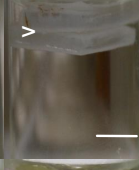
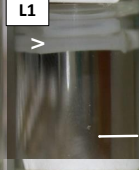


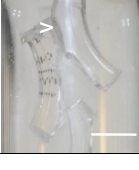
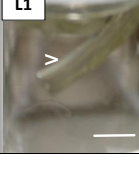
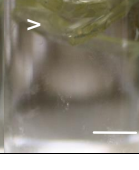
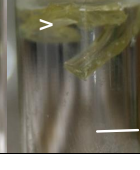

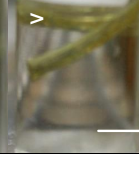
Supplement 1: Time series images of the digestion processes. Image series showing the gradual effects of $\text{HNO}_3\text{:HClO}_4$ to the respective plastic representative. White arrows point at the plastic item. Scale bars equal 0.5 cm. The images in one row always show the same item, sometimes with a slightly changed view angle.

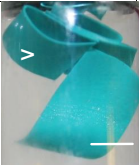


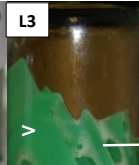
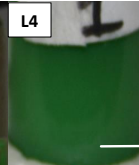

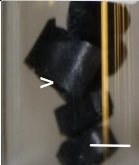
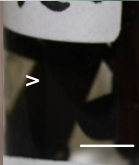
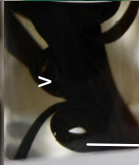

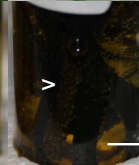
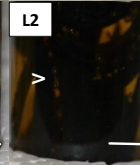
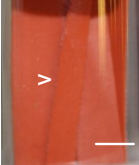

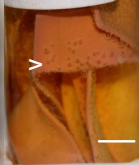
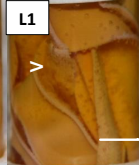
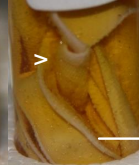




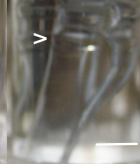

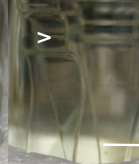
Supplement 2: Exemplary Raman spectra showing impacts of digestion chemicals. Spectra of each polymer are given in the order (from top to bottom): reference, after acidic treatment, after KOH treatment, after treatment with 30% dilution of KOH : NaClO 1:1 mixture. Missing spectra could not be measured due to severe degradation during digestions (i.e. complete dissolution).



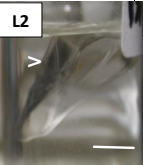
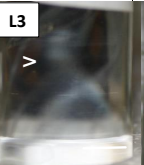
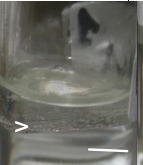








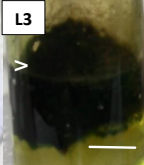
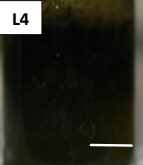



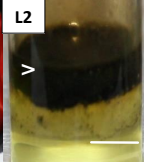
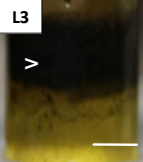


Supplement 1: Macroscopic impact of the the acid mix treatment $\text{HNO}_3\text{:HClO}_4$ (4:1)


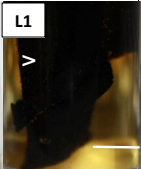
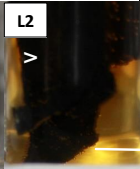
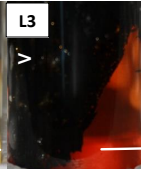
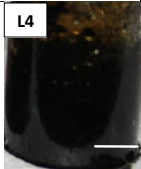
Type of plastic	Before trial	30 min	1 hour	5 hours	10 hours	20 min a 80°C	Comments
PP							No effect observed
LD PE							No effect observed
HD PE							No effect observed
PS							Yellowing after heat, solute stays clear

Type of plastic	Before trial	30 min	1 hour	5 hours	10 hours	20 min a 80°C	Comments
EPS							Slight yellowing after heat, solute stays clear
ABS							Darkening of original blue colour, later bleaching (greyish) and sponge-like bloating
PU							
PA							Complete dissolution within seconds to minutes

Type of plastic	Before trial	30 min	1 hour	5 hours	10 hours	20 min a 80°C	Comments
PA							Melting-like behaviour
EVA							No effect observed
PET							Transparency blurred
PC							Slight yellowing

Type of plastic	Before trial	30 min	1 hour	5 hours	10 hours	20 min a 80°C	Comments
Nitrite							
PVC 1							Leaching of dark colourant into solute, after 10 hours more softened appearance
PVC 2							
PVC 3							Slightly softened appearance after 10 h and 80°C

Type of plastic	Before trial	30 min	1 hour	5 hours	10 hours	20 min a 80°C	Comments
PMMA							Beginning dissolution creates mucous layer particle
PTFE							No effect observed
RE 1					n/a		
RE 2					n/a		

Type of plastic	Before trial	30 min	1 hour	5 hours	10 hours	20 min a 80°C	Comments
RE 3					n/a		

Supplement 2

Raman spectra of untreated plastics and after exposure to digestion treatments.

List of spectra:

Figure S1: Polypropylene (PP)

Figure S2: Polyethylene (PE)

Figure S3: Polystyrene (PS)

Figure S4: Acrylonitrile butadiene styrene (ABS)

Figure S5: Polyamide (PA)

Figure S6: Polyethylene terephthalate (PET)

Figure S7: Polycarbonate (PC)

Figure S8: Polyvinylchloride (PVC)

Figure S9: Polymethyl methacrylate (PMMA)

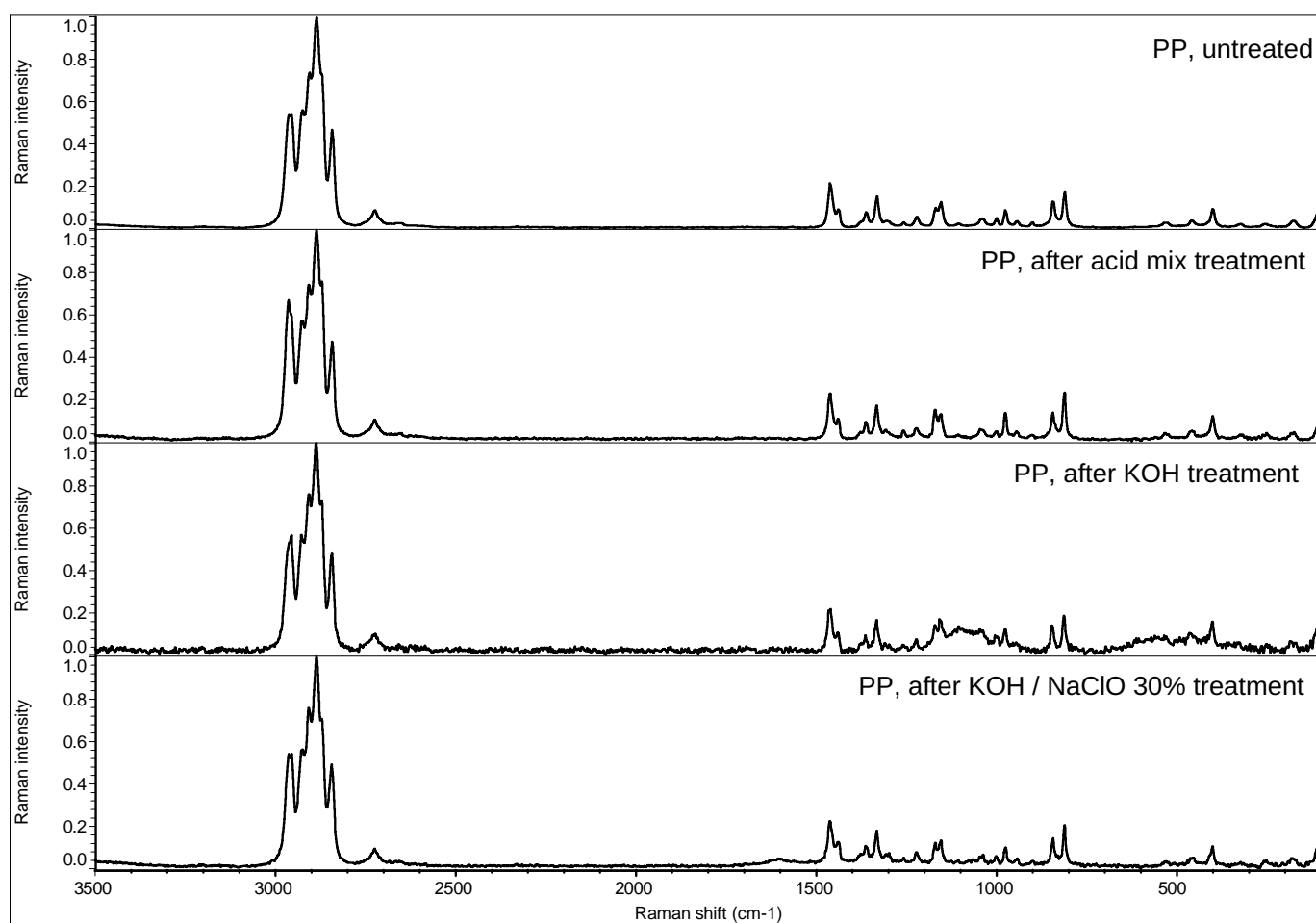


Figure S1: Spectra of polypropylene

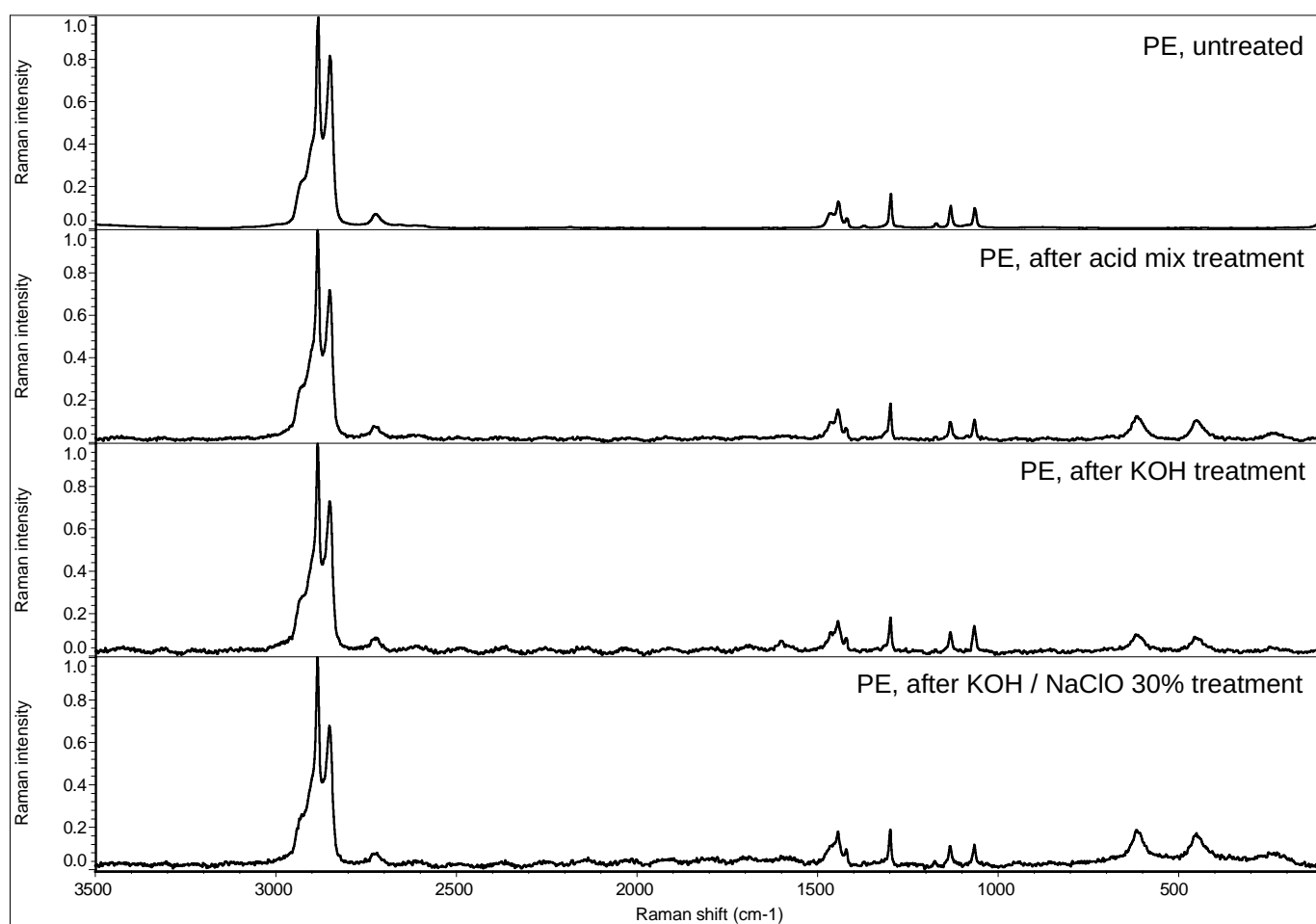


Figure S2: Spectra of polyethylene

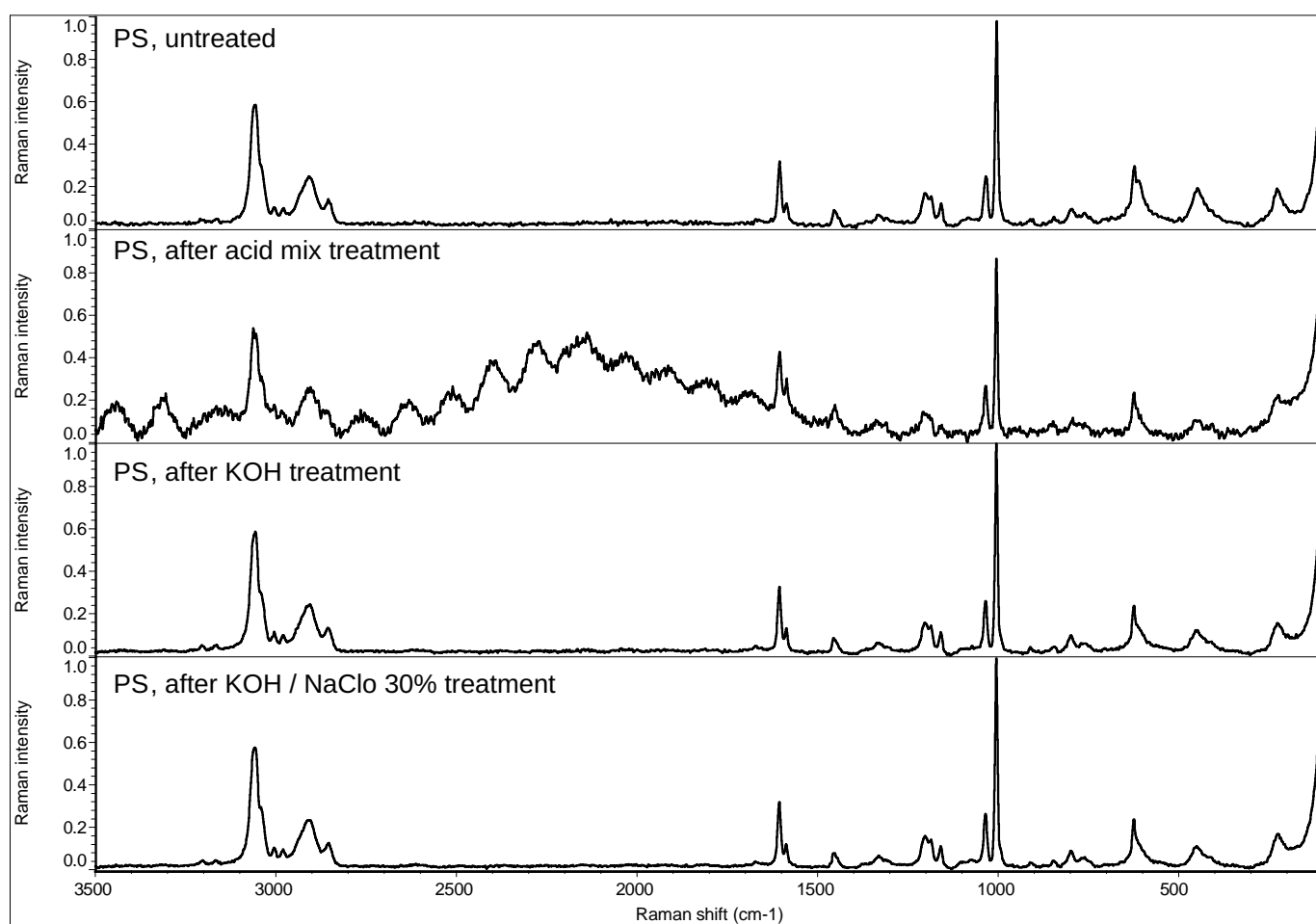


Figure S3: Spectra of polystyrene

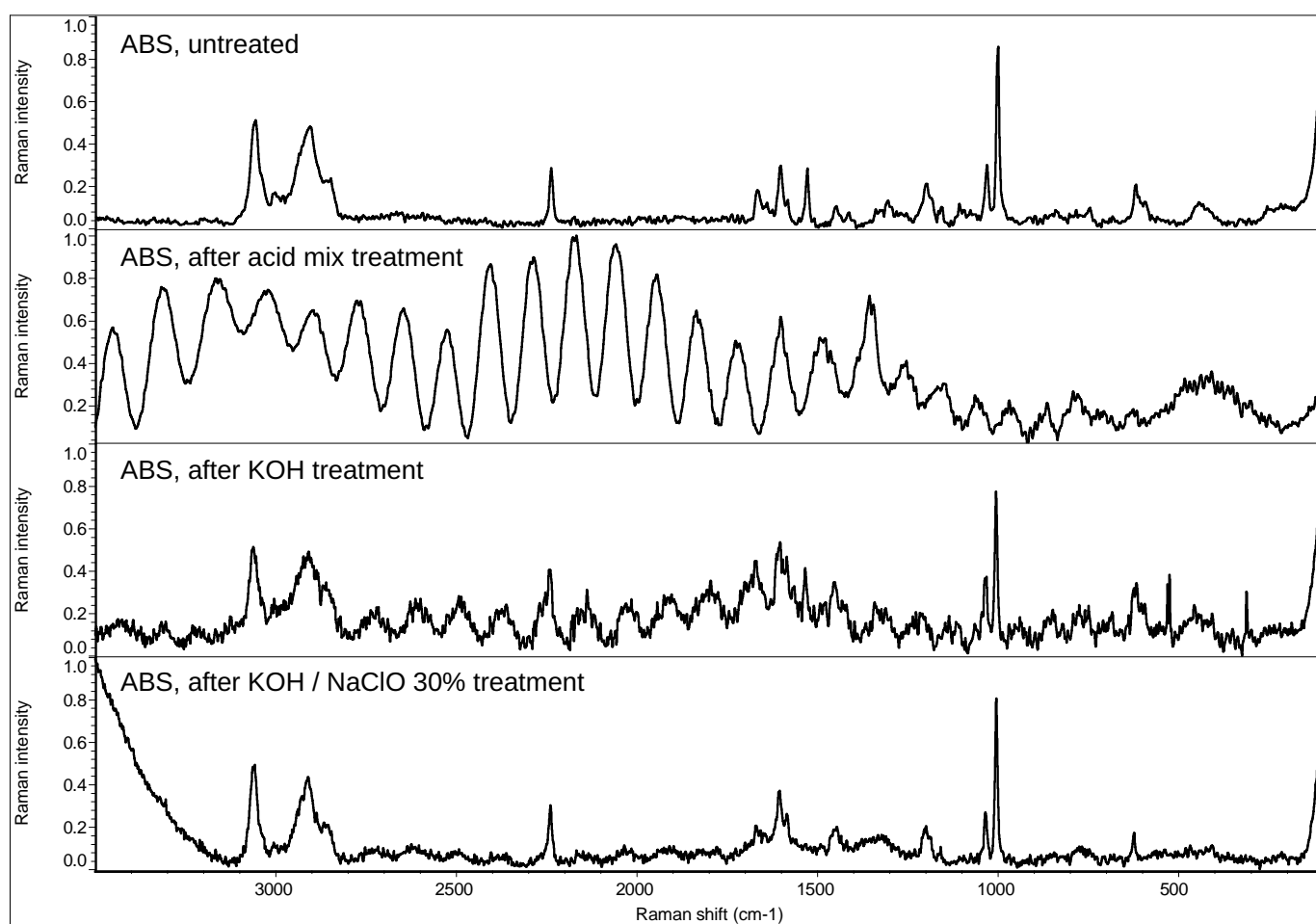


Figure S4: Spectra of acrylonitrile butadiene styrene

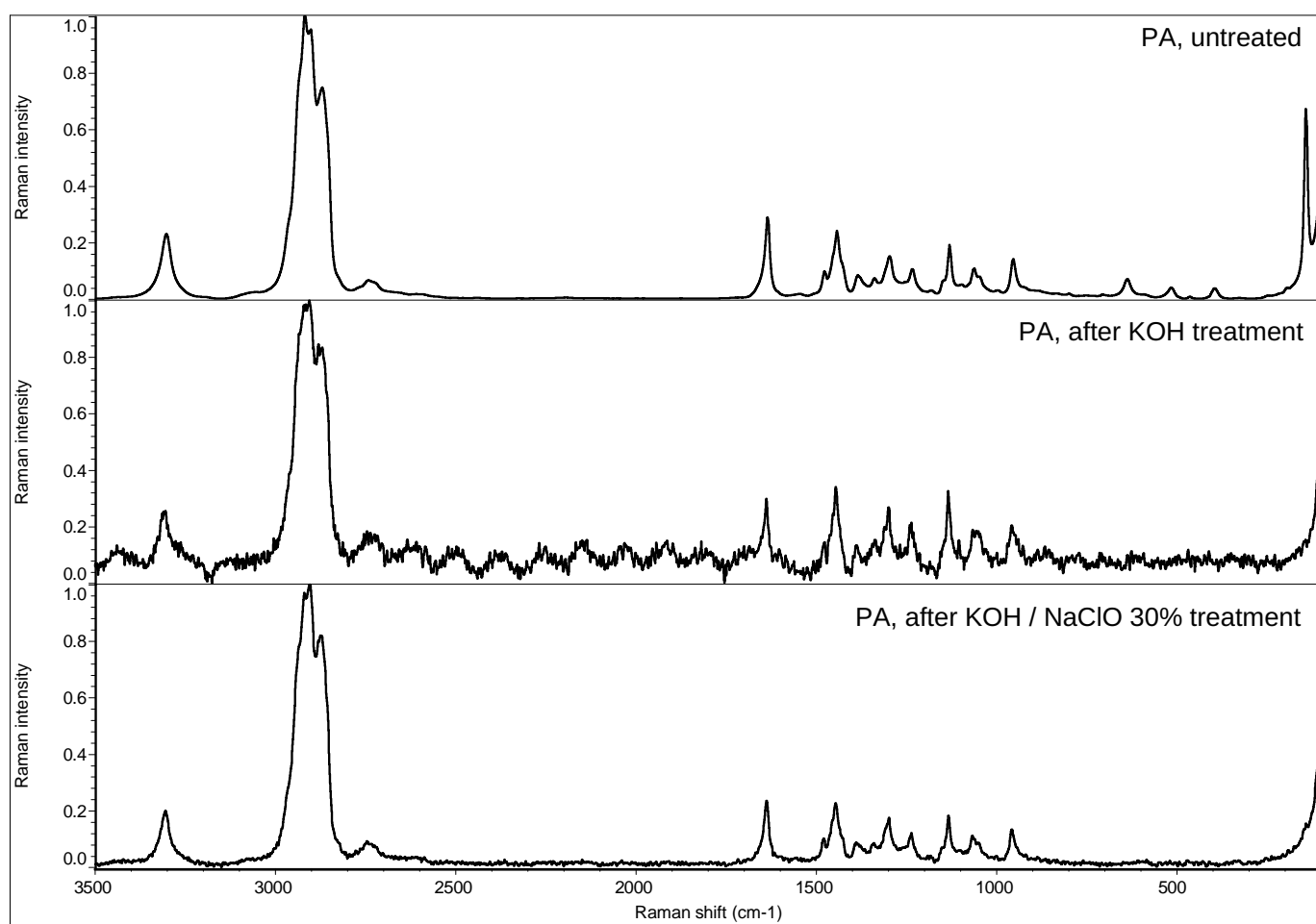


Figure S5: Spectra of polyamide

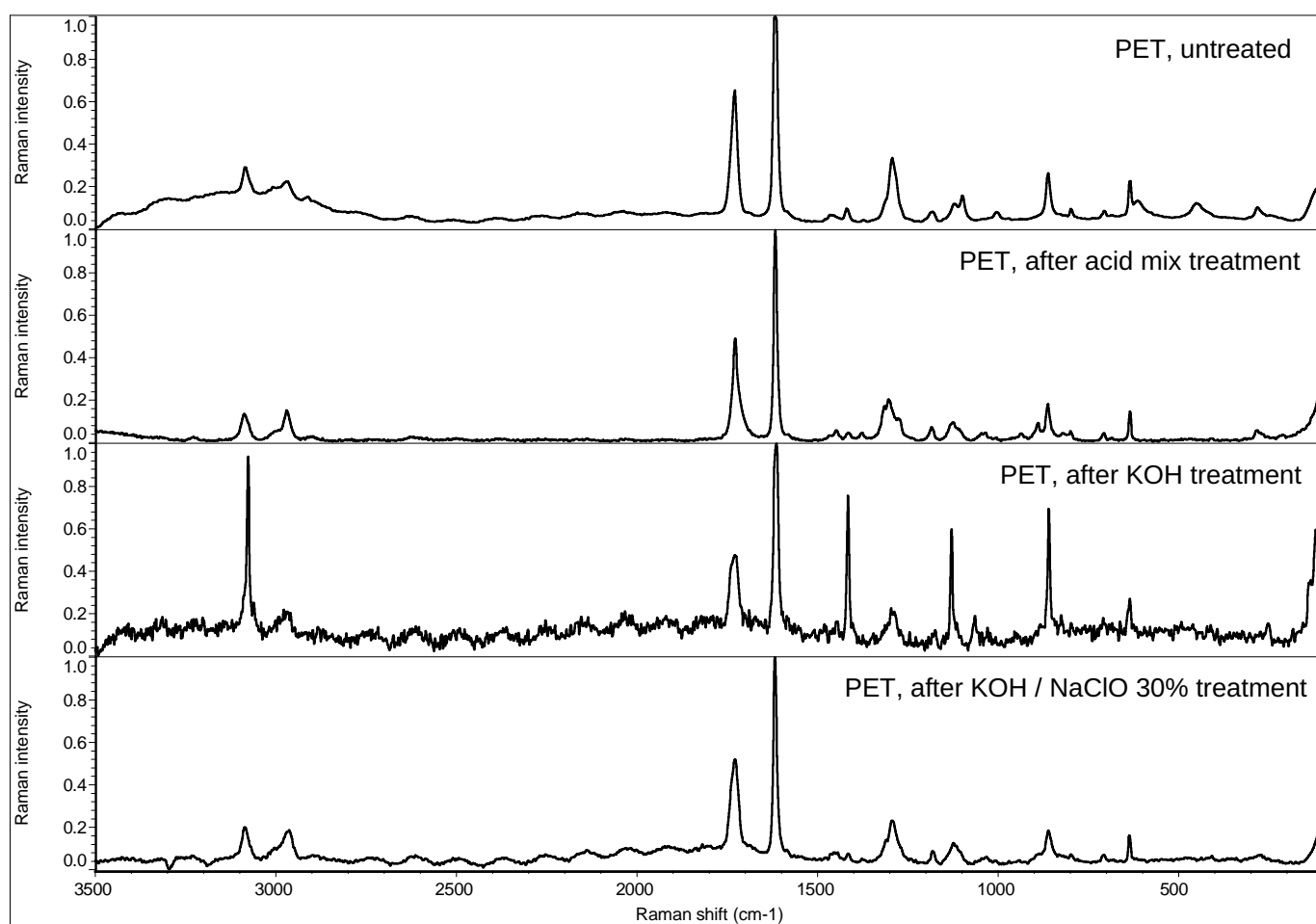


Figure S6: Spectra of polyethylene terephthalate

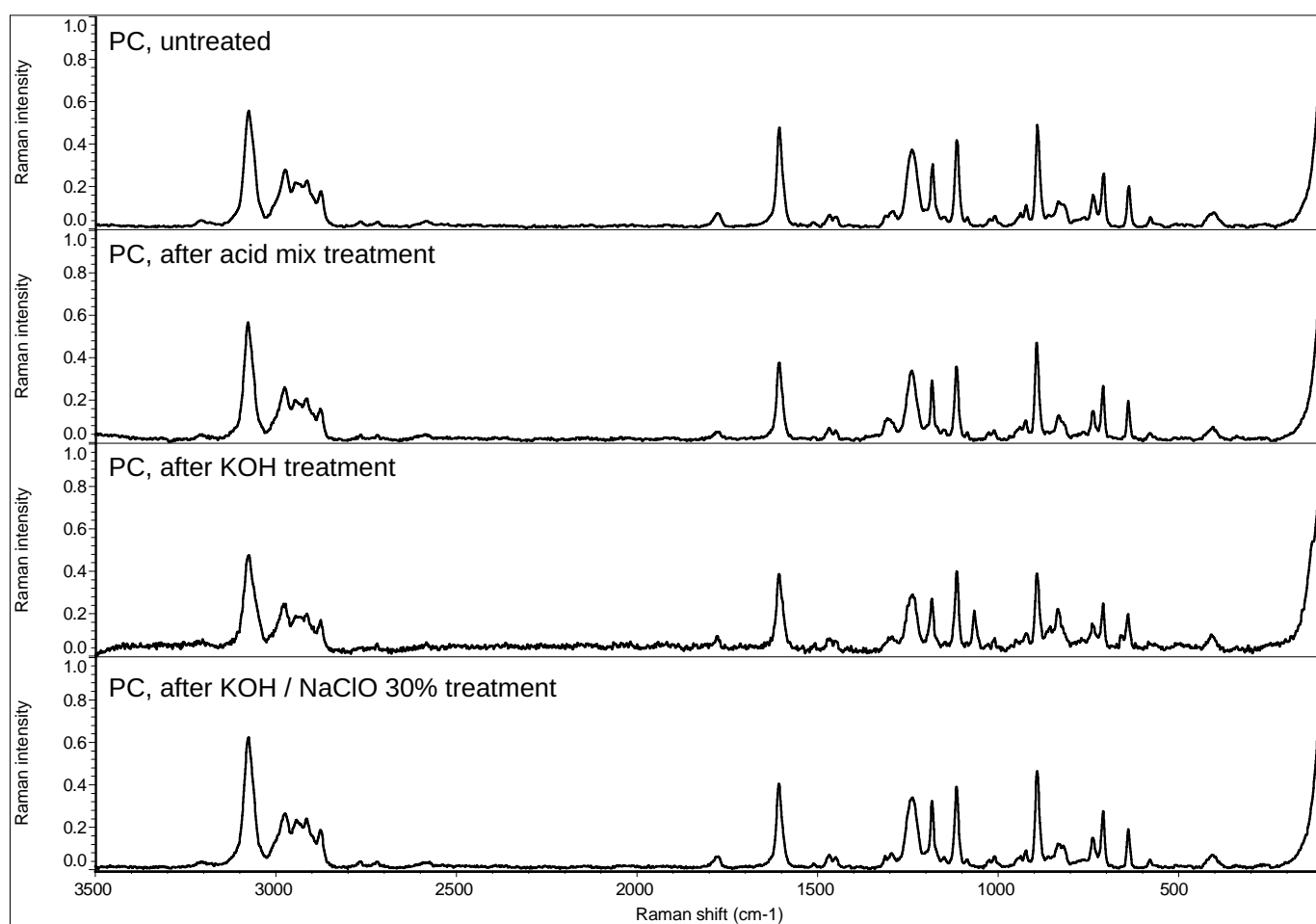


Figure S7: Spectra of polycarbonate

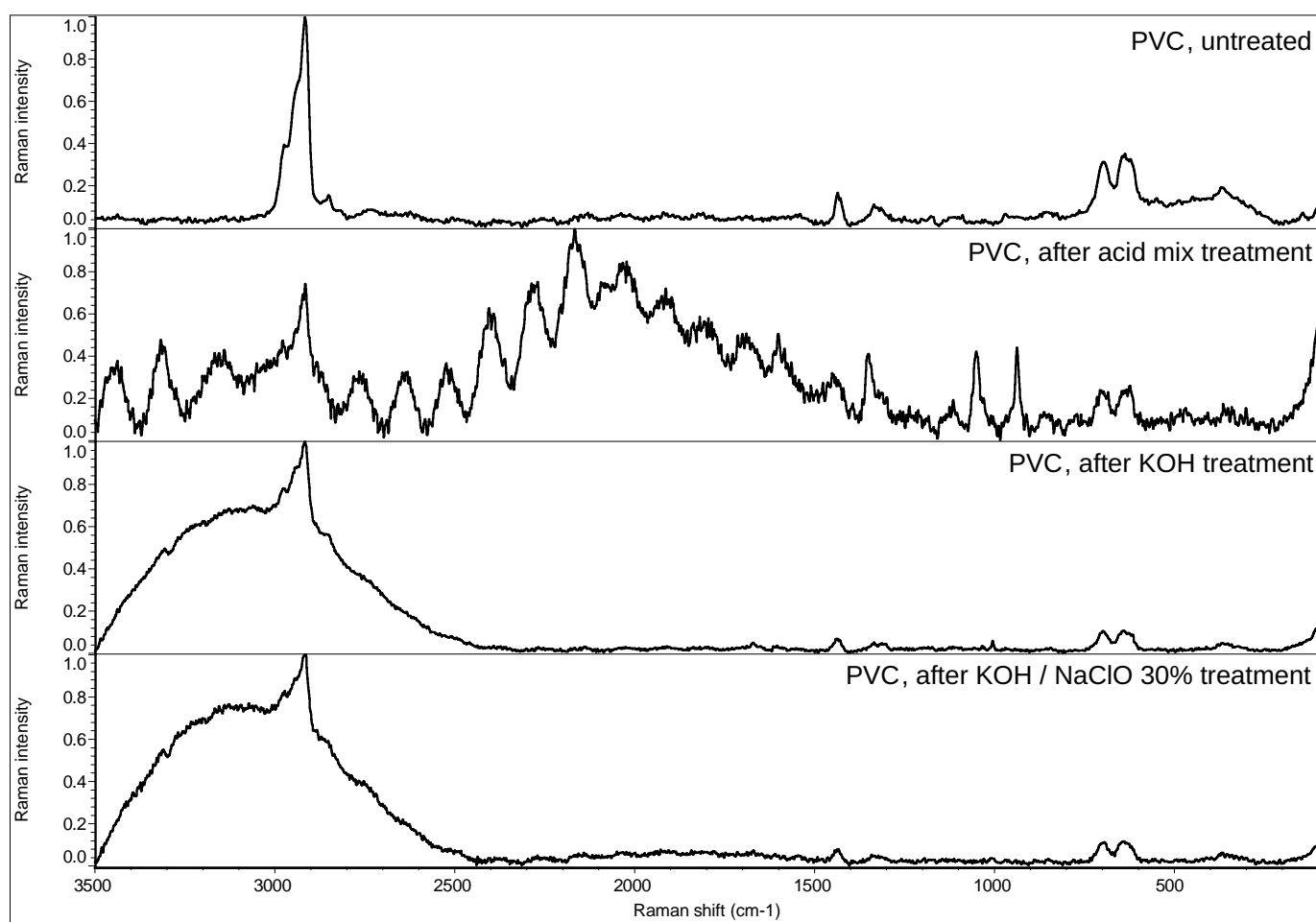


Figure S8: Spectra of polyvinylchloride

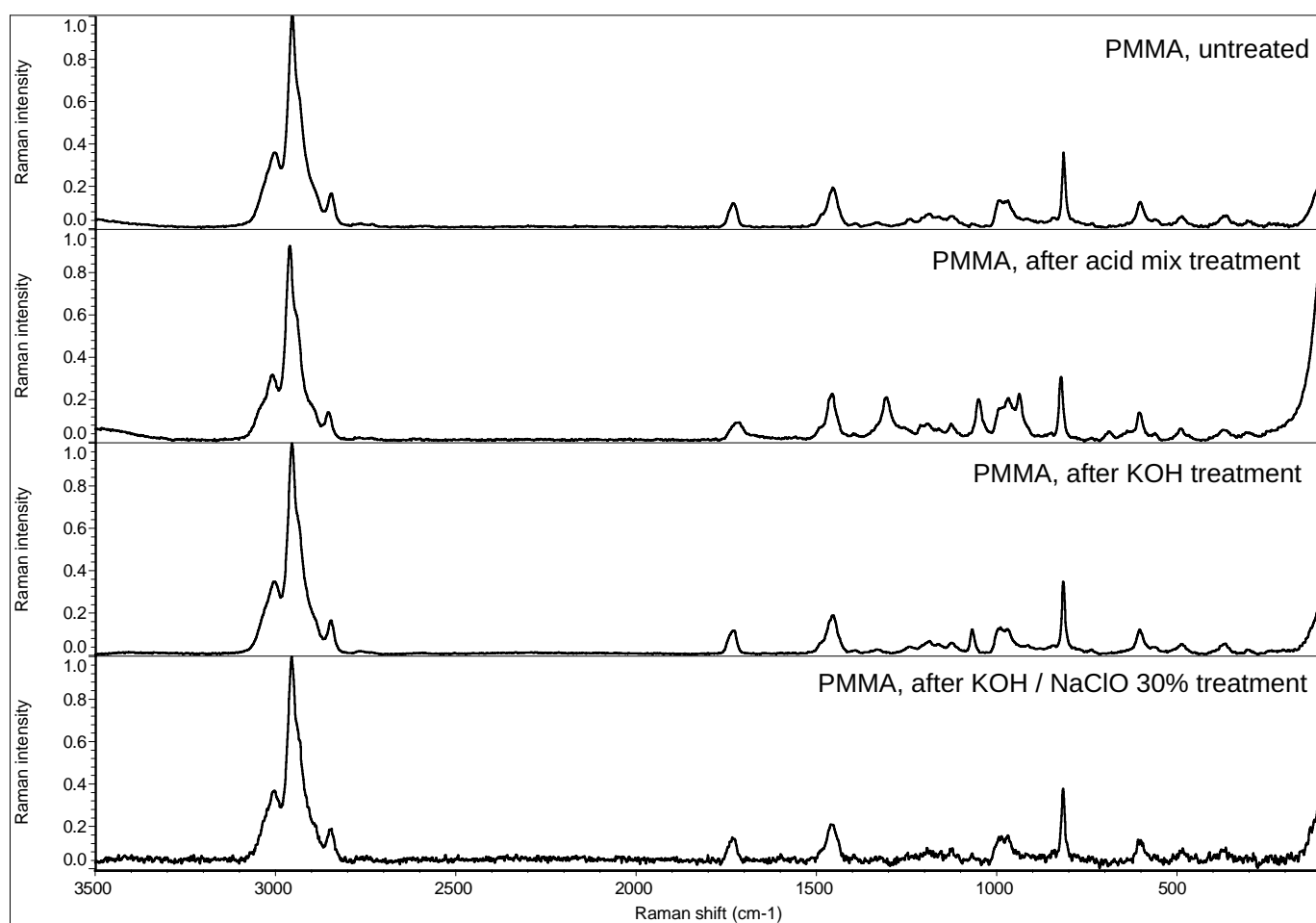


Figure S9: Spectra of polymethyl methacrylate

Microplastic exposure studies should be environmentally realistic

Robin Lenz^{a,1}, Kristina Enders^a, and Torkel Gissel Nielsen^a

To understand the impact of microplastic (MP) pollution to aquatic ecosystems, it is important to identify the mechanisms of interaction with organisms. Exposure experiments, like the study of Sussarellu et al. (1) recently published in PNAS, may provide such insights. However, the results of dose–response experiments must always be interpreted in light of environmental concentrations, and the experimental concentrations examined by Sussarellu et al. (1) and several others (2–8) are orders-of-magnitude higher than those reported from field studies (Fig. 1).

Experimental studies on effects of MP on mussels (2, 3), lugworms (4), copepods (5–7), and oysters (1) have documented reduced feeding, survival, and fecundity, as well as promoted polychlorinated biphenyl bioaccumulation linked to MP uptake. In addition, nano-sized plastic particles may reduce body size and lead to reproductive malfunctioning in *Daphnia* (8), and to reduced CO₂ uptake and enhanced production of reactive oxygen species in algae (9).

All of these experimental studies use MP concentrations far above the levels documented in the marine environment (Fig. 1). Many of those studies used MP beads smaller than those reported from the field, but even if one extrapolates field-measured concentrations of MP particles to the size range used in experiments, experimental and expected field concentrations are very far apart. Studies that determined concentrations for micro-bead exposures from field measurements of larger-sized MP assumed a mass-conserving fragmentation (Fig. 1), which compares to a theoretical 3D fragmen-

tation process, where numbers of particles will scale inversely with the particle radius to the power of 3. In contrast, the environmental concentrations documented in studies appear to follow a slightly lower exponent (2.67) (Fig. 1), possibly caused by size-dependent removal processes, lower dimensional breakdown (i.e., of flakes, sheets, and fibers), or considerable influence of new MP input of larger sizes. Additionally, decreased detection accuracy of applied sampling methods in their respective lower size ranges might play a role.

Experimental exposure concentrations tend to be between two to seven orders-of-magnitude higher than environmental levels. The most recent study (1) used concentrations closest to those found in nature. However, Sussarellu et al. calculate their MP concentrations based on sediment data from a pollution hot-spot area close to a ship-breaking yard in India (8, 10); thus, these data are unlikely to be representative of general concentrations beyond the local area.

Microplastic research is an emerging field, and there is a lot of misunderstanding and in some cases over-reaction or misinterpretation of results from MP science in the public. We therefore strongly suggest that future studies of MP impact on marine ecosystems should also include concentrations that have been documented in the environment to yield more realistic estimates of sublethal effects.

Acknowledgments

The authors thank Thomas Kiørboe and Mary Wisz for helpful comments on this letter.

^aSection for Marine Ecology and Oceanography, National Institute of Aquatic Resources, Technical University of Denmark, 2920 Charlottenlund, Denmark
Author contributions: K.E. and T.G.N. designed research; R.L. performed research; T.G.N. provided scientific leadership; and R.L. and K.E. wrote the paper.

The authors declare no conflict of interest.

Data deposition: A fully referenced version of the data review has been deposited at figshare.com, accessible under: https://figshare.com/articles/Size_and_concentration_comparison_for_microplastics_between_reported_environmental_levels_and_laboratory_exposure_studies/3206449.

¹To whom correspondence should be addressed. Email: roble@aqu.dtu.dk.

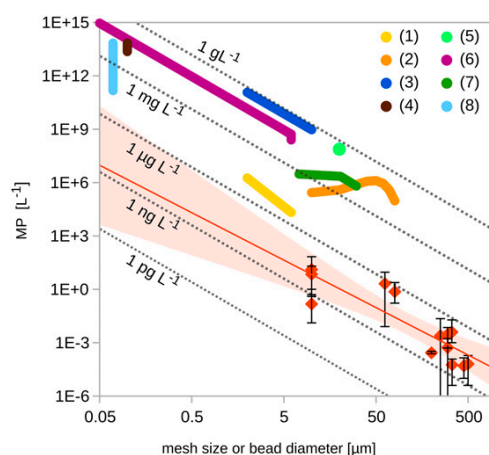


Fig. 1. Comparison between MP concentrations used in exposure studies (fat colored lines) and observed environmental levels (red diamonds: average concentrations; error bars: minimum and maximum concentration). The red line extrapolates the field data with best fit using a power law regression ($y = 3,188 \cdot x^{-2.67}$; 95% confidence intervals as pale red areas). The dotted gray isolines show equal mass concentrations for particles density = $1.04 \text{ g} \cdot \text{cm}^{-3}$. The x-axis scale is the diameter of the micro beads in exposure experiments and the mesh size used in environmental studies, respectively.

- 1 Sussarellu R, et al. (2016) Oyster reproduction is affected by exposure to polystyrene microplastics. *Proc Natl Acad Sci USA* 113(9):2430–2435.
- 2 von Moos N, Burkhardt-Holm P, Koehler A (2012) Uptake and effects of microplastics on cells and tissue of the blue mussel *Mytilus edulis* L. after an experimental exposure. *Environ Sci Technol* 46(20):11327–11335.
- 3 Browne MA, Dissanayake A, Galloway TS, Lowe DM, Thompson RC (2008) Ingested microscopic plastic translocates to the circulatory system of the mussel, *Mytilus edulis* (L.). *Environ Sci Technol* 42(13):5026–5031.
- 4 Besseling E, Wegner A, Foekema EM, van den Heuvel-Greve MJ, Koelmans AA (2012) Effects of microplastic on fitness and PCB bioaccumulation by the lugworm *Arenicola marina* (L.). *Environ Sci Technol* 47(1):593–600.
- 5 Cole M, Lindeque P, Fileman E, Halsband C, Galloway TS (2015) The impact of polystyrene microplastics on feeding, function and fecundity in the marine copepod *Calanus helgolandicus*. *Environ Sci Technol* 49(2):1130–1137.
- 6 Lee KW, Shim WJ, Kwon OY, Kang JH (2013) Size-dependent effects of micro polystyrene particles in the marine copepod *Tigriopus japonicus*. *Environ Sci Technol* 47(19):11278–11283.
- 7 Cole M, et al. (2013) Microplastic ingestion by zooplankton. *Environ Sci Technol* 47(12):6646–6655.
- 8 Besseling E, Wang B, Lüring M, Koelmans AA (2014) Nanoplastic affects growth of *S. obliquus* and reproduction of *D. magna*. *Environ Sci Technol* 48(20):12336–12343.
- 9 Bhattacharya P, Lin S, Turner JP, Ke PC (2010) Physical adsorption of charged plastic nanoparticles affects algal photosynthesis. *J Phys Chem C* 114(39):16556–16561.
- 10 Reddy MS, Basha S, Adimurthy S, Ramachandraiah G (2006) Description of the small plastics fragments in marine sediments along the Alang-Sosiya ship-breaking yard, India. *Estuar Coast Shelf Sci* 68(3–4):656–660.

Supplementary Information for

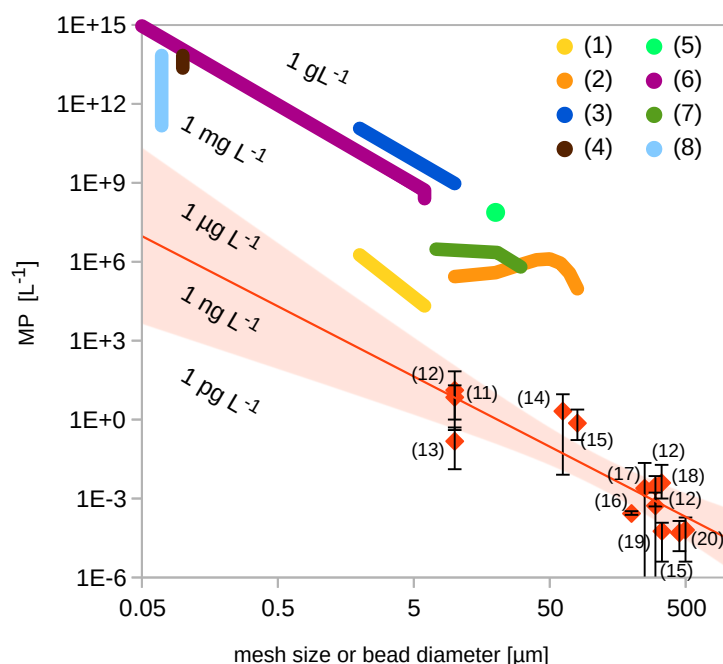
"Microplastic exposure studies should be environmentally realistic"

Authors: Robin Lenz^a, Kristina Enders^a,
and Torkel Gissel Nielsen^a

Affiliations:

^aSection for Marine Ecology and Oceanography,
National Institute of Aquatic Resources,
Technical University of Denmark,
2920 Charlottenlund, Denmark

Content: Fig. 1 with additional references.



References

1. Sussarellu R, Suquet M, Thomas Y, Lambert C, Fabioux C, Pernet MEJ, et al. Oyster reproduction is affected by exposure to polystyrene microplastics. *Proc Natl Acad Sci* . 2016;113(9):201519019. Available from: <http://www.pnas.org/lookup/doi/10.1073/pnas.1519019113>
2. von Moos N, Burkhardt-Holm P, Koehler A. Uptake and Effects of Microplastics on Cells and Tissue of the Blue Mussel *Mytilus edulis* L. after an Experimental Exposure. *Environ Sci Technol* . 2012 ;46(20):327–35. Available from: <http://pubs.acs.org/doi/abs/10.1021/es302332w>
3. Browne MA, Dissanayake A, Galloway TS, Lowe DM, Thompson RC. Ingested microscopic plastic translocates to the circulatory system of the mussel, *Mytilus edulis* (L). *Environ Sci Technol* . 2008 Jul 1;42(13):5026–31. Available from: <http://www.ncbi.nlm.nih.gov/pubmed/18678044>
4. Besseling E, Wegner A. Effects of Microplastic on Fitness and PCB Bioaccumulation by the Lugworm *Arenicola marina* (L.). *Environ Sci Technol* . 2012 ;47:593–600. Available from: <http://pubs.acs.org/doi/abs/10.1021/es302763x>
5. Cole M, Lindeque P, Fileman E, Halsband C, Galloway TS. The Impact of Polystyrene Microplastics on Feeding, Function and Fecundity in the Marine Copepod *Calanus helgolandicus*. *Environ Sci Technol* . 2015 Jan 6 ; Available from: <http://www.ncbi.nlm.nih.gov/pubmed/25563688>
6. Lee K, Shim WJ, Kwon OY, Kang J. Size-Dependent Effects of Micro Polystyrene Particles in the Marine Copepod *Tigriopus japonicus*. *Environ Sci Technol* . 2013 Oct;47(19):11278–83. Available from: <http://pubs.acs.org/doi/abs/10.1021/es401932b>
7. Cole M, Lindeque P, Fileman E, Halsband C, Goodhead R, Moger J, et al. Microplastic ingestion by zooplankton. *Environ Sci Technol* . 2013 Jun 18;47(12):6646–55. Available from: <http://www.ncbi.nlm.nih.gov/pubmed/23692270>
8. Besseling E, Wang B, L??rling M, Koelmans AA. Nanoplastic affects growth of *S. obliquus* and reproduction of *D. magna*. *Environ Sci Technol* . 2014 Oct 21;48(20):12336–43. Available from: <http://pubs.acs.org/doi/abs/10.1021/es503001d>
11. Norén F, Naustvoll L-J. Pilot study: Survey of microscopic anthropogenic particles in Skagerrak . Lysekil, Sweden; 2011. Available from: <http://www.miljodirektoratet.no/old/klif/publikasjoner/2779/ta2779.pdf>
12. Norén F, Norén K, Magnusson K. Marint mikroskopiskt skräp Undersökning längs svenska västkusten . 2014. Available from: <http://www.lansstyrelsen.se/vastragotaland/SiteCollectionDocuments/Sv/publikationer/2014/2014-52.pdf>
13. Enders K, Lenz R, Stedmon CA, Nielsen TG. Abundance, size and polymer composition of marine microplastics ≥10μm in the Atlantic Ocean and their modelled vertical distribution. *Mar Pollut Bull* . 2015 Nov;100(1):70–81. Available from: <http://linkinghub.elsevier.com/retrieve/pii/S0025326X15300370>
14. Desforges J-PW, Galbraith M, Dangerfield N, Ross PS. Widespread distribution of microplastics in subsurface seawater in the NE Pacific Ocean. *Mar Pollut Bull* . Elsevier Ltd; 2014 Jan 4 ; Available from: <http://www.ncbi.nlm.nih.gov/pubmed/24398418>
15. Norén F. Small plastic particles in Coastal Swedish waters. . 2007. Available from: [http://www.kimointernational.org/WebData/Files/Small plastic particles in Swedish West Coast Waters.pdf](http://www.kimointernational.org/WebData/Files/Small%20plastic%20particles%20in%20Swedish%20West%20Coast%20Waters.pdf)
16. Cole M, Webb H, Lindeque PK, Fileman ES, Halsband C, Galloway TS. Isolation of microplastics in biota-rich seawater samples and marine organisms. *Sci Rep* . 2014 Jan 31 ;4:4528. Available from: <http://www.ncbi.nlm.nih.gov/pubmed/24681661>
17. Lusher AL, Burke A, O'Connor I, Officer R. Microplastic pollution in the Northeast Atlantic Ocean: Validated and opportunistic sampling. *Mar Pollut Bull* . Elsevier Ltd; 2014 Sep ; Available from: <http://linkinghub.elsevier.com/retrieve/pii/S0025326X14005530>
18. Lattin GL, Moore CJ, Zellers a F, Moore SB, Weisberg SB. A comparison of neustonic plastic and zooplankton at different depths near the southern California shore. *Mar Pollut Bull* . 2004 Aug ;49(4):291–4. Available from: <http://www.ncbi.nlm.nih.gov/pubmed/15341821>
19. Law KL, Morét-Ferguson S, Maximenko NA, Proskurowski G, Peacock EE, Hafner J, et al. Plastic accumulation in the North Atlantic subtropical gyre. *Science* . 2010 Sep 3 ;329(5996):1185–8. Available from: <http://www.ncbi.nlm.nih.gov/pubmed/20724586>
20. Doyle MJ, Watson W, Bowlin NM, Sheavly SB. Plastic particles in coastal pelagic ecosystems of the Northeast Pacific ocean. *Mar Environ Res* . Elsevier Ltd; 2011;71(1):41–52. Available from: <http://dx.doi.org/10.1016/j.marenvres.2010.10.001>

Appendix

Abbreviations

Abbreviation	Definition
ABS	acrylonitrile butadiene styrene
DOM	dissolved organic matter
EPM	empirical predictive modelling
EVA	ethylene-vinyl acetate
EU	European Union
FAIR	Findable, Accessible, Interoperable, and Reusable
FTIR	Fourier Transform Infrared Spectroscopy
GEPARD	Gepard Enabled PARTicle Detection
GLM	generalised linear model
HDPE	high-density polyethylene
HELCOM	Helsinki Commission (Baltic Marine Environment Protection Commission)
HNM	hydrodynamic numerical modelling
ICES	International Council for the Exploration of the Sea
LDPE	low-density polyethylene
MARPOL 73/78	International Convention for the Prevention of Pollution from Ships
ML	machine learning
MP	microplastics
MPDB	Marine Plastic Database
MSFD	Marine Strategy Framework Directive
NCV	nested cross-validation
NIXVEGS	Nested Iterative (stratified) X-Validation-to-Ensemble-modelling through Grid Searches
OSPAR	Oslo and Paris Convention for the Protection of the North-East Atlantic
PA	polyamide
PAH	polycyclic aromatic hydrocarbons
PC	polycarbonate
PCB	polychlorinated biphenyls
PCo1	first principal coordinate
PE	polyethylene
perc_MUD	percentage of mud fraction
PET	polyethylene terephthalate
PMMA	polymethylmethacrylate
POM	particulate organic matter
PP	polypropylene
PS	polystyrene
PTFE	polytetrafluoroethylene
PU	polyurethane
PVC	polyvinyl chloride
QuEChERS	Quick, Easy, Cheap, Effective, Rugged, and Safe
RF	random forest
WWTP	wastewater treatment plant
XGB linear	extreme gradient boosting (linear base learner)
XGB tree	extreme gradient boosting (tree-based base learner)

Statement on the usage of language tools

In the preparation of this synopsis, language assistance tools including dict.cc, Linguee.com, DeepL.com and ChatGPT were consulted to support the refinement of English grammar, style, and readability, in instances of linguistic uncertainty. ChatGPT was additionally employed on occasion for preliminary literature searches, with all outputs subsequently verified through manual in-depth review, for a final typographical check and verification of the completeness of the abbreviation list.

Eigenständigkeitserklärung

Doktorandinnen/Doktoranden-Erklärung gemäß § 4 Absatz 1 Buchstaben g und h der Promotionsordnung der Mathematisch-Naturwissenschaftlichen Fakultät der Universität Rostock

Name: **Kristina Enders**

Ich habe eine Dissertation zum Thema

Analogies Between Microplastics and Natural Particles for Inventory Mapping in Aquatic Sediments

an der Mathematisch-Naturwissenschaftlichen Fakultät der Universität Rostock angefertigt.

Dabei wurde ich von Herrn **Prof. Dr. Matthias Labrenz** betreut.

Ich gebe folgende Erklärung ab:

1. Die Gelegenheit zum vorliegenden Promotionsvorhaben ist mir nicht kommerziell vermittelt worden. Insbesondere habe ich keine Organisation eingeschaltet, die gegen Entgelt Betreuerinnen/Betreuer für die Anfertigung von Dissertationen sucht oder die mir obliegenden Pflichten hinsichtlich der Prüfungsleistungen für mich ganz oder teilweise erledigt.
2. Ich versichere hiermit an Eides statt, dass ich die vorliegende Arbeit selbstständig angefertigt und ohne fremde Hilfe verfasst habe. Dazu habe ich keine außer den von mir angegebenen Hilfsmitteln und Quellen verwendet und die den benutzten Werken inhaltlich und wörtlich entnommenen Stellen habe ich als solche kenntlich gemacht.

Rostock, den

.....

Acknowledgement

The rules require me to declare that I have worked independently on this thesis - yet, it is also clear that this work would not have been possible without a large supportive network around me. As specific scientific or technical support has already been acknowledged in each of the respective publications, I would like to complement here on a more personal level.

Special thanks to my supervisor, Matthias Labrenz, who has granted me the independence to develop and follow my own research pathway. Thanks for your confidence. My other thesis committee members with their fields of expertise reflected the intriguing interdisciplinarity of my PhD topic: Sonja Oberbeckmann (microbiologist), Helge Arz (marine geologist) and Colin A. Stedmon (marine chemist). Besides the constructive individual and committee discussions I had with all of you, I highly appreciated your exceptionally critical scientific views, which gave me the confidence, that if I would postulate nonsense, you would notice. A special thanks to Sonja for your dedication in landing and coordinating the MICROPOLL project. I would also like to thank Hans Burchard (marine physicist), not only for his profound expertise and fruitful discussions, but also for his inspiring view on science as a kind of art.

I would like to thank the entire IOW, a research institute with short distances, mentally and spatially, between specialists' doors in which this thesis could evolve. Juliana A. Ivar do Sul and Alexander S. Tagg thanks so much for the good time we shared in our micro-room of high brainpower and MP abundance per m² and your helping hands whenever needed. Franziska Klaeger, thanks for being the truly irreplaceable coordinator, formally, and the informal ombudswoman, holding everything together. Along those lines, thanks also to the Spectroscopy and Microplastics group at the IPF (Andrea K  ppler, Franziska Fischer, Julia L  tsch, Melinda Arnold, Anne R  dinger, Josef Brandt, Dieter Fischer, Klaus Eichhorn, Mareike Schumacher und Lilly Lotzmann), a collaboration that persists already since my Master thesis. It has always been a pleasure to get into deeply detailed analytical debates. To Dieter Fischer, I greatly appreciate your trust and support, which allowed me to complete my PhD while embarking on new projects in your group.

For our life-collaboration, Robin, I thank you for going this path together in this kind of a 'parallel PhD trial design' and along the special PhD oscillation curve meandering between enthusiasm and exhaustion. Especially thank you for being my complementary counterpart for literally any discussion that a research idea, of technical or conceptual nature, needed to develop and reminding me to focus, when the researcher's thoughts ran too wild.

A very warm thank you to our families for the happy baby sitting. Thanks, Lotta, just for being with us.

The research in this thesis was primarily based on received funding from BONUS MICROPOLL project, supported by BONUS the joint Baltic Sea research and development programme (Art 185), funded jointly by the European Union and the German Federal Ministry of Education and Research (BMBF), Grant No. 03F0775A.